THE APPLICATION OF FINITE ELEMENT ANALYSIS TO THE DESIGN OF EMBEDDED RETAINING WALLS

RICHARD IAN WOODS

School of Engineering

University of Surrey

Volume 2

A Thesis submitted for the degree of
Doctor of Philosophy

September 2003

CONTENTS

CHAPTER 3 THE CRISP FINITE ELEMENT PACKAGE APPLIED TO RETAINING WALL ANALYSIS

CHAPTER 5 CONSTITUTIVE MODELLING AND PARAMETER SELECTION

CHAPTER 6 MODELLING OF CONSTRUCTION AND LONG TERM EFFECTS

NOTATION

A	cross-sectional area (of wall, soil sample, etc.)
A, B	Skempton's pore pressure coefficients
A,B,C	coefficients in the Jardine *et al.* non-linear elastic model
A	matrix linking element stresses to nodal forces
B	ratio defined in terms of principal effective stresses σ_1', σ_2', σ_3'
B	matrix relating element strains to nodal displacements
C_v	coefficient of consolidation (vertical drainage)
D	depth of penetration of wall below formation level
D	matrix relating element stresses to strains
E	Young's modulus (drained E′ or undrained E_u)
E*	constrained (oedometric) modulus
E_h	Young's modulus in horizontal direction
E_o	Young's modulus at ground surface
E_v	Young's modulus in vertical direction
E_w	Young's modulus of wall material
F	nodal force
F	vector of nodal forces
$\mathbf{F_{exc}}$	vector of nodal forces representing unloading due to excavation
G	shear modulus
G_{vh}	shear modulus in v-h plane
H	retained height (depth of excavation)
	gradient of Hvorslev surface in q : p′ space
	layer thickness
H_L	height by which pore water pressure head has been lowered (by drainage)
I	second moment of area
J	yield criterion type
J	Jacobian matrix
K	finite element stiffness matrix
K	bulk modulus
$\mathbf{K^e}$	element stiffness matrix
K_a	coefficient of earth pressure : active condition
K_f	bulk modulus of equivalent pore fluid
K_i	coefficient of earth pressure post-installation
K_o	coefficient of earth pressure at rest ($= \sigma'_h/\sigma'_v$)
K_{ot}	coefficient of earth pressure at rest in terms of total stress ($= \sigma_h/\sigma_v$)
K_p	coefficient of earth pressure : passive condition
K_r	stiffness ratio between soil and structure
K_w	bulk modulus of water
L	length (of wall, or structural member)
L	flow matrix in coupled analysis
LR	non-dimensional geometric ratio defining mesh grading
LR_{95}	value of LR at which parameter is 95% of "true" value
LR_{99}	value of LR at which parameter is 99% of "true" value

M	wall bending moment (+/- prefix signifies +ve or -ve moment)
M_t	bending moment at toe of wall
N	number of increments in a block
	number of elements in a mesh
N	matrix of interpolation (shape) functions
N_e	number of increments for pore water pressure equalization in a coupled analysis
N_i	shape function for stress smoothing
NN	number of nodes in a finite element mesh
OCR	overconsolidation ratio ($=\sigma'_{vmax} / \sigma'_v$)
P	point load or force
	axial force in prop (compressive) or anchor (tensile)
P_o	prestress load (in an anchor)
	out-of-balance force at a node
Q	shear force (in wall)
Q, T	characteristic mesh dimensions used in grading studies (r-refinement)
R	non-dimensional geometric ratio for FE mesh (X/H or Y/W)
R_i	diagonal decay ratio
R(i)	load increment ratio ($\Sigma R(i) = 1.0$)
R_{95}	value of R at which parameter is 95% of "true" value
R_{99}	value of R at which parameter is 99% of "true" value
S	vertical ground surface movement (+/- prefix signifies +ve or -ve Y direction)
S	global smoothing matrix
$\mathbf{S}^e$	element smoothing matrix
T_e	time for pore water pressure equalization
T_v	time factor for consolidation (vertical drainage)
U_v	average degree of consolidation (vertical drainage)
V	excavation heave
W	half-width of excavation
X	distance from back of wall to far edge of mesh
Y	distance from formation level to base of mesh
Y_o	reference elevation for parameter varying with depth
YR	yield ratio (growth of Cam-clay yield locus)

a, b	Henkel's pore pressure coefficients
a_o, a_1, ..	displacement approximation function coefficients
a, b, c	polynomial function coefficients
a_i	length of an element side
a	vector of nodal displacements
b	depth of web on 'T' section wall panel
b	body force vector
c′	effective cohesion
c_u	undrained shear strength
c_{uo}	undrained shear strength at ground surface
c_w	wall adhesion

d	diameter (of a pile)
	depth of web on 'T' section wall
d	vector of displacements at a point within an element
e	voids ratio
err	equilibrium error
$\mathbf{f}_b$	vector of equivalent nodal loads for body forces
f	yield function
f_d	correction factor for heave calculation
$\mathbf{f}^e$	RHS vector in smoothing process
$\mathbf{f}_\sigma$	ditto
$\mathbf{f}_t$	vector of equivalent nodal loads for applied tractions
g	acceleration due to gravity
h	thickness of prop slab
	total head
	height of element centroid above a particular elevation on a wall
	interval size in finite difference method
	node spacing in finite element method
k	coefficient of permeability
k_h	coefficient of permeability in horizontal direction (or k_x)
k_i	mesh grading ratio
k_v	coefficient of permeability in vertical direction (or k_y)
k_n	normal stiffness (of an interface)
k_s	shear stiffness (of an interface)
m	mesh grading element side length ratio
	rate of increase of Young's modulus (E′ or E_u) with depth
m	a multiplying vector containing 1s or 0s
m_q m_r m_s	mesh grading element side length ratios in particular regions
m_v	coefficient of volume compressibility
n	degree of anisotropy = E_h/E_v
p	mean stress invariant (axisymmetry)
	applied pressure
p'_c	maximum previous mean effective stress
q	deviatoric stress invariant (axisymmetry)
r	element aspect ratio
s	mean stress invariant (plane strain)
	gradient of tensile crack line in q:p′ space
	spacing of piles (centre to centre)
s_h	horizontal spacing or props
$\mathbf{s}_n$	vector of local consistent stresses
t	wall thickness
	time
	thickness of an interface element
	deviatoric stress invariant (plane strain)
t_e	time taken for pore water pressure equalization in a coupled analysis
t	vector of applied tractions

u	pore water pressure
	displacement in x direction
u_e	excess pore water pressures
u_f	final pore water pressure
u_o	initial pore water pressure
v	displacement in y direction
w	Gaussian integration weighting value
	width of 'T' section panel
	intensity of UDL loading
x, y	Cartesian co-ordinate directions
z	depth below ground surface
z′	depth below formation level
z_w	depth to ground water
Δ_σ	percentage error in computed stress
Φ	matrix term depending on excess p.w.p. gradients in coupled analysis
Γ	value of output parameter
Γ^*	"true" value of output parameter
Λ	ratio of current stiffness E_u to that at a reference strain
α	ratio of K_w to K′
	finite difference grid spacing ratio
	coefficient in the Jardine *et al.* non-linear elastic model
χ	degree of nonhomogeneity of soil stiffness
δ	wall horizontal displacement
δ'	effective angle of soil-wall friction
δx	incremental x displacement
δy	incremental y displacement
ε	normal strain
ε_v	volume strain
ε	strain vector
ϕ	angle of internal friction
	arbitrary shape function
γ	shear strain
	unit weight
	coefficient in the Jardine *et al.* non-linear elastic model
γ_{conc}	unit weight of concrete
γ_w	unit weight of water
η	local co-ordinate
ν	Poisson's ratio
θ	rotation (at a node)
	angle of rotation of stress axes
	Lode angle (stress invariant)
	factor in two-point finite difference approximation ($0 \leq \theta \leq 1$)
	angle of inclination (to the horizontal) of a ground anchor tendon

σ	normal stress
σ	stress vector
τ	shear stress
τ_f	shear strength
ξ	local ordinate
ψ	angle of dilation
2×2	(reduced) numerical integration rule for 2-D elements
3×3	(full) numerical integration rule for 2-D elements

subscripts etc.

a	axial
ave	average
c	centroidal
e	excess
	equalization
	excavated (side of wall)
h	horizontal
m	mean
max	maximum
min	minimum
i	initial, post-installation
o	initial (in-situ)
	at (ground) surface
r	retained (side of wall)
r, s	rough, smooth (boundary)
u	undrained
v	vertical
	volumetric
x, y, z	x, y, z direction (Cartesian)
95, 99	95, 99 %

superscripts

e	element
	elastic
p	plastic
′	effective

prefixes

Δ	increment (large)
δ	increment (small)
d	increment (infinitesimal)

suffixes

(x)	varying as a function of horizontal distance; a profile
(z)	varying as a function of depth; a profile

ABBREVIATIONS

AGS	Association of Geotechnical Specialists
APM	applied pressure method
AR	global aspect ratio of finite element mesh
ASCE	American Society of Civil Engineers
BEM	boundary element method
BFC3m	best-fit curve smoothing (of 3×3 Gauss point stresses in multiple elements)
BFL2	best-fit line (of 2×2 Gauss point stresses)
BFL3	best-fit line smoothing (of 3×3 Gauss point stresses)
BFP3	best-fit plane smoothing (of 3×3 Gauss point stresses)
BMD	bending moment diagram
BRE, BRS	Building Research Establishment, or Station
CAD/CAM	computer-aided design/computer-aided manufacture
CIRIA	Construction Industry Research and Information Association
CSSM	critical state soil mechanics
CSB	constant strain bar or beam
CSL	critical state line
CST	constant strain triangle
CuST	cubic strain triangle
d.o.f.	degree(s) of freedom
DTp	Department of Transport
ECSMFE	European Conference on Soil Mechanics and Foundation Engineering
EPBM	earth pressure bending moment
EPSF	earth pressure shear force
EPSRC	Engineering and Physical Sciences Research Council
ESP	effective stress path
FDM	finite difference method
FE / FEA / FEM	finite element / finite element analysis / finite element method
FIM	full installation method (of modelling wall construction)
FL	formation level
FHWA	Federal Highways Administration (US)
GWL	ground water level
HILE	homogeneous isotropic linear elastic
HPA	horizontal plan analysis
ICE	Institution of Civil Engineers
IP	integration point (Gaussian)
ITMF	flag indicating uniform (=0) or varying (=1) time intervals
LHS	left-hand side (of an equation)
LSB/LST/LSQ	linear strain bar (beam) / triangle / quadrilateral

LSTp/LSQp	linear strain triangle / quadrilateral with excess pore water pressure d.o.f.
LSBF	least-squares best fit
MIT	Massachusets(?) Institute of Technology
MNR	modified Newton-Raphson
MOM	multiple-overlay method
NAFEMS	National Agency for Finite Element Methods and Standards
NINC	total number of increments
NLR	nonuniform load ratios
NOIB	total number of increment blocks
OCR	overconsolidation ratio
OoB	out-of-balance (load)
PCG	preconditioned conjugate gradient (solution method)
RHS	right-hand side (of an equation)
SA3	simple averaging
SFD	shear force diagram
SI	site investigation
SSI	soil-structure interaction
T[R]RL	Transport [and Road] Research Laboratory
TSP	total stress path
UDL	uniformly distributed load
ULR	uniform load ratios
VSA	vertical section analysis
WIP	wished-in-place
WSBM	wall stress bending moment
WSSF	wall stress shear force

Computer programs

CRISP	CRItical State Program
FLAC	Fast Lagrangian Analysis of Continua
FREW	Flexible REtaining Wall program
ICFEP	Imperial College Finite Element Program
WALLAP	WALL Analysis Program

CHAPTER 6
MODELLING OF CONSTRUCTION AND LONG-TERM EFFECTS

6.1 Introduction

Once decisions have been made regarding the finite element mesh, constitutive model(s) and associated material parameters, attention then focuses on how to model the physical process of constructing the wall and support system, and their subsequent behaviour in the longer term. This can be broken down into five distinct phases:

i) installation of the wall,
ii) excavation of soil in front of the wall,
iii) installation of props/anchors (and removing them if they are temporary),
iv) long-term equalization of pore water pressures (i.e. dissipation of excess pore pressures), and
v) possible future fluctuations of groundwater and/or piezometric levels.

Phase (i) will occur ahead of any of the others, and will involve construction techniques such as diaphragm walling and bored piling (see Chapter 3). There will be an interlacing between (ii) and (iii), especially in cases of multiple propping/anchoring - there is also the possibility of temporary soil berms being left in place against the wall for a specified period. Walls which are singly propped at the crest (e.g. Bell Common tunnel, Hubbard *et al.*, 1984) will tend to have the permanent props installed early on, prior to bulk excavation - often in shallow, transverse trenches dug at the appropriate spacings - to keep wall movements to an absolute minimum. Walls which are singly propped at formation level in the long-term (e.g. Aldershot Road Underpass, Carder *et al.*, 1997) will usually have one or more levels of temporary support (props or anchors installed as excavation proceeds), which are removed when final dig level is reached and the permanent prop has been constructed.

Sometimes it is only the construction phase (short term) which is of interest to the analyst. This would be the case if the retaining wall was part of the temporary works, supporting a deep excavation until a permanent structure was built (perhaps incorporating the temporary walls within it). Under these circumstances the long-term equalization of pore water pressures, phase (iv), may not be of particular concern. However, it is more common for the

long-term case to be of equal importance as the short term, because excavation stability generally deteriorates with time. It is unlikely that long-term equalization will be accompanied by changes in wall geometry or support, so phase (iv) can be considered in isolation.

Fluctuating groundwater and/or piezometric levels, phase (v), are a feature of several urban areas in the world, such as Paris, New York, Tokyo, and London. Water pressures in underlying confined aquifers, depressed by abstraction for industrial use in the last century, are now recharging to former levels following the cessation of pumping activities. This has implications for a range of buried structures, including tunnels, piled foundations, deep basements, and retaining walls. In the writer's experience, the explicit modelling of rising groundwater levels in embedded retaining wall analysis is not common, but where it has been taken into account the effects have been significant (e.g. A406 Walthamstow, Appendix A).

Numerical experiments have been conducted by the writer to establish the potential errors which might be introduced into the results of an analysis, through the way(s) in which construction and long-term equalization are modelled. These experiments will be described in the following sub-sections. Because the individual topics embraced by this chapter are quite distinct and not all have been investigated by other workers, a review of previous work is given at the beginning of each section before detailing the analyses conducted and the results obtained. Every effort has been made to ensure that work conducted by the writer is clearly separated from the earlier contributions of others.

6.2 Wall Installation

6.2.1 Previous work

It is now generally accepted (e.g. Symons and Carder, 1993; Powrie and Kantartzi, 1996) that the diaphragm wall process (and, to a lesser extent, contiguous bored pile installation) leads to a reduction in lateral earth pressures during wall construction. This can be quantified by a post-installation coefficient of lateral earth pressure (K_i) which may be significantly lower than the "at rest" value, K_o. This is obviously of great importance to the designer, as it will lead to a reduction in wall thickness and propping requirements. In fact, the use of (undisturbed) K_o has become accepted as being partly responsible for the overestimation of wall movements, bending moments, and prop loads often observed in FE analyses.

As identified in Chapter 2, when modelling the installation of an embedded wall with finite elements, there are three different strategies that might be adopted:

a) begin the analysis with the wall already installed (so-called "wished-in-place") - the wall elements are part of the primary mesh and are present in the analysis from the in-situ stage,

b) begin with original undisturbed ground and then swap the relevant soil and concrete elements in the same increment block - the wall elements are part of the parent mesh (as "overlays") but are removed ("ghosted out") prior to the in-situ stage, or

c) begin with the original undisturbed ground and then simulate the excavation of soil under bentonite slurry support (from top-down), the placing of wet concrete via tremie (from bottom-up), and the subsequent hardening of the concrete - multiple overlay elements are defined in the parent mesh, ghosted out at the in-situ stage, and swapped in as requested.

Kutmen (1986) appears to have been one of the first to investigate the effects of wall installation on lateral stress distributions. Analysing a diaphragm wall in plane strain, Kutmen performed coupled-consolidation analyses with the following stages:

i) excavate under bentonite support (soil elements out, bentonite pressure applied to sides and base)
ii) allow delay (up to seven days) before concreting
iii) tremie in wet concrete from the bottom, displacing bentonite upwards (applied pressure distribution on sides and base of trench adjusted)
iv) allow concrete to set ($0 \rightarrow 12$ hrs)
v) install hard concrete (fix sides and base of trench/hole against further movement)
vi) allow consolidation/swelling of surrounding ground for up to 1 year

The sides of the trench were considered permeable during the wet concrete stage (only). An axisymmetric analysis was also carried out to represent a single bored pile - identical stages, except no bentonite support. The analyses showed that lateral stresses do not totally recover after concreting (only 30-50% for a bored pile), and that delays in concreting accentuated the effects of installation. No firm suggestions were made on a post-installation K (i.e. K_i), and neither was subsequent bulk excavation in front of the wall investigated. Some key results were later presented by Gunn and Clayton (1992), as supervisors of Kutmen's research.

Higgins *et al.* (1989) used ICFEP to compare different installation strategies in a re-analysis of the secant bored pile walls forming the Bell Common tunnel. Their installation method treated the line of piles as an equivalent plane strain slot and involved (post-installation in italics):

a) excavate slot without bentonite slurry support (remove soil elements)
b) fill with wet concrete (apply pressures on sides and base of trench/hole simultaneously with reaching full-depth excavation)
c) install hard concrete (swop in elements)
d) *bulk excavation in front of wall (remove elements)*
e) *switch from undrained to drained long-term conditions (impose pore pressure changes)*

Even though their analyses were uncoupled (and thus inferior to Kutmen's), they showed that the inclusion of installation effects produced much better agreement with field observations. As the walls comprised secant bored piles, they also compared plane strain and axisymmetry representations as a separate exercise, and were able to show a genuine "bracketing" of field measurements. They concluded that further improvement of prediction would require full 3D analysis, whilst accepting that this was impractical in design situations.

Gunn *et al.* (1993) extended the work of Kutmen (1986), again using the more rigorous coupled-consolidation approach afforded by CRISP. They too examined the Bell Common tunnel walls and used the following strategy (post-installation in italics):

a) excavate soil under bentonite support (soil elements out, bentonite slurry pressure applied to sides and base)
b) tremie in wet concrete from the bottom, displacing bentonite upwards (applied pressure distribution on sides and base of trench adjusted)
c) allow concrete to set, with water migration into clay permitted
d) allow 28 days during which surrounding ground can consolidate/swell
e) *bulk excavation in front of wall, with or without top prop (remove soil/install prop)*

This was very similar to Kutmen, but with the addition of a bulk excavation stage. Considering only the post-excavation bending moments, they found that installation effects were not so important for a cantilever wall, but made a big difference if a top prop was in place prior to excavation. The effect became greater as the in-situ ground water level was lowered. They pointed out that, as precise site procedures are rarely known in advance, it may be better to conduct bracketing analyses, as a ".. best shot is unlikely to hit the target.."

De Moor (1994) pointed out that the WIP and FIM assumptions in plane strain would over- and underestimate the post-installation lateral stress respectively. As an alternative, she presented CRISP analyses involving a plan (horizontal) section through a series of wall panels, instead of the vertical cross section normally used. De Moor's analyses were coupled, plane strain (implying that σ_v could reduce), and went directly from bentonite slurry pressure to hardened concrete. Investigation focused on the stress conditions behind a particular wall panel at a fixed depth of 15m as both it (and subsequent adjacent panels) were constructed. Panel width and K_o were varied in a sensitivity study. The results showed a consistent and credible pattern of stress change with time, and the agreement with available field data (e.g. Symons and Carder, 1993) was reasonable. An excavation ratio was proposed in terms of current and initial lateral stress and bentonite pressure, enabling non-dimensional charts to be plotted, from which more realistic values for K_i could be estimated. De Moor's work attracted some criticism (Simpson and Ng, 1995; St John *et al.*, 1995), but the basic idea of using complementary 2D analyses showed promise.

Ng *et al.* (1995) took the concept a step further by performing both a horizontal plan analysis (HPA) in plane stress and a vertical section analysis (VSA) in plane strain. First, the HPA of a single wall panel showed a drop in lateral stress at the centre of the panel, but a big increase just beyond the ends. Construction of two further (adjacent) panels produced an oscillating profile of σ_h and a permanent inward horizontal displacement δ_h ($\approx$ 3mm) at the soil/wall interface after concrete setting. It also suggested that horizontal arching (by itself) was merely a temporary load transfer mechanism, with the average lateral stress σ_h eventually returning to near its original value. Downward load transfer was postulated as being the key mechanism, with σ_h on the wall reducing but σ_h just below the toe increasing. In the VSA, the permanent deformation δ_h was imposed as a prescribed boundary displacement - the intermediate bentonite and wet concrete stages being omitted. Reasonable agreement with field data from the Lion Yard excavation (Ng, 1992) was shown, but full 3D work was advocated as the only way to make further progress.

The first full 3D FE analysis of wall installation effects was carried out by Gourvenec (1998), and reported by Gourvenec and Powrie (1999). A sequence very similar to that used by Gunn *et al.* (1993) was employed, except in full 3D. Imposed wet concrete pressures were bilinear, following the recommendations of Lings *et al.* (1994). A wall comprising nine bays was constructed, with panels constructed on a "hit and miss" (i.e. staggered) basis. Panel length

could be varied, and K_o was inversely proportional to depth. Results presented were profiles of coefficient of lateral pressure, wall movements, and zones of significant stress reduction. They showed that the reduction in horizontal stress ($-\Delta\sigma_h$) near the centre of a panel and the increase ($+\Delta\sigma_h$) just below the toe were partly reversed by adjacent panel construction. Panels further away had diminishing impact on $-\Delta\sigma_h$, but $+\Delta\sigma_h$ was almost fully reversed - in stark contrast to plane strain analysis. For full 3D effects to occur in the field, they recommended that $L/H \leq 3$. They also suggest that a 2D plane strain analysis in which a displacement profile was imposed on a wall already in-place would give acceptable accuracy in a design situation.

Ng and Yan (1998) although using the finite difference method (FLAC 3D), analysed the construction sequence of a single diaphragm wall panel in stiff clay. They found significant stress reduction behind the centre of the panel, attributed to downward load transfer ($\approx 1/3$) and horizontal arching ($\approx 2/3$). These results tended to confirm what was seen in the uncoupled HPA/VSA work of Ng *et al.* (1995) but, as they were only for a single panel, their usefulness was limited. Extension to three adjacent panels (Ng and Yan, 1999), again with FLAC, resulted in smaller $-\Delta\sigma_h$ behind the panel and much smaller $+\Delta\sigma_h$ below the toe, corroborating the main findings of Gourvenec and Powrie (1999).

The current state of the art is represented by the full 3D installation method of Gourvenec and Powrie, but this will be beyond the ability and resources of practitioners for many years to come. The needs of industry are perhaps better served by establishing the usefulness of simpler methods. In this connection, the approaches attempted by De Moor and Ng *et al.* are commended by the writer - they embody the philosophy set out in this thesis; namely to use existing tools/ technology in a way which challenges assumptions and provides new insight into old problems. In view of this, it was decided not to conduct rigorous and sophisticated 3D/coupled FIM for this thesis. Instead, simple comparisons will be made of the strategies (a)-(c) above, in the context of plane strain analysis, to reveal how they affect the key outputs of interest to the designer.

6.2.2 Wished-in-place method

The "wished in place" (WIP) wall has, in fact, been used in all of the analyses reported so far in this thesis, and these provide a base set of results with which to compare the other two methods.

The only restriction which is placed on the WIP method in CRISP is that the wall material must have the same unit weight as the surrounding soil. If this is not done, an equilibrium error will be flagged up at the in-situ stage due to there being a heavier inclusion in the mesh[1]. This error may be quite small and may not have any major consequences for the rest of the analysis, but it is good practice to avoid gratuitous errors of this sort. If there is a genuine error in the input data which would cause lack of equilibrium at the in-situ stage, the user does not want this masked by another unwanted (and unnecessary) error.

There are no obvious aspects of the WIP method which can usefully be investigated, as there is only one way in which it can be carried out. It is usually implicit that the full in-situ earth pressure will be acting upon the wall prior to excavation (i.e. $K_i = K_o$), and there is no softening of adjacent soil due to the ingress of water from wet concrete, etc. It probably represents a "worst case" in that it will always be conservative and lead to higher σ_h acting on the wall just prior to excavation. The exception would be if a reduced K_o (= K_i) was used a means of reflecting installation effects. As the in-situ stress profile in CRISP can only conveniently be defined on one single vertical profile (which applies across the full width of the mesh), K_i would apply from wall to boundary. This is contrary to field data, which shows localized reductions in σ_h. The full consequences of adopting a global reduction are unknown at present and could only be evaluated by comparison with full 3D methods. Time has not permitted this for the present thesis, but the other two installation strategies will now be considered.

6.2.3 Element swopping method

To investigate the influence of element swopping, one of the mesh geometry files, and several associated analysis data files used in the boundary location investigations were adapted for element swopping. Mesh x10y10 was used, with free cantilever conditions, Fig. 4.5.

---

[1] All along the base of the mesh, $\sigma'_v + u$ (= σ_v) as input by the user in the in-situ records must equate to $\Sigma\gamma.h + q$ based on layer thicknesses, unit weights and applied surcharges. The computed overburden on the base immediately below the wall will be somewhat higher than at points some distance either side. This lateral variation in σ_v is difficult to accommodate in the in-situ stress definitions provided by CRISP, and a constant σ_v along the base must be in error somewhere - unless the unit weight of the wall material is the same as that of the soil in which it is embedded.

The geometry data file required an additional column of "overlay" elements to be defined over the existing wall, Fig. 6.1. Subsequently in the analysis data file, the wall elements were marked for removal from the parent mesh in order to form the primary mesh. The new soil elements were, of course, present in the primary mesh.

Four different sets of (undrained) soil parameters were chosen for the preliminary analyses; sets 1, 3 (elastic) and 12, 13 (elastic-perfectly plastic) to give a reasonable range of soil behaviour (see Tables 4.3-4.8). The incoming concrete elements were given the same properties as in the WIP analyses; i.e. very stiff linear elastic, and with the same unit weight as the soil. This latter aspect was not, of course, necessary - the incoming concrete could have been given the more typical unit weight of 24 kN/m^3 - but the purpose of the present analysis was to investigate the differences between element swapping and wishing-in-place.

The results were, at first, a little surprising in that there were no significant differences whatsoever between the two strategies. This was true regardless of the nonhomogeneity of the E_u profile, or the amount of yielding which could be expected to take place. Comparisons were made on full profiles of horizontal wall displacement, bending moment, excavation heave, and ground surface movement - and nowhere could a difference in excess of ±0.5% be found. Further consideration of the finite element equations coded within CRISP, however, helped to identify why this should be so.

When an element is removed, the resultant nodal forces $\mathbf{F_{exc}}$ which must be applied to the mesh comprise terms representing internal stresses, body forces, and surface tractions:

$$\mathbf{F_{exc}} = \int_V \mathbf{B}^T \boldsymbol{\sigma}\, dV - \int_V \mathbf{N}^T \mathbf{b}\, dV - \int_S \mathbf{N}^T \mathbf{t}\, dA \qquad (6.1)bis$$

where all terms were defined in Section 3.3.2. The stiffness matrices of the outgoing elements are cancelled (removed) from the global stiffness matrix at the beginning of the increment block in which the removal is specified. Incoming elements, however, are not allowed to bring any internal stresses or boundary tractions with them - physically this is equivalent to saying that the concrete wall elements cannot be prestressed in any way, nor can they have surcharge loads applied to them at the time of installation. All that an incoming element is allowed to "bring" with it is stiffness and self weight. Body forces are calculated from the middle RHS term of Eqn 6.1 and added to the mesh; the stiffness matrix of an incoming element is added to the

global matrix at the beginning of the increment block in which the element addition is specified.

If the excavated soil elements were replaced by overlay soil elements with the same material properties, then the sides of the trench would move in. The body forces cancel out, as do the equivalent stiffnesses, but the internal stresses of the excavated elements are not balanced by the added elements, as the latter have no internal stresses when installed. Hence, inward movement of the trench would occur, proportional to the in-situ K_o in the excavated elements. However, if the incoming elements were very much stiffer than those which have been excavated (which is certainly the case when concrete replaces soil), then these "lost" internal stresses go unnoticed. The new elements are able to hold the trench sides in place by virtue of their stiffness, and the trench bottom by virtue of their self weight.

The only real justification, therefore, for adopting the soil/wall element swop approach is if the concrete was required to have a different unit weight to the soil. When the analyses described earlier were repeated with a unit weight of 24 kN/m^3 for the concrete, some differences (albeit very small) were observed between the two strategies. It is debatable whether or not extra effort in defining overlay elements and incorporating an increment block for the element swopping is actually worthwhile. What is clear is that if element swopping is used, just one increment is perfectly adequate if $\gamma_{conc} = \gamma_{soil}$, but may not be otherwise (depending on the effect which the increased vertical loading will have at that point in the mesh).

This argument is valid provided the wall installation is the first significant event in the analysis. In the writer's experience there are several cases where this is not so, and it would be misleading to have the stiffening effect of the wall present at too early a stage. Fig. 6.2 illustrates an example (from the RPR Junction Slip Road 5 - Appendix A) where significant bulk excavation took place prior to the construction of one of the walls. Another case would be where some previous construction event is being modelled prior to the present wall installation, such as the construction of basement walls on the site of an existing structure, which must first be demolished above and below ground.

6.2.4 Complete sequence

There would seem to be at least two ways of modelling the complete wall installation process with a high degree of realism. First, there is the approach used by Gunn *et al.* (1993), where

the slurry and wet concrete were modelled by applying an equivalent pressure distribution to the sides and base of the trench (after excavating the soil elements, and prior to placing full-strength concrete wall elements). The pressure distribution down the sides of the trench is hydrostatic, and this can be modelled in CRISP in a straight-forward fashion. The slurry pressures are applied in the same increment block as that in which the soil elements are removed, so as to prevent any undue movement of the wall into the trench. The pressures from the wet concrete will be higher than those from the slurry, but in CRISP all loads are incremental, so the additional pressures to be applied in the increment block where wet concrete is placed is the difference between the bentonite and concrete pressure distributions. This method will be termed the "applied pressure method" (APM).

Gunn *et al.* used a coupled formulation, with typical time steps being assigned to each of the operations (e.g. wall concreting 4 hours, concrete setting 12 hours, etc.). In addition it was also possible to specify whether or not water could flow into or out of the wall area - e.g. the bentonite was considered to form an impermeable boundary at the sides of the trench, whereas fresh concrete would allow the passage of water in either direction. A simpler variant would be to carry out all of the operations under undrained conditions, which would eliminate the need to specify time steps and permeabilities, and avoid the lateral pore water pressure oscillations which have sometimes been observed (Kutmen, 1986).

A second approach might be to have four sets of overlay elements superimposed on the wall position - original soil, bentonite slurry, fresh concrete, and hardened concrete - and to swop these in/out as appropriate. This would seem a logical approach and it does avoid the need to calculate and then specify applied pressures - at the expense only of some additional geometry preparation. However, it raises questions about the material properties which would be specified for the "fluid" materials (slurry and fresh concrete). In addition to possessing self weight (density), fluids are unable to carry shear stresses (which implies that G, and hence E, = 0) but may well be virtually incompressible[2], with a very high bulk modulus K (which implies that $\nu \approx \frac{1}{2}$). Care would need to be taken to avoid numerical problems (e.g. ill-conditioning, see Chapter 7) if such low stiffnesses were used. This method will be termed the "multiple overlay method" (MOM).

---

[2] Incompressible in the sense of no volume change due to applied mean stress - of course, in a trench the bentonite and wet concrete are unconfined at the top, with inward squeezing of the trench resulting in an upward movement of the fluid surface.

Both approaches have been tried, and have been compared with the WIP wall as a standard case. Again, mesh x10y10 was used in a free cantilever configuration. The applied pressure method (APM) required one set of overlay elements in the wall position, and the geometry data file used in the simple element swopping method sufficed without further modification. The multiple overlay method (MOM) required a further two sets of overlay elements (and associated material zones) which was straightforward to do, and resulted in a parent mesh of just under 700 elements.

6.2.4.1 Multiple overlay element method

The analysis steps in CRISP were as follows (Fig. 6.3):

Block	Activity
1	remove original soil elements - install bentonite "fluid" elements
2	remove bentonite elements - install fresh concrete "fluid" elements
3	remove fresh concrete elements - install full-strength concrete wall elements
4	excavate soil in front of wall to the required formation level

Just two sets of undrained isotropic elastic soil parameters were chosen (sets 1, 3) for initial comparison of the methods. The bentonite and fresh concrete materials were assumed homogeneous linear elastic, with the following parameters:

Material	E (kPa)	G (kPa)	ν	γ (kN/m^3)
Bentonite	1	1	0.497	12
Fresh concrete	1	1	0.497	24
Hard concrete	20×10^6	8.3×10^6	0.200	24

(Note: the values of 1 kPa for E and G were nominal non-zero values, the intention being to model a heavy, virtually incompressible fluid.)

Elastic Analyses

Selected profiles of wall displacement, wall bending moment, excavation heave, and ground surface movement are shown in Fig. 6.4(a)-(d). There is one curve for the WIP method, but up to four for the multiple overlay method - most of which are self explanatory. The curve labelled "diff" is the numerical difference between the full-strength concrete and excavation

profiles; i.e. the additional wall movement or excavation heave etc., that occurs between those two increments. This curve should be compared with that for WIP for wall displacements and excavation heaves; changes will occur in the ground due to making the trench (under slurry support) and it is not appropriate to establish a datum for structural wall behaviour until the wall is actually in place. Excavation heave, similarly, only becomes relevant once formation level has been reached. (Bending moments cannot be generated from the analysis until the wall is in place, so this problem does not arise.)

The preceding argument does not hold for ground surface movements; it will be important to be aware of them as soon as they commence. Sensitive structures nearby will be affected by ground movements from the outset, regardless of whether or not the wall is in place.

In general, there were huge differences between the multiple overlay and WIP methods; presumably this is due to the reduction in lateral stress afforded by the former, prior to actual wall installation. If the comparisons were based on the absolute profiles at the end of excavation (rather than incremental profiles) the discrepancies would apparently have been even greater. It was wall displacements and bending moments which showed the main differences - tending always to be of smaller magnitude - whereas excavation heaves and surface movements were not affected greatly. This accords with expectation; reductions in lateral stress will have the greatest influence on the lateral behaviour of the wall, and the least on vertical ground movements. The differences were most apparent in the bending moment diagrams, which showed virtually no moment at all above formation level (which is hardly credible in reality, but is theoretically possible in a wholly elastic analysis).

On reflection, there were good reasons why the multiple element overlay method would not work very well. A description of the way in which CRISP handles element removals/additions has been given earlier. The concept of heavy fluid elements is physically appealing, but incoming elements can only contribute self weight (i.e. body force) effects through:

$$\mathbf{F} = \int \mathbf{N}^T \mathbf{b} \; d(\text{vol}) \qquad (6.2)$$

so, the intended lateral fluid pressure (to support the trench sides) is simply not produced.

Gunn (1995) has also criticized the "fluid element" approach, principally because the mid-side nodes on the top and bottom of the slurry / wet concrete elements will be capable of large deformations associated with some (unknown) mode of shearing. He believes that the technique might work better with 4-noded elements, as these relatively unrestrained side nodes would then not be present. If the unwanted modes of shear deformation could be restrained, then the "fluid elements" should be able to generate hydrostatic pressures on the sides of the trench from self weight effects.

In order for the multiple overlay approach to work with 8-noded elements, Gunn suggests that the fluid should be given a finite shear stiffness which is low compared with the soil, say $G_{soil}/G \approx 100$, and that internally the fluid "material" should have $K/G \approx 100$. For parameter set 1, this could be achieved by setting $E = 300$ kPa and $\nu = 0.497$ (which would give $K =$ 16,666 kPa), and $G = 166$ kPa (in comparison with the soil $G = 50 / 2(1+.497) = 16{,}700$ kPa).

The analyses were re-run with these values and much closer correspondence with the WIP was observed. This could be expected because, by making the overlay elements for bentonite and fresh concrete stiffer, the method is tending toward straight element swopping as described in Section 6.2.2.

Elastic-perfectly plastic analyses

The opportunity was also taken to incorporate plastic yielding of the soil, by re-running the multiple overlay analyses with parameter sets 12 and 13 (see Table 4.7); the "fluid" elements were given the properties suggested by Gunn (1995) namely, $K/G \approx 100$. The elastic-perfectly plastic analyses produced profiles significantly different to those obtained with the WIP method, again predominantly in the form of reductions in wall displacements and bending moments. Reductions in excavation heave and ground surface movement (-S) were also observed, though to a lesser degree.

Doubts about the multiple overlay element method are inevitable. The motivation in testing it was to find a simple means of modelling installation effects, but this approach may not really be suitable. It is not clear if there are any advantages over the WIP method if the results obtained are the same as for WIP - which is the case if the suggestions of Gunn are followed. Final judgement will be reserved until later in this section, after the applied pressure method has been investigated.

6.2.4.2 Applied pressure method

The analysis steps in CRISP were (Fig. 6.5):

Block	Activity
1	remove original soil elements - apply pressure distribution due to bentonite fluid to sides and base of trench = $\gamma_{bent}.z$
2	increase pressures due to introduction of fresh concrete by amount = $(\gamma_{conc} - \gamma_{bent}).z$
3	install full strength concrete wall elements - cancel pressures by applying a distribution = $-\gamma_{conc}.z$
4	excavate soil in front of wall to the required formation level

Steps 1 - 3 were each done in one "lift" - e.g. there was no attempt to build up from the bottom to model the gradual introduction of tremied concrete.

Four sets of undrained soil parameters were chosen; two isotropic linear elastic (sets 1, 3) and two isotropic linear elastic-perfectly plastic (sets 12, 13). The hydrostatic pressures for the bentonite and fresh concrete materials were based on the same unit weights used in the MOM analyses; i.e. 12 and 24 kN/m^3 respectively. Selected profiles of wall displacement, wall bending moment, excavation heave, and ground surface movement are shown in Figs 6.6 (elastic) and 6.7 (elastic-perfectly plastic). On each figure, there is one curve for the WIP method and up to four for the APM, plotting the same analysis steps as for the MOM method.

Elastic analyses

The APM gave results which were much closer to the WIP than the MOM had been, showing rather smaller (though still significant) differences than when using multiple overlays. Wall displacements were consistently smaller, with the biggest reduction at the crest and zero reduction at the toe. Bending moment profiles were scaled down on both +M and -M sides by about 20% at the most - not just the lateral shift of the profile seen in some of the multiple overlay results. Excavation heaves showed no change, and surface ground movements were virtually unaffected.

Elastic-perfectly plastic analyses

Compared with the WIP, computed wall deflections were significantly smaller at all points along the wall. Bending moment profiles were scaled down on both +M and -M sides by

about 20% for $E_u = E_o+mz$, but there was no change for $E_u = mz$. Excavation heaves showed little reduction for $E_u = E_o+mz$, but a major (≈50%) drop for $E_u = mz$. (It should be recalled that $E_u = mz = 1000c_u$ is on the passive limit at the in-situ stage, so slightly unusual results might be expected, especially on the passive side). Surface movement profiles were shifted upward for both E_u profiles, but not by a great amount.

6.2.5 Summary

The full installation method employed by Gunn *et al.* (1993) in 2D is too complex for routine design; the 3D method of Gourvenec and Powrie (1999) even more so. Simpler alternatives are (a) the adoption of K_i ($< K_o$) above the wall toe prior to wall installation, or (b) imposition of a prescribed horizontal displacement δ_h at the soil-wall interface after the wall has been wished in place. However, it seems that a full 3D analysis may be required initially in order to determine appropriate values for K_i or δ_h; the tentative guidance provided by De Moor (1994) and by Gourvenec and Powrie is not general enough and much further work is required.

The APM may offer a suitable compromise, given that element swopping offers no advantage over WIP in the modelling of installation effects. However it is open to the same criticism as the plane strain work of Gunn *et al.* - namely the implication that an infinitely long slot is open during wall excavation, leading to over-relaxation of horizontal stress. As Higgins *et al.* (1989) showed for Bell Common, axisymmetric and plane strain analyses bounded the true behaviour of secant bored piling, and may well do so for diaphragm walls where alternative panels are excavated on a "hit and miss" pattern. The use of axi-symmetry may improve the APM, but further investigation is needed.

The WIP method does not permit any lateral stress reduction and will give the highest post-excavation wall deflections, bending moments and prop forces. Ultimately, the designer may be content with the knowledge that the WIP will produce these upper limits - given all the other uncertainties, this conservatism may be welcome.

6.3 Bulk Excavation

6.3.1 Previous work

Reference has been made earlier (Section 3.10.2) to some of the issues and problems associated with finite element modelling of the excavation process. All methods which have been proposed recognize that, from the overall FE mesh, there is a region of soil to be excavated (E) and a region which will remain in place (R), Fig. 6.8(a). If the elements comprising the zone to be excavated were removed from the mesh, it should be possible to find a distribution of stresses (surface tractions) on the excavated boundary which would produce the same effect on R as if E were still present, Fig. 6.8(b). Excavation is then simulated by cancelling these tractions to produce a stress-free boundary. Where the methods diverge is in how they compute the tractions, and whether or not the elements to be excavated are ever actually present in the mesh. The benchmark which any method must satisfy is that, for a time-independent linear elastic material, the solution must be independent of the excavation sequence followed to reach the final profile. Although an intuitive result, Ishihara (1970) appears to have been the first to provide a formal proof of this, using the virtual work theorem.

Where the in-situ stress conditions are relatively simple and the excavation profile straightforward, the initial mesh could be defined with the post-excavation profile already formed, and boundary tractions applied from the outset. In effect, this is replacing the soil to be excavated with a dense fluid possessing no shear strength or stiffness ($\tau_f \approx G \approx 0$). Depending on how σ_h is reduced on the side of the excavation, the heavy fluid is either being drawn down (location at which $\sigma_h = 0$ falling) or made weightless (γ scaled down). The former is more correct but both approaches ignore the shear strength and stiffness of the soil yet to be excavated, suggesting that greater movements into the excavation could take place. The main advantage of this method is that it can be done with virtually any FE code.

The more general (and preferred) method for modelling excavation is that of changing geometry, where equivalent nodal forces for the elements to be excavated are calculated within the program and removed from the mesh in the appropriate sequence. It is a numerical analogue to the physical removal of soil. The first published example of this was Christian and Wong (1973), who used a method of interpolating stresses in elements either side of the excavation boundary in order to obtain the required tractions. However, their results were

clearly dependent on step size, even for a linear elastic excavation analysis - furthermore (and paradoxically) the error increased with number of increments, whereas intuitively it would be expected to reduce. They suggested that the problem arose from using interpolating polynomials of too low an order and, although aware of Ishihara's work, stated that uniqueness in a linear elastic case should not be expected to apply in finite element analysis. Chandresakaran and King (1975) demonstrated otherwise, and presented an alternative formulation for excavation which gave results which were truly independent of number of increments. Insufficient details were given in their paper, but it would appear that they correctly identified the need to take account of the body force term ($\int N^T b$) as well as the internal stress term ($\int B^T \sigma$) in calculating the equivalent nodal forces for excavation.

The lessons appear not to have been learned, however. Some 10 years later, Desai and Sargand (1984) published results from a hybrid FE method for excavation which again showed dependency on step size for a 1D elastic excavation. Furthermore, in reply to discussion on their paper by Chow (1985), they rejected the latter's explanation that the error arose from omitting the $\int N^T b$ term and, in any event, did not accept that there was an error. Interestingly, CRISP had a correct implementation at least as early as 1982, but the method does not appear to have been published.

Fortunately, at about this time, two separate but equally correct and fully explained methods of excavation analysis appeared almost simultaneously, due to Ghaboussi and Pecknold (1984) and Brown and Booker (1985). Both dispensed with stress extrapolation and started with the virtual work equations, including terms due to internal stress, body force and external tractions. Numerical examples were presented to demonstrate that a stage-independent method had been achieved. Early errors were now clearly identified as the inconsistent determination of equivalent nodal forces from element boundary tractions, which would only work if element stresses satisfied local equilibrium (as in the exact solution). The last significant innovation in this area came from Borja *et al.* (1989) who presented a method of simulating excavation in elasto-plastic soils which produced a unique solution independent of the number of excavation stages. The non-linear FE equations were derived from a variational formulation which accounted for time-varying problem domains and boundaries.

At the present time, it is reasonable to assume that the early mistakes are now understood and should no longer be present in finite element analysis of retaining walls (Ho and Smith, 1991).

However, when presented with an unfamiliar code, the user should test it to check that it is insensitive to number of increments in linear elastic analyses. Other validation tests can and should be devised for non-homogeneous, anisotropic, and non-linear materials/situations. If using results (published or otherwise) from older codes, it should be borne in mind that errors in excavation may well exist.

6.3.2 Description of analyses

Before describing the investigations which were carried out, it will be helpful to consider how CRISP handles sequential layer removal. One or more elements can be marked for removal within an increment block, which can be divided into several increments. The contribution which those elements make to the global stiffness matrix is lost at the very beginning of the increment block, so the resistance which would otherwise have been there to help prevent wall movement is removed immediately. However the unloading (from forces representing internal stresses, surface tractions and body forces) is spread evenly over all the increments in the block (or according to some specified weighting through the load ratio facility in CRISP).

For an excavation of total depth H in elasto-plastic soil, all of the elements comprising the various rows could be marked for removal in just one increment block. If the block was split into a large number of increments, it is conceivable that the unloading could be in small enough steps to ensure a satisfactory response of the remaining soil, even with a tangent stiffness solution scheme. However, this would probably not be true for the other effect of excavation and element removal - i.e. loss of stiffness. Excavation in layers produces an ever-changing geometry (and hence stiffness of soil remaining in the excavation) to accompany the gradual load reduction, and this can never really be equivalent to complete removal of the soil in one operation.

To test out this hypothesis, a short series of numerical studies was carried out. An unpropped cantilever wall (mesh x10y10) excavated under undrained conditions was considered, with soil parameter sets 11, 12 and 13 (Table 4.7). When this combination of wall configuration and soil properties was used for other studies reported earlier in the thesis (e.g. for boundary location analyses), some decision had to be taken at that stage on total number of increments and blocks. In fact, each of the 8 layers of soil (1m thick) comprising the excavation was removed in a single increment block, making 8 blocks in total for the excavation stage. A total

of 40 increments was used, being 5 increments per block with uniform loading ratios (i.e. one fifth of the unloading caused by removing 1m of soil was applied in each individual increment).

The number of 40 increments was decided on the basis of some preliminary analyses in which 1, 2, 5 and 10 increments per block (i.e. 8, 16, 40 and 80 increments in total) were used. Whole profiles of wall displacement, bending moment, etc., were compared in much the same way as for the boundary location analyses. Very little additional improvement in the results was obtained beyond 40 increments, and the equilibrium errors at the end of each increment were well below acceptable limits (<< 1%).

In the analyses reported in Chapter 4 which were investigating the effect of mesh grading or degree of nonhomogeneity (for example), no errors should have been introduced through having insufficient numbers of increments. However, what is being investigated in more detail here is the sensitivity to

a) number of increment blocks NOIB (with a fixed total number of increments), and
b) total number of increments NINC (with a fixed number of increment blocks)

6.3.2.1 Number of increment blocks

To test the effect of total number of increment blocks, the earlier figure of 40 increments (i.e. NINC = 40) was retained, but the number of blocks (NOIB) was varied as follows (Fig. 6.9):

Scheme	NINC	NOIB	NINC/NOIB
a	40	1	40
b	40	2	20
c	40	4	10
d	40	8	5

The results of these analyses (not presented here) were contrary to expectation; the number of increment blocks used made no discernible difference to the profiles of horizontal wall displacement, wall bending moment, or ground surface movement. It was only the excavation heave which showed any effect, and this was in the form of a more angular profile next to the wall when NOIB $\leq$ 2, as compared with the smooth curve seen when NOIB >2. Maximum heave values were more or less the same.

From the argument advanced earlier, greater sensitivity to total number of increment blocks would have been expected. It is possible that, with a sufficiently large number of increments, it would make little difference if the layers were taken out singly or *en masse*. To test this, variations on the scheme were set up, as follows:

Scheme \ Variation	NOIB	I	II	III	IV
		NINC / NOIB			
a	1	64	32	16	8
b	2	32	16	8	4
c	4	16	8	4	2
d	8	8	4	2	1
Total NINC =		64	32	16	8

For example, in scheme Ib the excavation would be carried out in a total of 64 increments over 2 blocks, with 32 increments per block. It was decided to start with the coarsest analyses first, i.e. IVa to IVd, in which the excavation was carried out in a total of 8 increments.

Some of the computed profiles are shown in Fig. 6.10(a)-(d), from which it can be seen that, even with as few as 8 increments in total, there was not much influence from the number of increment blocks. The biggest effect was seen on the profiles of excavation heave, which were generally flatter across the excavation and steeper adjacent to the wall when NOIB $\leq$2. Wall displacements were affected when the soil stiffness and strength were constant with depth, but not otherwise. Bending moment profiles showed very little change, and ground surface movements were similarly unaffected.

To confirm these observations, analyses IIIa to IIId were run, using 16 increments for the excavation. The plots are not reproduced here because the profiles for 1, 2, 4 and 8 increment blocks were virtually identical (regardless of soil parameters), except for excavation heave, which showed the same trends as for analyses IVa to IVd. In the light of these observations it was deemed unnecessary to carry out the series I or II runs.

Why are the effects of number of increment blocks so small in general? Considering the heave profiles (which were most affected by NINC), it is clear that the average value of heave is about the same, which would indicate that magnitude of vertical unloading is of prime

importance. The alterations to the heave profile near the wall when only one or two blocks were used was almost certainly caused by the loss of stiffness of the overlying soil.

This loss of stiffness ought to have affected the deflections and curvature of the wall, but it is possible that the wall was too stiff (relative to the soil) for the stiffness of unexcavated soil in front of the wall to make much difference. In other words, the lateral stresses in the soil to be excavated had a bigger effect than its stiffness. It is conceivable that this would not be the case for a more flexible wall, such as steel sheet piling, but for diaphragm and contiguous pile walls the wall stiffness does appear to make load removal the most important aspect of excavation. If this is the case, then greater sensitivity to total number of increments should be apparent, and this will be considered next.

6.3.2.2 Total number of increments

To test the effect of total number of increments, the number of increment blocks (NOIB) was fixed at 8, but the number of increments (NINC) was varied as follows:

Scheme	NOIB	NINC	NINC/NOIB
p	8	8	1
q	8	16	2
r	8	32	4
s	8	64	8

Profiles of wall displacement are shown in Fig. 6.11(a), from which a moderate effect from total numbers of increments is shown, over the range considered. For parameter set 12 ($E_u = E_o+mz$), the curves for different NINC had a constant offset, whereas for set 13 ($E_u = mz$) the offset was greatest at the crest and was zero at the toe. The upper half of the bending moment profiles showed very little sensitivity to total number of increments, and it was only for set 13 that any significant sensitivity was shown below formation level, Fig. 6.11(b).

Excavation heave profiles generally coincided at either end (excavation centreline and wall face) but deviated in between according to total number of increments, Fig. 6.11(c). Set 12 gave the largest differences between heave profiles. Something unusual was noted in these profiles when compared with those obtained when the number of increment blocks was varied (fixed total number of increments). In that earlier series of analyses, reducing the number of

blocks (which would generally be regarded as making things worse) caused the profile to flatten off over a greater width and exhibit a steeper gradient near the wall; in the present series of analyses, a similar effect was achieved when the total number of increments was increased (which would generally be regarded as making things better). No explanation can be offered for this.

Ground surface movements behind the wall, Fig. 6.11(d), showed a small dependence on number of increments. Generally, more increments caused the ground to settle a little more; especially near the wall.

6.3.3 Summary

In practice, most designers/analysts would probably excavate a mass of soil this size in about 20 increments. The evidence from this short series of analyses is that as few as 15 increments would give reasonable answers for most of the results likely to be of interest to the designer - even with elastic-perfectly plastic behaviour and the potential for significant yielding. Certainly, using more than 15 would not appear to offer significant improvement in the results.

Individual increment blocks tend to involve the removal of reasonably large thicknesses of soil - perhaps 2-3m on average - or on the vertical distances between temporary/permanent props and/or anchors (if this is smaller). However, it would appear that the choice of number of increment blocks is not critical. The simplified wall and support geometry used in these studies, which had a clear excavation run from original ground surface to formation level, is probably the only situation in which removing the soil in one increment block could be contemplated. Even so, the above results suggest that a relatively small number of increments would yield acceptable results.

These analyses were all undrained, and were carried out in terms of total stress. When an excavation is part of a more extensive coupled analysis (which will proceed to examine long-term effects), the excavation will still be effectively undrained, although carried out in terms of effective stresses. The conclusions drawn here concerning numbers of increments and of increment blocks for total stress analysis are thought to be just as valid for effective stress analysis. Comparisons of the total and effective stress approaches to undrained excavation are presented later in the thesis (see Section 7.4).

6.4 Temporary Propping

6.4.1 Previous work

There appear to be no specific studies reported in the literature on the various issues facing the analyst, namely:

a) the way in which the prop will be modelled (point fixity, bar element, solid element); especially the wall connection detail,
b) the manner in which the prop is installed (together with how the soil is excavated), and
c) the manner in which the prop is removed.

The various forms of prop and connection detail (Item a) were summarized in Section 3.4.3 (Fig. 3.8). Decisions on what transferable actions should be included will be dictated by the expected construction details. The limits (e.g. full or zero moment transfer) can be modelled readily, and the designer/analyst may use these results to predict likely behaviour in between these limiting cases.

It was deduced in Section 3.10.3 that there were few (if any) uncertainties regarding the options available for interleaving the prop installation and excavation (Item b). Schemes A and B depicted in Fig. 3.24 are identical, and studies in the previous section have established that CRISP handles the former correctly.

Considering the matter of prop removal (Item c), nothing relevant has been found in the literature, and so a series of numerical studies has been carried out and will now be described.

6.4.2 Description of analyses

A small suite of numerical experiments was described in Section 6.3, in which the number of increments and increment blocks was investigated in the context of bulk excavation - which represents vertical unloading plus the loss of some lateral support in the vicinity of the wall. Prop removal is principally a lateral unloading event (although there would be significant vertical unloading in the case of an inclined ground anchorage being de-stressed). In view of this, although some similarities may be expected between the two (concerning the effects of numbers of increments/blocks), there could be key differences. Therefore a separate series of numerical studies into prop removal has been conducted.

Mesh x10y10 was used with the provision for both top and formation level props - referred to as the alternately-propped wall in Section 4.2.2 (Fig. 4.3). As a brief recap, the construction sequence for the alternately propped wall is as follows:

Block	Activity
1	Install wall (wished-in-place) together with temporary top level prop
2	Excavate to formation level
3	Install permanent formation level prop
4	Remove top level prop

In earlier numerical experiments which used this type of wall, the top level prop was taken out (block 4) in about 10 increments. This was selected on the basis of examining the incremental equilibrium errors, and ensuring they remained well below 1%. However, in an elastic-perfectly plastic analysis, quite large equilibrium errors (say 5-10%) do not necessarily mean that the analysis is invalid - they are simply a measure of the amount of yielding which has taken place in a given increment, and an indication of how much out-of-balance force needs to be redistributed (as correcting loads) in the next increment. Provided such redistribution has, in fact, been requested by the user (via the CRISP input data file) the analysis should be quite admissible. More stringent controls would need to be exercised in the presence of critical state based models, as no stress corrections are applied for them (see Section 3.6.3).

A more detailed study of the influence of increments in prop removal will now be described. The study is not exhaustive, but should be sufficient to establish useful guidelines. The mesh and propping arrangements have already been described. Excavation under conditions of undrained loading in terms of total stress (i.e. non-coupled) has been considered, together with soil parameter sets 11 and 13 (Table 4.7). The prop was removed in just one increment block, but different numbers of increments were used, as follows:

Scheme	NINC	Scheme	NINC
a	1	d	10
b	2	e	20
c	5	f	50

6.4.3 Results of analyses

Selected profiles of key results are shown in Fig 6.12(a)-(d). Wall displacements did not show much sensitivity to numbers of increments, and there was no significant change beyond NINC = 10. Similar observations can be made regarding bending moment profiles, which were also fairly constant for NINC $\geq$ 10.

Excavation heaves showed virtually no dependence at all on numbers of increments, with no changes beyond NINC = 2, Fig. 6.12(c). Ground surface movements showed a fair degree of sensitivity to the number of increments employed for prop removal, Fig. 6.12(d). Within a distance of 2H from the wall in particular, the profiles were very erratic for NINC $\leq$ 2 evidencing some numerical problems or at least a suspect (i.e. inadmissible) analysis. By the stage NINC = 10 the profiles had settled down to a reasonable pattern and did not change with the additional of further increments. Beyond 2H from the wall, there was no change to surface movement profile.

6.4.4 Summary

Prop modelling in CRISP is fairly straightforward and should cause few problems, but it must be done in an appropriate manner, or errors will be introduced into the analysis. However, there are few contentious issues here, and nothing which (in the writer's opinion) requires numerical investigation. Similar comments apply to prop installation on the whole. The removal of props, however, is certainly an aspect of retaining wall analysis which, at first sight, may need care and attention. A wall rigidly propped from the start of bulk excavation has a lot of lateral stress locked in - which will be substantially reduced by removing the prop (depending on wall rigidity and embedment).

The apparent insensitivity of wall deflection and bending moment to numbers of increments for prop removal may partly be explained by the fact that stress paths behind the wall are largely within the elastic region (having unloaded from relatively high K_o values in the in-situ stage), Fig. 6.13. The response of the wall may therefore be governed more by elastic soil behaviour - the small differences in prop unloading effects that can be seen between parameters set 11 (E_u/c_u = 500) and set 13 (E_u/c_u = 1000) would tend to support this. However, if this was the case, surface movements near the wall might also be expected to be relatively unaffected.

Excavation heave could be expected to show little sensitivity to temporary prop removal, when there is a virtually rigid prop in place at formation level. The wall can pivot about this lower prop when the top prop is removed, but it cannot translate into the excavation. Consequently the passive soil mass undergoes little additional change of load.

6.5 Partial Drainage

6.5.1 Previous work

If it is considered that construction may be partially undrained, and/or there is a requirement to investigate long-term conditions as part of one continuous analysis, then it will be necessary to set up a coupled-consolidation analysis (see Sections 3.5 and 3.11). This is another topic where questions confront the analyst, but for which answers do not appear to exist in the literature. Issues include:

a) which elements should have excess pore water pressure degrees of freedom?
b) where should drainage boundaries be located?
c) what type of drainage boundary condition should be specified?
d) should drainage conditions be imposed before, after, or concurrently with applied loadings and element changes?
e) how big/small should the time steps be?

Items (a) to (c) have been addressed in Sections 3.8.2 and 3.11.1. Item (d) is unlikely to be important - initial drainage boundary conditions are specified at the beginning, and moving boundaries (i.e. the excavated surface) will only need attention if the rate of change to the geometry is slow. Even then, as the drainage allowed would take place mostly within the soil mass just about to be excavated, there may be little justification for doing it. Final drainage boundary conditions are fixed once the ultimate geometry is reached.

Item (e) is an uncertainty, and it arises in two separate phases of the analysis - during bulk excavation and during post-construction equalization/equilibration. In each place the nature and implications of the question are somewhat different. During bulk excavation the size of Δt will govern where behaviour falls in the spectrum between undrained and drained. During equalization, the size of Δt will determine the speed with which the long-term steady state is

attained. The former is investigated here, whereas long-term equalization is reserved for Section 6.6.

6.5.2 Description of analyses

To investigate the size of Δt required to achieve (a) undrained, and (b) drained conditions in a coupled analysis, mesh x10y10 (cantilever configuration) was used together with parameter sets 2d & 3d (elastic), and 12d & 13d (elastic-perfectly plastic). Mass permeabilities for the soil were $k_y = 1 \times 10^{-9}$ m/s and $k_x = 4k_y$. Bulk excavation took place over 8 increment blocks (i.e. excavation layer thicknesses of 1m), with the same time interval Δt taken for each layer of excavation. The Δt used varied from 1 second to 100 years, stepping up approximately in orders of magnitude as follows:

Δt	Δt	Δt
1 sec	1 day	5 yrs
10 sec	1 wk	10 yrs
1.5 min (0.001 day)	1 mth	20 yrs
15 min (0.01 day)	1 yrs	50 yrs
2.5 hrs (0.1 day)	2 yrs	100 yrs

6.5.3 Results of analyses

The results extracted for consideration were

- the wall deflection profile at the end of excavation (δ:z)
- the pore pressure distribution adjacent to the wall below formation level (FL), at the end of excavation (u:z′)
- equilibrium error at the end of each increment (err_x) (see Section 3.12 for definition)

Wall deflection was selected as a practical design output; pore water pressure because the generation and dissipation of excess values is at the heart of a coupled analysis. Equilibrium error was extracted in case this was able to identify the onset of any numerical problems. Results will be presented and discussed in the contexts of lower and upper limits on Δt.

Lower limit on Δt

With the lower Δt used, differences in the δ:z profiles were only apparent between $1 \rightarrow 0.1$ days; for Δt below 0.1 days the profiles were indistinguishable and could be safely assumed to be at the undrained limit, Fig. 6.14(a). This held for both E′ profiles, and was unaffected by whether or not plastic yield was permitted.

The pore water pressure profiles (u:z′) in the elastic analyses looked reasonable for 1 day $\leq \Delta t \leq$ 1 month but became erratic/oscillatory for $\Delta t < 0.1$ day. The computed pore water pressure always remained positive but dropped by 50 kPa at most. For the elasto-plastic analysis, no oscillations in the u:z′ profile were observed at low Δt, although a kink occurred 2m below FL for all $\Delta t \leq 1$ day (straightening out for $\Delta t \geq 1$ week). For all $\Delta t \leq 0.1$ day, profiles were inseparable. Much negative pore pressure was in evidence in this case (as low as -140 kPa), Fig. 6.14(b), suggesting that both Δp and Δq were negative.

Equilibrium error (err_x) though steadily accumulating throughout the analysis, remained below 0.05% for all $10^{-4} \leq \Delta t \leq 1$ day. However, the growth of err_x during the analysis became noticeably erratic for $\Delta t < 10^{-4}$ days - suggesting the onset of numerical instability.

Upper limit on Δt

The big differences between the δ:z profiles which appeared once $\Delta t > 1$ week had, in the elastic case, vanished once $\Delta t \geq 10$ years, Fig. 6.15(a). In the elasto-plastic case, there were still significant differences between Δt of 50 and 100 years.

Pore pressure profiles in the elastic analyses were identical for $\Delta t \geq 20$ years; in fact, little difference could be seen for $\Delta t \geq 10$ years. There was no question that the FE response was drained as the profiles followed $u = 10z = 10(z'+8)$ - implying a flooded excavation (because formation level had not been set as a drainage boundary). In the elasto-plastic case, all u:z′ were positive for $\Delta t \geq 50$ years, but even u:z′ at $\Delta t = 100$ years was less than the hydrostatic [$u = 10z$] expected for the fully drained case, Fig. 6.15(b). This is probably due to the continued yielding of soil in front of the wall, which does not have a stable propping configuration.

Equilibrium error grew with each passing increment, reaching an ultimate value at the end of bulk excavation which increased as Δt increased. The maximum observed value of err_x was 2.5%, at increment 40 and $\Delta t = 100$ years.

6.5.4 Discussion

It is interesting to consider whether or not theoretical bounds for Δt can be established, to verify (or otherwise) the results just described. The routine way to estimate equilibration times is via Terzaghi's one-dimensional consolidation theory. This will need generalization to at least 2D to be applicable to the case at hand - drainage can be in both directions (x and y), and there may be anisotropy of stiffness and permeability. The normal definition of coefficient of consolidation involves m_v but can be slightly generalized thus:

$$C_v \quad = \quad k \; / \; \gamma_w \, m_v \quad \approx \quad k \, E' \; / \; \gamma_w \qquad (6.3)$$

Degree of consolidation (excess pore water pressure dissipation) is related to time factor, the latter being defined by Terzaghi (1943) as:

$$T_v \quad = \quad C_v \, t \; / \; d^2 \qquad (6.4)$$

A suitable drainage path length (d in Eqn 6.4) must now be established for an embedded retaining wall geometry. One option would be to consider the stress "bulbs" arising from an applied strip load of width B, where the 20% vertical stress bulb penetrates to 3B. For the retaining wall herein, B is the full width of the excavation (= 2W = 16m), and FL is the surface to which a uniform (un)loading has been applied. The drainage path might extend from this depth to the nearest available drainage boundary - the ground surface - hence, $d = 3 \times 16 + 8 = 56$m. The average E′ at this depth is $= 40 + 4 \times 56/2 = 152$ MPa, and with $k = 1 \times 10^{-9}$ m/s and $\gamma_w = 9.81$ kN/m^3, C_v is computed as 1.34 m^2/day (= 488 m^2/yr). Terzaghi's theory for most 1D cases suggests that if $T_v \geq 1.50$, then $U_v \geq 95\%$. Manipulation of Eqn (6.4) leads to the requirement of t = 9.6 years for at least 95% excess pore water pressure dissipation (equilibration) to have occurred - i.e. effectively drained conditions. At the lower end, Terzaghi's theory suggests that $T_v \leq 0.001$ is required for $U_v \leq 5\%$, which leads to t = 2.2 days for ≤5% dissipation to have occurred - a reasonable definition of undrained behaviour.

The above calculations are <u>very</u> approximate, but the CRISP analyses suggested that $0.1 < \Delta t < 1$ day per excavation layer was required for an undrained response; this converts to $0.8 < t < 8$ days for the whole excavation, which brackets the 2.2 days estimated above. At the drained end, agreement is also reasonable (at least with the elastic analyses) - CRISP indicates that $\Delta t = 20$ years is required for virtually complete drainage but that Δt = 1-2 years might suffice for

the 95% condition; this equates to t = 8-16 years for the whole excavation, comparing favourably with the 9.6 years estimated from Terzaghi theory.

The apparent influence of yielding on the time required to obtain a drained response was unexpected. Possibly it is because yielding leads to a reduction in operational E′, which in turn causes C_v to drop (Eqn 6.3) and hence the time to achieve a given T_v is longer (Eqn 6.4).

6.5.5 Summary

Undrained conditions ($\Delta\varepsilon_v \approx 0$) can be achieved with time steps of the order of 0.1 days (2.5 hrs) per 1m layer of excavation, for $k = 10^{-9}$ m/s (typical of clays). With this size of Δt there is no risk at all of numerical instability, which does not evidence itself until time steps are less than 0.001 day (1.5 min) at which point err_x becomes noticeable. However, u:z′ profiles appear somewhat erratic for $\Delta t < 0.1$ days, so a compromise would be to use $\Delta t = 0.1$ days. Anything slower (i.e. more) than 1 day per layer and partial drainage will start to occur.

With bigger Δt, larger changes in effective stress ($\Delta\sigma'$) are permitted in a given increment and, depending on the non-linearity of the stress-strain response, this could lead to inaccurate results in a tangent stiffness solution scheme. The use of a bigger Δt should probably be accompanied by more increments - which may necessitate more increment blocks, as a maximum of 50 increments are permitted in any one block in CRISP.

6.6 Long-Term Equalization

6.6.1 Previous work

After bulk excavation is complete and all permanent supports are in place, the designer may need to investigate behaviour in the years that follow: short term (1-2 years), medium term (2-20 years) and long term (>20 years). Again this will require a coupled analysis, and the following decisions must be made:

a) how long should be allowed for equilibration (t_e) ?

b) how many increments should be allowed for equilibration (N_e) ?

c) in what way should the individual time steps (Δt_i) be weighted ?

Item (a) has been discussed in Section 3.11.3, and it was concluded that this is quite likely to be fixed by external factors (e.g. design life of retaining structure). Results in the previous section suggest that full drainage may take longer than expected if yielding occurs.

The question of the number of increments (Item b) is difficult - other than a qualitative notion that more increments will give greater accuracy, the most appropriate number is uncertain. Sections 6.3 and 6.4 presented investigations on number of increments for bulk excavation and prop removal, respectively, and something similar is needed here.

The only published recommendation on time step weighting (Item c) is to use a logarithmic scale (Britto and Gunn, 1987). The writer has used this in the past but has also devised two other strategies. The first is an arithmetic progression of the form $\Delta t_i = \lambda.\Delta t_{i-1}$, in which the first time step is specified, and the factor λ adjusted until $\Sigma\Delta t_i = \Delta t_1 (1 + \lambda + \lambda^2 + \lambda^3 + ... \lambda^N) = t_e$ The second is to use a power law of the form $\Delta t_i = A(i)^m$, with the exponent m fixed at the desired (integer) value, and then a numerator found such that $\Sigma A(i)^m = t_e$. (Uniform Δt is a special case, in which $A = t_e/N_e$ and m=1.)

6.6.2 Initial studies

The investigations centered initially on the weightings of the Δt used during the equilibration phase. Mesh x10y10 with unpropped and top-propped wall configurations were used together with soil sets 12d and 13d (Table 4.8); excavation was carried out quickly enough to be undrained in 8 stages of five increments each.

run	set	prop	Series 1			Series 2		Series 3	
			$N_e = 15$			$\Delta t_1 = 1$ day		$N_e = 50$	
TF152	12d	none	**variant**	Δt_1	λ	**variant**	N_e	**variant**	**m**
TF153	13d	none	A	1 hour	2.5909	F	20	M	2
TF162	12d	top	B	1 day	2.0026	G	30	N	3
TF163	13d	top	C	1 week	1.7274	H	40	O	4
TF182	12d	twin				J	50	P	5
TF183	13d	twin				K	100		
			(in all cases $\Sigma\Delta t = t_e = 100$ years)						

Immediately after excavation, formation level was set as a drainage boundary. The number of equilibration increments (N_e) was fixed at 15, and the time for equilibration (t_e) was fixed at 100 years. The size of the first time step (Δt_1) was set variously at 1 hour, 1 day and 1 week, and the λ-method was used to generate the remaining Δt, such that $\Sigma \Delta t = t_e = 100$ years. Wall deflection profiles (δ:z) and equilibrium error plots (err_x : inc) were extracted for inspection; only one or two are shown herewith..

The choice of Δt_1 (and hence λ) had a significant effect on wall deflection - larger Δt_1 resulting in greater final displacement of the wall at t_e, Fig. 6.16(a). However, it was unclear if larger δ:z implied greater accuracy; earlier studies (e.g. on mesh size) demonstrated that larger δ generally indicated a more accurate analysis, as finite element models are usually too stiff. In this context, however, the use of more increments and longer elapsed time might be expected to lead to more accurate results, and it was less clear why changing Δt_1 and λ should give this also. A possible explanation is that small Δt_1 implies large Δt in the latter stages of equalization (when excess pore pressure gradients are low), producing small effective stress changes in an increment. Large Δt_1 leads to large Δt in the early stages when excess pore pressure gradients are high, leading to large effective stress changes (and hence larger δ) during an increment.

The plot of err_x : inc showed a local peak at start of equilibration (i.e. at Δt_1), falling quickly to a trough ($\approx 0\%$) before climbing through the remainder of the equilibration phase to values between 3-6%. $\Delta t_1 = 1$ hr (the shortest) usually gave the highest err_x, suggesting that there are numerical issues which may need investigating at small Δt (see Section 7.4).

In the next phase of investigation, Δt_1 and t_e were kept fixed (at 1 day and 100 years respectively) and N_e was increased from 15 to 20, 30, 40, 50 and 100 increments. In all cases, wall deflection was bigger for $N_e = 100$; as much as 190% increase was observed in going from 20 to 100 increments for run TF152; only 30% for TF163. As N_e was increased, the difference between successive δ:z profiles became less, and suggested that $N_e = 100$ would be adequate in most cases Fig. 6.16(b).

The third phase was to fix N_e at 50 and t_e at 100 years (Δt_1 was no longer fixed), and then to vary the weightings according to a power law $\Delta t = A(i)^m$. (Higher m basically gives smaller Δt at the start, and bigger Δt towards the end of the equilibration phase.)

The results confirmed that Δt weighting could have a very significant effect; m = 2 gave the largest δ:z at the end of equilibration (and also gave the lowest err_x), with reductions in δ as great as 30% as m varied from 2→5 in the unpropped case, Fig 6.16(c). With the inclusion of top-propping the differences were much smaller (≤5%). This would suggest that, with prop configurations that suppress soil yield (and more of the response being elastic), the weighting of Δt is less important and any reasonable scheme will suffice. The pattern of behaviour was unaffected by the profile of E′.

The data were then re-plotted to show the evolution of wall deflection with time (δ_{max}:t) - analogous to a dissipation curve - and neither the unpropped or top-propped walls showed that they had reached a long-term equilibration state by 100 years. In the unpropped case this was not unexpected (marginally stable, etc.); certainly it was the worst in terms of the δ_{max}:t curve not leveling out. However, dissipation for the top-propped wall was clearly not complete either. There was a suggestion that higher "m" in the power law gave faster convergence to the steady state, but not unequivocally.

The fourth phase comprised increasing time t_e beyond 100 years to determine when the steady state would be reached. Equalization times of 200, 400 and 800 years were all used, achieved by adding more increments so that $\Sigma\Delta t$ (power law) eventually reached the specified t_e whilst preserving Δt size in the early stages of the analysis. Results indicated that wall deflections in the unpropped case were continuing to increase even after 800 years of dissipation, but the excessive levels of movement (δ_{max} = 2m) tended to invalidate this particular analysis. The insertion of a top-level prop reduced the overall magnitude of movement very significantly (δ_{max}≤150mm) and the δ_{max}:t curve suggested that the dissipation of excess pore water pressure was occurring more rapidly, Fig. 6.16(d). Higher values of "m" in the power law produced slightly faster dissipation, but converged on δ_{max} values that were smaller (and possibly less accurate).

In view of the fact that movements were still quite large with the top-propped wall, it was decided to introduce double propping, and re-run this fourth phase of analyses. A top-level prop was present from the start, and a formation-level prop was inserted at the end of bulk excavation. The results for this propping configuration indicated that equilibration had definitely been reached by 800 years - in fact, the δ_{max}:t curve had leveled off by 250 years; overall movements were credible, with δ_{max} ≤35mm.

Overall, these magnitudes of equilibration time were unexpectedly large. For comparison, a representative selection of analyses were re-run as wholly elastic (simply by setting $c' = 10^8$ kPa). The δ_{max}:t curves indicated that a steady state could be reached within 20 years - perhaps faster than expected, but more realistic than the hundreds of years implied by the elastic-perfectly plastic analyses. Final wall deflection profiles were identical, regardless of the Δt weighting scheme employed. Of course, the end-result in a linear elastic system is path independent, so identical computed results would be expected at comparable elapsed times.

6.6.3 Description of analyses

Guided by these initial runs, a further suite of analyses was devised to investigate N_e, T_e and m in further detail. Due to the unpropped wall being marginally stable when fully drained, it was not used any further. Furthermore as results for $E' = 40+4z$ and $E' = 4z$ were very similar, only the former stiffness profile (= set 12d) was used. Analysis identifiers were as follows:

run	N_e	t_e (yrs)	run	N_e	t_e (yrs)	run	N_e	t_e (yrs)
TFnnnX1m	25	100	TFnnnY1m	50	100	TFnnnZ1m	100	100
TFnnnX2m	"	200	TFnnnY2m	"	200	TFnnnZ2m	"	200
TFnnnX4m	"	400	TFnnnY4m	"	400	TFnnnZ4m	"	400

where nnn = 162 (top-propped) or 182 (doubly-propped), m = 2, 3, 4 or 5 (exponent in power law)

Only wall deflection was extracted as an indicator of how these three different questions affected the analysis, as equilibrium error had revealed nothing of note in the initial studies.

6.6.3.1 Equalization time

Top-propped

Allowing 100 increments for equilibration (which might be considered adequate in situations with modest non-linearity), this propping configuration showed significant differences between δ:z profiles for t_e = 100, 200 and 400 years (50% increase in δ_{max} over this time range), Fig. 6.17(a), which was not unexpected following the earlier work reported in Section 6.6.2. From the δ_{max} : t curves it was quite clear that, even after 400 years, significantly less than 95% equilibration had occurred, although the δ_{max} :t curves for t_e = 100 and 400 years agreed very

well in the range $0 \leq t \leq 100$ years. This particular propping configuration, together with steady-state seepage to formation level produced wall deformations which were capable of continuing for a very long time in an elastic-perfectly plastic (Mohr Coulomb) analysis.

Double-propped

Moving to a more stable configuration (top + FL props), the analyses were repeated with N_e = 100. The additional FL prop reduced t_{95} very significantly and brought the δ:z closer together (10% increase in δ_{max} between 100 $\rightarrow$ 200 years; <2% between 200 $\rightarrow$ 400 years). In this case t_e = 200 years would be adequate, with t_{95} somewhere between 100 - 200 years, Fig. 6.17(b). Even this double propping configuration was somewhat unrealistic as the excavated surface was able to swell freely, instead of reacting against a full-width slab or similar - with such restraint, t_{95} could be 100 years or less. The trend noted above for sensitivity to changes in N_e at high t_e was still apparent, but the differences/divergences were much smaller.

These analyses cannot be said to have shown what value of t_e would be adequate for a given case; indeed, it is probably not possible to establish general rules for retaining wall analysis. However, they <u>have</u> shown that it is not only the coefficient of permeability and the location of drainage boundary conditions which governs the rate of equilibration - clearly propping plays a significant role, because of the amount of yielding it allows (or prevents). Also it should be remembered that mass permeability in the field may be a lot higher (by orders of magnitude) due to partings and fissures (especially those opening up following stress relief), so that the actual t_{95} in practice will be a lot faster than theoretical estimations.

6.6.3.2 Number of equalization increments

Top-propped

With t_e fixed at 400 years (thought to be adequate for complete equalization), there were obvious differences in the δ:z profiles between N_e = 25, 50 and 100 increments - the discrepancy in δ_{max} was about 25% between 25 and 100 increments, and key differences showed up in the δ_{max} : t curves too. However, it was known that this case had not reached t_{95} (or even approached it). This sensitivity to N_e was less pronounced as t_e dropped to 200 and then 100 years. Insufficient N_e (e.g. N_e = 25) lead to a marked mismatch of δ_{max} : t curves for t_e = 100 and 400, Fig. 6.18(a), whereas with N_e = 100, the curves overlaid each other quite closely in the range $0 \leq t \leq 100$ years. Differences in the δ:z occurred in the opposite sense.

The δ_{max} : t curves appeared to be leveling off faster at larger t_e with smaller N_e - presumably because the coarser Δt (which results from small N_e) leads to an overestimation of true system stiffness and the analysis is converging on a smaller (false) δ_{95}.

Doubly-propped

With a more stable doubly-propped configuration, the results for $t_e = 400$ years suggested very little dependence of δ:z on N_e, Fig. 6.18(b), and this was a case which was definitely known to have reached t_{95}. If t_e was set lower than 400 years, the discrepancies in δ:z became even less. Insufficient N_e led to a mismatch of δ_{max} : t curves, although not so pronounced as with the top-propped wall. One way of checking the sufficiency of number increments might, therefore, be to overlay the δ_{max} : t curves for different t_e and compare them.

6.6.3.3 Weighting of time steps

It was decided to examine only the power law variation in weightings, using m = 2, 3, 4 or 5 (in combination with $N_e = 25$, 50 or 100 and $t_e = 100$, 200 or 400 years).

Top-propped

Starting at $t_e = 400$ years and $N_e = 100$ (expected to be the most accurate) there was a small difference in the profiles of δ:z as $m = 2 \rightarrow 5$, with the higher powers of m resulting in lower deflections (no worse than 10% reduction in any case). Differences were more noticeable with the δ_{max} :t curves. Keeping N_e at 100 and reducing t_e basically brought the curves closer together until, at $t_e = 100$ years, they were virtually indistinguishable from each other, Fig. 6.19(a). Fixing t_e at 400 years and reducing N_e to 25 served to accentuate the differences in the δ:z profiles and the deviations between the δ_{max} :t curves, but only by a small amount.

Doubly-propped

Starting at $t_e = 400$ years and $N_e = 100$ there was no perceptible difference in the δ:z profiles as m changed from $2 \rightarrow 5$. Fixing t_e at 400 years and reducing N_e to 25 served to accentuate slightly the differences in the δ:z profiles and the deviations between the δ_{max} :t curves, Fig. 6.19(b).

6.6.4 Summary

Two key findings emerged from these analyses. Firstly, if insufficient time is allowed for equalization to occur, it would be possible to believe (incorrectly) that a small number of increments is adequate. However, the insufficiency of time would be revealed through an insensitivity to the weighting of the time steps Δt.

Secondly, if the number of increments is insufficient and only the δ:z profiles were compared, it could be judged that the use of small t_e was acceptable. It is only in overlaying the δ_{max} : t curves that the error would become apparent - and this seems to be the only satisfactory test, because insufficiency of N_e is <u>not</u> revealed by varying the weightings on Δt.

6.7 Groundwater Fluctuations

6.7.1 Previous work

As mentioned in Section 3.11.2, groundwater fluctuations are normally modelled by the appropriate manipulation of drainage boundaries. Incorporating this phenomenon into a finite element analysis is not as common as the other matters investigated in this chapter, but the writer suggests that it will become more important and will be taken into account increasingly.

The literature contains little (if anything) on the application of finite elements to this sort of retaining wall problem, let alone any guidance on the modelling issues. Particular points which need to be addressed are:

a) boundary conditions for imposing rising/falling levels,
b) time steps, and
c) shortcomings of the drainage boundary manipulation approach compared with more rigorous techniques.

The manipulation of drainage boundary conditions (Item a) has been addressed in Section 3.11.2. The rules concerning time step (Item b) are unlikely to be any different to those detailed in Section 3.11.3. There is, however, one issue that is not well understood and it combines aspects of Items (a) and (b) above in two different approaches to recharge:

- instantaneous recharge - specify the full expected increase of pore water pressure on the base of the mesh (boundary C - Fig. 3.20a) and possibly on the remote vertical side(s) (boundary B - Fig. 3.20a) in one increment block, and use the time steps in that block to allow equilibration to some new steady state, or
- gradual recharge - divide the full expected increase of pore water pressure into a number of smaller increments (of, say, 1-5 years duration) and specify these on boundary C (and possibly B) in individual increment blocks, using one last block for final equilibration.

It is not clear if there would be major differences between the instantaneous or gradual recharge approaches, in terms of what took place in and around the wall itself. Given that the changes are occurring on boundaries which are usually remote from the wall, it may not matter greatly which approach is followed. It would be relatively easy to compare the two in a design situation, but it is doubtful whether guidance of sufficient generality could be generated without running a large number of analyses. Therefore this will not be investigated.

6.7.2 Moving phreatic surfaces

The modelling of moving phreatic surfaces via finite element methods has been studied for many years in the context of transient seepage problems (well pumping, drawdown in earth dams, etc). One can either use a fixed mesh where permeability is made artificially low above the phreatic surface to restrict flow, or a variable mesh which attempts to keep the phreatic surface (the upper flow line) coincident with a line of nodes. Such analyses were aimed at seepage studies and did not consider the deformation or stress changes in the soil mass. More rigorous methods take account of storage and the (hysteretic) variation of permeability with degree of saturation, and couple the flow with volumetric strains in the soil. CRISP considers only fully saturated materials, where the volume of water entering (or leaving) corresponds to an increase (or reduction) in the volume of voids. Thus it cannot cope with unsaturated soils, the study of which has intensified greatly over the past decade.

However, work jointly supervised by the writer under an EPSRC research grant has led to the development of a computer code which can handle moving phreatic surfaces in the presence of unsaturated/saturated flow. This code has the capacity for more rigorous modelling of retaining wall problems where moving phreatic surfaces are involved (Mavroulidou, 1999). It is still a research level code and its features are some way off incorporation in a commercial program such as CRISP, but it could be a useful direction for further work to pursue.

6.7.3 Numerical studies

In the absence of any obvious fundamental studies which could be carried out on groundwater fluctuations, some results of analyses conducted with CRISP on two different practical problems will be presented herein. The first is taken from Case 1 in Appendix A, the A406 Walthamstow, which comprised a contiguous bored pile wall in London clay, singly propped at formation level, forming the sides of an underpass. The current pore water pressure profile was hydrostatic from 1m below ground level to 10m below ground level, below which the gradient of $\partial u/\partial z$ was only 4 (rather than 10) kPa/m, thus showing significant under-drainage. In the analysis, following bulk excavation and permanent prop installation, the ground was allowed to come into equalization over 120 years with the current (under-drained) pore water pressure profile, with a drainage layer at formation level - referred to as Stage LT1 (long term 1). Then, remote boundary pore water pressures were manipulated to model aquifer recharge such that the ultimate pore water pressure profile was hydrostatic from 0m (ground level). A further 120 years equalization was modelled - Stage LT2.

Fig 6.20 shows plots of (a) wall deflection, (b) wall bending moment, (d)prop axial force, and (c) prop bending moment for three stages - post-construction, LT1 and LT2. Very significant changes can be seen to have been brought about by the rising groundwater level. Overall, the wall rotated back into the retained soil (about the formation level prop) as the resultant thrust from the pore water pressure increased and its line of action moved down. Stage LT1 showed higher δ_{max} at the crest (40mm) than LT2 (24mm) - a point noted by the consultant (for whom the writer conducted the analysis), as the contractor had commissioned FE analysis from another university (to support their preferred choice of bored piles versus diaphragm panels) and omitted this intermediate stage, claiming that $\delta_{max} \leq 25$mm throughout. Clearly it can be important to consider all stages in a construction sequence, and not just the final.

The second example is a typical deep basement structure identified as being at particular risk by Simpson *et al.* (1989) in a major study on the implications of rising groundwater in London. An FE model of this particular case was set up (see Fig. 6.21) and used to examine the changes in bending moment and shear force in the walls, columns and floor slabs of the deep basement - as a result of rising groundwater levels in the surrounding soils. Two broadly different types of under-drained pore water pressure profiles were used for the present-day condition, namely:

a) hydrostatic but with groundwater levels at varying depths z_w below the ground surface ($u = 10[z-z_w]$)

b) non-hydrostatic but originating from ground level ($u = m\,z$, where $0 \leq m \leq 10$)

In both cases, the pore water pressure profile after aquifer recharge was full hydrostatic from ground level ($u = 10z$).

Typical London clay stiffnesses and permeabilities were used; the basement was "wished-in-place" as it was only the groundwater level fluctuations that were of interest. Further details are provided by Woods *et al.* (1996). Selected bending moment diagrams for the outer wall and upper floor slab are shown in Fig. 6.22. Some of the changes in internal structural forces were very large, especially at connections, as summarized in the table below. The analyses suggest that Simpson *et al.* (1989) were justified in their concern about this particular case. Although the connections were modelled as rigid, the changes experienced in practice could still be expected to be very significant and potentially damaging.

Member	**Quantity**	**Maximum change**
outer wall W	bending moment	600 %
internal column C1	bending moment	150 %
upper slab S1	shear force	100 %
	bending moment	140 %
	shear force	70 %
lower slab S2	bending moment	30 %
	shear force	30 %

6.7.4 Summary

Rising groundwater levels are not uncommon (they are occurring in many major cities), and may increasingly be a feature in design studies. Indications (from the two different practical problems reported here) are that the effects of rising groundwater can be highly significant and should be included if there is any likelihood of it occurring. CRISP provides a straightforward way of modelling this phenomenon, and there are no really contentious issues.

The only area of legitimate concern is how the method used herein (boundary pore water pressure manipulation) might differ from a more rigorous analysis with genuine movement of phreatic surfaces. Comparisons could be conducted, but would require more sophisticated software for the latter. Calibration with field data would also be helpful in establishing the accuracy of each approach.

6.8 Discussion and Summary

One of the great strengths of finite element analysis applied to retaining walls is that it is able to model changes in geometry, time-dependent drainage (transient seepage), and global fluctuations in groundwater levels. This permits investigation of the entire construction phase and subsequent design life of the earth-retaining structure.

Changing geometry

It has become clear over the past decade that, not only do lateral earth pressures relax as a result of wall installation (before bulk excavation takes place), but that it is possible to model this faithfully with the finite element method. However, the designer/analyst must appreciate that such modelling, if it is to be successful, requires three-dimensional coupled analysis. This is not trivial. Alternative approaches exist, ranging from manipulation of the in-situ earth pressure coefficient K_o (reduced to a post-installation value, K_i), through modified plane strain analysis (the MOM and APM presented herein), to coupled plane strain / plane stress strategies. Provided the strengths and weaknesses of each approach are understood, they are all a valid part of the "toolbox".

Geometric alterations are intuitive when modelled via element removal/addition. CRISP and most modern codes may now be considered to calculate correctly the equivalent nodal forces due to excavation, but tests and benchmarking are still good practice. The use of equivalent heavy fluid pressure on final excavated geometries provides a sensible cross-check. The independence of the final result on the number of increments and sequence of excavation in an elastic analysis has been proven by Ishihara (1970) and can be used as an acid test - unfortunately no parallel exists for elastic-perfectly plastic or CSSM models. If props/anchors are being installed, the overall system stiffness is changing and Ishihara's proof no longer applies (even if all materials are elastic). With intricate excavation and propping sequences,

sensible benchmarking will be difficult, but some kind of sensitivity checking on results is in order. In Section 6.3 it was shown that the influence of number of increments and increment blocks was minimal in the cases examined, but these were fairly simple analyses.

Finite element analysis is particularly good at tackling the questions relating to temporary props - how many, what level(s), when installed, when removed, etc. The direct analogue of adding/removing elements is physically appealing. The removal of a prop (or temporary berm) corresponds to the release of significant horizontal stress, and should be handled with the same degree of refinement (e.g. number of increments used for removal) as bulk excavation. If the soil is overconsolidated, the lateral stresses on the retained side will be closer to the passive limit (than to the active) prior to bulk excavation, and horizontal unloading will be largely in the elastic region (and thus not particularly sensitive to number of increments).

Time-dependent drainage

Where delays in construction are expected, or where construction may takes a considerable time, it may be important to analyse this phase with a coupled analysis. Partial drainage may take place in the field and this is more onerous than the fully undrained conditions which might otherwise be assumed. A coupled analysis will require (a) selection of consolidation elements, (b) definition of initial drainage boundary conditions (and any subsequent changes to them), and (c) specification of time steps. Execution time will be extended because the system of equations is bigger (additional excess head d.o.f.s at many of the nodes). The designer/analyst must decide if this refinement is warranted, but often the only way to verify this is to run both types of analysis and compare the results.

In practice, there is likely to be some reluctance towards running an undrained analysis first, then altering the mesh and analysis data in order to run a coupled analysis second. However, the writer believes there is a case for doing just that. If a coupled analysis model is set up right from the start, and very small time steps Δt (or very high permeabilities k) are used to recover the undrained case, errors could creep in due to ill-conditioning of the overall equations. The coupled formulation gives the facility of investigating the full spectrum of behaviour. This would be particularly useful if re-analysing a retaining wall system contemporaneously with construction, as part of the observational method of approach (Peck, 1969). But it would still be important to start at one well-defined limit (e.g. undrained, constant volume conditions) in order to provide some benchmark for subsequent, more refined analyses. The user should not

be deterred from the more complicated analysis, but should understand its strengths and its limitations. This is a similar argument to that advanced for starting with simple constitutive models and adding in the extra layers of sophistication later. It may not be a popular message but it is an important one.

Undrained conditions can be obtained with small Δt without risking numerical instability. Moving to larger Δt (or higher k) will promote partial drainage but care must be taken with drainage boundaries as these may activate during excavation - especially on freshly excavated surfaces. Larger Δt will result in larger $\Delta \sigma'$ and, depending on the non-linearity of the stress-strain response, may require many more increments.

Many users would consider that modelling long-term equalization (equilibration, dissipation) simply comprises selecting an arbitrarily large time interval (e.g. 50-100 years), several tens of increments and some suitable weighting of time steps (usually a logarithmic progression) and letting the analysis wind forward. The development of δ, M, S etc. with time can be followed by extracting profiles at the appropriate times. But the analyses herein have shown that the time allowed, number of increments, and the weightings adopted, can all have a significant effect on the results. The introduction of plastic yielding complicates the issue further, and many practical analyses do now include this feature of constitutive behaviour as standard. To understand the nature and magnitude of these effects requires sensitivity studies, and these are rarely done in design practice owing to time constraints.

Groundwater Fluctuations

With many urban areas now under threat from rising groundwater level, it is inevitable that embedded retaining structures may need to withstand pore water pressure changes that are independent of post-construction dissipation/equilibration. Limited investigation suggests that there can be very significant effects in the internal structural forces. In view of this, any possible groundwater fluctuations should be taken into account and included in the modelling sequence. CRISP provides a very convenient facility for modelling such fluctuations, which will be perfectly adequate in many situations. It is unable to model moving phreatic surfaces with any rigour, but this is unimportant in the context of earth-retaining structures (compared with, say, the analysis of borehole pumping and drawdown).

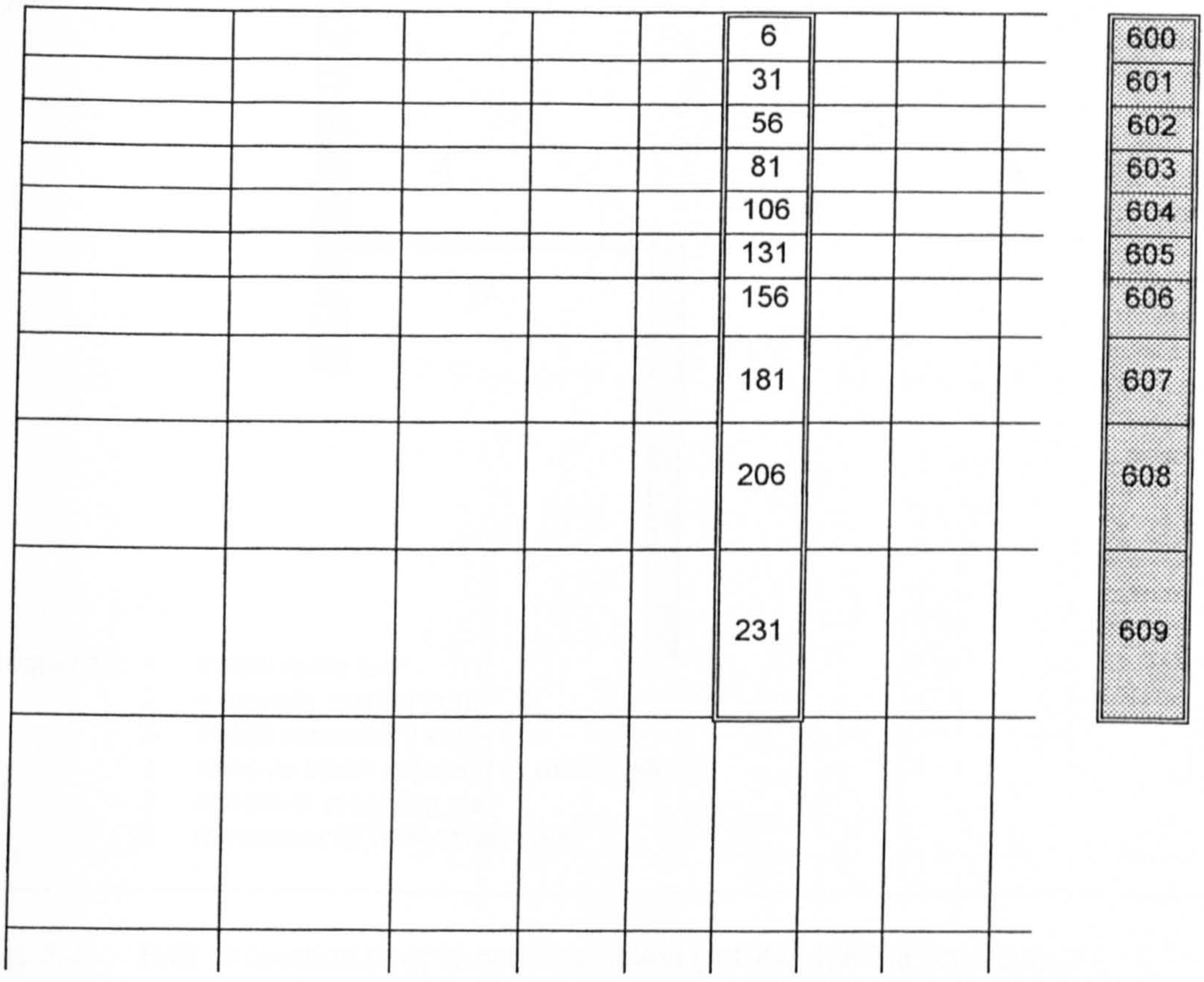

(a) original mesh (b) overlays

Notes:

1. Elements 6, 31, ... 231 are soil elements in the original mesh - they are present in the in-situ mesh.

2. Elements 600 - 609 are defined by exactly the same nodes as elements 6, 31, ... 231 - but have different material type - they are not present at the in-situ stage

3. Elements 6, 31, ... 231 are removed from the mesh - and elements 600 - 609 are added to it (in some future increment block in the analysis) to simulate wall installation.

Fig. 6.1 Wall installation by element swopping method

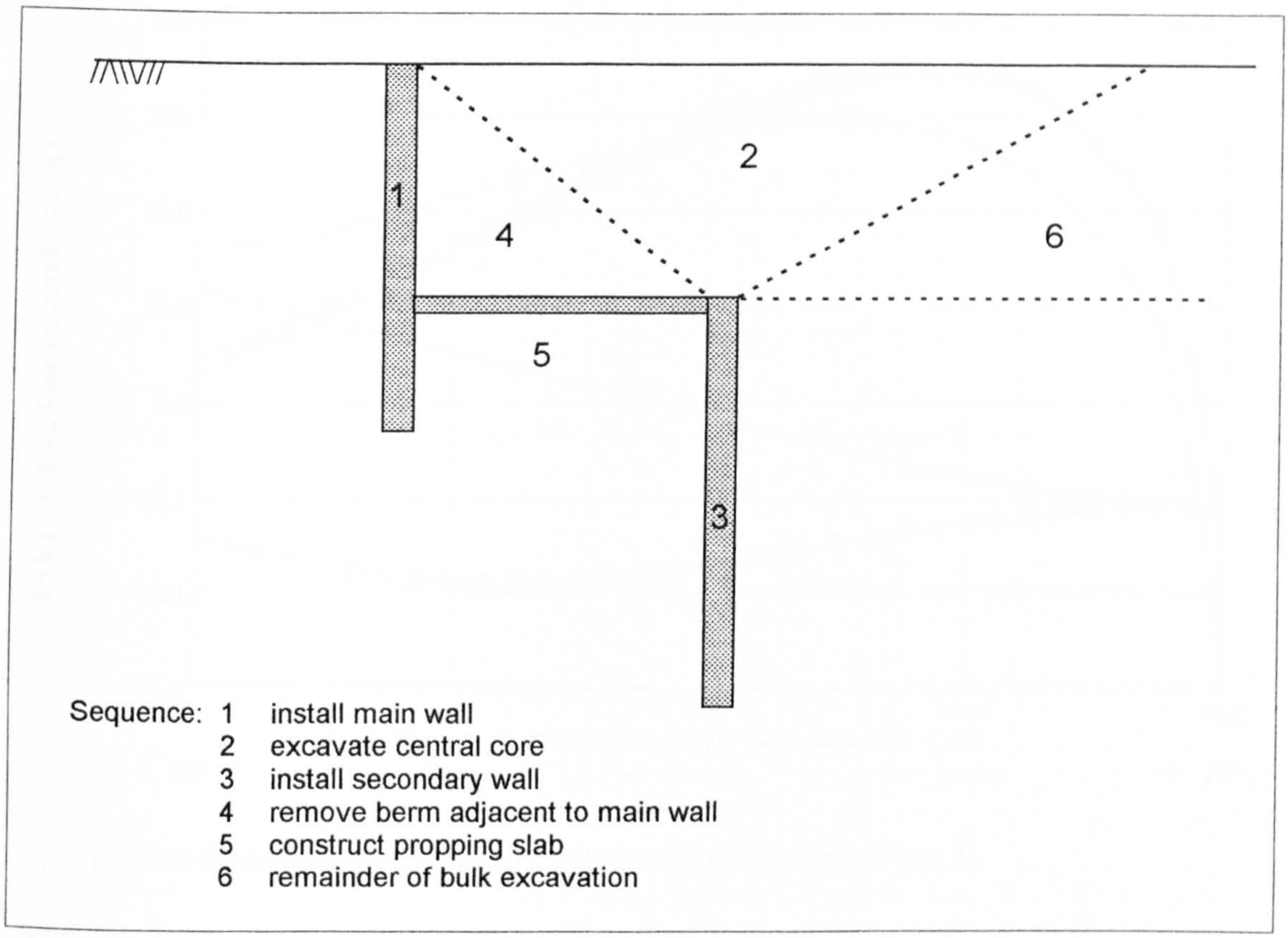

Sequence:
1 install main wall
2 excavate central core
3 install secondary wall
4 remove berm adjacent to main wall
5 construct propping slab
6 remainder of bulk excavation

Fig. 6.2 Bulk excavation prior to wall installation (A406/A1/A598 Junction)

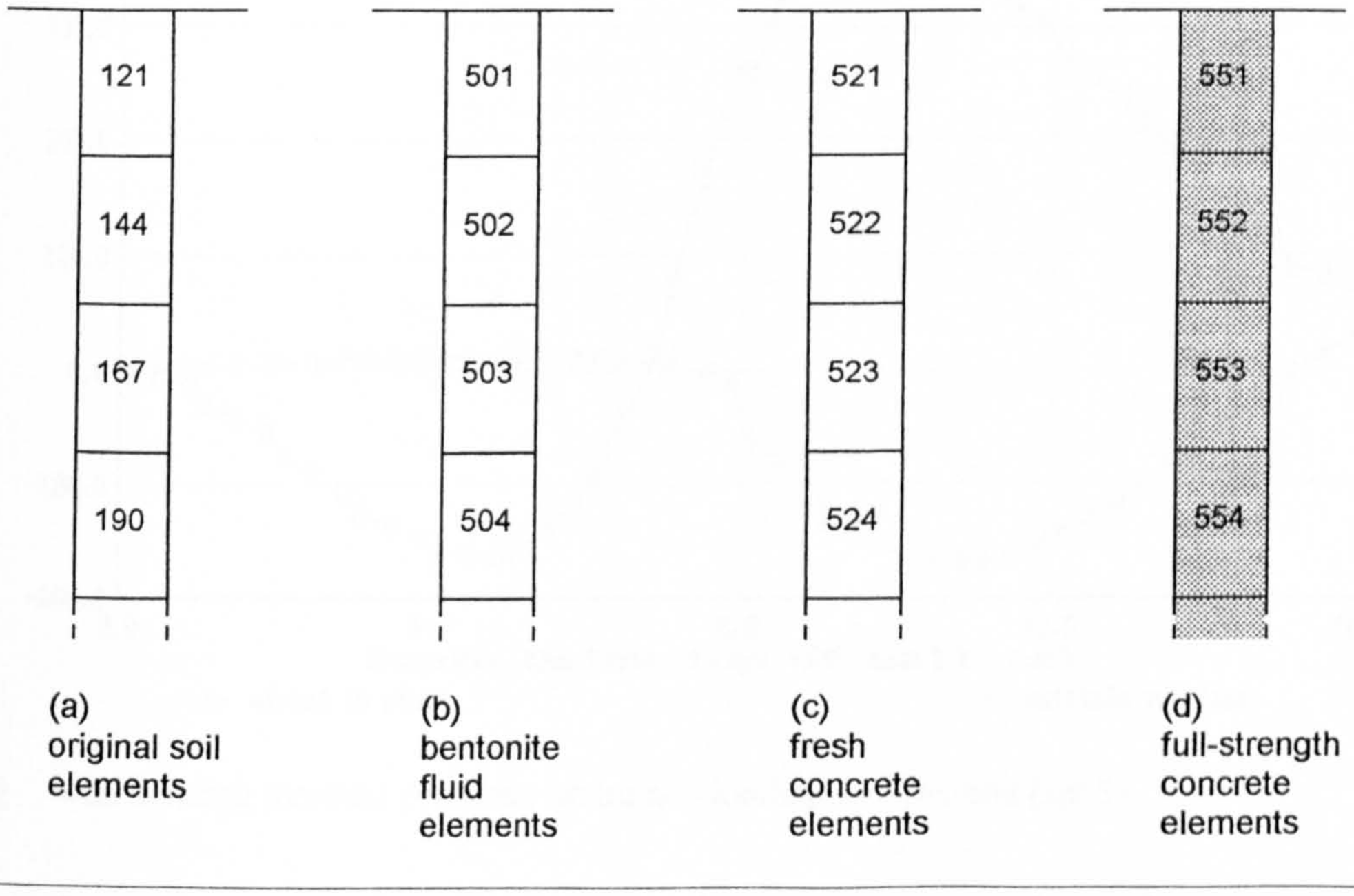

Fig. 6.3 Steps employed in the multiple overlay method (MOM) of wall installation

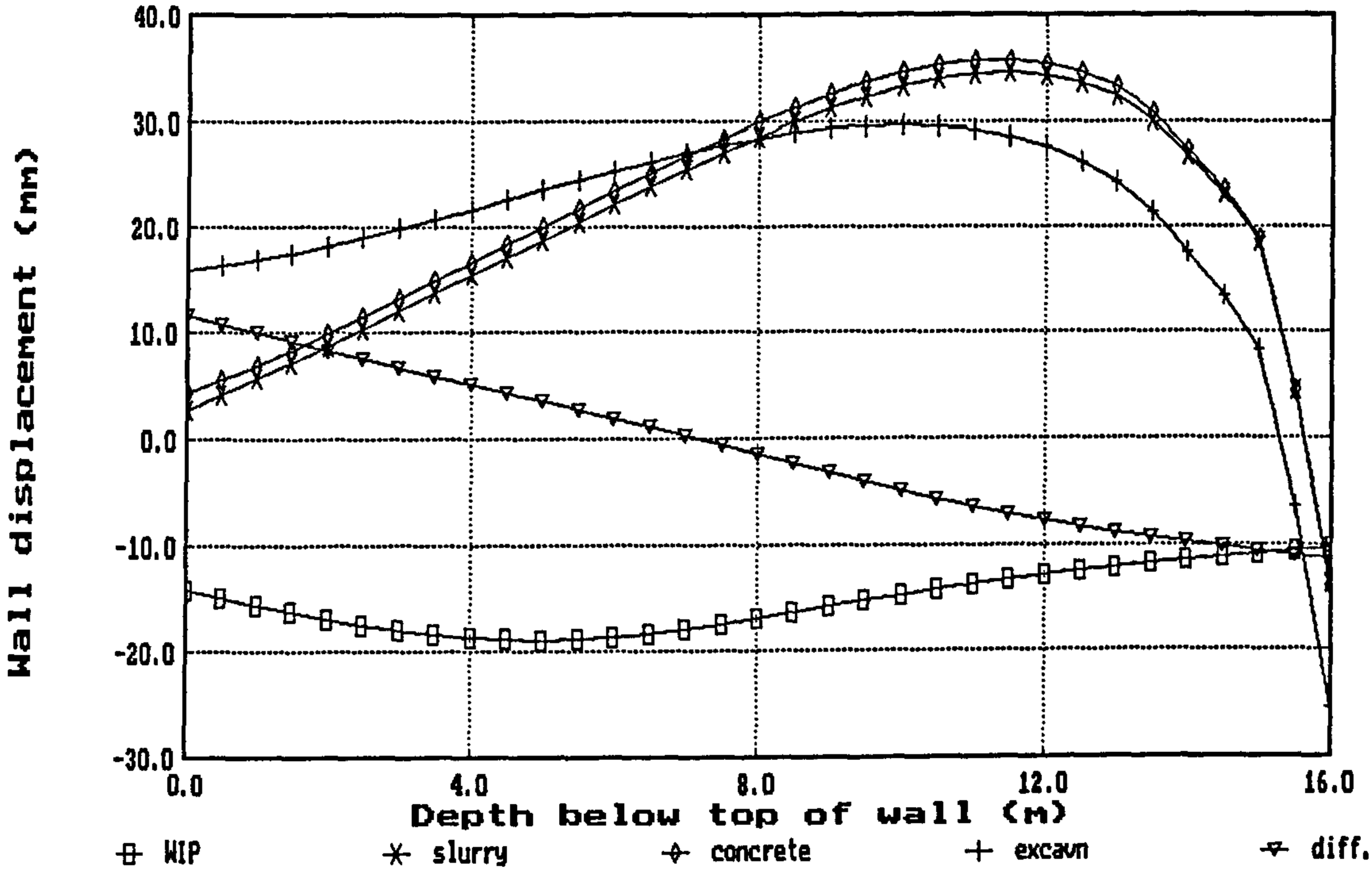

(a) wall displacement profiles : undrained loading / elastic soil (set 1)

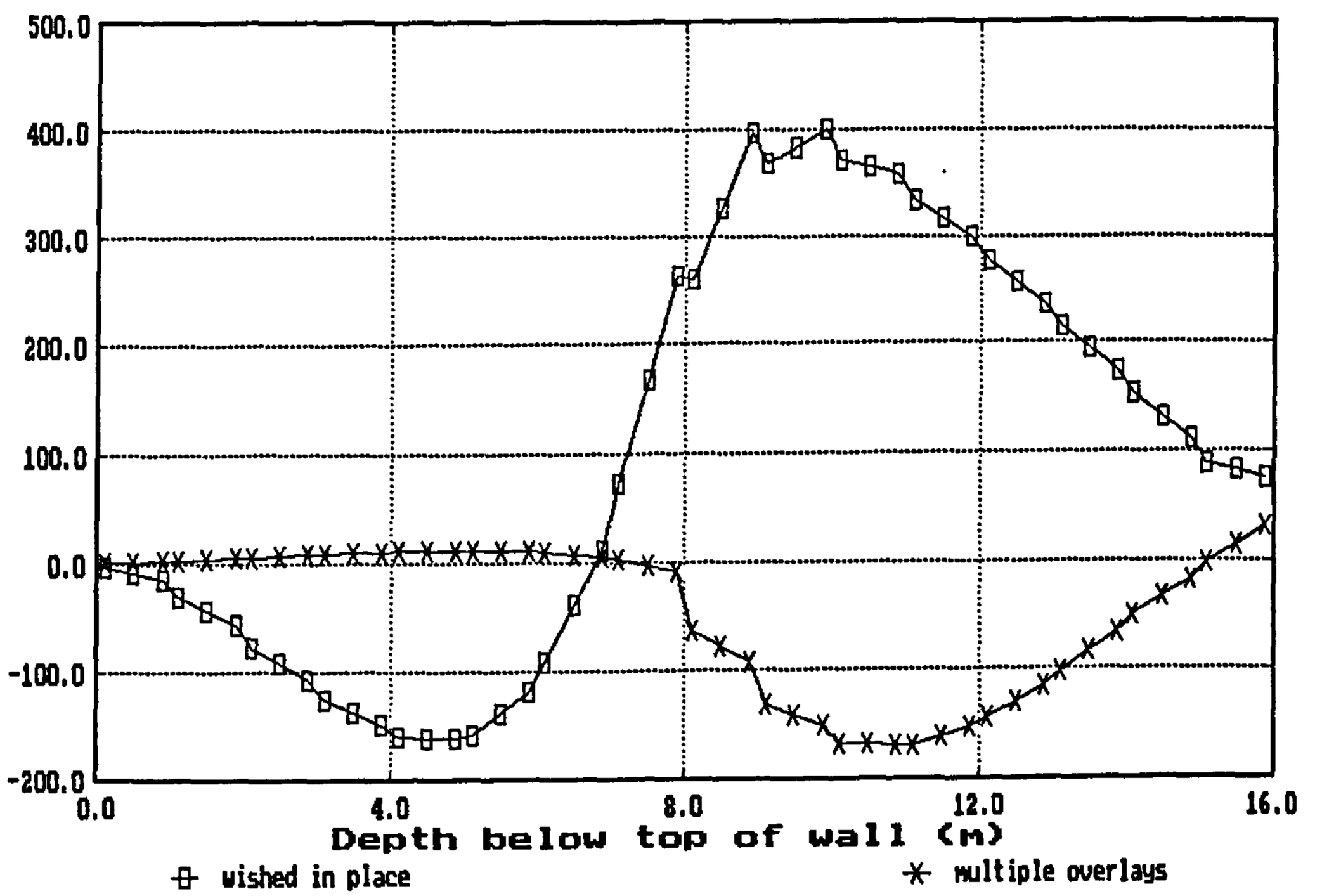

(b) wall bending moment profiles : undrained loading / elastic soil (set 3)

Fig 6.4 Comparison of multiple overlay and wished-in-place methods of wall installation for a cantilever wall

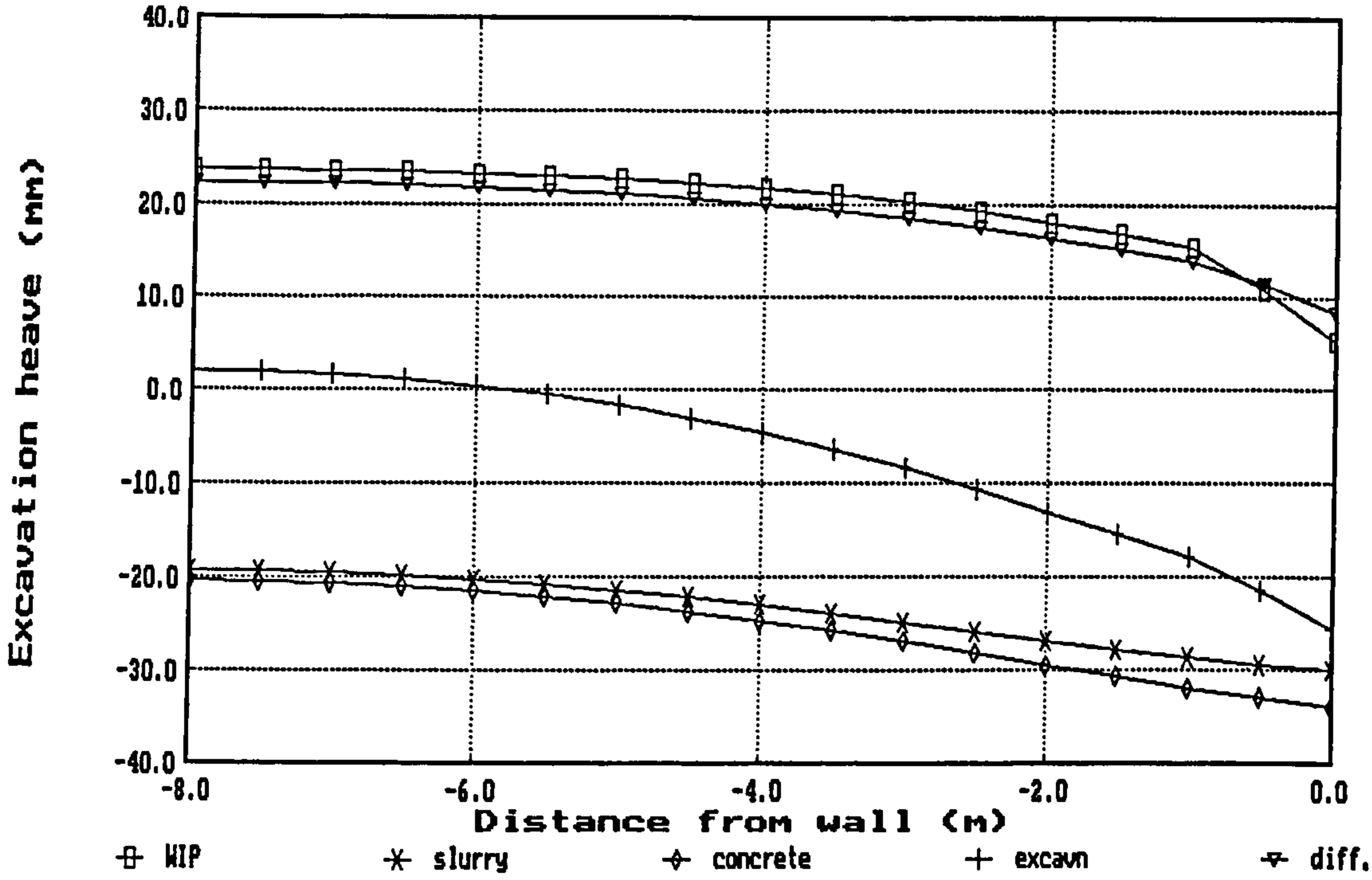

(c) excavation heave profiles : undrained loading / elastic soil (set 3)

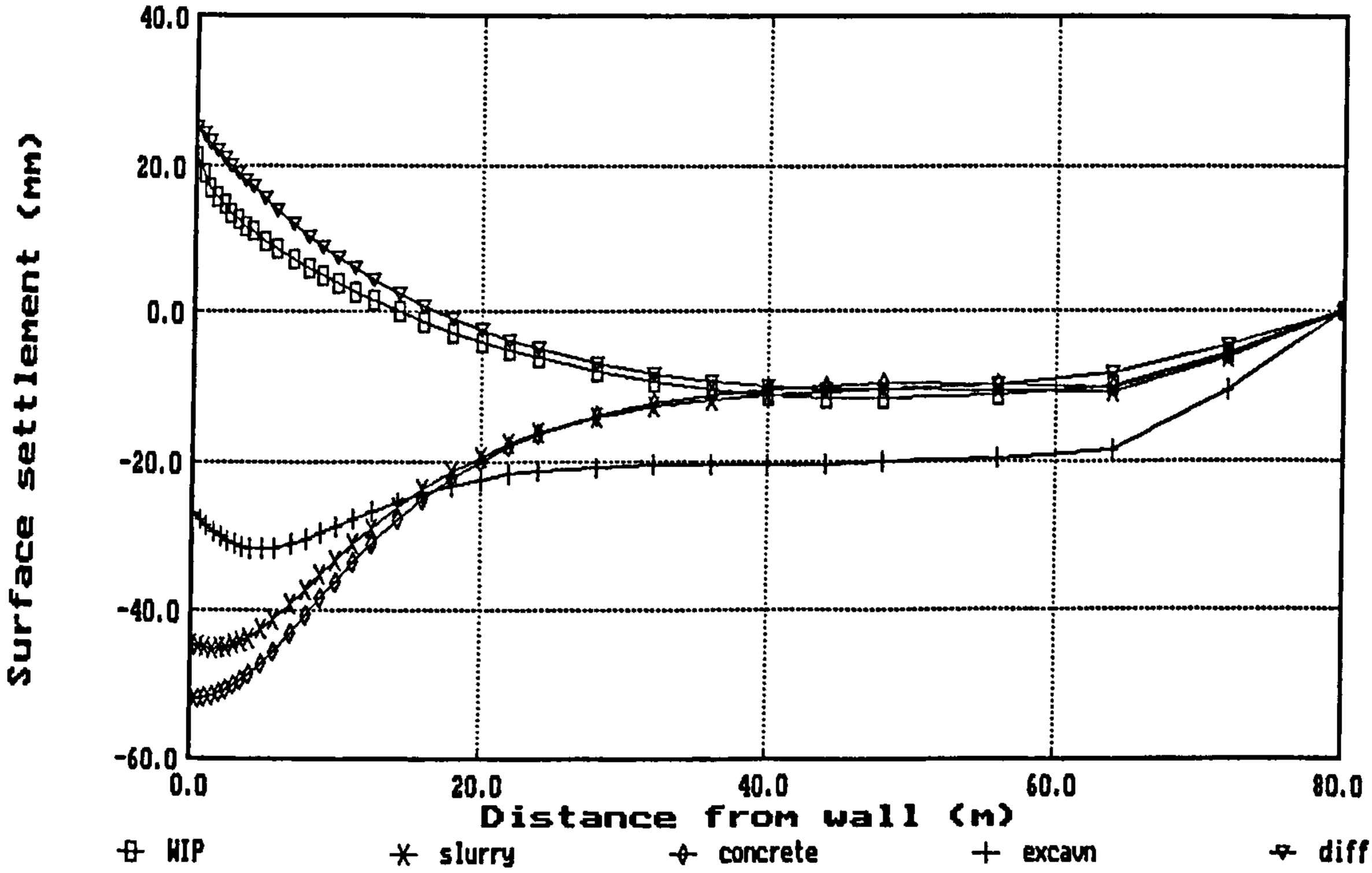

(d) ground surface movement profiles : undrained loading / elastic soil (set 1)

Fig 6.4 Comparison of multiple overlay and wished-in-place methods of wall installation for a cantilever wall (contd)

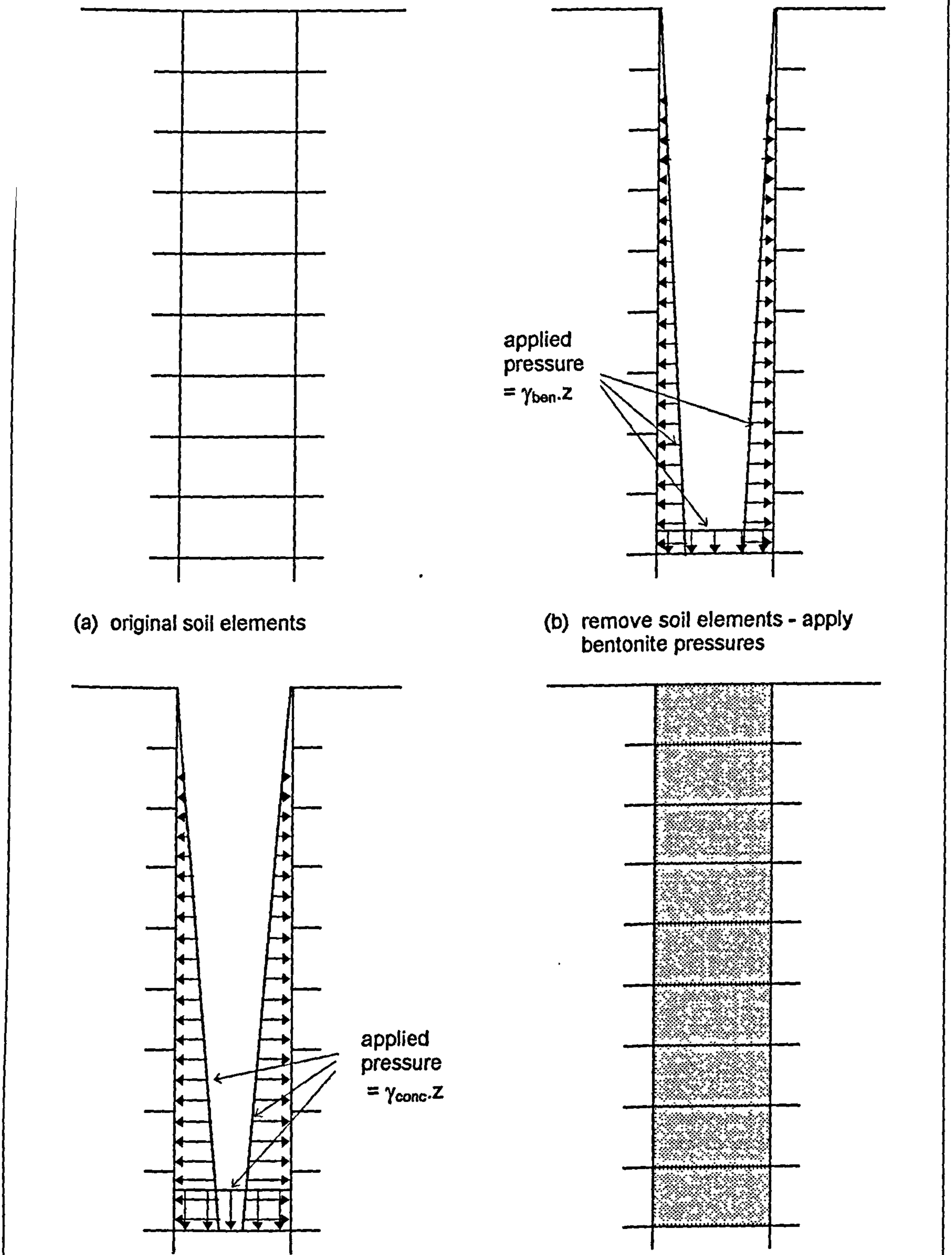

(a) original soil elements

(b) remove soil elements - apply bentonite pressures

(c) replace bentonite pressures with wet concrete pressures

(d) cancel wet concrete pressures - install concrete wall elements

Fig 6.5 Steps employed in the applied pressure method (APM) of wall installation

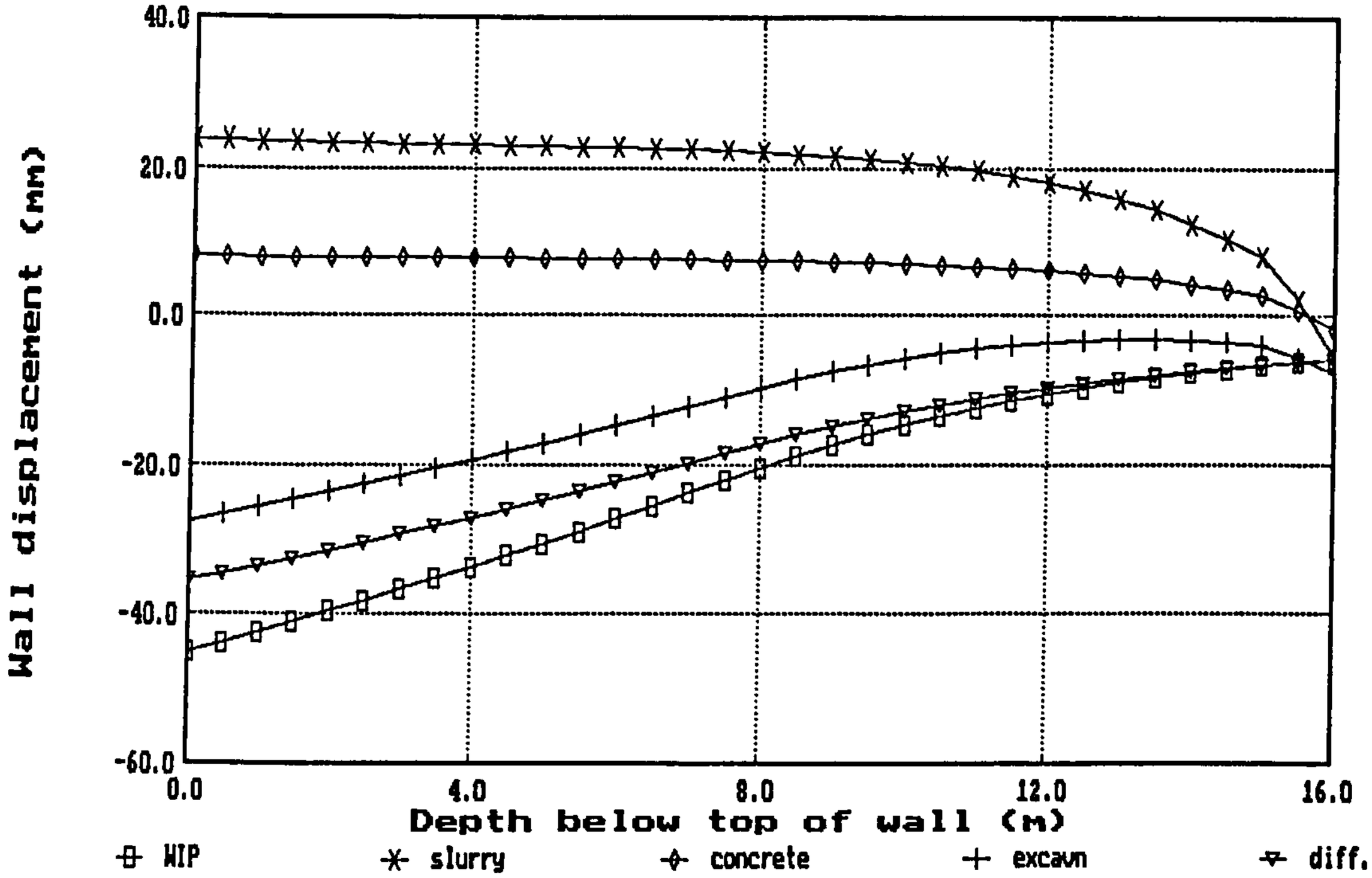

(a) wall displacement profiles : undrained loading / elastic soil (set 3)

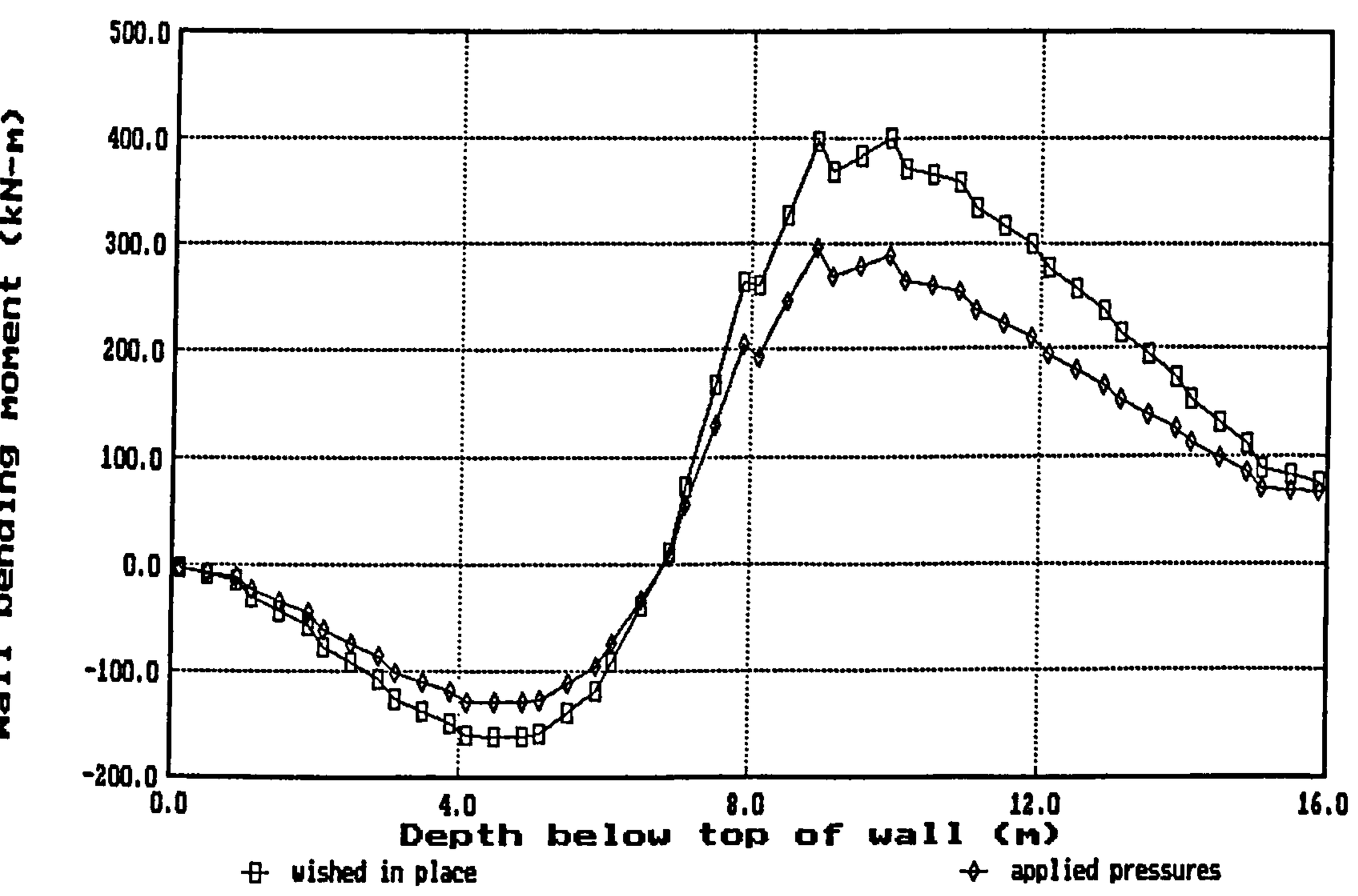

(b) wall bending moment profiles : undrained loading / elastic soil (set 3)

Fig 6.6 Comparison of applied pressure and wished-in-place methods of wall installation for a cantilever wall

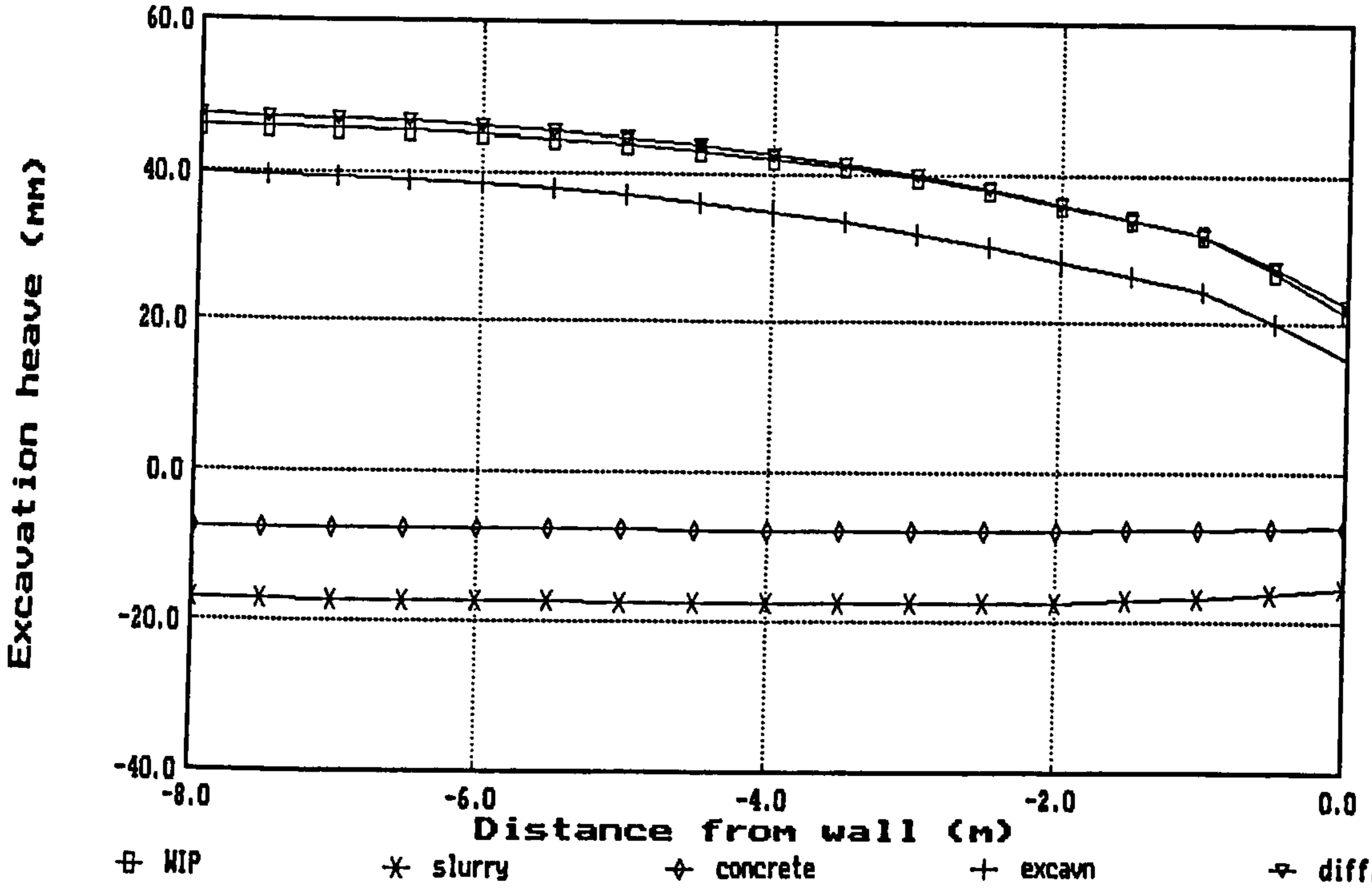

(c) excavation heave profiles : undrained loading / elastic soil (set 1)

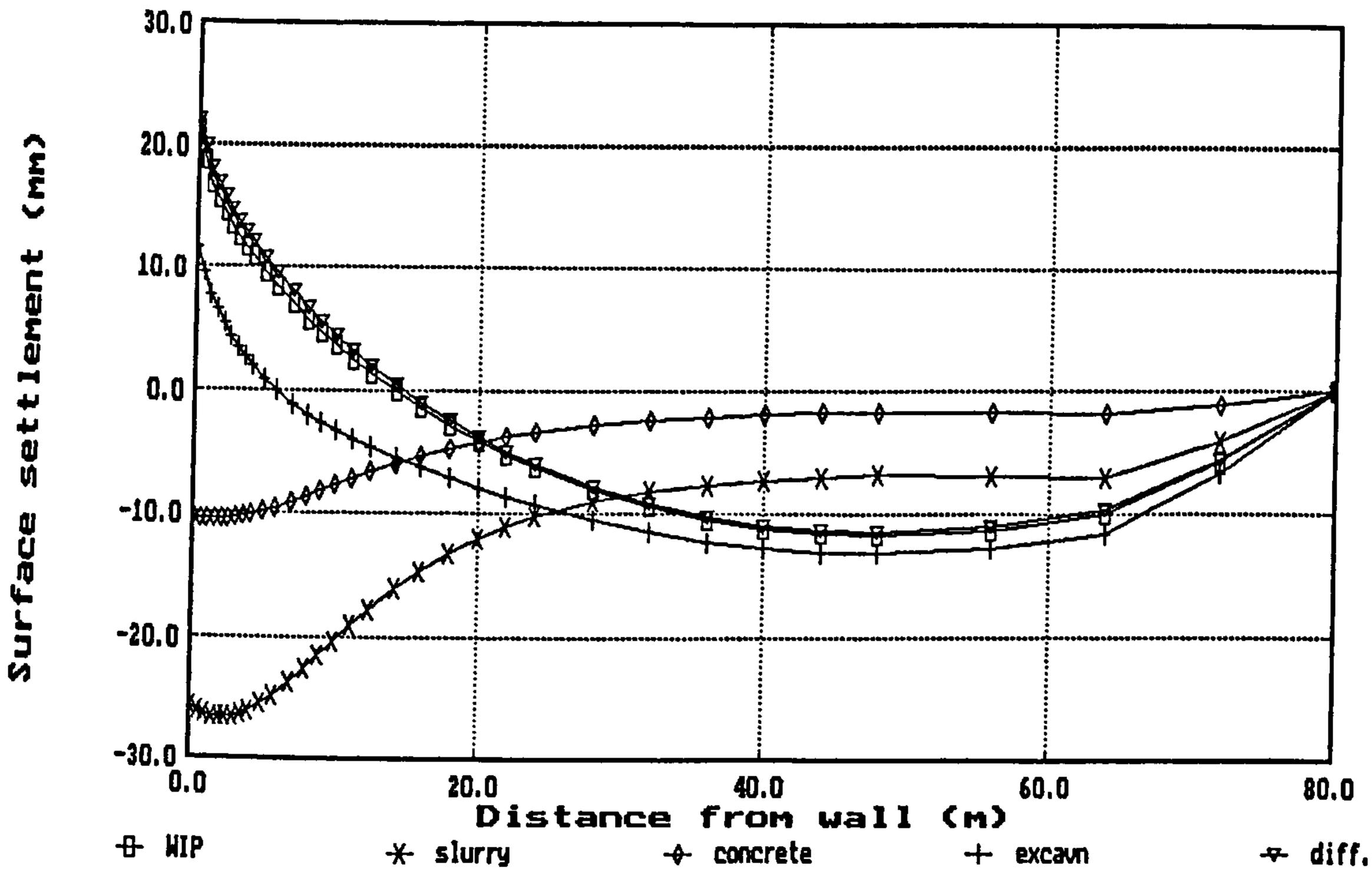

(d) ground surface movement profiles : undrained loading / elastic soil (set 1)

Fig 6.6 Comparison of applied pressure and wished-in-place methods of wall installation for a cantilever wall (contd)

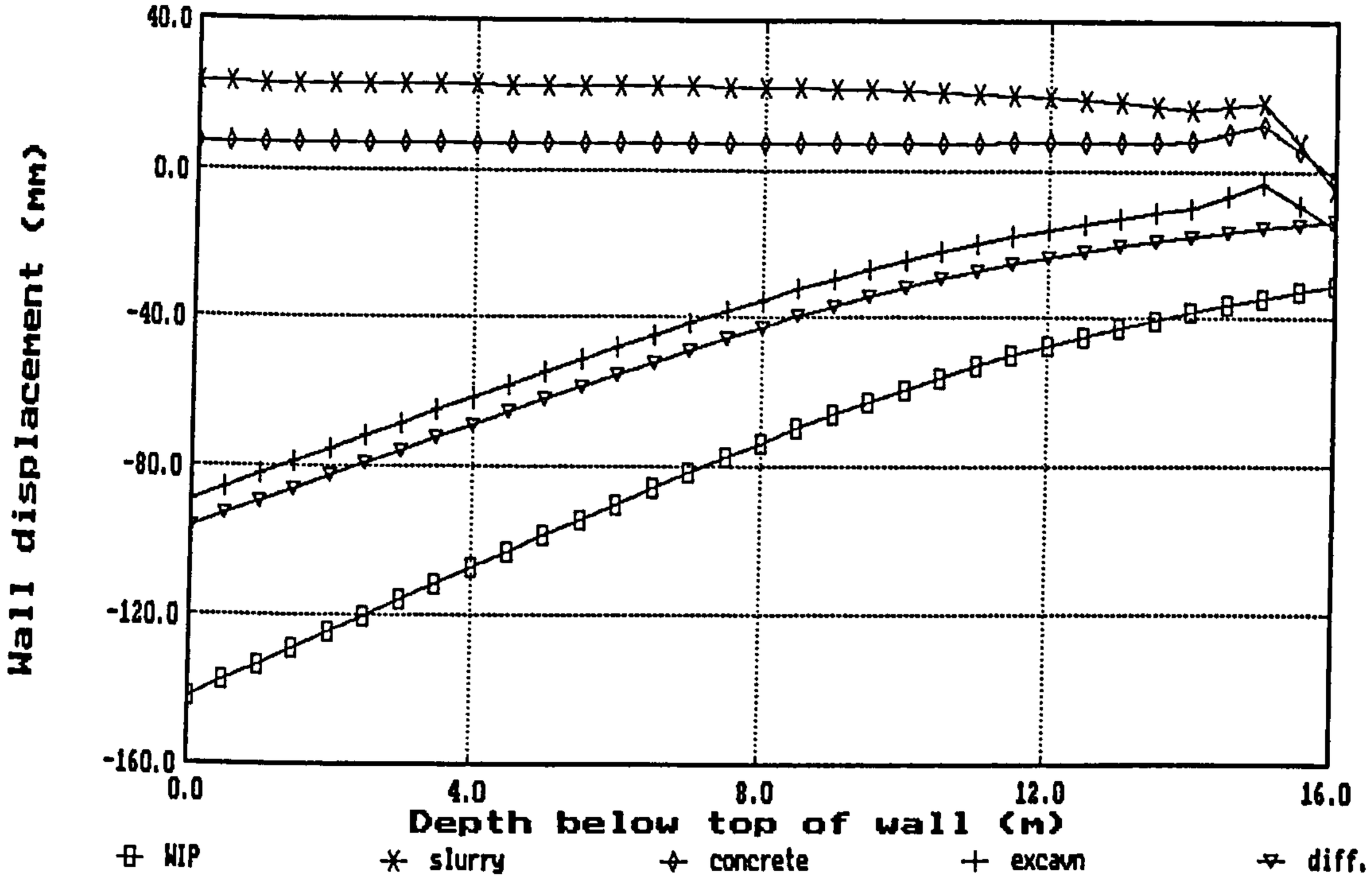

(a) wall displacement profiles : undrained / elastic-perfectly plastic soil (set 13)

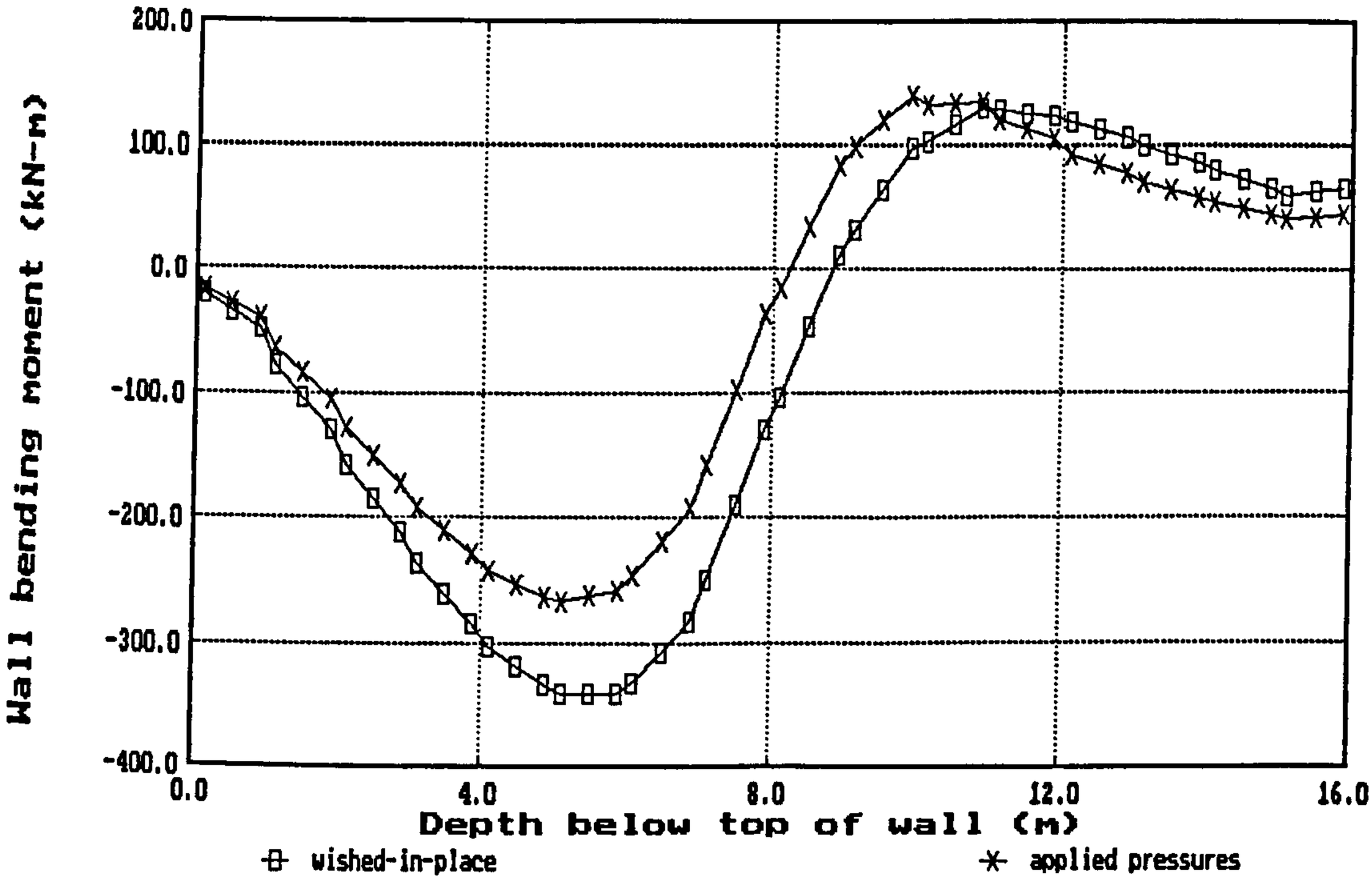

(b) wall bending moment profiles : undrained / elastic-perfectly plastic soil (set 12)

Fig 6.7 Comparison of applied pressure and wished-in-place methods of wall installation for a cantilever wall

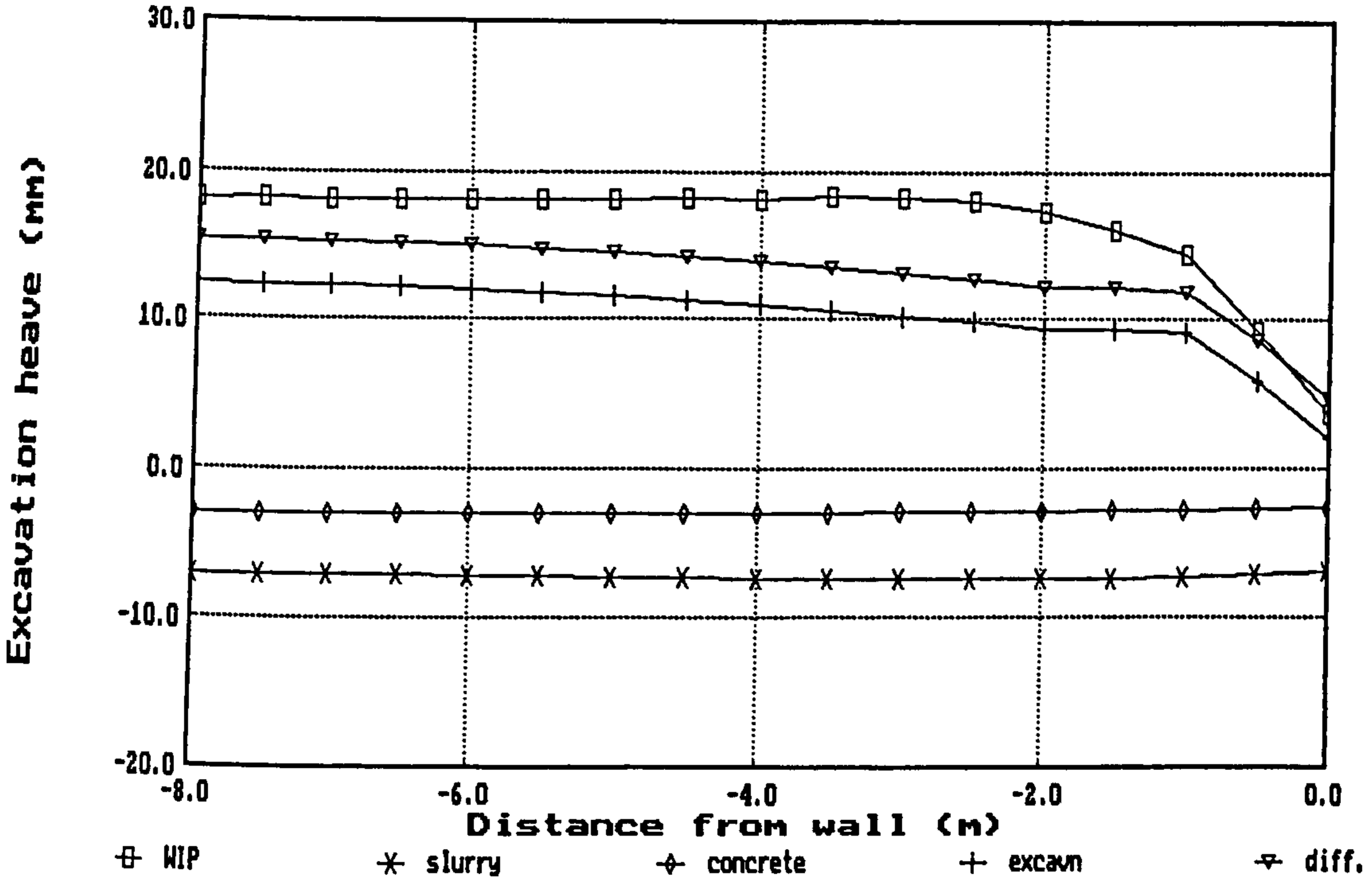

(c) excavation heave profiles : undrained / elastic-perfectly plastic soil (set 12)

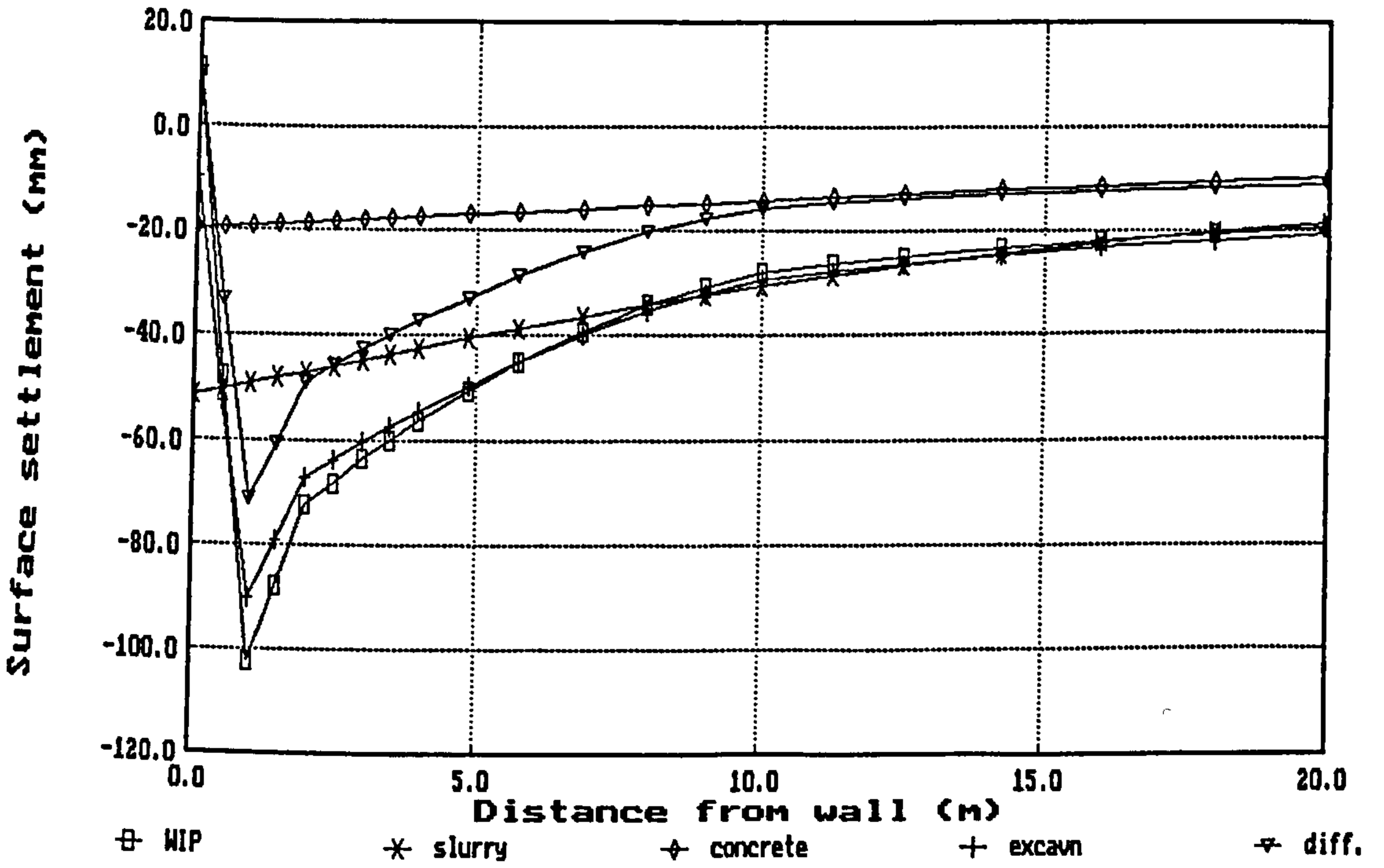

(d) ground surface movement profiles : undrained / elastic-perfectly plastic soil (set 13)

Fig 6.7 Comparison of applied pressure and wished-in-place methods of wall installation for a cantilever wall (contd)

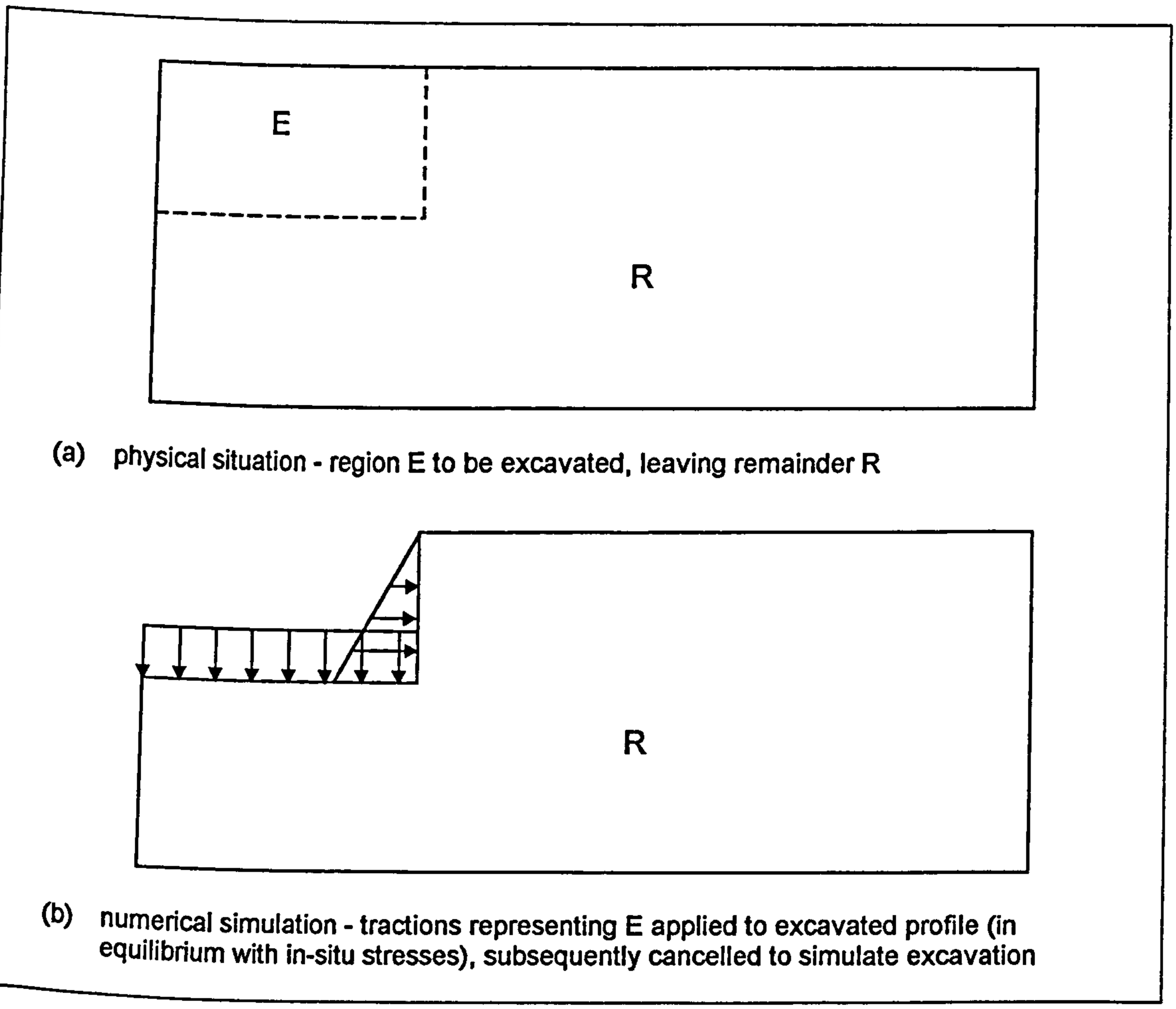

(a) physical situation - region E to be excavated, leaving remainder R

(b) numerical simulation - tractions representing E applied to excavated profile (in equilibrium with in-situ stresses), subsequently cancelled to simulate excavation

Fig 6.8 Simulation of bulk excavation by canceling applied tractions

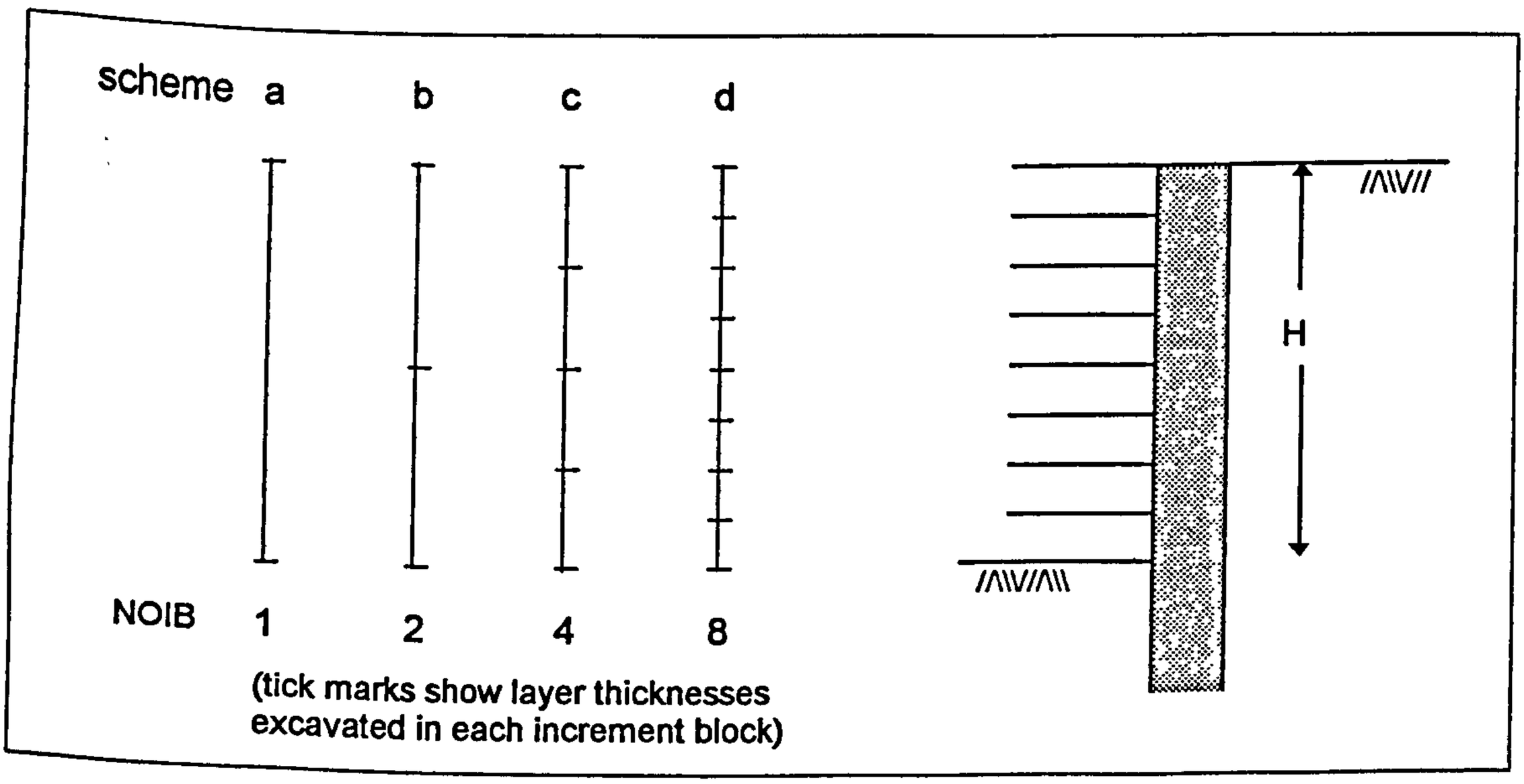

Fig 6.9 Excavation schemes using different numbers of increment blocks (NOIB)

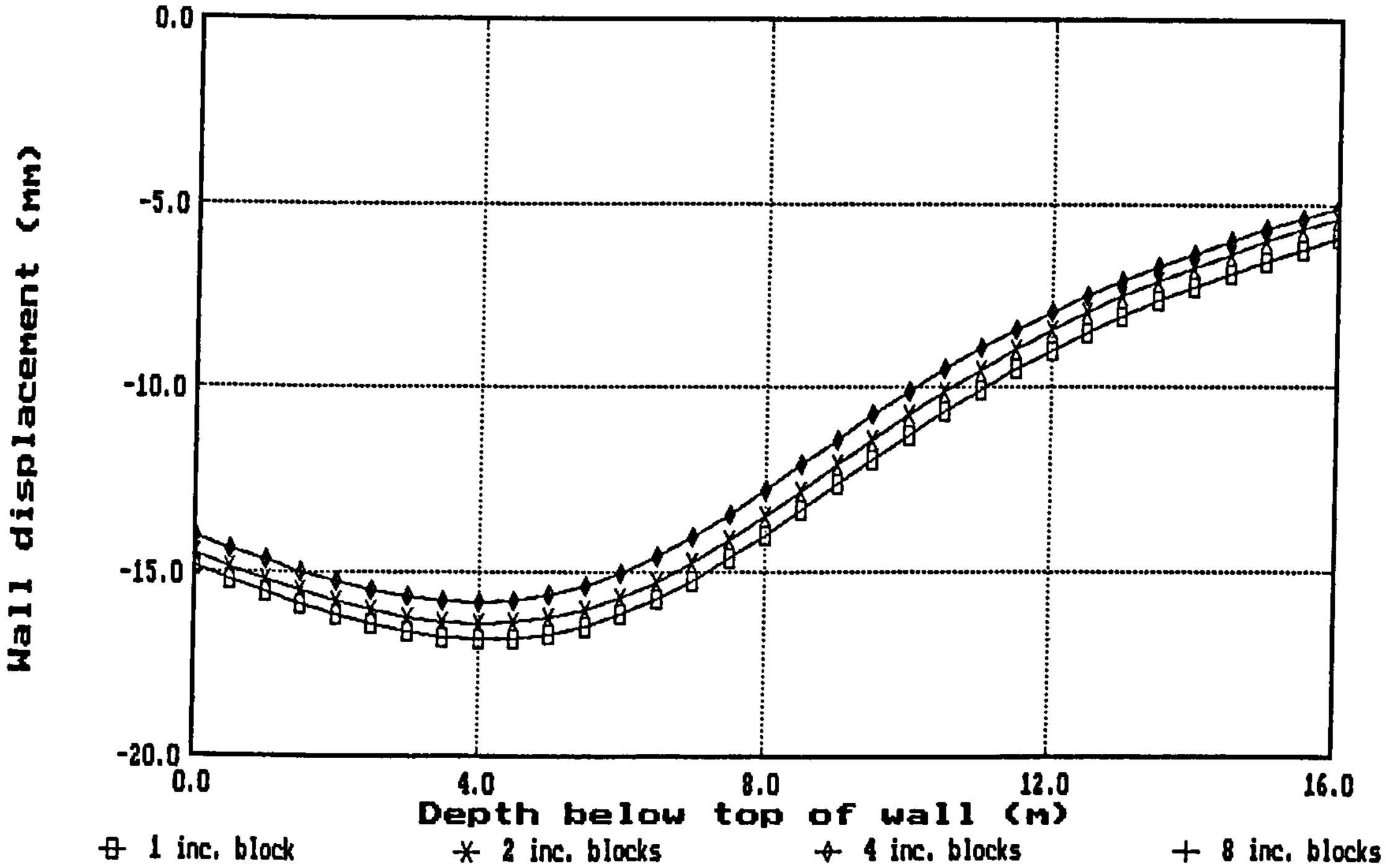

(a) wall displacement profiles : set 12

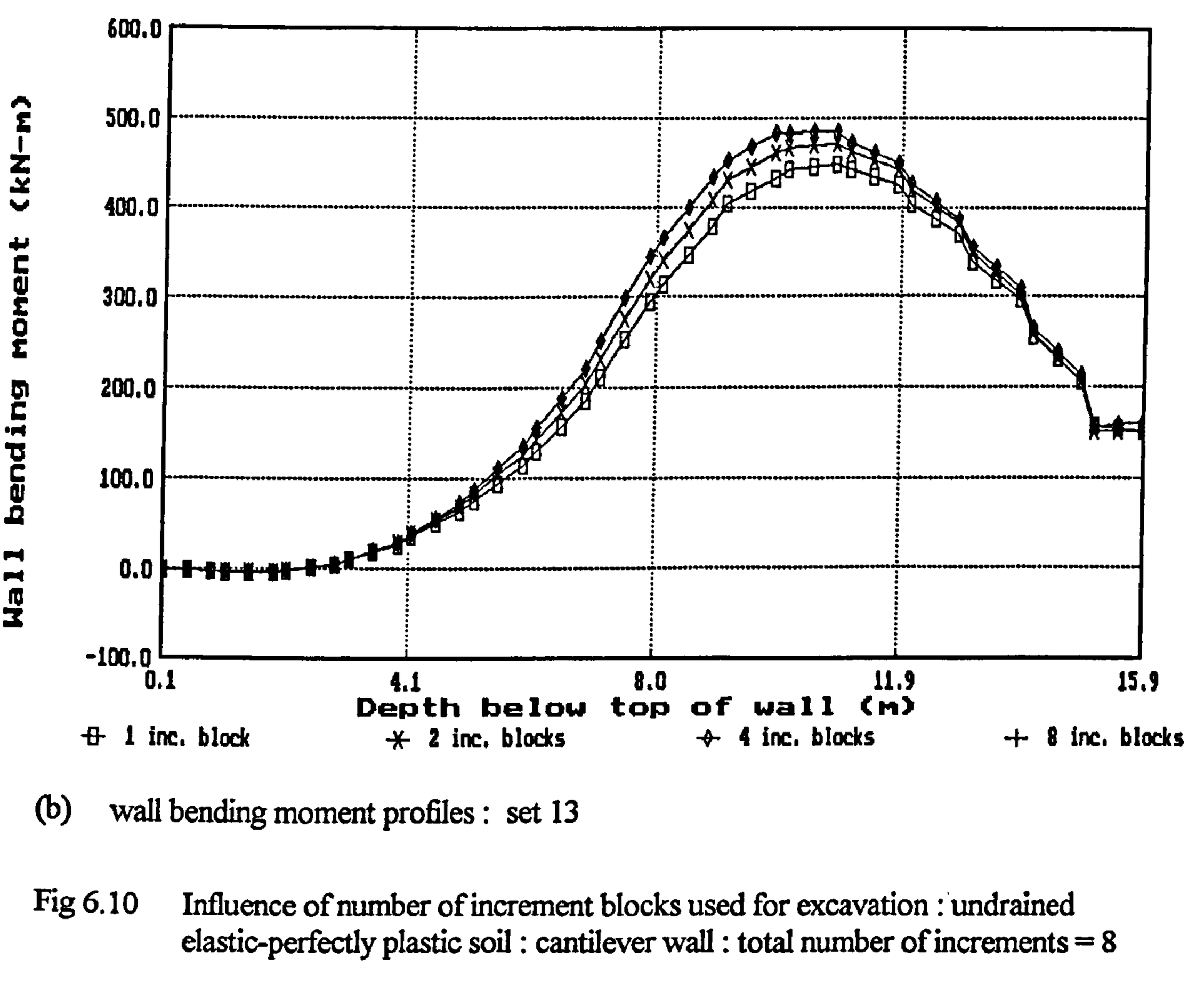

(b) wall bending moment profiles : set 13

Fig 6.10 Influence of number of increment blocks used for excavation : undrained elastic-perfectly plastic soil : cantilever wall : total number of increments = 8

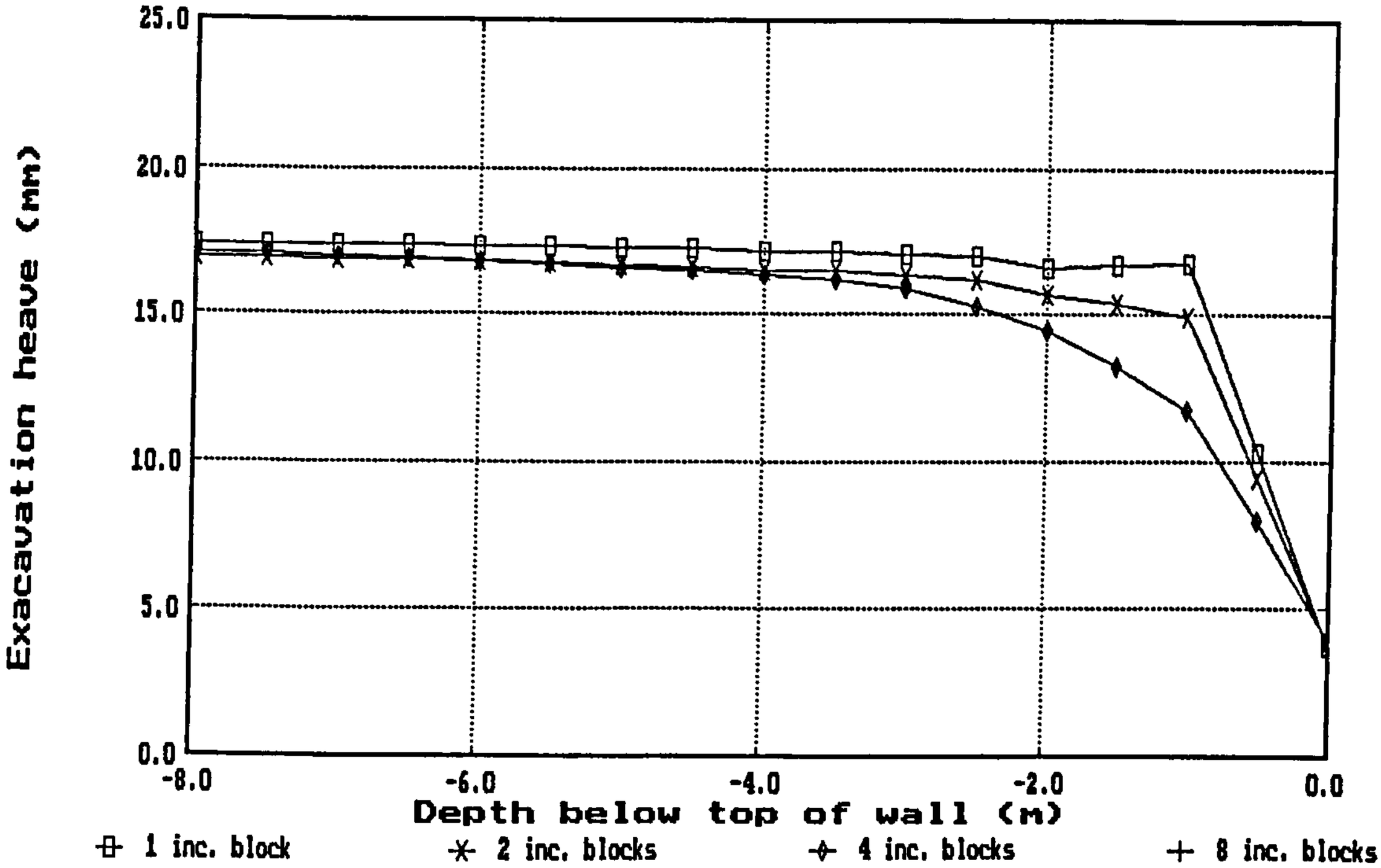

(c) excavation heave profiles : set 12

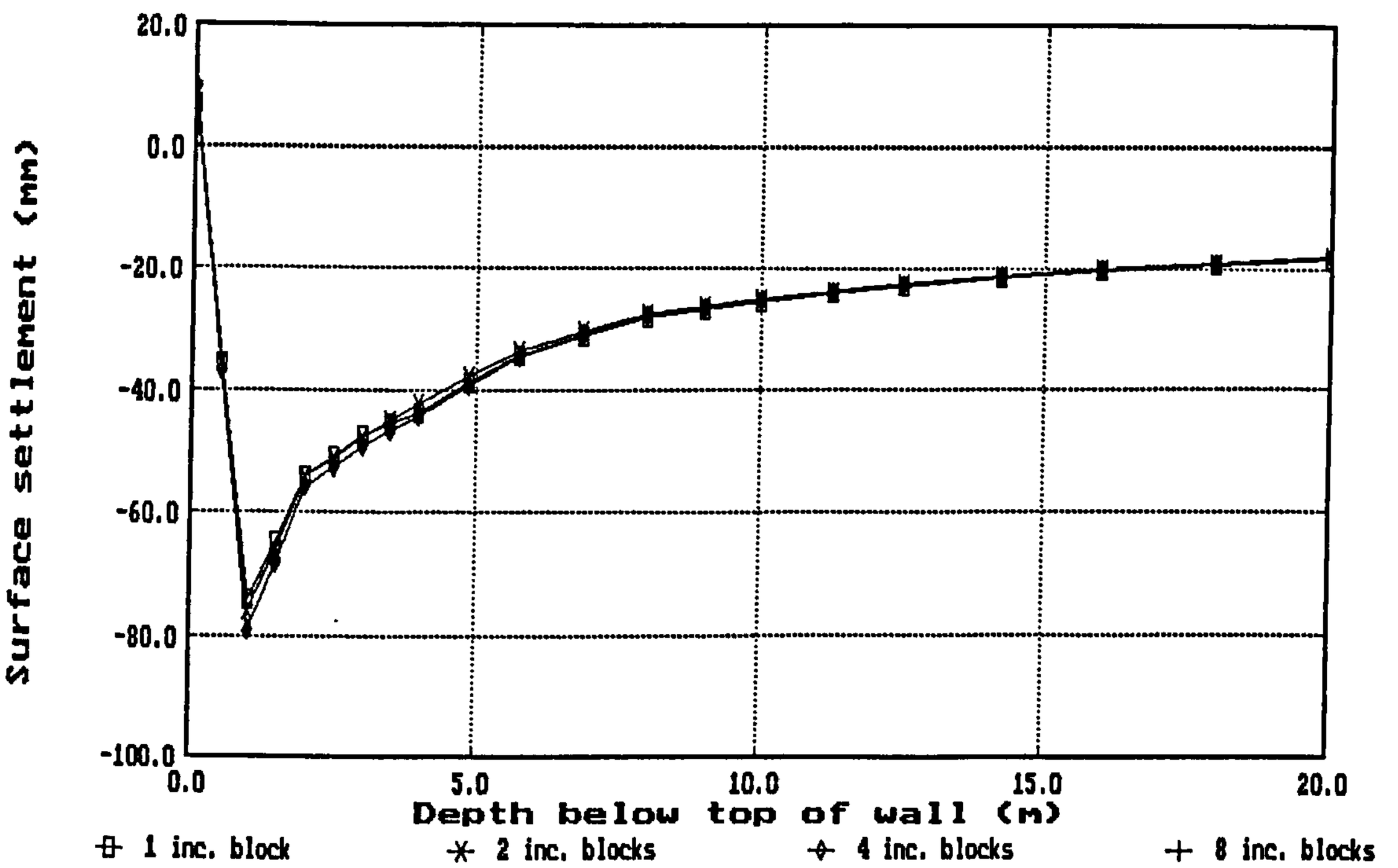

(d) ground surface movement profiles : set 13

Fig 6.10 Influence of number of increment blocks used for excavation : undrained elastic-perfectly plastic soil : cantilever wall : total number of increments = 8 (contd)

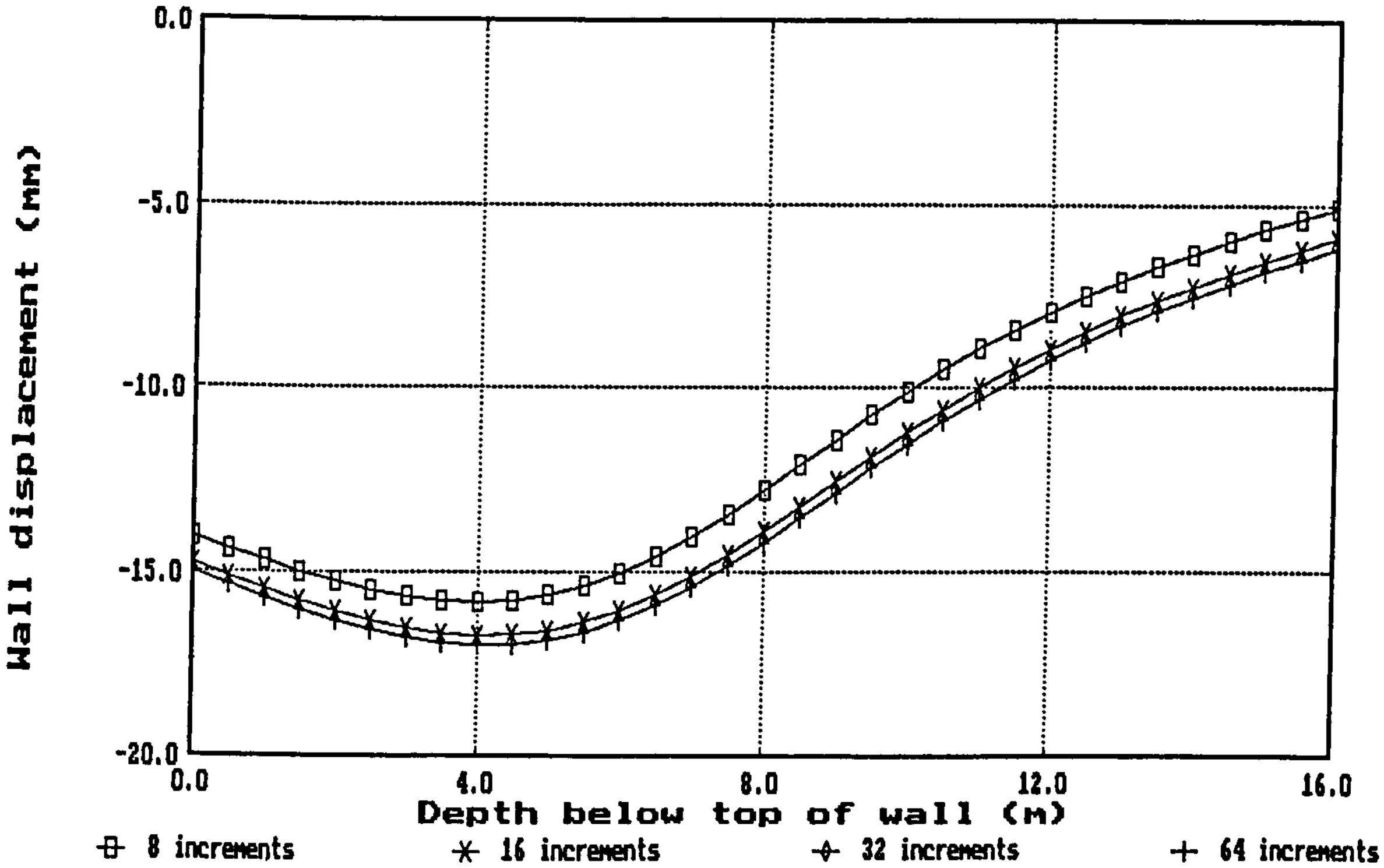

(a) wall displacement profiles : set 12

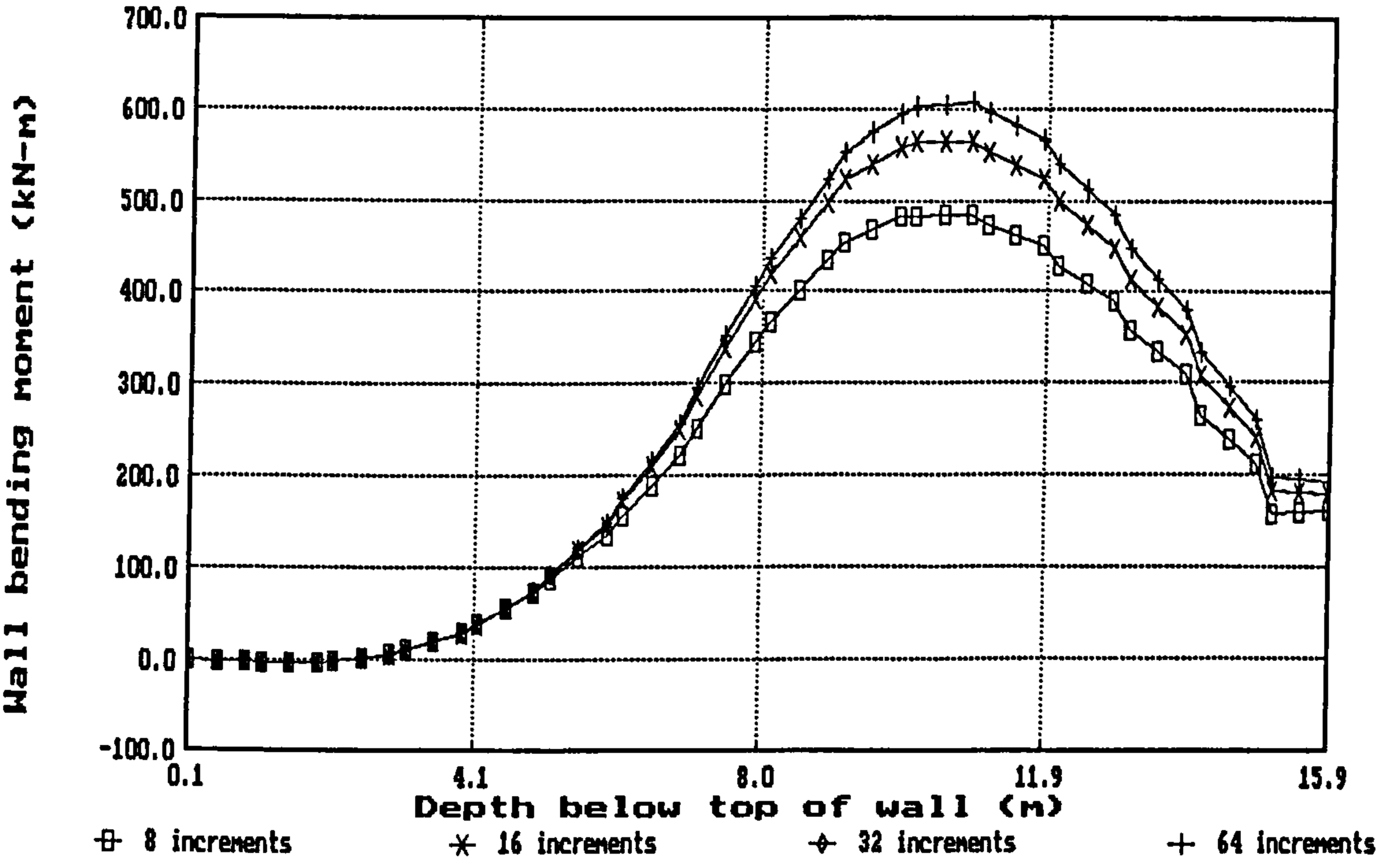

(b) wall bending moment profiles : set 13

Fig 6.11 Influence of number of increments used for excavation : undrained elastic-perfectly plastic soil : cantilever wall : number of increment blocks = 8

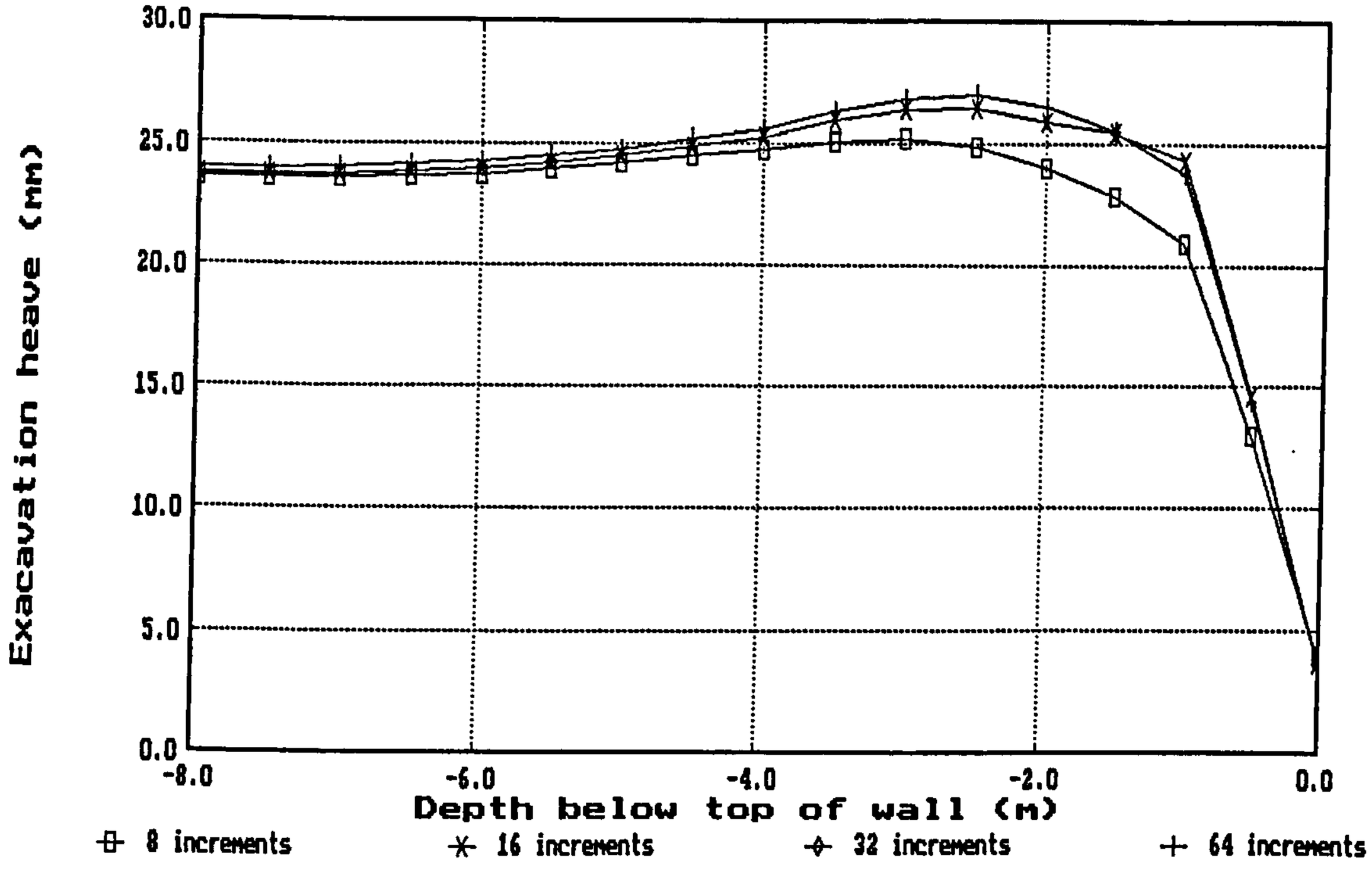

(c) excavation heave profiles : set 11

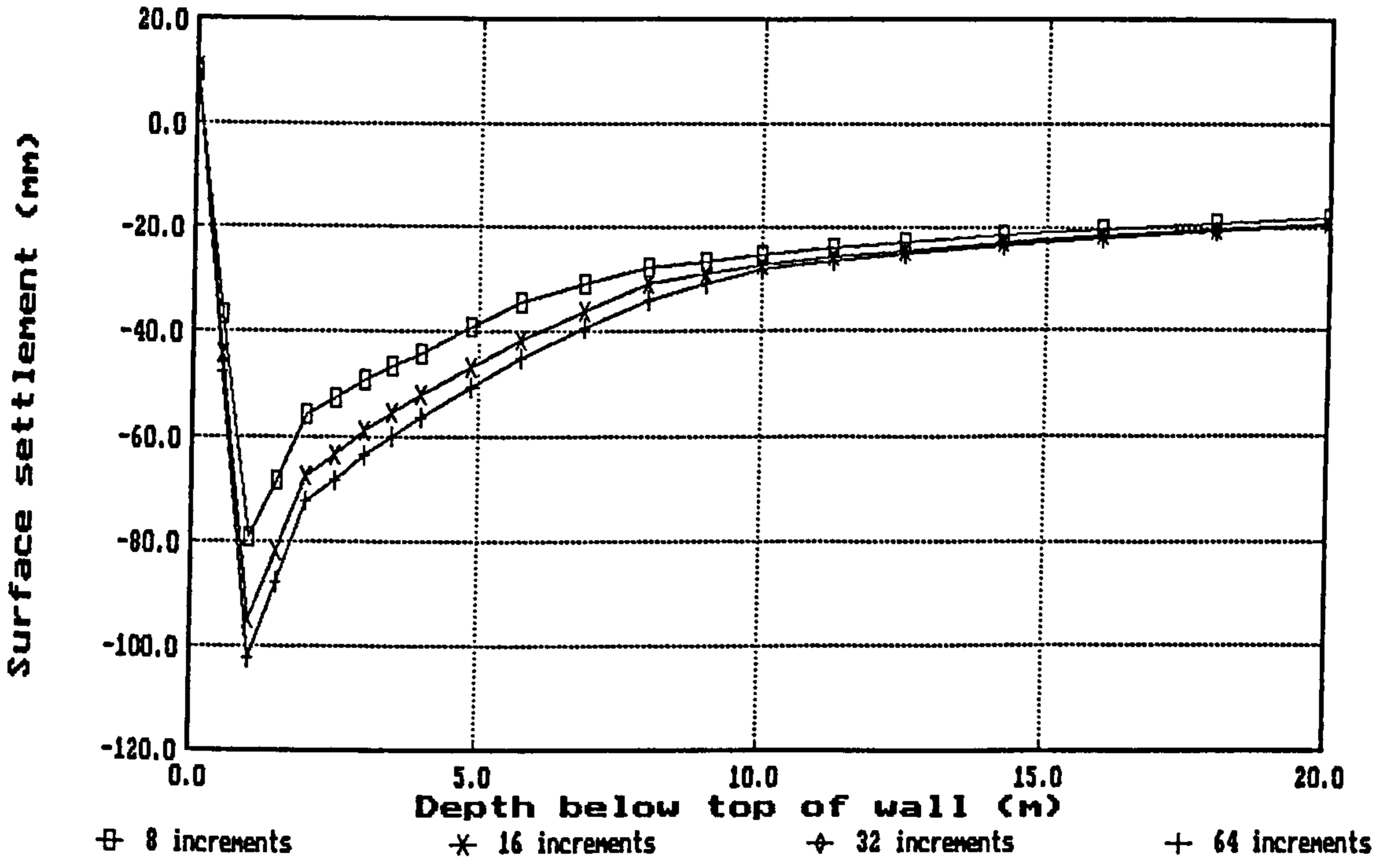

(d) ground surface movement profiles : set 13

Fig 6.11 Influence of number of increments used for excavation : undrained elastic-perfectly plastic soil : cantilever wall : number of increment blocks = 8 (contd)

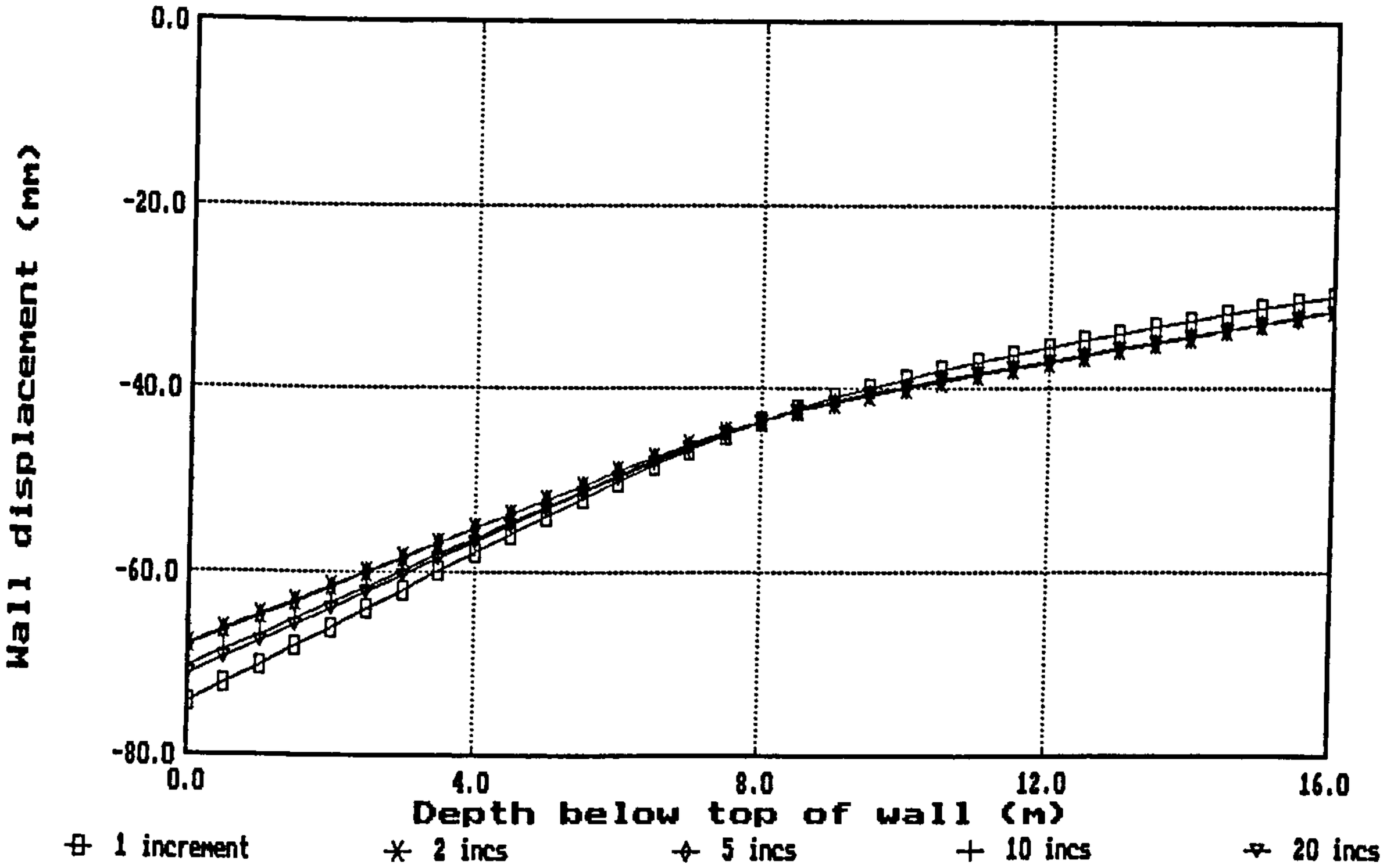

(a) wall displacement profiles : set 13

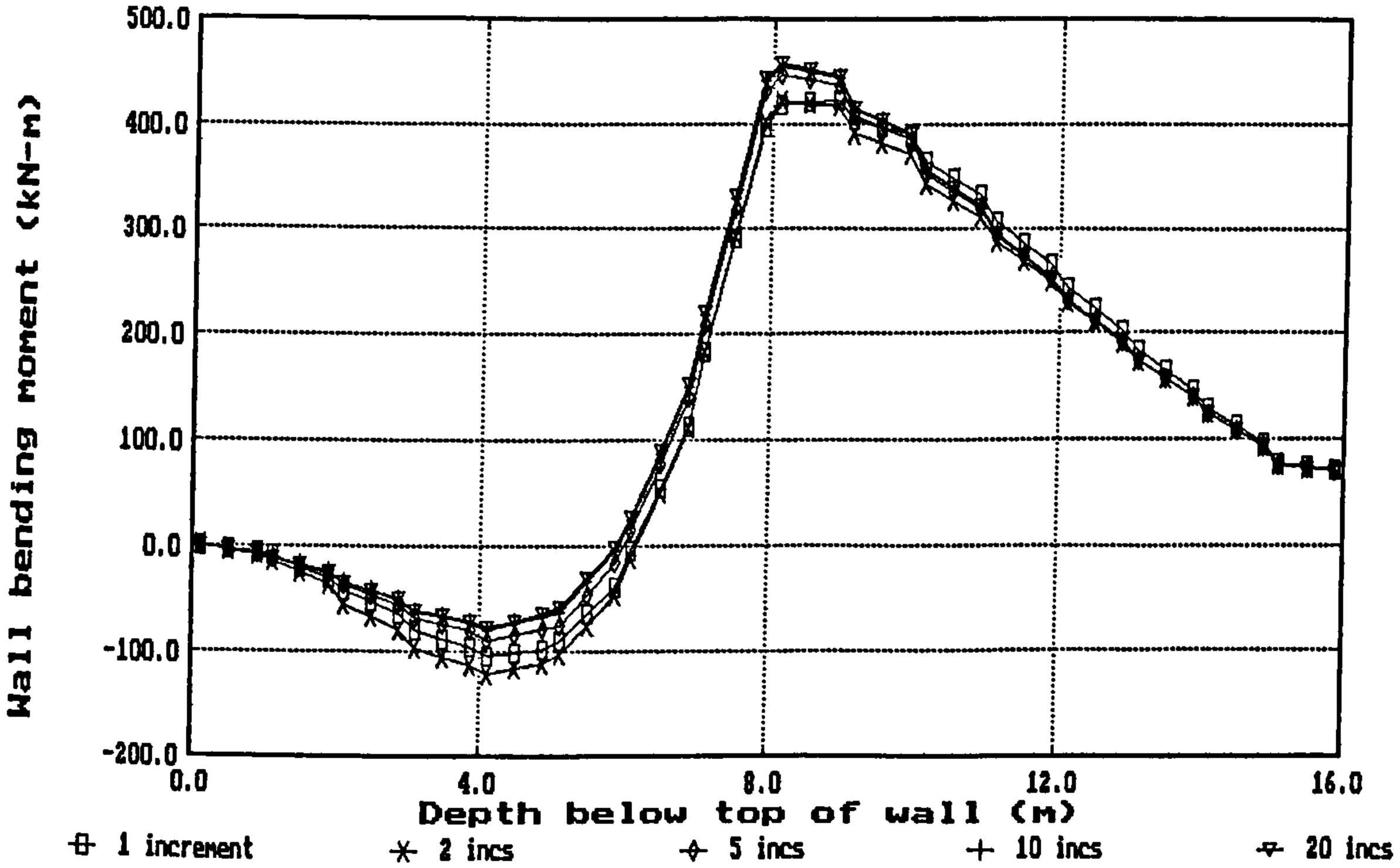

(b) wall bending moment profiles : set 11

Fig 6.12 Influence of number of increments used for temporary prop removal : undrained elastic-perfectly plastic soil : alternately-propped wall

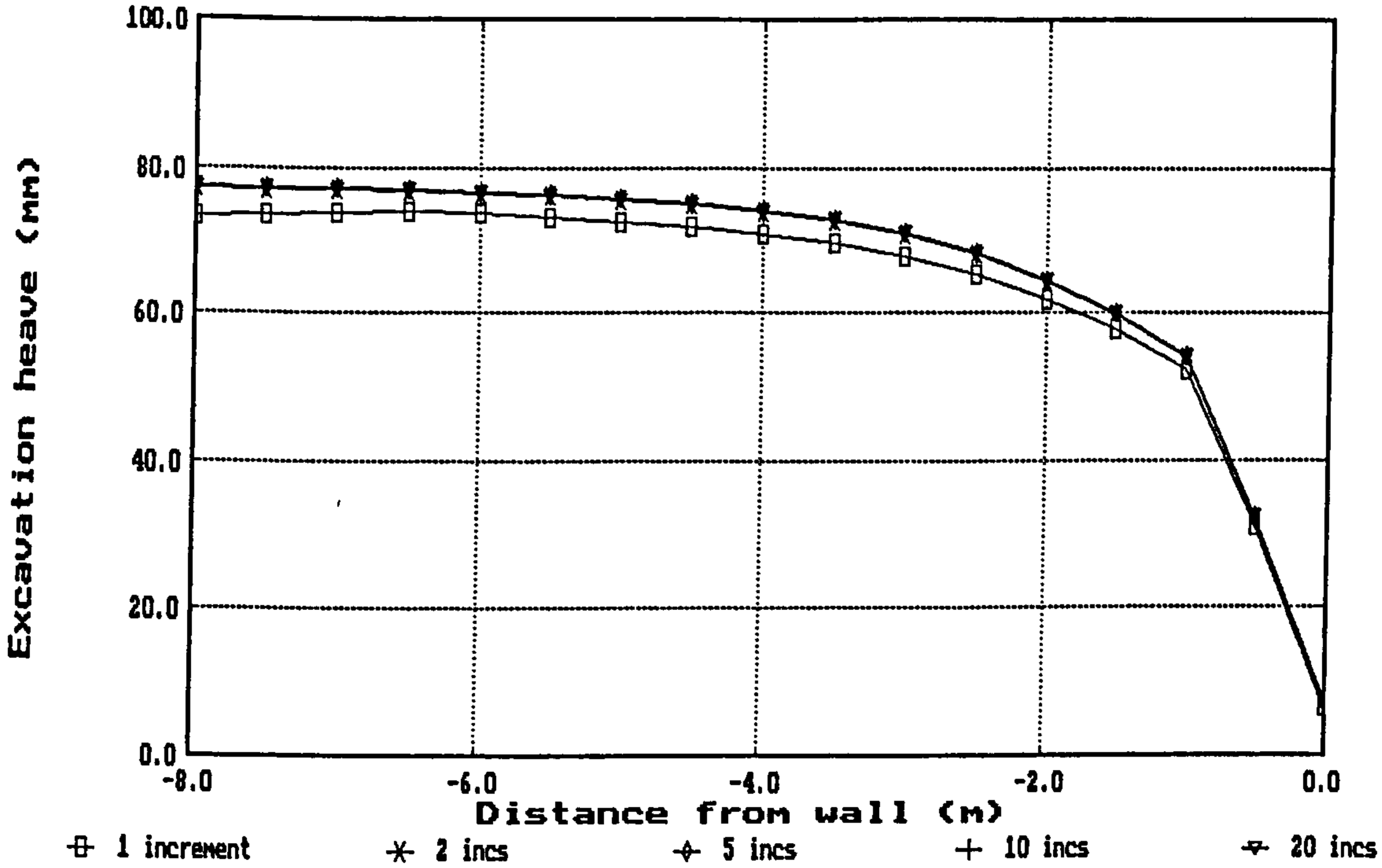

(c) excavation heave profiles : set 13

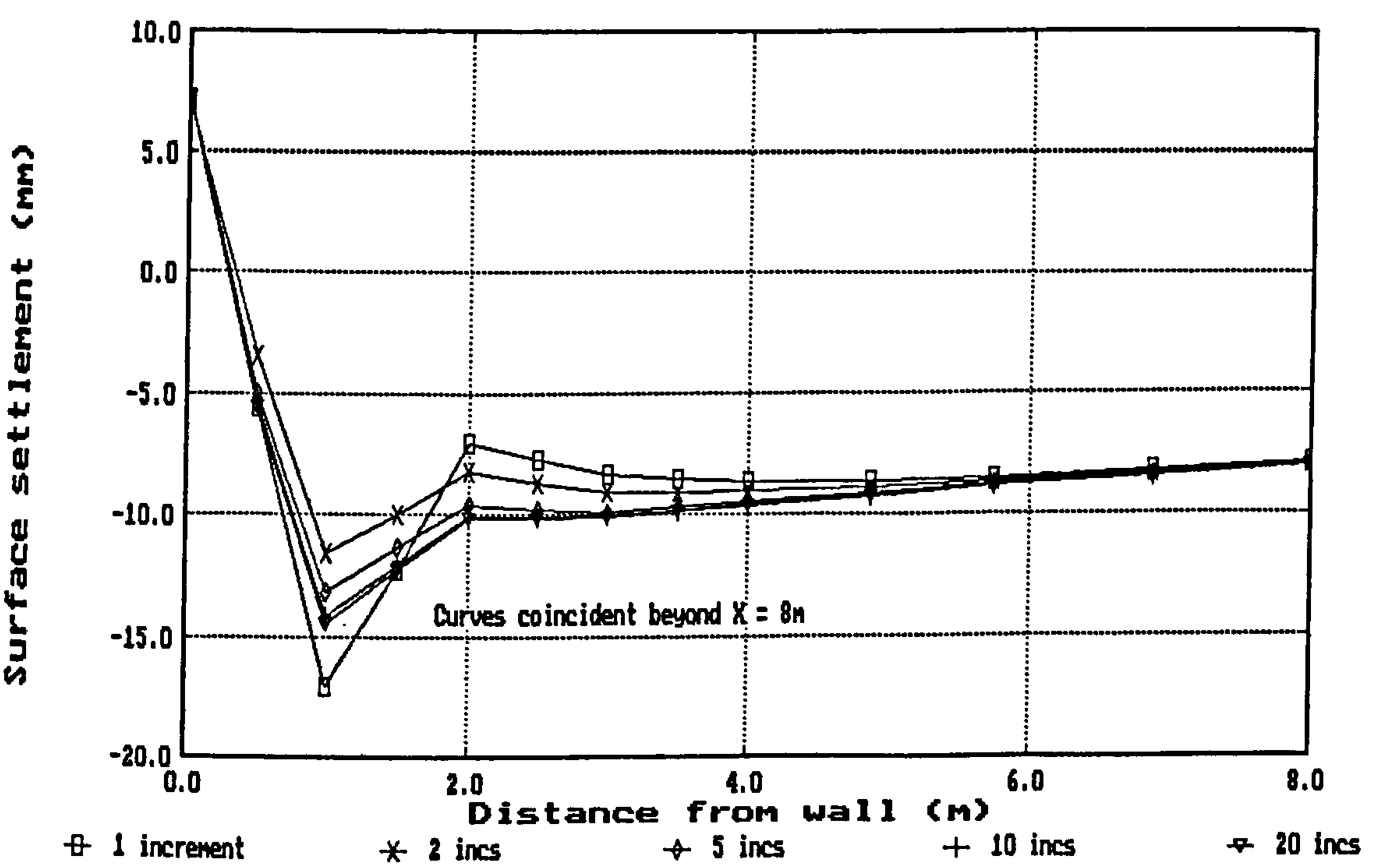

(d) ground surface movement profiles : set 11

Fig 6.12 Influence of number of increments used for temporary prop removal : undrained elastic-perfectly plastic soil : alternately-propped wall (contd)

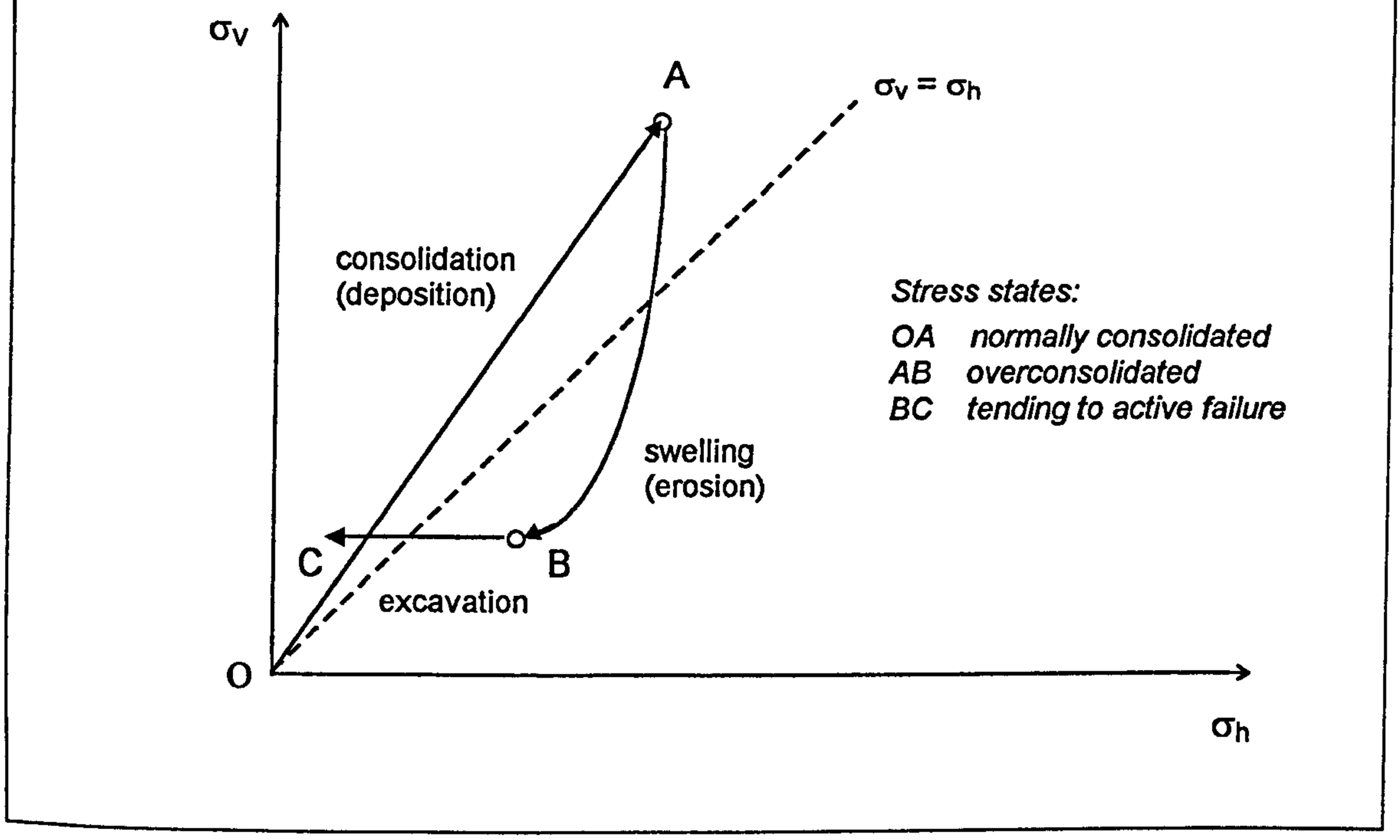

Fig 6.13 Approximate total stress paths in an element of soil behind an embedded retaining wall in stiff overconsolidated clay: geological processes of deposition and erosion, followed by present day excavation.

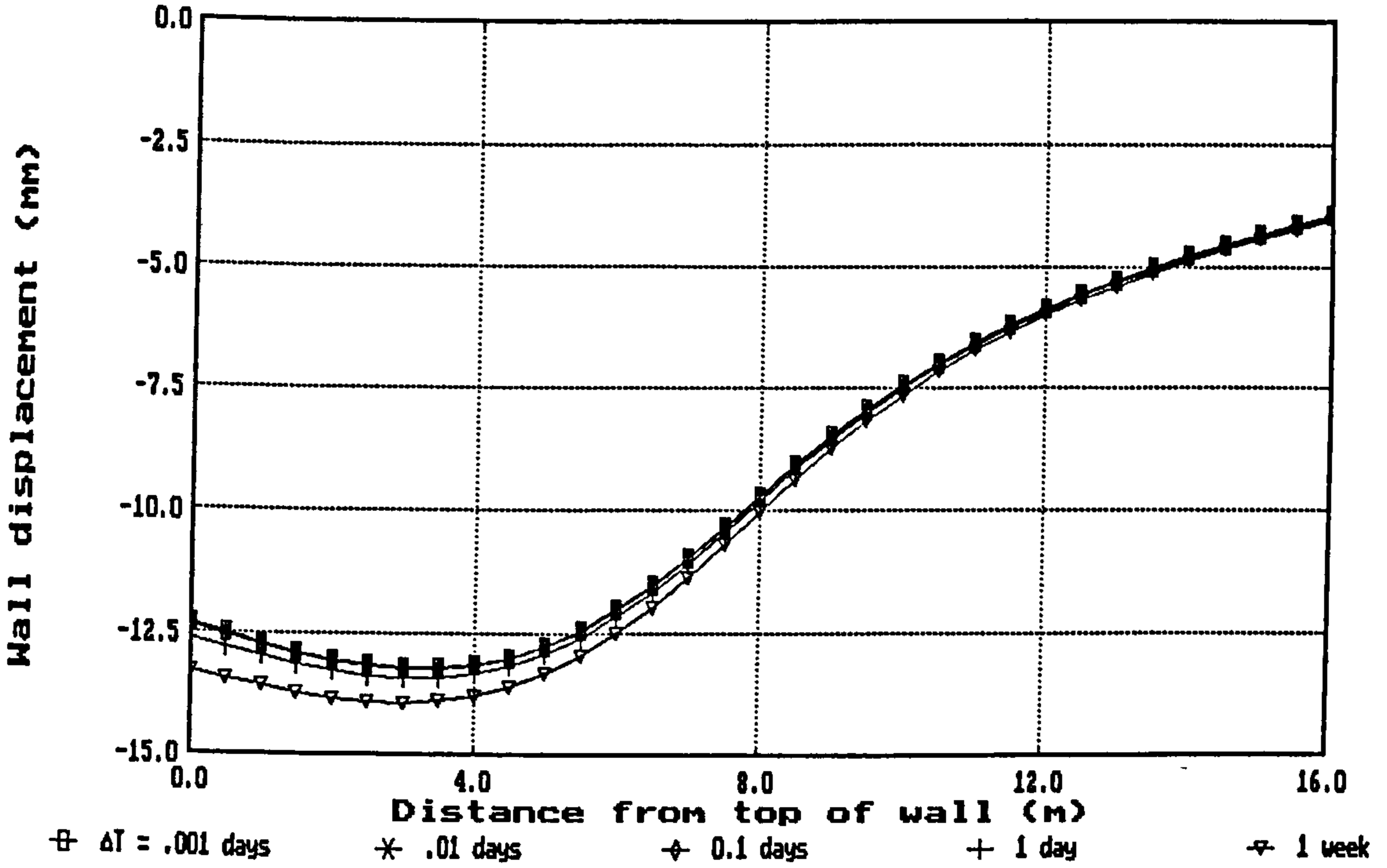

(a) wall displacement profiles

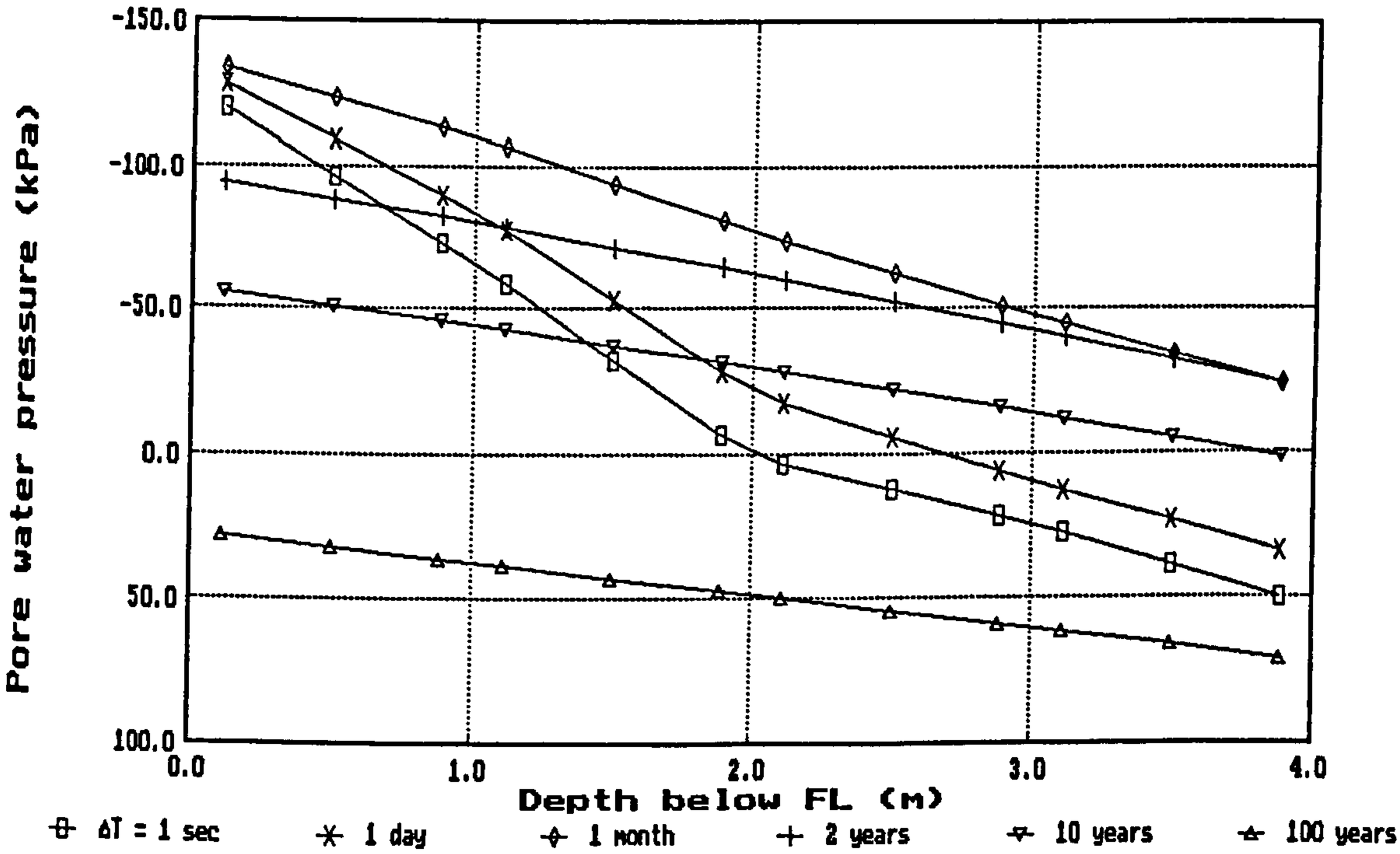

(b) excess pore water pressure profiles on excavated side

Fig 6.14 Lower limit on time step in a coupled analysis of partially drained excavation : cantilever wall : elastic-perfectly plastic soil : set 12d

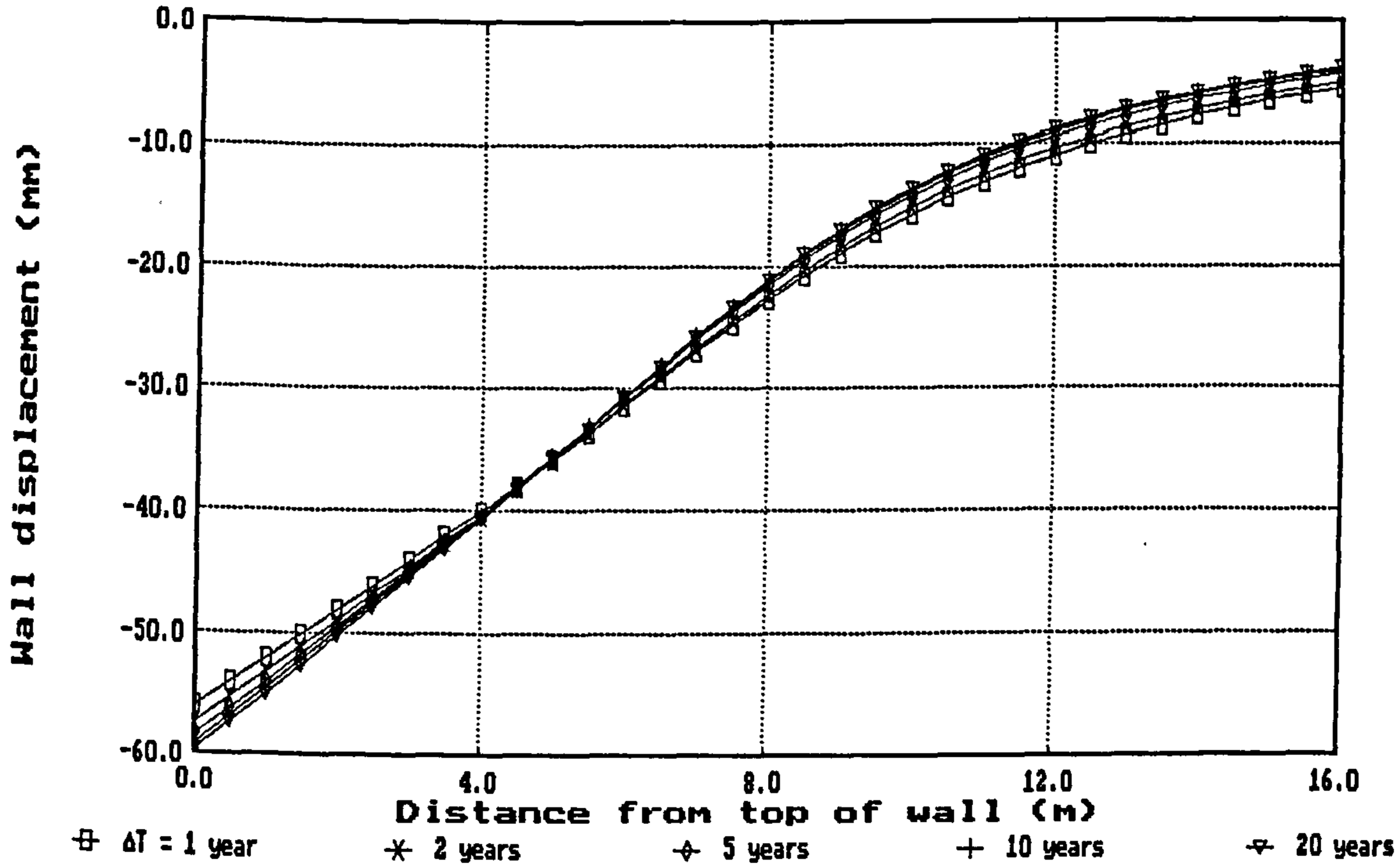

(a) wall displacement profiles : set 3d

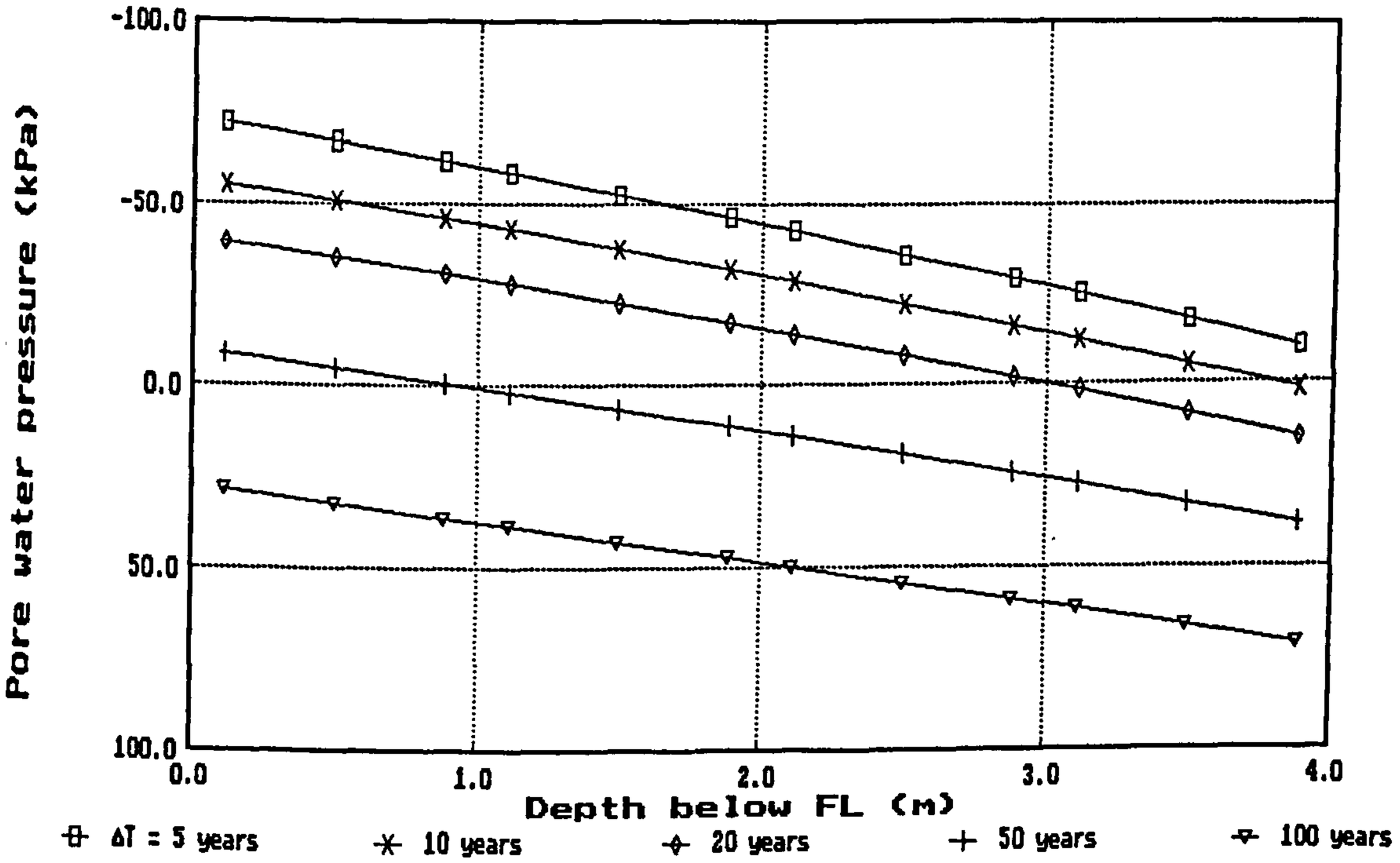

(b) excess pore water pressure profiles on excavated side : set 12d

Fig 6.15 Upper limit on time step in a coupled analysis of partially drained excavation : cantilever wall

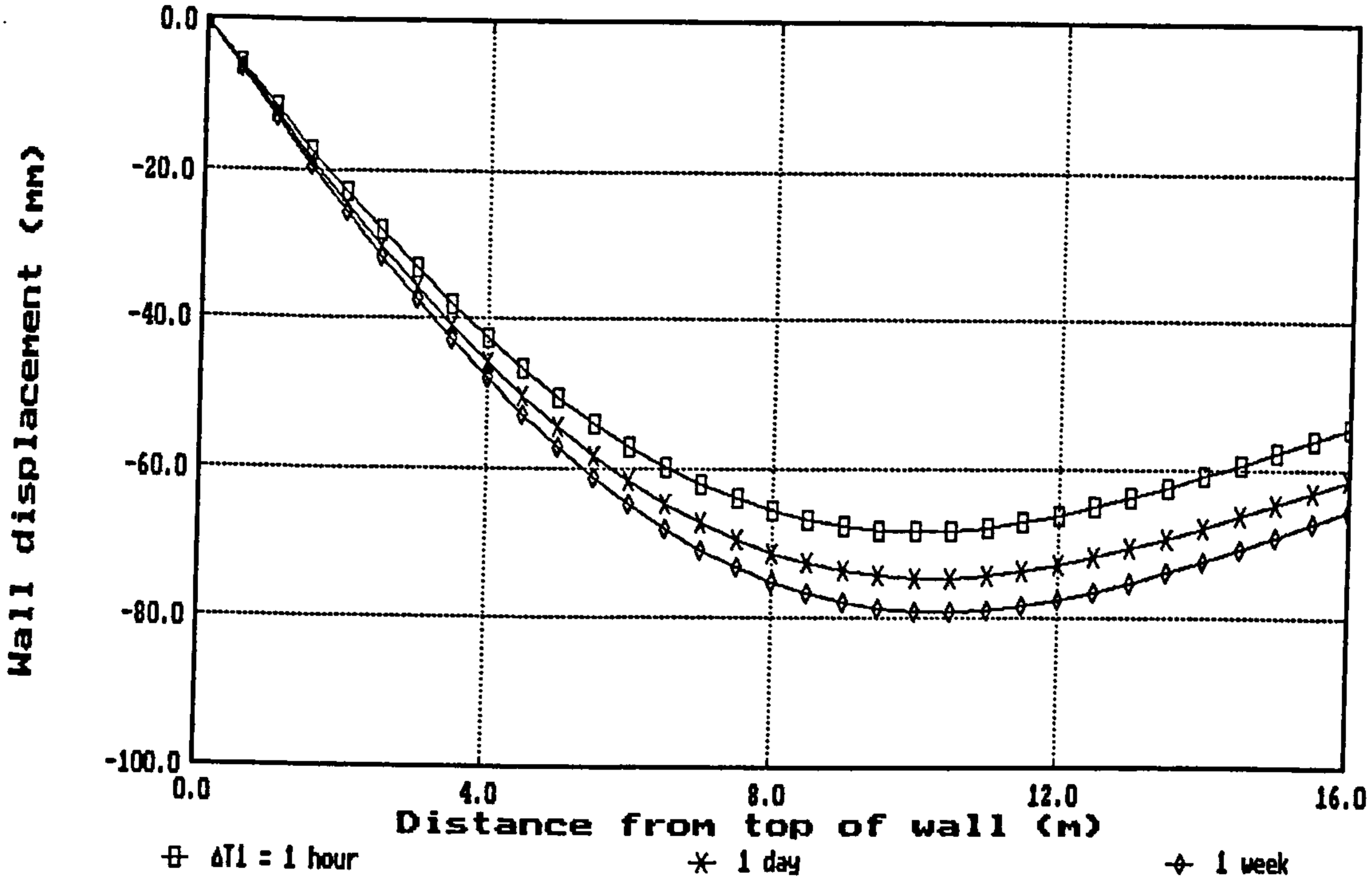

(a) wall displacement profiles for different Δt_1 : top-propped / set 13d

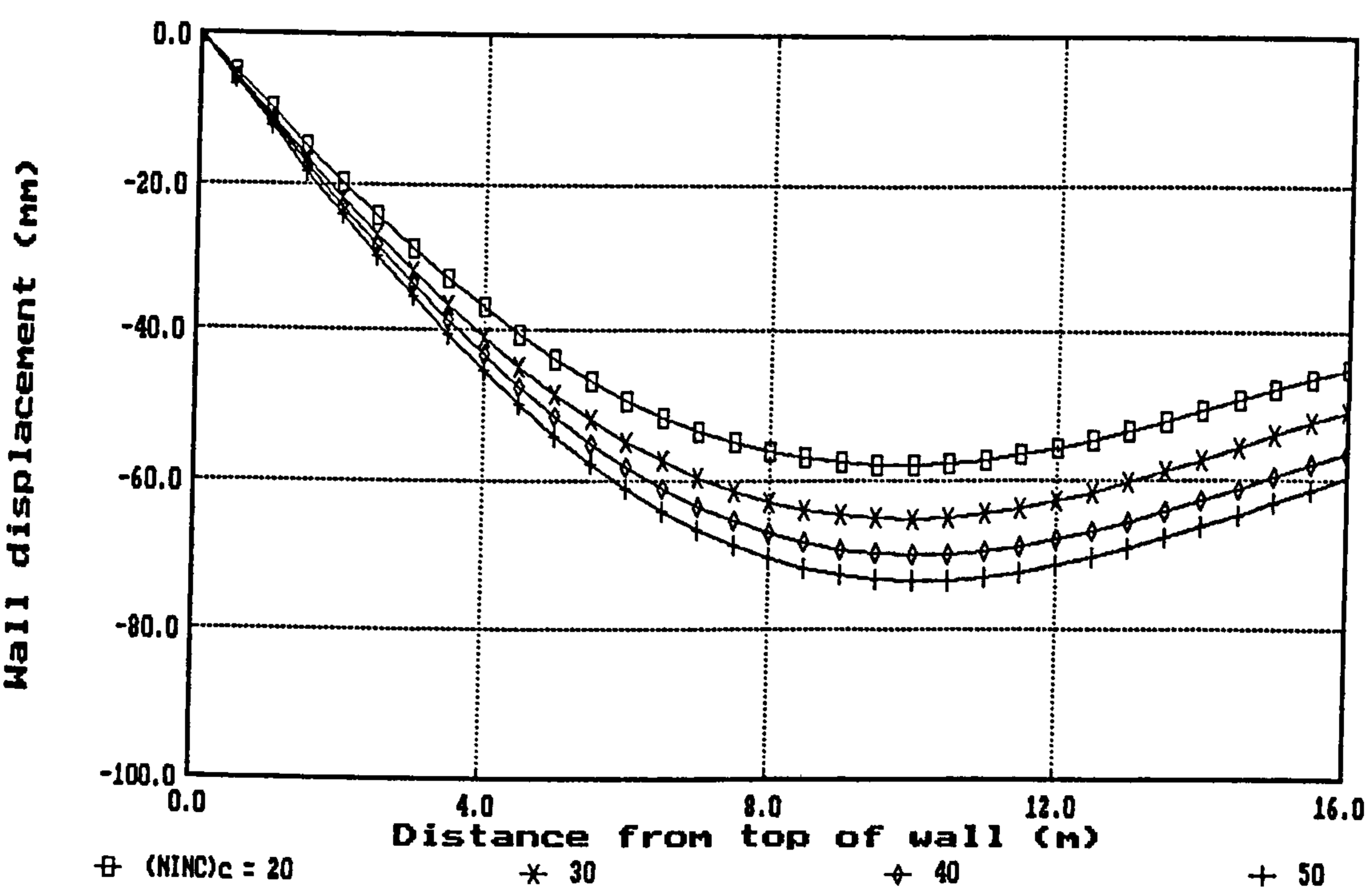

(b) wall displacement profiles for different numbers of increments : top-propped / set 12d

Fig 6.16 Initial studies of long-term equalisation in a coupled analysis : elastic-perfectly plastic soil

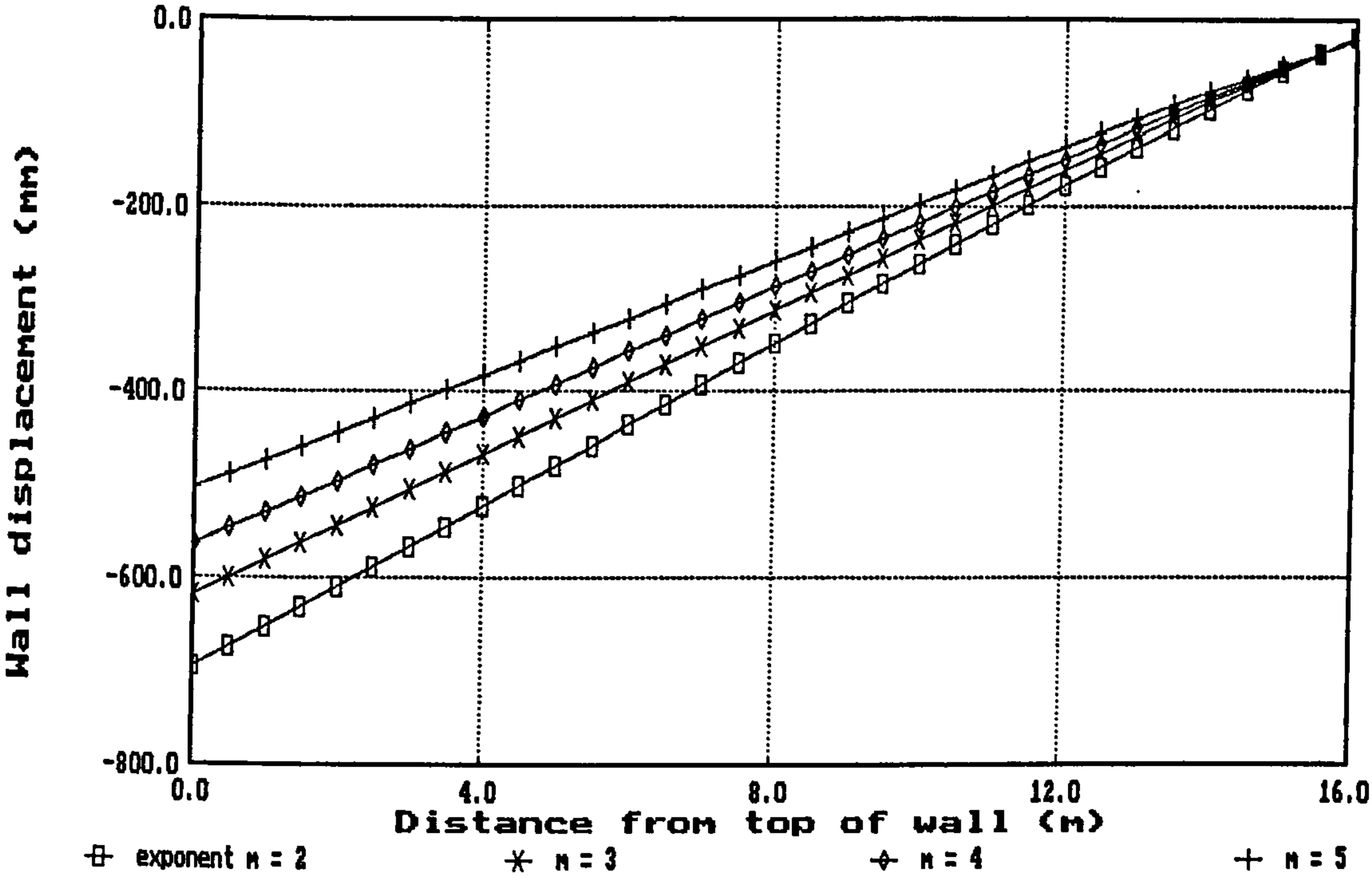

(c) wall displacement profiles for different values of exponent "m" : cantilever / set 12d

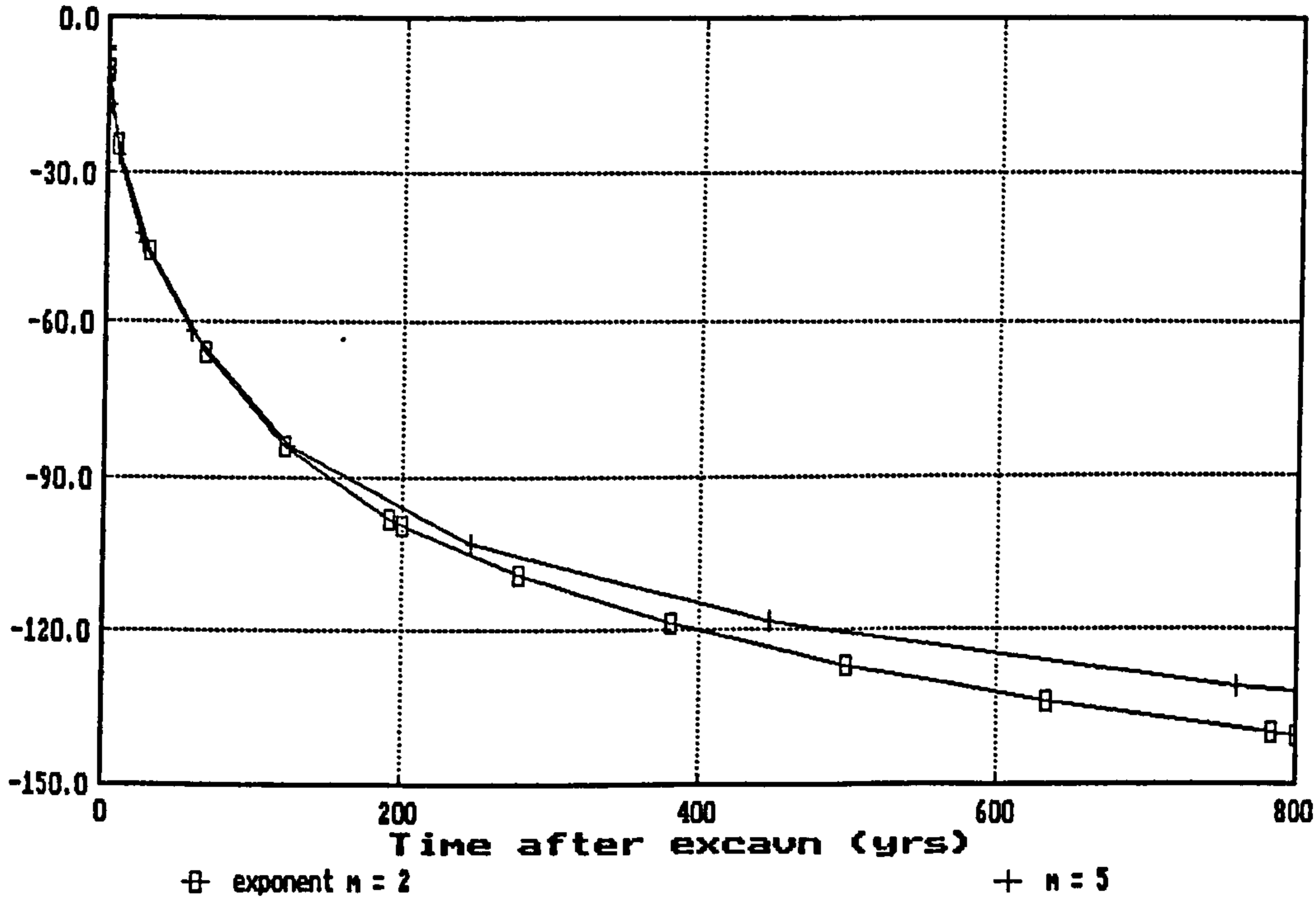

(d) max. wall displacement against time for different values of m : top-propped / set 12d

Fig 6.16 Initial studies of long-term equalisation in a coupled analysis : elastic-perfectly plastic soil (contd)

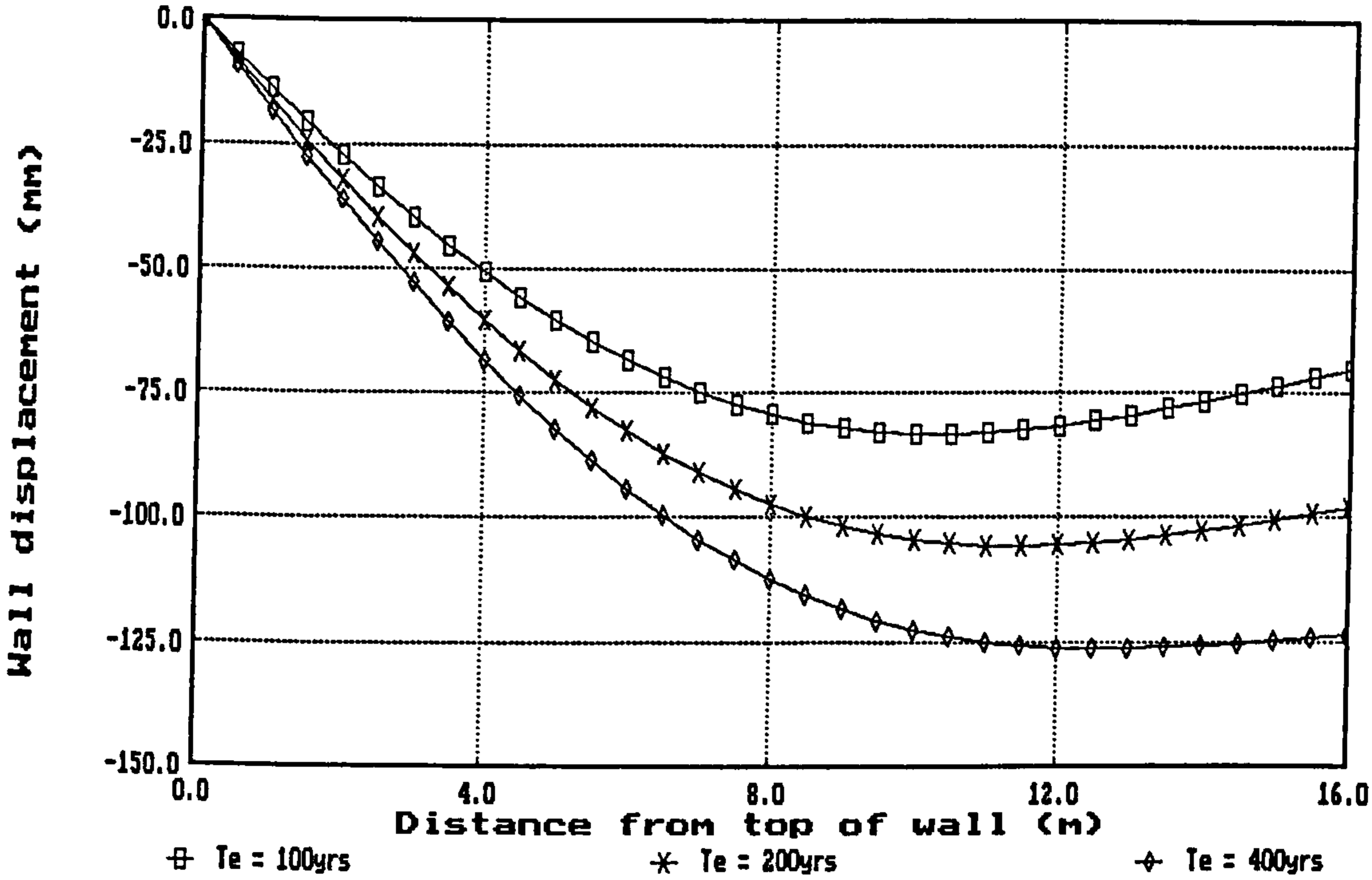

(a) wall displacement profiles : top-propped / set 12d

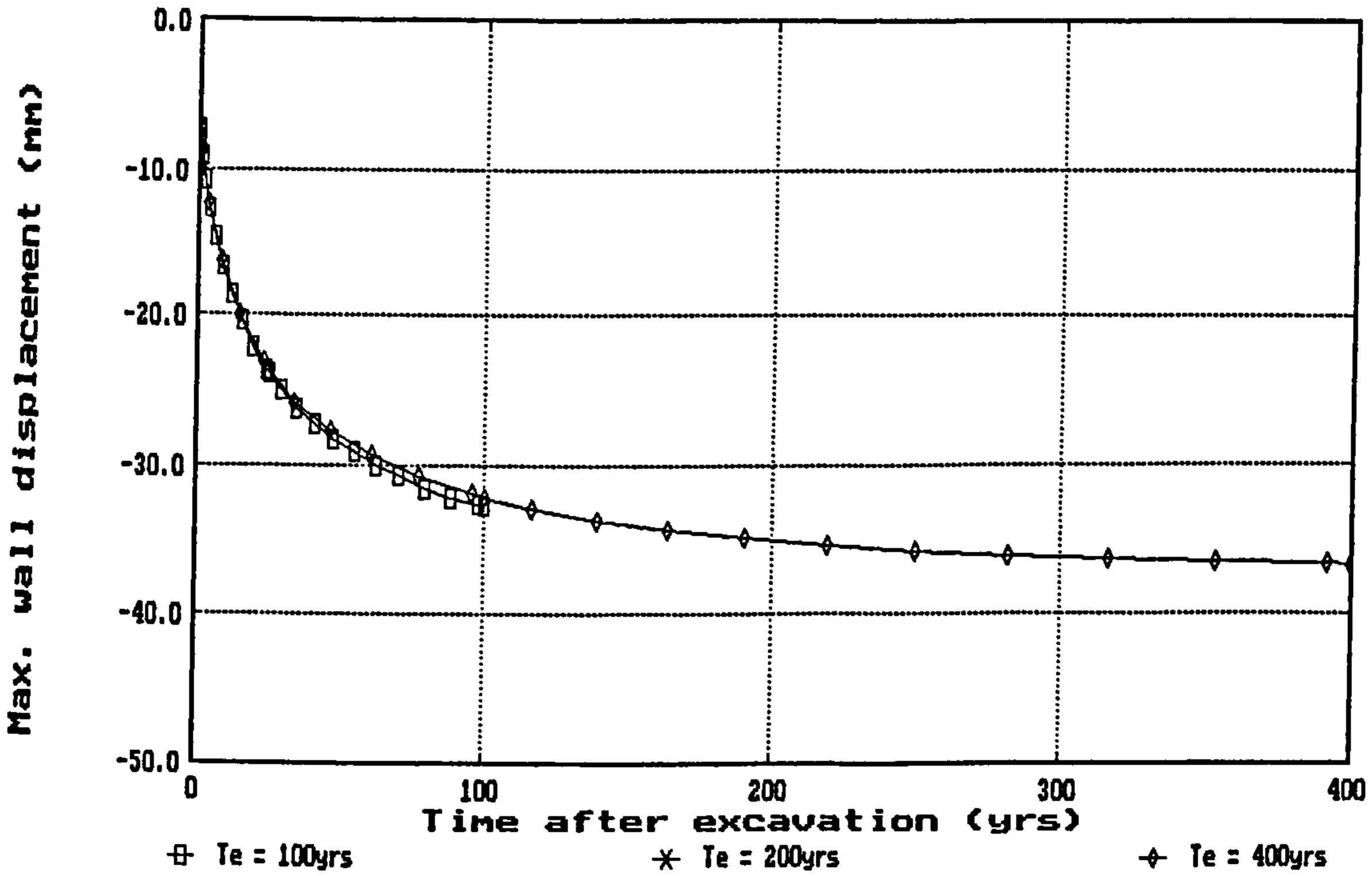

(b) maximum wall displacement against time : doubly-propped / set 12d

Fig 6.17 Influence of time allowed for pore pressure equalisation after construction in a coupled analysis ($N_e = 100$)

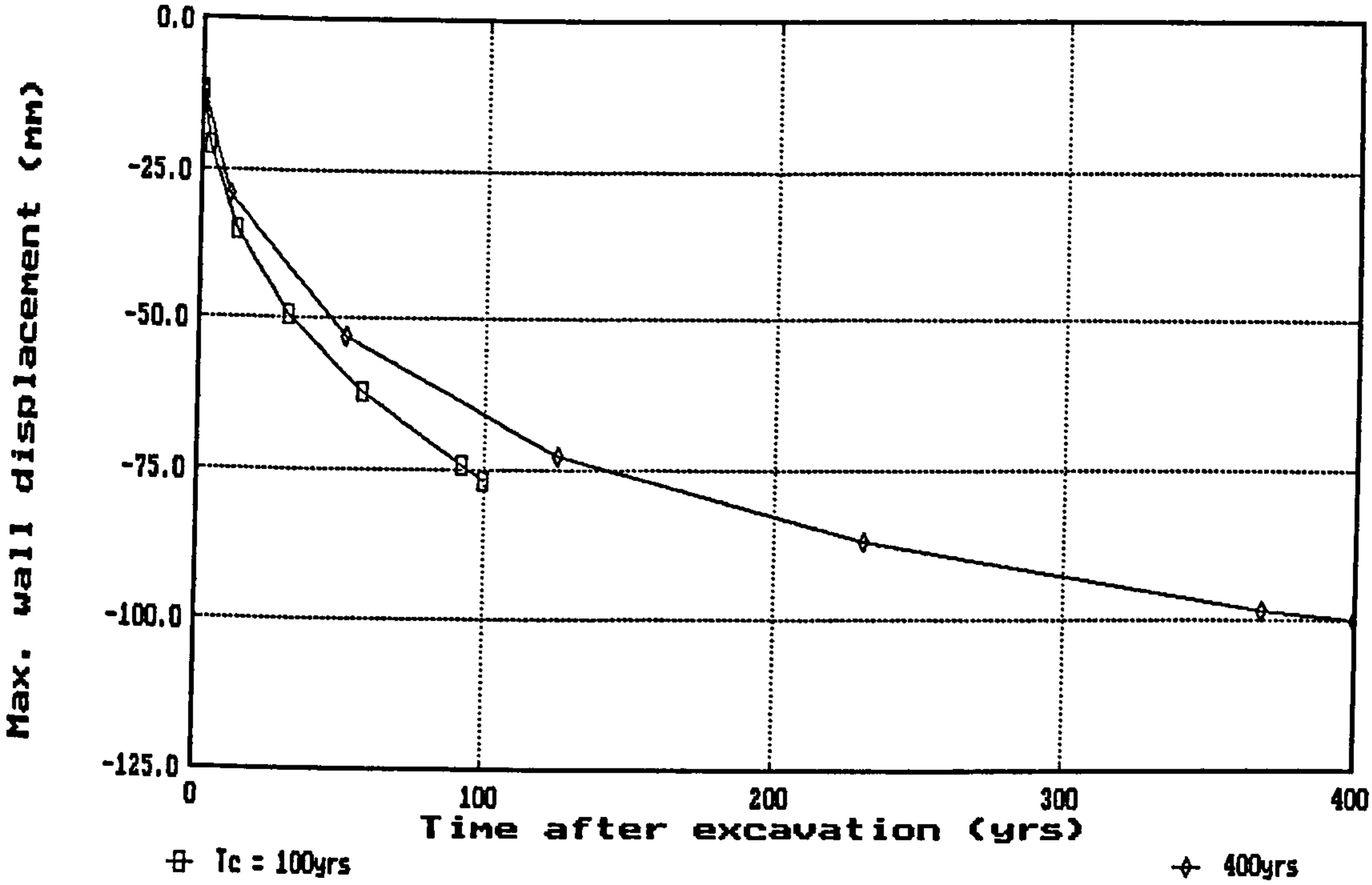

(a) max. wall displacement against time : top-propped / set 12d / $N_e = 25$ / variable t_e

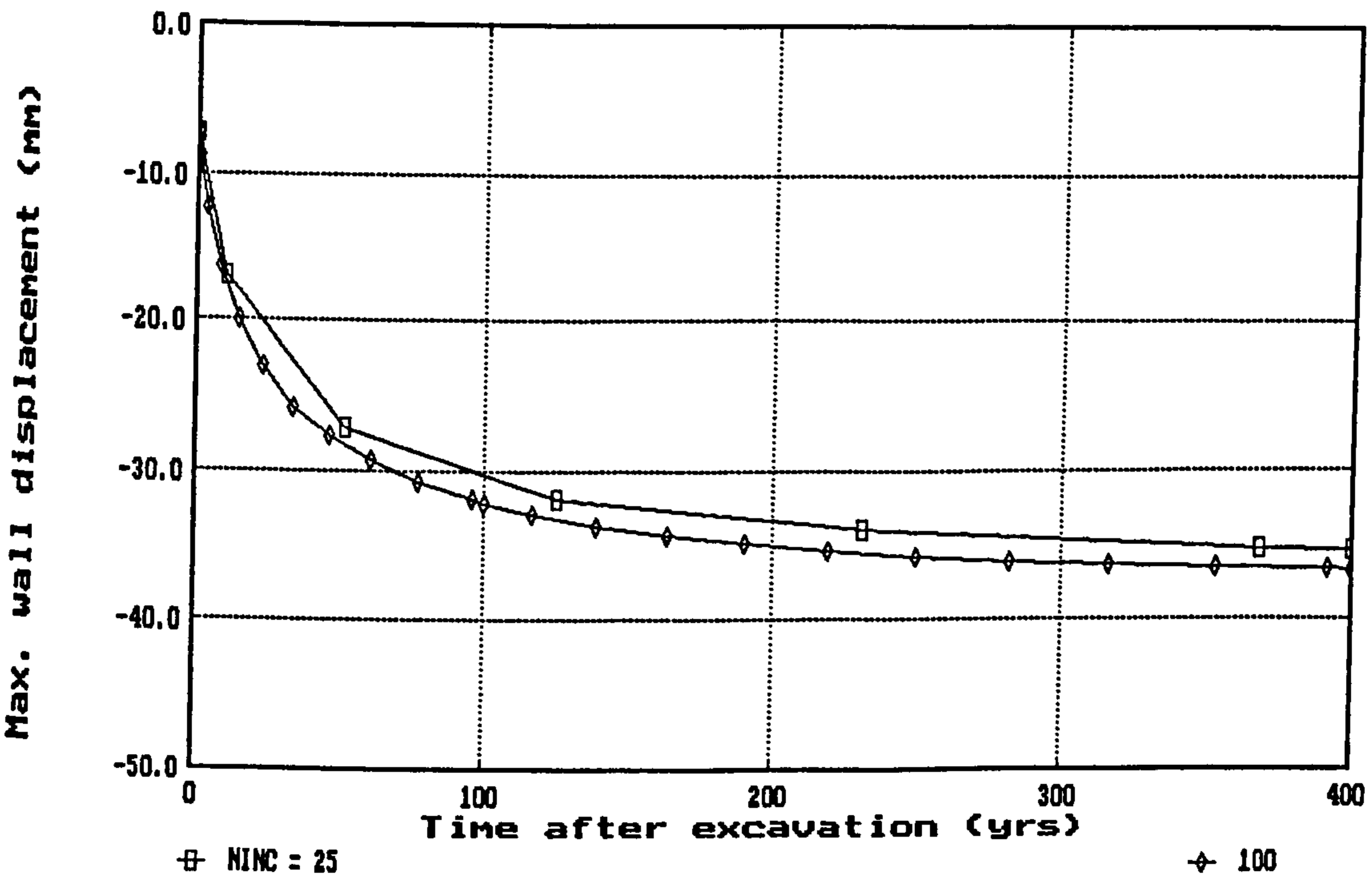

(b) max. wall displacement against time : doubly-propped / set 12d / $t_e = 400$ / N_e varies

Fig 6.18 Influence of number of increments allowed for pore pressure equalisation after construction in a coupled analysis

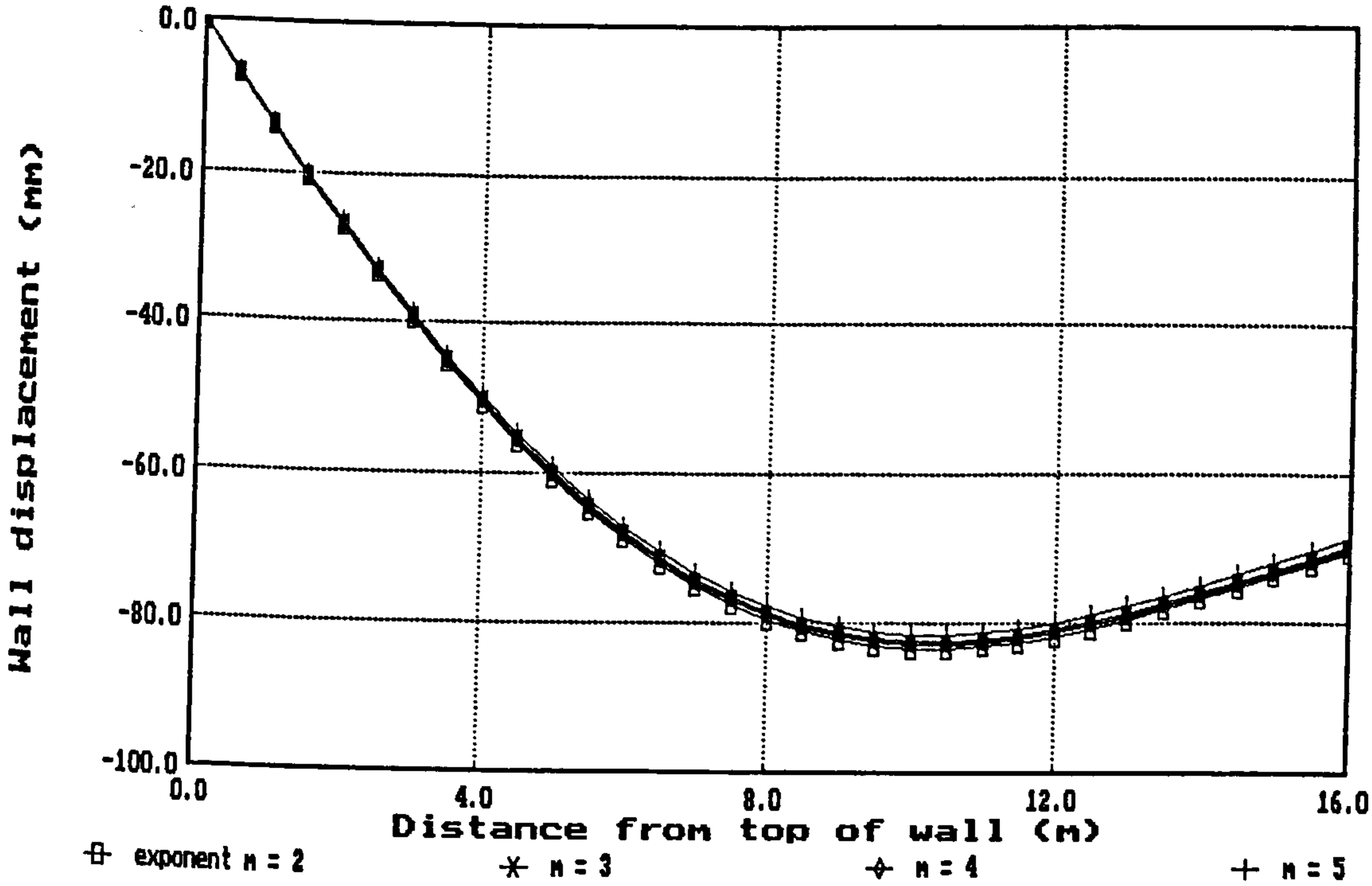

(a) wall displacement profiles : top-propped / set 12d / t_e = 100 yrs / N_e = 100

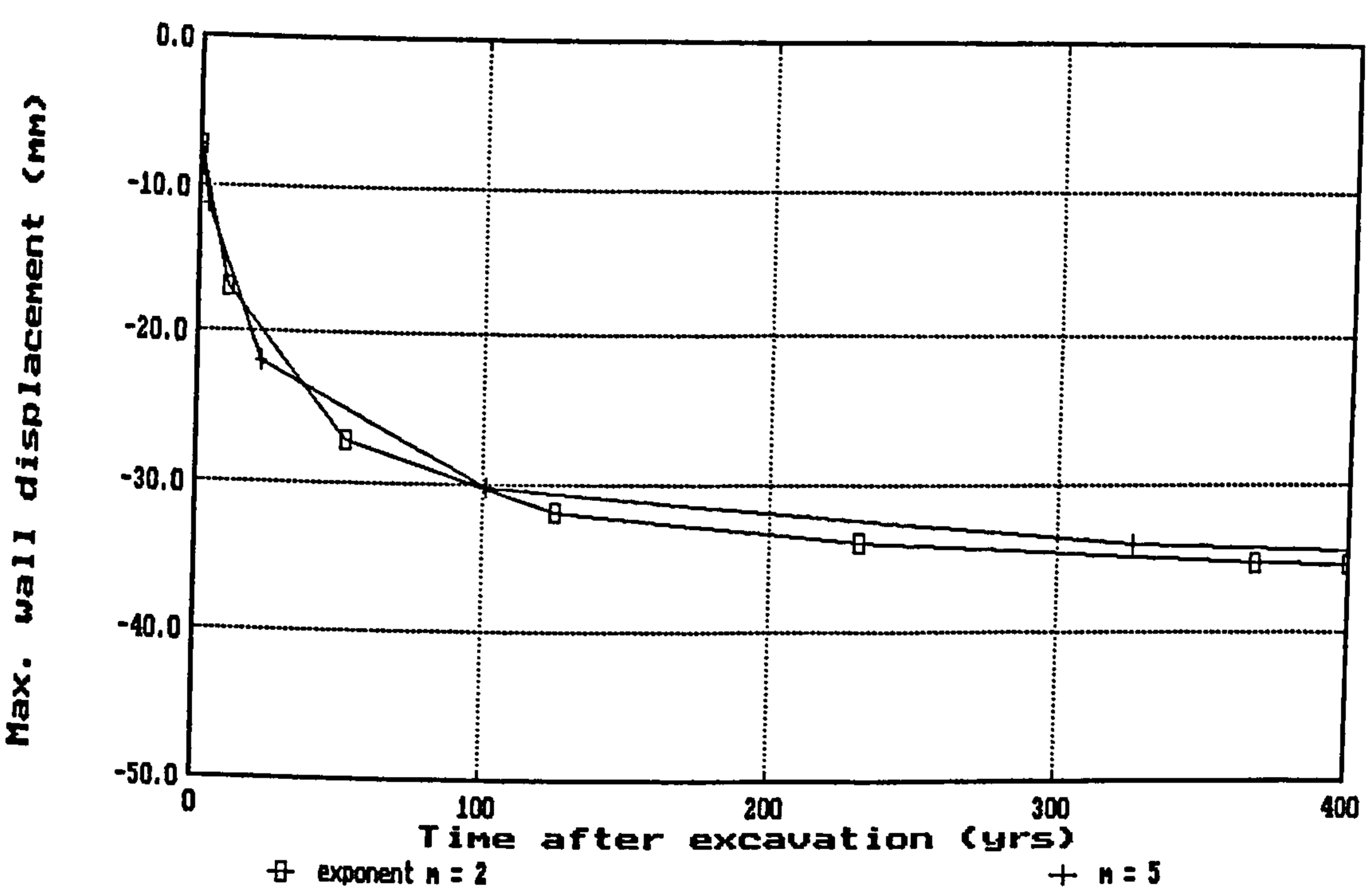

(b) max. wall displacement against time : top-propped / set 12d / t_e = 400 yrs / N_e = 25

Fig 6.19 Influence of time step weighting (power law exponent "m") used for pore pressure equalisation after construction in a coupled analysis

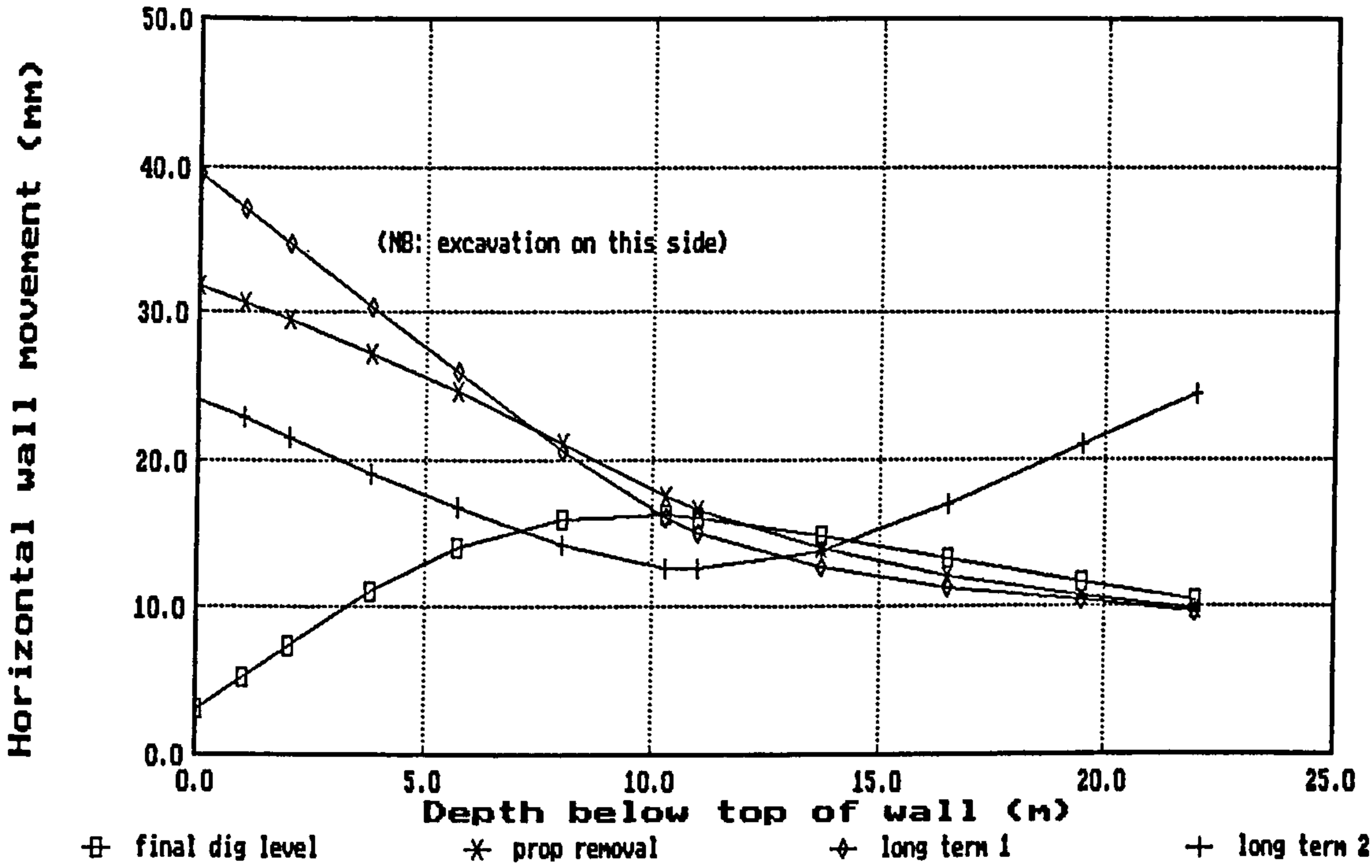

(a) wall deflection profiles

long term 1 = equilibration to underdrained p.w.p.
long term 2 = equilibration to hydrostatic p.w.p.

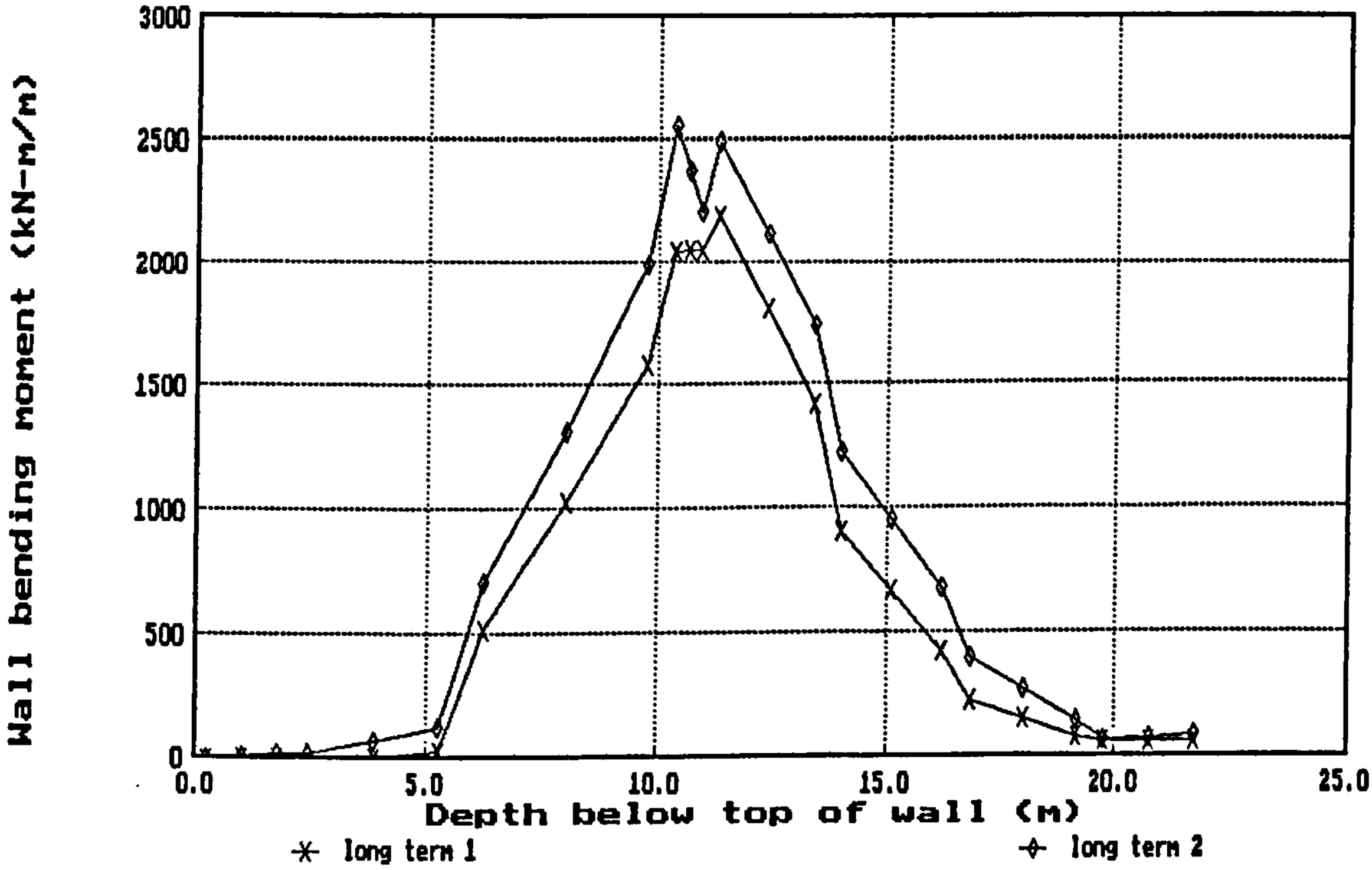

(b) wall bending moment profiles

Fig 6.20 Effects of rising groundwater on an embedded wall singly propped at formation level (A406 Walthamstow) : key results at various times after construction

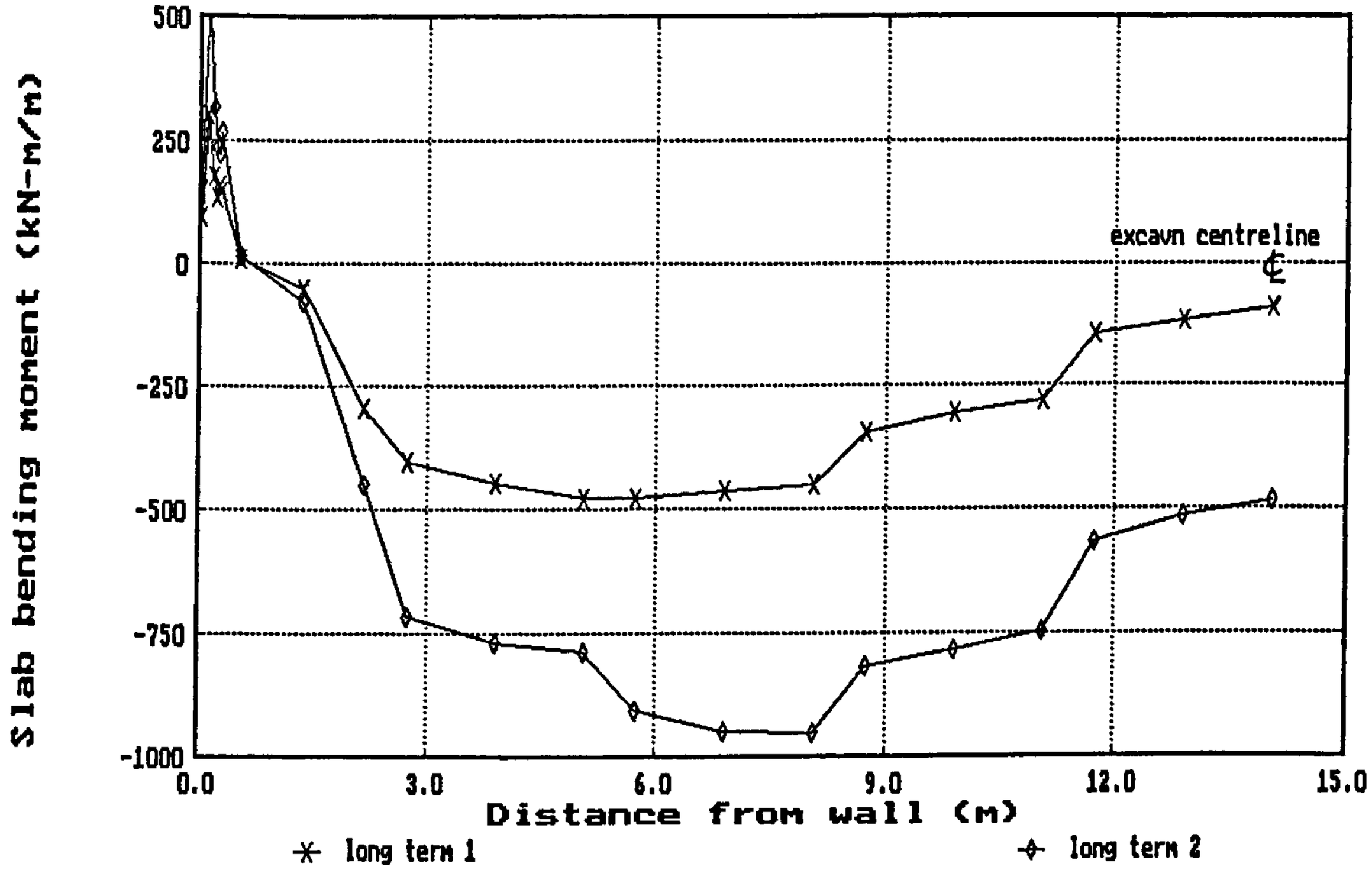

(c) prop slab bending moment profiles

long term 1 = equilibn to underdrained p.w.p.
long term 2 = equilibn to hydrostatic p.w.p.

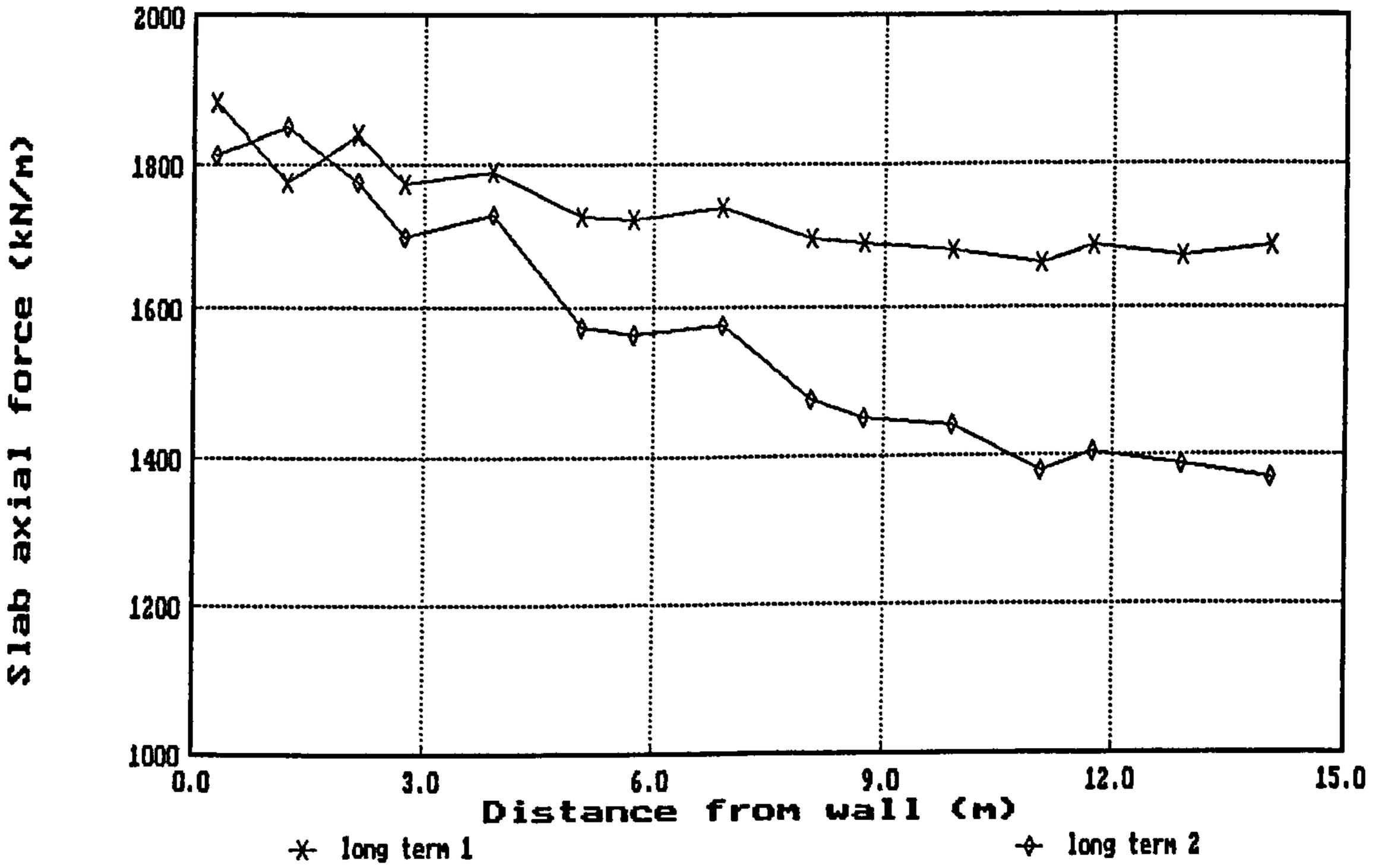

(d) prop slab axial force profile

Fig 6.20 Effects of rising groundwater on an embedded wall singly propped at formation level (A406 Walthamstow) : key results at various times after construcn (cont)

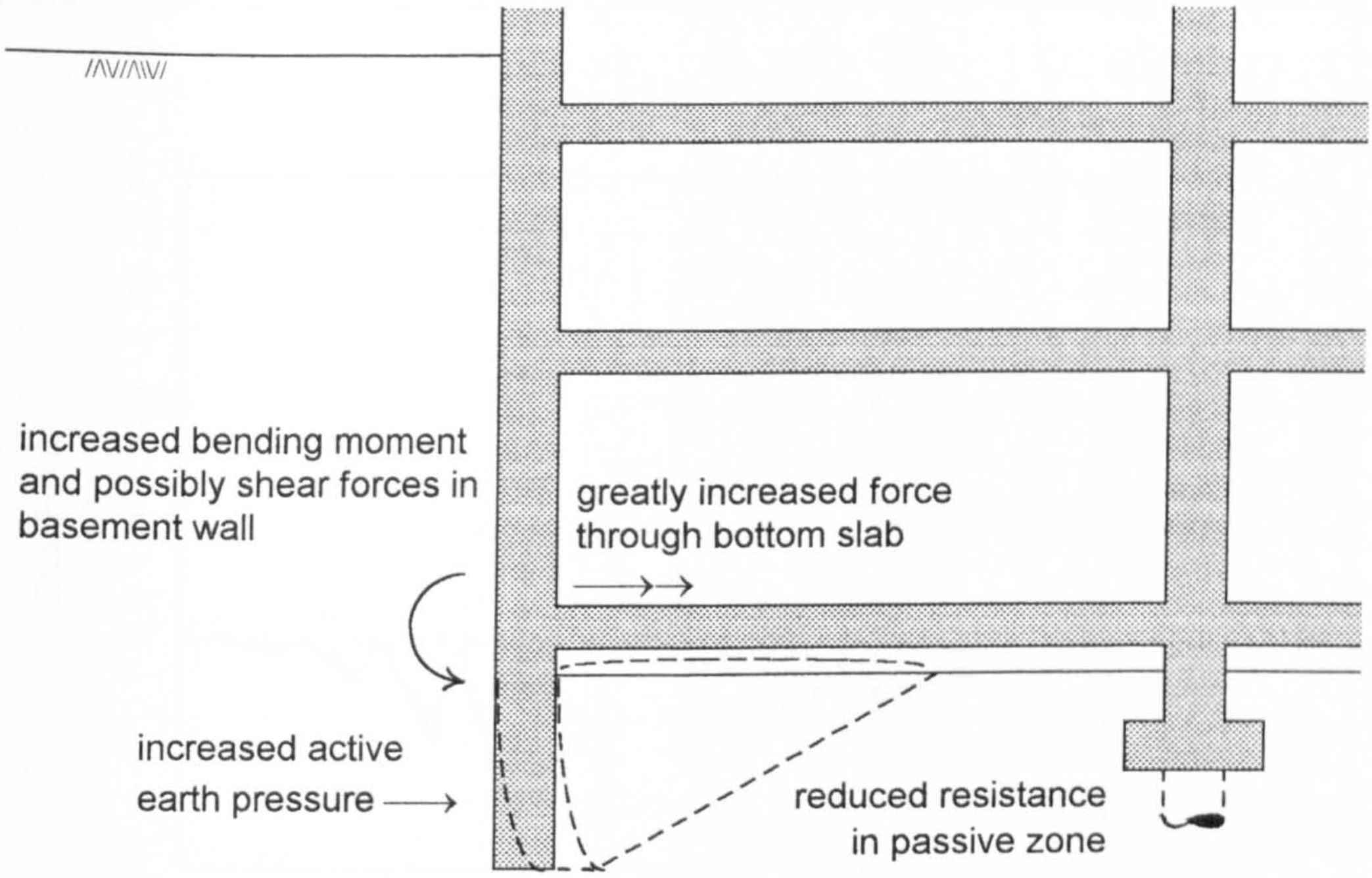

(a) Problems due to changes in ground stresses (after Simpson *et al.*, 1989)

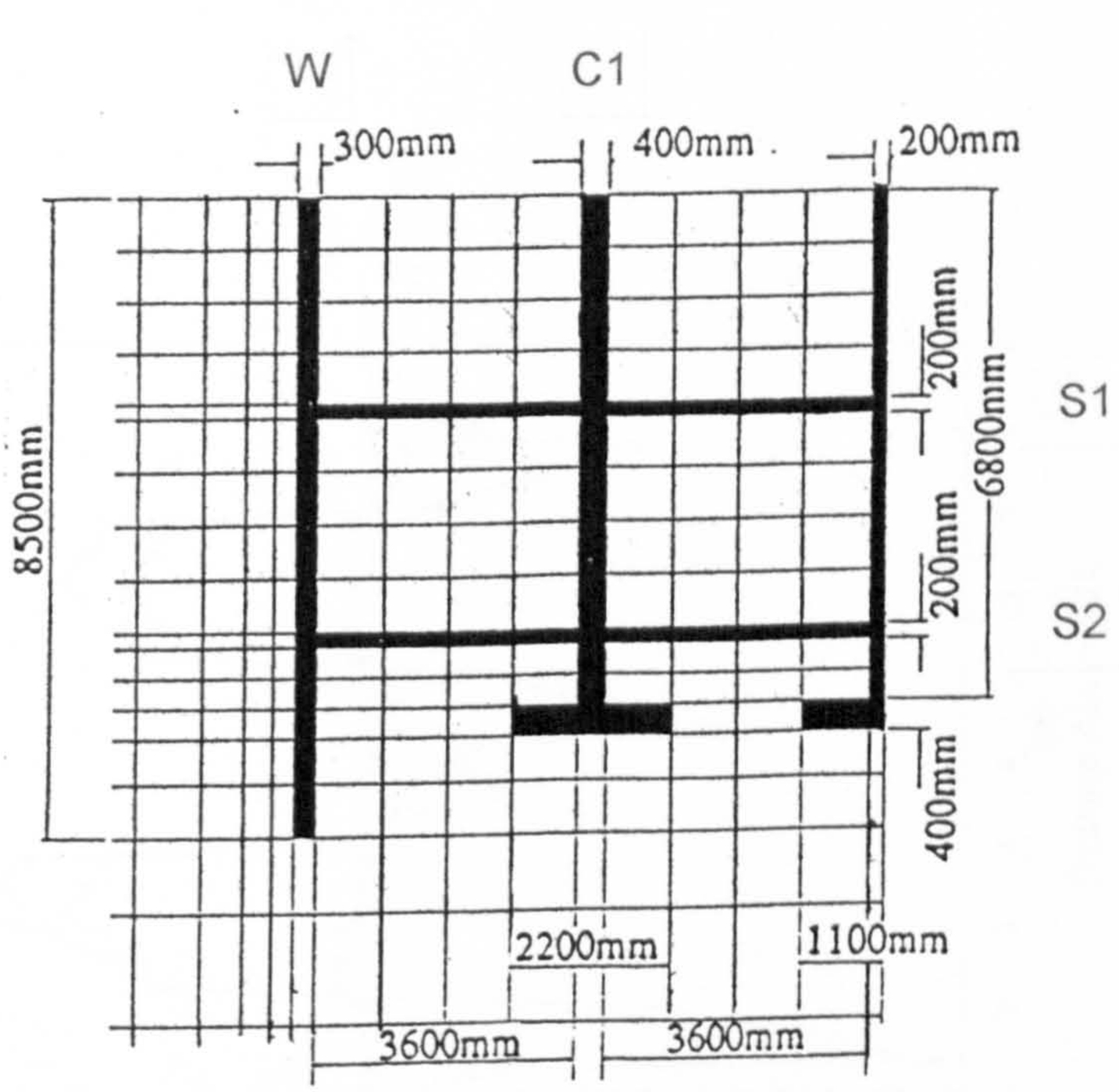

(b) finite element mesh : detail in and around basement

Fig 6.21 Deep basement configuration considered to be at risk from rising groundwater

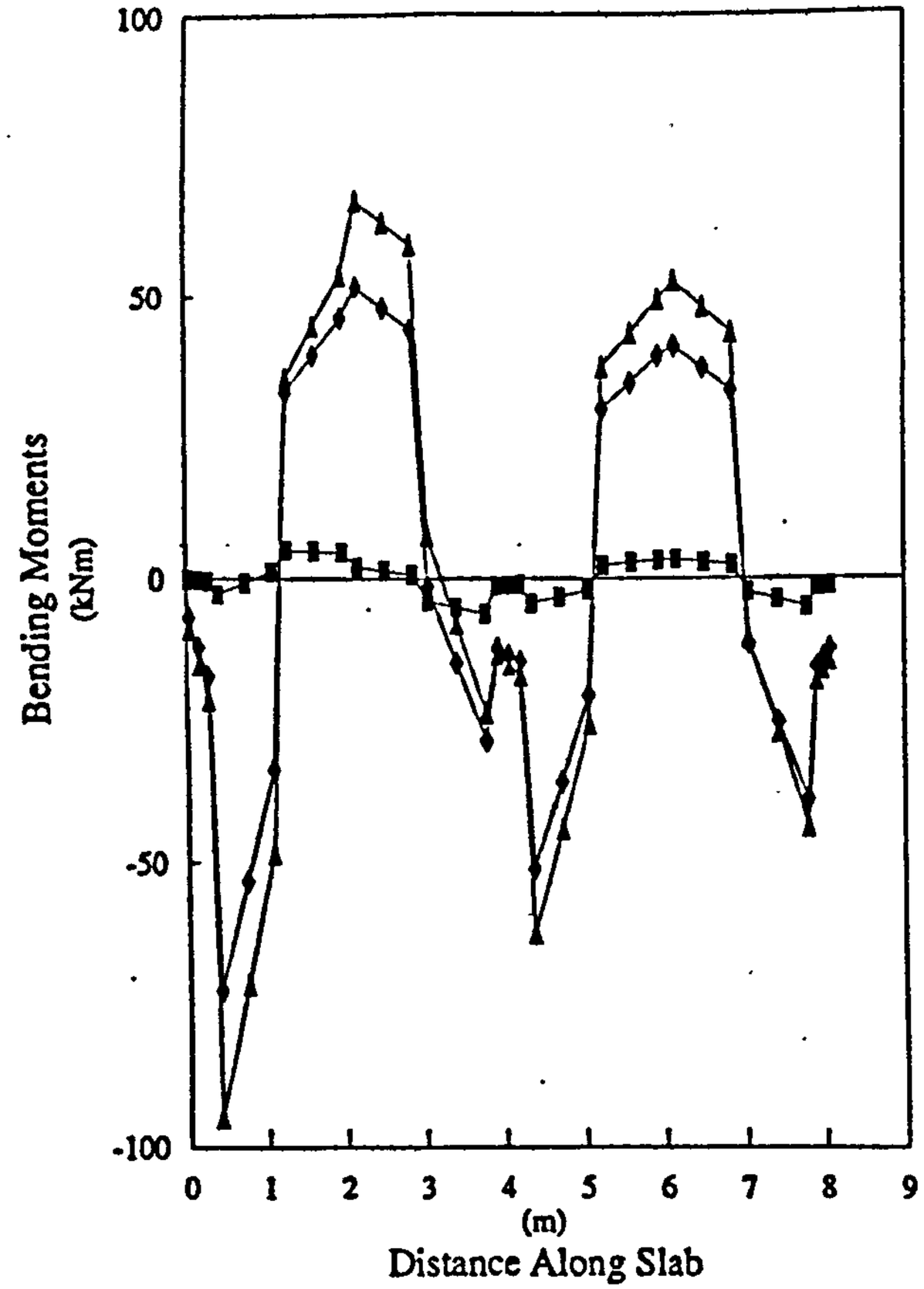

(a) bending moment profiles in lower slab

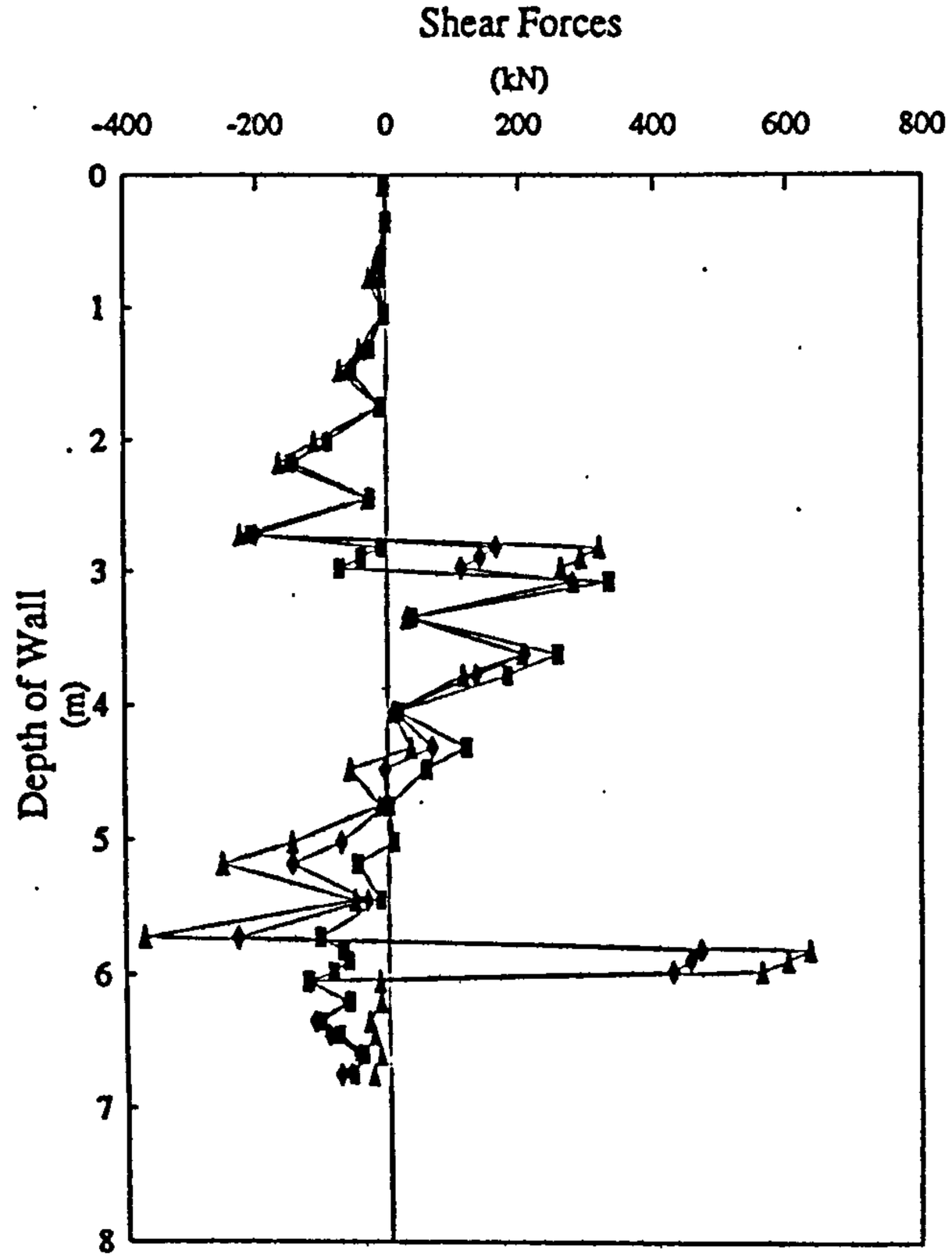

(b) shear force profiles in outer wall

Fig 6.22 Effects of rising groundwater on a deep basement : selected plots of structural forces, before/after aquifer recharge (after Woods *et al.*, 1996)

CHAPTER 7
COMPUTATIONAL DIFFICULTIES

7.1 General Introduction

Preceding chapters have dealt with the choices which must be made with respect to finite element mesh, material properties, construction processes, and long-term equalization. These choices are essentially of a modelling and discretization nature (as described in Chapter 1), and numerical experiments have addressed some of the errors and approximations that can be introduced into a retaining wall analysis. It can be argued that these errors have more to do with the analyst/operator than the computer itself, as they arise from human decisions.

The actual process of setting up and solving the finite element equations now takes place within the program itself, and this chapter considers issues which are of a specifically numerical and computational nature. These issues would almost certainly be beyond the understanding (except in broad terms) of a non-specialist, and yet they may have a profound effect on the accuracy (or even admissibility) of an analysis.

In the experience of the writer and of other users of CRISP, there are a number of specific problems of a computational nature which have been known to arise during retaining wall (and indeed all SSI) analysis. These are associated with:

- contrasting material stiffnesses,
- high element aspect ratios and distortions,
- effective stress representation of undrained loading conditions
- coupled analysis of undrained loading (in particular, problems with small time steps)
- oscillations and other anomalies in horizontal stresses
- tangent stiffness incremental scheme for non-linear analysis (esp. with elasto-plastic constitutive models)

Sometimes these problems manifest themselves in anomalous or bizarre output values and if they come to the attention of the designer they might lead to the analysis being discarded as wrong or worthless. Often these curious results are observed to occur in only a small region

of the mesh (perhaps in just a single element), and it is important for the designer to be able to judge whether or not the whole analysis is affected or just some part of it (and if so, which)[1]. This chapter will present some investigations which have been carried out in these different areas, in an attempt to establish their relative importance and influence on practical retaining wall analyses.

It will be helpful to start with a brief overview of the sort of errors which can occur in finite element computations, before focusing on the specific areas listed above. The following classification is due to Cook *et al.* (1989):

a) *Modelling Error* - refers to the difference between a physical system and its mathematical model. For example, seepage through a porous medium may be modelled by the Laplace equation, which may not be a wholly accurate representation. The mathematical model is then solved by a numerical solution scheme, and it is this scheme which is open to the following errors.

b) *Discretization Error* - refers to the error caused by representing the infinitely many d.o.f. of a continuous mathematical model by a finite number of d.o.f. in its discretized form. For example, the aforementioned porous medium is divided into finite elements, thus introducing discretization error. (In stress analysis, this is regarded as producing a model which is "stiffer" than the real system - or, more generally, a model in which the total potential energy is greater than that of the real system.)

c) *Round-off Error* - is caused by use of a finite number of bits or digits to represent real numbers in a computer. The last digit retained may be rounded or may be obtained by simple truncation (chopping). The round-off limit is the smallest floating point number ε such that, in the computer, $1 + \varepsilon > 1$.

d) *Inherited Error* - at any stage of the calculation, this is the sum of previous discretization and round-off errors.

---

[1] It is perhaps less important for the designer to know exactly why these anomalies arise - just how to recognize them, and avoid them if necessary.

e) *Manipulation Error* - refers to round-off error introduced by an algorithm. For example, a simultaneous equation solver performs numerical operations such as A_{22} - $(A_{21}/A_{11})*A_{12}$, where A_{ij} are matrix coefficients. The division and multiplication are each followed by rounding of the result to computer word-length, and the subtraction may lose several significant digits if A_{22} and $(A_{21}/A_{11})*A_{12}$ are almost equal.

In a finite element context, inherited error is present after very different element stiffnesses are added to form global stiffness matrix coefficients, and manipulation error is produced by solving the equations. Interestingly, a finer mesh means that more operations need to be performed - so whilst discretization error is reduced, manipulation error actually increases, and there is a trade off.

f) *Gross Error* - usually arises from a mistake or blunder in the basic input data. This is essentially a human factor and some gross errors are impossible to trap, even with sophisticated data checking routines in computer programs[2].

g) *Gratuitous Error* - refers to error introduced when numerical constants (such as Gauss point co-ordinates and weighting factors) are written into the code with fewer accurate digits than the machine can accommodate.

Errors from source (a) will be present in any FE analysis conducted, regardless of the FE package; details may vary, depending on which governing equations are used, but this thesis has not sought to address this area at all. Source (b), on the other hand, has been extensively investigated in Chapter 4 and it has been shown that care needs to be taken to minimize errors from this source in a retaining wall (or indeed any) analysis.

Computer hardware governs the extent of the error introduced through (c) and (d); levels of precision vary from one machine to another, quite apart from that requested in the code (e.g. single v double precision in Fortran). Much of this is fixed at compilation stage, and is generally beyond the control of the user. Errors in category (e) will be influenced by the way the FE program itself has been written - some statements and procedures will introduce more

---

[2] AGS (1995) has introduced the classification of (i) impossible, (ii) implausible and (iii) improbable values for input data - a program should never permit (i), and should always question both (ii) and (iii) before proceeding.

rounding/ truncation than others. This too is beyond the control of the user - and to some extent that of the programmer unless he/she is prepared to re-write code. All of the cases examined in this Chapter are due to errors introduced through (c), (d) or (e) in CRISP.

There really is no excuse for (g) - the programmer should ensure that the precision embodied in the code is greater than that likely to be accommodated by the machine. Based on an inspection of the Fortran source code, CRISP appears to be satisfactory in this respect[3].

Finally, (f) is largely in the control of the user, although the program can go some way to eliminating this, as described by AGS (1994). Irons and Ahmad (1980) make an ".... educated guess that as much as 50% of commercial FE runs lead to stillbirths, owing to a data error or misjudgement". CRISP is good at picking up certain kinds of data error (e.g. the provision of too few/too many items in a data record) but not others.

7.2 Stiffness and Aspect Ratio

In any finite element mesh, there is a limit to the difference in stiffness that can be tolerated between adjacent elements, before computational problems arise. This has potential implications for all soil-structure interaction problems, where materials with contrasting modulii (perhaps by 3-4 orders of magnitude) are being included in the same model.

Several investigators have reported problems with unacceptable equilibrium errors when applying CRISP to soil-structure interaction problems. Vaziri (1988) modelled a screw plate in sand and was forced to use double-precision arithmetic to handle the large modular ratio between steel and sand. Woods and Contreras (1988) analysed a circular steel plate on clay and found that stiffness ratios (steel : clay) in excess of 10^3 lead to high equilibrium errors. Similar problems can be expected to occur in the analysis of a steel sheet pile wall, if solid (rather than beam) elements are used.

---

[3] In fact, one of the strengths of CRISP is that it is probably the only commercial geotechnical FE program where the source code has been effectively placed in the public domain, allowing users to verify the implementation of constitutive models etc. - as well as enabling them to make their own modifications. Hence, true "glass box" testing is possible.

7.2.1 Ill-conditioning

An ill-conditioned set of equations is one in which the solution is sensitive to small changes in either the coefficient matrix or the vector of constants. Mathematically this means that the rows of the coefficient matrix are almost linearly dependent. In finite elements generally, ill-conditioning may be caused by (Cook *et al.*, 1989):

a) highly disparate material stiffness (especially rigid inclusions in a softer medium),
b) elements of large aspect ratio or severe shape distortion,
c) elements of markedly different size, and
d) a large number of elements.

In the context of a retaining wall analysis, all of these potential causes may be present. The steel or concrete wall is a rigid inclusion in the softer supporting soil; long, thin elements are sometimes used to model the wall and associated structural members; mesh grading is very common, with very large elements near the far boundaries and relatively small elements used for the wall and immediately surrounding soil; complex geometries may force the use of many hundreds (or several thousands) of elements.

It is mathematically possible to analyse successfully such cases via finite elements; the problems arise from the inability to store and process real numbers with infinite precision in digital computers (Dorn and McCracken, 1972). For example, adding the numbers 0.52E-1 and 0.83E4 should yield .8300052E4. In a machine which stores and handles numbers to only 6 significant figures[4], however, the trailing "2" would be lost. If this particular operation was part of the global stiffness matrix assembly, essential numerical information could be lost. The resultant system of equations might be ill-conditioned, and the situation would continue to worsen with subsequent floating point arithmetic (e.g. through Gaussian elimination). This particular problem is well known and has been investigated by several workers (Fried, 1971, 1972; Gallagher, 1977; Meyer, 1975; Rosanoff *et al.*, 1968; Tong, 1971).

Causes of ill-conditioning

To understand why cases (a) - (d) above can lead to ill-conditioning, it is necessary to examine the underlying equations. In the finite element (displacement) method, the applied loads **f** are related to the (unknown) displacements **d** through the global stiffness matrix **K**:

---

[4] Very crude by modern standards - this has been used simply to illustrate the point.

$$\mathbf{K}\,\mathbf{d} = \mathbf{f} \tag{7.1}$$

K is obtained by assembling the individual stiffness matrices $\mathbf{K}^e$ of each element, where:

$$\mathbf{K}^e = \int \mathbf{B}^T\,\mathbf{D}\,\mathbf{B}\;\; d(\text{vol}) \tag{7.2}$$

In this expression, **B** is a matrix of constants relating nodal displacements to internal strains. **B** is derived from the shape functions for the assumed displacement field of the element, and is thus influenced by its aspect ratio and distortion. The matrix **D** relates internal stresses to internal strains through various material parameters such as E and ν, or G and K. Variations in material properties therefore have a direct effect on the magnitude of the terms comprising **D**. Finally, the matrix product is integrated over the volume of the element, which brings into play the size of the element relative to others in the mesh.

Taking all these factors together, it can be seen that element geometry, size and material modulus all influence the magnitude of the coefficients of $\mathbf{K}^e$. In a retaining wall analysis, nodes along the soil-structure interface will share elements of very different stiffness. The modular ratio between a soil element and an adjacent structural element may be very high (typically $>10^3$ for concrete; $>10^4$ for steel). Global stiffness matrix assembly may then lead to just the sort of numerical problem described in Section 7.2.1, where fixed computer word-length results in the loss of significant digits.

Measures of ill-conditioning

a) Condition number

Classically, rounding and truncation error has been studied by investigating the sensitivity of the solution to changes in the stiffness matrix. From Eqn 7.1, if a change in stiffness $\delta\mathbf{K}$ causes a change in displacement $\delta\mathbf{d}$, then it is possible to write:

$$(\mathbf{K} + \delta\mathbf{K})\,(\mathbf{d} + \delta\mathbf{d}) \;=\; \mathbf{f} \tag{7.3}$$

Taking Euclidean norms of all vectors and matrices and assuming $|\delta\mathbf{K}| \,/\, |\mathbf{K}| \ll 1$, leads to:

$$|\delta \mathbf{d}| / |\mathbf{d}| < C(\mathbf{K}) |\delta \mathbf{K}| / |\mathbf{K}| \tag{7.4}$$

where $C(\mathbf{K})$ is the *condition number* (or spectral condition number) of the stiffness matrix $\mathbf{K}$, and is defined formally as the ratio of the maximum and minimum eigenvalues of $\mathbf{K}$:

$$C(\mathbf{K}) = \lambda_{max} / \lambda_{min} \tag{7.5}$$

$C(\mathbf{K})$ provides a numerical measure of the ill-conditioning of $\mathbf{K}$; it has been shown (Rosanoff *et al.*, 1968) that the number of accurate digits lost due to ill-conditioning is approximately equal to $\log_{10} C(\mathbf{K})$. If this number is compared to the word length of the machine, then some idea of the reliability of the solution may be obtained.

Unfortunately, Eqn (7.5) does not provide a convenient means of assessing the condition number prior to conducting a finite element analysis. The evaluation of the minimum and maximum eigenvalues of $\mathbf{K}$ (e.g. through the "power method"; Kreyszig, 1999) can require considerable computational effort (and hence cost). The use of approximate methods is desirable, and several have been suggested (Tong, 1971; Fried, 1972; Meyer, 1975). For example, Fried suggests that the condition number may be estimated from:

$$C(\mathbf{K}) = b \, (h_{max}/h_{min})^{2m-1} \, N^{2m/n} \tag{7.6}$$

where b = a positive constant
h_{min} = smallest node spacing in any element of the mesh
h_{max} = greatest node spacing in any element of the mesh
N = number of elements
$2m$ = order of governing differential equation
n = dimensionality of problem (1, 2, or 3D)

Of particular relevance to geotechnical finite elements is that the condition number may be strongly affected by Poisson's ratio ν (Fried, 1973). The constant b in Eqn (7.6) is inversely proportional to $(1-2\nu)$, with the consequence that the requirement of virtual incompressibility may increase $C(\mathbf{K})$ by several orders of magnitude. This has important implications for undrained analysis, where ν (in terms of total stresses) is set close to 0.5.

The condition number is not a practical means of assessing the degree of ill-conditioning in finite element equations. Simpler and less expensive indications of stiffness matrix condition have been proposed (Irons and Ahmad, 1980). The two most important of these are the *diagonal decay* and *residual* criteria.

b) Diagonal decay

Solution methods such as Gaussian elimination process each row of **K** in turn. In each successive step, the diagonal coefficient K_{ii} of row i (known as the pivot) is used to eliminate terms corresponding to degree of freedom (d.o.f.) i further down in the matrix. Due to previous elimination operations, the value of a diagonal coefficient just prior to its use as a pivot may be very different to its original value. A pivot may have accumulated considerable round-off error by the time it is used for further elimination, thus spreading damage throughout the matrix. The diagonal decay criterion involves taking the ratio R_i between the initial and pivotal values of each diagonal coefficient, as it is about to be used. The number of accurate digits lost is given approximately by $\log_{10}(R_i)$. There would be cause for concern if $R_i > 10^4$. Higher values (say $R_i > 10^{10}$) suggest a major blunder in the model, such as insufficient kinematic restraints.

A form of diagonal decay test is relatively easy to implement, and could give warning of impending difficulty. CRISP is programmed only to detect when a pivot is zero, and stops program execution before it attempts to divide through by this pivot. This is unsatisfactory because it does not give the user the opportunity to take corrective action before the analysis is aborted, and it does not indicate the actual cause of the error. For example, ill-conditioning may arise from gross errors such as failure to prescribe sufficient kinematic restraints (i.e. boundary fixities) to the mesh. Such a case would cause difficulties regardless of computer precision. If a full diagonal decay check were implemented in CRISP, an additional N terms would have to be stored, where N is the number of d.o.f. in the problem. These terms would be the K_{ii} and there would be book-keeping implications to ensure that it was synchronized with the frontal solution method.

c) Residuals

After the finite element equations (Eqn 7.1) are solved to yield the displacements **d**, residuals $\Delta\mathbf{f}$ may be calculated from:

$$\Delta \mathbf{f} = \mathbf{f} - \mathbf{K}\,\mathbf{d} \qquad (7.7)$$

If the original equations were well conditioned and/or unlimited precision was used by the computer, then the residuals would be zero. In practice the residuals provide an *a posteriori* check on the reliability of the solution. A sufficiently small $\Delta \mathbf{f}$ indicates that resisting loads $\mathbf{K.d}$ generated by the deforming mesh are almost balancing the applied forces $\mathbf{f}$.

CRISP adopts a slightly different approach to the residuals test. After a solution is obtained, an "out-of-balance force" P_o is calculated for each unrestrained node in the mesh:

$$\mathbf{P_o} = \int_S \mathbf{N}^T \boldsymbol{\tau}\, d(\text{area}) + \int_V \mathbf{N}^T \mathbf{w}\, d(\text{vol}) - \int_V \mathbf{B}^T \boldsymbol{\sigma}\, d(\text{vol}) \qquad (7.8)$$

The terms on the right hand side of Eqn (7.8) represent edge tractions, self weight, and internal stresses respectively. To provide an index of the numerical error in the solution, the worst out-of-balance force found at any node within the mesh is expressed as a percentage of the largest applied load at any node within the mesh. The resulting *equilibrium error* may be used as a yardstick for assessing a particular analysis and comparing one analysis with another. This choice of scaling or normalizing the out-of-balance forces may appear somewhat arbitrary - however, some nodes will have no applied loads (e.g. internal nodes), so it seems sensible to use one single value of nodal load (i.e. the largest in the mesh) to perform the normalization. It is not easy to identify a limiting value on equilibrium error which would ensure acceptable results from CRISP in all cases. The type of constitutive model used, and whether or not stress corrections are carried out after each load increment will have a bearing on this. For example, a 5% error may be unacceptable in a purely elastic analysis, whereas it would be quite permissible in an elastic-perfectly plastic case if the error arose from yielding and would subsequently be "iterated out".

In some boundary value problems, large out-of-balance forces may be confined to a very small region of the mesh, in which case the overall integrity of the solution may not be too adversely affected (for example, at the edge of a loaded plate at the soil surface). Thus, whilst negligible out-of-balance forces throughout a mesh indicates a solution free from ill-conditioning, the presence of significant out-of-balance forces may not necessarily indicate a flawed analysis[5].

---

[5] Of course, on rigorous theoretical grounds one could argue that any error should result in the analysis being rejected, but in a practical design context this may be wasteful and unnecessary.

Further investigation would be required to ascertain how the results (stress distributions, nodal reactions, bending moments, etc.) were being affected. This test is a necessary (but not sufficient) criterion for a good analysis.

Summary

Ill-conditioning is both a hardware and a software issue. An FE model may be presented to two different programs on a given machine, and because of differences in programming language precision, solution algorithms etc. ill-conditioning may cause problems in one package and not the other. Similarly, the same FE model analysed with the same program may run into trouble on one machine but not another, due to differences in internal (machine) precision.

Ideally, computers would possess unlimited precision, and ill-conditioning would not occur. In practice, it is important to know not only when ill-conditioning is present, but also to have some idea of how it is affecting the quality of the analysis. Some ill-conditioning may be tolerable, provided it does not affect the answers which are of prime interest. In the following sections, results will be presented from a series of numerical experiments which have been carried out to investigate ill-conditioning and how it may affect the quantities of prime interest to a retaining wall analyst.

7.2.2 Description of analyses

In an attempt to assess the level (and potential consequences) of ill-conditioning in retaining wall analyses performed with CRISP, a short series of numerical experiments has been conducted. Simple two-element models in plane strain were used to investigate the influence of both disparate material moduli and aspect ratio on the conditioning of the finite element stiffness equations. Such simple models are an essential starting point in attempting to unravel the principal features of a complex situation (Robinson, 1976).

Mesh and element types

The two-element mesh used is shown in Fig. 7.1. The 8-noded linear strain quadrilateral (LSQ) was used for both elements in the model, as this is probably the most commonly used element in 2D soil-structure interaction analysis. The element employs full 3×3 Gaussian integration; no attempt has been made to examine reduced 2×2 integration in this context.

The dimension B was fixed at 1m, and five different aspect ratios (t/B) for the structural element were adopted; 1/2, 1/4, 1/8, 1/16, and 1/32. The latter two aspect ratios are extreme but are included here as they are relevant to elements representing a sheet pile wall.

Boundary conditions

Each of the five different aspect ratios was initially used in conjunction with four different types of displacement boundary condition, Fig. 7.2(a)-(d). Type A represents simple uniaxial compression, type B cantilever bending, type C one-dimensional compression, and type D fixed-end beam bending. These boundary conditions were selected to represent some of the different constraints which may be met in soil-structure interaction analysis.

A uniform normal stress of 100 kPa was applied along the vertical side of the soil or structure element (as appropriate), giving a total force of 100 kN per metre run. The actual magnitude of the load was unimportant; CRISP simply needs a reference against which to calculate percentage equilibrium errors (see Section 3.3.6). Merely assembling the element stiffness matrices in a fixed word-length computer is sufficient to cause numerical damage, but in the absence of applied loads and/or body forces the seriousness of the damage cannot be assessed using the existing indicators within CRISP.

Subsequently, two variants of boundary condition type B were selected for more detailed study as they most closely represented the conditions likely to be found in a small segment of a retaining wall. The first of these was type B1, which was identical to B except the external normal stress was applied to the soil element, Fig. 7.2(e). The second was type B2 - identical to type B1 except that fixities along the side of the soil element were removed, Fig. 7.2(f). This latter condition constrained all of the applied load to be transmitted to "earth" through the fully-fixed edge of the structural element.

Modular ratio

In studying the influence of relative stiffness in soil-structure interaction problems, it is normal to define a stiffness ratio K_r. One convenient definition used for raft and plate problems is due to Brown (1969):

$$K_r = (E_p/E_s)\,(1-\nu_s^2)\,(t/B)^3 \qquad (7.9)$$

where E_p and E_s are the Young's modulus for the plate and the soil respectively, and ν_s is the Poisson's ratio of the soil. Eqn 7.9 recognizes the role of both the *modular ratio* (E_p/E_s) and the *aspect ratio* (t/B). However, in the present study, these two ratios have been distinguished so that their influence can be considered separately. The material properties of the two elements were selected to give modular ratios in the range 10^{-2} to 10^{7}; a Poisson's ratio of 0.25 was used for both. Hereafter the term E_p will be retained for its familiarity, even though a wall is being considered rather than a plate. Furthermore - aspect ratio is considered to increase when t/B becomes numerically smaller. Thus an aspect ratio of 1/8 is "greater" (i.e. worse) than 1/2, because $8 > 2$ even though $1/8 < 1/2$.

Computer precision

To investigate the influence of computer type and computational precision, CRISP was run on a Prime 9750 and on a Gould PN9005 (using both Single and Double Precision arithmetic on each machine), and on Intel 486 and Pentium PCs (Single Precision only). The former architectures are typical of smaller mainframes available in the early 1990s whereas the latter are more typical of desktop computers of the late 1990s and early 2000s.

Evaluation of results

Percentage equilibrium error (in the horizontal direction) was extracted in the first instance, because it is a basic indicator available to the user of CRISP no matter what type of analysis is being conducted. However, equilibrium error alone does not give a good indication of how particular aspects of the finite element results may be affected. In an attempt to gain further information from the simple two-element mesh study, three other quantities were extracted for examination. These were the distributions of nodal reaction along the fixed boundary, the normal stresses in the soil, and the bending moment in the structural member.

7.2.3 Results of analyses

7.2.3.1 Equilibrium errors

The results are shown in Figs 7.3 (a-d), in the form of log-log plots of equilibrium error against modular ratio, E_p/E_s. The different aspect ratios are shown as different curves on the same plot, enabling the relative influence of t/B and E_p/E_s to be distinguished. The results will be discussed on the basis that 1% is a desirable maximum equilibrium error, and 5% is the upper limit of acceptable error. The purpose in adopting this approach is to apply the sort of

criteria that practising engineers might consider reasonable. A figure of 1% also ties in with the accuracy levels typically being sought by investigators of adaptive mesh refinement (Zienkiewicz and Taylor, 1989).

Boundary condition type A

Unacceptable equilibrium errors began to occur for modular ratios in the range 10^3 (at t/B = 1/32) to 10^5 (at t/B = 1/2), Fig. 7.3(a). At any given value of E_p/E_s, the range of aspect ratios considered altered the equilibrium error by about 1.5 orders of magnitude. Equilibrium errors for all the different computer architectures employed were very similar. The use of Double Precision, however, suppressed equilibrium errors dramatically, with even the most unfavourable combinations of E_p/E_s and t/B producing insignificant errors (< .001%).

Boundary condition type B

Unacceptable equilibrium errors occurred only for aspect ratios exceeding 1/16, Fig. 7.3(b), and the overall pattern was quite different to that for Type A. Intuitively this did not seem reasonable, because worse performance would have been expected from the cantilever-type conditions (Irons and Ahmad, 1980). The curves for lower aspect ratios were quite flat, showing very little influence from modular ratio. By contrast, the influence of t/B was very marked, especially at higher modular ratios. At $E_p/E_s = 10^3$, for example, the range of aspect ratios considered altered the equilibrium error by over 4-5 orders of magnitude. The variation of overall equilibrium error with modular and aspect ratio for types B1 and B2 was very similar to that obtained for type B, and so has not been shown.

Boundary condition type C

The spread and distribution of equilibrium errors for Type C were very similar to those for Type A boundary conditions (Figs 7.3(c) and (a)). Again, unacceptable errors began to manifest themselves for E_p/E_s in the range 10^3 to 10^5, and increasing t/B from 1/2 to 1/32 altered the equilibrium error over 1-2 orders of magnitude. The different types of computer architecture yielded essentially the same results.

Boundary condition type D

Equilibrium errors were acceptable at all aspect ratios over the entire range of modular ratio considered, Fig. 7.3(d). The overall pattern was similar to that for Type B, though never

approaching the magnitude of error achieved for some cases with those boundary conditions, Fig. 7.3(b).

7.2.3.2 Nodal reactions

The results obtained were examined in two different ways;

a) distributions of nodal reaction along fixed element edge(s), and

b) total out-of-balance reaction.

The distributions were considered simply by plotting the computed reactions along the restrained edge; different modular ratios with a fixed aspect ratio were considered, and *vice versa*. Two of these - plotted in the form of a comparative bar-chart - are included with this chapter; type B1 with t/B=1/4 (Fig. 7.4a), and type B2 with t/B=1/16 (Fig. 7.4b). The out-of-balance reaction ΔR was calculated by summing up the computed reactions at each node along the fully-fixed edge, and subtracting this from the applied load of 100kN. The variation of ΔR with modular ratio E_p/E_s for types B1 and B2 is summarized on Fig. 7.5.

Boundary condition type B1

In this type, it was possible for some reaction to be transmitted through the boundary at the base of the soil element, due to the specified fixity. In general, the distribution of nodal reaction along the soil element boundary (nodes a, b and c in Fig. 7.1) was fairly uniform, although the actual value depended fairly heavily on both t/B and E_p/E_s, Fig. 7.4(a). Crossing the boundary between the soil and the structural element (node c) caused a big jump in the profile, and the reaction distribution was very oscillatory thereafter.

Judging by the out-of-balance reactions, aspect ratios of 1/2, 1/4, and 1/8 appeared to give overall satisfactory performance across the range of modular ratios being considered, Fig. 7.5(a). Aspect ratios $\geq$ 1/16 gave noticeable out-of-balance reactions as soon as E_p/E_s exceeded 10^2. For the case of t/B = 1/32, the out-of-balance reaction reached over 2kN (i.e. 2% of the applied load of 100kN) when $K_r = 10^3$. Comparing this with the corresponding plot of equilibrium error (Fig. 7.3b), at the same combination of E_p/E_s and t/B the equilibrium error was approximately 4%.

Boundary condition type B2

In this case it was <u>not</u> possible for any reaction to be transmitted through the soil element boundary; all transfer took place along the structural element boundary, Fig. 7.4(b). At $E_p/E_s \leq 10^{-1}$, all of the 100 kN was taken to reaction by the first node (at the soil-structure interface). As E_p/E_s was increased from 10^{-2} to 10^3, the observed oscillation of reaction along the fixed element edge became increasingly exaggerated. For example, at t/B = 1/4 and $E_p/E_s = 10^{-1}$ the reactions at nodes c, d, e, were approximately -90, 0, -10 kN respectively, whereas at $E_p/E_s = 10^3$ they were approximately -205, 295, -190 kN. In each case the FE model achieved reactions summing to -100 kN, but differences between the individual reactions became greater as both modular and aspect ratios were increased.

Visual inspection of the nodal reactions shows that they are non-intuitive. If an engineer had extracted these forces from CRISP output, and was working out how to use them (perhaps in calculating shear force at a wall section), he/she could easily be confused. This sort of occurrence is not uncommon in FE, where consistent nodal loads for uniform boundary tractions and body forces are, at first sight, often surprising (see Section 3.3.6). The spatial oscillation of the reactions shown in Fig. 7.4 became more extreme as t/B worsened.

The out-of-balance reactions ΔR showed a very similar trend to Type B1, with noticeable force imbalance occurring for stiffness contrasts as low as $E_p/E_s \geq 10^2$, Fig. 7.5(b).

Relevance to practical problems

Nodal reactions may be used in computing wall bending moments so it is important to know how ill-conditioning may affect this computed quantity. In a retaining wall analysis, a pair of elements either side of the soil-wall interface would fall somewhere between the models represented by boundary conditions B1 and B2 (nearer to B2 as K_r increased). The modular ratio (E_p/E_s) would not need to be particularly high in order to give rise to large oscillations in the nodal reactions across the stiffer (i.e. wall) elements. Aspect ratio (t/B) seemed not to greatly affect the distribution of reactions at a particular modular ratio until E_p/E_s exceeded 10, when the effect was very pronounced.

7.2.3.3 Normal stresses in soil

It is entirely reasonable that an engineer might wish to extract the soil stresses calculated by CRISP, perhaps to compare with the simplified distributions assumed in design. This is a potential minefield which is discussed more fully in Chapter 8; here attention is focused on how finite element stresses near an embedded wall are influenced by modulus and aspect ratio.

Only boundary condition type B2 (Fig. 7.2f) was considered to be meaningful in this context. Normal stress profiles were examined on three sections, through the sections of Gauss points that are adjacent (near), central, and remote (far) from the structural element, Fig. 7.1. In a retaining wall context, these would be the lateral earth pressures. Summary plots have also been produced for the central section of Gauss points, showing the effect of varying t/B at a constant E_p/E_s (Fig. 7.6a) and of varying E_p/E_s at a constant t/B (Fig. 7.6b).

At no stage did the Gauss point distributions coincide with the applied uniform 100 kPa. All distributions oscillated either side of the reference by a minimum of ±5 kPa; in some cases as much as ±50 kPa deviation was seen. Unexpectedly (because there ought not have been much ill-conditioning), $E_p/E_s = 1$ gave the worst discrepancies. Furthermore, the stress distribution became more oscillatory with increasing proximity to the wall. Hitherto, the writer had always considered that a profile through the central section of Gauss points would give the most reliable stress distribution on an embedded retaining wall (and perceives this to be a widely held view), but it is not borne out by the results obtained here.

The central profiles for all t/B considered at $E_p/E_s = 1000$ (a typical ratio for concrete walls in clay), have been brought together in Fig. 7.6(a). The initial stress oscillations at t/B = 1/2 appeared to attenuate as t/B → 1/8, but then worsen at t/B = 16. Not only that, but there was a switch in the position of the "point of coincidence" relative to the 100 kPa reference line; for t/B ≤ 1/4 it was below the reference, but for t/B ≥ 1/8 it was above. The oscillation of the profile nearest the wall was again worst; perhaps not surprisingly the profile through points furthest from the wall bore the most resemblance to a uniform 100 kPa. Fig. 7.6(b) plots the centre profiles for all E_p/E_s considered at t/B=1/4, which shows clearly that patterns become more uniform at higher modular ratios.

What is being observed here is the kind of stiffness oscillation that has prompted many previous workers to experiment with stress smoothing procedures. Ways of improving the

stress distributions in and around a retaining structure are discussed in Chapter 8; here it is the causes of the oscillations which are being studied.

7.2.3.4 Bending moments in structure

Thus far in this thesis, bending moments in the wall have been used as one way of studying the influences of various modelling decisions. It should be remembered that bending moment is not a primary output quantity from an FE analysis - it is derived from primary (or even secondary) output values. In Chapter 8, this is explored further as there are several different ways in which wall bending moments might actually be calculated.

Bending moments were calculated in two different ways - (a) using transverse stress distributions in the structural element (generally regarded as being the most reliable - see Section 3.4.2), and (b) using normal pressure distributions in the soil (used in routine hand calculation methods such as fixed-earth support). In the latter approach, the resultants of active and passive thrust (and any known prop/anchor forces) are multiplied by their lever arms above a particular elevation in the wall, Fig. 7.7. In order to use this approach it was necessary to take a profile of normal stress through the soil element next to the wall. The decision is then whether to use the column of Gauss points near the structure, those in the centre of the element, or those furthest from the structure[6]. All three were compared with each other and with the analytical bending moment, given by $\frac{1}{2}w(B-y)^2 = 50.(1-y)^2$.

With $E_p/E_s = 1$, transverse stress bending moments were greatly in error, with M_{max} being (at best) only 20% of the analytical value when t/B = 1/2, Fig. 7.8(a). The transverse stress bending moment was virtually zero everywhere when t/B = 1/16.

At $E_p/E_s = 1000$ the agreement between the transverse stress bending moment and the analytical distribution was quite good at t/B = 1/2, but steadily deteriorated as aspect ratio increased. At t/B = 1/16 the agreement was very poor, and M_{max} was only 25% of the analytical value and showed little variation along the element, Fig. 7.8(b). This may be attributed to the poor bending performance of an 8-noded quadrilateral as the aspect ratio becomes high. The results for intermediate values of E_p/E_s showed a consistent trend.

---

[6] Another way would be to use 'smoothed' stresses, extrapolated from Gauss point values up to the nodes on the soil-wall interface. This is explored further in Chapter 8.

Bending moment profiles based on soil stresses were much closer to the analytical values, with very little evident influence from the t/B ratio. The distributions tied in well with each other, with only a small discrepancy between them which increased as the fixed end was approached. Best agreement was with the bending moment calculated from soil stresses on the "far" section of Gauss points, but presumably this was because it was closest to the boundary on which the 100 kPa was applied.

Alternative plots were also produced showing the influence of E_p/E_s on transverse stress bending moment (only) at a constant t/B; representative examples (for t/B=1/2 and 1/16) are shown in Fig. 7.8(a)&(b). These show reasonably clearly that a combination of high modular ratio and low aspect ratio was required to produce the best agreement between transverse stress bending moments and the analytical solution, Fig. 7.8(a). Also, reducing E_p/E_s and t/B both had the effect of flattening the transverse stress bending moment diagram, forcing it closer to zero everywhere, Fig. 7.8(b).

7.2.4 Discussion and summary

The simple two-element model analyses would tend to suggest that ill-conditioning may not arise much in the case of concrete diaphragm walls in firm to stiff clay, where aspect ratios (for sensible meshes) are not likely to exceed 1/4 and E_p/E_s will typically be in the range 10^3 to 10^4. In the case of steel (e.g. sheet pile) retaining walls and plates, much higher values of t/B and E_p/E_s are likely to arise and the likelihood of ill-conditioning is correspondingly much greater. The different computers used exhibited similar amounts of ill-conditioning, and double precision arithmetic provided adequate remedy in all cases investigated. (In addition, 1D beam elements should be used to represent something as slender as a sheet pile wall.)

This has not been an exhaustive study of modular and aspect ratio effects in retaining wall analyses, but it has served to indicate some of the problems which may exist. Numerical problems which arise from machine precision may simply not be an issue with some computer architectures. True 64-bit workstations (e.g. the Fujitsu HALstation 300 series) have been available since the late 1990s and the precision (as well as speed) of these computers is continually redefining the standards.

The two-element model is arguably too onerous a test, and may not be sufficient on which to construct a set of general recommendations (e.g. $t/B \geq 1/4$ to ensure good computation of

bending moments). However, it will not be too far from the true situation in a full-scale finite element model. There is a suggestion here that bending moments calculated from soil stresses may be more reliable than those from wall stresses. This is contrary to the findings of others (e.g. Gunn and Ponnampalam, 1990) and will be explored more fully in Chapter 8.

If high stiffness contrasts exist in the finite element model, then one obvious way to ascertain the severity of the effects would be to re-run the analysis with the stiffness of the more rigid materials reduced by an order of magnitude. This has some drawbacks however - the displacements and stress distributions of interest will be affected by such changes as they depend on relative stiffness. The possible effects of ill-conditioning may thus be hard to distinguish from genuine interaction effects.

The percentage equilibrium errors reported by CRISP may include out-of-balance loads arising from plastic yielding (with the elastic-perfectly plastic models, for example). It may be considered that the errors are due entirely to stress points going outside the yield surface and, provided they are not excessive, that they are being dealt with satisfactorily by the stress correction algorithm. Thus, equilibrium errors arising from ill-conditioning may be masked by those due to plastic yielding. This can be detected fairly easily by re-running the analysis as purely linear elastic, so that the contribution to out-of-balance loads from stiffness and aspect ratio can be isolated.

How should the retaining wall designer/analyst proceed? Most analysts probably work on the assumption that ill-conditioning is absent - until the program announces its presence, perhaps by crashing in mid-analysis. However, it is prudent to assume that some degree of ill-conditioning will be present in any soil-structure interaction analysis. In the same way that adjusting mesh density should show if adequate refinement has been achieved, adjusting modulus contrasts should indicate if ill-conditioning is present. Elements with high aspect ratio should always be avoided in the vicinity of high modular ratios and stress gradients.

Routine use of double precision is one solution, but this effectively halves the size of problem (in terms of d.o.f.) that can be stored in computer memory at any one time. Automatic use may, therefore, prove inefficient and wasteful.

7.3 Effective Stress Method

7.3.1 Introduction

Many geotechnical finite element codes (including CRISP) use the effective stress method for both drained and undrained loading. The bulk modulus of the pore fluid K_w is set either to zero (to give a drained response) or to an arbitrarily large number (to give an undrained response). Further details have been given earlier in this thesis (see Section 3.3.2).

It is generally believed that the actual magnitude of K_w used for undrained analysis is unimportant, provided it is greater (at least by a factor of 100) than the drained bulk modulus K' of the soil skeleton. If the value of K_w is too low, then the behaviour modelled is similar to that of a partially saturated ($B < 1$) - or perhaps partially drained[7] - soil, with some load being taken in effective stress even in the short term. However, if K_w is too high, Ponnampalam (1990) found that computed horizontal stress distributions following wall installation can be very erratic. Kutmen (1986) had similar problems with wall installation analysis, using a fully coupled formulation, though this was probably due to small time steps.

It would seem that K_w should neither be too high nor too low, relative to the drained bulk modulus of the soil, but it is not clear that there will always be a satisfactory range between these limits, for all combinations of geometry and soil properties. The problem is analogous to that of selecting a value of Poisson's ratio ν close (but not exactly equal) to 0.5 for undrained analysis in terms of total stresses. In the analyses reported in earlier chapters a value of $\nu = 0.497$ was used without any formal justification, but it is typical of what is used in practice (which tends to fall in the range 0.495-0.498).

The lower limit on K_w (i.e. ensuring that partial saturation or drainage is not unintentionally implied) is, in a sense, a soil mechanics problem. It has been noted earlier in the thesis that the assumption of undrained behaviour during retaining wall construction may be incorrect, as

---

[7] From a soil mechanics perspective, the ability to undergo some volume change upon loading could indicate that there was some air in the pore water ($B < 1$) causing a significant increase in compressibility, or that the drainage characteristics were such that some expulsion of the pore water could take place during loading, or that the skeletal compressibility was low, and approaching that of the water. In an FE context there is no continuity of volume change unless a coupled formulation is being used (i.e. if water leaves one element it must drain into adjacent elements). So, strictly speaking, a low K_w (e.g. $\approx 10K'$) replicates partially saturated behaviour.

some drainage may occur even in low permeability soils (due to laminations of coarser material, fissures opening up due to stress relief, etc.). So it may be advantageous to use a value of K_w (or ν) which implies that some volume change can indeed take place during construction. The upper limit on K_w, in contrast, is a finite element numerical problem; the analyst simply wishes to produce relatively incompressible behaviour, and may intuitively believe that, the higher the value selected for K_w, the better.

7.3.2 Description of analyses

To investigate some of the problems which can arise and the effect that they might have on quantities of interest to the designer, a series of CRISP analyses has been carried out on an unpropped cantilever wall. Mesh x10y10 was used, Fig. 4.1, together with soil parameters in terms of effective stress. Both elastic (sets 1d and 3d) and elasto-plastic (sets 12d and 13d) soil models were used, though in the case of set 12d the strength parameters were c'=53 kPa and ϕ'=19.5°. This was to ensure coincidence of the yield envelopes described by the total and effective stress approaches to undrained behaviour, as discussed in Section 5.8.2.

Unlike previous analyses where these parameters were used (see Chapters 4 and 5), K_w was set to a non-zero value so that the response was no longer fully drained. The wall was installed "wished-in-place" (WIP) to remove any influence from that aspect of the construction process, and the numbers of increments used in the excavation sequence were more than adequate according to the findings of Section 6.3. The aim was to ensure that the only major influence was from the compressibility of the pore water.

It is suggested by the authors of CRISP (e.g. Britto and Gunn, 1990) that K_w should be set to approximately $100 \times K'$ to obtain an undrained response. This is a straightforward calculation when soil stiffness is constant, but most real soils are nonhomogeneous, with E' (and hence K') increasing with depth. In such cases, it is not clear whether it is best for the designer to attempt to satisfy $K_w/K' \approx 100$ at the top, bottom or middle of the wall. It would be much more satisfactory if the user was able to specify the ratio K_w/K' as input data, rather than the absolute value of K_w. Indeed, this was implemented in the "book" version of CRISP (Britto and Gunn, 1987), but not in any of the major commercial releases (CRISP 8x, 9x or SAGE).

Another potential problem in specifying a constant value for K_w would be if a non-linear stiffness model (defined in terms of effective stress) was employed. If E' can vary with stress

and/or strain level, it would be virtually impossible to guarantee an undrained response throughout the analysis unless the ratio K_w/K' could be defined instead. This strengthens the argument to adopt a ratio rather than an absolute value in the input data.

For the present purpose, estimations of an appropriate value for K_w were based on set 1d, where $E' = \text{constant} = 40$ MPa and $\nu' = 0.2$. In consequence, when $E' = 4z$ the ratio of K_w/K' was rather higher than 100 for $z < 10$m (i.e. roughly over the upper half of the wall), but less than 100 for $z > 10$m. Because K_w/K' approaches infinity as $E' \rightarrow 0$, results were scrutinized for possible signs of ill-conditioning near the soil surface. For a stiffness profile of $E' = 40 + 4z$ (set 12d), K_w/K' was less than 100 at all points below the ground surface. At the toe of the wall, E' was approximately $2.5 \times E'_o$ and so the ratio K_w/K' dropped from 100 to about 40. Using Eqn 3.11, for $E' = 40$ MPa and $\nu' = 0.2$, $K' \approx 2 \times 10^4$ kPa. This value of K' for set 1 was used subsequently as a reference for normalizing K_w, even though it only applied at $z = 0$ for set 2 and at $z = 8$m for sets 3 and 13.

Following the advice of Britto and Gunn (1990), K_w was set to $100\ K' = 2 \times 10^6$ kPa. Using this as a reference value, it was decided to investigate values of K_w several orders of magnitude either side of 2×10^6 kPa. The separate cases selected are tabulated below:

case	K_w (kPa)	K_w/K'	case	K_w (kPa)	K_w/K'
KW01	2×10^3	0.1	KW04	2×10^6	100
KW02	2×10^4	1	KW05	2×10^7	1000
KW03	2×10^5	10	KW06	2×10^8	10000

7.3.3 Results of analyses

A complete set of full profiles of wall displacement, bending moment, excavation heave and ground surface movement for the different K_w values are shown in Appendix B, Figs B8-11. Additionally, convergence on the maximum value, Γ^*_{max}, for each individual quantity (δ, $\pm M$, V and -S) has been plotted as a function of K_w, Fig. 7.9(a)-(d), as a way of summarizing the main results. Γ^*_{max} was based on the relevant values of δ, $\pm M$, V or -S at $K_w = 2 \times 10^7$ kPa, rather than 2×10^8 kPa; clear evidence of ill-conditioning at the higher value of K_w rendered

the results unreliable. In addition, only the numerically larger of $+M_{max}$ and $-M_{max}$ was used in creating these convergence plots.

To provide further insight into what was happening at high K_w/K' ratios, two additional K_w values of 2×10^9 and 10^{10} kPa were included, and profiles of σ'_h, u, and σ_h on the retained side of the wall were examined. Profiles of pore water pressure (only) are shown in Fig. B12, based on Gauss point values in the centre of the column of elements adjacent to the wall (this is returned to in Chapter 8). To provide a means of comparison, percentage errors in stress Δ_σ relative to the reference case were computed thus:

$$\Delta_\sigma = \max(\sigma_i - \sigma_i^*) / \max(\sigma_i^*) \times 100\% \qquad (7.10)$$

where σ_i is the stress (σ'_h, u or σ_h) at point i on the wall for a given K_w, and σ_i^* is the stress at the reference K_w of 2×10^6 kPa ($K_w/K' \approx 100$) at the same point i. The variation of Δ_σ with K_w/K' has been plotted in Fig. 7.10(a)-(d), providing some indication of the errors introduced.

Horizontal wall displacement

The plotted profiles confirm that the "rule of thumb" value of $K_w/K' = 100$ provided a satisfactory prediction of wall displacements (Fig. B9). The curve obtained for the equivalent total stress analysis (with $\nu = 0.497$) has not been reproduced, but showed good agreement with the effective stress analysis. The curves for K_w/K' values between 10 and 1000 were clustered close together, but there was some evidence that the profile was beginning to diverge away at $K_w/K' = 10^4$ in the elastic analyses. This can also be seen in Fig. 7.9(a), which plots ($\delta_{max} / \delta^*_{max}$) against K_w and indicates problems developing at high K_w values.

The sensitivity to K_w appeared to be more pronounced for the elastic-perfectly plastic analyses, but it should be remembered that the unpropped wall was rotationally unstable under fully drained conditions for parameter set 13d (when $E'=4z$; $\phi'=19.5°$), so the displacements at lower K_w values (tending towards the drained limit) were, not surprisingly, rather large.

Wall bending moment

The bending moment profiles also provided confirmation that $K_w/K' = 100$ seemed to give a sufficiently undrained response, Figs B9 and 7.9(b). The errors introduced by having K_w too

low were more pronounced below formation level than above, with less sensitivity to K_w over the upper half of the wall; especially for sets 1d and 12d. Profiles were clustered together in the range $10 < K_w/K' < 1000$ and, like wall displacements, there was a clear deterioration of the results for $K_w/K' = 10^4$.

Excavation heave

From Figs B10 and 7.9(c), it would seem that excavation heave was relatively much more sensitive to the compressibility of the pore water than wall behaviour. Heave profiles did not reach steady values until $K_w/K' \geq 100$, the sensitivity being more pronounced when the soil was permitted to yield. It was only for the homogeneous E′ case that there was any evidence of possible numerical problems at high K_w.

Ground surface movement

The profiles of surface heave/settlement showed very clearly the importance of selecting the right magnitude for K_w, Figs B11 and 7. 9(d). As with excavation heaves, $K_w/K' = 100$ appeared to give an adequate undrained response, but only just. $K_w/K' = 10$ would have lead to significant error in the computed surface movements. The profile obtained when E′ = constant and $K_w/K' = 10^4$ indicated the onset of serious ill-conditioning, Fig. B11(a).

Horizontal effective stress

Recalling that effective stresses cannot change during undrained loading in an elastic analysis provides a means of checking the computed profiles of σ'_h. When $10^2 \leq K_w/K' \leq 10^4$, the profiles correctly followed the line $\sigma'_h = K_o \sigma'_v = 20z$. However, for $K_w/K' > 10^5$, σ'_h began to oscillate across this line in the elastic analyses, and these results were therefore discarded as unreliable. (NB: the elastic-perfectly plastic analyses crashed due to serious ill-conditioning after just 2-3 increments when $K_w > 10^5$, and therefore these σ'_h profiles could not be plotted.) Fig. 7.10(a) suggests that a 20% discrepancy could arise at high K_w/K'.

Pore water pressure

In an undrained analysis, the pore water pressures are expected to change. Behind the wall, where lateral stress relief leads to a reduction in mean total stress, the pore water pressures will reduce. This trend can be seen in Fig. B12. However, these plots convey a rather alarming picture of how the pore water pressure profile can degenerate if K_w/K' is taken much

above 100. Such was the degree of oscillation when $K_w/K' \geq 10^5$ that the profiles for K_w/K' 10^5 and 10^6 been omitted from most plots so as not to obscure the detail. However, the trend which is developing has become quite clear by the time $K_w/K' = 10^5$. Fig. 7.10(b) underlines this, and indicates that discrepancies as high as 2000% may arise when $K_w/K' = 10^6$.

Deterioration in computed stress components as a material becomes nearly incompressible has also been studied by Naylor (1974), for a number of simple boundary value problems. Increasing errors were shown both in total stress analyses with ν approaching 0.5, and in effective stress analyses with K_w approaching ∞. The nature of the problem lies in the fact that, with full numerical integration (3×3 for 8-node quadrilaterals), the number of constraints may exceed the number of degrees of freedom in an undrained analysis. Similar conclusions were reached by Sloan and Randolph (1982). Reduced integration is one solution to this, but users of CRISP do not have this facility in commercially available releases of the program. (Naylor's findings are also relevant to the investigations of Chapter 8; specifically, the quality of stress distributions computed by the finite element displacement method.)

Horizontal total stress

Profiles of σ_h also showed oscillation, but this was a direct consequence of the problems with pore water pressures noted already. The trends in Fig. 7.10(c) are very similar to those in Fig. 7.10(b), though the discrepancies are not quite as severe.

Comparison with total stress analyses

To verify that $K_w/K' = 100$ was giving an undrained response for the cases being considered here, the elastic analyses were re-run using total stresses and the key results compared.

Horizontal wall displacement and wall bending moment did not appear to be particularly sensitive to K_w/K' for values ≥10, which recovered essentially the same solution as the total stress approach. Excavation heave and ground surface movement required $K_w/K' \geq 100$ in order to produce similar results to the total stress analysis, and even then the agreement was not as close as that obtained for the wall movements and bending moments.

7.3.4 Discussion and summary

The effective stress method is a very convenient way of switching between drained and undrained analyses, simply by adjusting one single parameter. Of course, the total stress approach could be used with E_u and $\nu_u \approx ½$ but then the pore water pressures are not explicitly calculated. The convenience of the effective stress method may tend to disguise its main pitfall; i.e. that there is actually an optimum value for K_w. If K_w is set low, partial saturation is modelled, whereas if it is too high, numerical instability may result. Some users might tend to the view that, if a large number is required for K_w, then 10^{10} (or higher) might be ideal, in the belief that it would ensure completely undrained behaviour. (The writer has seen this being done, together with the use of $\nu_u = 0.4999$.)

If E′ (and hence K′) varies with depth (quite common in natural soils) then even the experienced user would tend to select a K_w on the high side to ensure that $K_w/K' > 100$ everywhere, and this could cause particular problems near the soil surface - often the area of greatest interest. Therefore, it is suggested that $\alpha = K_w/K'$ be an input parameter rather than K_w. It removes some of the possible errors which may occur due to K′ varying in the mesh.

7.4 Coupled Analysis

7.4.1 Introduction

Depending on the exact requirements, it is not unusual to commence a commercial retaining wall analysis in uncoupled mode. Separate undrained ($\nu_u \approx 1/2$ or $K_w >> 0$) and drained ($\sigma = \sigma'$) analyses can be performed to give the short and long term respectively, and the matter may rest there if time dependency is unimportant (and/or the data for more sophisticated analysis is not available). However, there is now ample evidence that coupled analyses can produce phenomena which are not in evidence if one simply takes the numerical difference between the corresponding drained and undrained results (e.g. Woods, 1986). Hence coupled analysis may well be called for.

If coupled analysis is required, elements in the original mesh can be converted to the type with excess pore pressure d.o.f. Additional information is then specified in the input data file (e.g. coefficients of permeability, drainage boundary conditions, time steps) and the FE model is

ready. The first task might well be to benchmark the coupled analysis against an equivalent uncoupled analysis. It should be possible to recover the undrained case with small time steps Δt (and/or low k), but how small? The drained case can be recovered with large Δt (and/or high k), but how large? This section will examine if expectations of equivalence are justified.

7.4.2 Description of analyses

To investigate the equivalence of coupled and uncoupled analyses at the limits of drainage, mesh x10y10 was used to perform five different types of analysis:

Code	Type	Modulus	ν	K_w	k	Δt
(a)	uncoupled; drained	E′	0.2	0	n/a	n/a
(b)	uncoupled; undrained (σ′)	E′	0.2	≈100K′	n/a	n/a
(c)	uncoupled; undrained (σ)	E_u	0.497	0	n/a	n/a
(d)	coupled; undrained	E′	0.2	n/a	10^{-9}	$\rightarrow 0$
(e)	coupled; drained	E′	0.2	n/a	10^{-9}	$\rightarrow \infty$

In all but (c), stiffness profiles E′ =40+4z and E′ =4z MPa were used; in (c) the corresponding profiles E_u = 50+5z and E_u =5z MPa were adopted. Both elastic and elastic-perfectly plastic analyses were run, for comparison. The expectation *a priori* was that analyses (a) and (e) would yield the same results, and that (b), (c) and (d) would be virtually identical to each other.

7.4.3 Results of analyses

The only type of result extracted for each analysis was the wall displacement profile (δ:z) at the end of excavation, as this was considered sufficient to demonstrate equivalence (or otherwise) of the total stress and effective stress approaches.

Elastic analyses

Regardless of soil stiffness profile, the δ:z profiles for (a) and (e) were indeed identical and reflected the long-term drained response; for example Fig. 7.11(a), which is for E′ = 4z. The profiles for (b), (c) and (d) were similarly equivalent to each other - all giving the short-term undrained wall displacement profile.

Elasto-plastic analyses

With $E' = 40+4z$, the δ:z profiles for (b), (c) and (d) were only approximately equivalent, with noticeable differences at some wall elevations, Fig. 7.11(b). The δ:z profiles for (a) and (e) were very different from each other, with greater movement and wall curvature shown in (e). Considering $E' = 4z$, the lack of agreement between δ:z profiles for (b), (c) and (d) was even more pronounced, but the discrepancy between (a) and (e) profiles was not quite so much.

7.4.4 Discussion and summary

The results from the elastic analyses confirmed what had been intuitively expected; namely that a coupled analysis with small Δt gives the same results as undrained/uncoupled analysis, and that a coupled analysis with large Δt gives the same results as drained/uncoupled analysis. However, the lack of agreement between coupled and uncoupled analyses in the presence of plastic yielding was unexpected (especially for the drained case). Had the coupled wall displacements been smaller than the uncoupled, it might have suggested that insufficient time had been allowed to elapse (i.e. the individual Δt and cumulative $\Sigma\Delta t$ were too small). But the reverse case was true, indicating that the drained/uncoupled analysis may <u>not</u> be an upper bound on calculated behaviour, and that the coupled analysis provides for different modes of behaviour and new possibilities.

A possible explanation is provided by the nonuniform volume changes which can occur throughout the domain during a coupled analysis. Excess pore water pressure are generated wherever there is the tendency for volume strain $\Delta\varepsilon_v$ - these excess pressures are normally relieved by drainage towards prescribed boundaries. Net water movement permits distortion (through continuity) and hence changes in effective stress σ'. If drainage was to formation level as well as to the original ground level, and/or the wall was assumed to be a partial drainage boundary, then different patterns of drainage would emerge, leading to different patterns of strain and stress change, and hence different permanent displacements.

Time has not permitted more detailed investigation of the reasons behind the phenomena observed herein. But the investigation has served a useful purpose by demonstrating that equivalence between coupled and uncoupled analysis cannot be guaranteed by making time steps large (or small) enough. This confirms the earlier findings of the writer (Woods, 1986) albeit for a very different type of boundary-value problem.

7.5 Horizontal Stresses

7.5.1 Introduction

Horizontal stresses are an important output quantity which a designer may wish to extract from a retaining wall analysis; perhaps to compare with a profile obtained from classical theory (e.g. Rankine). It is often emphasized that the simplified earth pressure distributions assumed in such theories bear little resemblance to those pertaining in practice - especially under working conditions. However, the use (and interpretation) of stresses from an FE analysis is far from clear-cut and it would be misleading if FE advocates were to claim otherwise. Stress in an element is a secondary quantity, in that it is derived from the primary solution (i.e. nodal displacements) through the relationship:

$$\Delta\sigma = \mathbf{D}\,\Delta\varepsilon = \mathbf{B}\,\mathbf{D}\,\Delta\mathbf{a} \tag{7.11}$$

It should be recalled that, in the FE (displacement) method, it is only the equilibrium of nodal forces which is required. The stresses inside any element may not necessarily be in equilibrium; i.e. they may not satisfy the differential equations of equilibrium, viz.:

$$\begin{aligned}
\frac{\partial\sigma_x}{\partial x} + \frac{\partial\tau_{xy}}{\partial y} + \frac{\partial\tau_{xz}}{\partial z} + F_x &= 0 \\
\frac{\partial\tau_{yx}}{\partial x} + \frac{\partial\sigma_y}{\partial y} + \frac{\partial\tau_{yz}}{\partial z} + F_y &= 0 \\
\frac{\partial\tau_{zx}}{\partial x} + \frac{\partial\tau_{yz}}{\partial y} + \frac{\partial\sigma_z}{\partial z} + F_z &= 0
\end{aligned} \tag{7.12}$$

Furthermore, stresses in neighbouring elements are not required to balance across mutual boundaries. Stress discontinuities often exist across these boundaries (and indeed can be used as an *a posteriori* check on the adequacy of mesh density). Equilibrium is satisfied in an average sense, however, through the nodal equilibrium equations:

$$\int_V (\mathbf{B}^T\mathbf{D}\mathbf{B})dV\,\mathbf{a}^e = \int_V (\mathbf{N}^T\,\mathbf{b})\,dV + \int_S (\mathbf{N}^T\,\mathbf{t})\,dA \tag{7.13}$$

The topic of horizontal stress can be considered to have two different perspectives - (i) the quality and reliability of the computed stresses, and (ii) the use and interpretation of such stresses in a design context. The investigation and discussion of the former (which is primarily of a numerical nature) takes place in the present chapter, whereas the latter is addressed in Chapter 8 (which deals with obtaining design output).

Three specific numerical problems relating to computed horizontal stresses have been identified in CRISP analyses of retaining walls:

a) tensile active stresses
a) passive pressure concentrations
c) horizontal stress oscillations

7.5.2 Tensile active stresses

For walls which are unpropped above final excavation level, "negative" bending moments (tension face on excavated side) sometimes occur in the upper portion of the wall. This implies the existence of tensile total stresses across the soil-wall interface on the retained side, which develop as the wall attempts to move towards the excavation. According to Powrie and Li (1990b), this effect is particularly pronounced when elastic-perfectly plastic soil models are used, and becomes worse with higher soil stiffness (E′). They state that the effect can be minimized by using the Schofield soil model, but were unsure if this was due mainly to the "no tension" cut-off, or pressure dependent stiffness (E′ α p′) incorporated in this model. A final point made by Powrie and Li is that although the transmission of tensile stresses can be prevented by the use of interface elements[8], this does not seem to overcome the problem of negative bending moments. This is probably because there is still downward shear on the back of the wall (present even if interface elements are used, where $\tau = c'_w + \sigma' \tan\delta'$).

7.5.2.1 Description of analyses

In order to examine in detail the conditions under which tensile active stresses can arise and the effect that they might have on dependent quantities, a series of undrained CRISP analyses has been carried out on an unpropped cantilever wall. (It was considered that an unpropped wall would give the most severe situation in terms of the tendency to develop tensile stresses.)

---

[8] interface elements themselves have to be used with caution as they have been known to cause other problems Powrie and Li (1990).

Mesh x10y10 was used, Fig. 4.1, so that mesh boundary location and element grading effects were minimized. The wall was installed "wished in place" and a sufficient number of increments were used for excavation (based on the findings of investigations reported in Chapter 6).

Soil parameter sets 12d and 13d (Table 4.8) were used, with $c' = 0$, 5, 20, 50 and 10^8 kPa (the last giving the elastic condition, and referred to hereinafter as $c' = \infty$). Undrained analyses were conducted first, with K_w set to 2×10^6 kPa ($\approx 100K'$) in order to give the optimum representation of undrained conditions. These were followed by fully coupled analyses to investigate the changes in horizontal stress as end-of-construction excess pore water pressures were allowed to dissipate. The changes to the original FE model were to:

a) convert soil elements to LSQp type
b) specify coefficients of permeability ($k_v = 1 \times 10^{-10}$ m/s ; $k_h = 4.k_v$ - typical of London clay)
c) impose initial drainage conditions (constant head) on remote boundaries
d) specify time steps Δt for each increment
e) create a drainage boundary at formation level at the end of excavation
f) allow dissipation of excess pore water pressures for 100 years

In step (c) the original ground level was impermeable until drainage to the excavated formation level was permitted - this allowed more direct comparison with the previous (uncoupled) undrained analyses up until the end of excavation, with excess pore water pressures then being released from that point onward. In step (d), Δt was set at 1m of excavation per day (therefore full excavation would take 8 days) - a typical speed for an underpass project, for example. Larger time steps would have led to significant drainage occurring during excavation, thus obscuring the comparison.

7.5.2.2 Results of analyses

If $\sigma_h < 0$, then it follows that $\sigma'_h + u < 0$, which means either that σ'_h and u are both negative -or that just one is negative (but is numerically larger that the other). Therefore, it will be necessary to examine all three quantities σ_h, σ'_h and u in attempting to discern the source of the tensile active stress phenomenon.

The results were extracted in the two different forms of (i) pressure distributions, and (ii) stress paths - during excavation and subsequent equilibration. Profiles of horizontal effective

stress σ'_h, pore water pressure u, and horizontal total stress σ_h over the upper portion of the wall were plotted and inspected, based on Gauss point values in the centre of the column of soil elements immediately behind the wall. Total and effective stress paths (σ_v:σ_h and σ'_v:σ'_h) were plotted at these same Gauss points, for the uppermost two elements. Many plots were thus produced; only a representative few are reproduced with this chapter to illustrate key points. Furthermore, stress paths from the coupled analyses showed more consistent trends than the uncoupled and so only these will be shown and discussed. The main findings were as follows.

Horizontal effective stress distribution

a) $E'_o > 0$

With $c' = \infty$ (elastic) σ'_h became negative over approximately the top 0.5m of the wall, dropping as low as -20 kPa at the completion of bulk excavation, Fig. 7.12(a). During equilibration, σ'_h dropped to -70 kPa (significantly more than during excavation) and was negative down to 4m. As c′ reduced to zero, σ'_h actually began to increase from the in-situ value over the top 3m of wall, whilst still reducing below this depth, changing in such a way that the post-excavation profile was at an almost constant value over this depth (and was positive everywhere), Fig. 7.12(b). During equilibration, the σ'_h profile reduced by between 25-75 kPa and was negative over the top 1.5m, reaching a minimum of -50 kPa.

b) $E'_o = 0$

With $c' = \infty$, σ'_h dropped only a small amount ($\leq$ 10 kPa) from its in-situ value during excavation, and remained positive at all depths. During equilibration, however, the top 4m of the σ'_h profile became negative, with a minimum value of -25 kPa. As c′ dropped to 0, the change in σ'_h during excavation switched from one of reduction to one of increase above the in-situ value and thus moved away from the tensile region. There was a significant reduction in effective stress during equilibration, but σ'_h remained positive at all stages post-excavation.

Pore water pressure distribution

a) $E'_o > 0$

With $c' = \infty$ (elastic) pore water pressures showed marked oscillation, becoming negative down to a depth of 5m, and averaging about -20 kPa at the end of excavation. At the end of equilibration, pore water pressures returned almost to the in-situ profile (actually, slightly less

than $u_o(z)$ on account of steady-state seepage occurring around the wall). As c′ reduced to 0, the post-excavation oscillation became less pronounced, but u was negative down to 6m, Fig. 7.13(a). Average pore pressures at the end of excavation were more negative in the coupled analysis than in the uncoupled (-60 compared with -25 kPa), thus putting in doubt the equivalence of the two different approaches. In the long term, pore water pressures again dropped to slightly less than $u_o(z)$ due to seepage.

b) $E'_o = 0$

Uncoupled pore water pressures in the elastic case again showed marked oscillation about the $u_o(z)$ line, but remained positive always. However, the coupled analysis showed negative end-of-excavation pore water pressures (around -35 kPa), though without oscillation. Reducing c′, the oscillations remained but the average value shifted towards the negative until, at $c' = 0$, there were some peaks (-15 kPa) within the top 2m, Fig. 7.13(b). Pore pressures in the coupled analysis dropped to -60 kPa at the end of excavation. In the long term, a profile just less than $u_o(z)$ was recovered once again.

Horizontal total stress distribution

a) $E'_o > 0$

With $c' = \infty$, as a consequence of what happened to σ'_h and u, σ_h was negative over the top 1m, reaching a maximum of -50 kPa at crest level by the end of excavation, Fig. 7.14(a). In the long term, following dissipation of excess pore water pressures, σ_h varied linearly from -60 kPa to 0 over the top 2.5m of the wall. This profile was not too different to that achieved at the end of excavation, suggesting that total stress varied little during equilibration. As c′ reduced to 0, post-excavation tensile stress at the top of the wall virtually disappeared, with σ_h being positive at nearly all points. In the long term, σ_h was negative over only the top 1m of the wall, with a minimum value of -50 kPa.

b) $E'_o = 0$

With $c' = \infty$, σ_h was positive at all depths in the uncoupled analysis, and simply oscillated ±10 kPa about the in-situ profile $\sigma_{vo}(z)$. In the coupled analysis σ_h dropped to a small negative value ($\approx$ -10 kPa) between 0-2m and remained there during equalization, Fig. 7.14(b). As c′ reduced to 0, σ_h always remained >0 in the uncoupled analysis, though continued to oscillate and tended to reduce from the in-situ value below 2m depth. In the coupled analysis σ_h

dropped from σ_{ho} to approximately zero over the top 2m, increasing back to substantial positive values during equalization, but always < σ_{ho}.

Effective stress paths

a) $E'_o > 0$

With $c' = \infty$, effective stress paths (ESPs) during excavation were generally at constant mean effective stress (s′) following a gradient of $\Delta\sigma'_v:\Delta\sigma'_h \approx 1:-1$, as required by elastic theory. During equalization, ESPs were generally inclined at $\Delta\sigma'_v:\Delta\sigma'_h \approx -1:-1$ to -1:-3 depending on depth below crest, showing major reductions in σ'_h. With $c' = 50$ kPa, all excavation ESPs were again almost all constant s′, because of the significant elastic region; an example is shown in Fig. 7.15(a). As c′ reduced, the ESPs progressively became very different - the constant s′ portion gradually reduced in length and switched over to approximately constant stress difference t′ ($\Delta\sigma'_v:\Delta\sigma'_h \approx 1:1$), as plastic yield occurred at lower deviatoric stresses. During equilibration, ESPs retraced themselves first and then continued dropping at a shallower gradient ($\Delta\sigma'_v:\Delta\sigma'_h \approx -1:-2$), probing well into the negative quadrant of stress space. For points deeper below ground, ESPs increased in σ'_v before falling parallel to the excavation path.

At $c' = 0$, the excavation ESP indicated the onset of yield as it crossed the isotropic line, well below the prescribed active failure line (i.e. $\sigma'_h = K_a\sigma'_v - 2c'\sqrt{K_a}$); for example Fig. 7.15(b). This looked intuitively wrong, from a 2D plane strain viewpoint - which does not take account of τ_{xy} and σ'_z in determining yield. Recalling the Mohr-Coulomb yield function as coded in CRISP (Eqn 5.10) the analyses were checked by substituting output values of σ'_x, σ'_y, σ'_z and τ_{xy} into the function. This did indeed evaluate to zero at the point indicated on the ESP, and remained at approximately zero as yield continued, thus verifying this part of the code.

b) $E'_o = 0$

With $c' = \infty$, all excavation ESPs were constant s′ with $\Delta\sigma'_v:\Delta\sigma'_h \approx 1:-1$, switching to -1:-2 during pore pressure equilibration, Fig. 7.15(c). As c′ reduced to 50 kPa, then 20, 5 and 0, ESPs started off as constant s′ but then began to turn to $\Delta\sigma'_v:\Delta\sigma'_h \approx 2:1$ as yield commenced at a progressively earlier stage - particularly in Gauss points near the top of the wall; an example is in Fig. 7.15(d). Equilibration ESPs for $c' \rightarrow 0$ first relaxed in σ'_h and then ran down parallel to the excavation ESP, but generally staying in the positive quadrant of σ_v: σ_h space.

Total stress paths

a) $E'_o > 0$

With $c' = \infty$, total stress paths (TSPs) during excavation at the top six Gauss points nearest the ground surface were quite variable in the uncoupled analysis, proceeding in different directions. They were more consistent in the coupled analysis. The uppermost Gauss point showed the TSP diverging from the ESP during excavation to give large negative pore pressure changes, at a gradient $\Delta\sigma_v:\Delta\sigma_h \approx -1:-2$; see Fig. 7.15(a). During equilibration, TSPs were relatively short, and were of the order $\Delta\sigma_v:\Delta\sigma_h \approx 2:-1$ (perpendicular to, and shorter than, excavation TSPs). Reducing c' to 0, TSPs converged on the ESPs, intersected them, and then kept falling at $\Delta\sigma_v:\Delta\sigma_h \approx -1:-3$; Fig. 7.15(b). During equilibration, TSPs rejoined the ESPs before dropping at $\approx -1:-2$ to the long term equilibrium point.

b) $E'_o = 0$

With $c' = \infty$, excavation TSPs showed a predominant reduction in σ_h, falling at -1:-3; as seen in Fig. 7.15(c). As c' reduced to 0, TSPs during excavation were very similar to the elastic case ($c' = \infty$). During dissipation of excess pore pressures, TSPs showed an increase in σ_h (not quite to the initial value) plus some increase in σ_v; Fig. 7.15(d).

7.5.2.3 Discussion and summary

The development of tensile total stresses behind the wall arises from the combined response of the effective stresses and pore water pressures. There is no evidence that the constitutive law has been violated, as the stress state is well within the yield locus defined by the shear strength parameters (where appropriate). The effect is more pronounced with higher E'_o and when there is a significant elastic region, confirming the observations of Powrie and Li (1990b).

What are the practical consequences? Taking $E'_o > 0$ and $c' = \infty$ as an example, a crude calculation shows that the bending moment at a depth of 2.5m below the top of the wall would be approx. ½ × 2.5m × -60kPa × 2/3 × 2.5m = -125 kN-m/m. Whilst this is not a particularly large value, the effect of these tensile horizontal stresses on wall bending moment becomes amplified further down the wall, as the lever arm increases. For instance, at dig level, the moment effect would be ½ × 2.5 × -60 × (2.5 × 2/3 + 5.5) = -537 kN-m/m.

7.5.3 Passive pressure concentrations

Soil elements closest to the wall on the excavated side (just below final dig level) have been known to exhibit high horizontal effective stresses, after the removal of elements to simulate excavation. It appears to be possible to obtain stress states outside of the specified failure envelope near soil surfaces where the soil has undergone swelling. This phenomenon has been observed in elasto-plastic retaining wall analyses with CRISP by Clarke and Wroth (1984), Ponnampalam (1990), and Powrie and Li (1990b). The writer has observed it in various analyses, including most of those reported in Appendix A. It can also be seen in the results obtained by Rodrigues (1975) and Creed (1979) for other FE codes - this is particularly noteworthy because these codes were wholly elastic and did not incorporate plastic yielding.

A typical distribution of horizontal stress on the passive (excavated) side following excavation is shown in Fig. 7.16. It is evident that the element immediately in front of the wall just below the excavated surface has some rather severe restraints imposed on it; it is in contact with a more rigid material, there may be high shear stresses on the soil-wall interface, and formation level propping (if present) may impose limitations on how much vertical movement (swelling) can take place. The virtual incompressibility imposed by an undrained analysis may also be part of the problem, as it imposes further restraint on possible displacement patterns. It may also be that, if stress states are moving outside the failure envelope, too few increments are being used to allow yielded states to come back onto the yield surface (see Section 3.3.8 for a description of how CRISP does this).

A useful starting point in unravelling the problem is to consider the approximate total stress paths followed by this element (or different points within it). The major change of total stress experienced by the element is that of vertical unloading, accompanied by some increase in horizontal stress. The former component is unequivocal and arises from overburden removal, whereas the latter (which is harder to quantify) is caused by the wall tending to move outward following excavation. The horizontal component $\Delta\sigma_h$ could be expected to lie between the limits $0 \leq \Delta\sigma_h \leq \Delta\sigma_v$, as shown in Fig. 7.17(a). Total stress paths are shown in both σ_v:σ_h space (better suited to showing field conditions) and t:s space (more useful for distinguishing deviatoric and mean stress components).

Sketching effective stress paths requires a knowledge of pore pressure response, and a convenient way of doing this is to use pore pressure parameters written in invariant form[9], leading to $\Delta u = b(\Delta s + a.\Delta t)$. For a fully saturated soil then $b = 1$; if the soil is also elastic then $a = 0$, and the change in pore pressure is equal to the change in mean stress Δs. For the case of $\Delta\sigma_h = 0$, Δs is negative and the effective stress path converges with the total stress path. If $\Delta\sigma_h = \Delta\sigma_v$, Δs is zero and the effective stress path is parallel to the total stress path. Consequently, the effective stress path is the same in both cases, Fig. 7.17(b). In the absence of any yield criterion, it can be seen that as the effective stress path approaches the σ_h axis, high horizontal stresses (passive pressure concentrations) are predicted as the vertical stress tends to zero.

If the soil is permitted to yield, however, the parameter "a" is no longer zero but will depend on whether the soil skeleton tends to dilate ($a < 0$) or collapse ($a > 0$) on shearing. If a Mohr-Coulomb criterion is assumed, the yield (failure) envelope can be added to both σ_v:σ_h and t:s space. As noted in Chapter 5, the classical Mohr-Coulomb model in CRISP assumes normality which implies strong dilation with $\psi = \phi'$. At yield the tendency would be for $\delta\varepsilon^p_v < 0$, but in an undrained situation it is not possible to have $\delta\varepsilon_v \neq 0$, $\therefore \delta u = K_w.\delta\varepsilon_v = K_w.(\delta\varepsilon^e_v + \delta\varepsilon^p_v)$. Because $\varepsilon_p >> \varepsilon_e$, the strongly negative $\delta\varepsilon^p_v$ will produce negative δu, which means that σ'_n (or more generally, p′ or s′) must increase and the stress state will migrate along the Mohr-Coulomb envelope, Fig. 7.17(c). The absolute pore pressure will reduce until the total and effective stress paths meet; further reduction will create a negative absolute pore pressure. The key point, however, is that effective stresses can continue to rise - apparently unchecked. They will do so in such a way that high horizontal stresses (passive pressure concentrations) can, again, be sustained at low vertical stress - though not as much for wholly elastic soil.

7.5.3.1 Description of analyses

The above reasoning was tested by examining the stress paths in the element(s) where the passive pressure concentrations arise. Specifically, this has been done through a series of undrained analyses of an unpropped cantilever wall; the same analyses as were used in the previous section on tensile active stresses. The only difference is that the profiles of σ'_h, u,

---

[9] Attributed to Henkel by Naylor *et al* (1984), and differing from the more familiar parameters A and B due to Skempton (1954) which are based on principal stress changes and are more appropriate to triaxial test conditions.

and σ_h were extracted from the central column of Gauss points in the elements adjacent to the wall on the passive side (0.5m from the wall), below formation level (FL). Effective and total stress paths were considered in the element just below FL (element "x" in Fig. 7.16a), at the shallowest Gauss point. As before, both uncoupled analyses (excavation only) and coupled (excavation and equilibration) were performed. Finally, profiles and stress paths on sections a little further from the wall (at 1.5m and 2.5m) were also examined, for comparison purposes.

7.5.3.2 Results of analyses

It was found that results for $E' = 40+4z$ (set 12d) and $E' = 4z$ (set 13d) were very similar, and so the following comments on the results are applicable to both stiffness profiles. Significant differences between the uncoupled analyses and fully coupled analyses were observed by the end of excavation - largely due to pore water pressure distributions in the uncoupled analysis being much more oscillatory (discussion on this is deferred to Section 7.5.4). As in the precious section, many plots were created but only a few are reproduced here.

Horizontal effective stress distribution

With $c' = \infty$ (i.e., elastic) σ'_h increased to +300 kPa ($\approx 2 \times \sigma'_{ho}$) just below FL at the end of excavation, Fig. 7.18(a). Following the dissipation of excess pore water pressures, σ'_h increased further to +480 kPa ($\approx 3.5 \times \sigma'_{ho}$). At $c' = 0$, the maximum value of σ'_h post-excavation was +380 kPa, Fig. 7.18(b), though the profile didn't fall away quite so much with depth. The peak reduced a little to +340 kPa after pore pressure equilibration, but stood out very sharply as an anomaly because $\sigma'_h \approx -100$ kPa at the Gauss point immediately beneath.

At 1.5m and 2.5m from the wall, post-excavation profiles showed no peak just below FL; in fact σ'_h values increased with depth regardless of the value of c'. In the long term, the values of σ'_h either increased a little ($c' = \infty$) or dropped a lot ($c' = 0$) over the first 2m below FL.

Pore water pressure distribution

With $c' = \infty$, pore water pressures in the uncoupled analysis showed marked oscillation post-excavation, with a large positive value of approx. +200 kPa ($\approx 2.5 \times u_o$) just below FL, but with -100 kPa at the next two Gauss points further down, Fig. 7.19(a). The coupled analysis had the same maximum value of +200 kPa post excavation, but very little oscillation with depth. As c' reduced to 0, the post-excavation oscillations remained in the uncoupled analysis,

but the large positive pore pressure disappeared and the first 3m of the profile was in the negative region, averaging around -300 kPa just below FL. In the coupled analysis, pore pressures were negative over the first 2m of the profile, with a minimum value of -130 kPa, Fig. 7.19(b). Regardless of c′, the final pore pressure profile at the end of equilibration was almost hydrostatic (du/dz just less than γ_w) in accordance with steady seepage conditions.

Some distance from the wall, pore pressures generally reduced by a greater amount during excavation. With $c' = \infty$, the profile was always positive, but with $c' = 0$ it was negative down to 4m, being -125 kPa at FL[10]. Post-dissipation, profiles were virtually identical to those adjacent to the wall.

Horizontal total stress distribution

After excavation with $c' = \infty$, σ_h increased to +480 kPa ($\approx 2 \times \sigma_{ho}$) just below FL, with the (uncoupled) profile oscillating about $\sigma_{ho}(z)$, Fig. 7.20(a). The coupled analysis showed a similar peak value but no real oscillation, Fig. 7.20(b). After excess pore pressure dissipation, this peak value remained the same; in fact, the whole profile showed little change during equilibration. When $c' = 0$, the whole profile dropped <u>below</u> $\sigma_{ho}(z)$ following excavation, though the fall was greater in the uncoupled analysis than in the coupled, which showed $\sigma_h \approx \sigma_{ho}$ at the top Gauss point, and $\sigma_h(z) \approx \sigma_{ho}(z)$ - 30 kPa elsewhere. Following equilibration, σ_h peaked at +340 kPa in the Gauss point below dig level, but σ_h values at greater depths were well below post-excavation values (up to +200 kPa lower).

Further from the wall, post-excavation profiles were very different from those near to the wall over the first 2m in the elastic case ($c' = \infty$), though again showed little subsequent change during dissipation. When plastic yield was allowed ($c' = 0$), post-excavation profiles were not much different from those near to the wall over the first 2m, whereas long term profiles were very different - the large peak in σ_h seen adjacent to the wall was not present 2.5m away.

Effective stress paths

With $c' = \infty$ in the coupled analysis, the ESP (at Gauss point just below FL) showed increasing σ'_h with little change in $\Delta\sigma'_v$ for the first three-quarters of the excavation, after which much

---

[10] In practice, cavitation would limit negative pore water pressure to -101.25 kPa, but CRISP does not apply any such limit.

larger changes occurred at constant s′ ($\Delta\sigma'_v:\Delta\sigma'_h \approx -1:1$), Fig. 7.21(a). During dissipation of excess pore pressure, the ESP moved at ≈1:1 (constant t′), converging on the corresponding TSP, after which they both showed a small increase in horizontal stress. As c′ reduced to 0, the constant s′ portion disappeared and the path switched to $\Delta\sigma'_v:\Delta\sigma'_h \approx 1:2$, as yield occurred at an earlier stage of excavation. During equilibration, the ESP travelled straight to the origin, where it joined the corresponding TSP. Both paths then subsequently climbed together at a slope of 2:3 (following the passive failure line), maintaining a small pore water pressure.

Further from the wall, the elastic case ($c' = \infty$) showed the ESP straightening out to become constant s′ throughout the excavation stage, followed by constant σ'_v during equilibration. With $c' = 0$, the trend essentially comprised both σ'_v and σ'_h increasing at 1:3 during excavation, initially backtracking at -1:-3 during the dissipation stage, and finally climbing at 1:3 - returning almost to the start point, Fig. 7.21(b).

Total stress paths

In the fully elastic case, the excavation TSP near the wall just below FL broadly showed a major increase in σ_h with $\Delta\sigma_v \approx 0$, Fig. 7.21(a). During dissipation of excess pore pressure, the TSP moved at ≈ -1:-1 to converge with the ESP (as noted above when describing the ESP). As $c' \rightarrow 0$, yield became more significant and the TSP showed a reduction in σ_v (and $\Delta\sigma_h \approx 0$ overall) by the end of excavation. Much larger stress changes occurred during equilibration - both σ_h and σ_v fell approximately to zero (at -1:-3), before rising (at 1:2) to large positive values approximately the same as those pertaining at the end of excavation.

Further from the wall, the TSP just below FL for the elastic case was largely one of reducing σ_v (at almost constant σ_h) during excavation, switching to a path of increasing σ_h (at constant σ_v) during pore pressure dissipation. With $c' = 0$, σ_v and σ_h both reduced at a ratio of -2:-1 during excavation, followed by reducing σ_h (at constant σ_v) during equilibration, as the TSP converged on - and joined - the ESP, Fig. 7.21(b).

7.5.3.3 Discussion and summary

Overall, it is clear that peak σ_h (and σ'_h) can develop in both fully elastic and elasto-plastic cases - though much higher values can be sustained in the former (in the absence of any limit on stress). Away from the wall, high σ_h do not develop when $c' = 0$; there is a continual

reduction in the $\sigma_h(z)$ profile through the excavation and equilibration stages. But with $c' = \infty$, high positive values of σ'_h can still be sustained 2-3m from the wall, with the long-term $\sigma'_h(z)$ greater than the in-situ profile.

The pore water pressure response depends heavily on whether or not yielding occurs - full elasticity causes a big increase in pore water pressure during excavation whereas yielding causes a massive reduction, indicating strong dilation. However, the post-excavation $\sigma'_h(z)$ are considerably greater in the latter case, and subsequent equilibration to the same long term u(z) profile means that high σ_h develops in both cases.

The high values of σ'_h at shallow depth could be due to mechanisms of overconsolidation. Consider, for example, one-dimensional excavation to 8m depth over a large area, using the same parameters listed in Section 7.5.2.1. At 0.1m below FL, $\sigma'_{vo} = 8.1x(\gamma-\gamma_w) = 81$ kPa, $\sigma'_{vf} = 0.1x(\gamma-\gamma_w) = 1$ kPa, and hence $OCR = \sigma'_{vo} / \sigma'_{vf} = 81$. Using Parry's (1982) proposal that $K_o = K_{nc}(OCR)^{\phi}$ gives $K_o = 3.928$. But even with this large K_o, to generate the very high σ'_h values seen in the FE analyses would require substantial σ'_v. In the early analyses with $c' = \infty$, σ'_v dropped from +80 to -60 kPa by the end of excavation, and then climbed to +60 kPa during equilibration; on the other hand, with $c' = 0$, σ'_v rose from +80 to +190 kPa after excavation, then fell to 0 before climbing to +215 kPa at the end of equilibration. The analyses show that these large σ'_v actually do occur in the FE model, although this seems unreasonable at shallow depths.

The evolution of σ'_x ($= \sigma'_h$), σ'_y ($= \sigma'_v$), σ'_z, τ_{xy}, u, K_o, B, and *f* (yield function) during the analysis was studied by plotting each quantity against increment number. These plots showed that the out-of-plane stress σ'_z did not change much during the analysis, and so probably did not have much of a role in the observed phenomena. Shear stress τ_{xy} did, however, increase from 0 to 100 kPa by the end of excavation, indicating significant rotation of principal stresses at this Gauss point. K_o rose from 2.00 to 7.66 in the elastic case, but dropped from 2.00 to 1.55 in the elasto-plastic case. B, which is the ratio $(\sigma'_2 - \sigma'_3)/ (\sigma'_1 - \sigma'_3)$, started at 1.00 and dropped to 0.39 (elastic), and from 1.00 to 0.20 (elasto-plastic).

7.5.4 Lateral stress oscillations

In Section 7.3.3 a form of stress oscillation was described in the context of problems arising with the effective stress method of analysis. These oscillations were in the horizontal effective stresses on a vertical section just behind the wall on the active side. A different form of oscillation is that seen when horizontal effective stress is plotted on a horizontal section at a fixed elevation on the active side. Such a profile is useful when studying the variation of horizontal stress as the wall is approached laterally from a distant point, and was first reported by Kutmen (1986).

Kutmen carried out an important study in which CRISP was used to investigate the installation effects of diaphragm and bored pile walls. He was particularly interested in the horizontal total and effective stresses acting on the wall/pile before, during and after the installation process. The analyses were coupled-consolidation, elastic-perfectly plastic - plane strain for the diaphragm wall, and axisymmetry for the bored pile[11]. In the axisymmetric case, Kutmen observed that the horizontal effective stresses showed oscillations on a lateral profile - particularly in the element immediately adjacent to the wall, Fig. 7.22. (The lateral profiles given by Kutmen for the plane strain case are also far from smooth).

Kutmen likened his findings to those of Naylor (1974), who found similar oscillations using 8-node quadrilaterals in the analysis of nearly incompressible elastic materials. A significant difference between Kutmen's and Naylor's analyses was that the former was using a coupled-consolidation formulation, but with small time steps this is essentially modelling a nearly undrained event. It is the difficulty of modelling zero volume change (especially in axisymmetry) which would appear to be at the heart of the problem. Undrained axisymmetry is notorious for causing poor results in a different context - that of obtaining good estimates of collapse loads for circular footings (Sloan and Randolph, 1982). Solutions to such difficulties tend to focus on the use of reduced integration techniques, higher order elements (such as the 15-node cubic strain triangle), or finite elements with "mixed" variables such as displacements and mean normal stresses. In effect, coupled-consolidation is an example of the latter, where unknown displacements are mixed with excess pore water pressure. Kutmen's results show

---

[11] In an axisymmetry analysis, only a single bored pile is being analyzed rather than a row of piles forming a wall.

that stress oscillation is not completely suppressed by using a coupled formulation, but in comparison with Naylor's results the oscillation is confined to the element adjacent to the wall.

In view of the amount of previous investigation of this form of stress oscillation, it can be considered that the causes and remedies for it are reasonably well established. The vast majority of retaining wall analyses will assume plane strain conditions, where (on the basis of Kutmen's observations) the problem is not so acute. Reduced integration is not an option in the commercially available versions of CRISP, and 15-noded triangles are probably excessive for retaining wall analysis. A compromise solution would appear to be to use a coupled formulation (which is often the case anyway) together with elements immediately adjacent to the wall having a thickness in the range 50-100% of that of the wall.

It is unfortunate that a case of considerable importance to geotechnical engineers (i.e. the undrained response) is known to be troublesome in a numerical context. However, the measures which need to be taken to avoid serious problems and inaccuracies are not onerous. The particular issue here, namely that of lateral stress oscillations, is likely to have more implications for how earth pressure distributions are inferred from a finite element retaining analysis of a wall, and this is considered further in the next chapter.

7.6 Solution Scheme

7.6.1 Introduction

As described in Section 3.3.8, CRISP uses an incremental (tangent stiffness) solution scheme. For elastic-perfectly plastic models, corrections are applied to elements that have yielded in order to bring the stress state back to the yield surface. For the critical state family of models no such correction is carried out as the process would be considerably more complex and has been found to be unstable (Britto and Gunn, 1987)[12]. It is therefore relatively easy to produce an invalid analysis using CSSM models in CRISP unless the increment size is sufficiently small.

---

[12] Britto and Gunn point out that others report to have had no difficulty in applying iterative techniques to critical state models (e.g. Zienkiewicz *et al.*, 1975; Potts, 1981), but that they (along with Naylor, 1975) have encountered problems both with convergence and with attempting to recover known analytical solutions.

The alternative, which has been adopted by other geotechnical FE codes (for example, ICFEP and VISAGE) is to use an iterative solution strategy such as modified Newton-Raphson (MNR), which can provide good solutions with only a few increments per loading stage. However, there is an analogy here with the debate concerning low versus high order elements. High order elements offer better accuracy and, in principal, fewer (larger) elements would be needed in an analysis to yield a given level of accuracy. However, in some problems the size of element will be dictated by the complexity of the geometry and larger numbers of (smaller) low order elements will be called for. In other words, a practical consideration may negate the need for (or diminish the benefit of) a level of sophistication in a particular part of the model.

A similar argument may apply to non-linear solution strategies. Consider the example of an embedded cantilever wall retaining a deep excavation in soil of highly non-linear stiffness. With an FE package which uses an iterative scheme, the excavation could be modelled as one load step, within which many tens (or hundreds) of iterations could take place until some predefined convergence tolerance was satisfied. The wall deformations etc. at the end of excavation could be expected to be correct, as the iterative scheme would ensure that the material non-linearity was catered for properly. The user can predefine the level of accuracy which will be acceptable, and the program will return the desired results (if possible). With an FE package using an incremental scheme (such as CRISP), the same excavation would be split up into a number of smaller increments within which linear behaviour was assumed. Without performing tests of the sort described in Chapter 6, the analyst cannot be sure that he/she has chosen sufficient increments to achieve the desired accuracy. This is a clear case where an iterative scheme would win over an incremental.

However, the excavation may involve several intermediate stages, with props being installed/removed, anchors being placed and prestressed. Most designers would wish to plot wall movements, etc., at the intermediate stages as well as final dig level, and this would require a number of load stages (or increment blocks) regardless of solution scheme. The multi-stage nature of the analysis lends itself quite naturally to the incremental method. Certainly, within each stage the iterative method will always offer an extra level of confidence, but the advantages are not so persuasive as with the single-stage deep excavation.

It is possible to conduct a crude study into incremental versus iterative solution with CRISP, by making use of the load correction facility in conjunction with the elastic-perfectly plastic

models. The basis of the load correction was described in Section 3.3.8, but one feature which has not been discussed in any depth hitherto is that of "load increment factors".

In CRISP, the effects of applied loads, changing geometry, etc., in an increment block are spread over the increments in that block. If there are N increments, the default is that each increment experiences (1/N)th of the total load change in that block. In other words, the load change is distributed uniformly between the increments. However it is possible to specify the proportion that each increment will experience through a list of load ratios or increment factors, R_i, where $\Sigma R_i = 1$. For example, in a block which had 5 increments, any of the following might be used:

a)	.2	.2	.2	.2	.2	← *(the default)*
b)	.1	.3	.4	.1	.1	
c)	.45	.25	.15	.1	.05	
d)	.01	.05	.14	.3	.5	

One choice which is, perhaps, not so obvious is the following:

e)	1.	0.	0.	0.	0.

This would have the effect of forcing MNR-type iterations in the 2nd to 5th increments of the block, following the load change which has taken place in the 1st increment. To make this clearer, consider scheme (a). If there were any out-of-balance (OoB) loads at the end of increment 1, they would be applied as correcting loads in increment 2, *in addition to* the 1/5th of the total load which is to be applied. Any OoB loads at the end of increment 2 would similarly be applied as correcting loads in increment 3, in addition to the load increment already specified, etc. However, in scheme (e), any OoB loads at the end of increment 1 will be applied as correcting loads in increment 2, and would be the <u>only</u> load applied in that increment. Any further (hopefully much smaller) OoB loads at the end of increment 2 will be applied as correcting loads in increment 3, again being the only load applied in that increment. If applying all the load in one increment was thought too severe, suitable alternative increment factors might be:

(f)	.5	.5	.0	.0	.0
(g)	.33	.33	.34	.0	.0
(h)	.4	.3	.2	.1	.0

7.6.2 Description of analyses

To investigate the influence of load ratios upon the outcomes of a retaining wall analysis, a short series of analyses was conducted. Mesh x10y10 was used with two different load ratio schemes - ULR (uniform load ratios) and NLR (nonuniform load ratios), defined as follows:

$$\text{ULR:} \quad R_i = 1/N \quad \text{for } i = 1 \text{ to } N \tag{7.14}$$

$$\text{NLR:} \quad R_i = 1 \quad \text{for } i = 1; \quad = 0 \quad \text{for } i = 2 \text{ to } N \tag{7.15}$$

where N is the number of increments in the block (= NINC in CRISP terminology)

The wall was wished in place and the analyses were run only as far as the excavation stage; the soil types, propping configurations, and numbers of blocks and increments used are summarized below:

Run	Soil type	Prop	Drainage	No. of excav^{n} blocks	No. of increments per block	Total no. of increments
SC102_1	12	none	undrained	1	1, 2, 4, 8, 16, 32	1, 2, 4, 8, 16, 32
SC103_4	13	none	undrained	4	1, 2, 4, 8	4, 8, 16, 32
SC103_8	13	none	undrained	8	1, 2, 4, 8	8, 16, 32, 64
SC152_1	12d	none	drained	1	1, 2, 4, 8, 16, 32	1, 2, 4, 8, 16, 32
SC152_8	12d	none	drained	8	1, 2, 4, 8, 16	8, 16, 32, 64, 128
SC162_1	12d	top	drained	1	1, 2, 4, 8, 16, 32	1, 2, 4, 8, 16, 32
SC162_8	12d	top	drained	8	1, 2, 4, 8, 16, 32	8, 16, ... 128, 256

NB: soil type 13 with one excavation block was numerically unstable

7.6.3 Results of analyses

The results extracted for these brief studies were wall displacement profile (δ:z) at the end of excavation, and the variation of horizontal equilibrium error (err_x) throughout the analysis.

Undrained analyses

SC102_1 : (See Fig. 7.23) For the ULR case, significant changes in the δ:z profile were observed up to NINC=8, after which changes were imperceptible and the profile could be considered to have converged on the final result. Equilibrium error err_x was 2% if only one

increment was used in the excavation block, reducing to 0.5% or less with NINC≥8 - but the error was always >0 and never completely disappeared.

For NLR, convergence of the δ:z profiles was much more rapid and only took 2 increments - the profile for NINC=4 was indistinguishable from that for NINC=32. The profile with only 2 increments was more accurate than that for the ULR analysis with 4 increments - yet took only half the computational effort. Equilibrium error err_x was <0.5% for NINC≥2, and virtually zero for NINC≥8. Of course, having zero stress residuals is not in itself a sufficient condition (the analysis may have converged on the wrong answer if the model is otherwise deficient), but it is a necessary condition. The err_x v increment plots show that the additional increments reduce err_x .

SC103_4 : (See Fig. 7.24) This run needed at least 2 increments per block, otherwise the analysis failed (regardless of load ratio scheme). Using ULR, differences in the δ:z profiles were still apparent between 4 and 8 increments per block (i.e. 16 and 32 total increments), with err_x never dropping below 0.1%. However, with the NLR scheme, only 4 increments per block were sufficient for an accurate δ:z profile, and for err_x to reduce to zero. As with run SC102_1, the NLR analysis with only 4 increments was more accurate than the ULR with 8 increments.

SC103_8 : Differences in the δ:z profiles were only apparent up to 4 increments/block with the ULR scheme, at which point err_x was very small. With excavation being in relatively fine layers (8 × 1m thick), the NLR analyses gave results which were indistinguishable from the ULR.

Drained analyses

SC152_1 : Starting with the ULR, big changes in the δ:z profiles were evident, even between 16 to 32 increments per block; equilibrium error err_x steadily worsened throughout the analysis and was barely below 2% by the end. Switching to NLR, the changes in the δ:z profiles (between the different numbers of increments) were just as big, although err_x <2% for NINC≥4. Another observation was that wall displacements were much bigger than for ULR analyses when comparing results for similar numbers of increments - probably because this unpropped cantilever wall is unstable under drained conditions (as noted in earlier chapters).

SC152_8 : With ULR, noticeable changes were evident in the δ:z profiles, even up to 16 incs/block; equilibrium error err_x steadily increased through each of the analyses but was always < 1% for NINC≥8 per block. Using NLR, changes in the δ:z profiles were even bigger than in ULR; err_x <1% for NINC≥4. Wall displacements in NLR were greater than those in ULR using twice the number of increments ($\delta_{NLR(NINC)} > \delta_{ULR(NINC/2)}$), therefore offering an improvement for no extra computational time.

SC162_1 : (See Fig. 7.25) Differences between the δ:z profiles were observed all the way up to 32 increments/block for ULR; err_x steadily worsened throughout each analysis, but was always <1% for NINC=32. Some change in δ:z profiles between 8 and 16 increments/block were observed for NLR, but little between 16 to 32, so once again NLR has produced more rapid convergence. For NINC≥4, err_x <1%.

SC162_8 : Using ULR, some increase in δ:z profiles between 4 → 8, 8 → 16, and 16 → 32 increments/block was observed; err_x was always < 1% for NINC≥4, but always tended to increase throughout each analysis. With an NLR scheme, some improvement could be seen in the δ:z profiles between 4 and 8 increments/block, but very little thereafter. Equilibrium error err_x iterated to zero fairly quickly once NINC≥8.

7.6.4 Discussion and summary

Common practice, as perceived by the writer, is for ILDF=0 and a ULR scheme to be used. A good test for sufficiency of NINC would appear to be to rerun the analysis with ILDF=1 and NLR [1, 0, 0, ...0]. In elastic-perfectly plastic (Tresca yield criterion), major changes in δ_{max} will be detected if number of increments (and/or number of increments per block) is too small. Even bigger changes in the elastic-perfectly plastic (Mohr-Coulomb yield criterion) will be observed, when the wall and support configuration are inherently on the limit of stability. Even with top-propping, and a good number of increment blocks, switching to ILDF=1 will reveal if NINC is insufficient..

The definition of NLR given by Eqn 7.15 is not unique, and it could be that other weightings may be optimal. Consequently four additional non-uniform load ratio schemes were examined with run SC152_1, spanning between NLR and ULR as follows:

NLR	1	0	0	0	0	0	0	0
↓	1/2	1/2	0	0	0	0	0	0
	1/3	1/3	1/3	0	0	0	0	0
	1/4	1/4	1/4	1/4	0	0	0	0
	1/5	1/5	1/5	1/5	1/5	0	0	0
ULR	1/8	1/8	1/8	1/8	1/8	1/8	1/8	1/8

A variation on SC162_1 was devised, in which each of the above schemes was implemented as run SC162_1R. The δ:z and err_x:inc plots, Fig. 7.26, confirmed that NLR [1, 0, 0 ...0] gave the best performance, and there was no evidence of an optimum configuration of weightings lying between ULR and NLR. To some extent this was slightly surprising because the original NLR was the most extreme, with all load applied in the first increment. However, this was a helpful finding and it suggested that it was unnecessary to search any further.

Two main conclusions can be drawn from these limited analyses (in the context of performing bulk excavation in front of a retaining wall). Firstly, using NLR leads to better (faster) convergence of the analyses when increasing the number of increments used in a block. Secondly, using NLR produces more accurate results than ULR for a given number of increments - indeed it can produce better results for substantially fewer increments. A test for sufficiency of number of blocks would be to vary the load ratios adopted - if there are sufficient, the analysis will not be sensitive.

7.7 Discussion and Summary

Errors in finite element analysis have many sources. Some arise at the programming stage and users have to recognize that "bug-free" software is very difficult to achieve. Systematic testing and benchmarking are essential with all "off the shelf" software, but even this may not trap any errors in the code. Other errors are totally in the hands of the user as they arise from mistakes in the input data, inappropriate use of the program, and/or poor modelling choices. Yet other errors may be machine dependent and thus beyond the control of programmer and user alike, but the onus is on the user to be aware of their existence and how significant they might be. There is some overlap; for example, poor choice of mesh can produce elements with high aspect ratio, leading to ill-conditioning. In a commercial setting, there is a risk that ill-conditioning will not be spotted, as no one is looking for it and its effects may be indistinguishable from genuine soil-structure interaction phenomena. Unless users acquire the habit of carrying out checks (re-running as purely elastic,

reducing stiffness of structural elements, etc) they may never be aware of the problem. Default operation in double precision is one solution, but it might create a false sense of security - and in many cases may be unnecessarily wasteful of computer memory.

Calculations of undrained loading using the effective stress method should be cross-checked with total stress analysis to ensure that an appropriate value for bulk modulus of water K_w has been selected. As the stiffness of soil frequently varies with depth, it would be better to specify the ratio K_w/K' to produce a uniformity of drainage response throughout the soil stratum concerned.

Coupled analysis provides an elegant means of modelling the full life-span of an embedded retaining wall and the surrounding soil, both during and after construction. It allows the designer to incorporate a realistic time-line in the analysis, and the ability to study the consequences of project delays, etc. However, attempts to benchmark against a non-coupled analysis need to be carefully considered so as not to draw potentially misleading conclusions. Undrained behaviour appears relatively straightforward to match, but faster rates of drainage (with respect to loading rate) are more difficult to equivalence.

Horizontal stresses, whether whole distributions or values at specific locations, can often appear unreasonable or counter-intuitive. This is particularly disappointing in a retaining wall context as earth pressure distributions play a big role in preliminary design (determining embedment depths, anchor loads, etc) and engineers believe that they have a good "feel" for them. However, it must be remembered that the finite element method requires equilibrium of forces (only) at the nodes, and that the computed stresses do not have to satisfy the differential equations of equilibrium. Anomalous stresses can be legitimate output in a theoretical sense, but clearly must be treated with caution when interpreting an analysis.

As soon as any form of non-linearity enters the finite element model, the solution scheme becomes important. The user needs to have a good grasp of the solution method in the program he/she is using; what size load steps should be used; what (if any) corrections and/or iterations can or will be applied - and how the user can control this - etc. Investigating the consequences of different choices (on the part of the user) is not difficult, and may provide valuable insight into the overall model - provided that genuine behaviour can be distinguished from that which is only apparent.

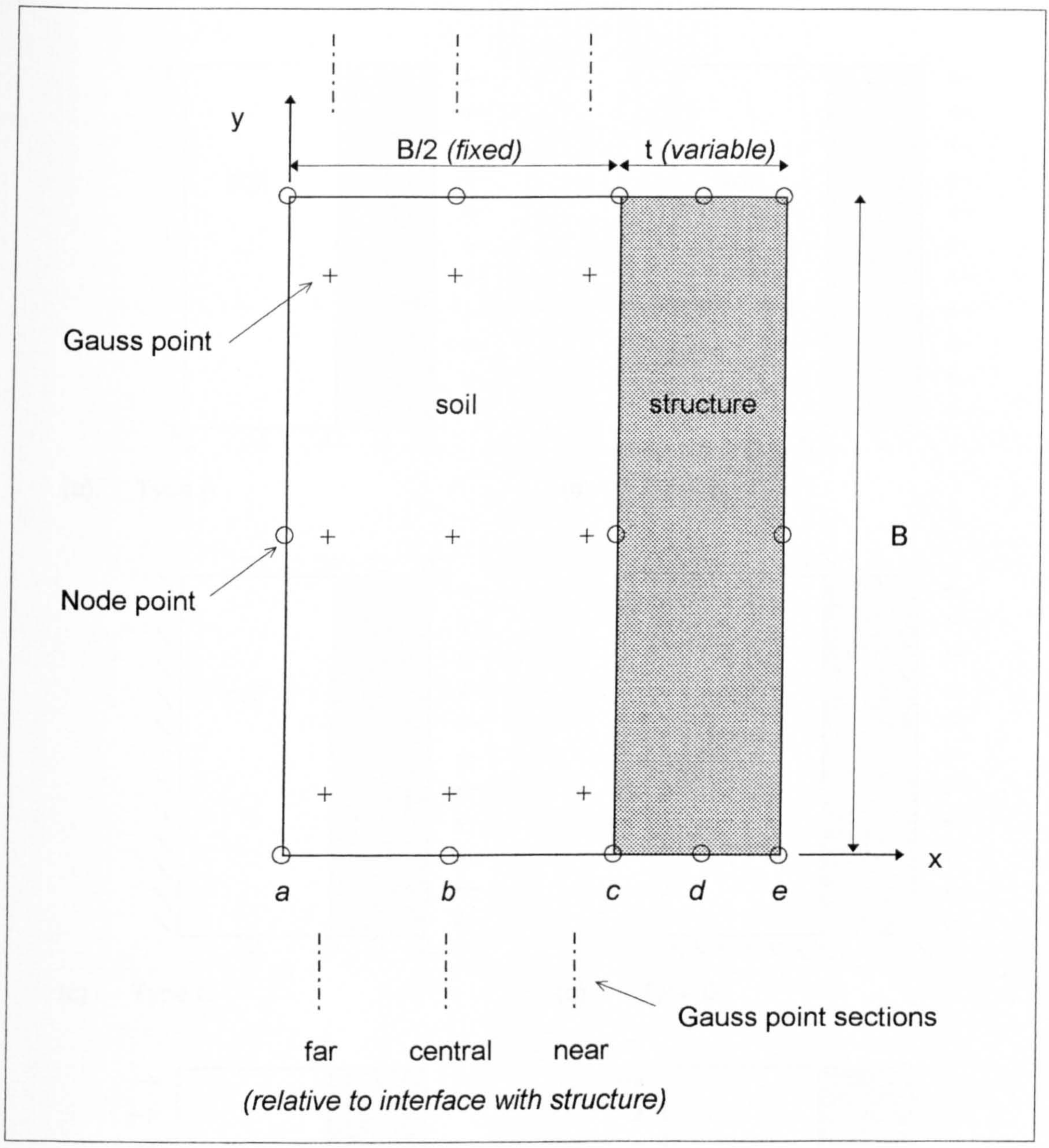

Fig 7.1 Simple two-element mesh used in studies of ill-conditioning

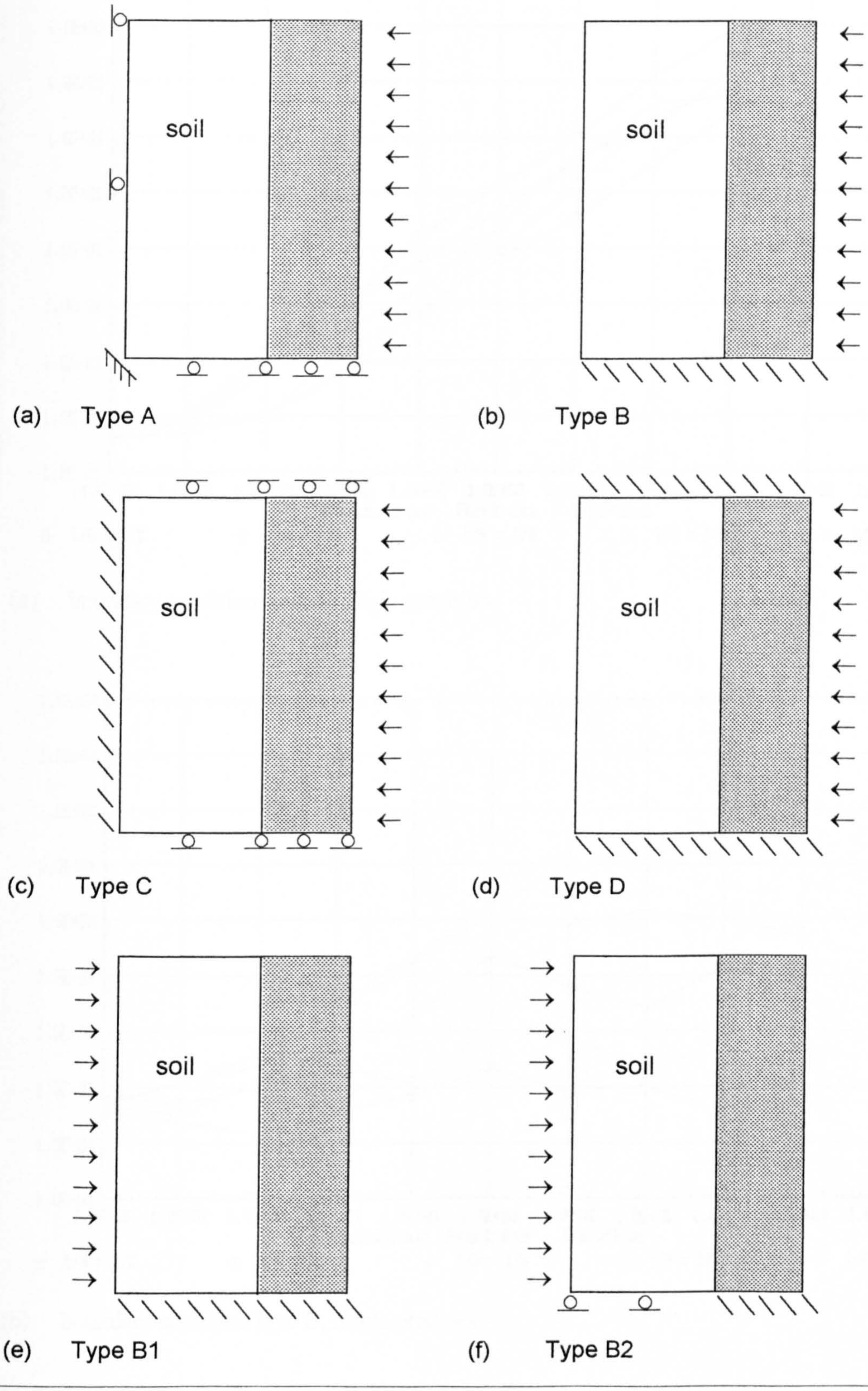

Fig 7.2 Boundary conditions for displacement and loading in two-element mesh

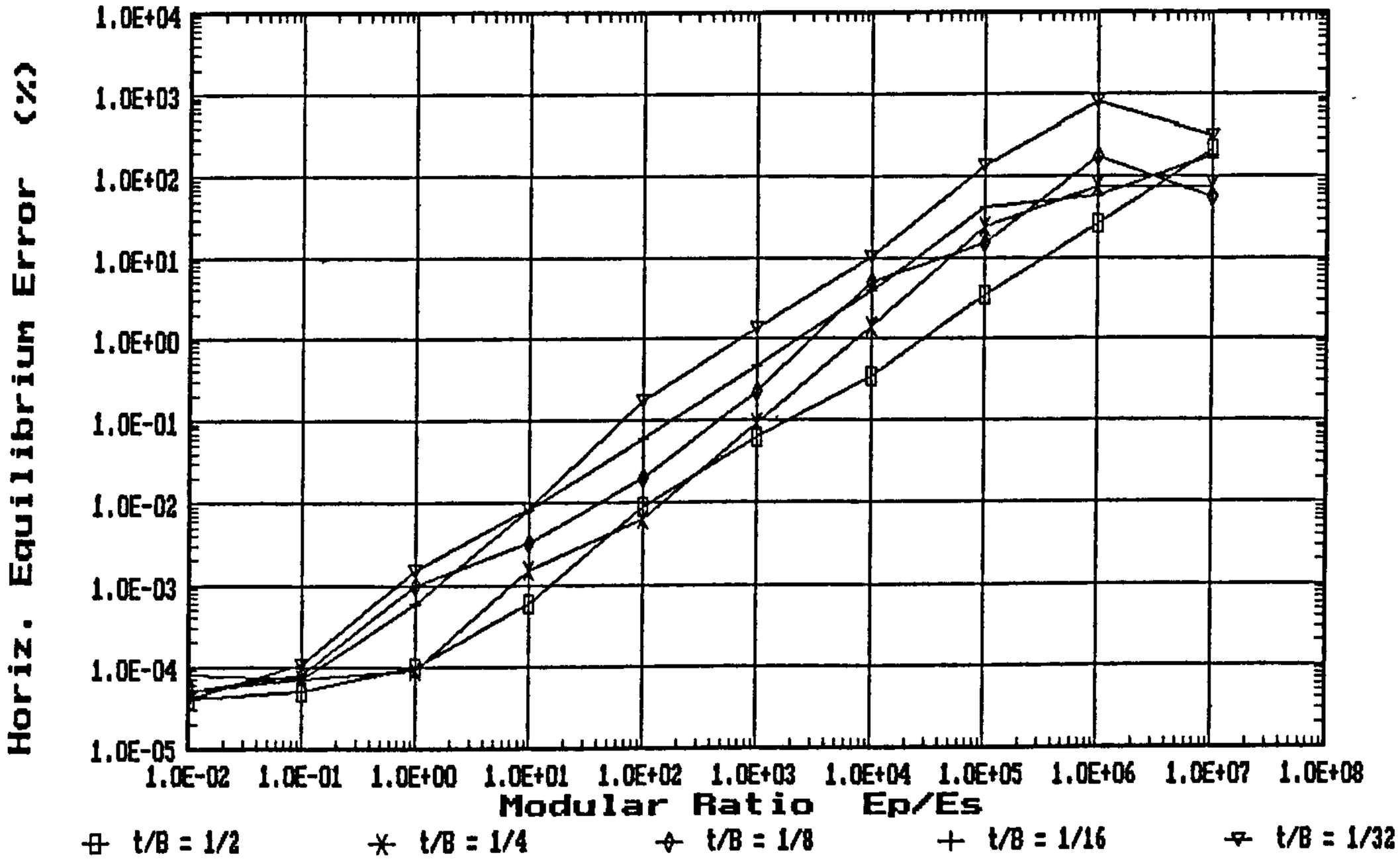

(a) boundary condition type A, single precision

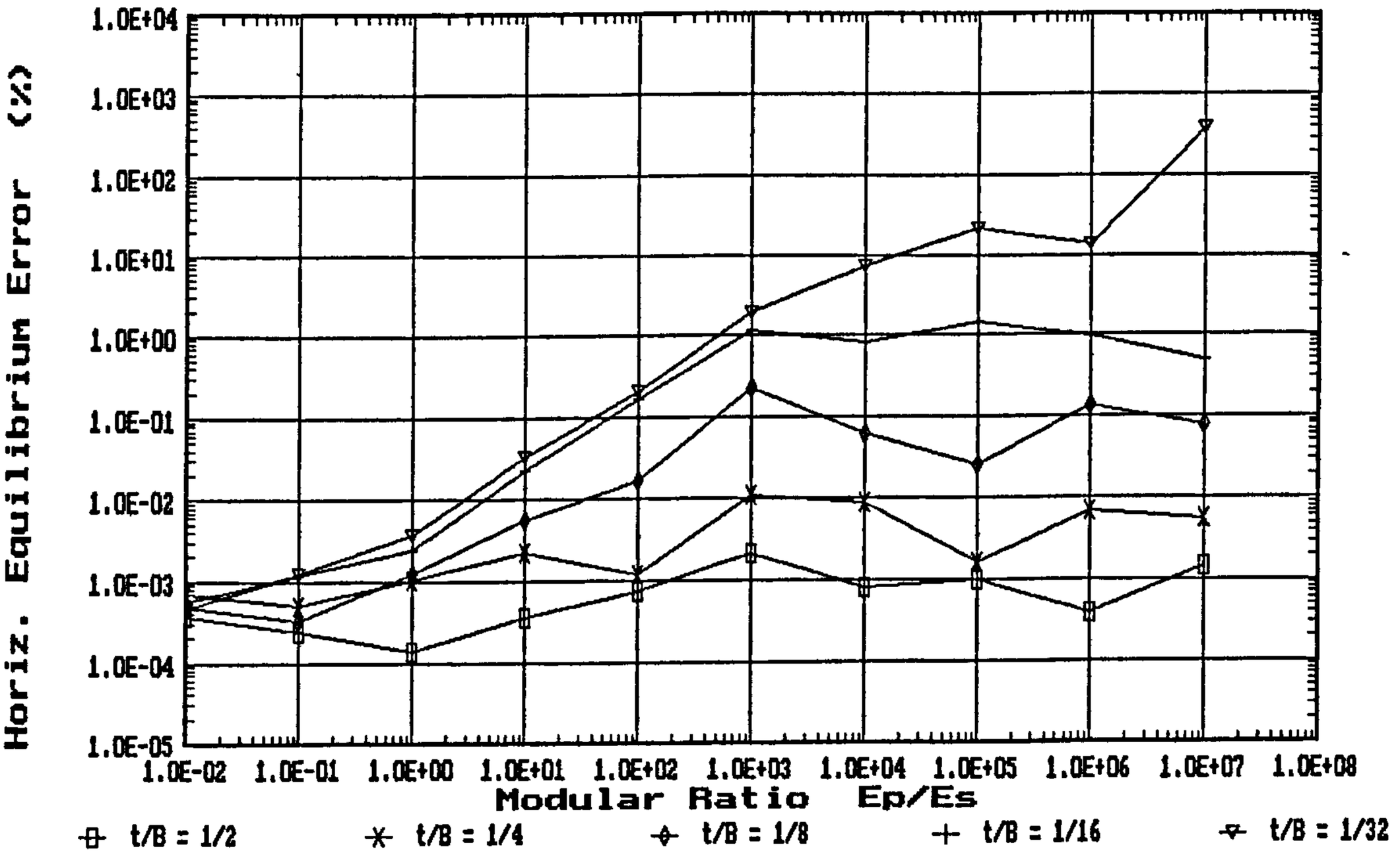

(b) boundary condition type B, single precision

Fig 7.3 Effects of ill-conditioning in two-element mesh: percentage equilibrium error against modular ratio, for different aspect ratios

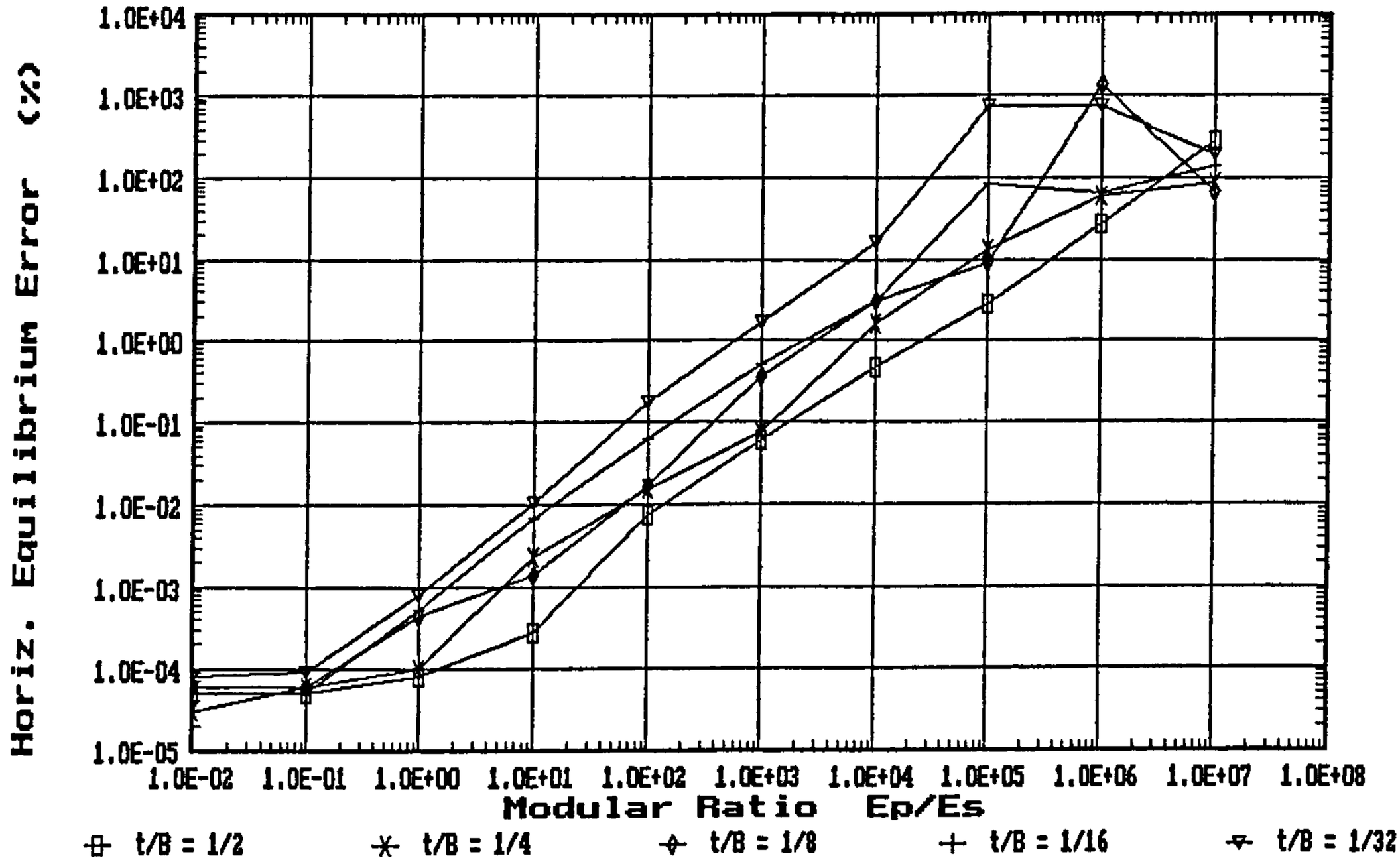

(c) boundary condition type C, single precision

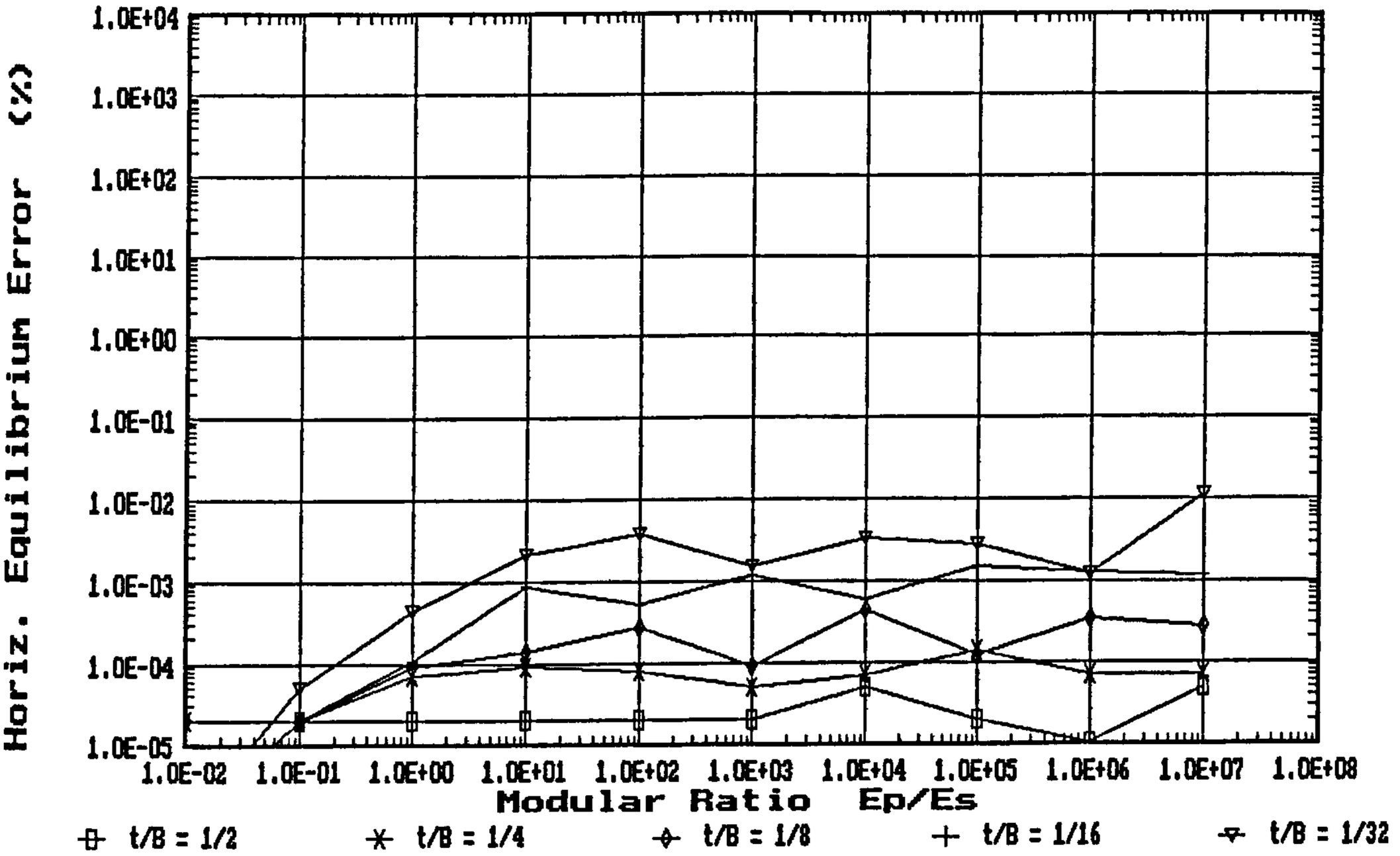

(d) boundary condition type D, single precision

Fig 7.3 Effects of ill-conditioning in two-element mesh: percentage equilibrium error against modular ratio, for different aspect ratios (contd)

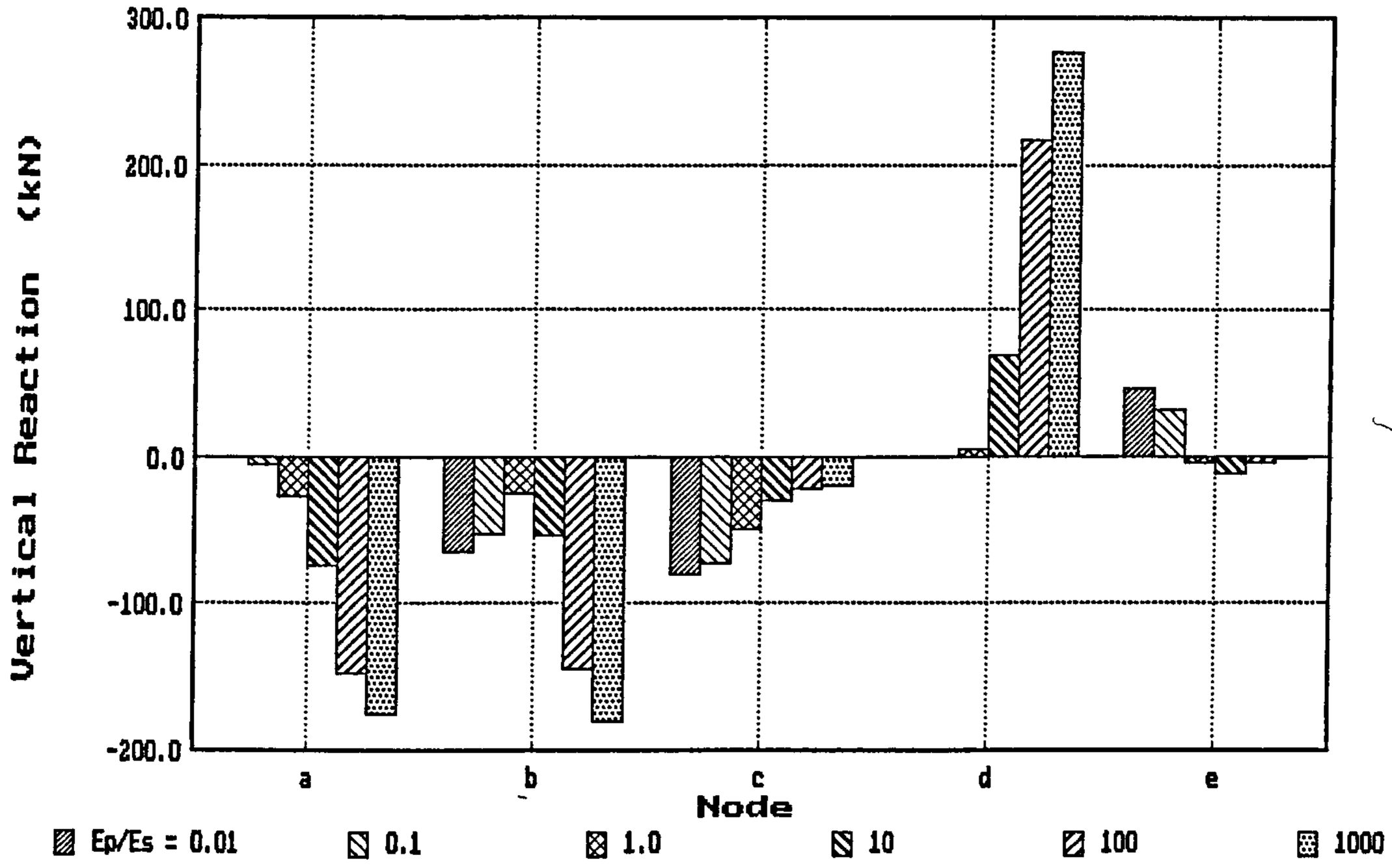

(a) boundary condition type B1, with t/B = 1/4

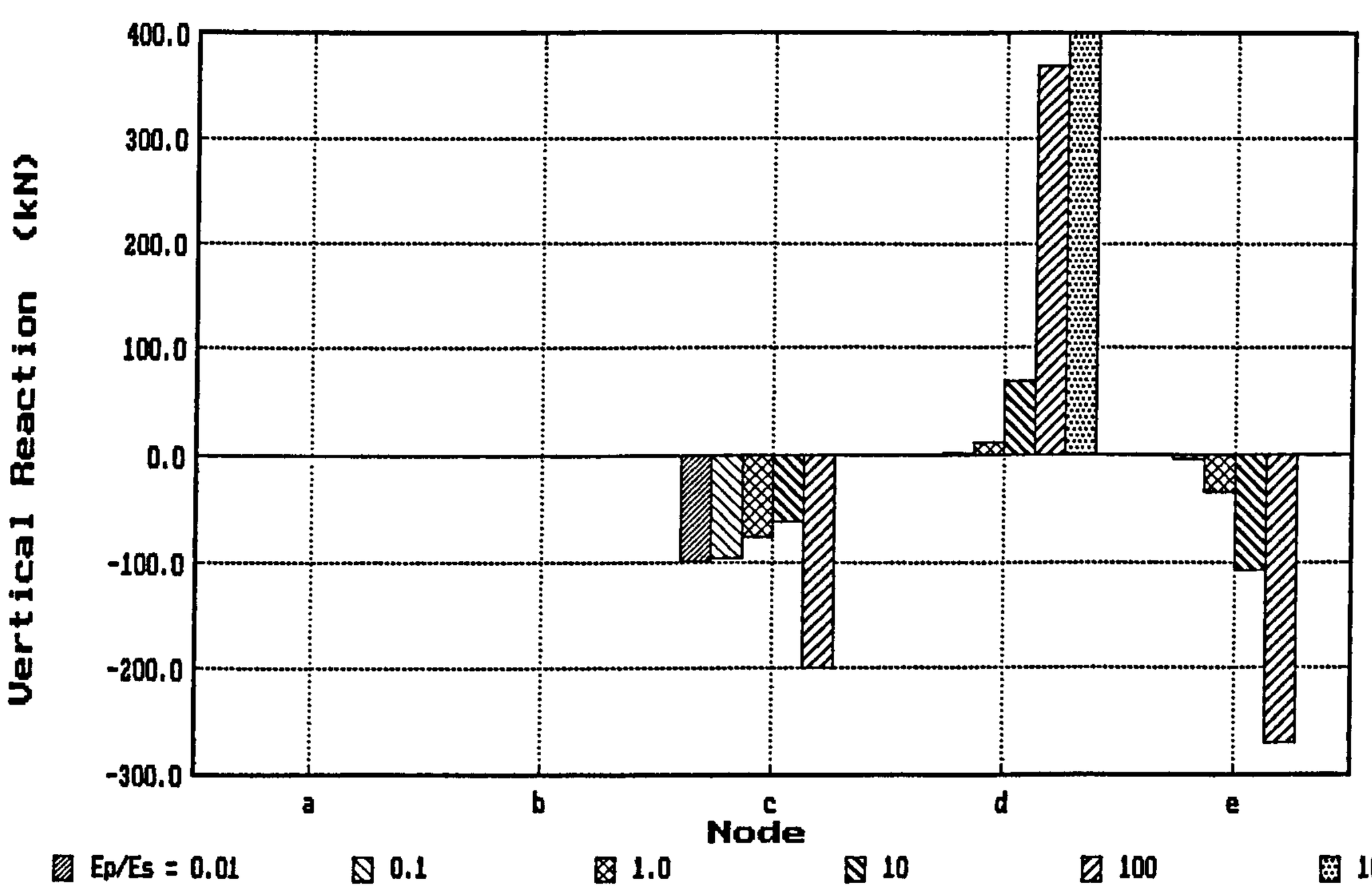

(b) boundary condition type B2, with t/B = 1/16

Fig 7.4 Effects of ill-conditioning in two-element mesh: distributions of nodal reaction along fixed element edge, for different modular and aspect ratios

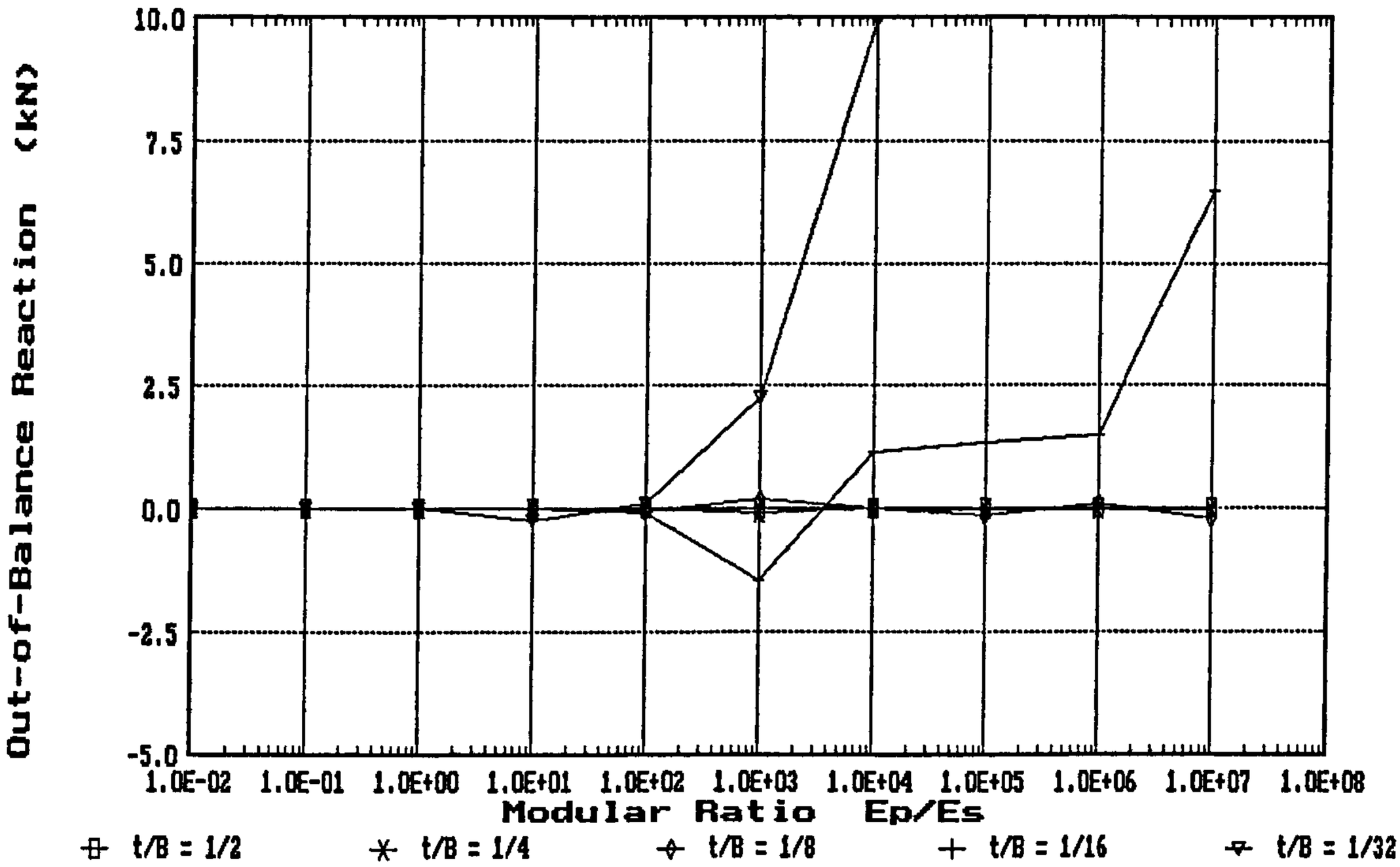

(a) boundary condition type B1

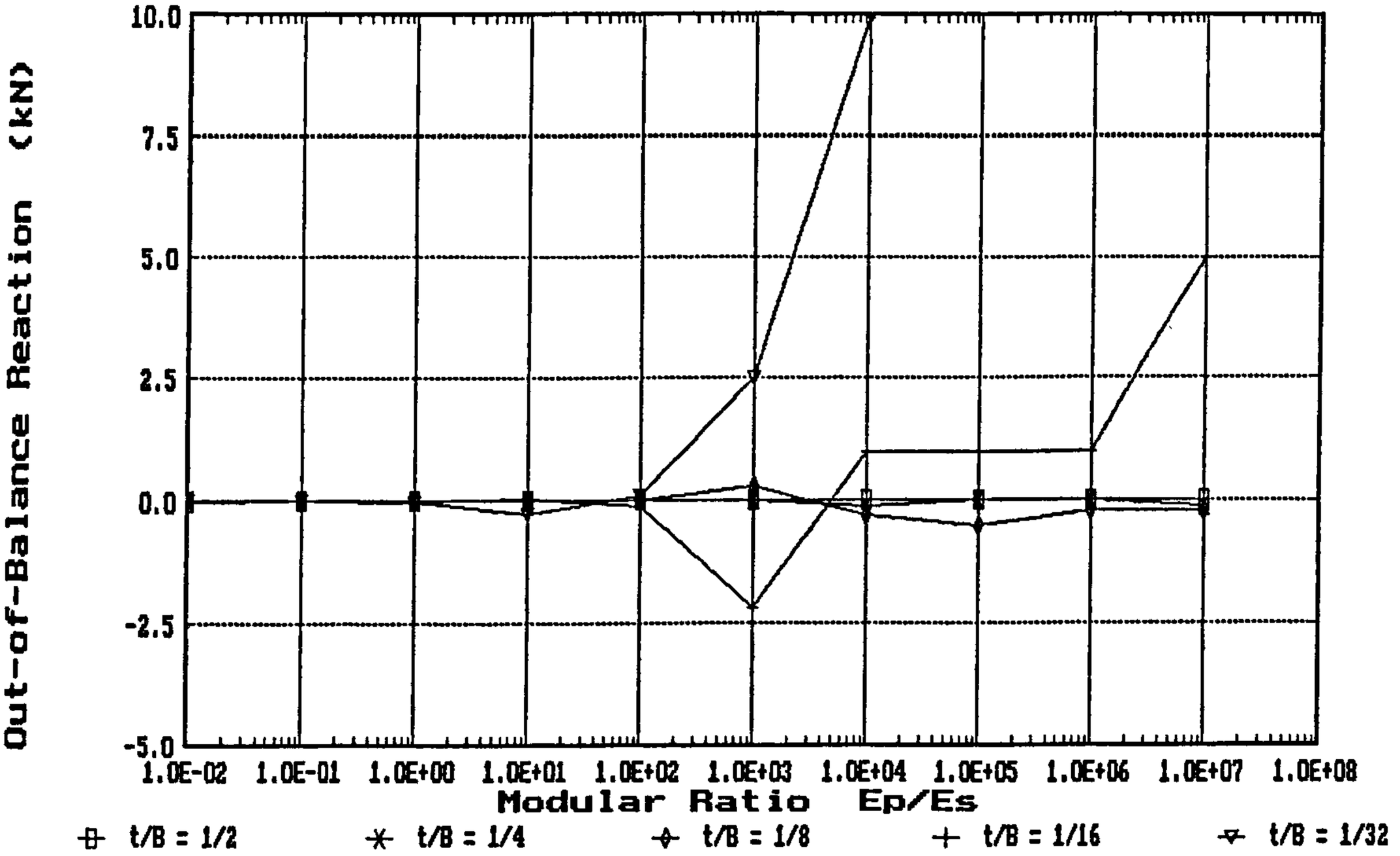

(b) boundary condition type B2

Fig 7.5 Effects of ill-conditioning in two-element mesh: total out-of-balance reaction against modular ratio, for different aspect ratios

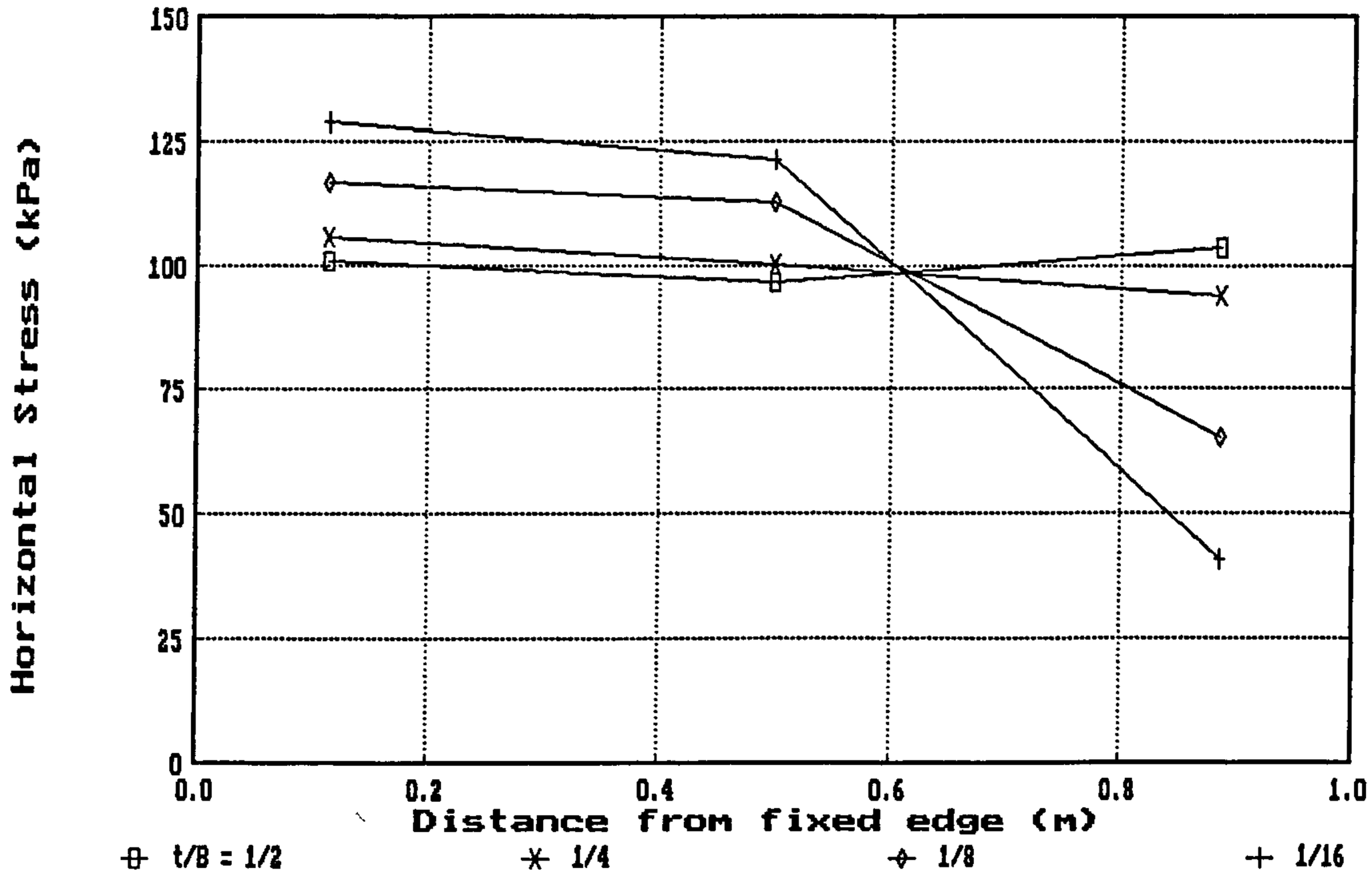

(a) Ep/Es = 1000, with different aspect ratios

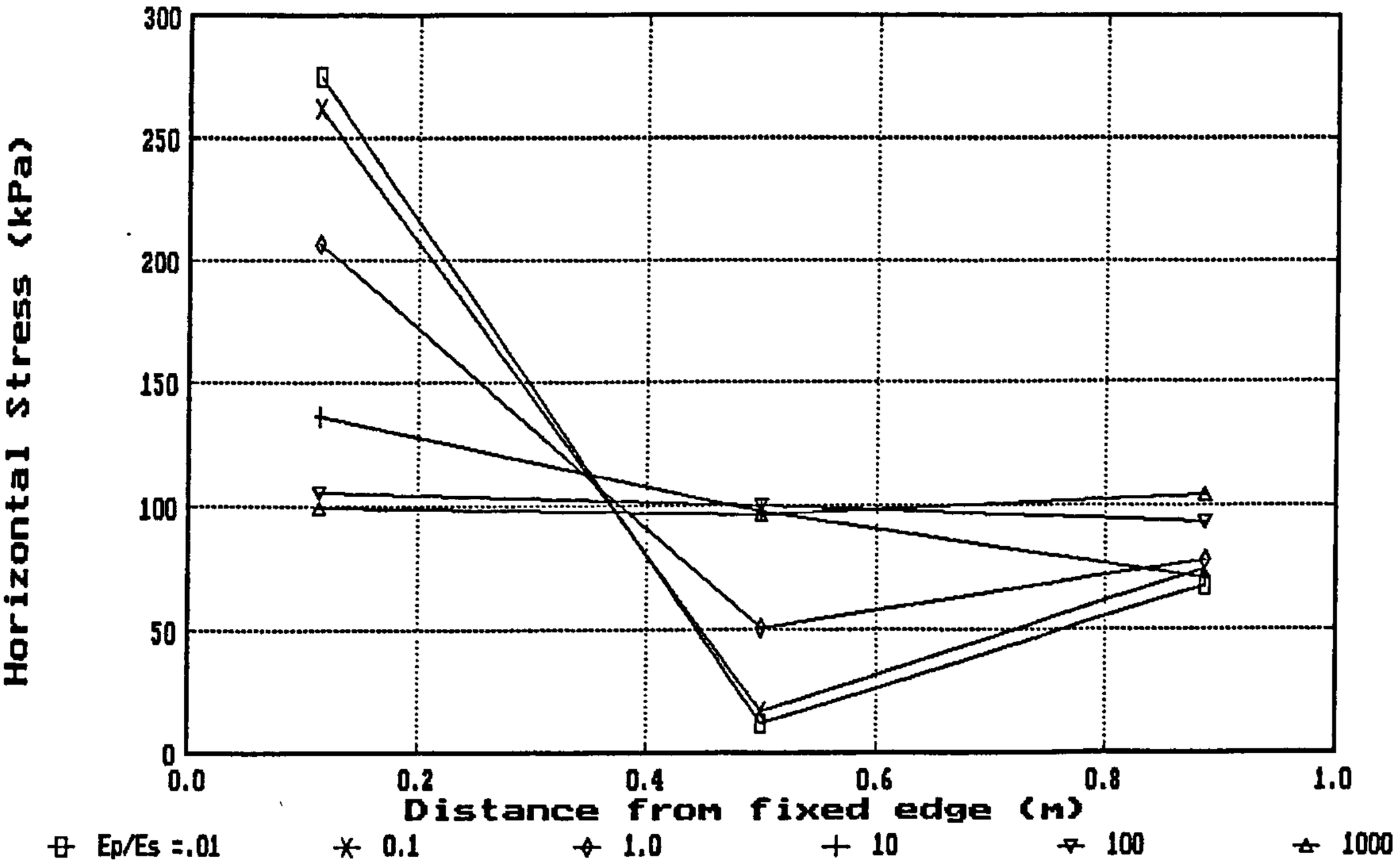

(b) t/B = 1/4, with different modular ratios

Fig 7.6 Effects of ill-conditioning in two-element mesh: horizontal stress distribution in soil on centre Gauss point section, for boundary condition type B2

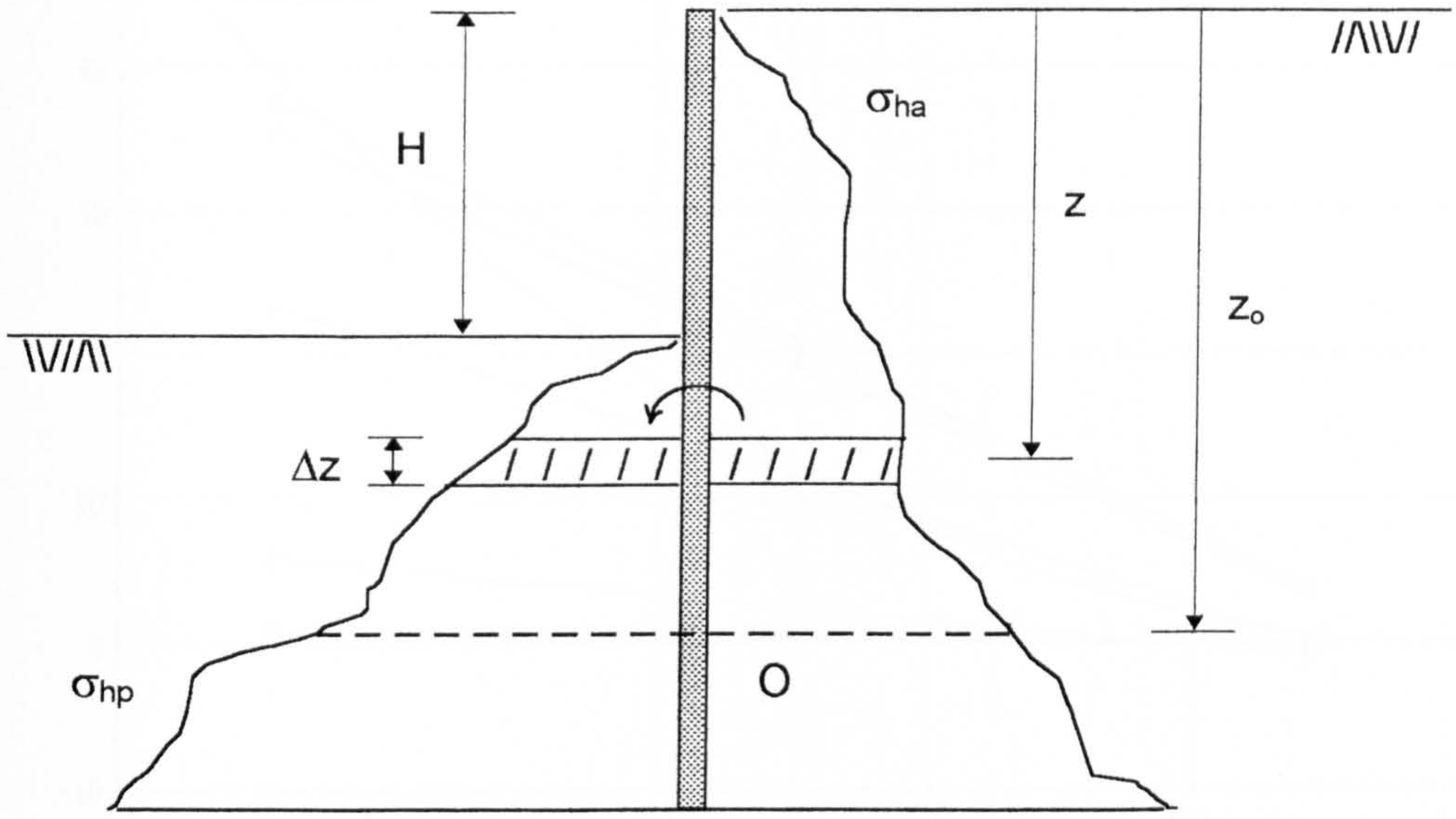

Bending moment about O (ignoring soil-wall shear stresses) is estimated as:

$$M = P_a L_a - P_p L_p$$

$$= \int_o^{z_o} \sigma_{ha} (z_o - z)\, dz - \int_H^{z_o} \sigma_{hp} (z_o - z)\, dz$$

$$\approx \sum_o^n \sigma_{hai} (z_o - z)\, \Delta z - \sum_o^m \sigma_{hpi} (z_o - z)\, \Delta z$$

(NB: $n = z_o / \Delta z$, $m = n - H/\Delta z$)

Fig 7.7 Approximation of wall bending moment from horizontal soil stresses

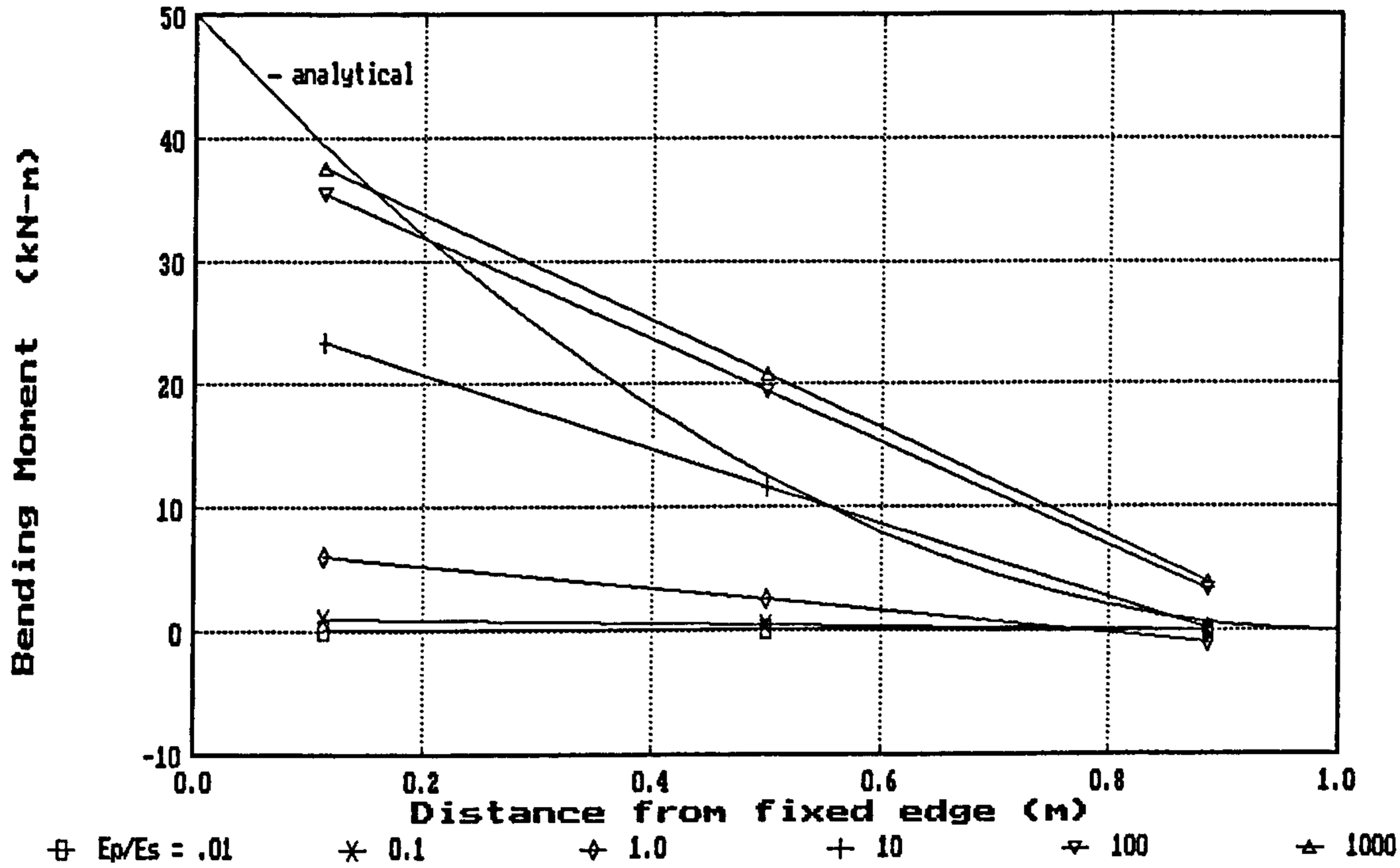

(a) aspect ratio t/B = 1/2

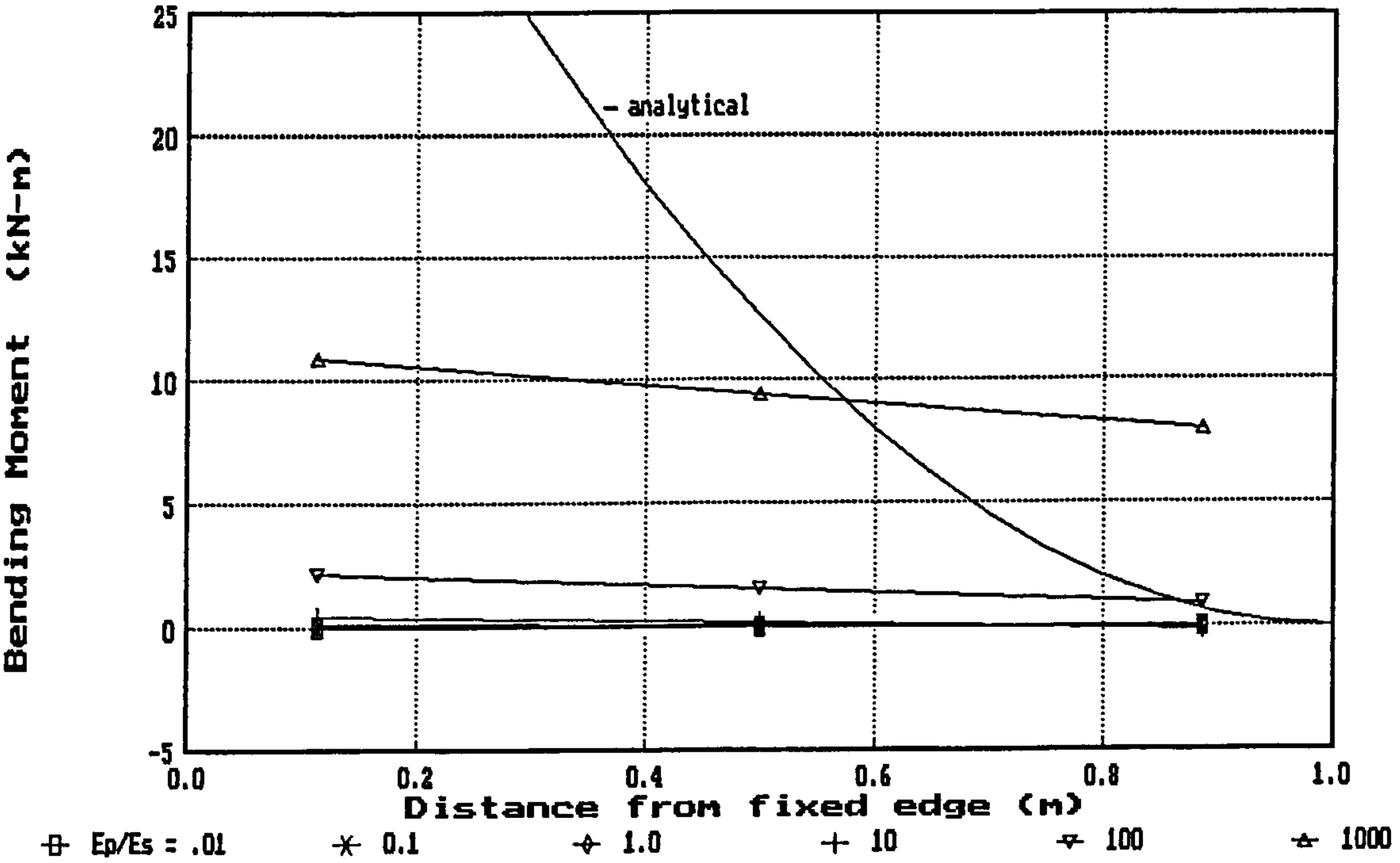

(b) aspect ratio t/B = 1/16

Fig 7.8 Effects of ill-conditioning in two-element mesh: bending moment distribution (based on stresses in structure), for type B2 with different modular ratios

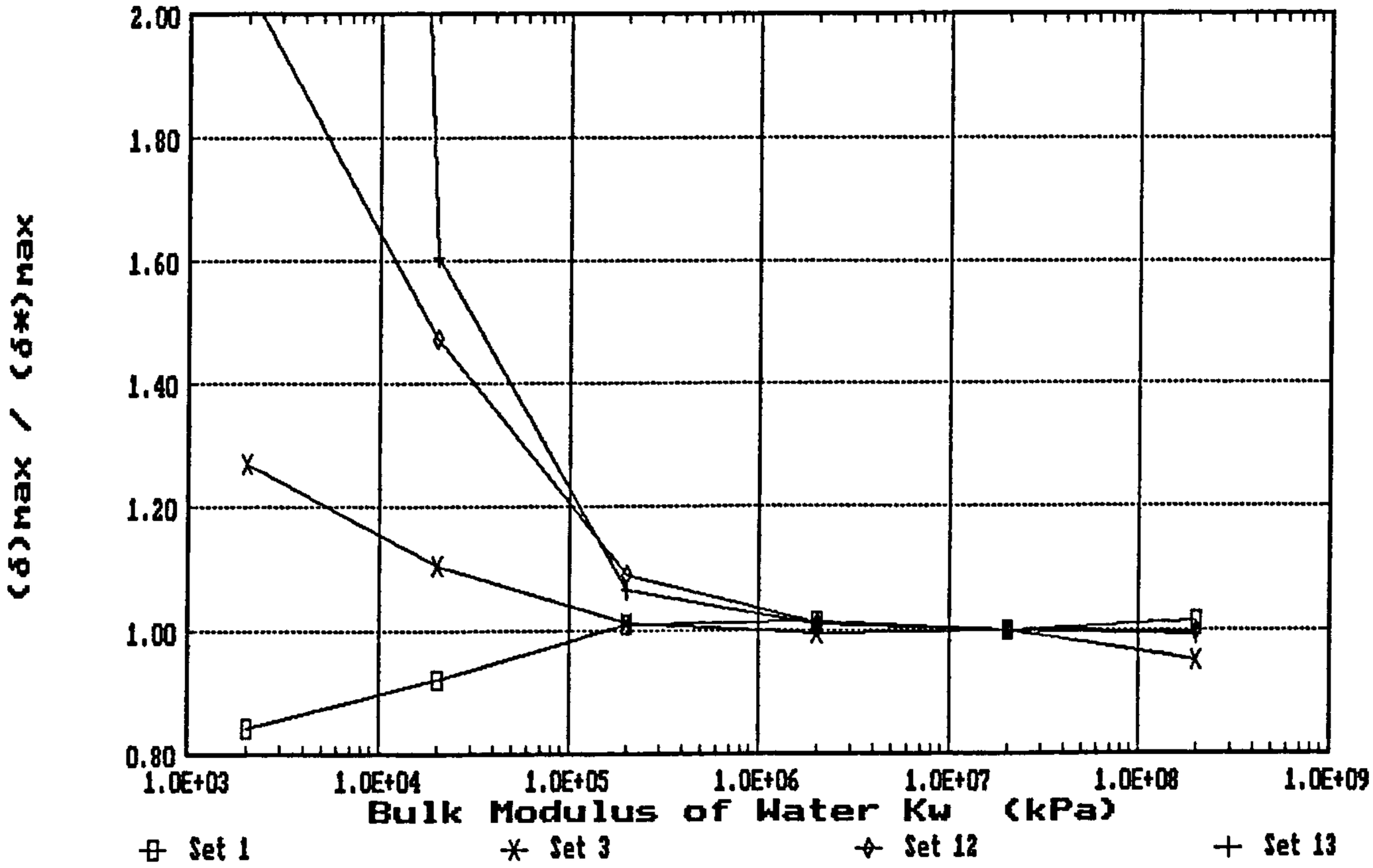

(a) horizontal wall displacement

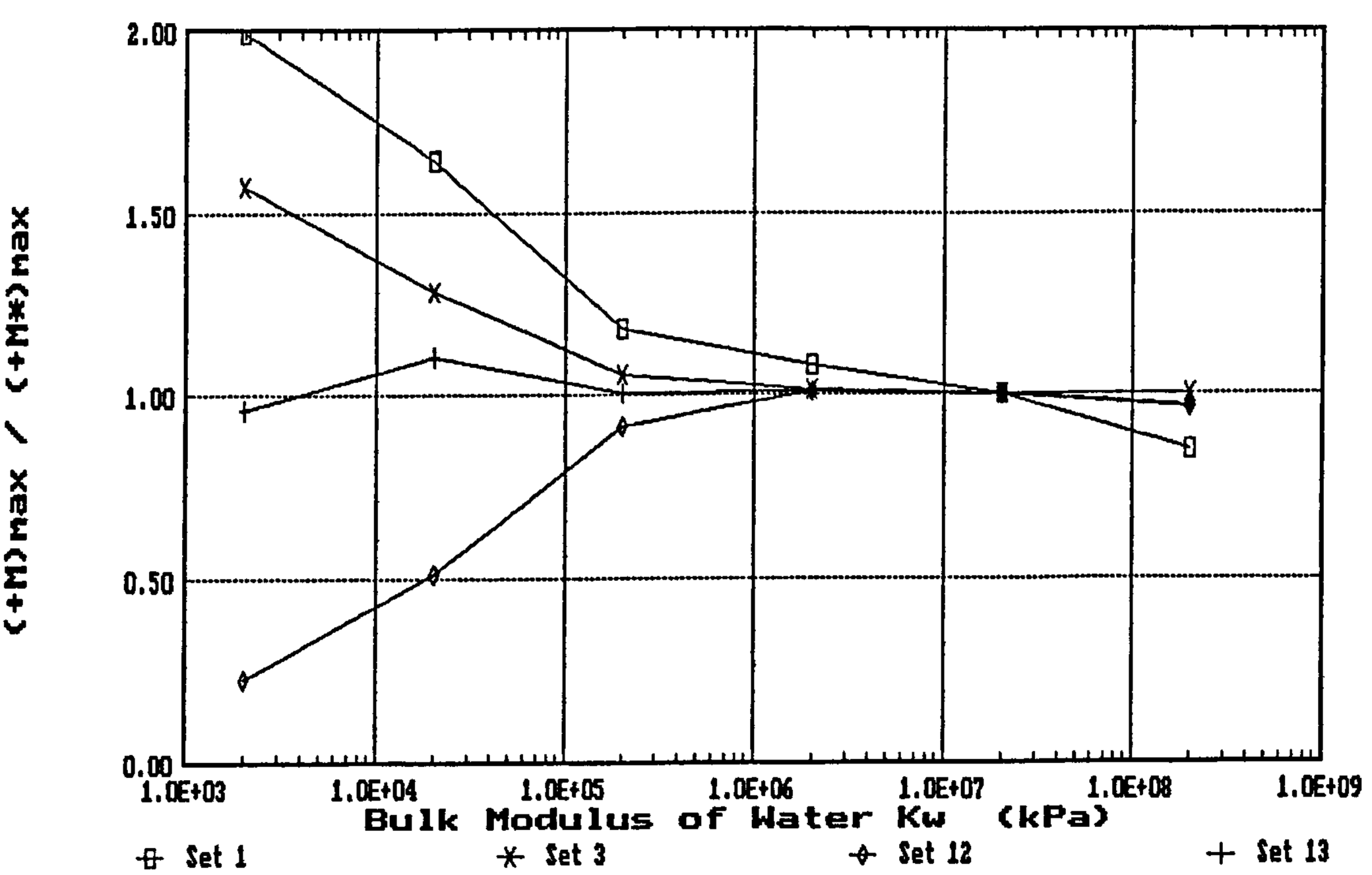

(b) wall bending moment

Fig 7.9 Influence of pore fluid compressibility on a cantilever wall analysis: normalized characteristic value against bulk modulus of water

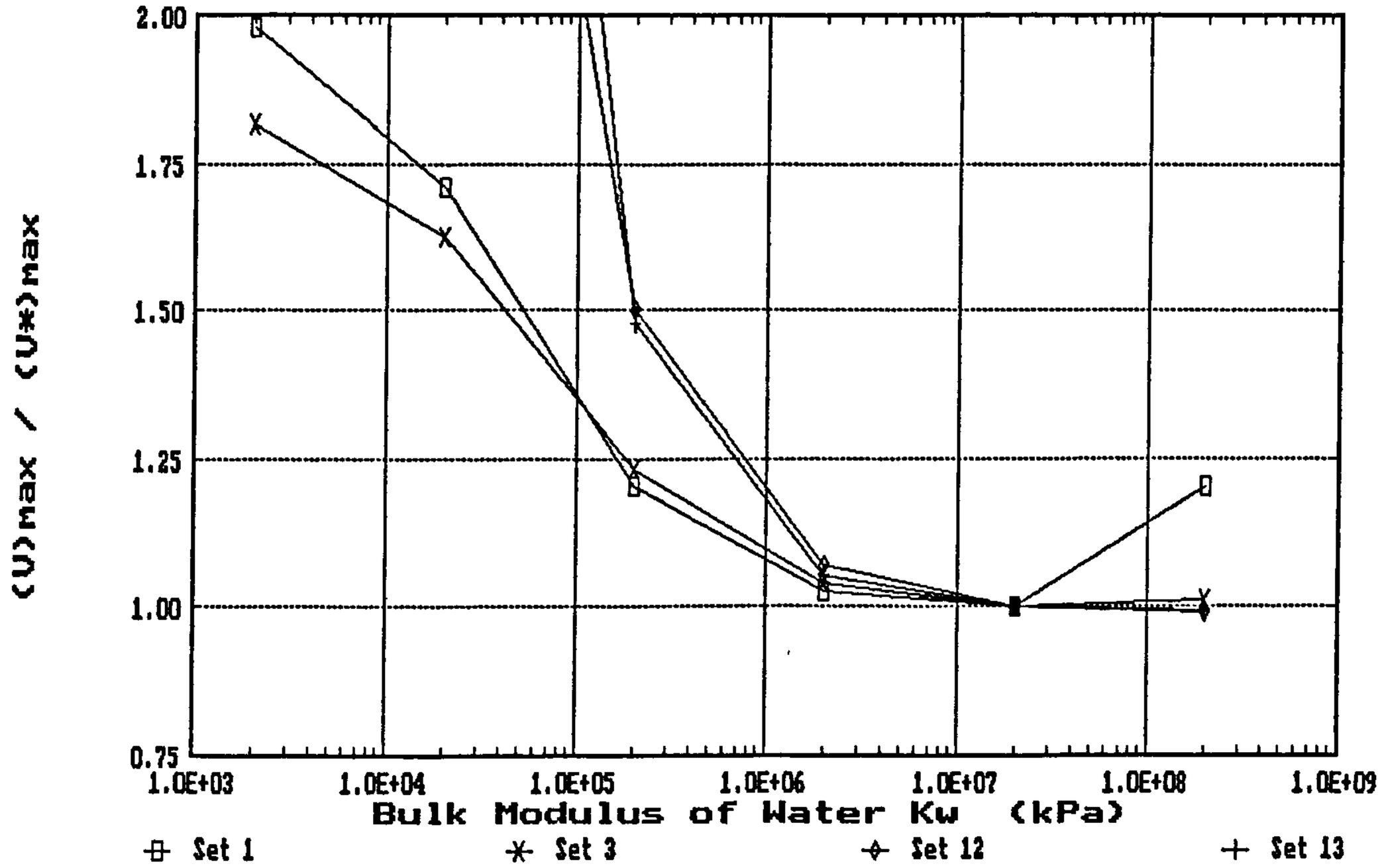

(c) excavation heave

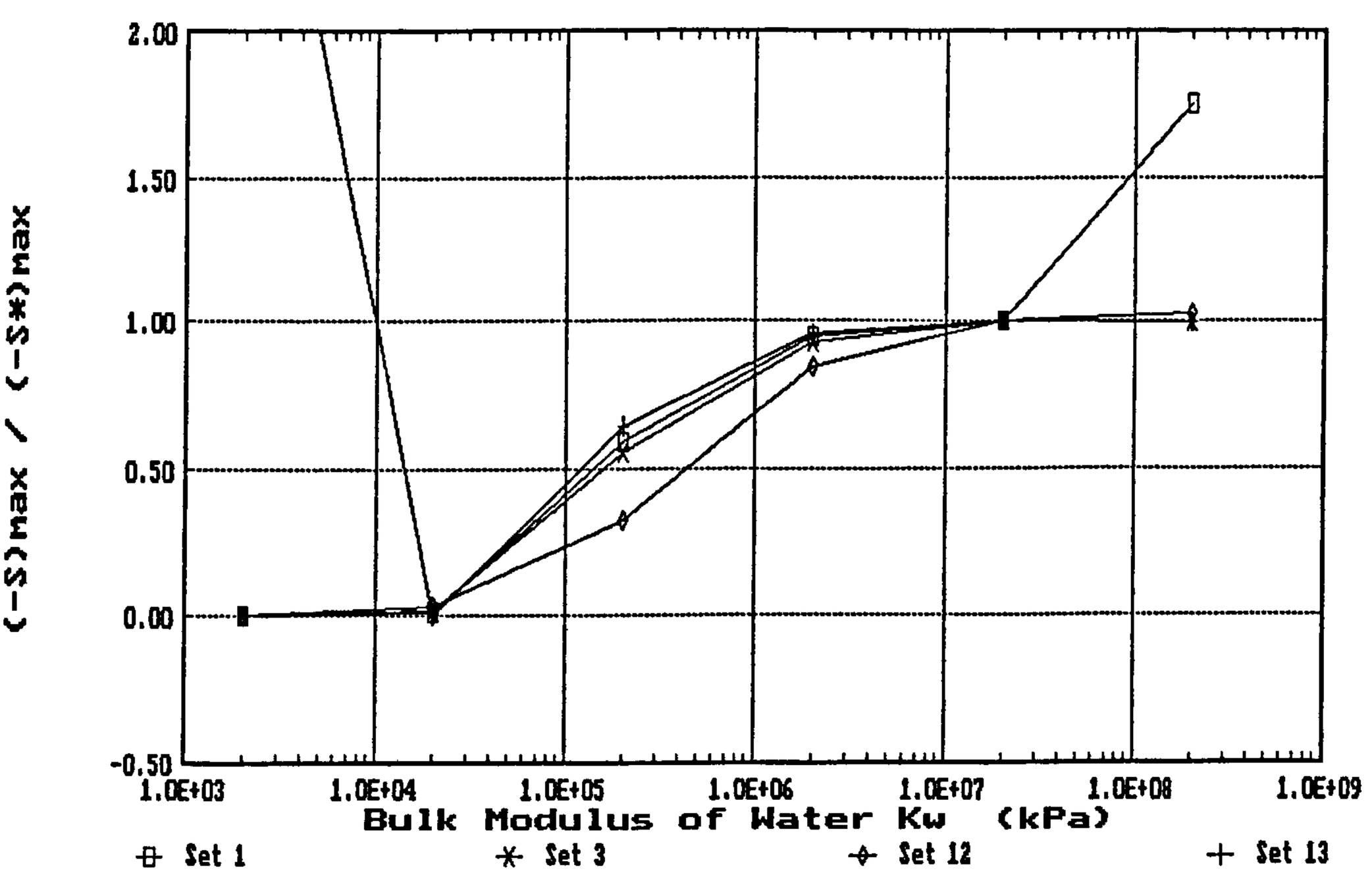

(d) ground surface settlement

Fig 7.9 Influence of pore fluid compressibility on a cantilever wall analysis: normalized characteristic value against bulk modulus of water (contd)

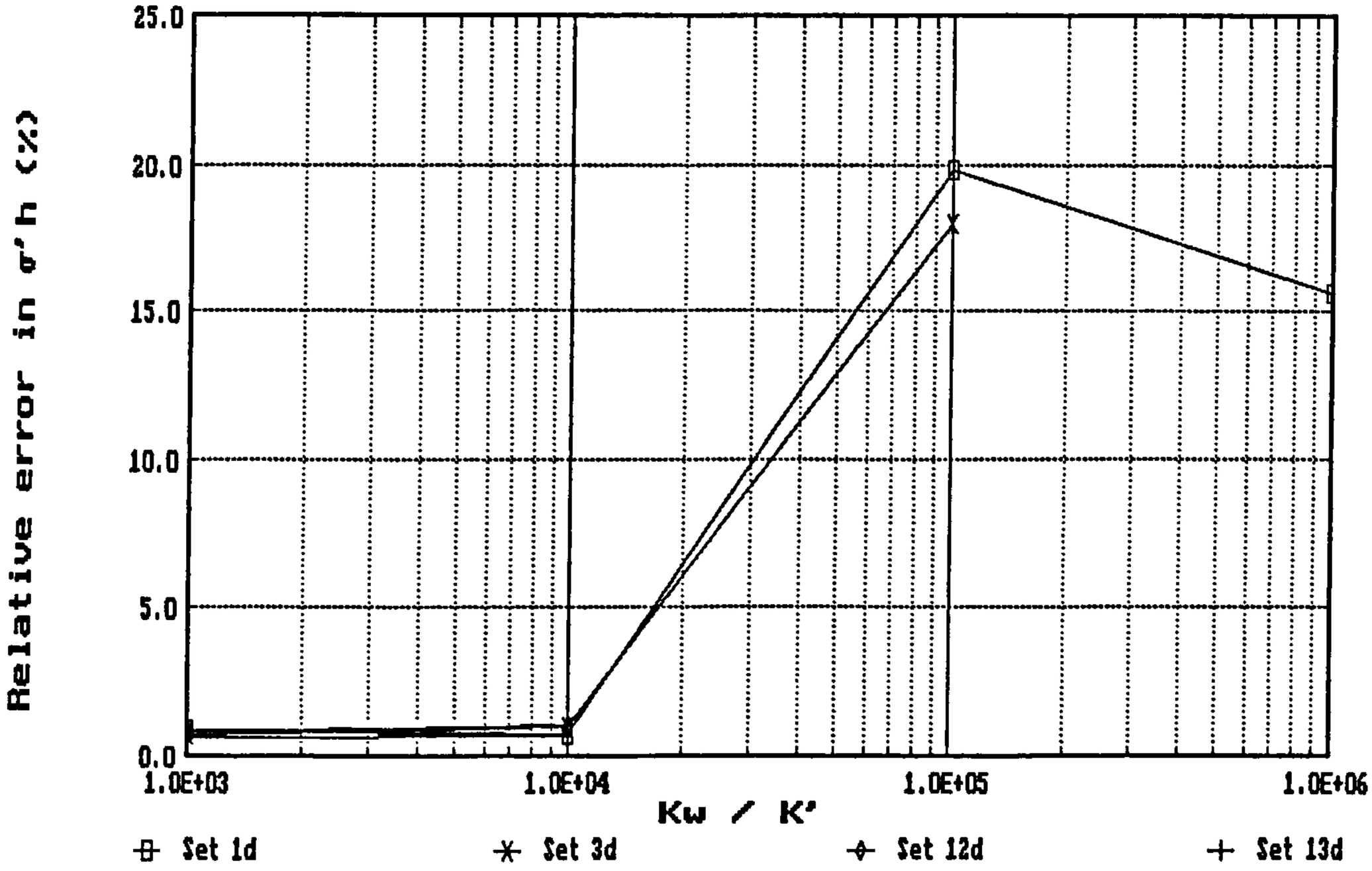

(a) horizontal effective stress on retained side

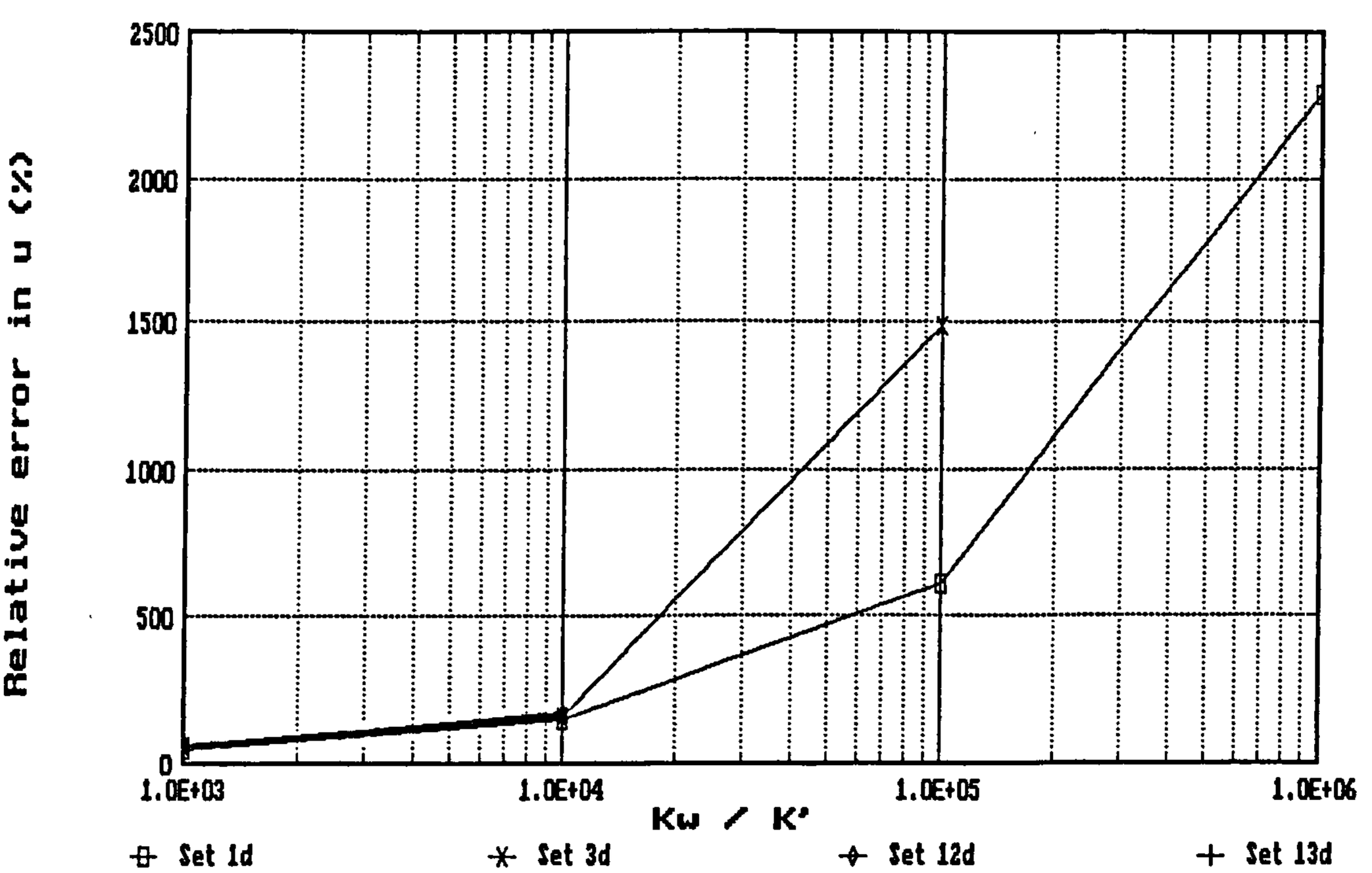

(b) pore water pressure on retained side

Fig 7.10 Influence of pore fluid compressibility on a cantilever wall analysis: relative error in computed stress against ratio of bulk moduli

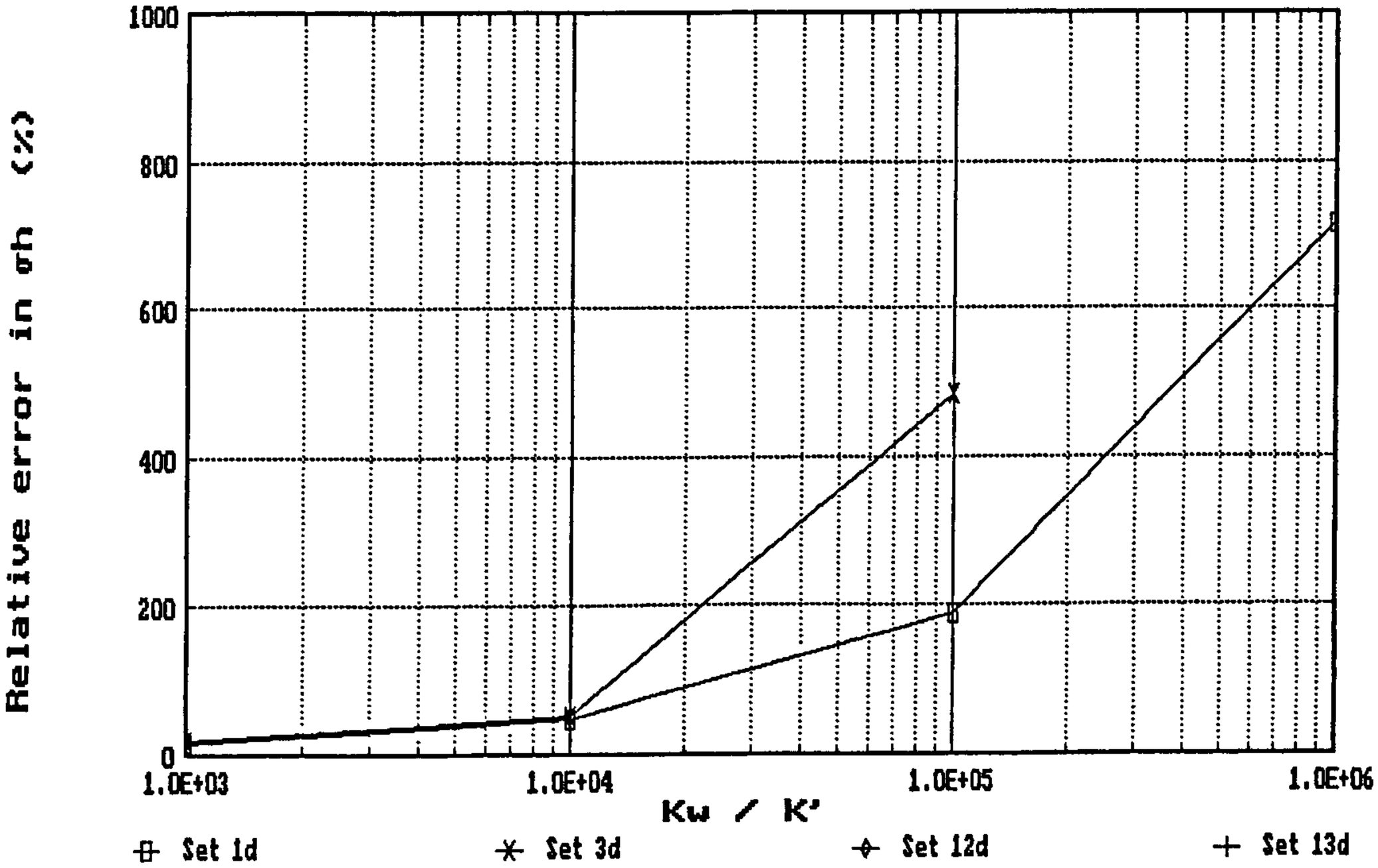

(c) horizontal total stress on retained side

Fig 7.10 Influence of pore fluid compressibility on a cantilever wall analysis: relative error in computed stress against ratio of bulk moduli (contd)

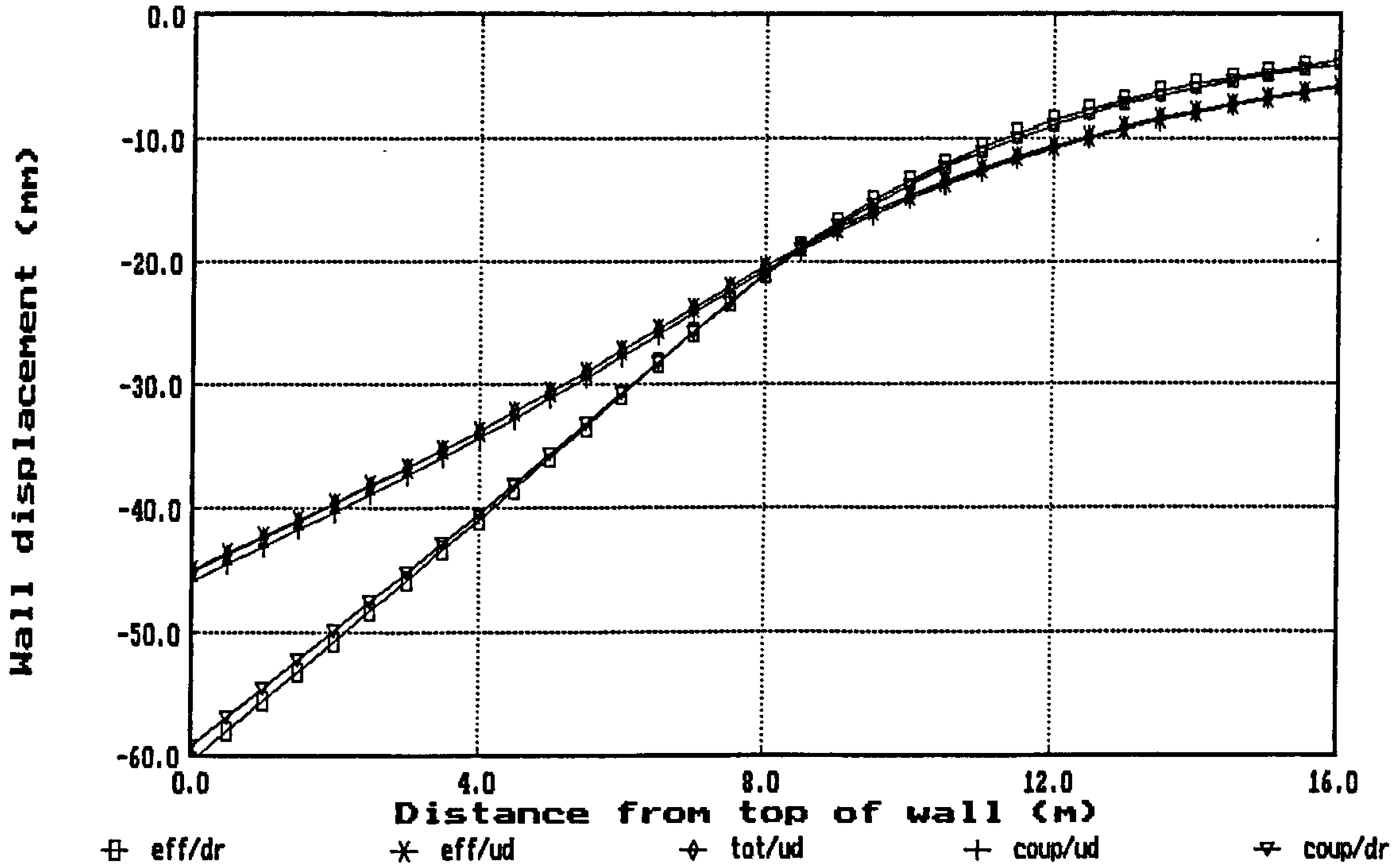

(a) elastic analysis, with $E' = 4z$ (effective stress) or $E_u = 5z$ (total stress)

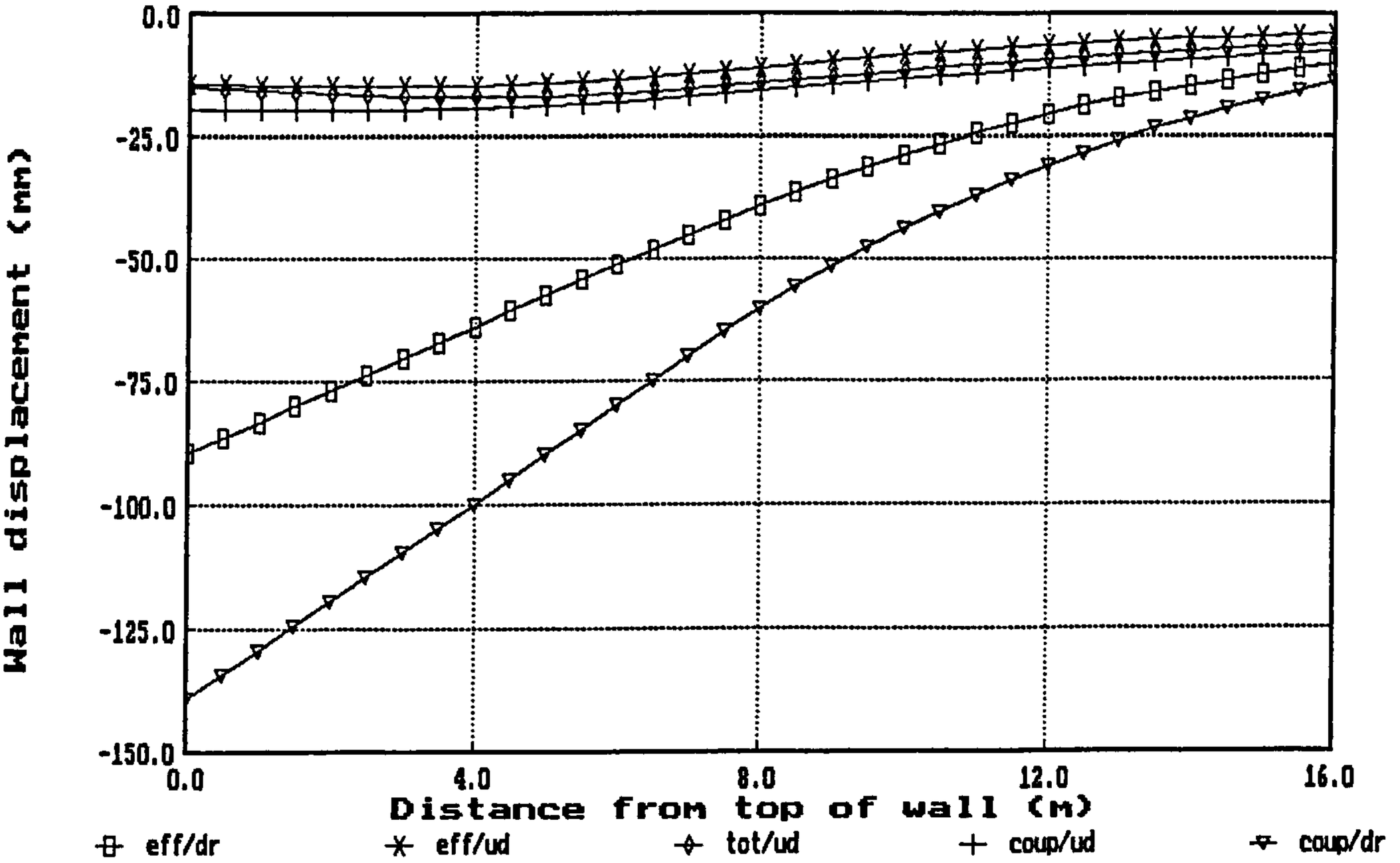

(a) elastic-perfectly plastic analysis, with $E' = 40+4z$ (effective) or $E_u = 50+5z$ (total)

Fig 7.11 Comparison of wall displacement profiles from coupled and non-coupled analyses of a cantilever wall

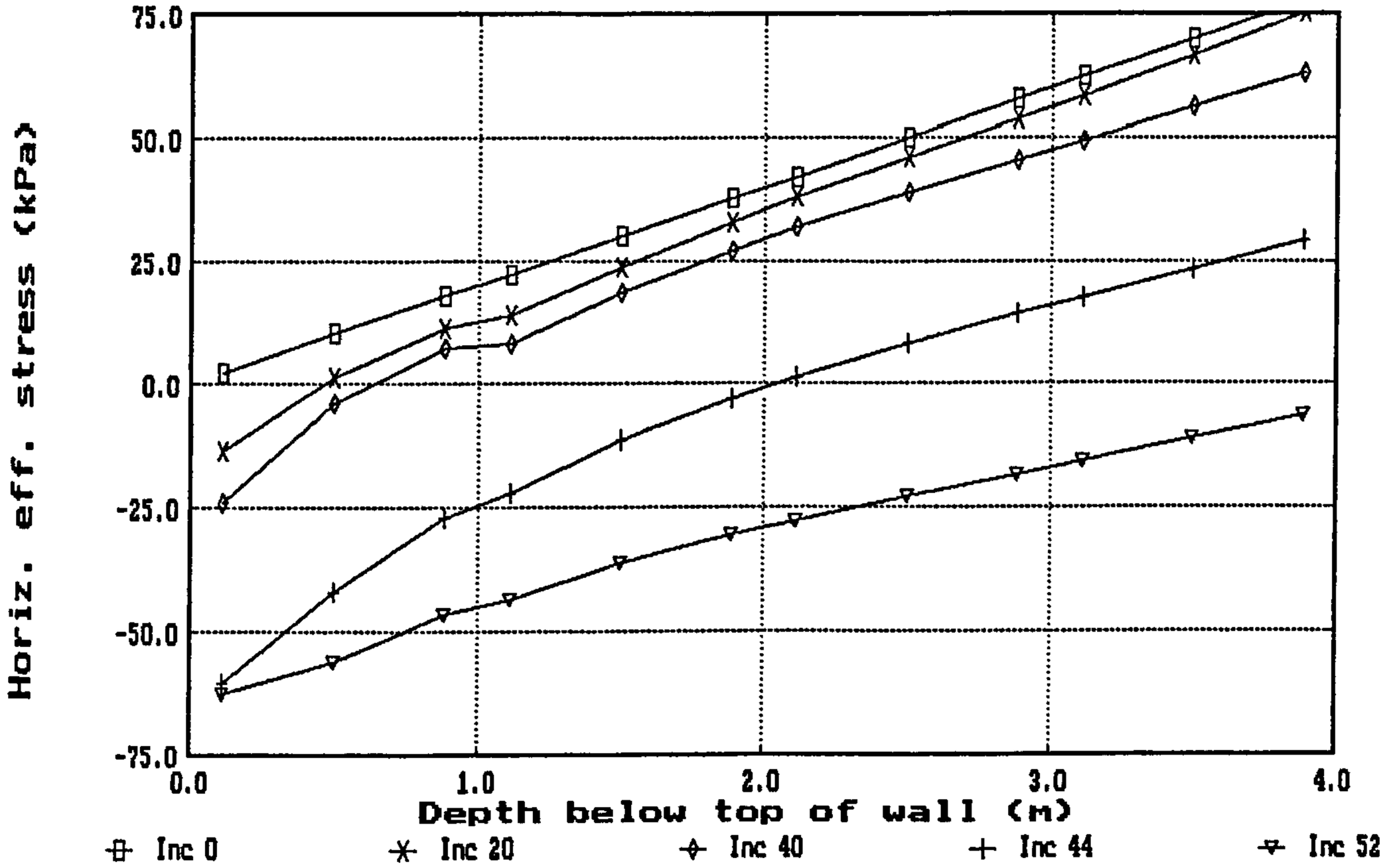

(a) elastic analysis, with $E'_o > 0$

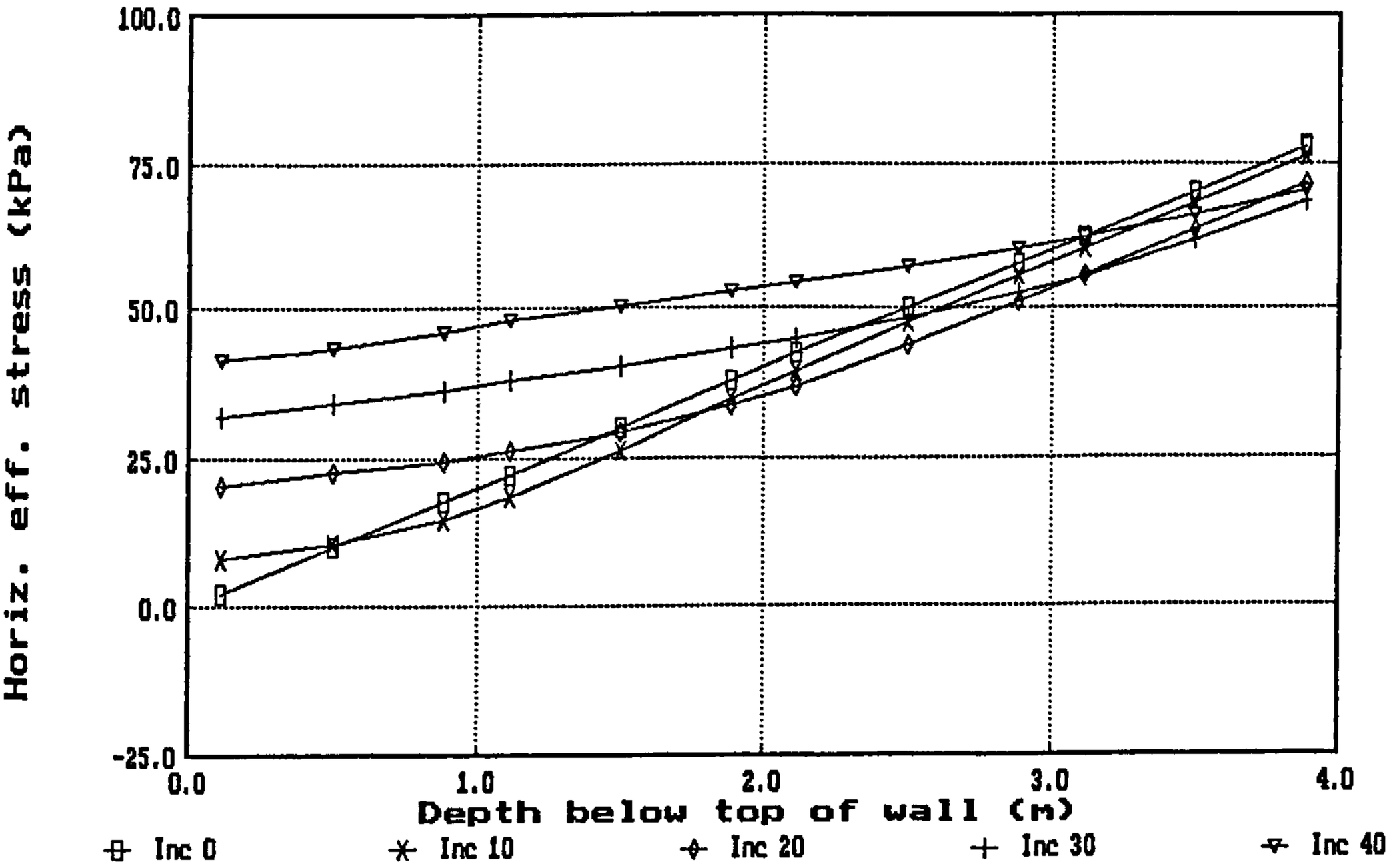

(b) elastic-perfectly plastic (Mohr-Coulomb) analysis, with $E'_o > 0$, $c' = 0$: uncoupled

Fig 7.12 Investigation of tensile active stresses on the retained side of a cantilever wall: effective horizontal stress profiles near the top of the wall

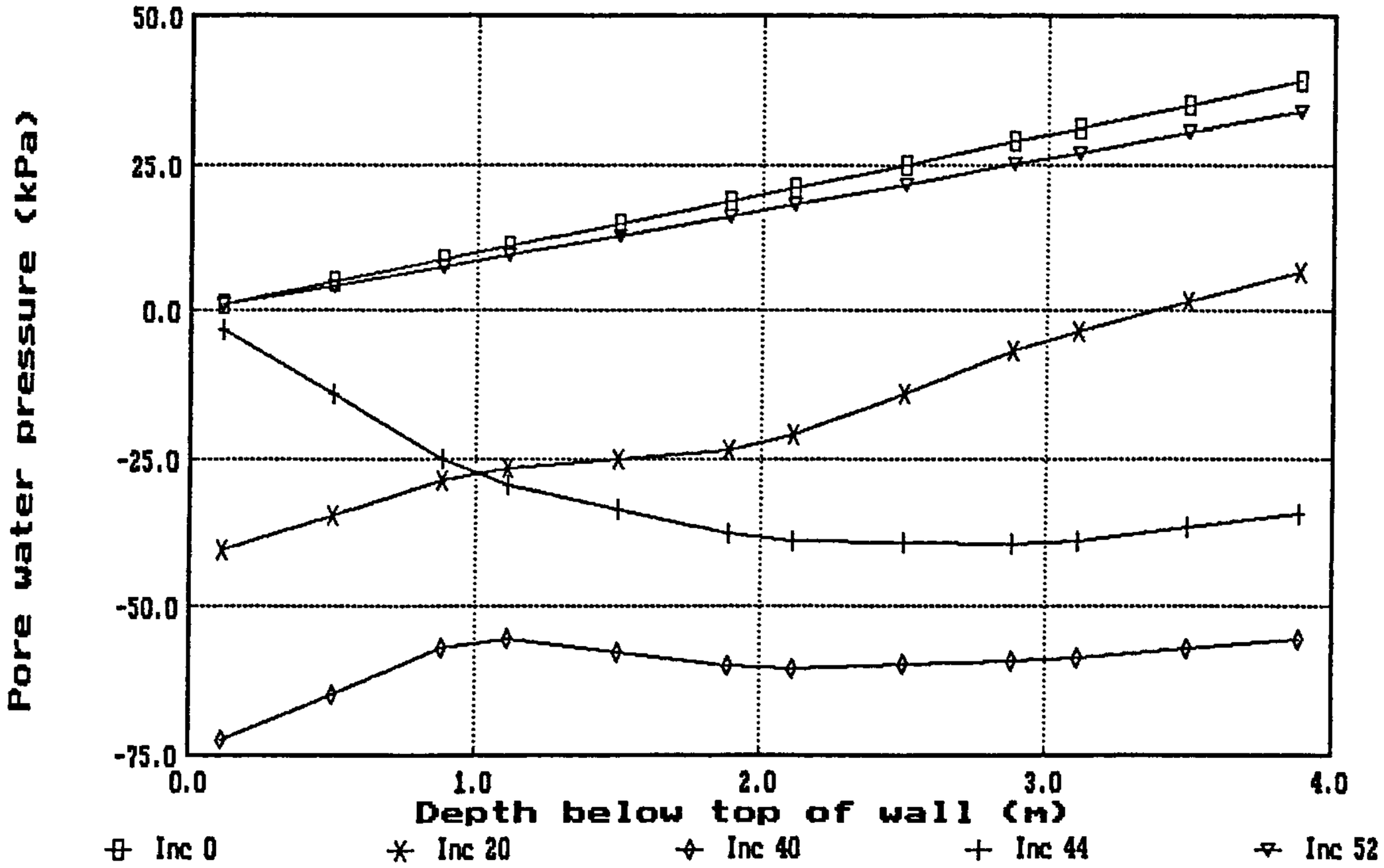

(a) elastic-perfectly plastic (Mohr-Coulomb) analysis, with $E'_o > 0$, $c' = 0$

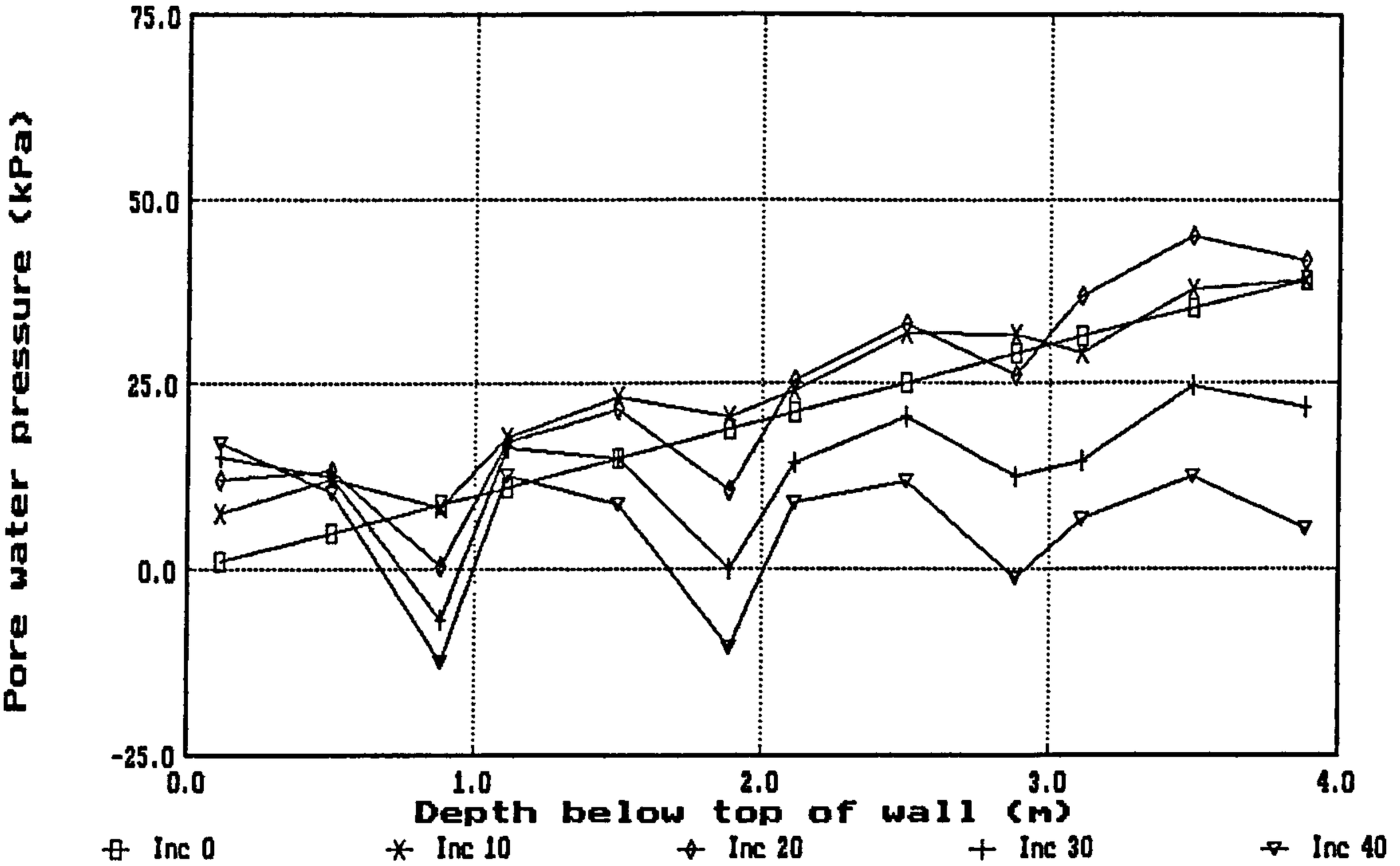

(b) elastic-perfectly plastic (Mohr-Coulomb) analysis, with $E'_o = 0$, $c' = 0$: uncoupled

Fig 7.13 Investigation of tensile active stresses on the retained side of a cantilever wall: pore water pressure profiles near the top of the wall

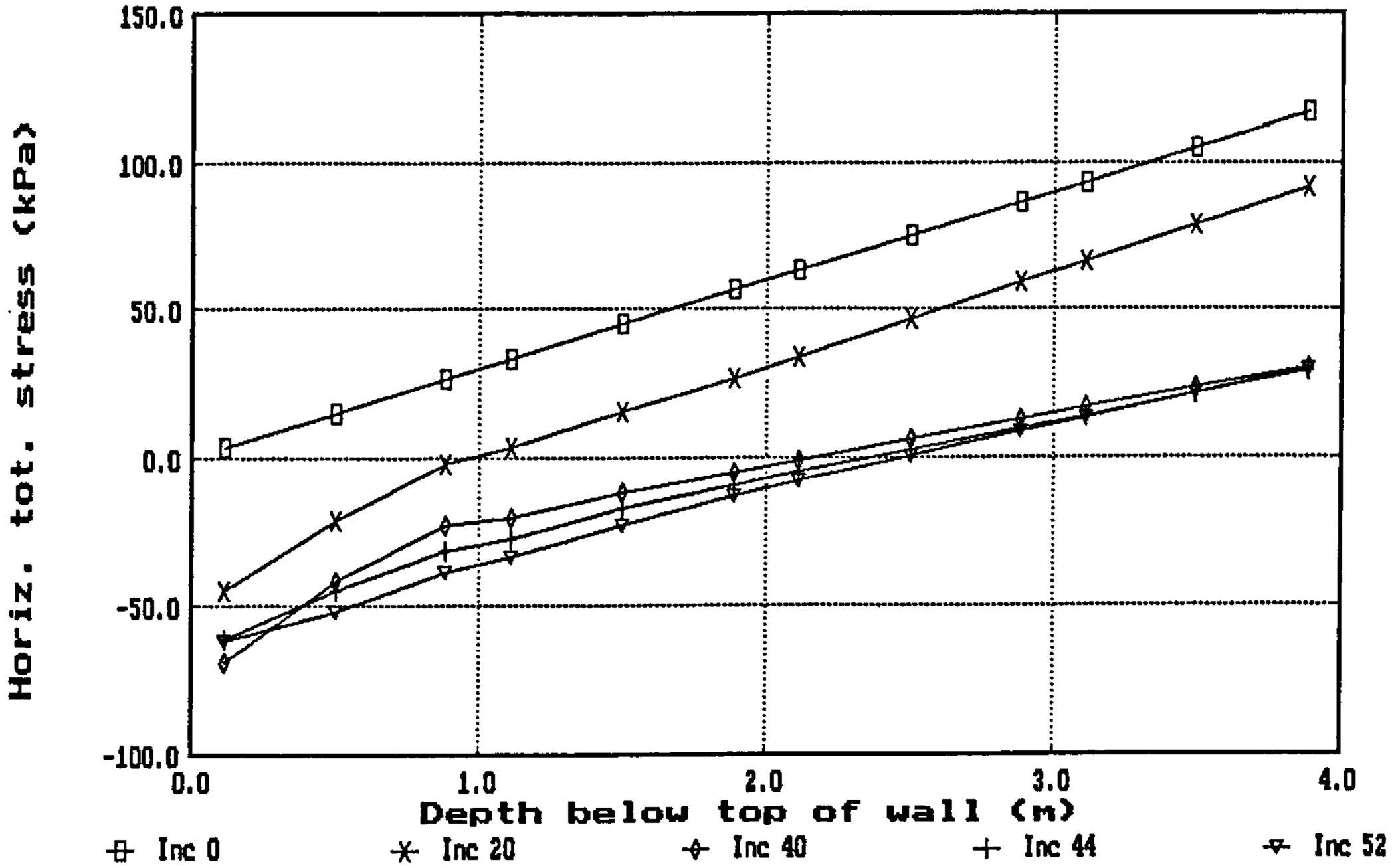

(a) elastic analysis, with $E'_o > 0$

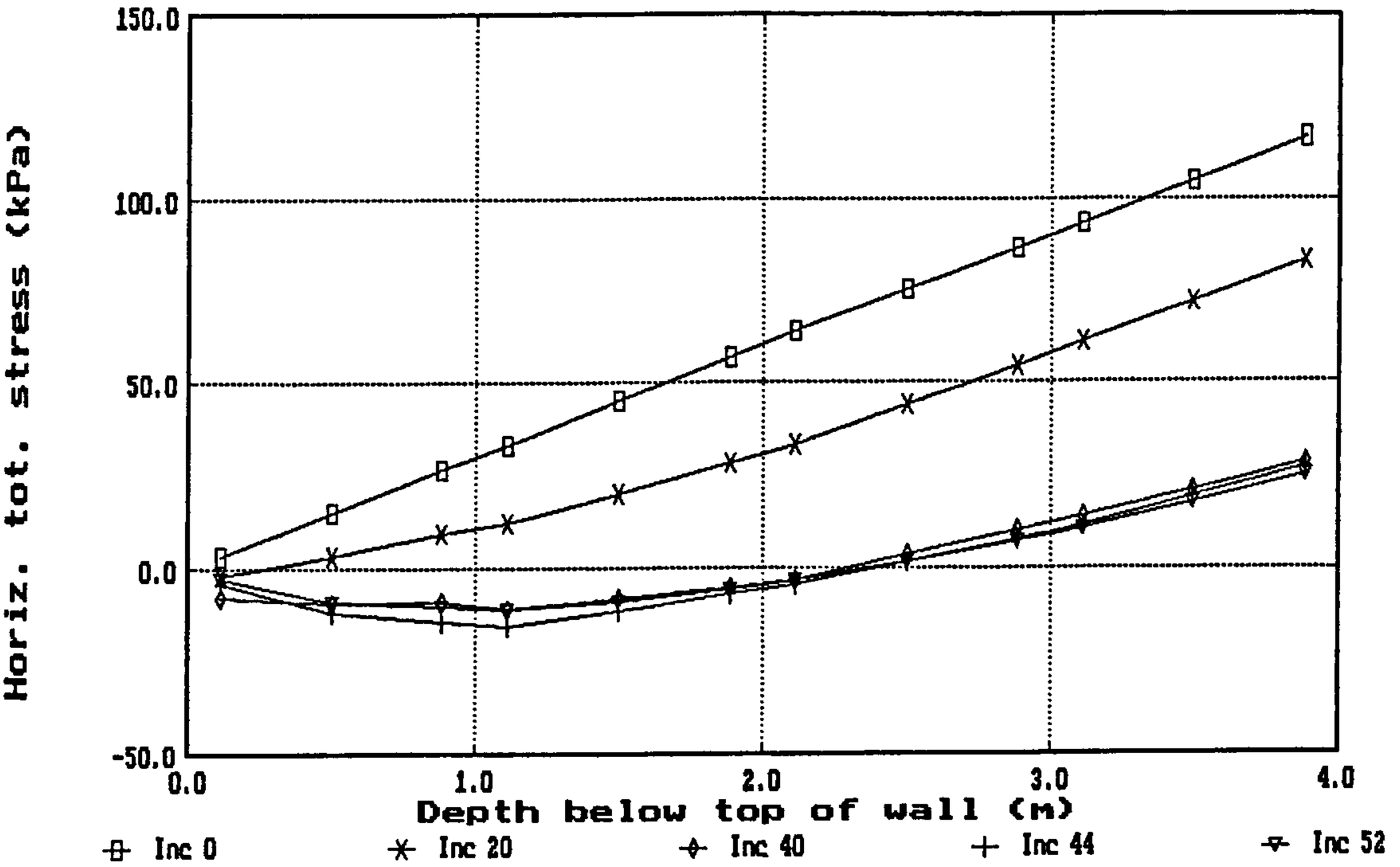

(b) elastic analysis, with $E'_o = 0$

Fig 7.14 Investigation of tensile active stresses on the retained side of a cantilever wall: total horizontal stress profiles near the top of the wall

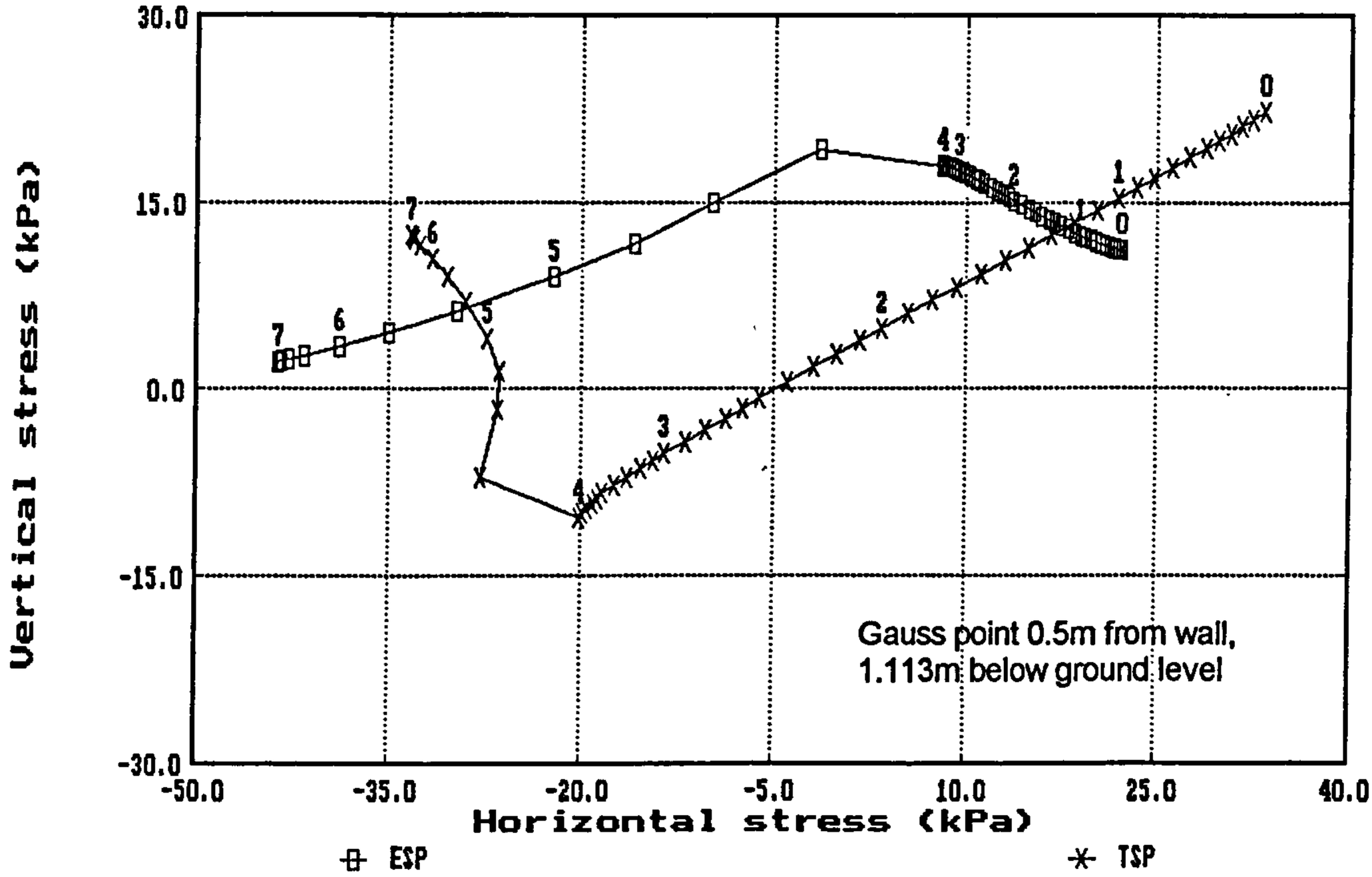

(a) elastic-perfectly plastic (Mohr-Coulomb) analysis, with $E'_o > 0$, $c' = 50$ kPa

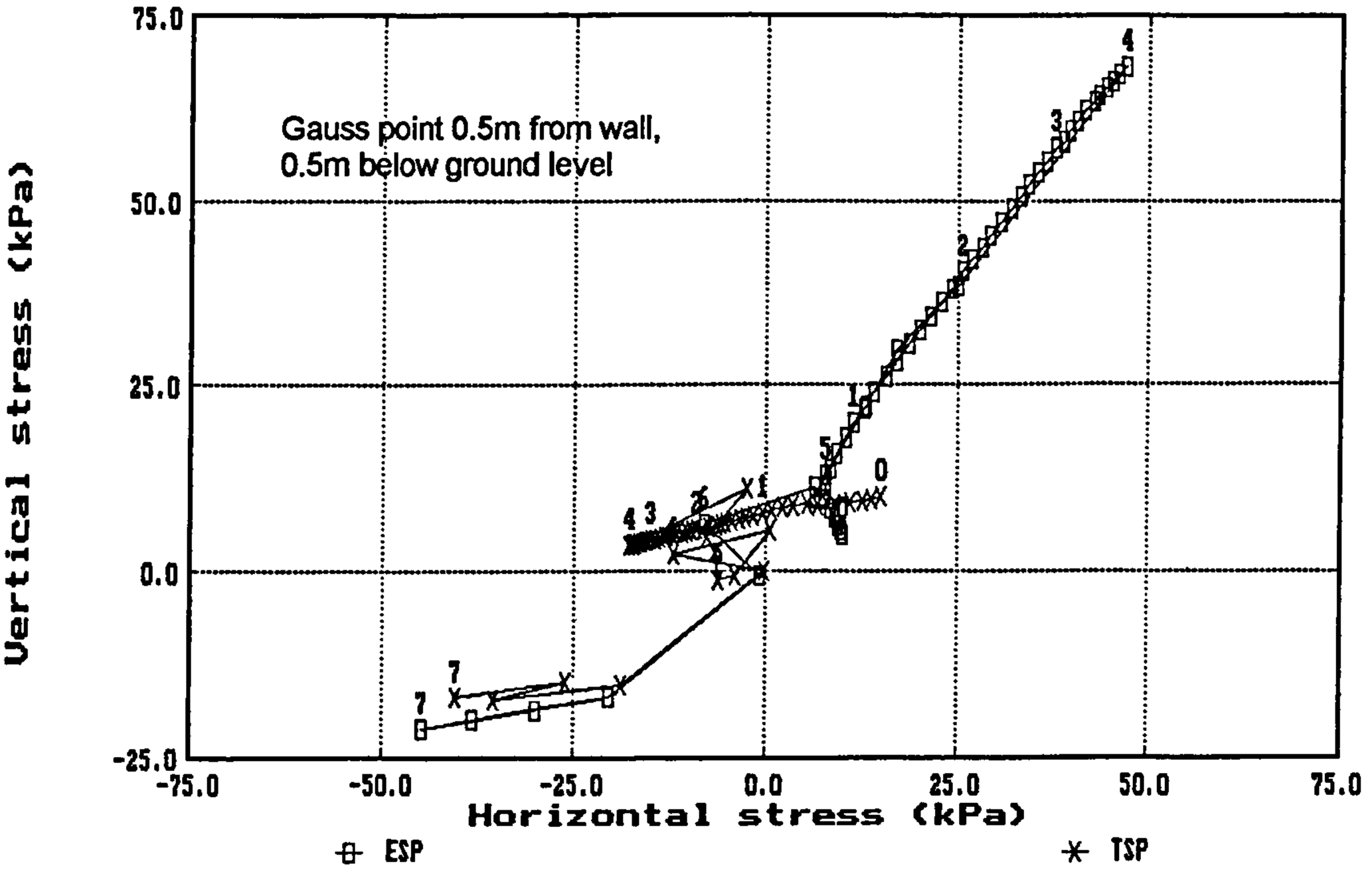

(b) elastic-perfectly plastic (Mohr-Coulomb) analysis, with $E'_o > 0$, $c' = 0$

Fig 7.15 Investigation of tensile active stresses on the retained side of a cantilever wall: effective and total stress paths

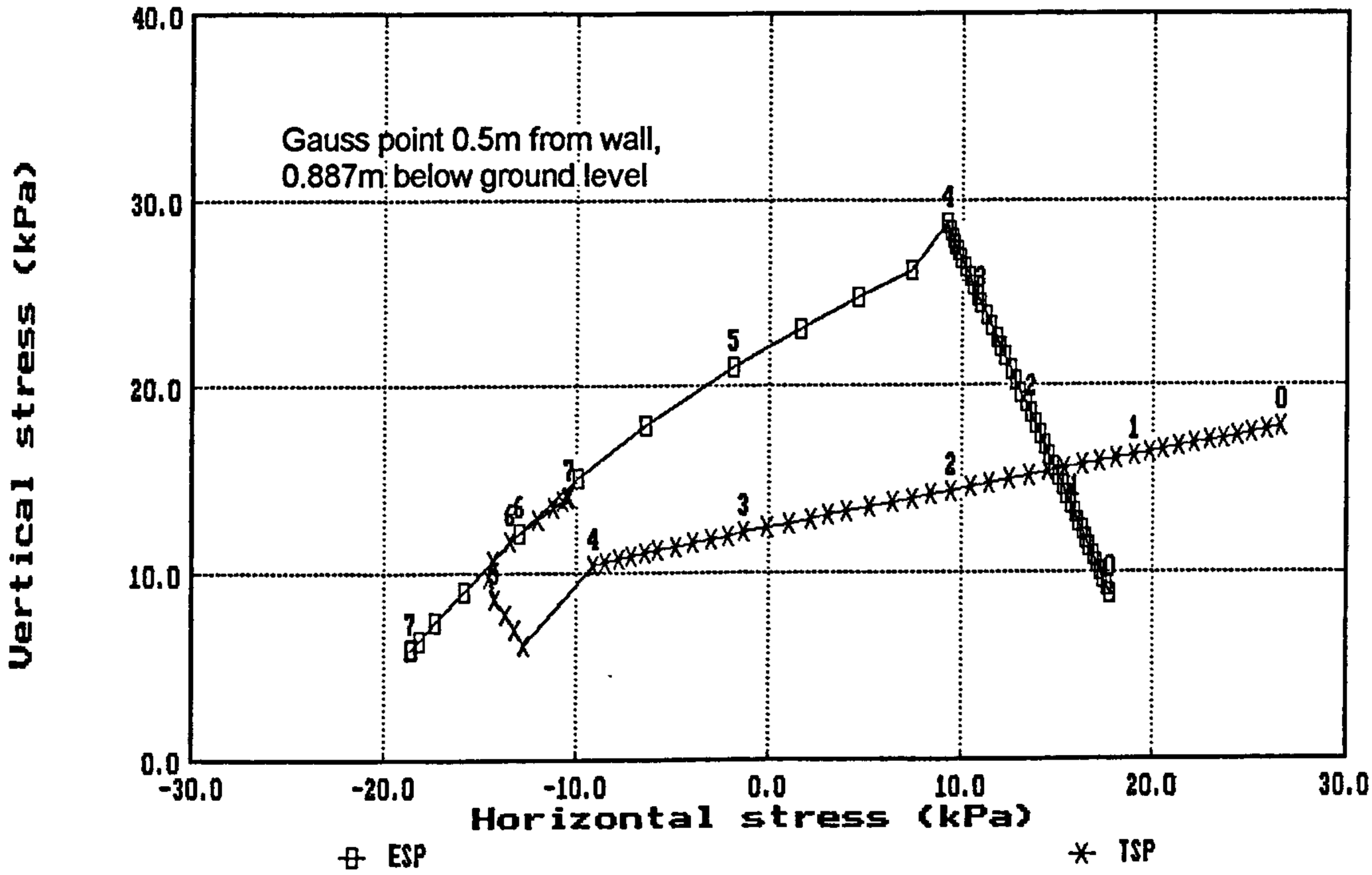

(c) elastic-perfectly plastic (Mohr-Coulomb) analysis, with $E'_o > 0$, $c' = 50$ kPa

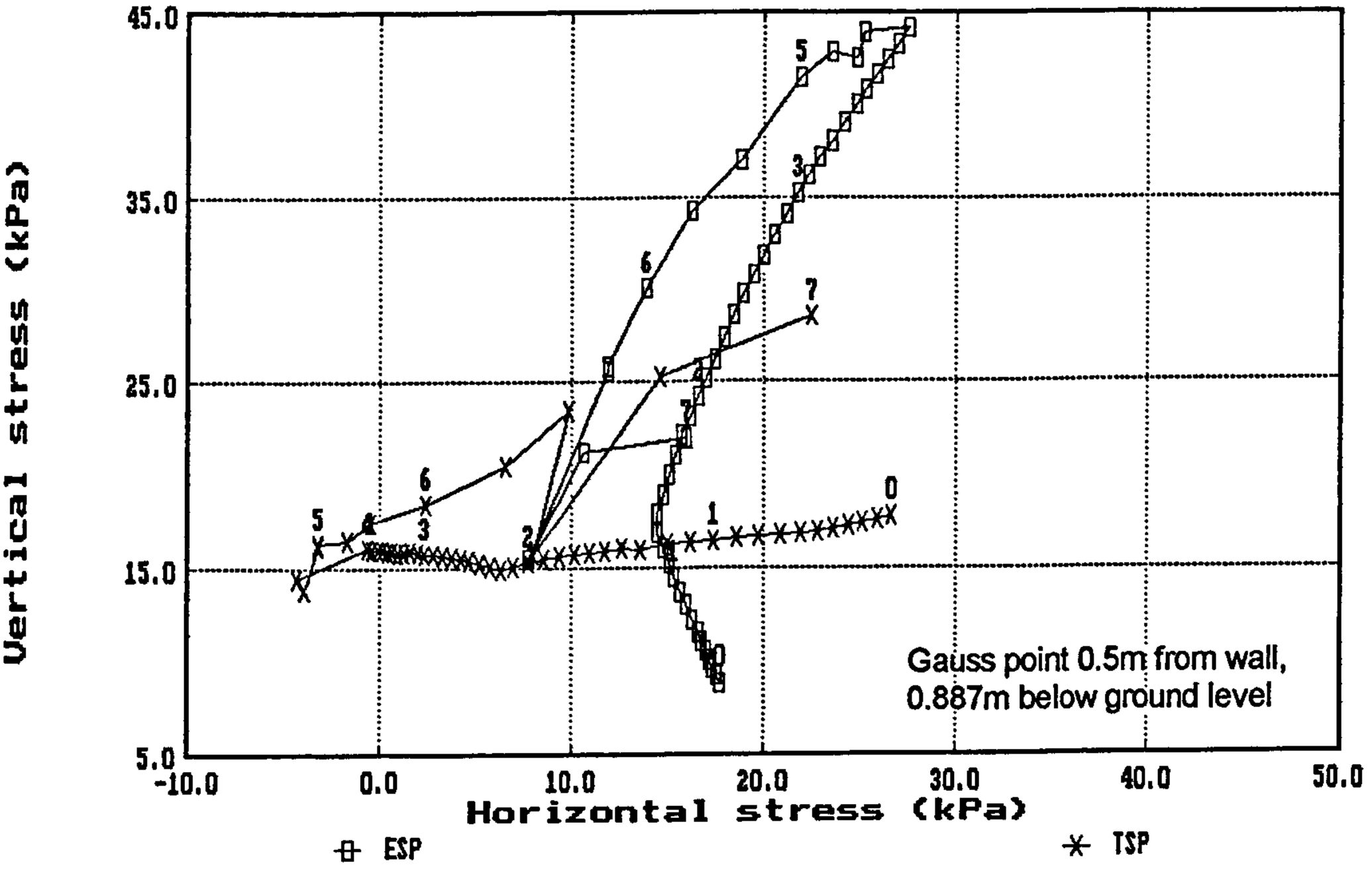

(d) elastic-perfectly plastic (Mohr-Coulomb) analysis, with $E'_o > 0$, $c' = 0$

Fig 7.15 Investigation of tensile active stresses on the retained side of a cantilever wall: effective and total stress paths (contd)

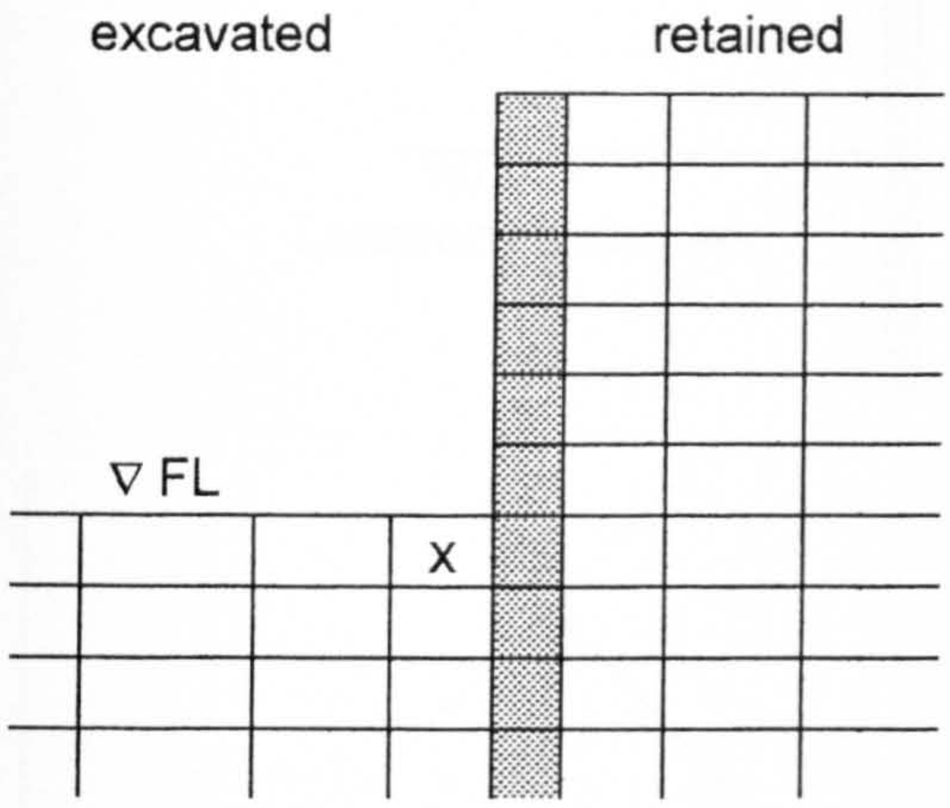

(a) mesh detail near wall

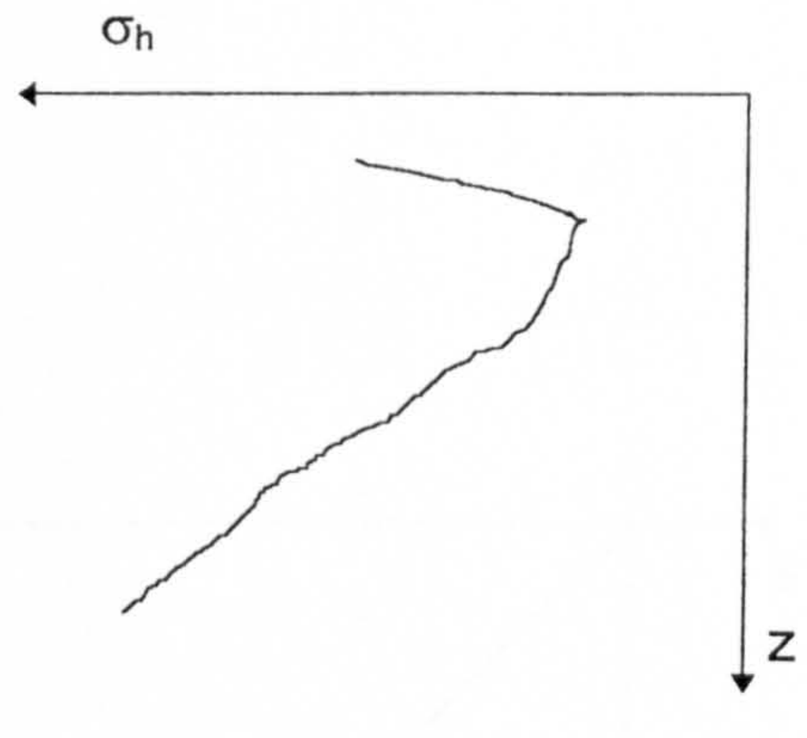

(b) anomaly in σ_h profile below formation level (FL)

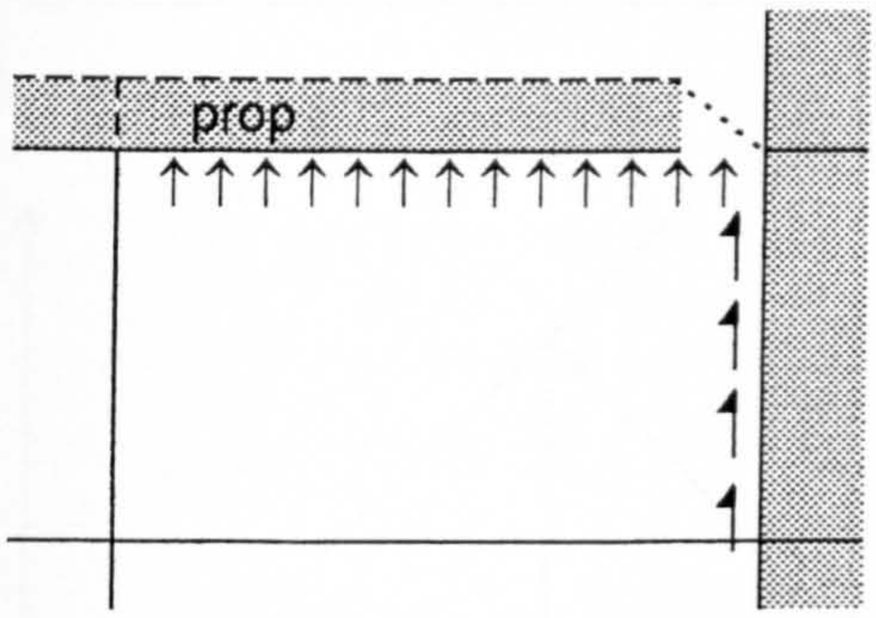

- stiffness contrast (soil:wall)
- shear stresses on interface ↑
- formation level prop (if present) prevents swelling ↑↑↑

(c) particular problems in element 'x'

Fig 7.16 Anomaly in horizontal soil stress (passive pressure) on the excavated side of an embedded retaining wall

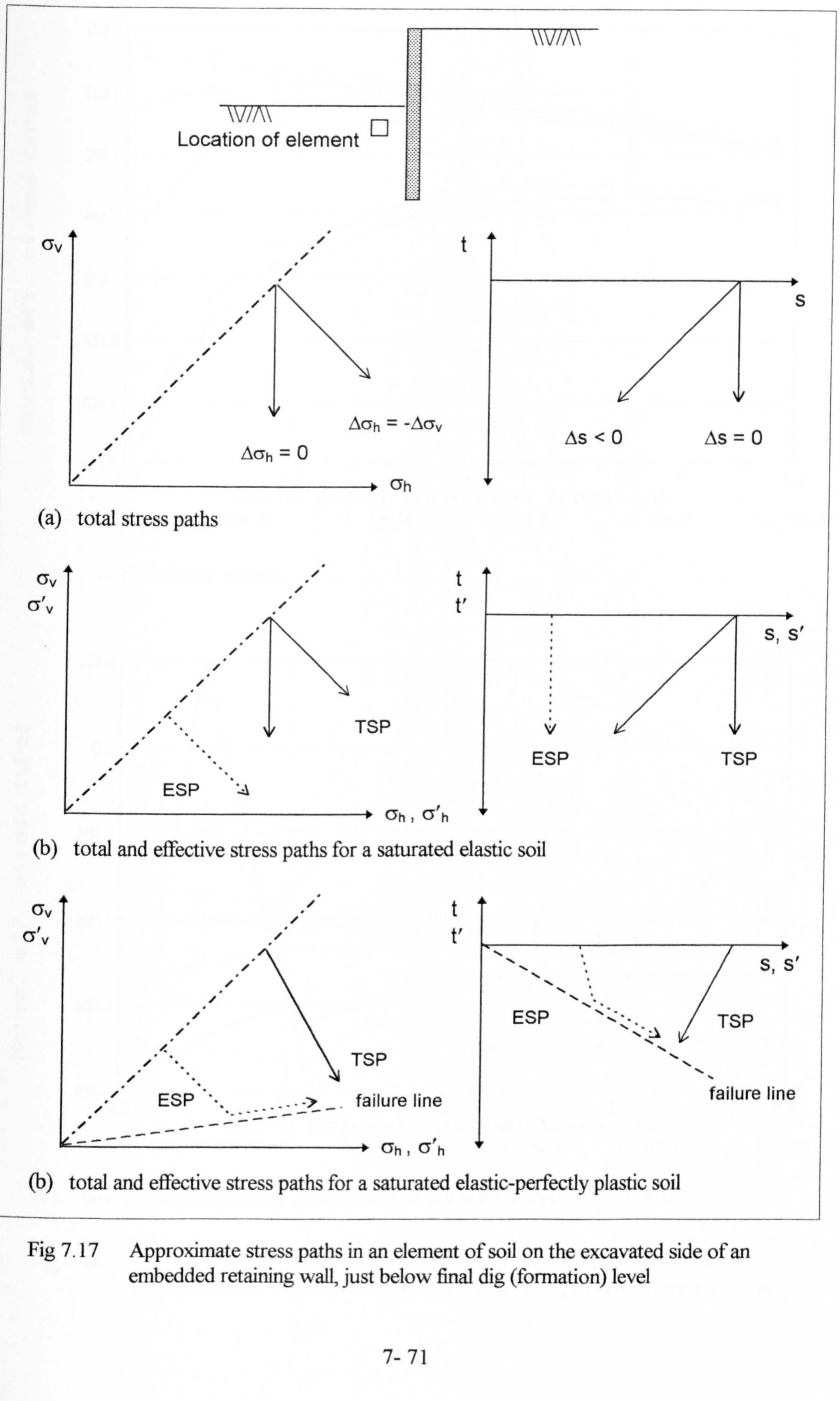

(a) total stress paths

(b) total and effective stress paths for a saturated elastic soil

(b) total and effective stress paths for a saturated elastic-perfectly plastic soil

Fig 7.17 Approximate stress paths in an element of soil on the excavated side of an embedded retaining wall, just below final dig (formation) level

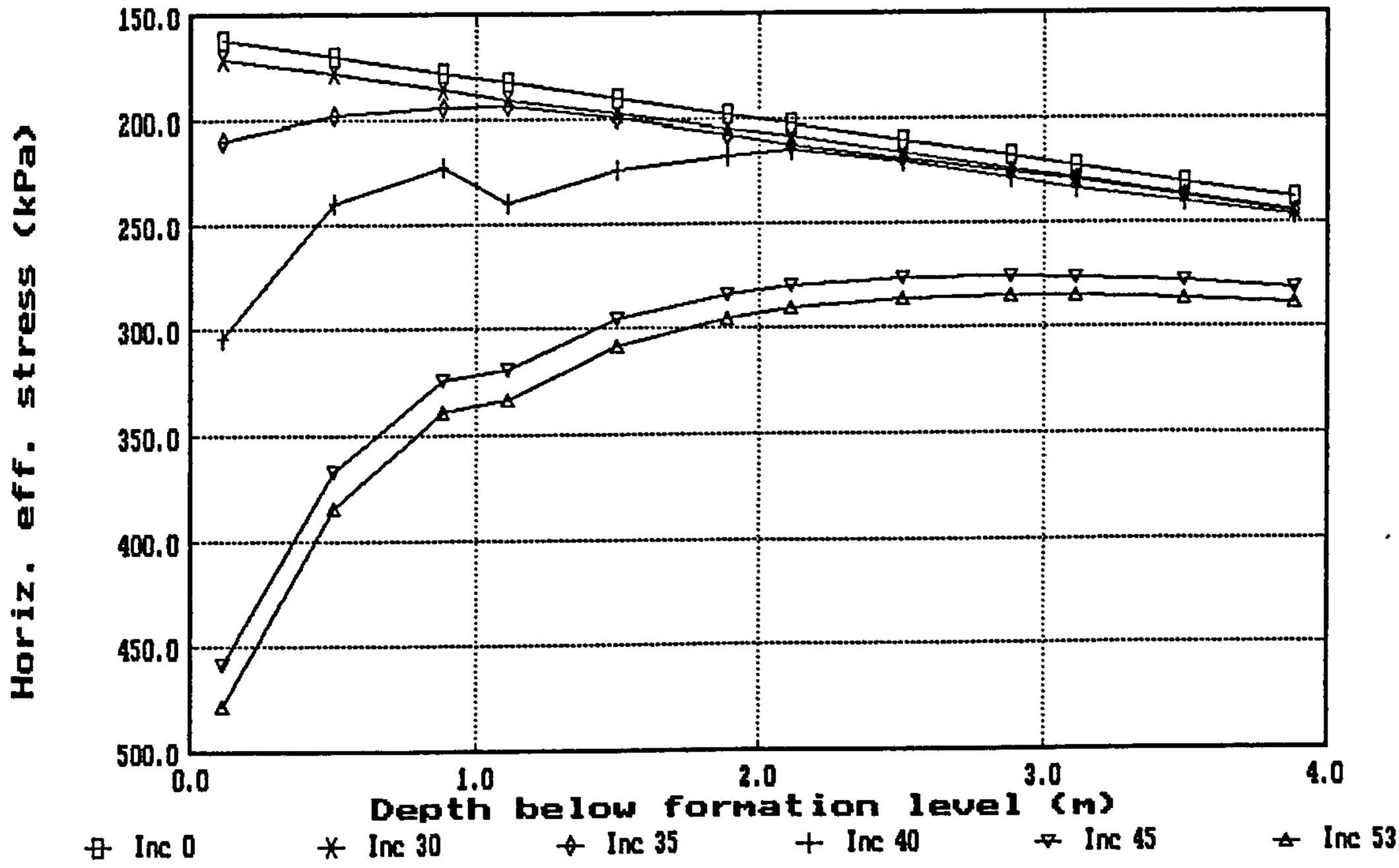

(a) coupled elastic analysis

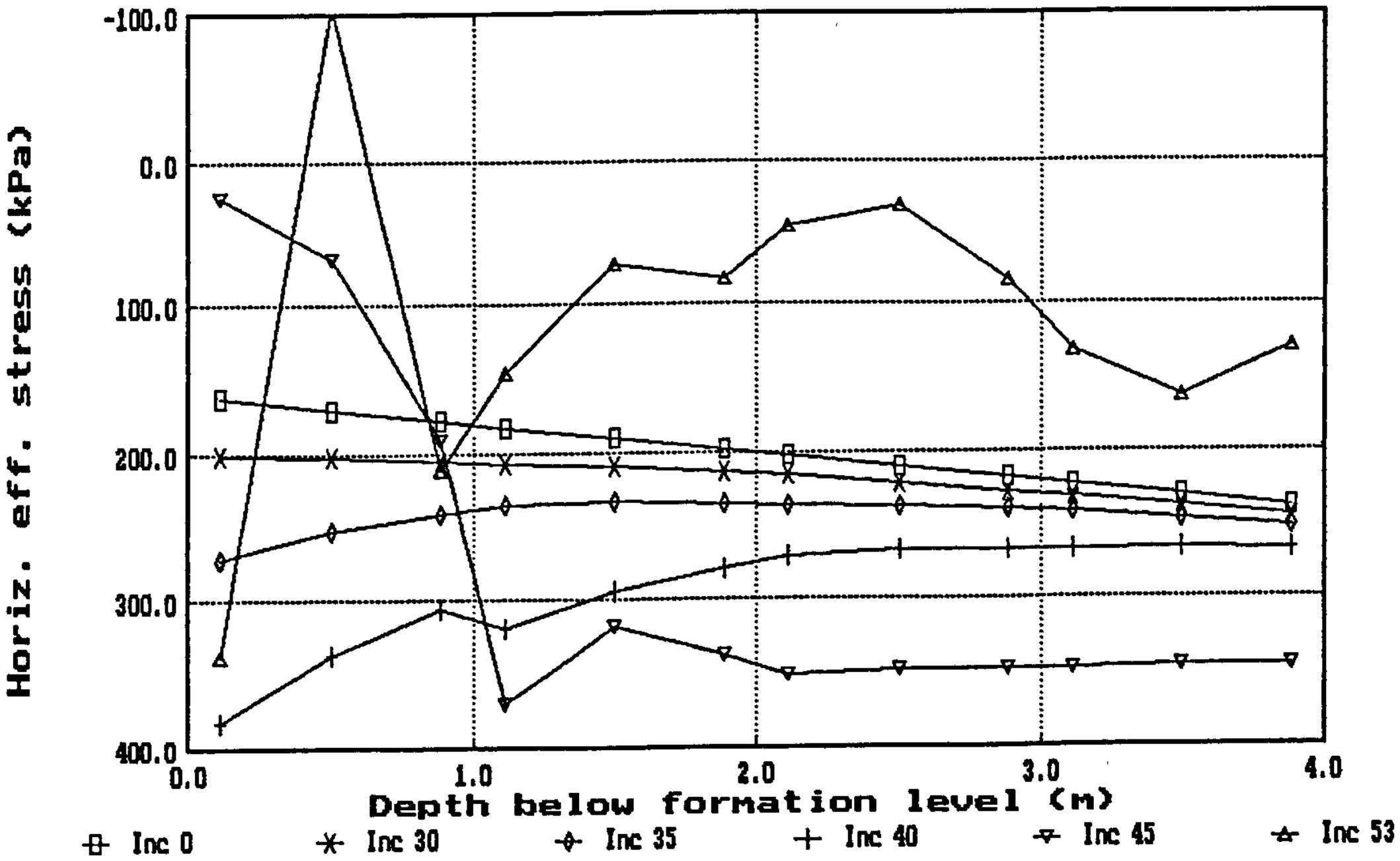

(b) coupled elastic-perfectly plastic (Mohr-Coulomb) analysis, with $c' = 0$

Fig 7.18 Investigation of passive pressure anomaly on the excavated side of an embedded wall : effective horizontal stress profiles just below formation level

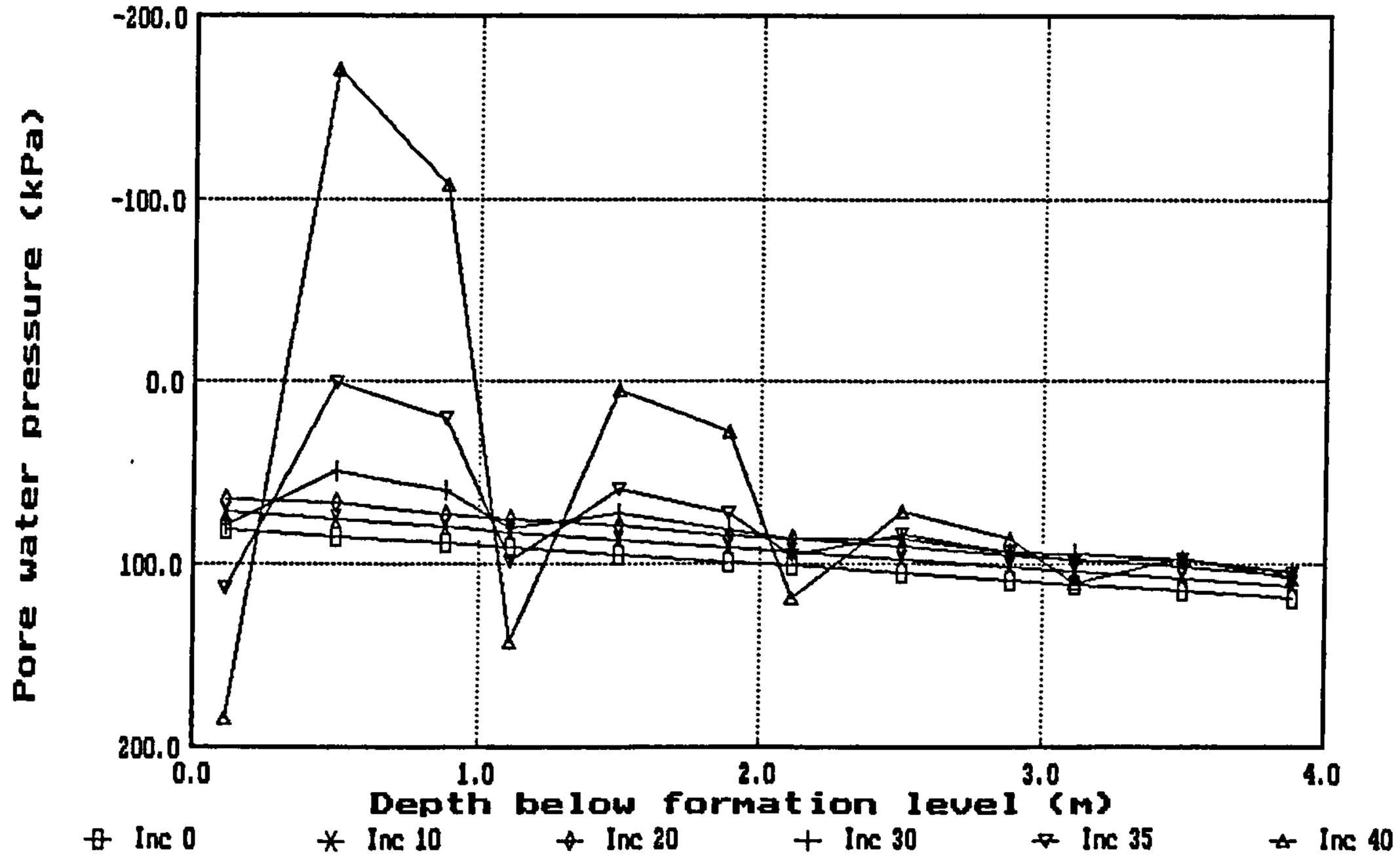

(a) uncoupled elastic analysis

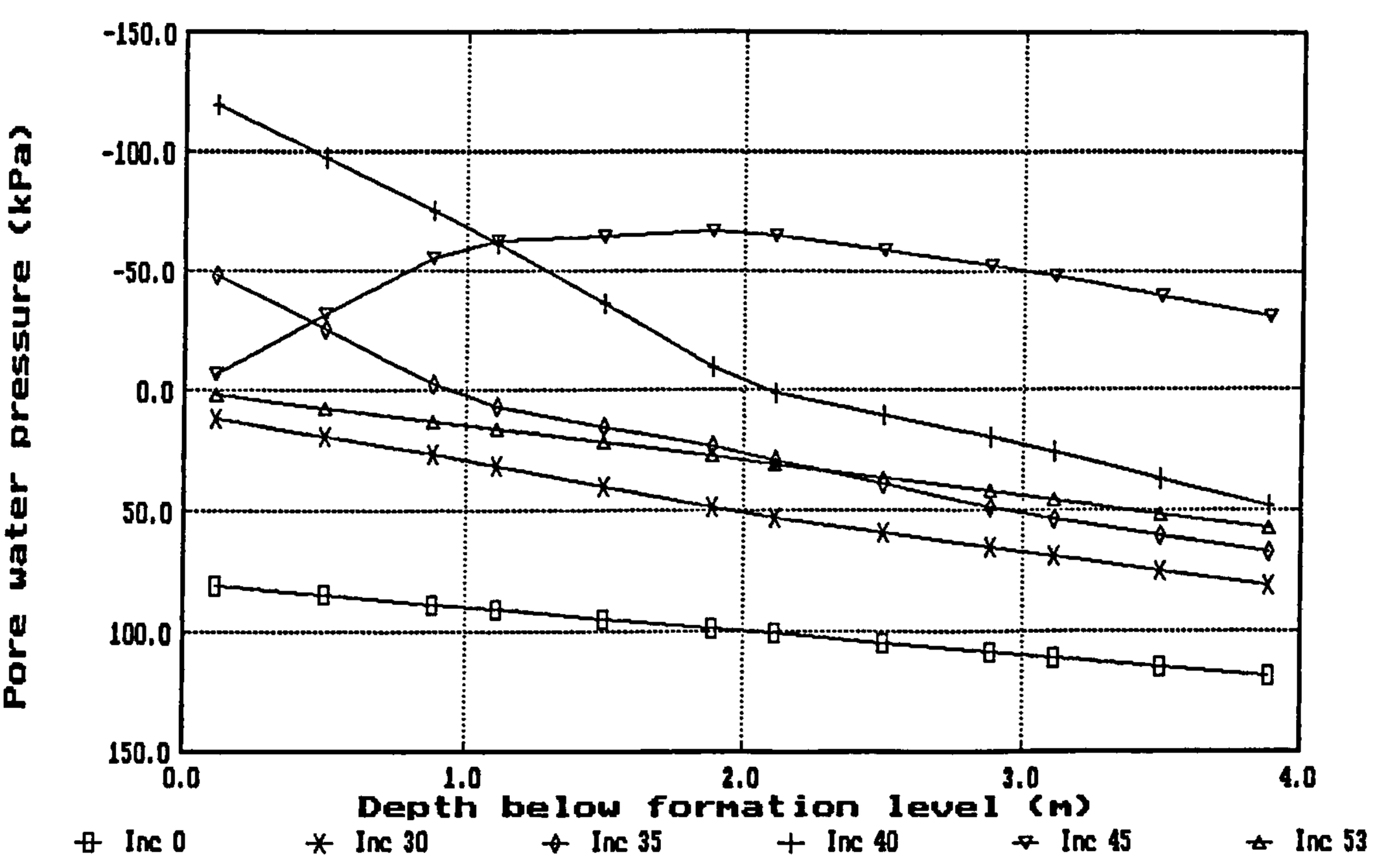

(b) coupled elastic-perfectly plastic (Mohr-Coulomb) analysis, with $c' = 0$

Fig 7.19 Investigation of passive pressure anomaly on the excavated side of an embedded wall : pore water pressure profiles just below formation level

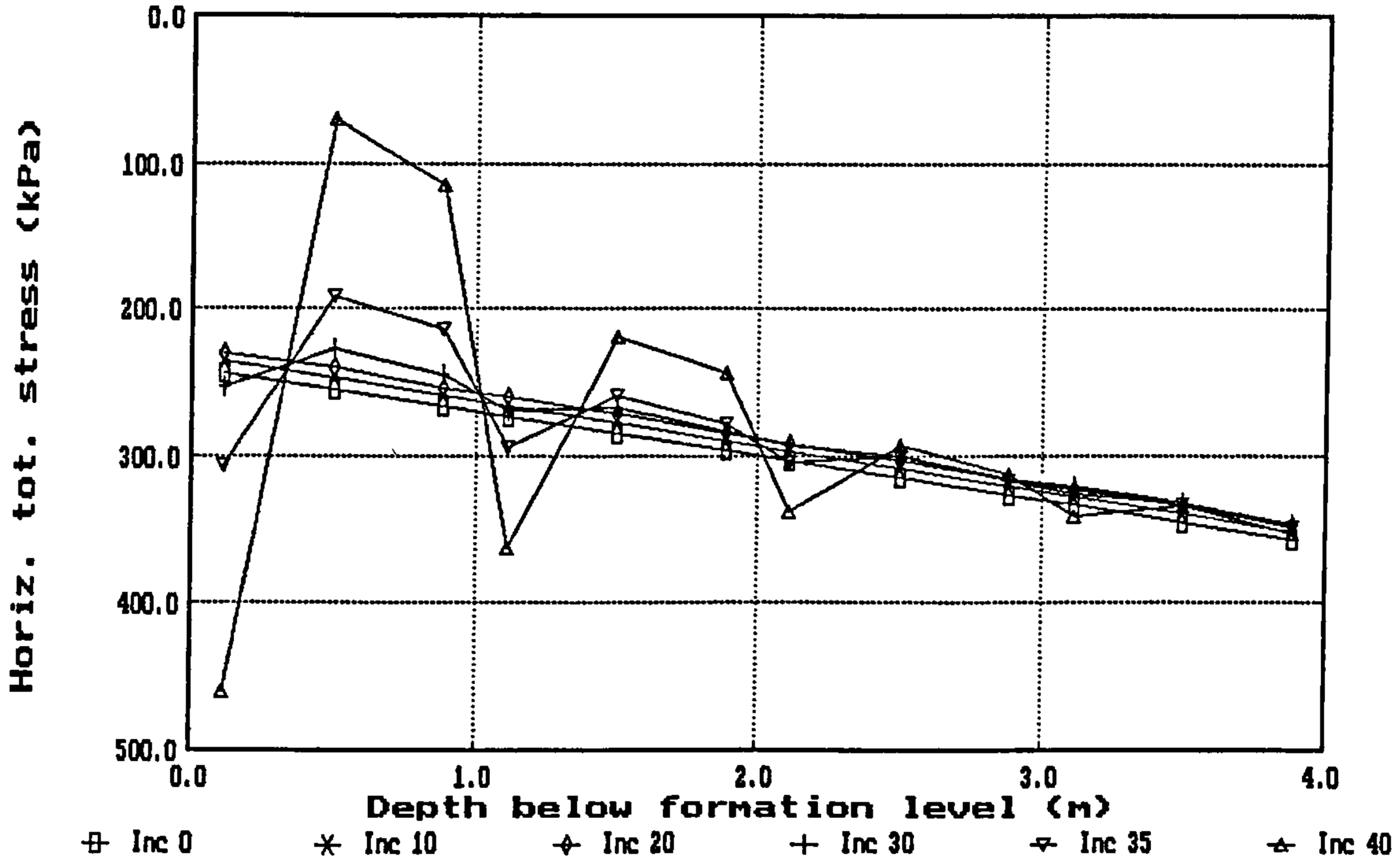

(a) uncoupled elastic analysis

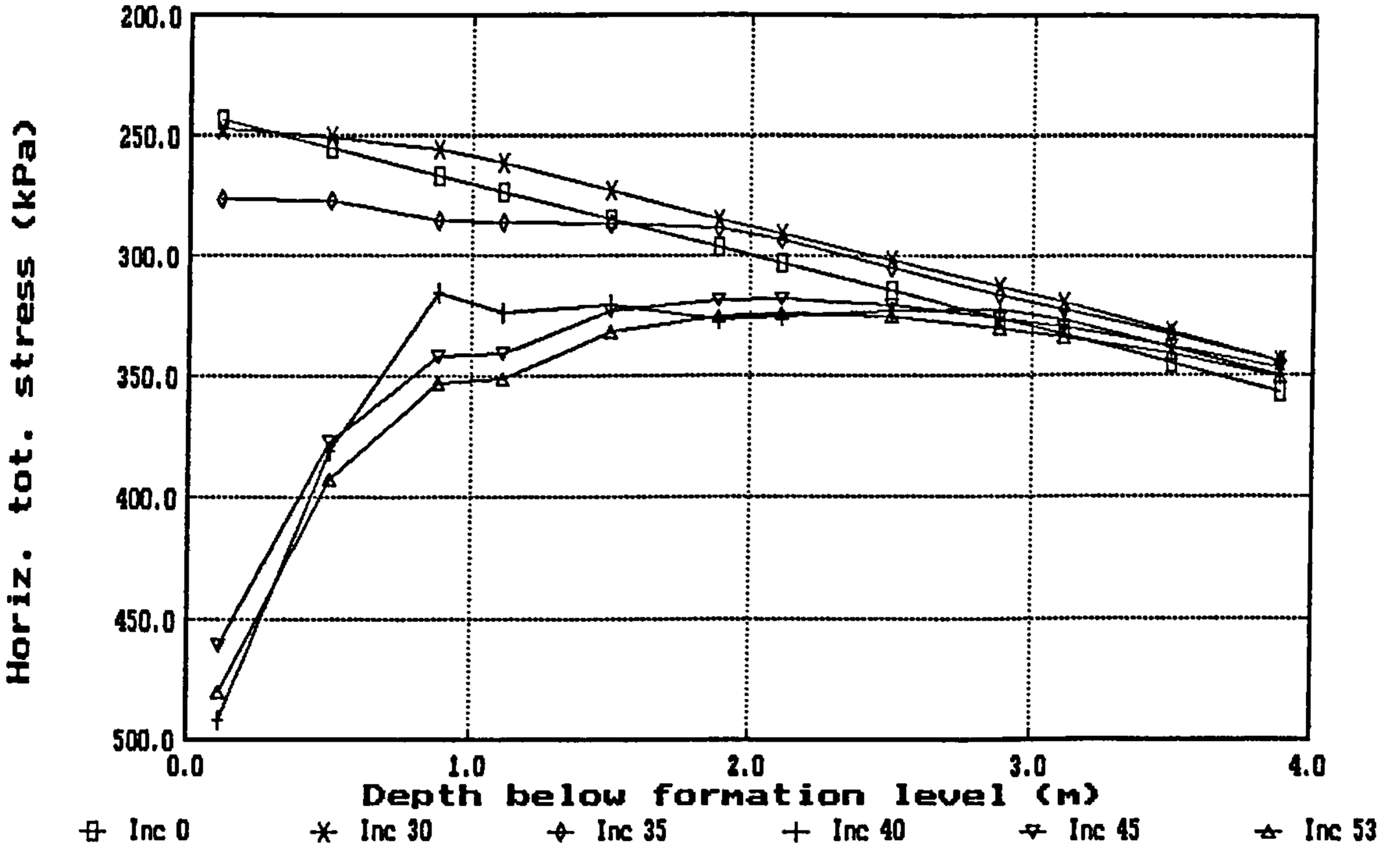

(b) coupled elastic analysis

Fig 7.20 Investigation of passive pressure anomaly on the excavated side of an embedded wall : total horizontal stress profiles just below formation level

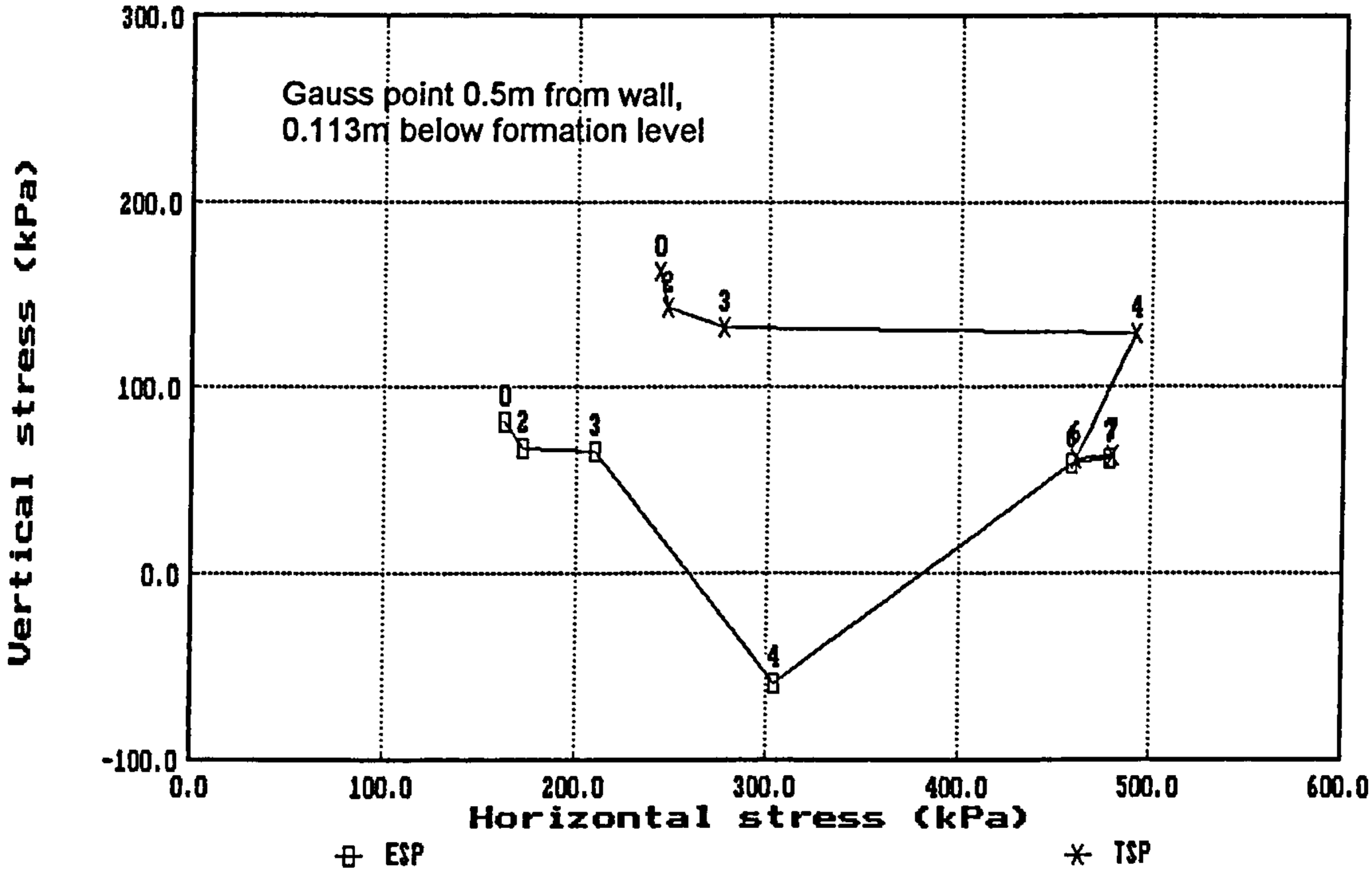

(a) coupled elastic analysis

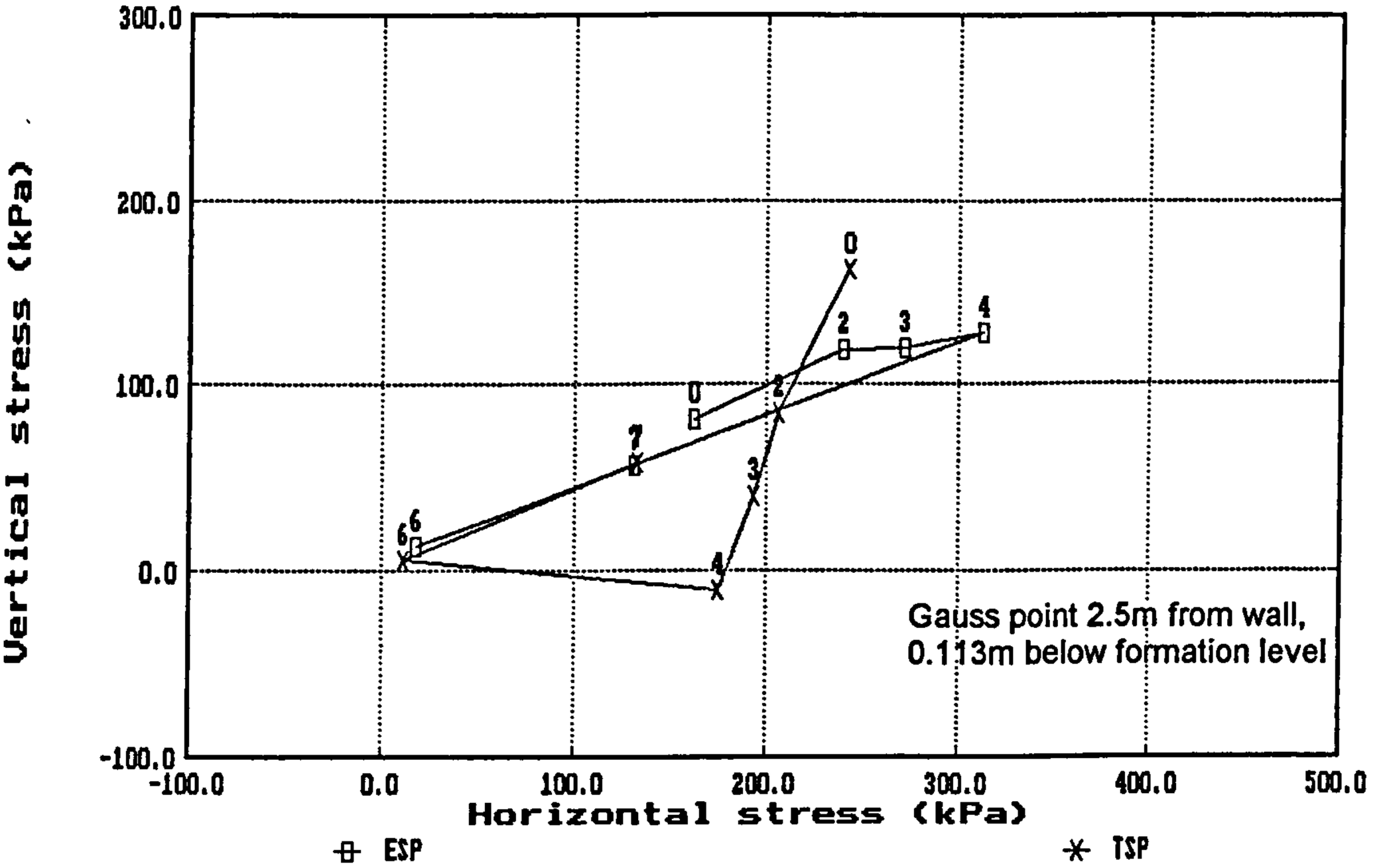

(b) coupled elastic-perfectly plastic (Mohr-Coulomb) analysis, with $c' = 0$

Fig 7.21 Investigation of passive pressure anomaly on the excavated side of an embedded wall : effective and total stress paths during excavation and equilibration

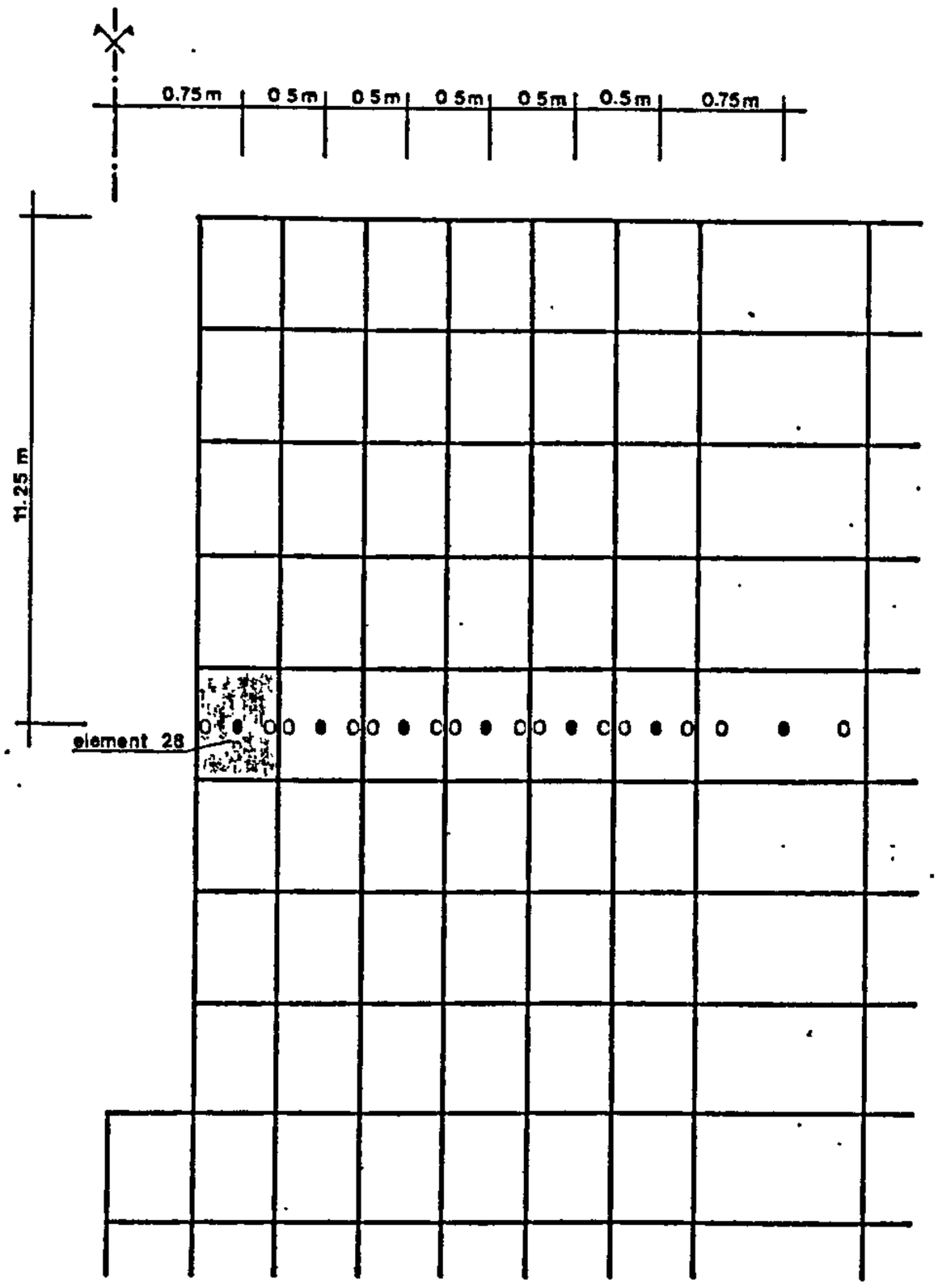

(a) Locations of integration points considered in plot (b)

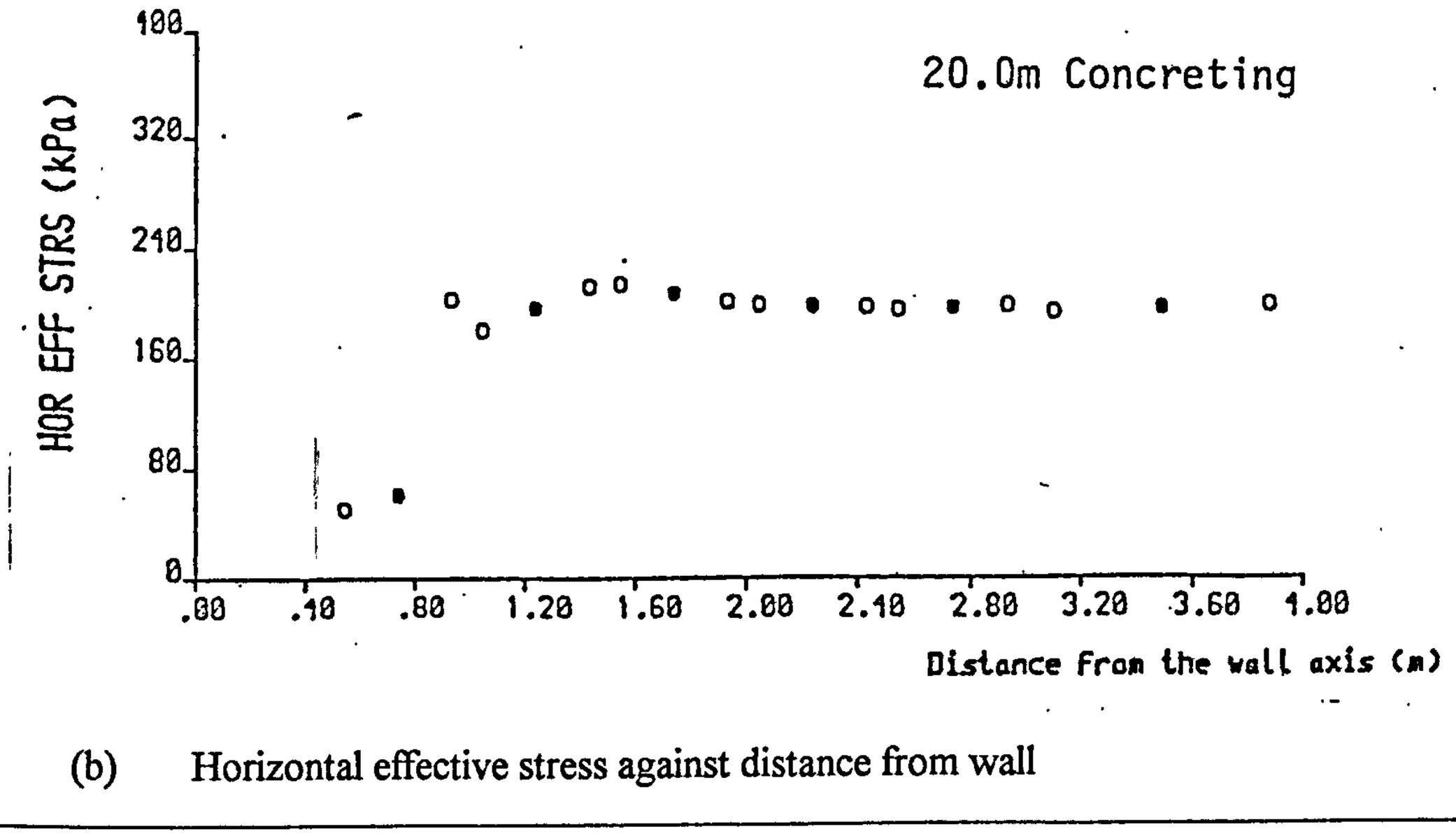

(b) Horizontal effective stress against distance from wall

Fig 7.22 Lateral oscillations in horizontal effective stress on the retained side of an embedded wall (after Kutmen, 1986)

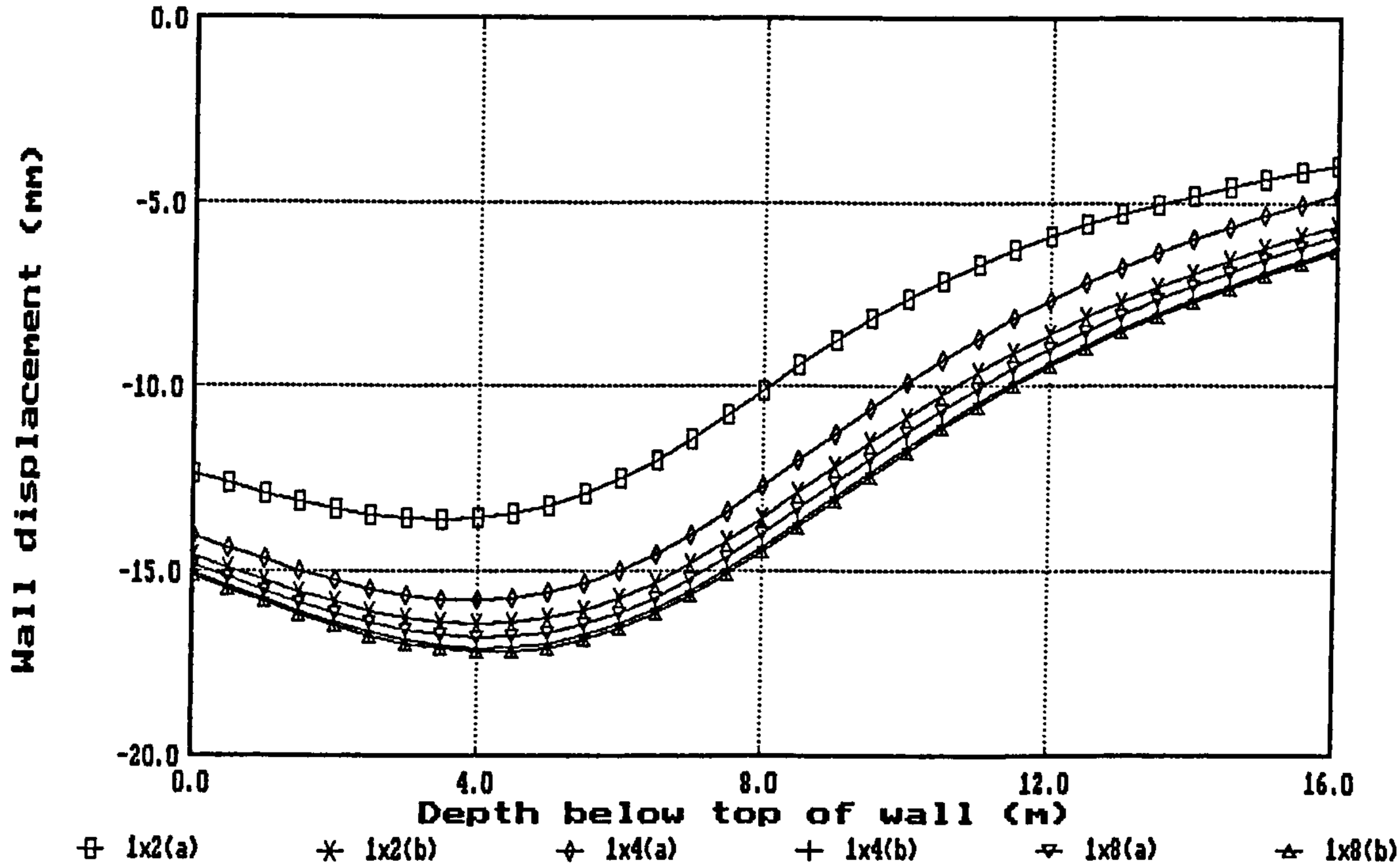

(a) wall deflection profiles

NB: 1x2 ⇒ 1 incr. block @ 2 incrs per block, etc
(a) = uniform load ratios [ULR] (b) = nonuniform [NLR]

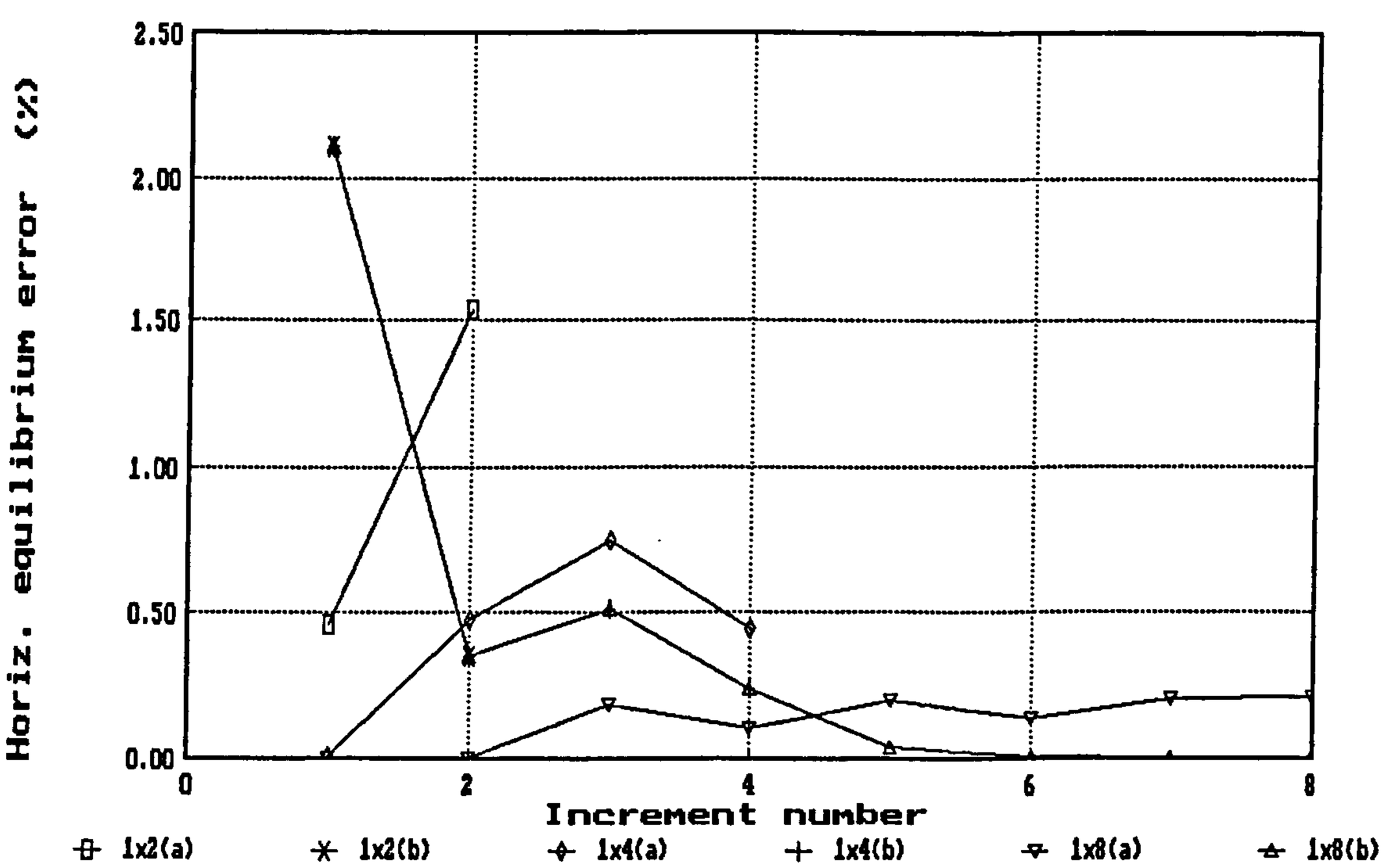

(b) evolution of equilibrium error during the analysis

Fig 7.23 Influence of load ratio (increment factor) scheme on an elastic-perfectly plastic analysis of a cantilever wall: run SC102_1

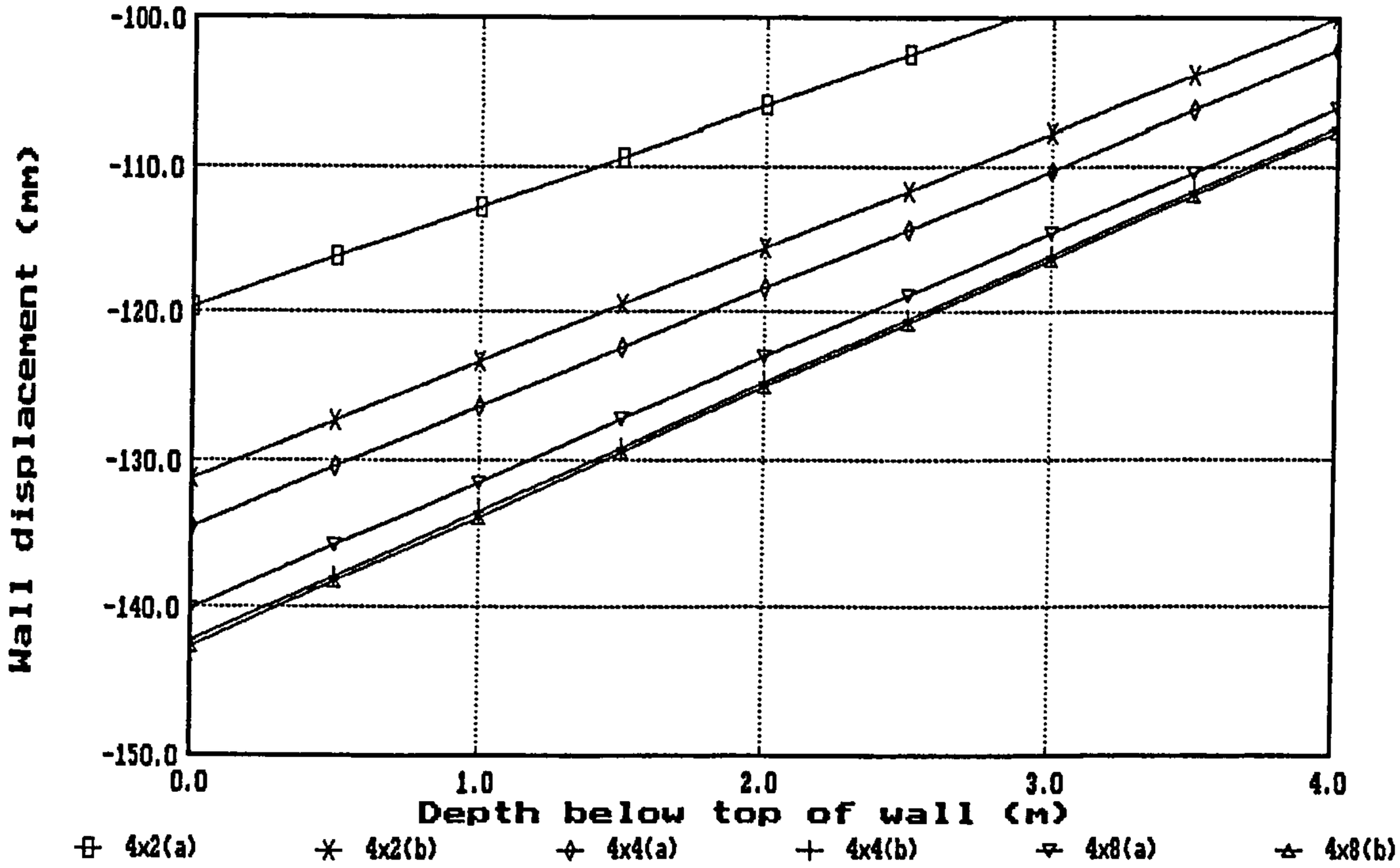

(a) wall deflection profiles (top 4m of wall only)

NB: 4x2 ⇒ 4 incr. blocks @ 2 incrs per block, etc
(a) = uniform load ratios [ULR] (b) = nonuniform [NLR]

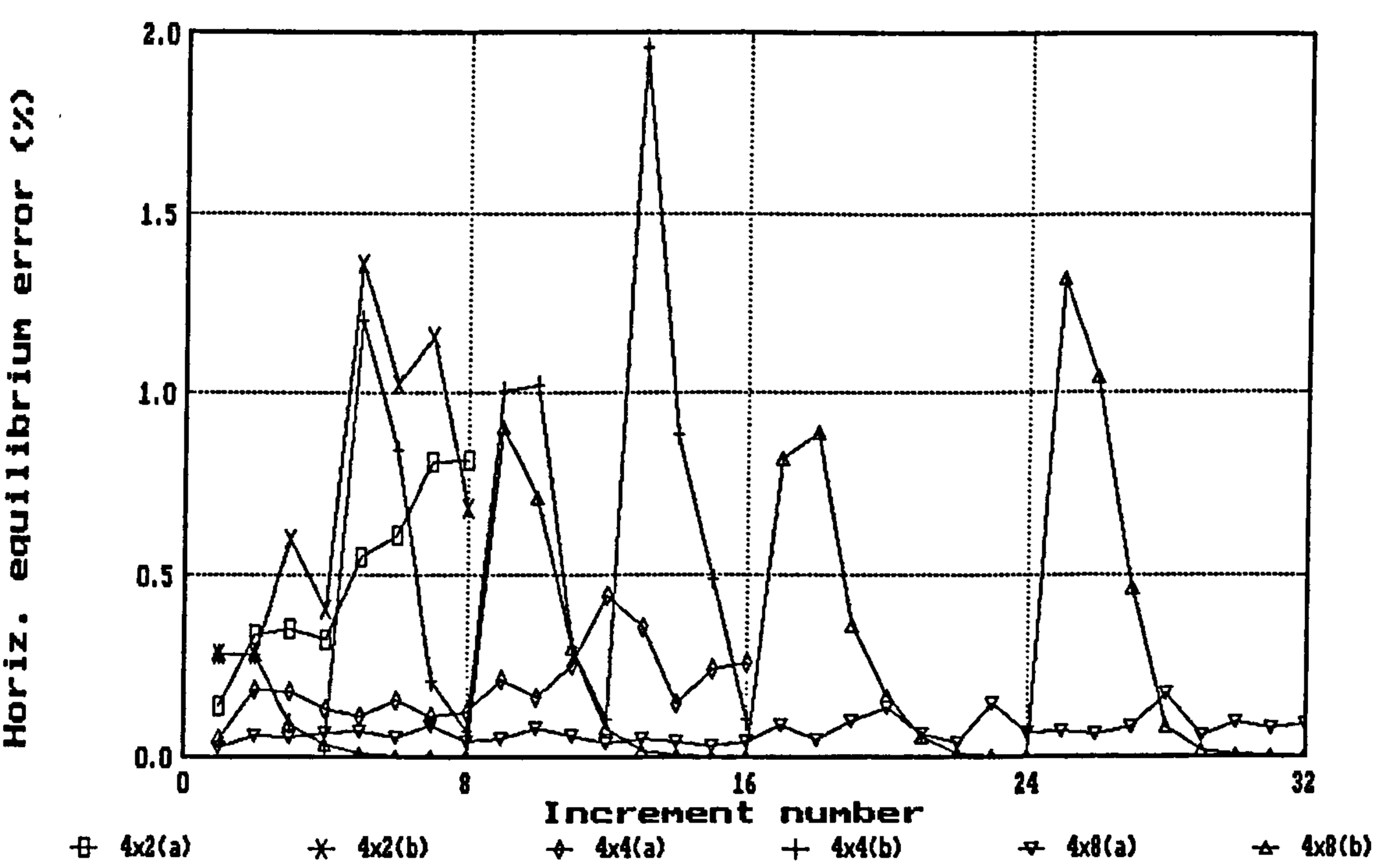

(b) evolution of equilibrium error during the analysis

Fig 7.24 Influence of load ratio (increment factor) scheme on an elastic-perfectly plastic analysis of a cantilever wall: run SC103_4

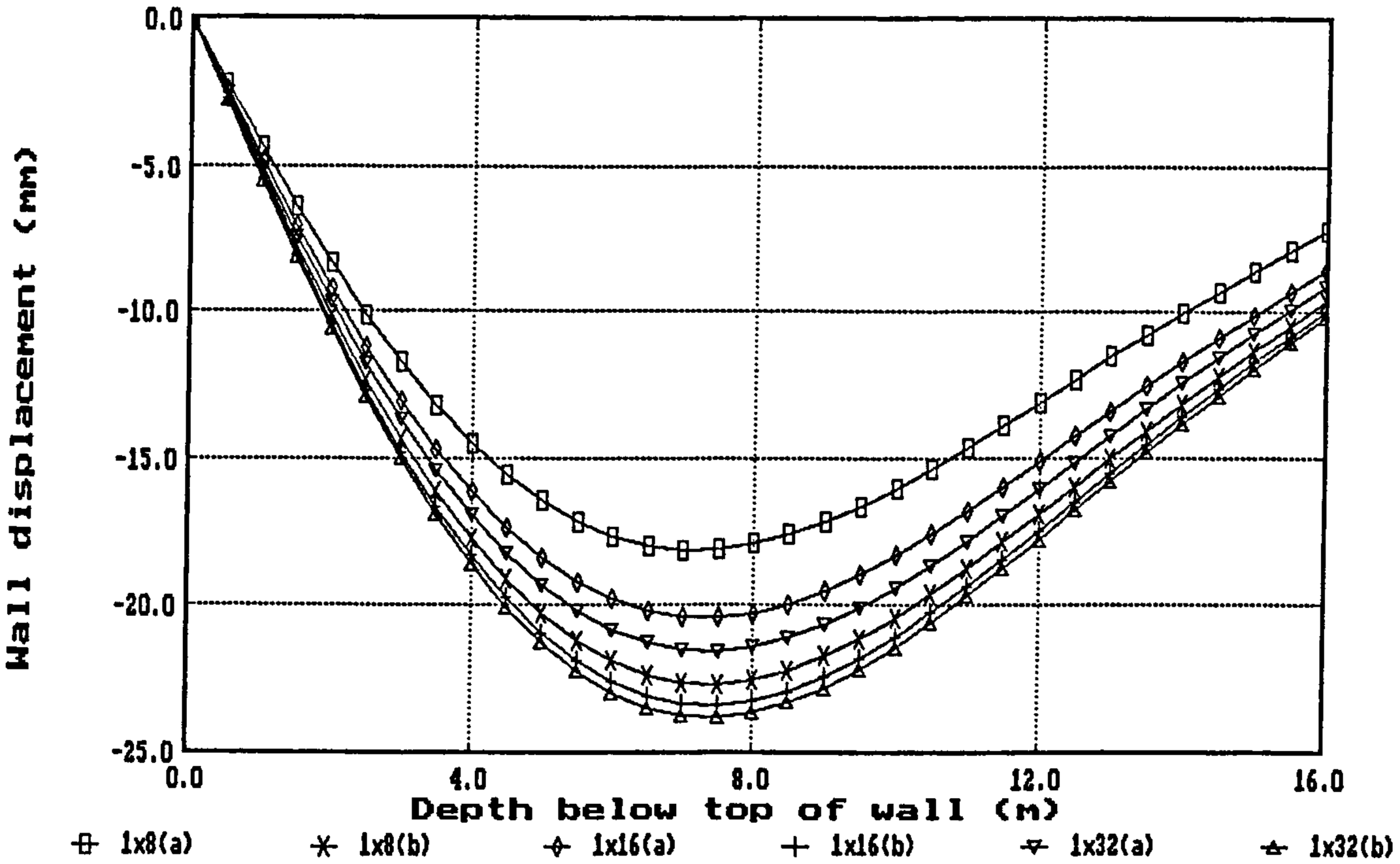

(a) wall deflection profiles

NB: 1x8 ⇒ 1 incr. block @ 8 incrs per block, etc
(a) = uniform load ratios [ULR] (b) = nonuniform [NLR]

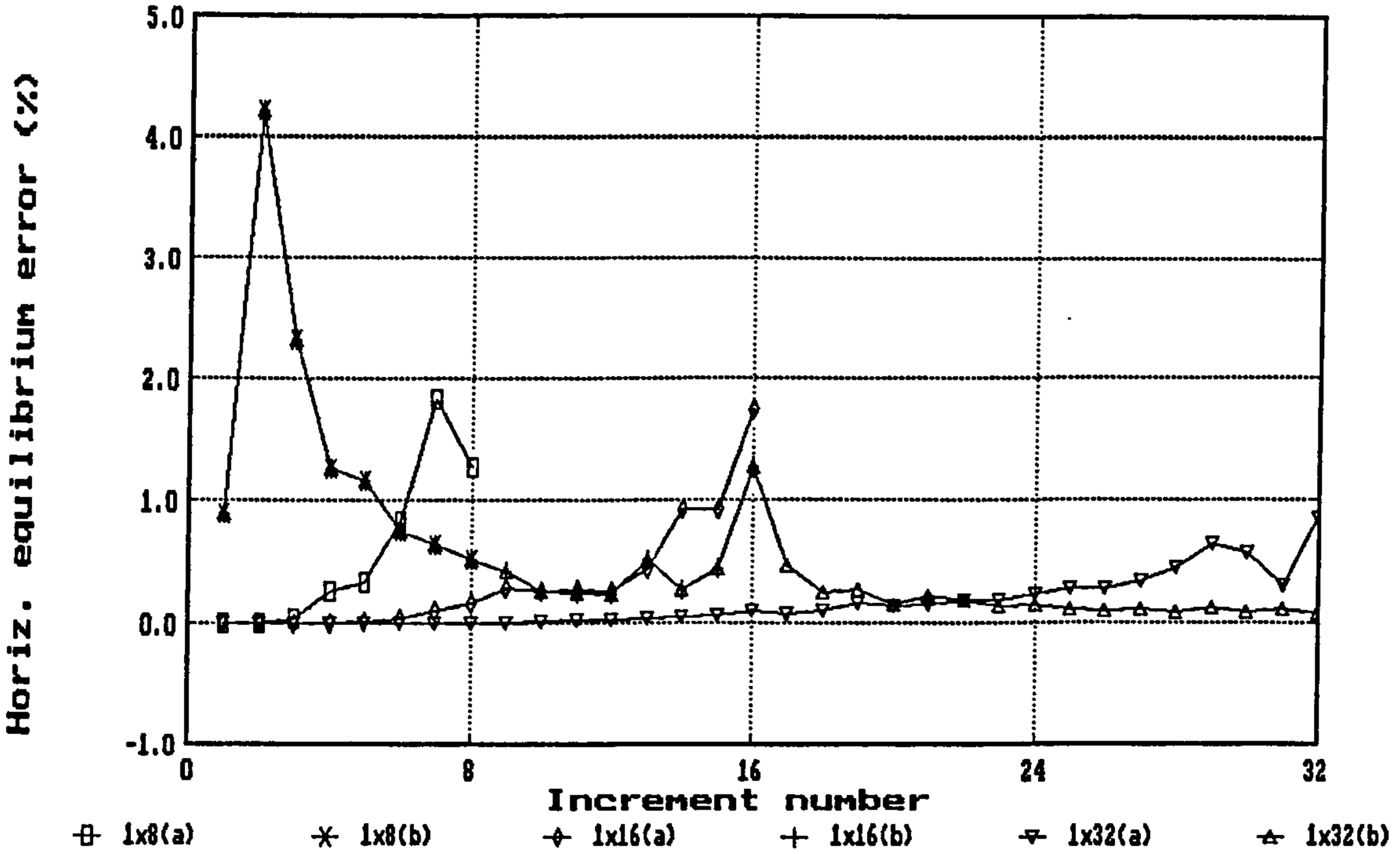

(b) evolution of equilibrium error during the analysis

Fig 7.25 Influence of load ratio (increment factor) scheme on an elastic-perfectly plastic analysis of a top-propped wall: run SC162_1

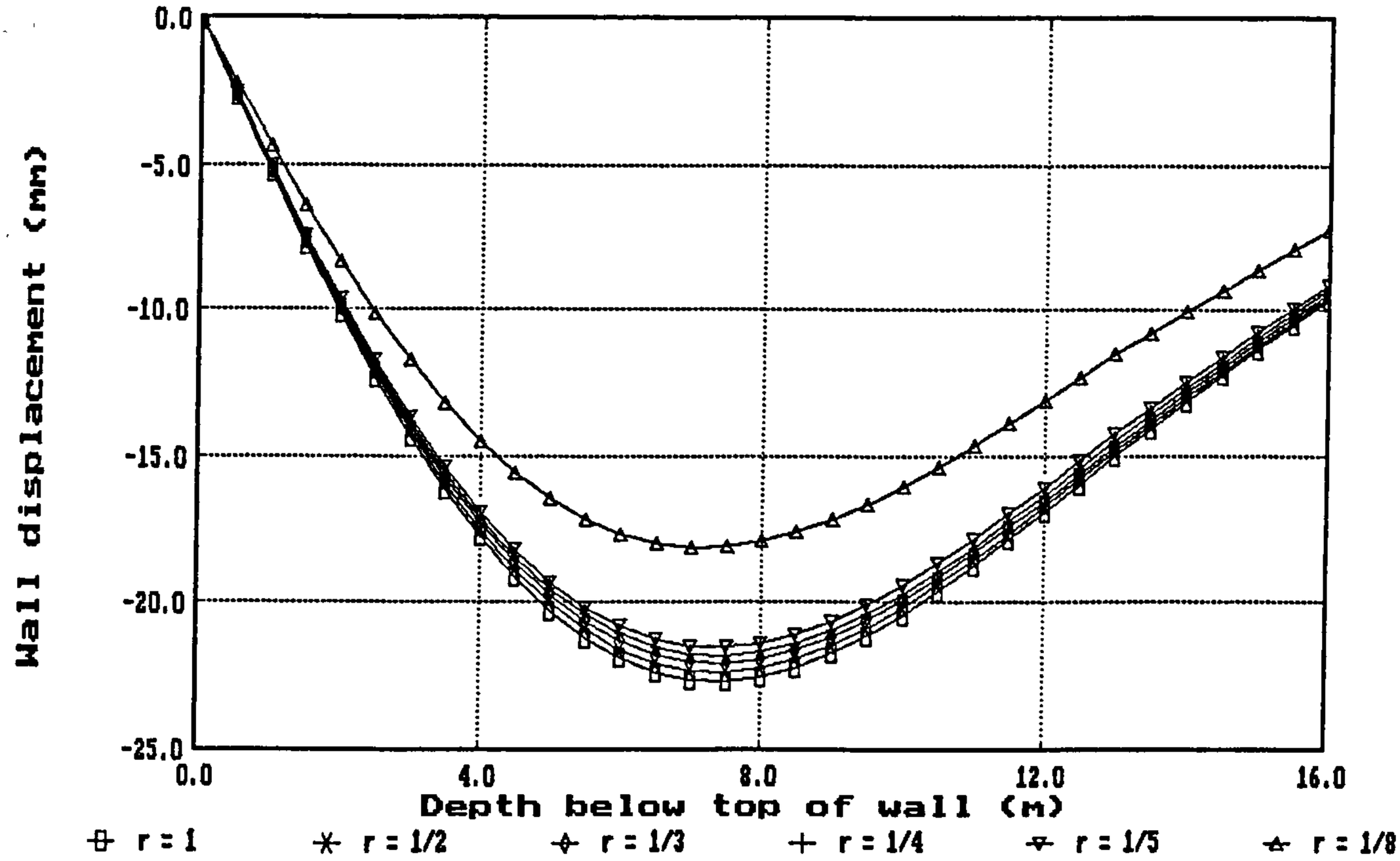

(a) wall deflection profiles

NB: value of "r" defines the initial load ratio(s) used:
1 ⇒ 1 0 0 ... 0, 1/2 ⇒ ½ ½ 0... 0, 1/3 ⇒ ⅓ ⅓ ⅓ ...0

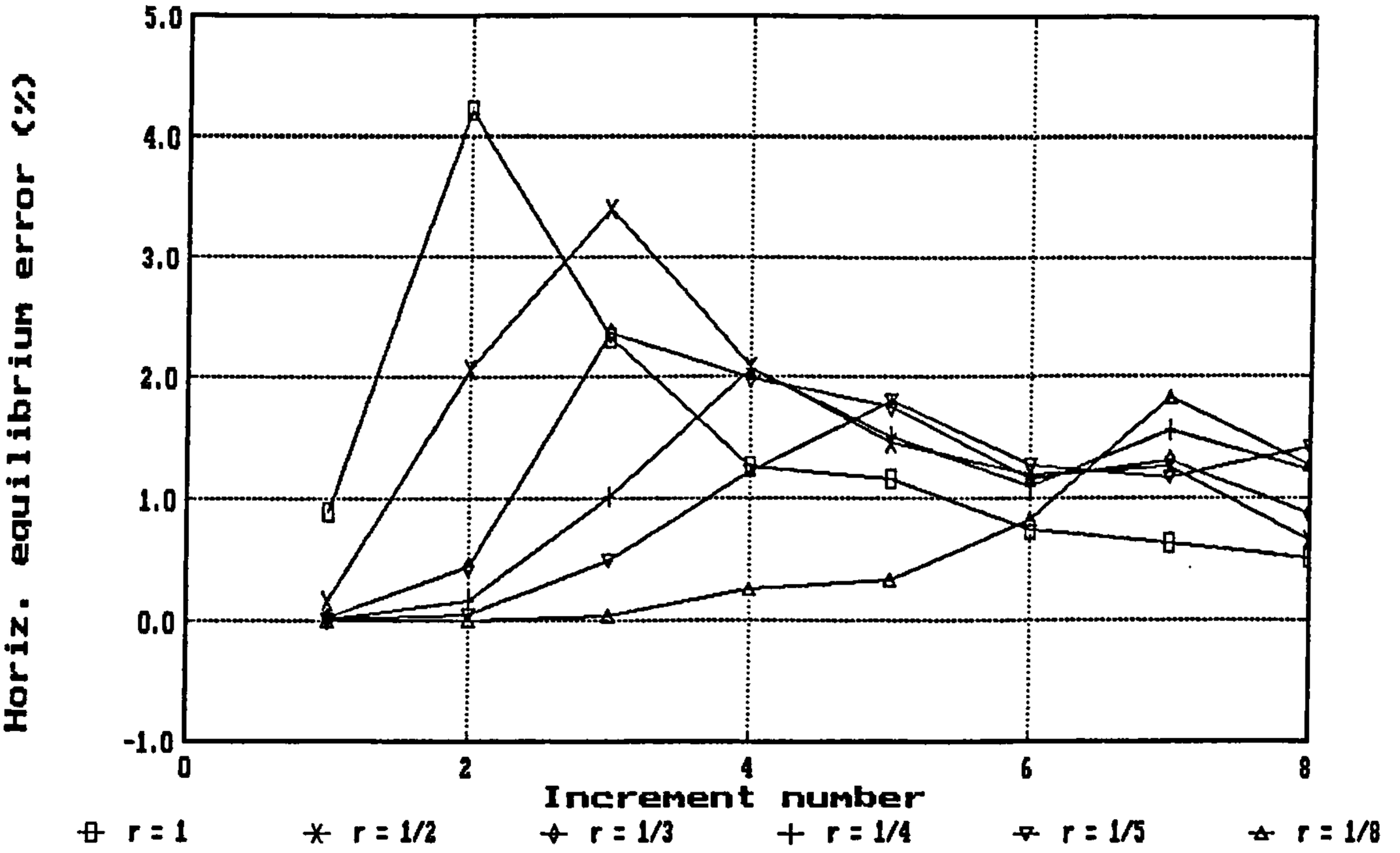

(b) evolution of equilibrium error during the analysis

Fig 7.26 Influence of load ratio (increment factor) scheme on an elastic-perfectly plastic analysis of a top-propped wall: run SC162_1R

CHAPTER 8
OBTAINING REQUIRED DESIGN OUTPUT

8.1 General Introduction

The designer of a retaining wall must ensure that the wall and its support system can safely carry the loads imposed on it, without excessive deflection and without causing damage to adjacent structures. The ability of the wall to meet all of these criteria can be assessed with finite element analysis. However, a great deal of information is produced compared with design-oriented software such as WALLAP (GeoSolve), FREW (Ove Arup/Oasys) or ReWaRD (Geocentrix). Furthermore, FE results are not in an immediately useable form - some post-processing must always take place in order to convert the raw output into something which is meaningful and capable of being understood by design engineers. This is always one of the main "culture shocks" awaiting the novice FE modeller - there is a substantial amount of information which has to be examined (sometimes just to ascertain whether or not the analysis is valid) before going on to interpret the results.

The quantities which the retaining wall designer may be interested in can be grouped into three principal categories:

a) displacements - of wall and surrounding ground
b) stresses/pressures - in soil and pore water
c) internal structural forces - in wall and support system

Further subdivision is possible (and indeed is done in this chapter), but these categories reflect increasing degrees of manipulation of the primary solution obtained by the finite element method. In other words, they reflect greater levels of approximation added to the most basic quantity which is output from the finite element (displacement) method. Some of the salient points of these output quantities will now be outlined, prior to presenting numerical investigations carried out for this thesis.

8.1.1 Displacements

Displacements are the primary unknowns obtained directly by the finite element method. No post-processing is required; no manipulation or smoothing is necessary. The FE method guarantees continuity of displacement across element boundaries through the choice of

approximation function. For example, in a 6-noded (linear strain) triangle, displacements u and v (in the x- and y-direction respectively) vary quadratically:

$$\begin{aligned} u &= a_o + a_1 x + a_2 y + a_3 x^2 + a_4 y^2 + a_5 xy \\ v &= a_6 + a_7 x + a_8 y + a_9 x^2 + a_{10} y^2 + a_{11} xy \end{aligned} \qquad (8.1)$$

(a_o .. a_{11} are found by substituting the co-ordinates of the six nodal points into these expressions in turn). The form of Eqn (8.1) ensures that the displacement field in one element will match up with those in adjacent elements along the common boundaries.

Of course, there are numerous influences which will affect the reliability of both the magnitude and pattern of displacements in a retaining wall analysis. These have been explored in earlier chapters and include geometric discretization, constitutive modelling, construction simulation, etc. Here it is assumed that the calculated displacements are available, and it is their overall quality (from a finite element viewpoint) which will now be explored.

Engineers are generally led to believe that the finite element method produces displacements which are too small, as the mathematical model is "stiffer" than its physical counterpart (due to having finite d.o.f.). In a retaining wall context, this could be interpreted as meaning that the maximum predicted displacement of a wall will always be too small. Strictly speaking, it is the total potential energy of the finite element model which is greater than that of the real system. This may mean that the displacement predicted at a particular point in the mesh is too small, but this cannot be generalized[1]. Studies reported in Chapter 4 showed that the changes in magnitude of displacements arising from mesh refinement, for example, were not always intuitively "correct".

Strains logically belong in the same category as displacements, as they are a measure of change of dimension. However, strains have gone through one stage of approximation more than displacements, as they are obtained by multiplying nodal displacements by differentiated shape functions (Section 3.3.2):

$$\boldsymbol{\varepsilon} = \mathbf{B}\,\mathbf{a} \qquad (8.2)$$

---

[1] If reduced integration is used, it cannot even be guaranteed that the minimum potential energy is bounded from above.

where **B** contains differentiated shape functions of the form $\partial(N_i)/\partial x$, ε is the vector of internal strains and **a** the nodal displacements (Section 3.3.2). One case where strains would be expected to be of poor quality is in large displacement problems, where the conventional definitions of strain (e.g. $\varepsilon_x = \partial u/\partial x$) are no longer sufficiently accurate, due to the increasing significance of second-order terms. CRISP offers an approximate solution to this through the option to update nodal co-ordinates; future versions may include a more rigorous formulation employing Green's strain tensor (Zienkiewicz and Taylor, 1989), but see Section 3.3.8.

Furthermore, although displacements are continuous across element boundaries, strains need not be continuous (although, as the mesh is refined, improved continuity would be expected). This is because there is no requirement of continuity in the displacement function derivatives (upon which strains rely).

On the whole, strains do not appear to be sought routinely by those using finite elements in practical retaining wall design. Movement criteria are more likely to be expressed in terms of a maximum allowable displacement (e.g. horizontal movement at top of wall), rather than a limit on strain levels in the surrounding soil. The writer has only been involved with one case where an estimate of operational shear strain levels around a deep basement excavation was required (Queensberry House - see Appendix A). This was in order to select appropriate stiffness parameters for a linear elastic analysis from continuous shear modulus versus axial strain data, before progressing to a full non-linear analysis.

8.1.2 Stresses and pressures

Stresses and pore water pressures are secondary (or perhaps even tertiary) quantities as they are derived from element strains, which in turn are based on displacements:

$$\boldsymbol{\sigma} = \mathbf{D}\,\boldsymbol{\varepsilon} = \mathbf{D}\,\mathbf{B}\,\mathbf{a} \qquad (8.3)$$

Stress distributions may be required for comparison with classical design methods, or perhaps with in-situ measurements. However, they may be unreliable as a basis for simple hand calculations of equilibrium, as unexpected patterns can occur on both sides of the wall (see Chapter 7), potentially confusing the inexperienced analyst. It must be remembered that the FE method only ensures equilibrium of nodal forces, and that in general there will neither be local equilibrium within an element nor equilibrium of stresses across element boundaries.

Gallagher (1977) has pointed out the irony that, for a technique which is so often used in stress analysis, the (displacement) finite element method produces rather poor predictions of stress. Attempts to improve output stresses through smoothing are well documented, and are examined in greater detail in Section 8.3. Improvements to stress computation through hybrid finite elements have also been established, but are beyond the scope of this thesis.

8.1.3 Internal structural forces

Internal forces comprise axial loads, bending moments and shear forces, which may be present in the wall and any of its supporting anchors or props (temporary and permanent). These quantities are obviously of prime interest to the designer who must ensure that there is an adequate reserve of strength against structural failure in all possible modes.

The manner in which the internal forces are computed is determined by the type of element which has been used for the structural component. Anchors and struts without bending stiffness are adequately modelled with 2-noded bar elements[2], which have axial stiffness only. Bar force is then given by standard relationships, involving the product of Young's modulus and cross-sectional area, EA. Force in a bar element is thus a secondary quantity, although directly linked to displacement without further approximation. For anchors, it is convenient to work in terms of excess force over the initial (pre-stress) value.

Struts which possess bending (in addition to axial) stiffness may be modelled with 2-noded beam elements, where EA is supplemented by the flexural rigidity EI, and bending moments are calculated at nodes using standard stiffness relationships. It is possible for the wall itself to be modelled this way, though this is not common unless it is a steel sheet pile wall. Permanent props in the form of concrete slabs are usually modelled by solid 2D elements, and the axial load at any section can be readily obtained from integrating the transverse stress distribution across the section. The calculation of prop/anchor forces is discussed further in Section 8.6.

The calculation of bending moments in walls modelled with 2D elements may be based on:

i) transverse stress distributions in the wall elements

ii) lateral pressures acting externally on the wall elements

---

[2] The 3-noded bar element is unsuitable, because of the requirement either to fix the middle node, or attach it to the mid-side of another element.

iii) nodal forces acting between wall elements

iv) nodal forces acting externally on the wall elements

v) double differentiation[3] of the wall displacement profile

Methods (i) and (ii) are intuitively reasonable and also quite convenient as they make use of stresses calculated at integration points in the relevant elements. However, as noted earlier, stress distributions in the soil can be far from reliable; furthermore method (ii) multiplies (possibly) inaccurate stresses by an increasing lever arm for sections further down the wall. Limited comparisons of methods (i) and (ii) have shown significant discrepancies (Swain, 1989; Gunn and Ponnampalam, 1990; Powrie and Li, 1990a). Methods (iii) and (iv), on the other hand, make use of nodal forces which can be expected to be rather more reliable. As these forces are not normally output to the user, some program modifications will be necessary. Method (v) is probably too error-prone to warrant serious consideration - it is sometimes used to infer bending moments in field structures when inclinometer profiles are available, though it is not nearly as reliable as using strain gauges to infer transverse normal stress distributions.

The calculation of wall shear forces where 2D elements have been employed may be based on the same ideas as methods (i) to (iv) above, with obvious modifications (use of shear rather than normal stress distributions, no lever arm, etc.). However, little previous work appears to have been done in this area. Investigations of bending moment and shear force computation are presented in Sections 8.4 and 8.5 respectively.

Fundamentally, the finite element method deals with nodal forces and displacements, but whilst the latter are commonly used and are of recognizable value, it is quite rare for the former to be used directly. Nodal forces may be used to make simple (hand) checks that the output satisfies force equilibrium, but this tends to be done automatically by the program and summarized for the user in the form of out-of-balance loads. There is the added complication that consistent nodal forces for typical distributions of boundary traction are far from intuitive, for elements other than constant strain type. Notably, nodal forces (other than reactions) have never been listed as an output option in CRISP - only "out of balance" loads which are a measure of equilibrium (see Section 7.2.3.1).

---

[3] Usually by finite difference techniques; but it should be noted that numerical differentiation is substantially less accurate than numerical integration.

8.1.4 Assessment v interpretation

There is a distinction between output which designers ultimately require for checking the sufficiency of their designs, and output which serves to demonstrate whether or not the analysis is admissible in its entirety. The two types of output rarely overlap and consequently, if time is short, the latter category is overlooked. A useful analogy exists with the Morgenstern and Price (1965) non-circular slope stability analysis - it is the factor of safety which is ultimately sought, but the implied position of the thrust line within the failing soil mass must be checked for admissibility before the analysis can be considered valid.

Following a similar approach, the authors of the SAGE CRISP interface have chosen to distinguish between output visualization and output interpretation tools (SAGE, 1996). SAGE describe *visualization* as helping the user identify regions of interest for more detailed examination. The tools of visualization are contour plots, deformed mesh and displacement vector plots, and status plots (stress state codes, principal directions, etc). However, most analysts already know what parts of the output they are interested in. Arguably visualization has a much more important role to play, and the writer prefers to think of it as the process of establishing that the analysis is both legitimate and the one which was intended, boundary conditions have been applied correctly, geometry changes (element removals/additions) are in the right place and sequence, overall patterns of movement appear reasonable, stress distributions are credible, equilibrium errors and/or yield ratios are within acceptable limits, etc. The term "assessment" is therefore considered to be more appropriate than visualization. An important point is that none of this is directly useful in the design context but it must be examined and checked. In the writer's experience, however, this seldom happens in practice.

Interpretation is the process of extracting data directly relevant to the application - in this case wall movements, prop forces, wall bending moments, earth pressures etc. The tools of interpretation are principally X-Y graphs of various quantities, one against another. SAGE (1996) distinguish two different types of graph, "instance" and "duration" graphs. An instance graph shows some part of the analysis at a particular increment, for example the vertical displacement of a line of nodes in some part of the mesh. A duration graph shows the variation of a quantity at a single point in the mesh over a specified range of increments; for example the decay of excess pore water pressure with time at a particular node. These are the plots which usually appear in final reports, for example, but their reliability can only be established after having viewed the assessment output (i.e. contour, status, vector and

deformed mesh plots - termed "visualization" by SAGE). However, in commercial situations, time pressures often dictate that instance graphs (only) are extracted and plotted quickly.

On the whole, the distinction between assessment and interpretation is a helpful one - whether or not engineers are consciously aware of it. The key point in the writer's opinion is that both are essential but, unless the analysis actually crashes, engineers rarely search for proof of its veracity. The usual stance is to accept finite element output unless it is obviously flawed. The attitude should actually be one of suspicion until the analysis can be shown to be correct (and that the inherent limitations of the method have not rendered the results meaningless) through proper assessment.

Having established the three principal output categories which are of interest to the retaining wall designer, each will now be subject to more detailed examination and discussion in the following sections of this chapter.

8.2 Displacements

8.2.1 Graphical representation

Deformed mesh plots

It is always advisable (though rarely done) to produce the first deformed mesh plot with no exaggeration at all. In this way, any excessive movement (arising from a gross error perhaps) will show up clearly. This is especially true when there is a plotting option to draw the deformed mesh such that the largest movement anywhere is specified, and all other movements are scaled *pro rata* (this avoids having to decide what exaggeration factor to select initially).

It is also important that deformation of the whole mesh should be shown before zooming in to a particular window. Otherwise it is possible to miss a problem which has occurred in a part of the mesh not in the main area of interest. An example of this was related by Bond (1996) for an analysis of a retaining structure on a slope, where the engineer immediately "zoomed in" on the upper part of the wall and saw only modest movements. However, the exaggeration which had been calculated automatically by the program in order to fit the plot on the screen was found to be <<1, indicating that displacements had been factored down heavily for plotting purposes. What the engineer had missed was that an overall failure mechanism had

formed in the slope, and the wall was moving monolithically as part of this failure. This was obvious to see after "zooming out" to view the deformations of the entire mesh.

The norm is for the resultant of both horizontal and vertical components of displacement to be used to produce deformed mesh plots. However, there are occasions (especially when high exaggeration factors are employed) where it would be better to show just the horizontal or vertical movements separately. One example of such a situation is when there has been large base heave and outward wall movement in an excavation; a conventional deformed mesh plot can produce overlapping elements at dig level near the wall, Fig. 8.1.

Overlay elements can also cause problems, especially if they incorporate new nodes. Fig. 8.2 shows a not uncommon situation in which soil was excavated to final dig level, and a hinged permanent prop slab[4] was installed. The slab had been defined by overlay elements, and when it was installed, nodes along the top edge initially had their displacements zeroed - whereas (common) nodes along the excavated soil surface had heaved. (The small settlement visible along the top edge of the slab was due to the surcharge it applied to the underlying soil). The overall effect was one of unreasonable element distortion - especially in the hinge location.

Displacement vector plots

Vector plots are much more effective at depicting the overall flow of movement than are deformed meshes. It is advisable always to create a vector plot for the whole mesh without exaggeration, before zooming in and/or exaggerating the displacements (for the type of reason mentioned above). It would also be useful to be able to plot horizontal and vertical vectors separately, for a better picture of the components of movement. However, the norm is to plot resultants and many post-processing packages only allow this.

There is one point unique to displacement vector plots which should be discussed here. When a vector is plotted, it is basically an arrow joining the two points (x_o, y_o) and $(x_o+\delta x, y_o+\delta y)$ - where δx and δy are the components of movement. The displacement vector plot will join the original and final positions of a node (over the range of increments considered) without tracking its overall movement. This is illustrated in Fig. 8.3, with the example of a node whose position after each of 5 successive increments is shown. In Fig. 8.3(a), the original and

---

[4] If not hinged in reality then perhaps modelled as such in order to give zero moment transfer.

final points are joined up, consequently missing the fact that the node has followed a curved displacement path. In Fig. 8.3(b), the points are joined up sequentially and the true pattern of movement is revealed. This form of representation may provide helpful insight into developing mechanisms, but it would require modification to the post-processing package.

Displacement contour plots

Contours of displacement, though not as general as strains, can be very useful. As it is normally possible to contour either horizontal (δx) or vertical (δy) displacement, these plots can be used to distinguish zones of net heave/settlement (separated by the $\delta y = 0$ contour) or net movement to left/right (separated by $\delta x = 0$). Post-processing software does not normally permit resultant displacement $\sqrt{(\delta x^2+\delta y^2)}$ to be contoured, but this is unlikely to be a major disadvantage. Resultants are very useful in depicting flow patterns but less meaningful as a scalar quantity for contouring. As noted earlier (Section 8.1.1) displacement contours can be expected to be smooth and continuous across the domain.

Contours of displacement provide immediate proof that boundary fixities are correct, evidenced by their coincidence with $\delta x = 0$ and/or $\delta y = 0$ contours as appropriate. Furthermore, inspection of contour spacing near the boundaries gives an immediate feel for whether or not the boundaries are too close to the retaining wall; high gradients would suggest that the boundaries are too close and may be influencing the analysis.

Instance graphs

In most cases, instance graphs are ultimately what the designer needs, and there are four principal types which can be extracted from a retaining wall analysis:

a) wall displacement
b) excavation heave
c) ground surface settlement and/or heave
d) horizontal ground movement

It is inadvisable that instance graphs be extracted without having first given the whole analysis a "health check": a movement profile might be accepted uncritically when there is a serious error in the finite element model. An example of this arose in the analysis of the Queensberry House deep basement (Appendix A) where the foundations of a neighbouring bank building were immediately adjacent to a party wall on the longitudinal section. The adjacent

foundation was modelled as two slabs with a void between them, reflecting the actual construction, Fig. 8.4. Bar elements were included every few metres to maintain vertical separation between the slabs. This would have been quite satisfactory except that the material zone number given to the slab overlay elements was initially incorrect, and instead of having the stiffness of concrete, the original soil (gravel) material properties were still active for these very long slender slabs. The result was that, in the FE analysis, the upper slab buckled in a concertina fashion and failed to prevent the top of the party wall moving backwards away from the excavation. This was not picked up until after profiles of wall movement, and horizontal and vertical ground movement along adjacent foundation level had been plotted and despatched to the client. This may seem an extreme case, but recall Irons and Ahmad (1980; cited in Chapter 1) who estimate that "... >50% of commercial runs are probably stillbirths....". Analysis assessment is a necessary part of the quality assurance process.

To generate instance graphs, one can either use a purpose-written plotting program (e.g. the SAGE CRISP post-processor) or something which essentially allows raw data to be exported to a spreadsheet (such as the CRISP-Lotus Interface provided with CRISP 9x). A spline could be used to join the data points, but should not be of an order higher than that used for the displacement approximation in the elements. The default for most spreadsheets is to joint points with line segments, which will give acceptable quality in most cases. (A "smoothing" option is often available, but should be used with caution as there is normally no way of controlling the curve-fitting order).

Horizontal and vertical sections passing through nodes are generally straightforward and convenient to define in a mesh comprising predominantly rectangular elements. Developed sections (e.g. tracing around a buried object such as a tunnel lining) are rather more time-consuming to set up. Some post-processors (e.g. FEMVIEW) have the facility to specify a any two points in the mesh by pointing and clicking with a mouse, and the nodes near to a line joining these points are automatically picked up and used.

Cumulative v incremental plots

It is normal to commence analysis assessment by viewing cumulative displacement plots, to obtain an impression of the total movement which has occurred since the start of the analysis. But this is not always the best approach and can sometimes be misleading - especially in multi-stage construction, where a wall and components of its support system can only actually

"move" after they have been installed. It is also unrealistic to use cumulative plots where the analysis has included modelling of past events - for example, previous construction which is to be demolished to make way for something new. Movements associated with present and future activities would have to be referenced to displacements at the end of the increments used to establish present day conditions.

Incremental displacement plots shows the differences between two specific increments in an analysis, and have several advantages over cumulative plots. For example, they would help overcome the problem described previously for apparently distorted overlay elements. They also prove useful in illustrating the effectiveness of propping, as displacements zeroed against the increment in which the prop was installed should show little (if any) subsequent movement between the propping positions.

Caution must be observed when producing incremental plots with CRISP in regions where the geometry has changed. Elements not actually present in the final increment may still be shown in the plot because they were present in the first increment.

8.2.2 Wall movement

The entire wall displacement profile is usually of interest, with the maximum value (δ_{max}) of particular importance. As the wall material will nearly always be linear elastic, it should show a smooth displacement profile without any discontinuities: deviation from this indicates an immediate problem. In an analysis undertaken by the writer (Southwark Station Ticket Hall - see Appendix A), the excavation of a row of soil elements accidentally included one taken out of the wall itself - a fact which would have been missed if only δ_{max} was extracted (although the excessive magnitude of δ_{max} due to the wall effectively being hinged at mid-height was adequate warning of a major error).

It might be more informative to produce displacement plots which have been normalized by the height of the wall. This gives a more general measure of movement, and facilitates comparison with other walls, checking against recommended limits, or applying methods such as that of Bolton *et al.* (1990).

Whole displacement profiles can offer particular insight with walls which are singly propped at foundation level, as cases have been reported where the sense of movement (i.e. rotation into

or away from the excavation) has changed during the course of the analysis. Such behaviour must be compared with the global direction of soil movement (displacement vector and deformed mesh plots) to establish consistency.

If wall installation modelling has been used (see Section 6.2.3), wall displacement must be zeroed against the nodal positions prevailing when (solid) concrete elements were introduced.

The complete wall displacement profile will be needed if any attempt is being made to predict bending moments from finite difference techniques (see Section 8.1.3). A second-order central difference approximation for the moment at node i would be appropriate, giving:

$$M_i \approx - EI\,(1/\Delta y^2)\,\{+\delta_{i-1} - 2\,\delta_i + \delta_{i+1}\} \qquad (8.4)$$

where δ is horizontal wall displacement, Δy is the vertical distance between nodes, and the subscripts i-1, i, i+1 denote adjacent nodes (variable Δy requires modification to Eqn 8.4).

8.2.3 Excavation heave

As the maximum heave (V_{max}) virtually always occurs on the excavation centreline, it can be extracted quite simply and it is thus not always necessary for the whole profile to be plotted. V_{max} is often compared with simple 1D calculations - either undrained or drained (using E_u or E′ as appropriate). One of the many elastic solutions (e.g. Butler, 1975; Carrier and Christian, 1973) may be used; these were originally derived for downward foundation loads, but are applicable (in reverse sense) to excavation unloading. A simple approximate check of V_{max} is given by integrating the quotient of stress change and soil stiffness with depth:

$$V_{max} = f_d \int_0^H \frac{1}{E^*(z)}\,\Delta\sigma_v(z)\,.\,dz \qquad (8.5)$$

where

f_d	is a correction factor for two- (or three-) dimensional conditions
H	is the layer thickness (or depth of influence of load, whichever is the lesser)
$E^*(z)$	defines the variation of constrained ("oedometric") modulus with depth z
$\Delta\sigma_v(z)$	defines the vertical stress change at depth z

Eqn (8.5) is easy to evaluate if either $E^*(z)$ and/or $\Delta\sigma_v(z)$ are assumed constant, but is more complex if both vary with depth. If $E^*(z) = E^*_o + m.z$, and assuming $\Delta\sigma_v(z) \approx \sigma_o/(1+z/W)$ for 2D plane strain, evaluating Eqn (8.5) leads to:

$$V_{max} = \frac{f_d \sigma_o W}{-E^*_o + W m} \left[\ln\left[\frac{E^*_o + mH}{W + H} \right] - \ln\left[\frac{E^*_o}{W} \right] \right] \qquad (8.6)$$

Such hand-checks should always be carried out, but as this may not be the case it would be helpful to include them in the post-processing system (see Section 8.6).

8.2.4 Ground surface settlement

The prediction of the settlement trough behind a retained excavation has become established as an important application for FE codes. Engineers generally turn to finite elements when, *inter alia*, they need to predict the surface settlement profile with some degree of accuracy. Other design-oriented software such as WALLAP and FREW concentrate solely on the wall and cannot (and do not purport to be able to) calculate adjacent ground movements.

Frequently, the focus in excavation-induced settlement has been on the soil constitutive model; especially non-linearity of stiffness. A well-known case is that of the deep excavation for the House of Commons (Palace of Westminster) Car Park, where the "Big Ben" clock tower either tilted away from (linear analysis; Ward and Burland, 1973) or towards (non-linear analysis; Simpson *et al.*, 1979) the excavation, depending on the model used, Fig. 8.5. However, work reported in Chapter 4 has demonstrated that mesh size, boundary conditions, and nonhomogeneity also have an influence on the shape of the settlement trough.

Whilst the absolute magnitudes of movement are important, designers are often more concerned with differential settlement. This is because damage predictions are carried out on the basis of comparing predicted curvature of ground surface with acceptable values for the type of construction concerned (e.g. Burland and Wroth, 1975; Boscardin and Cording, 1989). Thus, in addition to a surface settlement profile (S:x) another form of graph is needed, $(\Delta S/\Delta x) : x$, which is easily obtained with finite difference techniques. The backward, forward and central finite difference expressions are readily established: the central is more accurate (error of the order of h^2, where h is the interval size) but cannot be used at the first and last

nodes on the line. Considering three adjacent nodes (i, j, k) unevenly spaced at h_a and h_b on the ground surface boundary, Fig. 8.6, leads to:

$$\Delta S/\Delta x \approx 1/(2h_a)\,[-S_i + (1-\alpha)S_j + \alpha S_k] \qquad (8.7)$$

where $\alpha = h_a / h_b$.

It would be of great practical value to the analyst to have an immediate indication of how the finite element predictions compared with general expectations. In this respect, the approach adopted by ReWaRD (BSC, 1992) may prove helpful. ReWaRD uses a database of measured displacements normalized by excavation height, combining case histories published by Clough and O'Rourke (1990) and St John *et al.* (1993). Wall and ground movements are predicted empirically with reference to this database, an example of which is shown in Fig. 8.7. If CRISP output was normalized in similar fashion, one of these "envelopes" of movement could be used as an overlay to check for anomalous behaviour.

8.2.5 Horizontal ground movement

Horizontal movements in the ground (away from the wall) are probably not sought as often as vertical movements. They tend to be required where existing structures are immediately adjacent to the retained excavation, such as on the Queensberry House longitudinal section (Appendix A).

Differential horizontal ground movement will cause lateral compression (or tension) in those structures founded upon it. If a building moves towards an excavation more at the proximal end than at the distal end, tensile strains are set up at foundation level and the superstructure may crack. This tendency will be exacerbated if the vertical settlement trough is one of sagging, Fig. 8.8.

As with surface settlement, it is the differential horizontal movements and their rate of change with distance which are of most concern. An equation similar to Eqn (8.7) could be used to compute approximate gradients. Envelopes of horizontal movement have also been published by Clough and O'Rourke (1990), and their form is very similar to those for vertical settlement (Fig. 8.6).

8.2.6 Summary

Although displacement is the primary output of the finite element (displacement) method, the way in which it is viewed can be as important as the accuracy of its calculation. There is a little in the way of manipulation or smoothing that can be done, but there are various ways in which displacement results can be represented graphically. Each of these can contribute to understanding the overall behaviour of the earth-retaining structure system, and should be used. By isolating presumed features of interest too quickly, other important points can be missed. Comparing profiles of horizontal and vertical movement with minima/maxima based on case studies can also help to identify anomalous behaviour.

8.3 Soil Stress Distributions

Once displacements have been extracted and plotted, the designer usually proceeds to inspect the stresses in the soil immediately surrounding the wall and excavation. There are two different types of analytical solution which may be helpful in this context. The first are contours of stress change in the ground due to applied loading/unloading at the surface (so-called "pressure bulbs"), which give an indication of how adjacent structures may be affected, and whether or not compressible layers will experience significant strains. The second are lateral earth pressure diagrams, which are used to estimate overall wall stability, required penetration depth, etc. Geotechnical engineers are familiar with both and use them extensively in the design of foundations and earth-retaining structures, respectively. It would be natural for such solutions to be used to verify finite element analysis. It is, therefore, important to have an appreciation of how reliable the computed stresses might be.

Earlier chapters have documented some of the problems which have been encountered with CRISP when examining stresses from retaining wall analyses. The focus was on the apparent anomalies caused by factors such as high stiffness contrasts. In this section, issues of quality and methods of smoothing will be discussed. A considerable amount of work has been done in this area (e.g. by the Swansea group in the 1970s) but many of the lessons appear to have been forgotten in geotechnical FEA. This earlier work is reviewed, following which different techniques for stress smoothing implemented (by the writer) for CRISP are presented. Finally, the results of numerical experiments with these different techniques are given.

8.3.1 Previous work

Quality of computed stresses

In the finite element (displacement) method, stresses are calculated at integration points from $\sigma = \mathbf{D\,B\,a}$ (Eqn 8.3). These will be referred to hereinafter as "conventional" stresses. Melosh (1963) was one of the first to point out that, at best, these stresses represent only averages of the true stresses in a finite element. The common practice established by the mid-60s was to evaluate more reliable stresses at a node by computing a weighted average over the elements meeting at that node. However, there are obvious difficulties with this approach when a node lies at the boundary of two materials of different stiffnesses - such as at the interface between a wall and the soil it retains. The stresses either side of the interface may be very different, and an averaging process would tend to "smear" this and give a misleading impression.

The key point concerning conventional stresses is that, even in relatively simple cases, their accuracy may be rather low. Oden and Brauchli (1971) cited an example of a 1D bar, 6 units long, in axial compression under a prescribed longitudinal displacement of $u(x) = 1-x^2/36$. The Young's modulus E varied linearly according to $E(x) = E_o(1+x)$, and the exact internal stress distribution $\sigma(x)$ was given by $E(x).\varepsilon(x) = E(x).du/dx = -E_o x(1+x)/18$. The bar was represented by 6 elements of equal length with linear shape functions N of the form $1-\xi$ and ξ, with strain $\varepsilon = \partial N_i/\partial U_i + \partial N_j/\partial U_j$ and stress $\sigma = E(x).\varepsilon$. Exact and computed (conventional) stress distributions are shown in Fig. 8.9, where the discrepancies are evident - especially the discontinuities at the nodes, where the piecewise linear distributions in adjacent elements do not match up. However, there is agreement between exact and computed stresses at one point within each element - at the centroid, in this example.

Consistent stresses

In an attempt to provide a more powerful and elegant approach, Oden and Brauchli (1971) proposed that the theory of conjugate approximations could be used to obtain "consistent" stress fields in a finite element analysis. Consistent stresses were claimed to have the advantage of being continuous across element boundaries because their distribution was dictated by the displacement approximation functions (e.g. Eqn 8.1), which were themselves continuous. Furthermore, consistent stresses involved less mean error than those computed by the conventional approach (i.e. $\sigma = \mathbf{D\,B\,a}$). Continuity was achieved by using linear combinations of all of the local element approximation (shape) functions, to give conjugate functions which

were defined everywhere. The 1D bar under axial compression cited earlier was processed in this manner; the resulting distribution of stress is shown in Fig. 8.9 also.

Oden and Brauchli's procedure involved the formulation and solution of an ancillary set of linear equations of comparable order to the global stiffness matrix. It was thus a computationally expensive process, even if consistent stresses were generated only at the nodes (as opposed to a complete distribution). For problems where stresses are of interest everywhere in the mesh (e.g. stress analysis of an engine component) then this would be a reasonable approach - but it would become very inefficient for retaining wall problems, where the area of interest is normally confined to one or two parts of the mesh[5].

Appreciating the drawbacks, Oden and Reddy (1973) went on to simplify the method, by focusing on areas of high stress gradient in the mesh (arguing that where gradients were low, conventional estimates of stress were adequate for practical purposes). A central concept to this new method was that of a domain of stress influence; for a point at x^* having stresses $\sigma(x^*)$, the domain of influence encompasses all adjacent points for which $|\sigma(x)| \geq \alpha|\sigma(x^*)|$, where α is a constant ($0 < \alpha \leq 1$); the idea is illustrated in Fig. 8.10, using $\alpha = 0.3$.

In the simplified method, local consistent stress components in an element were first obtained from a local integration, and then summed up over all elements to give the global consistent nodal averages. (These averages indicated which nodal points have high stress gradients.) Next, α was selected and the domain of influence for each node with a high stress gradient was established. Finally, the approximate consistent nodal stresses were obtained by solving a set of equations of much reduced size, relative to the method of Oden and Brauchli. Further simplifications resulted if conventional nodal stress averages were used to identify high stress concentrations, as this yielded an even smaller system of equations to solve. Numerical examples given by Oden and Reddy suggested that these approximate consistent nodal stresses could be quite accurate.

---

[5] This is an obvious shortcoming of the FE method in any situation where some of the far field has to be modelled, even when it is not of direct interest - a shortcoming addressed by using infinite elements.

Stress smoothing

Hinton and Campbell (1974) also proposed methods of local and global stress smoothing, but based on least squares techniques rather than conjugate approximations. They observed that, in numerically integrated isoparametric elements (such as used in CRISP), the Gaussian integration points were the best place to sample the stresses, whereas the nodes (at which stress output would be more useful) were the worst. The principal reason cited for this was that approximation functions tend to behave poorly near the limits of the interpolation region. Hinton and Campbell also made the helpful observation that the displacement finite element method can be thought of as a weighted least squares error procedure, where the errors are the difference between the exact and finite element stresses[6].

The global method of Hinton and Campbell constructed a set of simultaneous equations over the whole finite element mesh, with the smoothed stresses as the unknowns. The equations were built up in a way analogous to the original finite element set, with a piecewise construction based on shape functions. The shape functions used for stress smoothing, $\tilde{N}_i$, were often of different order to the N_i those used in defining the element[7]. First, an "element smoothing matrix" $\mathbf{S}^e$ was built up of terms of the form $\iint \tilde{N}_i \tilde{N}_j |J| \, d\xi d\eta$ (where $|J| \, d\xi d\eta = dxdy$ in local terms). Then, a right-hand side vector $\mathbf{f}^e$ was assembled for the element using terms of the form $\iint \tilde{N}_i \sigma |J| \, d\xi d\eta$, where σ are the unsmoothed (conventional) stresses. Both $\mathbf{S}^e$ and $\mathbf{f}^e$ were evaluated numerically. Finally, a global system of equations was assembled and solved to yield smoothed stresses $\tilde{\sigma}$ for the whole domain:

$$\mathbf{S} \tilde{\sigma} = \mathbf{f} \tag{8.7}$$

Unfortunately, this method suffered from the same time and cost penalty as that proposed by Oden and Brauchli (1971), in that effectively a re-analysis of the finite element model was being performed. This led Hinton and Campbell to consider two local methods - function smoothing and discrete smoothing. In the former, a smoothing function was found which provided a least squares fit to the whole unsmoothed stress function, whereas in the latter the

---

[6] This helps to explain the stress oscillations often observed in finite element computations, as discussed in the previous chapter.

[7] In the coupled consolidation formulation, excess pore water pressures are permitted to vary in an order which is one less than that for displacements.

smoothing function needed only to provide an exact least squares fit at the Gauss points. Essentially, both lead to the same equation for smoothed stress (a single element version of Eqn (8.7)), because in function smoothing $\mathbf{S}^e$ and $\mathbf{f}^e$ were both evaluated by reduced numerical integration at the same Gauss points at which discrete sampling was made. For the case of a quadrilateral element with linear $\tilde{N}_i$ and a 2×2 integration scheme, nodal stresses $\{\sigma_1, \sigma_2 \ldots\}$ were obtained from Gauss point stresses $\{\sigma_i, \sigma_{ii} \ldots\}$:

$$\begin{bmatrix} \sigma_1 \\ \sigma_2 \\ \sigma_3 \\ \sigma_4 \end{bmatrix} = \begin{bmatrix} a & b & c & b \\ b & a & b & c \\ c & b & a & b \\ b & c & b & a \end{bmatrix} \begin{bmatrix} \sigma_i \\ \sigma_{ii} \\ \sigma_{iii} \\ \sigma_{iv} \end{bmatrix} \tag{8.8}$$

where $a = 1+\sqrt{(3)}/2$, $b = -1/2$, and $c = 1-\sqrt{(3)}/2$. The local methods did not produce unique values at the nodal points, and so the last stage was to compute nodal averages. Hinton *et al.* (1975) claimed that these averaged smoothed stresses were of consistently good accuracy in situations where averaged conventional stresses were of poor quality.

If 2×2 reduced integration was used, Hinton and Campbell showed that local smoothing would produce a value at the centre of the element which was equal to the mean of the unsmoothed Gauss point values. This conclusion was of practical value to designers using finite elements, as it suggested that simple averaging was just as good as costly smoothing procedures - provided reduced integration was used.

Another approach to stress smoothing was proposed by Cantin *et al.* (1978), who showed how the conventional finite element solution (displacements as well as stresses) could be improved iteratively, as follows. First, the global equations $\mathbf{K\,a = f}$ were solved and the conventional stresses obtained from $\sigma_o = \mathbf{D\,B\,a}$. Then, average stresses σ_n were calculated at each node based on contributions from all of the elements adjoining that node (effectively defining the domain of stress influence in the terminology of Oden and Reddy, 1973). Next, a set of interpolation functions was devised giving a stress field σ_1 on each element which was continuous at the element boundaries. A new right-hand side was evaluated from this field:

$$\mathbf{f}_\sigma = \int \mathbf{B}\,\sigma_1\,d(\text{vol}) \tag{8.9}$$

and then a re-solution of modified FE equations was performed thus:

$$\mathbf{K}\,\Delta\mathbf{a} \;=\; \mathbf{f} - \mathbf{f}_{\sigma} \tag{8.10}$$

Displacements and stresses were then updated:

$$\mathbf{a} \;=\; \mathbf{a} + \Delta\mathbf{a} \tag{8.11}$$

$$\sigma_o \;=\; \mathbf{D}\,\mathbf{B}\,\mathbf{a}$$

and the whole process repeated (starting with new average stresses σ_n) until satisfactory convergence was achieved; Cantin *et al.* claimed that 2-6 iterations would be sufficient. The accuracy of stresses in the numerical examples given by these authors was remarkably good, but the iterated displacements were actually larger than the exact values. This obviously went against the normal trend (i.e. displacements underestimated) and it was possible that the pursuit of smoother stresses had actually impaired the quality of results elsewhere.

Alternative formulations

Pursuing the above idea further eventually leads to another class of possibilities - i.e. that of re-examining the theoretical basis of the finite element equations themselves. Two such possibilities are alternative variational principles and hybrid element formulations. An example of the former would be to use a stress function (e.g. the Airy stress function) as the solution parameter in a complementary energy (rather than potential energy) formulation. However, Gallagher (1977) did not consider that this approach had much promise in geotechnical applications and history appears to have vindicated this viewpoint. Mixed variational principles are functionals containing both stress and displacement variables, which eventually become unknowns at the nodes. A popular mixed functional is that due to Reissner (1950), but as this does not demand inter-element equilibrium it would not appear to offer any particular advantages over the traditional displacement method.

This leaves the so-called hybrid finite elements, pioneered by Pian (1973). In a hybrid formulation, one field is described in terms of generalized parameters and the others in terms of nodal physical parameters. For example, in the hybrid stress method, an equilibrium stress field is written in terms of undetermined parameters, and a compatible displacement field for the element boundary is described independently in terms of nodal values. Conventional element stiffness matrices are produced, but few (if any) applications of hybrid finite elements in geomechanics have been reported.

Nodal forces

A different approach to the problem has been to consider how element stresses σ might be computed directly from nodal forces **f** through a matrix of coefficients **A**:

$$\boldsymbol{\sigma} = \mathbf{A}\,\mathbf{f} \tag{8.12}$$

This appears sound, because the reliability of nodal forces is fairly high (certainly higher than that of element stresses). A simple example would be in the case of 1D bar elements in axial tension, where σ = F/a - i.e. the matrix **A** in Eqn (8.12) would depend only on terms involving cross-sectional area.

Creed (1979) devised an approximate method of inferring pressure distributions from nodal loads, specifically in the context of lateral pressures on retaining walls. The nodal loads $\mathbf{f}_t$ equivalent to applied tractions **t** on the perimeter (or side s) of an element were given by:

$$\mathbf{f}_t = \int_s \mathbf{N}^T \mathbf{t}\, ds \tag{8.13}$$

For the 6-node triangle in Fig. 8.11, the explicit form of Eqn (8.13) was written as:

$$\begin{bmatrix} f_{tx1} \\ f_{tx4} \\ f_{tx2} \end{bmatrix} = L/30 \begin{bmatrix} 4 & 2 & -1 \\ 2 & 16 & 2 \\ -1 & 2 & 4 \end{bmatrix} \begin{bmatrix} t_{x1} \\ t_{x4} \\ t_{x2} \end{bmatrix} \tag{8.14}$$

(For the case of a uniform traction of unit value, this can be seen to give the established values of L/6, 2L/3, and L/6 for the equivalent nodal loads.) Applying Eqn (8.14) at each node along the rear face of a wall led to a set of linear simultaneous equations linking (unknown) soil pressures to (known) nodal forces:

$$\frac{L_i}{30}(-p_{2i-3} + 2p_{2i-2} + 4p_{2i-1}) + \frac{L_i}{30}(4p_{2i-1} + 2p_{2i} - p_{2i+1}) = f_{2i-1} \quad i = 1,n+1$$

$$\frac{L_i}{30}(2p_{2i-1} + 16p2_i - 2p_{2i+1}) = f_{2i} \quad i = 1,n \tag{8.15a}$$

where $L_o = L_{n+1} = 0$, 'p' signifies pressure and 'f' force. In matrix form:

$$\mathbf{S\,p} \;=\; \mathbf{f} \qquad (8.15b)$$

where S comprises purely geometric terms. Eqn (8.15) was solved to yield the required pressures - normal stresses from the horizontal forces and shear stresses from the vertical forces. In general, the pressure distribution thus computed was quadratic along each element boundary, and continuous from element to element, but without slope continuity. Creed suggested a procedure for smoothing out these discontinuities, but it was somewhat involved.

The main drawback with this method, however, is that it requires (unassembled) nodal forces to be output from the program, and this is not routinely done - either in CRISP or any other program. Specifically, it is the forces from the soil elements alone which are required for Eqn (8.15); the forces at any one node on the soil-wall interface from all contributing elements would simply sum to zero in vertical and horizontal directions (the equilibrium condition). However, as the finite element method deals primarily with force equilibrium, Creed's approach has the attraction of dealing with quantities which could be expected to be reliable.

Other possibilities

According to Naylor (1974), there are four different headings under which techniques to improve finite element stresses can be grouped, namely:

a) mesh refinement
b) reduction of Poisson's ratio
c) stress smoothing
d) location of stress output

Option (a) is always viable in a retaining wall analysis, and was the subject of investigation in Chapter 4. The investigations in that chapter did not consider stresses directly, although they were taken into account indirectly through wall bending moments. However, coupled with some of the findings in Chapter 7, there is every reason to suppose that the computed stress distributions around a retaining wall (and under a propping slab, if present) could be improved by mesh refinement. The question for the designer/analyst is: what is the most efficient form of mesh refinement in order to obtain, for example, improved lateral earth pressures?

Option (b) is included in Naylor's list as he was specifically investigating problems with nearly incompressible materials - where stress distributions are notoriously poor. It is akin to the

pore fluid compressibility issue explored in Section 7.3. Option (c) has been covered in the earlier summaries of the work of Oden and Brauchli (1971), Oden and Reddy (1973), Hinton and Campbell (1974), Hinton *et al.* (1975), and Cantin *et al.* (1978). Option (d) has been touched on in the references to Hinton and his co-workers. However it opens up a larger range of possibilities including stress sampling, nodal averaging, reduced integration etc.

8.3.2 Stress smoothing in CRISP

At present, the commercial user of CRISP has access only to raw Gauss point stresses - in isoparametric elements which are fully integrated. Distributions plotted from the "raw" 3×3 Gauss point stresses, without any smoothing or processing, are often unsatisfactory (e.g. see Section 7.5). Users can refine meshes, but reduced integration is not an option (unless they are prepared to modify the code itself).

Stress smoothing across the whole domain is unnecessary for a retaining wall - stresses are generally required only in the immediate vicinity of the wall and/or ground-bearing prop slabs. To apply a global smoothing procedure would be inefficient and would yield values in areas that would be of no real interest. The problem is localized and so requires a local smoothing method, such as that due to Oden and Reddy (1973) or Hinton and Campbell (1974). The former would need to be programmed into the FE code, and is rather complex.

Outputting conventional stresses at reduced (2×2) points would not be onerous - although (again) some programming would be required in the CRISP code. A convenient alternative would be to perform the necessary smoothing in the post-processing - i.e. to take the existing 3×3 stresses and then manipulate these in some way to obtain the desired values. A method to do this has been devised and implemented in CRISP by the writer, based on the findings of Barlow (1976) concerning the existence of optimal stress points. Starting with an 8-noded quadrilateral, interpolation functions are constructed for each of the 3×3 Gauss points, to allow a stress quantity to be interpolated anywhere within the area encompassed. Suitable shape functions are those of the 9-noded Lagrangian quadrilateral element (QU9). Typical vertex, mid-side and centre node shape functions are:

$$\begin{aligned} N_1 &= \xi(1-\xi)\eta(1-\eta)/4 \\ N_5 &= -(1-\xi^2)\eta(1-\eta)/2 \\ N_9 &= (1-\xi^2)(1-\eta^2) \end{aligned} \qquad (8.16)$$

With reference to Fig. 8.12, the 3×3 points in the parent element ($-1 \le \xi \le 1$, $-1 \le \eta \le 1$) are located at local abscissae 0, $\pm\sqrt{(3/5)}$. For a 2×2 scheme (reduced integration) the Gauss points are located at $\pm 1/\sqrt{3}$. If the 3×3 points are taken as the nodes of a QU9, and a transformation of axes is carried out such that these points lie at 0, ±1, then the 2×2 points would lie at $\pm (1/\sqrt{3})/\sqrt{(3/5)} = \pm\sqrt{(5)}/3$, Fig. 8.12. Hence, stress values at the 2×2 points can be obtained simply via $\sigma = \Sigma N_i \sigma_i$, using $\pm\sqrt{(5)}/3$ for ξ and η as appropriate. The Cartesian co-ordinates of the 2×2 points are found from:

$$\begin{aligned} x_i &= x_c \pm (x_2 - x_1)\sqrt{(5)}/6 \\ y_i &= y_c \pm (y_4 - y_1)\sqrt{(5)}/6 \end{aligned} \qquad (8.17)$$

With the "raw" (3×3) and "interpolated" (2×2) stresses thus available, it is possible to produce a profile of stress on the wall at the soil-wall interface. Five different *a posteriori* smoothing methods have been implemented by the writer for numerical comparison:

a)	simple averaging (3×3)	denoted SA3
b)	best-fit line (3×3)	" BFL3
c)	best-fit plane (3×3)	" BFP3
d)	best-fit line (2×2)	" BFL2
e)	best-fit curve (3×3 / multiple)	" BFC3m

Simple averaging (3×3) or *SA3* works with the Gauss points which line up on each of the three horizontal sections in a single (rectangular) soil element adjacent to the wall, Fig. 8.13(a). Using normal Gauss point numbering, these 3 sections (from the top) are labelled 4-7-3, 8-9-6 and 1-5-2. On the top section, for example, the (mean) stress is given by $(\sigma_4 + \sigma_7 + \sigma_3) / 3$ or $\Sigma\sigma_i /3$.

The best-fit line (3×3) or *BFL3* works with the same horizontal rows of Gauss points, but fits a line of the form $\sigma = a + b.x$ to the stress values, which is then extrapolated to the back of the wall, Fig. 8.13(b). Standard least squares techniques are employed to establish the coefficients a and b (see Appendix C for derivation):

$$\begin{bmatrix} N & \Sigma x \\ \Sigma x & \Sigma x^2 \end{bmatrix} \begin{bmatrix} a \\ b \end{bmatrix} = \begin{bmatrix} \Sigma\sigma \\ \Sigma\sigma.x \end{bmatrix} \qquad (8.18)$$

The best-fit plane (3×3) or *BFP3* seeks to fit a single plane of the form $\sigma = a + b.x + c.y + d.x.y$ to all 3×3 Gauss points in the element, Fig. 8.13(c). This plane is extrapolated to the back of the wall to produce the required soil stress distribution. Least squares techniques are used to determine a, b, c and d (see Appendix C):

$$\begin{bmatrix} N & \Sigma x & \Sigma y & \Sigma xy \\ \Sigma x & \Sigma x^2 & \Sigma xy & \Sigma x^2 y \\ \Sigma y & \Sigma xy & \Sigma y^2 & \Sigma xy^2 \\ \Sigma xy & \Sigma x^2 y & \Sigma xy^2 & \Sigma x^2 y^2 \end{bmatrix} \begin{bmatrix} a \\ b \\ c \\ d \end{bmatrix} = \begin{bmatrix} \Sigma\sigma \\ \Sigma\sigma.x \\ \Sigma\sigma.y \\ \Sigma\sigma.x.y \end{bmatrix} \qquad (8.19)$$

The best-fit line (2×2) or *BFL2* is identical to BFL3, but fits a straight line $\sigma = m+n.x$ to the stress values at the upper pair of interpolated 2×2 points (III and IV) and another line through the lower pair (I and II), Fig. 8.12(b). Both straight lines are then extrapolated to the back of the wall to give the stress at the soil-wall interface.

Finally, the best-fit curve (3×3 / multiple) or *BFC3m* also uses a least squares best-fit, but extended to multiple columns of (rectangular) elements adjacent to the wall. This approach was suggested by the shape of typical horizontal stress contours from CRISP, which become more oscillatory as they approach the back of the wall, Fig. 8.14. However, the oscillation was clearly either side of a mean value which could be fitted by a curve ($\sigma = p+q.x+r.x^2$) or line ($\sigma = s+t.x$). The coefficients p, q, r are obtained by solving (see Appendix C):

$$\begin{bmatrix} N & \Sigma x & \Sigma x^2 \\ \Sigma x & \Sigma x^2 & \Sigma x^3 \\ \Sigma x^2 & \Sigma x^3 & \Sigma x^4 \end{bmatrix} \begin{bmatrix} p \\ q \\ r \end{bmatrix} = \begin{bmatrix} \Sigma\sigma \\ \Sigma\sigma.x \\ \Sigma\sigma.x^2 \end{bmatrix} \qquad (8.20)$$

Using M columns of soil elements, it is possible to pick out rows of elements (M wide) behind the wall at different elevations. Within any one of these rows, the internal 3×3 Gauss points line up in 3 separate horizontal "tracks" in the top, middle and bottom of the row - giving 3 tracks of 3×M Gauss points. If the best-fit curve (or line) is extrapolated to the back of the wall, a further set of stresses (3 per element) are obtained at the soil-wall interface. In the present investigation, M=5 was used for both curves ($\sigma = p+q.x+r.x^2$) and lines ($\sigma = s+t.x$).

The first four smoothing methods work with the column of soil elements immediately adjacent to the wall and are thus "local" methods. The fifth involves elements near the wall, not only those adjacent to it, and so may be termed "superlocal". Hereafter in the text and figures, simple averaging (3×3) will be abbreviated to SA3, best-fit line (3×3) to BFL3, best-fit plane (3×3) to BFP3, best-fit line (2×2) to BFL2, and best-fit curve (3×3 / multiple) to BFC3m.

8.3.3 Description of analyses : horizontal stress

All smoothing methods described in Section 8.3.2 have been applied to a range of embedded retaining wall analyses, using mesh x10y10 (Fig. 4.1) in both cantilever and top-propped configurations, together with six different soil parameter sets (see Tables 4.3-4.8):

Case	Propping condition	Soil params	Case	Propping condition	Soil params
RW1	cantilever	1	RW61	top-propped	1d
RW3	cantilever	3	RW63	top-propped	3d
RW11	top-propped	1	RW102	cantilever	12
RW13	top-propped	3	RW103	cantilever	13
RW51	cantilever	1d	RW112	top-propped	12
RW53	cantilever	3d	RW113	top-propped	13

In addition, a variation on soil parameter sets 1 and 3 was run in which $\nu = 0.4999$ - a value which (from Chapter7) would be expected to cause large oscillations in total normal stress. This was in order to create an onerous test for the different smoothing methods. The cases where this has been done are denoted by a suffixed * (e.g. RW3*).

8.3.4 Results of analyses : retained side

For each of the analyses, plots of raw 3×3 stresses and interpolated 2×2 stresses were first extracted for initial inspection. In the former case, profiles from three vertical "tracks" of Gauss points in the column of soil adjacent to the wall (near, centre, far - see Fig. 7.1 and Section 7.2.3.3 for definitions) were plotted. In the latter just two vertical tracks (adjacent and remote) were plotted, although in most cases these produced stresses almost identical to each other over the wall length. For the local smoothing methods, only the stress profile at the soil -wall interface was available.

A considerable number of plots were generated from these analyses, of which only a few have been selected for inclusion in this Chapter; specifically Figs 8.15-8.21. The superlocal method is considered separately later.

Only total horizontal stress σ_h (total lateral earth pressure) is depicted on the plots. The reason for this comes from the observation in Chapter 7 that effective horizontal stress σ'_h distributions tend to be fairly regular and well-behaved whereas pore pressure and anything related to it (e.g. $\sigma_h = \sigma'_h + u$) sometimes exhibits a ragged and oscillatory profile. If the smoothing methods can cope with σ_h distributions satisfactorily, then they will be considered adequate for smoothing σ'_h and u.

Undrained elastic

Commencing with case RW1, the σ_h distribution was reasonable, although clearly erratic near the top of the wall, and significant differences (up to 150 kPa) existed between the near, centre and far Gauss points, Fig. 8.15(a). In contrast, σ_h for the two columns of interpolated 2×2 points were in better agreement with each other and produced a smoother distribution over the length of the wall. (The strongly negative σ_h values over the top 2m were able to occur because it was an elastic analysis with no strength limits.)

Improvement from using interpolated 2×2 stresses compared with the raw 3×3 values is also demonstrated in Fig. 8.15(a), which shows the BFL2 profile compared with the raw 3×3 on three vertical tracks of Gauss points. The four local methods are compared in Fig. 8.15(b) and all performed reasonably well. There were some differences over the top 2m, but no one method was clearly better (or worse).

To investigate the robustness of the local techniques in coping with highly erratic profiles, the σ_h oscillations in case RW1 were increased by setting $\nu = 0.4999$. The interpolated 2×2 stresses were again generally very good and compared well with the $\nu = 0.495$ case. The mean stress SA3 and best-fit line BLF3 suffered similar irregularities as the raw σ_h data, whilst the best-fit plane BFP3 and best-fit line BFL2 did a much better job of smoothing the stresses and removing these irregularities.

For case RW3 (with E_o=0), the 3×3 Gauss point values were not so erratic as case RW1 near the surface, but differences still remained between the centre and edge points. Interpolated

2×2 profiles appeared reasonable, whilst the four local smoothing methods produced broadly similar results to each other. The σ_h from BFL2 again provided a form of average through the raw Gauss point values, although some oscillation remained. Increasing ν to 0.4999 produced the expected deterioration in raw σ_h, but the interpolated 2×2 values remained steady, Fig. 8.15(c). BFP3 and BFL2 performed better than the other smoothing methods (see Fig. 8.15d) but started to show significant differences between each other - with the latter (BFL2) generally appearing more correct.

Changing from cantilever to top-propping (cases RW11 and RW13) produced broadly similar observations as above. The raw 3×3 σ_h profiles were poor, whilst the interpolated 2×2 were much better. All local methods produced acceptable results, but BFP3 and BFL2 appeared best, Figs 8.15(e) & (f).

Drained elastic

In all cases examined, switching to fully drained conditions smoothed out the raw 3×3 values very significantly. Consequently, all local methods worked well and produced virtually indistinguishable profiles. Even the massive σ_h discontinuity seen at the wall toe was no longer evident when $\nu = 0.2$. (Yet another case where the undrained condition [$\varepsilon_v = 0$] was shown to provide the more onerous condition for the FEM to model).

Undrained elasto-plastic

The introduction of limiting shear strength led to various changes in the horizontal stress profiles - in some cases the range between the centre and outer Gauss point values was reduced, but in others it was increased. The overall severity of stress oscillations was also seen to improve or worsen (with respect to the elastic case); there was no consistency. But the real issue was whether or not the smoothing methods appeared to work.

Indications were that the interpolated 2×2 method performed well and delivered consistent and well-behaved stress distributions. Fig. 8.16(a)&(b) shows results for the cantilever wall, soil parameter set 12, and Fig. 8.16(c)&(d) for the top-propped wall, parameter set 13. All smoothing methods offered an improvement over the raw 3×3 stresses, with BFL2 seemingly the best.

A number of drained/elastic-perfectly plastic analyses were also run, but have not been plotted here. These confirmed that the raw 3×3 σ_h profiles were reasonably smooth, and hence amenable to any of the local smoothing procedures described above.

Superlocal method

Assessment of the superlocal method has been presented last because of its different nature to the others, as it was using data from more than just the one column of elements adjacent to the wall. In plotting results, just two rows of elements were considered; row A at the top of the wall and row B just above FL. For each row of elements, the three horizontal "tracks" of 15 points yielded plots of lateral variation of σ_h with distance from wall (along each track). Plots of raw 3×3 Gauss point stresses, together with both best-fit curve BFC3m ($p+q.x+r.x^2$) and line BFL3m ($s+t.x$) were inspected before extrapolating the curve or line to the wall to give the final σ_h : z profile (which was then compared to the local methods).

Fig. 8.17 shows the plots for case RW1, row A; (a) is the variation of raw σ_h with distance from wall, (b) the best-fit line, (c) the best-fit curve, and (d) the full σ_h : z profile based on extrapolating all best-fit lines. The plots for row B were broadly similar though with less oscillation in σ_h : x as the wall was approached, and this meant that the best-fit line and curve were almost the same. The full σ_h : z profile based on extrapolated best-fit curves was broadly similar to that shown in Fig. 8.17(d) for best-fit lines, but just a little more oscillatory.

The superlocal method offered reasonable results, but there was little to suggest that it offered significant improvement over the other methods. Despite the fact that it clearly smoothed out the oscillations along a row of Gauss points as the wall was approached, there were still oscillations from one row to the next (down the wall). Considering that 400% more stress data were manipulated compared with the local methods, the results were rather disappointing and this approach would appear to have little to commend it. For subsequent analyses, this method was discontinued.

8.3.5 Results of analyses : excavated side

All four local stress processing methods described in Section 8.3.2 above have also been used on the excavated ("passive") side of the wall, where in-situ stress σ_{ho} is no longer zero at the ground surface, and $\sigma_h > \sigma_{ho}$ is expected to develop. The same soil parameters, drainage, and

propping cases used for the retained side have been examined. The profiles of raw 3×3 and interpolated 2×2 stresses extracted for inspection were plotted from FL downwards.

Undrained elastic

As noted in Chapter 7, σ_h on the excavated side just below final dig level often shows an anomalous peak, and this is evident in Fig. 8.18(a) for case RW1. There was a stress difference in excess of 500 kPa between Gauss points at the same elevation, and a similar variation in σ_h over the first 2m of depth on any column of Gauss points. The rather severe nature of the stress oscillation in this area provided a demanding test for the different stress smoothing methods. Interpolated 2×2 stresses were the most reasonable results, Fig.18(b), though all schemes were subject to large oscillations at shallow depths, Fig. 8.18(c). If the mid-points of each element on the smoothed curve were connected, a reasonable σ_h profile resulted, Fig. 8.18(d). The corresponding curves for case RW3 were identical.

Top-propping (cases RW11 and RW13) reduced the overall magnitude of σ_h a little, but the pattern was much the same as seen for the corresponding cantilever cases (RW1 and RW3).

Drained elastic

Switching to fully drained analysis produced less oscillatory raw 3×3 σ_h profiles (as observed previously for stress distributions on the retained side). Consequently all methods (except the SA3) produced smooth stress profiles. Changes in stiffness profile and propping arrangement had a noticeable effect on magnitudes of σ_h, but overall patterns were largely unchanged.

Undrained elasto-plastic

In the undrained elasto-plastic case, yield caused the oscillations in the raw 3×3 stresses to extend deeper below ground than the corresponding elastic case, and it was also observed that σ_h dropped below σ_{ho} in some places - especially on the centre "track" of Gauss points.

The σ_h profiles on individual tracks of Gauss points were not particularly erratic in themselves, but with $E_o = 0$ (cases RW103 and 113) a large gap (> 400kPa) opened up between the centre track and the other two. The different smoothing methods performed satisfactorily, with Fig. 8.19(a) and (b) showing, respectively, the raw 3×3 and locally smoothed σ_h profiles for case RW113.

8.3.6 Description of analyses : soil-wall shear stress

The designer may, from time to time, be interested in soil-wall shear stress (due to adhesion and/or friction). Of course, the actual magnitude of shear stress at the soil-wall interface in an analysis could be controlled by the use of suitable interface elements. However, these have not been used in this thesis despite the availability of the Goodman-type element in CRISP. Use of such interface elements in practice has frequently been marked by high equilibrium errors (e.g. Powrie and Li, 1991; Moulds, 1998) and although it is recognized that high shear stress reduces displacement and bending in a wall, the element needs more development before it is suitable for routine use. The engineer/analyst might, in fact, benefit from seeing what the implied shear stress distribution is from an analysis which does not employ slip elements. The main focus in this section is how to obtain reliable profiles of soil-wall shear stress from CRISP. The local methods described in Section 8.3.2 used to smooth σ_h have been used here for τ_{xy}.

8.3.7 Results of analyses : soil-wall shear stress

For case RW1, Fig. 8.20(a) shows the raw 3×3 shear stresses over the full wall depth (and beyond), whilst Fig. 8.20(b) gives the interpolated 2×2. It is immediately clear that there is a greater difference between the adjacent and remote profiles of interpolated 2×2 τ_{xy} than was ever observed for σ_h. Equally clear from Fig. 8.20(c) is that all methods of improving the quality of the τ_{xy} distribution agreed with each other very closely - except the SA3 method. The smoothed stresses lay outside of the raw 3×3 stresses, Fig. 8.20(d), rather than plotting through the middle - indicating that there was a continual increase in τ_{xy} across the element, rather than the "dished" variation seen previously for σ_h. With case RW3, the same comments are broadly applicable, though the shape of the profile was different (see Fig. 8.21a). Top-propping produced profiles different from those for the unpropped wall, but the performance of smoothing methods was unchanged; for example Fig. 8.21(b) which is for case RW13.

The imposition of limiting shear strength (plastic yield) caused the raw 3×3 Gauss points to be in rather better agreement with each other, compared with the elastic case. For example, with reference to Fig. 8.21(c) which is for case RW103, and which shows how the limiting shear stress ($c_u = 5z$ kPa) is followed by the near 3×3 and adjacent 2×2 Gauss point profiles very closely. All other cases (RW51-102 and RW112-113) were examined, but the overall patterns which emerged, and the conclusions drawn from them, were similar to RW103.

8.3.8 Summary

The stress distributions output directly from CRISP (the "raw" Gauss point stresses) are not particularly useful in a design context. Some form of smoothing is necessary, as has been recognized by investigators for several decades. Many different methods have been proposed and can be found in the literature.

For the retaining wall, it is only the stresses (σ and τ) acting on the wall (and perhaps on the underside of a formation level prop slab) which are of interest. There is no requirement to produce stress distributions throughout the mesh, as there might be in the finite element analysis of a jet engine component, for example. Therefore, local methods which do not involve the manipulation of large amounts of raw stress data would seem most appropriate. A number of such methods have been devised and implemented in CRISP as part of the present work. In keeping with the spirit of this thesis, none of them is particularly complex and would be readily understood and applied by most practitioners.

Based on the results presented in this section, the use of interpolation to obtain stresses at the 2×2 points from the raw 3×3 data (Fig. 8.12), and thence to extrapolate to the desired profile, provides a convenient and robust smoothing technique. Such interpolation requires no modification of the CRISP code and can be carried out in a spreadsheet post-processor (as done here.). It delivers one of the advantages of 2×2 integration (specifically more reliable stresses), without any of the drawbacks (e.g. uncertainty over whether the total potential energy is under/over-predicted). Even in cases where stress oscillations are high (typically as $\nu \rightarrow ½$) the interpolated 2×2 works well.

8.4 Wall Bending Moments

8.4.1 Elements in bending

The performance of the 8-noded quadrilateral (LSQ) element in bending is generally very satisfactory, provided element aspect ratios are in the range $½ \leq r \leq 2$, and internal angles are all 90°±5°. Zienkiewicz and Taylor (1989) show the effects of deviating from these angular limits on the computed deflection of a tip-loaded cantilever modelled with LSQs, and the deterioration of the finite element solution is very rapid. Livesely (1983) shows results which suggest that a relatively small number of elements can give high accuracy in bending

applications. Some of the work presented in Chapter 7 examined the performance of the LSQ in various (extreme) circumstances of geometry and stiffness ratio.

The analytical solution for the strain field in a vertical wall under pure bending is $\varepsilon_y = M.x/EI$, so at a given section where M, E and I are constant, ε_y varies linearly with distance x from the neutral axis. The LSQ assumes a displacement approximation with terms in 1, x, y, x^2, xy, y^2, x^2y, xy^2. Differentiation w.r.t. y gives terms in 1, x, 2y, x^2, 2xy. Therefore ε_y is actually capable of a quadratic variation in the x direction, which is one order higher than that required by the analytical solution. The element is, therefore, well able to handle the condition of pure bending, as well as bending with axial tension/compression.

The LSQs in CRISP are fully integrated with a 3×3 Gauss rule. LSQs with reduced integration are currently unavailable in CRISP, although their implementation is relatively straightforward. Reduced integration introduces other potential problems, such as "zero strain energy" modes, and although these can usually be spotted by characteristic "hour-glassing", it places the onus on the user to examine all of the deformed mesh before focusing on the results of interest. Another drawback is that the bounding quality of the analysis is lost - with 3×3 integration the FE model is always too stiff, whereas with 2×2 integration corresponding bounds cannot be established. A compromise might be to use 2×2 elements for the structural wall only - continuing with 3×3s in the surrounding soil. In keeping with the aims of this thesis, it was decided to work within the limitations of CRISP 9x and therefore to restrict the investigations to fully-integrated elements.

The performance of a LSQ element in bending is also known to deteriorate rapidly if it is used to represent a curved structural member, such as a tunnel lining. However, there are few conceivable circumstances in retaining wall analysis where such curved elements would be required - embedded walls are always straight (or are at least intended to be) by virtue of the construction processes used. Therefore, although the topic is of interest, curved LSQ elements will not be considered in this thesis.

A more relevant case is where two or more of the elements representing the wall are trapezoidal in shape: this is sometimes necessitated by the mesh detail near to a hinged wall-slab connection (e.g. A406 Walthamstow and A331 Aldershot Road Underpass; Appendix A).

It is generally possible to avoid trapezoidal elements in the wall by appropriate mesh refinement in the adjacent soil, so again this is not a priority for further investigation.

8.4.2 Calculation methods

The conventional method for calculating bending moments in wall elements is to integrate the product of transverse stress and distance from the neutral axis across the section, Fig. 8.22(a). The derivation for a 3×3 integration scheme was given in Section 3.4.2, leading to (Eqn 3.20):

$$M \approx t^2/4 \ (5/9) \sqrt{(3/5)} \ (\sigma_{yc} - \sigma_{ya}) \qquad (8.21)bis$$

This method (referred to hereinafter as the wall stress bending moment or WSBM method) appears to give satisfactory results. However, as it is not possible to know the absolute accuracy in a full retaining wall analysis, confidence must be established using idealized cases with known solutions. Comparisons with bending moments computed by an alternative method can be helpful, but there can be pitfalls (see Section 8.4.6).

If a reduced 2×2 integration scheme is used, then:

$$M \approx t^2/4 \ \{ \ (1).\ (-1/\sqrt{3})\ \sigma_{ya} \ + \ (1).\ (1/\sqrt{3})\ \sigma_{yb} \ \}$$

$$\approx t^2/4 \ (1/\sqrt{3}) \ (\sigma_{yb} - \sigma_{ya}) \qquad (8.22)$$

CRISP does not currently possess such elements, but the interpolated 2×2 stresses can be obtained from the 3×3 points using Lagrangian interpolation as described in Section 8.3.2.

A second (and fundamentally different) approach to the above is to calculate moments from horizontal soil stresses acting on the wall, and will be referred to as the earth pressure bending moment or EPBM method, Fig. 8.22(b). The procedure follows similar lines to typical hand calculations using idealized earth pressure diagrams, and a version applicable to a single element was used in Section 7.3.2.4 (see Fig. 7.7). The more general case leads to:

$$M = \int_{y_o}^{y_r} (\sigma_x)_r \ (y - y_o) \ dy \ - \int_{y_o}^{y_r} (\sigma_x)_e \ (y - y_o) \ dy$$

$$\approx \sum^{Nr} (\sigma_x)_{ri} \ (y_i - y_o) \ \Delta y \ - \sum^{Ne} (\sigma_x)_{ei} \ (y_i - y_o) \ \Delta y \qquad (8.23)$$

where y_o is the elevation of the section at which M is required, y_r and y_e are the heights of retained and excavated soil surfaces above the section, N is the number of elements, and subscripts 'r' and 'e' denote retained and excavated respectively. As the analyst may well have performed similar hand calculations at an early stage of the wall design, this would appear to be a sensible method with which to check bending moments based on wall stresses. It would seem obvious to use horizontal stresses from the column of Gauss points adjacent to the wall, but this could give very poor quality, as the raw 3×3 stresses have been shown to be erratic (see Section 8.3). The use of smoothed total horizontal stresses would be preferable. Horizontal stresses from the least-squares best-fit plane (BFP3 - see 8.3.2 for details) extrapolated to the wall on both the retained and excavated sides would be suitable. The discrete σ_x values can be joined up to form a series of trapezoidal areas, Fig. 8.23(a). The elevation of the centroid of each area y_i can be fixed using standard relationships, and the moment of each area about a section further down the wall is then calculated and summed. Eqn (8.23) could easily be applied to net pressures, as the elevations of the discrete points on each side of the wall usually coincide. Gunn and Ponnampalam (1990) employed a Lagrangian polynomial to fit stresses in a row of 3 Gauss points in an element, and then extrapolated this to the wall. This is similar in principle to the local best fit a+b.x method described in Section 8.3.2, but suffers from the drawback that a Lagrangian polynomial will be forced to pass through the Gauss point values, which can result in a highly curved trajectory. Least-squares best-fitting to an order n-1 (where n is the number of data points) is more appropriate, but results in the previous section suggest that even this is not entirely satisfactory.

If the wall is of significant thickness, it may be important to take account of the moment of the soil-wall shear stresses about the wall centreline. Retained soil tends to slump as the wall moves forward, causing a downward shear on the back of the wall; excavated soil tends to heave, causing upward shear on the front. On both sides, shear stress acts to reduce the moment due to retained soil pressure by an amount:

$$\Delta M = \int_{y_o}^{y_r} (\tau_{xy})_r \, t/2 \, dy \quad + \quad \int_{y_o}^{y_e} (\tau_{xy})_e \, t/2 \, dy \qquad (8.24)$$

For thin (sheet) walls, this is a second-order effect but for diaphragm walls it can be quite significant - especially if slip elements have not been used to limit the soil-wall shear.

A different formulation for calculating bending moments from earth pressures makes use of Gaussian integration rules. Considering the retained side only (Fig. 8.23b):

$$M = \int_{h-L/2}^{h+L/2} \sigma_x \, y \, dy - \int_{h-L/2}^{h+L/2} \tau_{xy} \, t/2 \, dy$$

$$\approx \int_{-1}^{+1} \sigma_x \, (\eta+h) \frac{L}{2} \frac{L}{2} \, d\eta - \int_{-1}^{+1} \tau_{xy} \frac{t}{2} \frac{L}{2} \, d\eta$$

$$\approx L^2/4 \left\{ \sigma_{xa} (-\alpha+h)(5/9) + \sigma_{xb} (0+h)(8/9) + \sigma_{xc} (\alpha+h)(5/9) \right\}$$

$$- t\,L/4 \left\{ (5/9) \tau_{xya} + (8/9) \tau_{xyb} + (5/9) \tau_{xyc} \right\} \qquad (8.25)$$

where $\alpha = \sqrt{(3/5)}$. The excavated side is treated similarly, for elements below formation level. Due to its formulation, this method can only be used conveniently at the base of each element, rather than through each section of Gauss points. Bending moments calculated from Eqns (8.23) and (8.25) have been compared by the writer, and are indistinguishable. Consequently, only results obtained with Eqn (8.23) are shown hereafter.

Nodal forces in the wall offer an alternative third approach. With reference to Fig. 8.22(c), forces F_{ya}, F_{yb} and F_{yc} can be obtained from $F = \int B^T.\sigma_y$, and thence:

$$M = \Sigma F_{yi} \, x_i = F_{ya}.(-t/2) + F_{yb}.0 + F_{yc}.t/2 = (t/2)(-F_{ya} + F_{yc}) \qquad (8.26)$$

Moments can be calculated at the top, bottom and middle of an element - a total of 3+2(N-1) sections in a column of N elements. This method would be expected to agree with the integration of wall stresses $\int \sigma_y.x.dx$, and a short series of analyses reported by Gunn and Ponnampalam (1990) suggest that this is indeed the case. However, in order to implement Eqn 8.26, unassembled nodal forces are required, and most programs do not make these available. FE codes are usually more concerned with demonstrating equilibrium (force balance) at each node by outputting ΣF_{xi} and ΣF_{yi}, as is the case with CRISP.

A fourth and final method is based on equivalent nodal loads from the earth pressure in adjacent soil elements. In Fig. 8.22(d), the lateral forces exerted by a soil element are given by $\int B^T.\sigma_x$, and vertical forces by $\int B^T.\tau_{xy}$, whence for the retained side:

$$M = \sum_{N_{LR}} F_{xi}\, y_i - \sum_{N_{LR}} F_{yi}\, t/2 \qquad (8.27)$$

where N_{LR} is the number of soil elements on the retained side. Forces on the excavated side are dealt with similarly (N_{LX}). As with Eqn (8.26), moments can be calculated at the top, bottom and middle of an element, but unassembled nodal forces are required. This method would be expected to agree with the integration of soil stresses $\int \sigma_x.y.dy$, although it does not appear to have been investigated by other workers. Owing to time constraints, it was not possible to implement this method, and so no studies have been carried out.

8.4.3 Benchmarking - wall stress bending moments

A column of 16 LSQ elements, each 1m high (such as used to represent the wall in the analyses reported in Chapters 4-6) has been isolated for a number of numerical tests. The column was fully fixed along the bottom edge (a much more onerous condition than applies to a full embedded wall), and subject to three separate load cases as follows (see Fig. 8.24):

A1 single UDL of 10 kN/m/m all along the right-hand side (RHS)

B1 double UDLs of 10 kN/m/m all along the RHS and 40 kN/m/m along the lower half of the left-hand side (LHS)

C1 double linearly varying loads - 6.67z ($=K_a\gamma z$) on the RHS and 60z ($=K_p\gamma z$) on the lower half of the LHS

Case C1 approximates the typical design earth pressures used in the free-earth support method. With the addition of a single mid-way prop half-way up the LHS, another 3 analysis cases (A2, B2, C2) were created.

The bending moments diagrams (BMDs) for these simplified cases are shown in Fig. 8.25(a-f), from which two key items are apparent. Firstly, the 3×3 and (interpolated) 2×2 integration schemes gave results which were indistinguishable, and secondly both schemes agreed extremely closely with the exact bending moment distributions.

Potential problems with wall stress bending moments (WSBM) do exist, however. For example, if case A1 (16m cantilever with single UDL) was rerun using LSQs only 0.25m thick (and not 1m as above), then the BMD was very inaccurate, Fig. 8.26. This was a numerical problem and was a function of the end fixity conditions and the overall slenderness ratio of the

cantilever, as LSQs of 0.25m thickness produced correct results when used to form cantilevers 8m, 4m and 1m long (meshes with 8, 4 and 1 LSQ elements respectively). Problems of this nature were discussed in Chapter 7; and provided appropriate aspect ratios and stiffness contrasts are maintained, there should not normally be a problem with the WSBM method.

8.4.4 Assessment - wall stress bending moments

To assess the WSBM method, the same retaining wall analyses used in Section 8.3.3. (cases RW1 to RW113) have been rerun, and wall stresses extracted to permit the bending moments to be calculated. Selected plots are included in Fig. 8.27(a-f).

Inspection of the BMDs reveals three main features. Firstly, although the moment was zero (or close to it) at the top of the wall, it was significantly non-zero at the toe in many cases: the bottom element often showed a "kink" in the diagram (e.g. Fig. 8.27a & e). Secondly, where the soil was drained the BMD tended to be smoother than the corresponding undrained analyses (compare Fig. 8.27c & a). Thirdly, the BMDs in elastic-perfectly plastic soil tended to be smoother than the corresponding elastic analysis (compare Fig. 8.27e & a)

The first observation suggests that the soil can sometimes offer a clamping effect at the toe of the wall. This is not unreasonable; a truly zero moment can only be expected at the end of a structural member if it is pinned at that point. Although soil is considerably less stiff than concrete (approximately by a factor of 10^3), it is able to offer some resistance to wall rotation. Interestingly, the drained cases (Figs 8.27c & d) showed virtually zero moment at the toe. As this cannot be explained simply by the difference between undrained and drained soil stiffness ($E'/E_u \approx 0.8$), it would appear that the constant volume (undrained) condition was responsible.

Supporting the constant volume hypothesis is the second observation; namely that the BMDs were more erratic in the undrained than the drained (elastic) cases, especially below formation level when the soil medium was on both sides of the wall (Figs 8.27a & b). In plane strain ε_x, ε_y and γ_{xy} are variables but as $\varepsilon_x + \varepsilon_y = 0$ only two strains are actually independent and this could, in turn, impose a form of kinematic restraint on the wall through common nodes on the soil-wall interface.

If BMDs are to be smoothed and non-zero toe moments are to be removed, an observation from Chapter 4 may be relevant. During mesh refinement studies (in particular r-refinement), it was noted that non-zero bending moment at the wall toe disappeared if the soil element immediately below the wall was modified so that it became much shorter than the wall element. At the same time, BMDs for undrained loading cases also became smoother if the column of soil elements adjacent to the wall was made thinner. In other words, local mesh geometry in the soil affects the quality of the BMD in the wall. Instead of changing the grading of the whole mesh (which was the case in Chapter 4) some localized refinement might be adequate. A suitable scheme would simply involve splitting into two the layer of soil elements adjacent to the wall.

8.4.5 Improvement - wall stress bending moments

A short series of analyses has been conducted to investigate the non-zero bending moment at the toe, and ways in which it might be removed. Firstly, the column of 16 LSQ elements used in Section 8.4.3 was modified to include six extra elements around the toe, Fig. 8.28. With the addition of a top prop on the LHS and a single UDL of 10 kN/m/m along the RHS, case A3 was created. The extra soil elements were given a stiffness E_s which was varied to give wall: soil stiffness ratios E_w/E_s of 1000, 100, 10 and 1. At $E_w/E_s = 1000$, a simply supported column with a lateral UDL was effectively created. At $E_w/E_s = 1$ a propped cantilever was produced.

If the soil elements were present below the toe only, the BMD remained smooth, but fixed-end moments at the toe (M_t) were generated as follows:

E_w/E_s	1000	100	10	1	
M_t (kN-m)	0	50	210	300	($\nu = 0.15$)
	0	75	240	300	($\nu = 0.497$)

The use of different Poisson's ratios served to highlight the influence of drainage which, from these results, can be seen to be modest.

If the soil elements were present below the toe and on either side of the wall for the lowest two elements, the BMD was smooth above these two elements, but the "kink" referred to in Section 8.4.4 was observed (see Fig. 8.29), even when $E_w/E_s = 1000$ and little influence from

the soil would be expected. The effect was most pronounced if the soil was undrained (which gave M_t = -50 kN-m); if drained, a smaller kink in the BMD was evident (with M_t = 0 kN-m).

The second investigation was carried out with a full embedded wall - case RW1 (defined in Section 8.3.3). In this instance, two different local mesh refinement schemes were adopted, both reducing the size of the soil element immediately below the wall toe, Fig. 8.30. The first scheme, which involved dividing the soil element into four 6-noded triangles, actually made the kink worse, Fig. 8.31(a). The second scheme, however, involved dividing the soil element below the wall toe into two LSQs and this virtually removed the kink. A small non-zero moment persisted, but the lower half of the BMD was noticeably smoother, Fig. 8.31(b).

The principal conclusion from these brief studies is that the soil around the toe of an embedded wall can indeed provide rotational restraint - but only if the soil is undrained, given the typical modular ratio (E_w/E_s) likely to be prevalent. Thus, non-zero bending moment can be expected and does not necessarily indicate a fault in the analysis. However, irregularity in the BMD (in the form of kinks) is more likely to be a function of mesh density, and this can be overcome with minor local refinement of the mesh, although some refinement schemes will perform better than others.

8.4.6 Assessment - earth pressure bending moments

The column of 16 LSQ elements used in Sections 8.4.3 and 8.4.5 were initially considered for benchmark studies. However, the earth pressure bending moment (EPBM) method requires external (soil) stresses and these would be the same as the stresses applied directly to the column of LSQs. Based on this, EPBMs would equal the exact values at all points. Several columns of soil elements could be included either side of the wall, with the UDLs applied on the far boundaries, but one might as well proceed directly to full embedded wall analyses.

Consequently, the analyses presented in Section 8.4.4 were reused, namely cases RW1 to RW113. This time, total horizontal soil stresses (σ_x) and soil-wall shear stresses (τ_{xy}) in the adjacent soil elements on both the retained and active sides were extracted from the output, rather than transverse bending stresses in the wall. Selected plots (out of the large number generated) are included in Fig. 8.32(a-f). The plots show the earth pressure bending moments (EPBM) compared with those based on wall stresses (WSBM). For the purposes of the discussion below, pressures on the retained side will be referred to as "active" and on the

excavated side as "passive" - though it is recognized that these terms relate to limiting conditions which are not achieved in these analyses (which relate to working conditions).

In all cases except RW112, the agreement between the WSBM and EPBM methods over the upper half of the wall was generally very good. However, agreement below formation level was at best very poor (and usually much worse). In virtually all cases the curves for the two different methods began to diverge significantly when formation level was reached, with the worst discrepancy at the toe. Such large non-zero moments are clearly incorrect and are in a different category to the problems of non-zero moment at the tow described in Section 8.4.5. Case RW112 (Fig. 8.32f) showed significant divergence developing from the top of the wall. A further point to note is that in the undrained analyses (RW1-RW13 and RW102-RW113) the EPBM tended to a large negative value at the toe (e.g. Fig. 8.32a), whereas in the drained analyses (RW51-RW63) it tended to a large positive value (e.g. Fig. 8.32d). Again, case RW112 was an exception to this, though for reasons which are unclear. Some comments on individual cases will now be made.

Case RW1 showed a very large negative (EPBM) moment at the toe, but this was not caused by soil restraining the wall - rather the modest active pressures were being opposed by very large passive pressures. There was some tensile active stress at the top, causing a significant negative moment (i.e. the side of the wall facing the excavation being in tension) which was only partly counteracted by the (positive) active pressures further down. There were no tensile stresses at the top in case RW3 (Fig. 8.32a), but large passive pressures again dominated the EPBM diagram over the lower half of the wall.

In RW11 (Fig. 8.32b) and RW13, the EPBM was virtually always negative, with a small negative region just below formation level, with passive pressures again being mainly responsible for the substantial movement towards high negative moments at the toe. Top-propping prevented tensile active stresses developing, as the wall could not move forward freely. The EPBM diagrams for RW11 and RW13 were quite similar to each other.

Switching to drained analyses (Figs 8.32c-d), the passive stresses were lower than in the undrained (in particular, the large peak just below formation level was not so pronounced) and this generally resulted in EPBMs remaining positive below formation level. Divergence between the WSBM and EPBM methods below formation level was not quite so severe as in the undrained case, but it was still far too great to be acceptable.

Introducing yield (Figs 8.32e-f) generally served to worsen both the discrepancy between the WSBM and EPBM methods at the wall toe and the divergence over the upper half of the wall, though it was the former which was more noticeable. Comparisons with the corresponding elastic analyses (RW1-RW13) showed similar patterns except in case RW112, which exhibited the worst agreement between the WSBM and EPBM methods in all of the cases examined (and for no obvious reason).

8.4.7 Summary

These analyses suggest that bending moments calculated from earth pressures are of limited reliability. Above formation level where σ_h is only present on one side of the wall, the agreement between WSBM and EPBM can be very good indeed, but below formation level where σ_h is on both sides, the EPBM method breaks down completely. As the maximum BM often occurs below formation level, a potentially useful cross-check on its magnitude is thus lost. Gunn and Ponnampalam (1990) reached a similar conclusion, although they were not able to obtain agreement over the upper portion of the wall (probably due to the method which they used to extrapolate stresses to the wall). The role of tensile horizontal stresses at the wall top, large peaks in horizontal stress below formation level, etc. - all have an effect on computed EPBM. Toward the wall toe, (possible) errors in stress are being amplified by an increasing lever arm, thus compounding the error in bending moment.

The EPBM is an obvious and intuitive check to carry out, but one which fails (at least in part) because of certain aspects of the finite element method. Even by taking steps (i.e. stress smoothing) to minimize one of the known sources of error, the result is still unsatisfactory. It underlines the need for totally independent corroboration, instead of relying on different output from the FE analysis in various cross-checking schemes. Consistency may well be demonstrated, but this would not be sufficient endorsement of the analysis itself.

For the time being, calculation of bending moments using transverse stress distributions in the wall elements would seem perfectly adequate, and its continued use is recommended. Using raw 3×3 or interpolated 2×2 stresses gives the same result, so the extra effort involved in the interpolation for the latter is not warranted.

8.5 Wall Shear Forces

8.5.1 Elements in Shear

The performance of the LSQ element in shear appears to have received significantly less attention than in bending, despite the fact that both modes are generally present. An engineer might assume that the behaviour is satisfactory, provided similar geometric restrictions are observed as for bending (see Section 8.4.1). The main problem (highlighted by Zienkiewicz and Taylor, 1989) is that the shear stresses show a parabolic variation in each LSQ element - providing an extremely poor representation of the actual stresses. However, shear stresses sampled at the reduced (2×2) points have been shown to be excellent. In embedded wall design, bending moments are sought more often than shear forces, but the latter are a valid design output and it is appropriate to enquire into their accuracy and reliability.

The shear strain field in an embedded wall of thickness w is given by $\gamma_{xy} = (Q/2GI)(w^2/4-x^2)$ (Livesely, 1983). At a given section where the shear force Q and the values G and I are constant, γ_{xy} reduces quadratically with distance x from the neutral axis, being zero at the extreme fibres (where x=w/2). As noted in Section 8.4.1, differentiating the assumed displacement approximation for the LSQ element with respect to y gives terms in 1, x, 2y, x^2 and 2xy, whereas differentiation with respect to x gives terms in 1, 2x, y, 2xy and y^2. Given that $\gamma_{xy} = \partial u/\partial y + \partial v/\partial x$, there is the potential for quadratic variations of γ_{xy} (and hence $\tau_{xy} = G.\gamma_{xy}$) in both the x and y directions. This is the order required by the analytical solution for the shear stress distribution across a transverse section, but the freedom to vary quadratically in the longitudinal direction (when only a linear variation is required) may lead to unwanted effects.

In this section, the performance of the LSQ in obtaining shear force diagrams (SFDs) in retaining walls is examined. As in the previous section, only straight-sided elements with all internal angles equal to 90° have been considered.

8.5.2 Calculation methods

Unlike bending moments, there appears not to be an established or conventional method for calculating shear force in wall elements. However, the logical approach would be to integrate

the shear stress distribution across the section, Fig. 8.33(a). The derivation for a full 3×3 integration scheme was given in Section 3.4.2, leading to (Eqn 3.21):

$$Q \approx t/18 \, (5 \, \tau_{yxa} + 8 \, \tau_{yxb} + 5 \, \tau_{yxc}) \qquad (8.28)bis$$

This method usually gives unsatisfactory results, with wildly oscillating shear forces. A typical example is shown in Fig. 8.34 which is the SFD for a top-propped wall with $E_u = 5z$ (case RW13). (The reasons for these poor shear forces are examined in detail in the next section.) The shear forces seem to fluctuate either side of a curve describing a reasonable SFD, and whilst it is not possible to know the absolute accuracy of computed shear forces in a full retaining wall analysis, the method can be verified against idealized cases for which the solutions are known. Comparisons with other calculation methods can also be helpful, provided potential pitfalls are recognized.

If a reduced (2×2) integration scheme is used, the weightings are unity, thus:

$$Q \approx t/2 \, \{ (1) \, \tau_{yxa} + (1) \, \tau_{yxb} \} \approx t/2 \, (\tau_{yxa} + \tau_{yxb}) \qquad (8.29)$$

In the absence of reduced integration elements, interpolated 2×2 stresses could be obtained from the 3×3 Gauss points, as explained in Section 8.3.2. Shear forces at any given section at elevation y_o can also be calculated from external soil stresses (Fig. 8.33b):

$$Q = \int_{y_o}^{y_r} (\sigma_x)_r \, dy - \int_{y_o}^{y_e} (\sigma_x)_e \, dy$$

$$\approx \sum_{N_r} (\sigma_x)_{ri} \, \Delta y - \sum_{N_e} (\sigma_x)_{ei} \, \Delta y \qquad (8.30)$$

where N is the number of elements and subscripts 'r' and 'e' denote retained and excavated. As was the case with bending moments, this would be a logical method for checking shear forces based on wall stresses. Smoothed total horizontal stresses using the best-fit plane (BFP3) can be extrapolated to the wall on both sides; soil-wall shear stresses are not required.

Making direct use of Gaussian integration rules, for a single element on the retained side whose centroid is at a height h above the section concerned (Fig. 8.23):

$$Q = \int_{h-L/2}^{h+L/2} \sigma_x \, dy = \int_{-1}^{+1} \sigma_x \frac{L}{2} d\eta$$

$$\approx L/2 \left\{ (5/9)\,\sigma_{xa} + (8/9)\,\sigma_{xb} + (5/9)\,\sigma_{xc} \right\} \qquad (8.31)$$

Summation is carried out for all elements above the section; on the excavated side, summation is done for elements below formation level. As was the case for bending moments (see Section 8.4.2), Eqns (8.30) and (8.31) yield identical values, so only shear forces calculated with Eqn (8.30) will be shown in the numerical studies.

Using equivalent nodal forces between the wall elements (Fig. 8.33c):

$$Q = \Sigma F_{xwi} = F_{xa} + F_{xb} + F_{xc} \qquad (8.32)$$

This value of Q would be expected to agree with the integration of wall shear stresses $\int \tau_{yx}.dx$, but the writer has found no such comparisons in the literature.

Finally, using equivalent nodal forces due to the lateral earth pressures from adjacent soil elements (Fig. 8.33d):

$$Q = \Sigma F_{xsi} = F_{xs1} + F_{xs2} ..... + F_{xsn} \qquad (8.33)$$

A priori it is difficult to say whether or not Q from Eqn 8.33 would agree with the integration of soil stresses above the section $\int \sigma_y.dx$, and there has been insufficient time to investigate further. It is not clear that there would be any major advantage with this method over the others.

8.5.3 Investigation - wall stress shear forces

The column of 16, 1m high x 1m wide LSQ elements described in Section 8.4.3 (Fig. 8.24) has been used in a further series of numerical tests. In the first instance, only case A1 has been extracted, to allow more detailed examination of the shear stress distribution. Fig. 8.35 shows the SFD for case A1 calculated with Eqn (8.28), from which it is clear that the shear force variation along any one element is following a parabolic trend. This arises from the parabolic variation permitted by the element formulation, as explained in Section 8.5.1 above. It is clear

that some form of smoothing could usefully be applied - either to the shear stresses before they are presented to Eqn (8.28), or to the calculated shear forces themselves. Two methods in the former category have been selected for further investigation:

a) fitting a least-squares best-fit plane to the raw 3×3 shear stresses (BFP3), and

b) obtaining the interpolated 2×2 shear stresses by fitting 9-node Lagrangian shape functions to the 3×3 Gauss points.

These methods were selected because they were shown to work well in preceding sections for smoothing both lateral soil stresses and transverse bending stresses in the wall.

8.5.4 Benchmarking - wall stress shear forces

Load cases A1 to C1 (simple cantilever) and A2 to C2 (singly propped cantilever) have been re-run, and the SFDs are shown in Figs 8.36(a-f). It is clear that the BFP3 and interpolated 2×2 schemes gave results which were indistinguishable, apart from in the element adjacent to the fixed end. In addition (and more importantly) both schemes agreed extremely well with the exact shear forces - in marked contrast to distributions based on the raw 3×3 stresses. In view of the fact that the BFP3 method worked well in all elements, this method was selected for further examination in the context of full retaining wall analyses.

8.5.5 Assessment - wall stress shear forces

The wall analyses described in Section 8.3.3 (RW1 to RW113) have been re-used, the wall shear stresses extracted and smoothed using the BFP3 method, and the shear forces calculated. Results of some selected cases are shown in Fig. 8.37(a-f). Shear force diagrams based on raw 3×3 stresses and on BFP3 are both shown for comparison.

Four main features are evident from the plots in Fig. 8.37. Firstly, the shear force was generally zero (or close to zero) at the top of the wall, except where the wall was top-propped. Secondly, the shear force at the toe was usually small (if not zero), except in the elastic-perfectly plastic cases with $E_u = mz$. Thirdly, the introduction of drainage and plastic yielding had little overall effect on the smoothness of the relevant SFDs, which were generally free of erratic behaviour in the corresponding undrained elastic analysis. Fourthly, the maximum shear force (and main discontinuity in the SFD) always occurred at formation level.

The first observation suggests that the change in calculated shear force at a prop location would be a useful cross-check on prop loads obtained by other methods (e.g. $\int \sigma_x.dx$).
The second observation suggests that the soil can sometimes offer horizontal restraint at the toe of the wall, which is reasonable because the toe is not completely free (compare with the argument advanced in Section 8.4.4). However, drainage does not appear to have much influence on this, as the toe shear forces Q_t in cases RW51-RW63 are similar to those in RW1-RW13. Indeed, the constant volume condition in the soil would <u>not</u> be expected to offer any additional resistance to shear distortion (recall that $G_u = G'$).

Consistent with this is the third observation; namely that the overall smoothness of the SFDs is not greatly affected whether the analysis is drained or undrained. In view of the absence of obvious anomalies in the diagrams presented here, it was considered unnecessary to investigate the influence of mesh refinement. However, it is reasonable to expect that mesh refinement of the type described in Section 8.4.5 (which leads to an improvement in BMD quality) could be carried out without impairing the SFD.

The fourth observation above simply shows how the lateral earth pressures on the retained ("active") side are suddenly counteracted by pressures on the excavated ("passive") side when formation level (FL) is encountered. The fact that an abnormally high passive lateral stress is observed just below FL in many analyses, explains why the discontinuity in the SFD is so pronounced. If this peak were not present, a more gradual change in SF gradient would be expected (e.g. see Fig. 8.36 which shows SFDs for the idealized K_a and K_p profiles).

8.5.6 Assessment - earth pressure shear forces

As with earth pressure bending moments, benchmarking of the form described in Section 8.5.4 is not feasible, so the embedded wall analyses RW1 to RW113 have been used once more. Total horizontal soil stresses (σ_x) in the adjacent soil elements on both the retained and active sides were extracted from the output, for use in Eqn (8.30).

Results for selected cases are plotted in Fig. 8.38(a-f), showing the earth pressure shear forces (EPSF) compared with those based on wall stresses (WSSF). As before, pressures on the retained and excavated sides will be termed "active" and "passive" for convenience.

In the majority of cases, the agreement between the WSSF and EPSF methods over the upper half of the wall was generally very good, if not excellent. The exceptions to this were some of the elastic-perfectly plastic cases where the agreement was, at best, reasonable. As with EPBM diagrams, it is below formation level that discrepancies between the two methods became very much worse - except for the drained analyses where the agreement was excellent at all points on the wall. Some comments on individual cases will now be made.

In case RW1 there was a fairly small and constant offset of 10 kN/m between the EPSF and WSSF diagrams down to formation level, below which they diverged to about 200 kN/m over the lower portion of the wall. A very similar pattern was observed for RW3 (Fig. 8.38a). With top-propping (RW11 and RW13, Figs 8.38b), agreement over the upper half was very good indeed, but a discrepancy of about 150 kN/m developed between formation level and the toe. Slightly closer examination revealed that the main "shift" in the EPSF diagrams occurred in the first element below formation level, indicating that the peak in passive horizontal stress was primarily responsible. That the discrepancy did not worsen towards the toe is because (unlike in the EPBM diagram) there was no lever arm to amplify the effect of the peak.

Under drained conditions, (RW51-RW63) agreement between the EPSF and WSSF methods was excellent at all points along the wall (Figs 8.38c & d). This was principally because the large passive total horizontal stress no longer existed, and the SFD did not undergo a shift just below formation level.

Introducing plastic yield had variable effects. In RW102 the discrepancy in the results form EPSF and WSSF was small ($\approx$ 20 kN/m) over the top half of the wall, gradually increasing to 100 kN/m between formation level and the toe. A variable difference of 20-75 kN/m was in evidence over the upper half in RW112 (Fig. 8.38f), but there was almost complete agreement over the lower half (recall that RW112 showed anomalous behaviour for EPBMs too). Finally, RW113 gave excellent agreement from wall top to formation level, but a worsening discrepancy between the two methods down to the toe where it reached 350 kN/m.

8.5.7 Summary

As with bending moments, the main conclusion to be drawn from the analyses presented here is that the reliability of shear forces calculated from earth pressures is limited, although the discrepancies are not quite as large as with bending moments. Above formation level, the

EPBM method could be used reliably to cross-check shear forces based on wall stresses, but it is only in drained cases where this could be claimed for the fully embedded portion of the wall.

Discontinuities in the SFD should occur at (and only at) the location of props; the magnitude of the prop level discontinuity provides a useful cross-check on calculated axial forces in those props.

There are problems in carrying out what might be considered an obvious cross-check (i.e. between WS and EP shear forces. The large peak in horizontal stress below formation level is thought to give rise to most of the discrepancy between the two methods; further improvements to the EPSF method are unlikely unless some way of removing this peak can be found. In view of the fact that the wall stress method appears to give reliable and accurate results, there is therefore little incentive to attempt to improve the earth pressure method.

8.6 Prop and Anchor Loads

8.6.1 Tension/compression

Elements forming a structural member in pure tension or compression do not, in general, pose any particular problems for output interpretation. The main factor which the user needs to be clear about is whether or not axial force is expected to remain constant along the length of the member.

Examples of where the force would be expected to remain constant are the free (debonded) length of a ground anchorage, and in free-spanning props (e.g. cut-and-cover tunnel struts). Whether modelled by 1D or 2D elements, the axial force should not vary along the member and this must be evidenced in the output.

Examples of where the axial force would be expected to vary in reality are along the fixed (bonded) length of a ground anchorage, and across a formation level prop slab. A fixed anchor is usually modelled by a number of bar elements in series, and it would be expected that the load in the bars would reduce from the proximal to the distal end (owing to load transfer), although the exact variation will depend on how the tendon-grout-ground interfaces are modelled (Barkhordari, 1998).

Prop slabs at formation level are cast against the underlying ground (or a drainage blanket), allowing for load transfer via shear stresses between the prop and the soil. Where the underlying soil has been modelled as elastic-perfectly plastic, there is a limit on the maximum shear stress which could develop on the underside of the slab (c_u or $\sigma'_n \tan\phi'$). Such a limit does not exist in an elastic analysis, and so more care would have to be taken in the interpretation. As the shear stress from the soil will always act in the opposite direction to that in which the prop slab is changing length, it will always be acting to reduce the axial load - whether compressive or tensile.

One-dimensional elements

The axial force is calculated by CRISP as the product of the axial rigidity EA and the axial strain, and is output directly. If the prop is inclined to the global co-ordinate system (x, y), the appropriate transformations will have been carried out automatically by the program. Care must be taken in the interpretation of loads output for 1D elements if any pre-stress has been applied prior to installation. If this is the case, CRISP outputs the change of load ΔP since the insertion of the prop in the mesh, and is thus relative to the prestress P_o. The total load at any point in the analysis is then $P_o + \Delta P$.

Two-dimensional elements

The derivation of axial force based on transverse stresses with a full 3×3 integration scheme was given in Section 3.4.3.1, leading to (Eqn 3.25):

$$P \approx h/18 \, (5 \, \sigma_{xa} + 8 \, \sigma_{xb} + 5 \, \sigma_{xc}) \qquad (8.34)\textit{bis}$$

where h is the section depth of the prop. With a 2×2 integration scheme:

$$P \approx h/2 \, (\sigma_{xa} + \sigma_{xb}) \qquad (8.35)$$

For props which are inclined to the horizontal (e.g. A406 Walthamstow and A331 Aldershot Road Underpass, Appendix A), the local element axes (ξ, η) are no longer aligned with the system axes (x, y). The σ_{xi} in Eqns (8.35) and (8.36) must be substituted by $\sigma_{\xi i}$, the normal stress in the local axial direction ξ. As CRISP outputs Cartesian stresses, the $\sigma_{\xi i}$ at the Gauss points must be obtained from standard formulae based on manipulation of Mohr's circle of stress. If the angle of inclination of the prop to the horizontal is θ, then:

$$\sigma_\xi = \tfrac{1}{2}(\sigma_x + \sigma_y) - \tfrac{1}{2}(\sigma_x - \sigma_y)\cos 2\theta - \tau_{xy}\sin 2\theta \qquad (8.36)$$

If θ is small (say <10°) then the correction is quite minor and can probably be neglected. The dimension h is the (true) depth of the element, measured normal to the local ξ axis, and not the vertical distance across (= h.secθ).

8.6.2 Bending and shear

One-dimensional bar elements (2- or 3-noded) are only capable of transmitting axial force, whereas beam elements can additionally carry bending and shear. Two-dimensional elements are able to transmit shear and bending in addition to axial force; the actions actually carried depend on geometry and end conditions. This is illustrated in Fig. 8.39 which shows 3 types of end connection between prop and wall (pin-pin, fixed-pin, and fixed-fixed), and the bending moment and shear force diagrams resulting from a unit vertical displacement of the RHS.

In the pinned-pinned case (Fig. 8.39a) it should be noted that, if the end triangles were not symmetrical about the axis of the prop, bending moment would be induced by axial load alone, due to the eccentricity. (This also occurs in a cranked prop slab, Fig. 3.9, even if both ends are pinned.)

One-dimensional elements

The bending moment is calculated using standard stiffness relationships involving the flexural rigidity EI and rotation θ. There is no choice for the user, nor any likelihood of problems occurring. If the prop is free-spanning, 3-noded beam elements must not be used or problems will arise with the mid-side node being unrestrained.

Two-dimensional elements

The options for computing bending moments and shear forces in a slab are identical to those in a wall (with the obvious difference that the former is generally horizontal while the latter is vertical). What can make a more significant difference is that prop slabs may be inclined to the horizontal and thus not aligned with the global x axis. Transverse normal stresses must therefore be obtained from the Cartesian stresses (σ_x σ_y τ_{xy}) via Eqn (8.36) before attempting to use them to calculate bending moments in the prop. Once this has been taken into account, the observations made and the conclusions drawn in Sections 8.4 and 8.5 would be relevant.

8.6.3 Summary

No numerical investigations have been carried out into prop and anchor loads for this thesis. The methods of obtaining the axial forces output from CRISP are straightforward and no specific problems have been reported in the literature. The only factors to take into account when interpreting output are (a) whether or not shear stress transfer can occur, and (b) if any prestressing has been performed. For bending moments and shear forces in 2D elements, methods based on internal (transverse) stresses are probably the best, and these have been investigated earlier in this chapter. For 1D elements, there are few (if any) contentious issues.

8.7 Discussion and Summary

This Chapter has examined that part of the finite element analysis which impacts ultimately on the design process - *viz.* the output. Earlier chapters have covered the modelling issues that are relevant during the set-up and execution of the finite element analysis - such as discretization, constitutive modelling, construction representation, and numerical problems. These earlier chapters have demonstrated that the calculated quantities can be influenced by a large number of factors - even before results are extracted, processed, and finally displayed. This chapter has attempted to show that there are further issues to be aware of when viewing program output, or using it for further calculations. A finite element analysis can take days to set up and run, and so there will be considerable pressure to expedite the production of plots and graphs for the design team - but this can result in a false economy of time.

Three principal categories of output have been examined:

a) displacements *(primary output)*
b) stresses/pressures *(secondary output)*
c) internal structural forces *(tertiary output)*

Correct interpretation and visualization are of key concern to practitioners, but the literature provides little if any advice on the matter. The numerical results presented in this chapter should go some way to addressing this deficiency, in a manner which is understandable by, and useful to, designers. The major points will now be summarized.

Displacements

Recommendations have been put forward based largely on the writer's experience, having performed many retaining wall analyses in a commercial context. The recommendations are not onerous to implement, and significant benefit would arise from following them, yet anecdotal evidence suggests that they are not being followed in current practice. An inadmissible analysis can be unwittingly passed if the displacements (deformed mesh, vectors, contours) are not scrutinized appropriately and thoroughly. There is a temptation to extract the wall displacement, ground surface settlement profile, etc as soon as the analysis is complete, but this should be regarded as negligent practice.

Stresses/pressures

Numerical analyses have been deployed to assess various alternatives for obtaining soil stress distributions (normal and shear) on the wall. Methods of varying levels of rigour were implemented and tested The methods which used a least-squares best-fit plane through the 'raw' 3×3 Gauss point stresses, or which interpolated the 2×2 (reduced integration) point stresses, gave a satisfactory degree of smoothing for the present purpose. These local element-by-element methods are not ideal, as they still leave some degree of "raggedness" in the profiles of horizontal total stress or soil-wall shear stress. Compromise approaches (e.g. the superlocal method in Section 8.3.4) would seem attractive, but the limited results presented herein have not been convincing. There may be more potential to explore than has been possible in the present work, and this may deserve further investigation.

Internal structural forces

Numerical experiments have been used to benchmark the methods normally employed to obtain wall bending moment and shear force - and also to assess the merits of various alternatives. Methods using transverse stress distributions in the wall have been confirmed as the most reliable. For bending moments, "raw" 3×3 Gauss point normal stresses are satisfactory, whereas for shear forces the 3×3 shear stresses are not suitable and a smoothing stage is required. The independent check sought from external soil pressures is logical and intuitive, and is thus arguably the kind of check that ought to be carried out - but unfortunately it breaks down and affords only limited corroboration in practice.

Customized pre-/post-processing

The basic CRISP "engine" released initially in 1982 was enhanced with a variety of in-house pre-/post-processing software or linked to commercial packages where users had already acquired them. Cambridge University produced the CRISP 90 engine plus interface in 1990, eventually superseded by SAGE CRISP in 1995. At present, a variety of practices and products exist, but there is a specific gap which no investigator has attempted to fill: the provision of pre/post-processing software aimed at particular types of analysis and design applications. For example, embankment modelling has different requirements to (say) tunnel analysis, which are different again to retaining walls - yet only a general interface is available. Errors due to ignorance or lack of experience could be minimized by "situation-specific" front/back ends (not necessarily using an expert knowledge-based system, though this may happen in time). Other commercial FE software appears to be evolving in this direction - for example, LUSAS release 14 (FEA, 1998) comes with various modules which recognize the particular demands of (for example) bridge analysis.

A retaining wall post-processing module might include:

i) empirical profiles for ground movement (vertical and horizontal) behind the wall, which can be superimposed on calculated results: the later being converted to non-dimensional form to allow proper comparison,

ii) interpolation to obtain stresses at reduced integration (2×2) points from the raw (3×3) Gauss point data in specified elements, for use in (iii) and (vi) below,

iii) one or more of the local stress smoothing methods presented in Section 8.3 - best-fit plane 3×3 (BFP3) and best-fit line 2×2 (BFL2) are recommended - in order to produce profiles on any given horizontal or vertical section in the mesh,

iv) simplified earth pressure diagrams for both retained (active) and excavated (passive) sides of the wall, which can be superimposed on calculated distributions (suitably smoothed) for comparison,

v) wall bending moment calculations using the wall stress method (WSBM) - with an option on the earth pressure method (EPBM) provided it carries an appropriate warning about probable inaccuracy,

vi) wall shear force calculations using the wall stress method (WSSF) - with an option on the earth pressure method (EPSF) carrying the same proviso as (iv) above,

vii) bending moment and shear force calculations as in (iv) and (v), but for props modelled with 2D continuum elements - corrected as appropriate for inclination to horizontal

viii) bending moment, shear force and axial force calculations for props modelled with 1D beam/bar elements

ix) axial tensions (relative to prestress load) for anchors modelled with 1D bar elements

Progress towards such a system is represented by various utilities (programs and spreadsheets) developed by the writer during the course of the present work - elements of (v), (vii) and (viii) have been present since CRISP 9x. However, significant further work remains to be done before something of sufficient robustness and commercial standard is available.

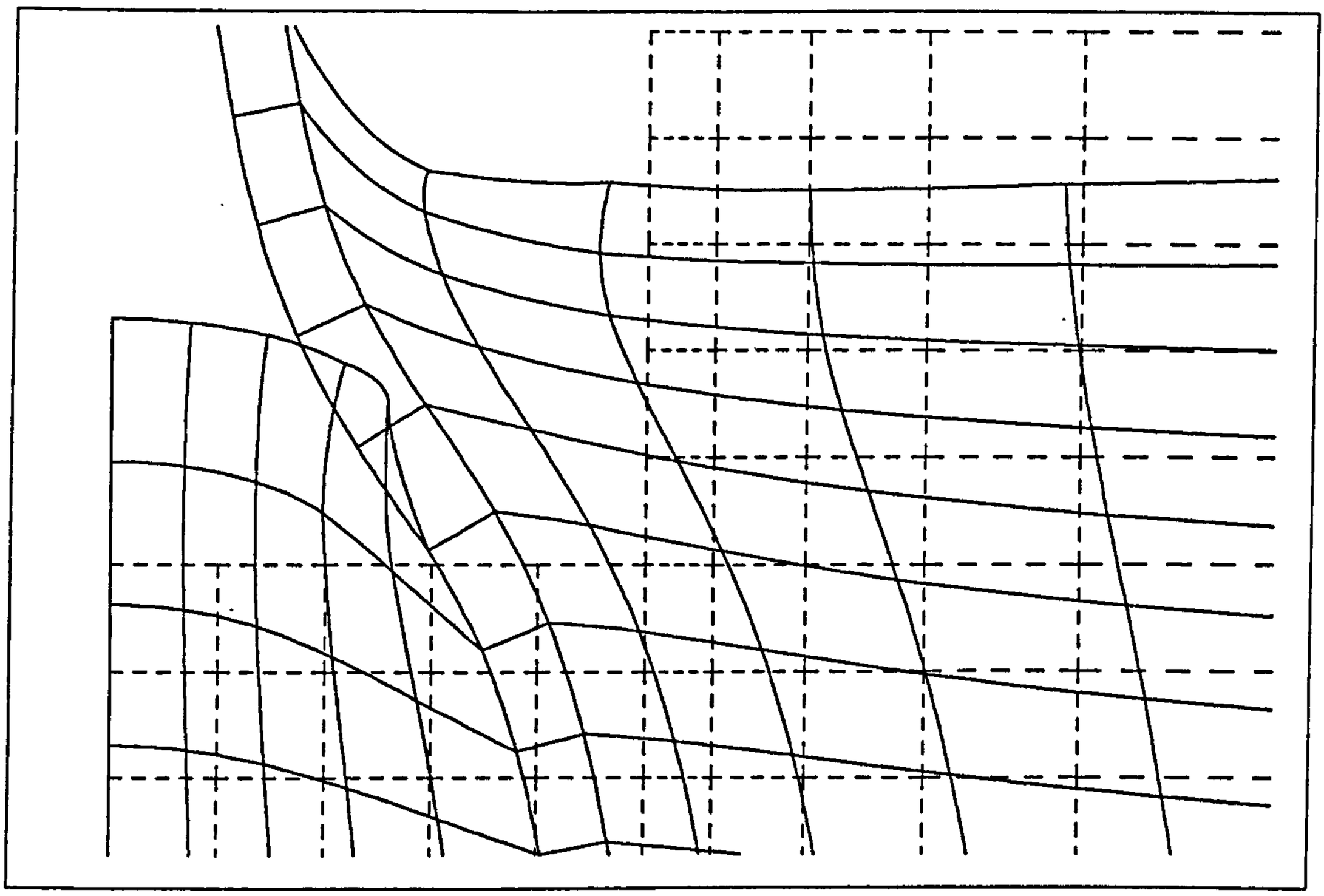

Fig 8.1 Example of apparently overlapping elements caused by exaggeration
(- - - - undeformed mesh —— deformed mesh)

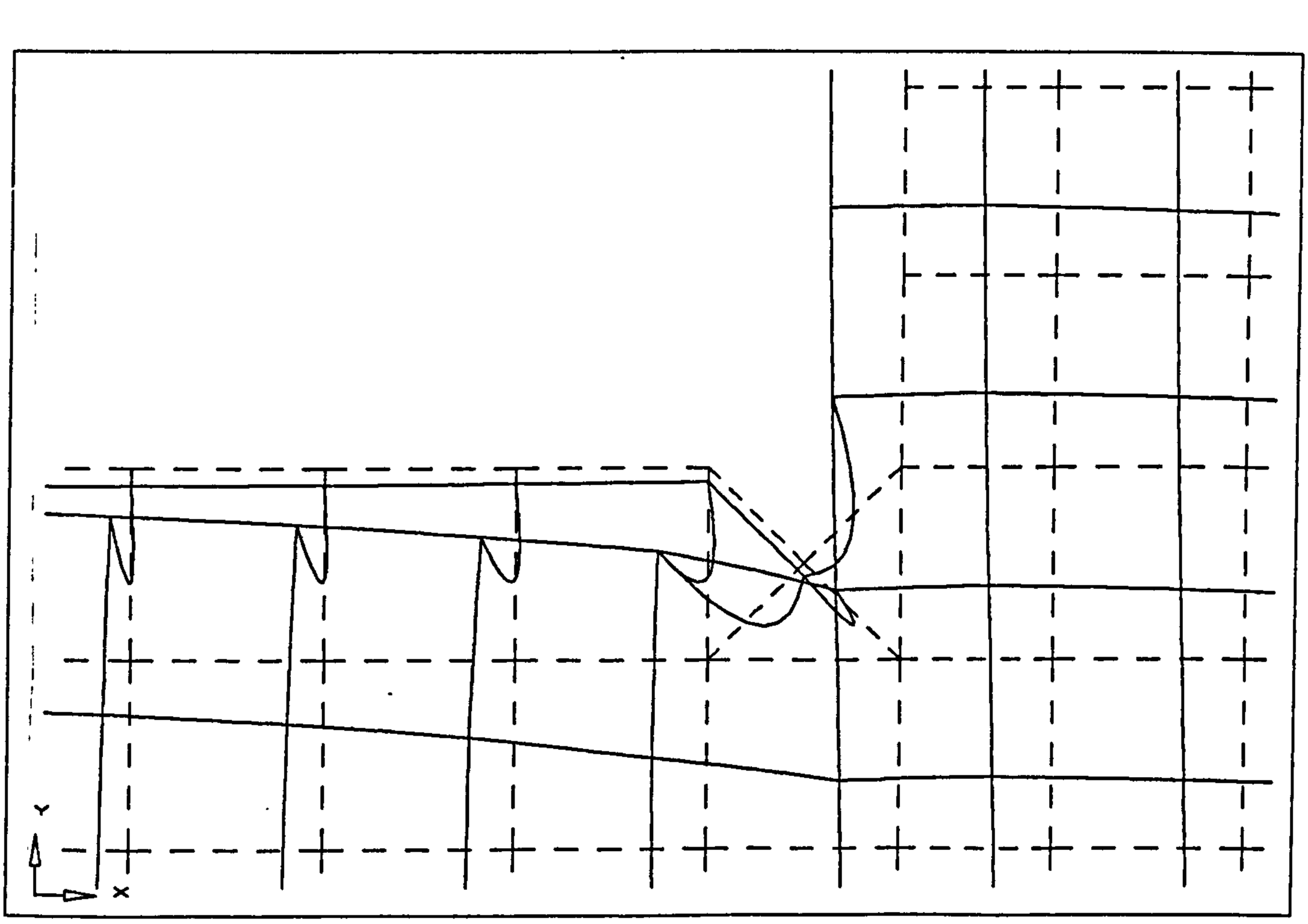

Fig 8.2 Example of excessive distortion which can occur with overlay elements

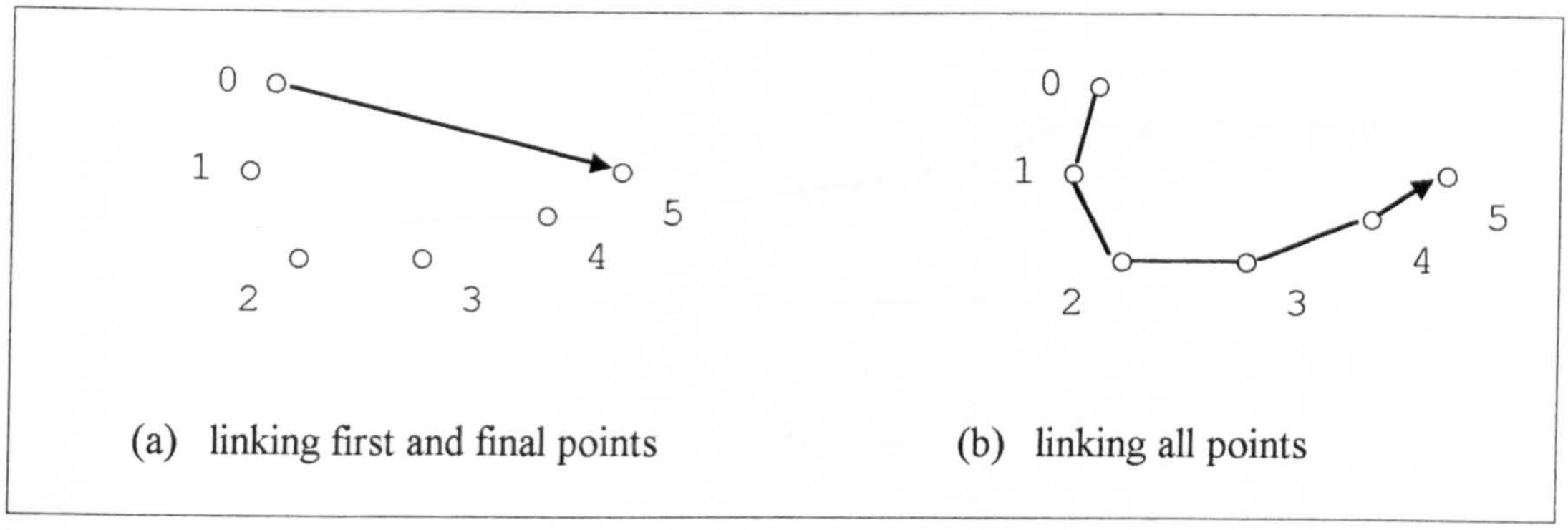

Fig 8.3 Two possible interpretations of displacement vectors

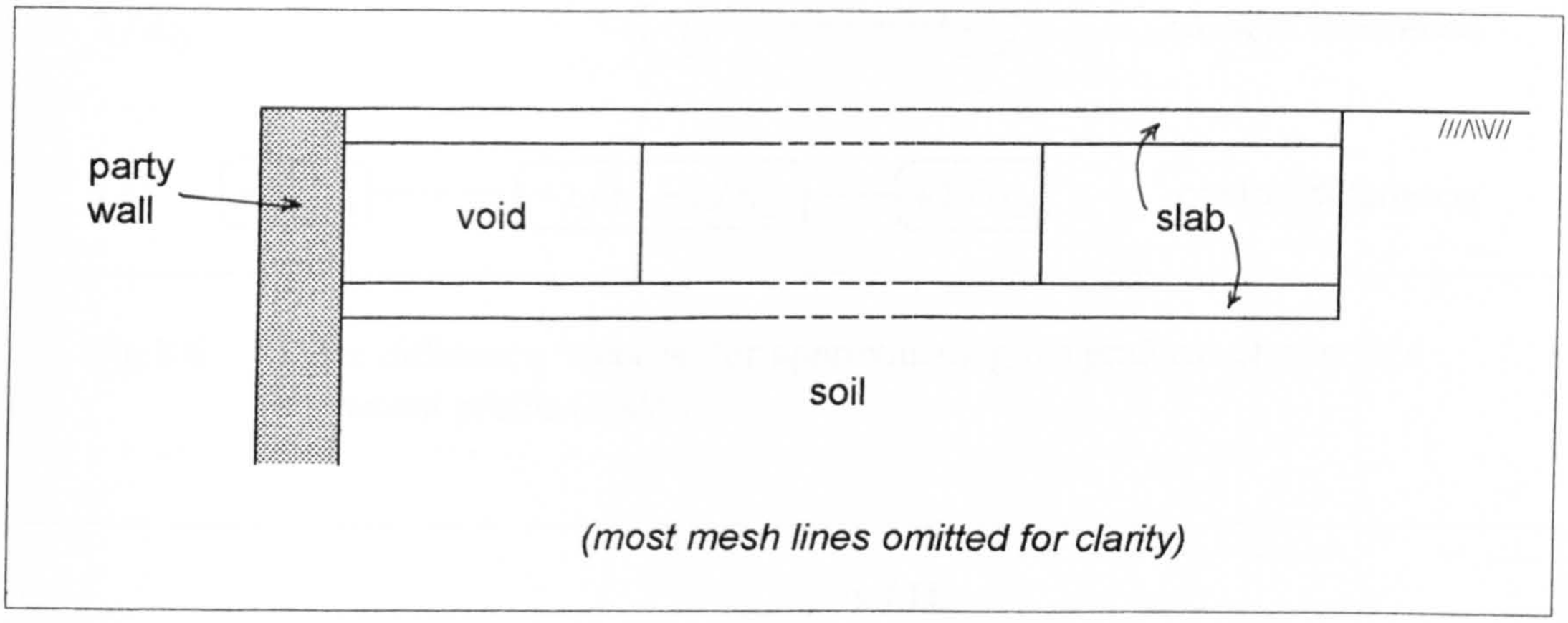

Fig 8.4 Queensberry House - mesh detail near party wall and adjacent basement

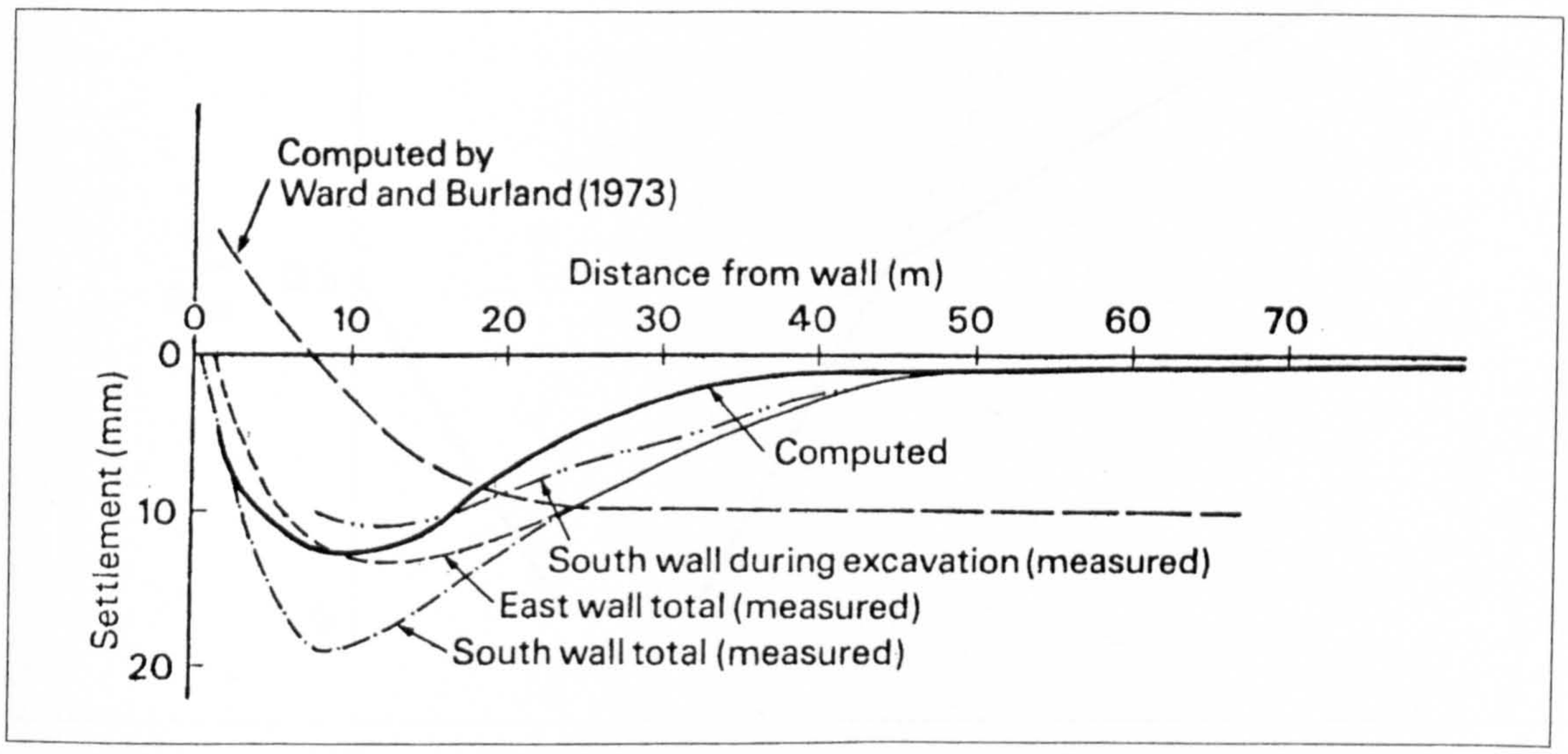

Fig 8.5 Comparison of settlement profiles predicted for the House of Commons Car Park. (after Simpson, 1981)

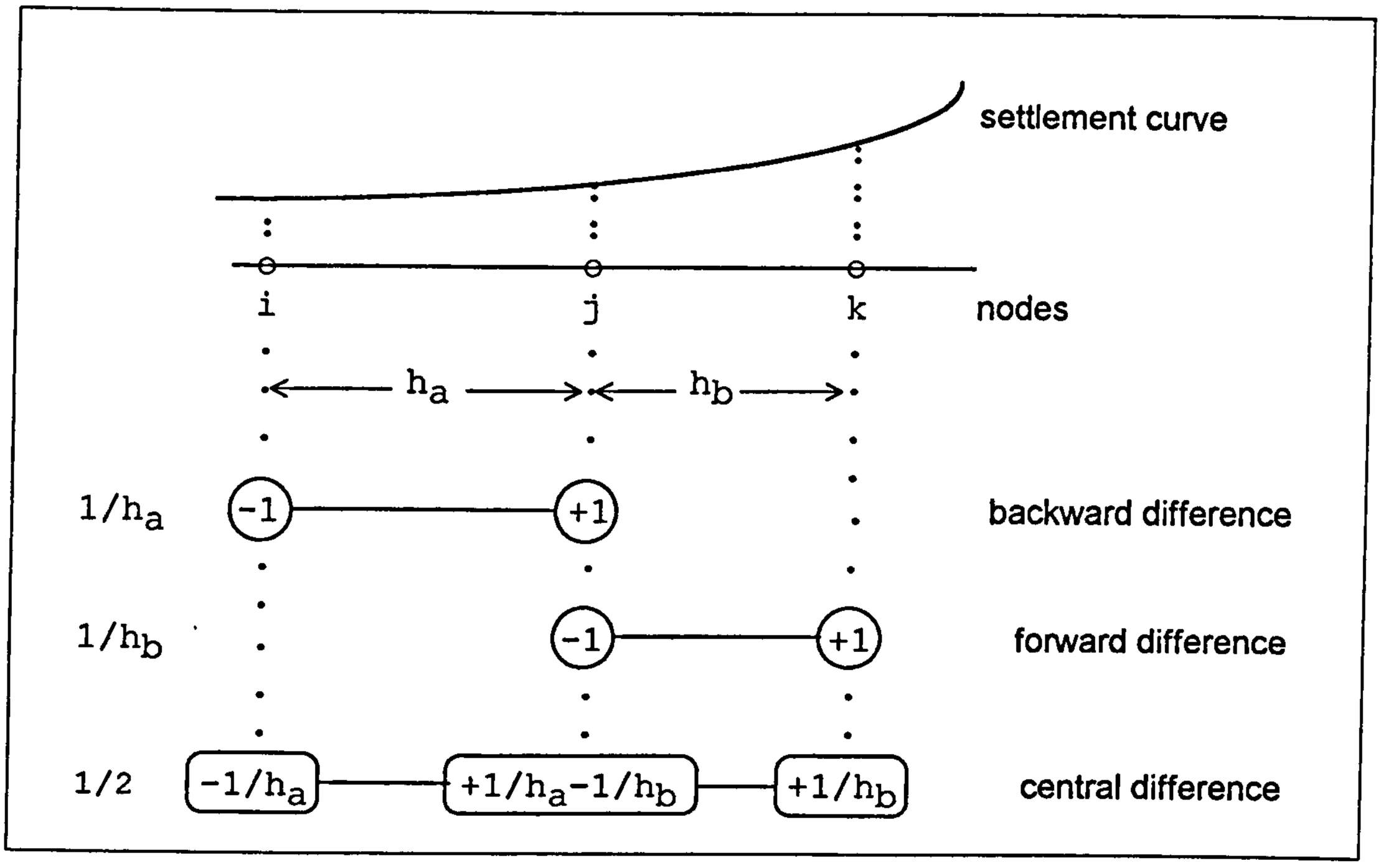

Fig 8.6 Finite difference 'stencils' for approximating the gradient of a surface settlement profile ($\Delta S/\Delta x$)

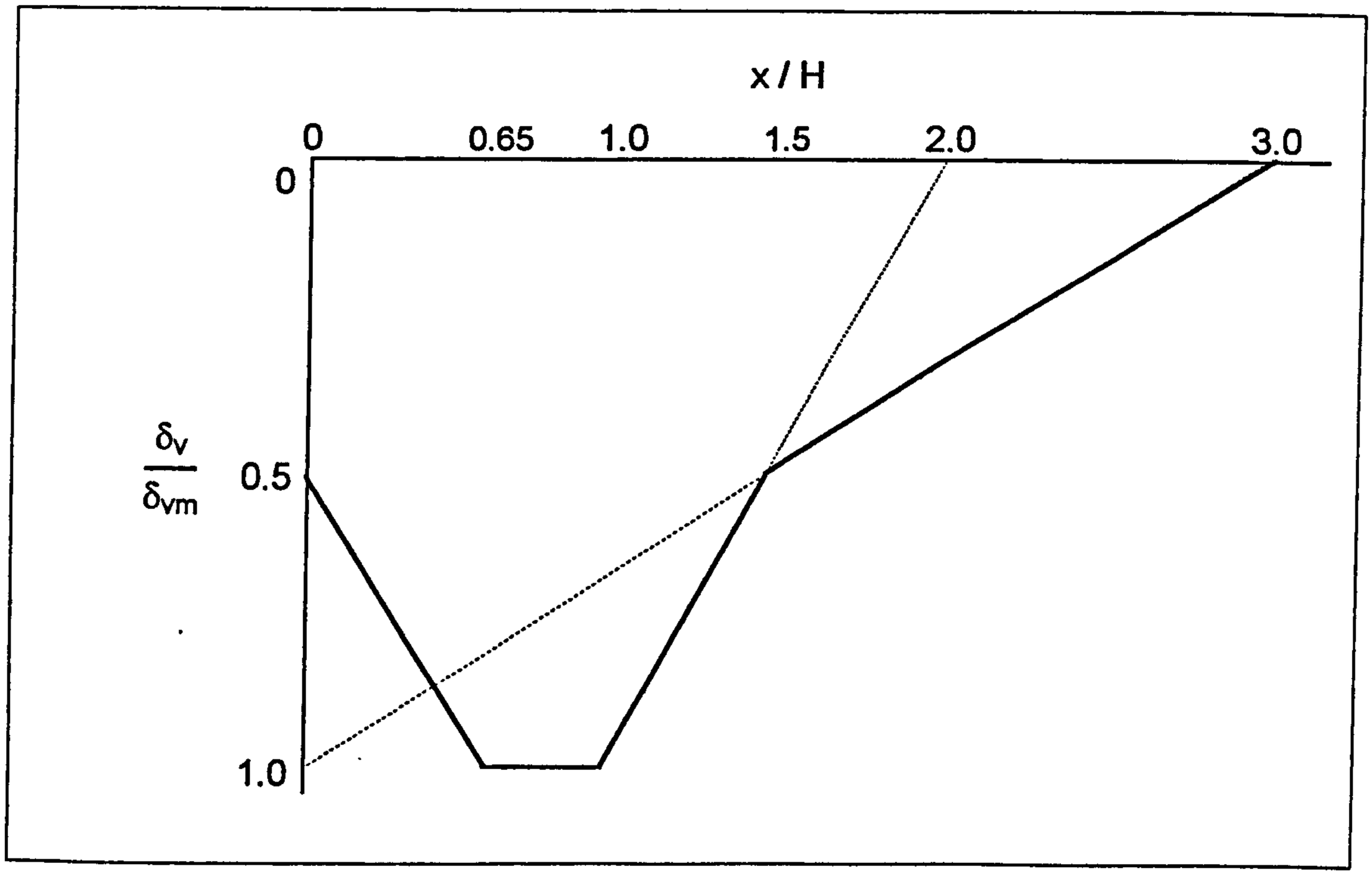

Fig 8.7 Envelope of normalized settlement for propped embedded walls in stiff clay (after Clough and O'Rourke, 1990)

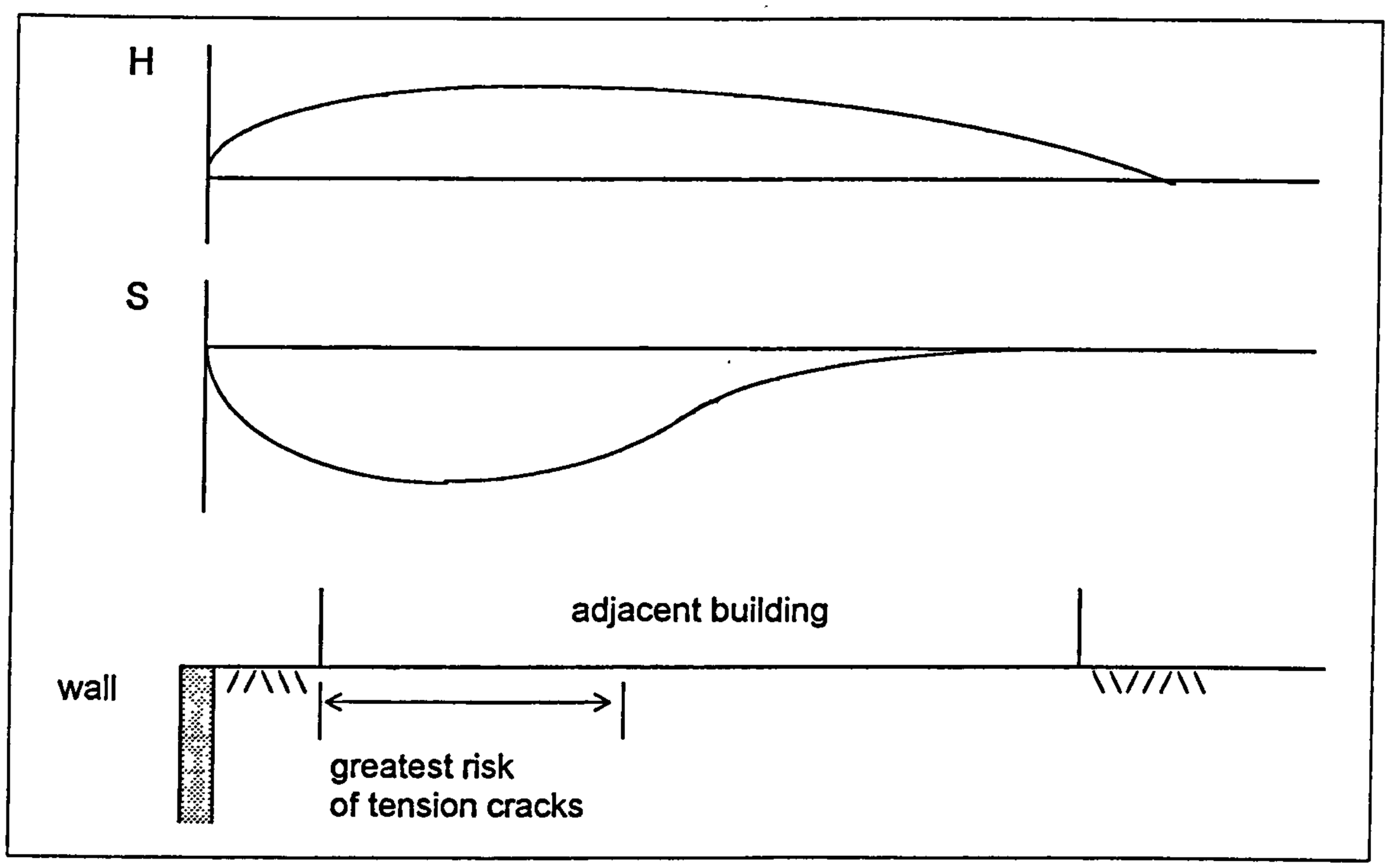

Fig 8.8 Differential ground movements : horizontal (H) and vertical (S)

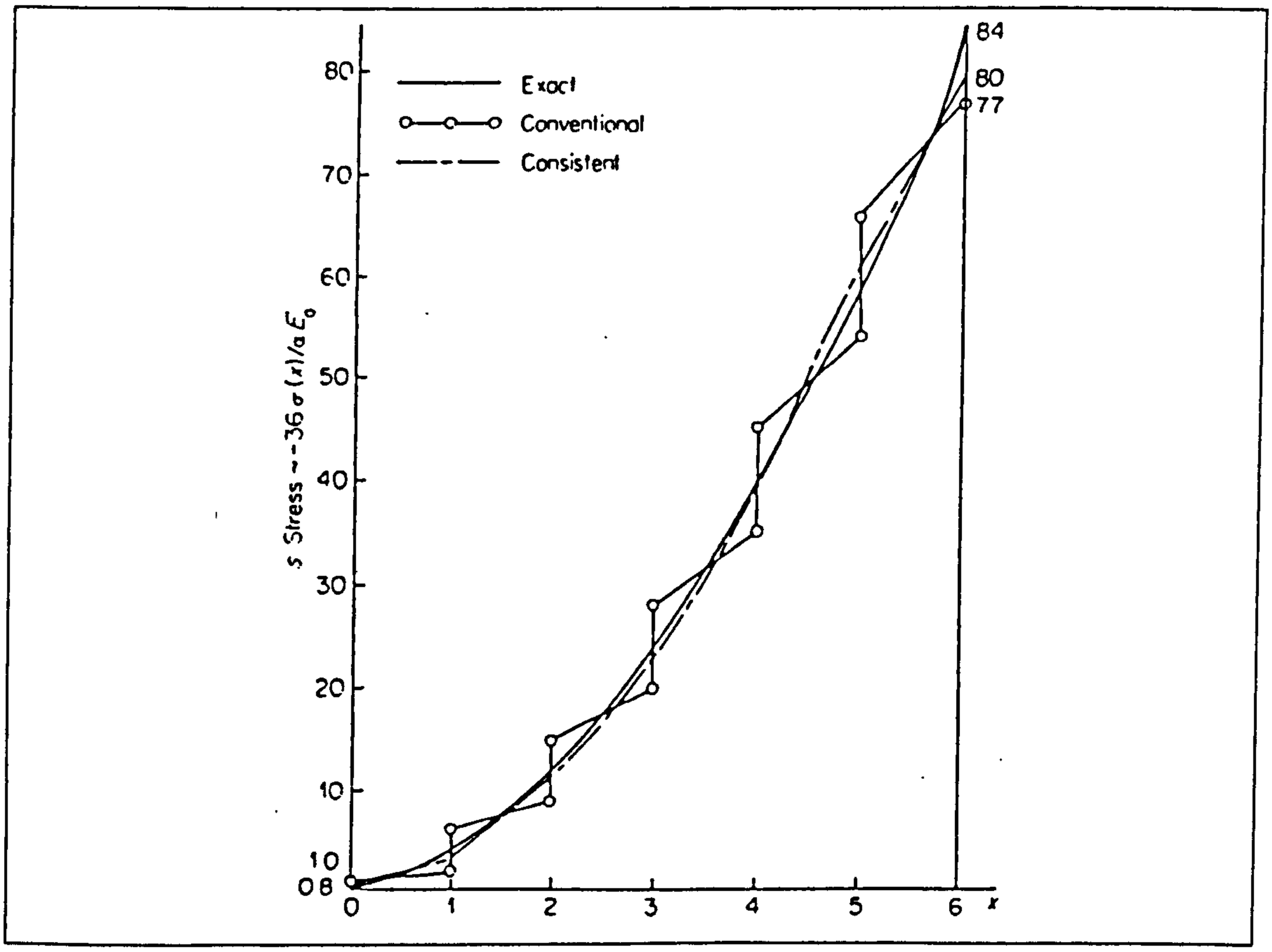

Fig 8.9 Comparison of conventional (FE) and consistent stresses with the exact solution, for a 1-D bar (after Oden & Brauchli, 1971)

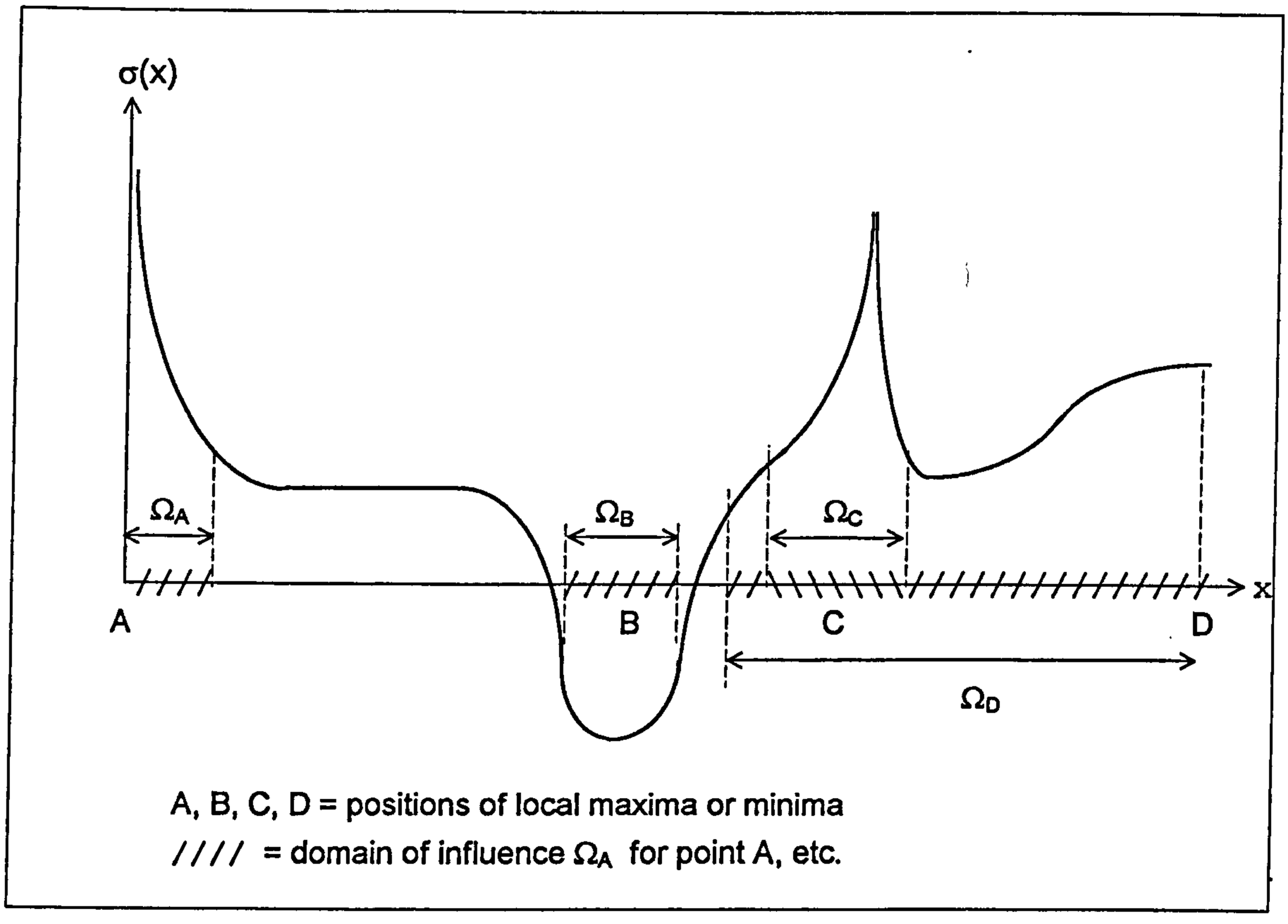

Fig 8.10 Illustration of domains of stress influence (after Oden and Reddy, 1973)

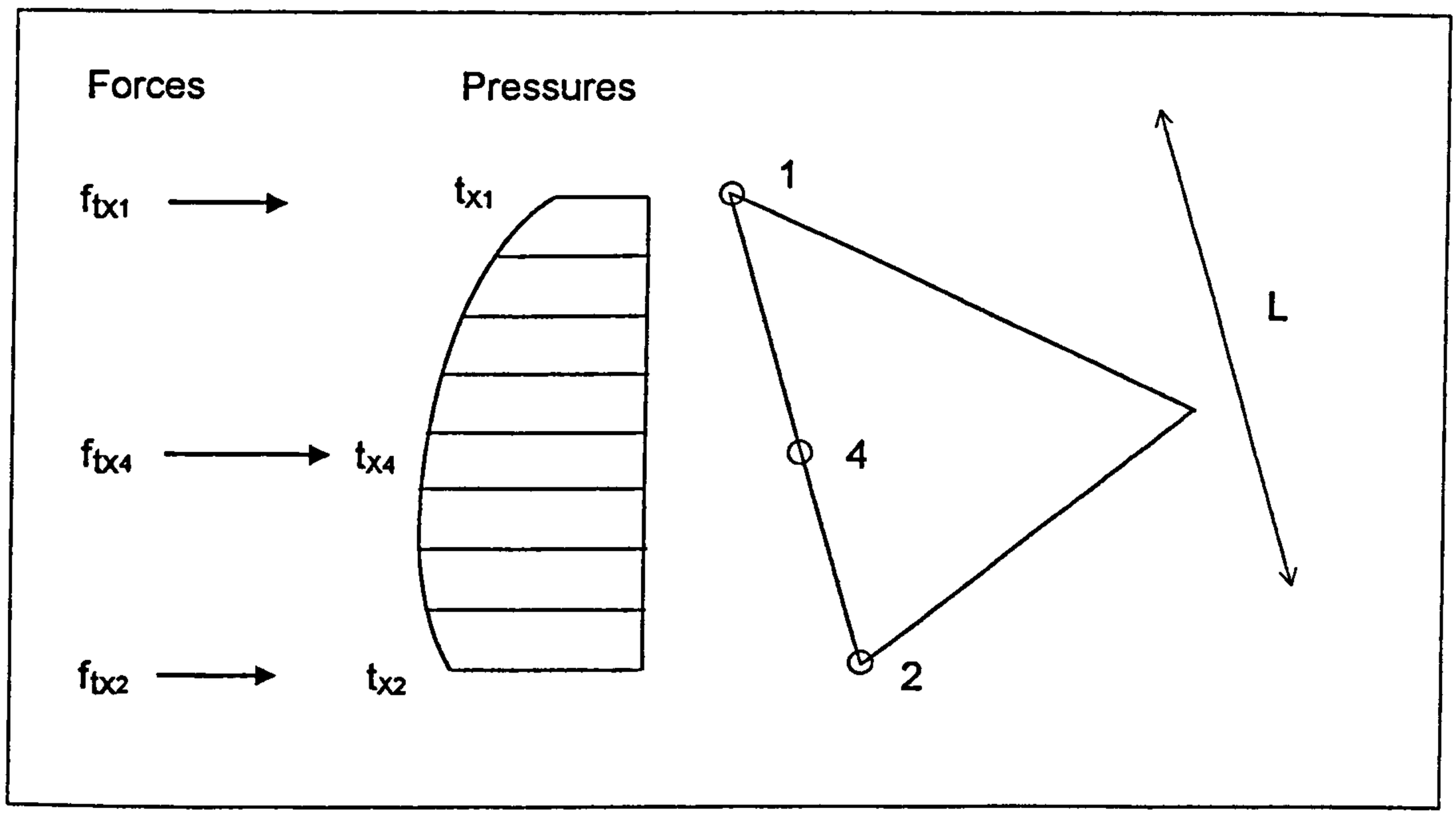

Fig 8.11 Earth pressure distributions on an element side based on nodal forces (after Creed, 1979)

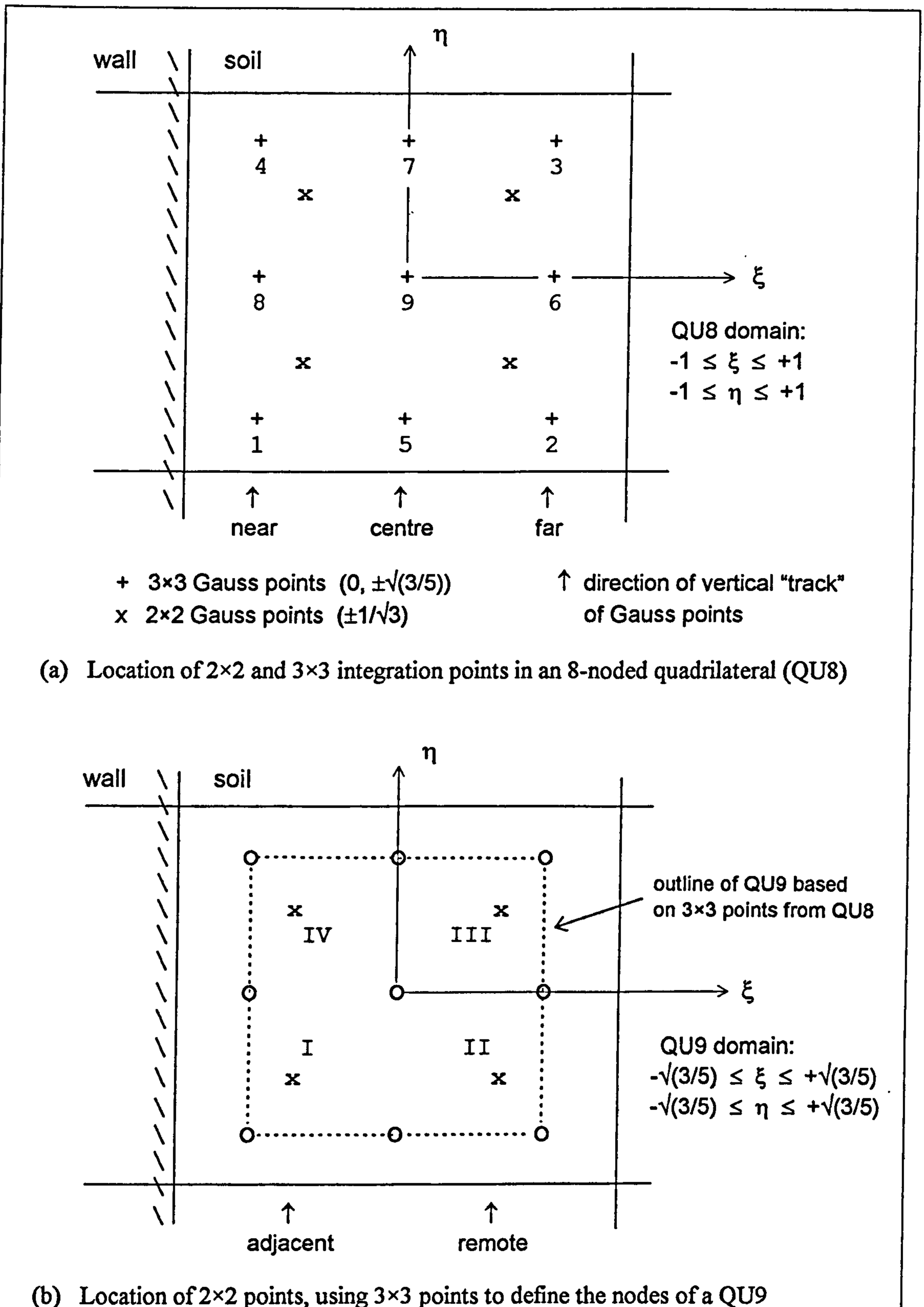

(a) Location of 2×2 and 3×3 integration points in an 8-noded quadrilateral (QU8)

(b) Location of 2×2 points, using 3×3 points to define the nodes of a QU9

Fig 8.12 Interpolation within 8- and 9-noded quadrilateral elements

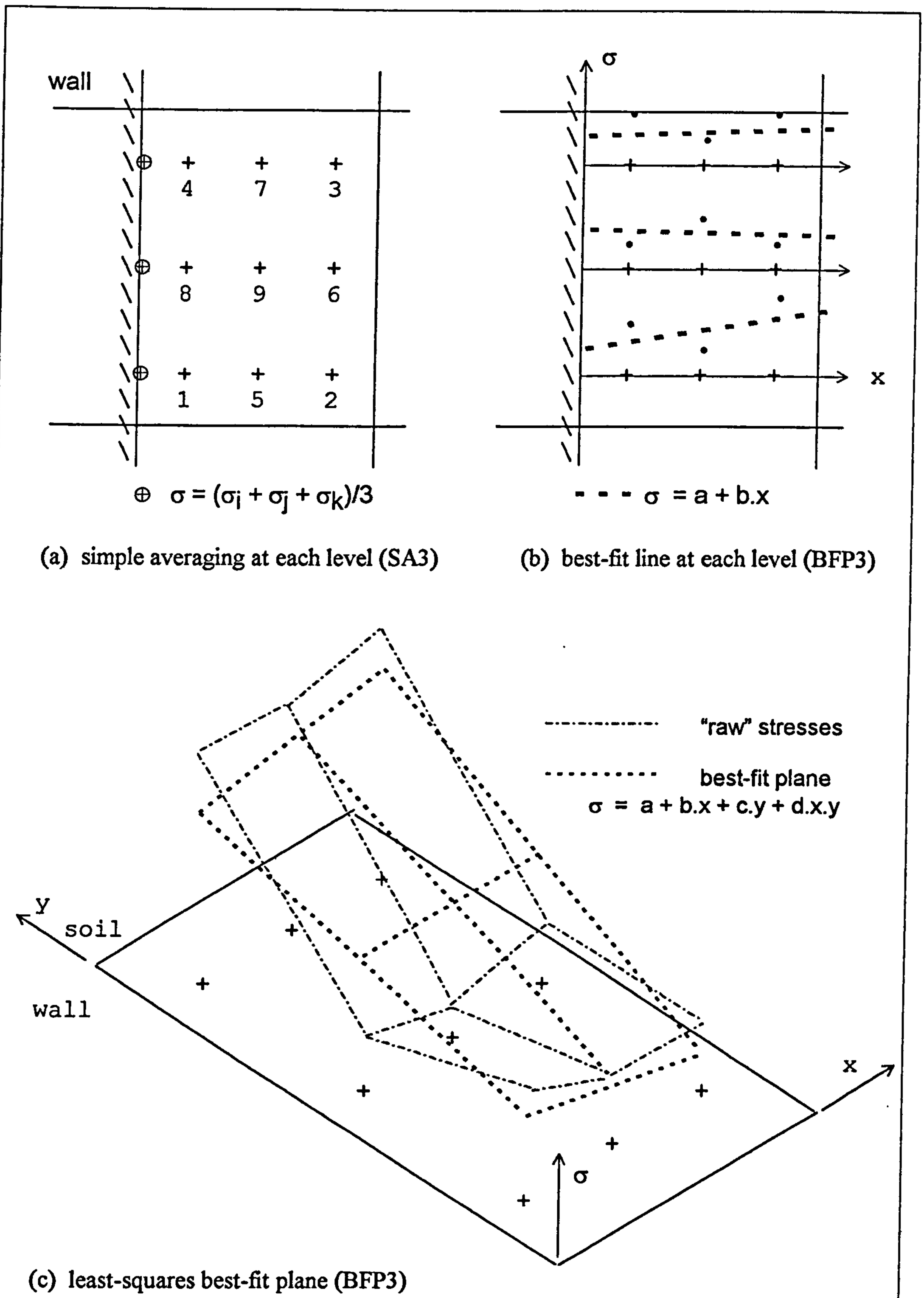

(a) simple averaging at each level (SA3)

(b) best-fit line at each level (BFP3)

(c) least-squares best-fit plane (BFP3)

Fig 8.13 Local stress smoothing methods based on averaging and least-squares best-fit techniques, using "raw" stresses at Gauss points in soil elements

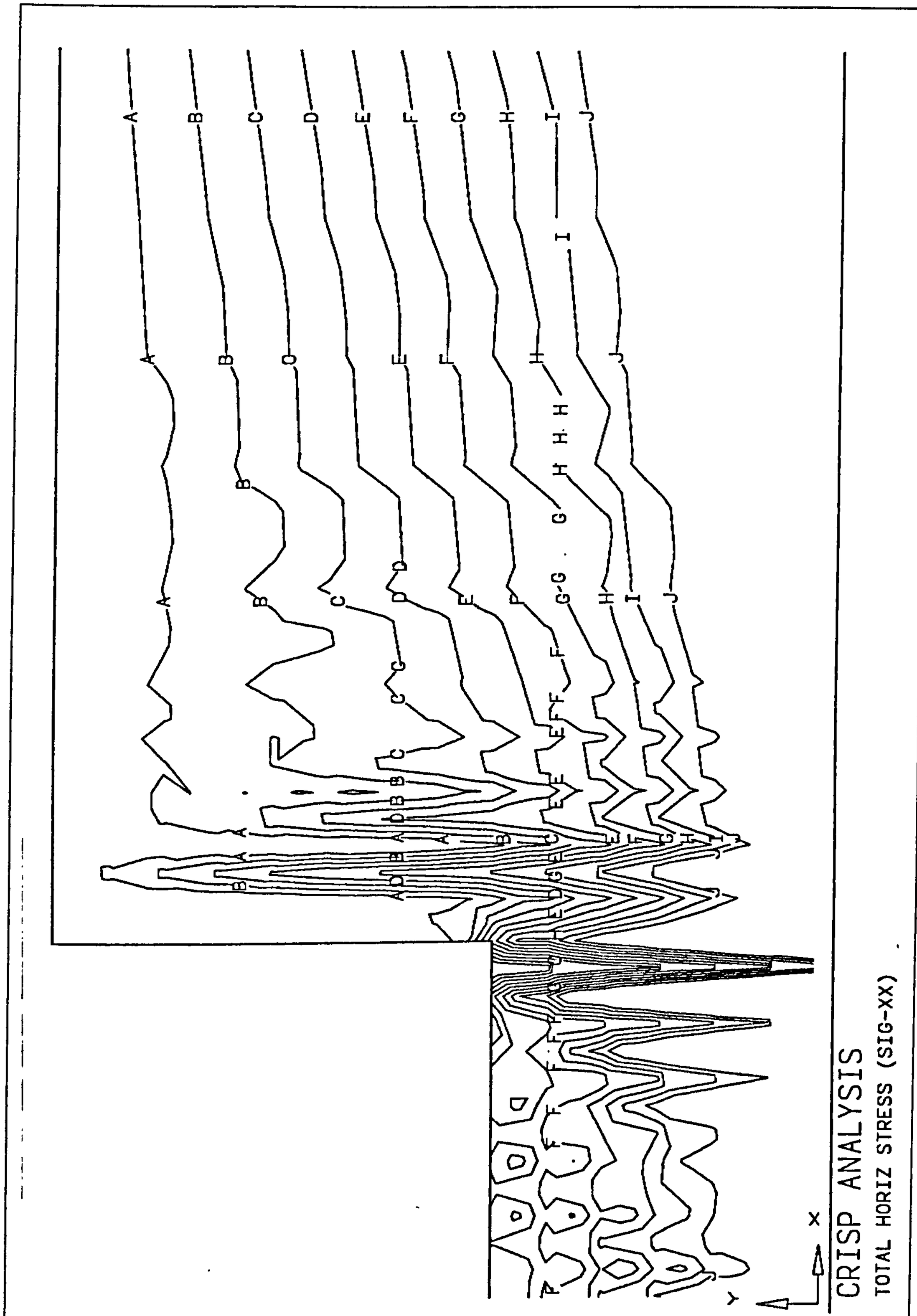

Fig 8.14 Typical contours of horizontal stress near an embedded retaining wall

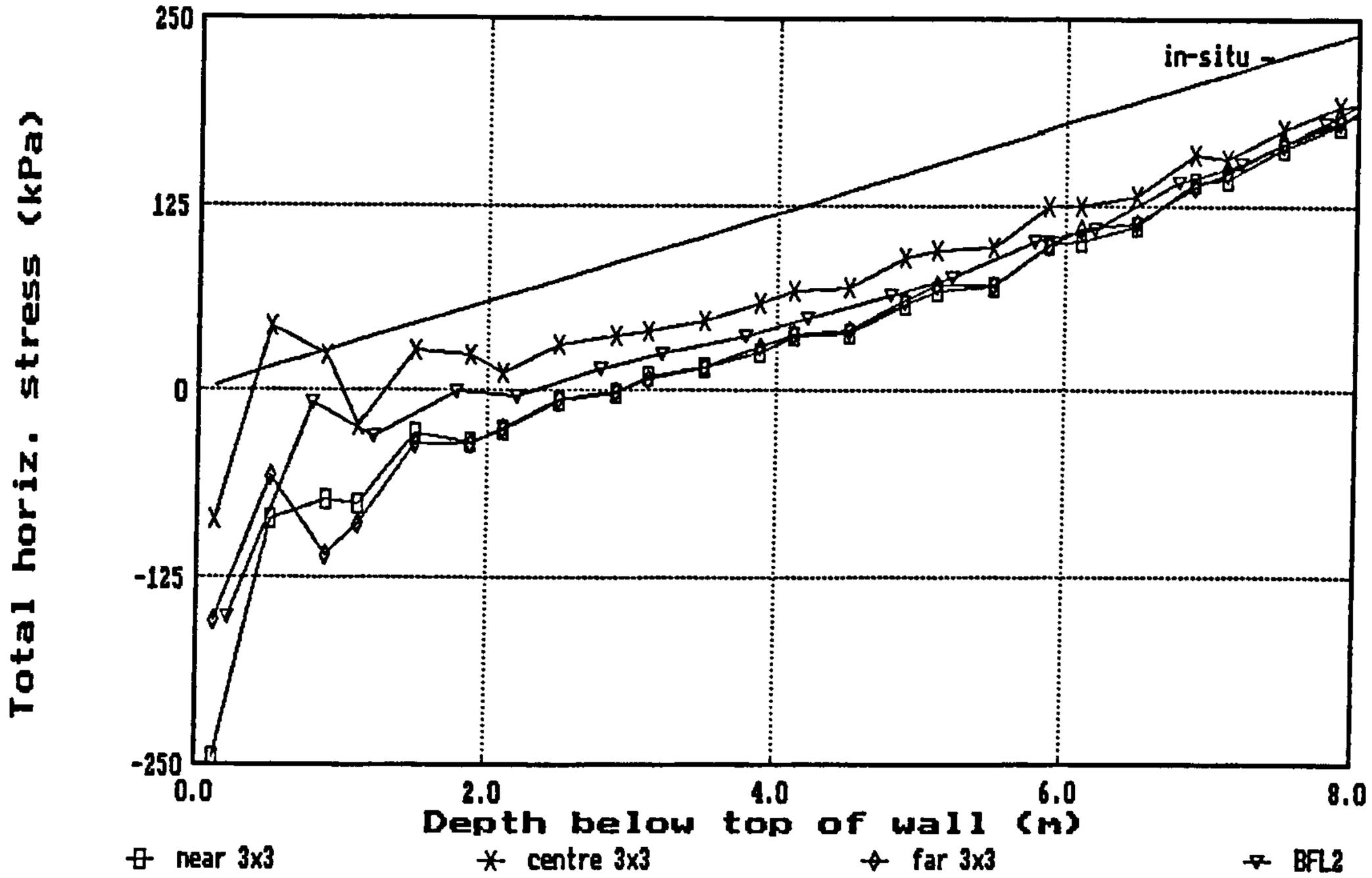

(a) Case RW1 - raw 3×3 stresses on near, centre and far sections compared with smoothed (BFL2) distribution

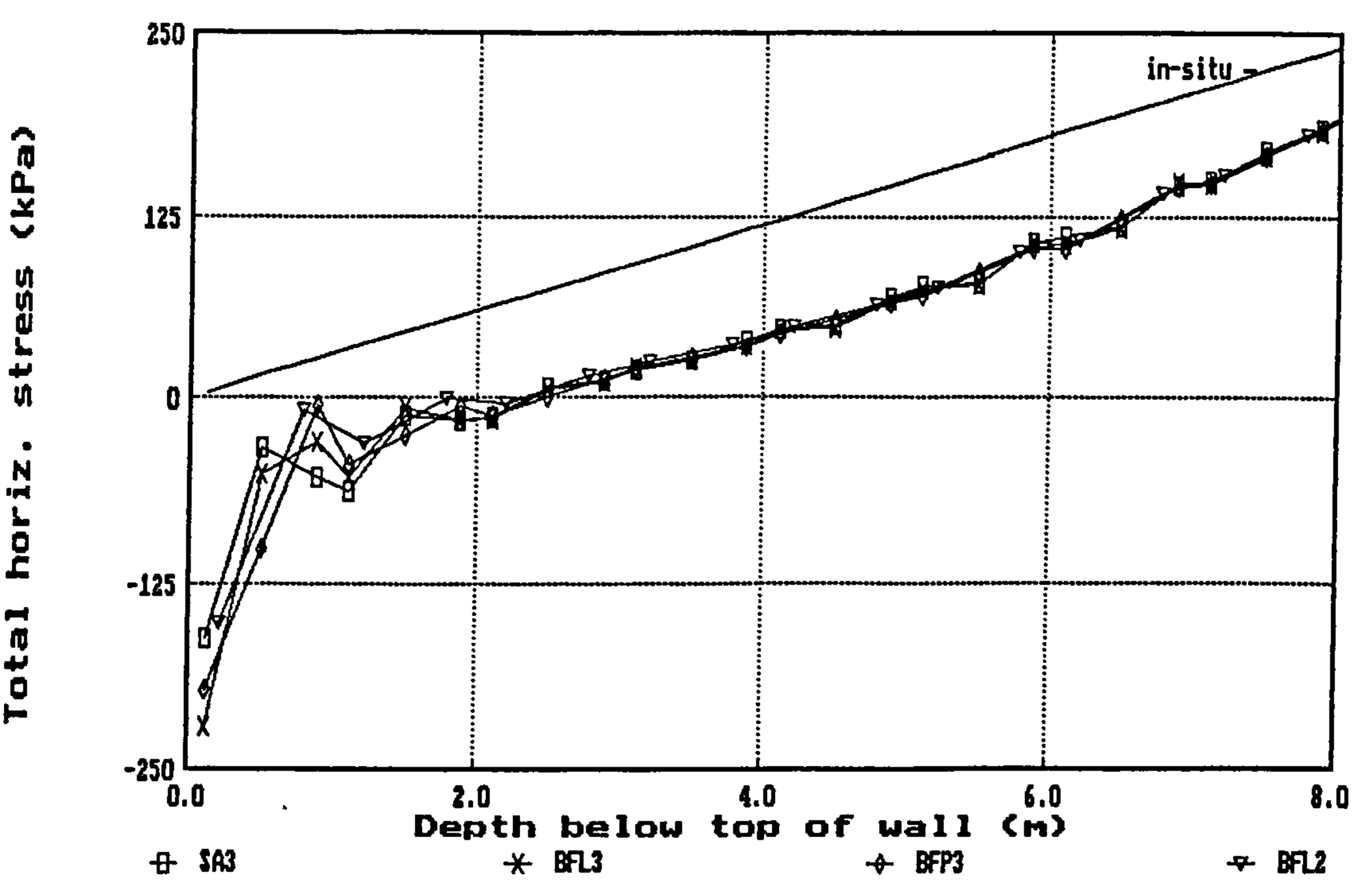

(b) Case RW1 - comparison of local smoothing methods

Fig 8.15 Total horizontal stress distributions on the retained side of an embedded wall - undrained elastic analysis

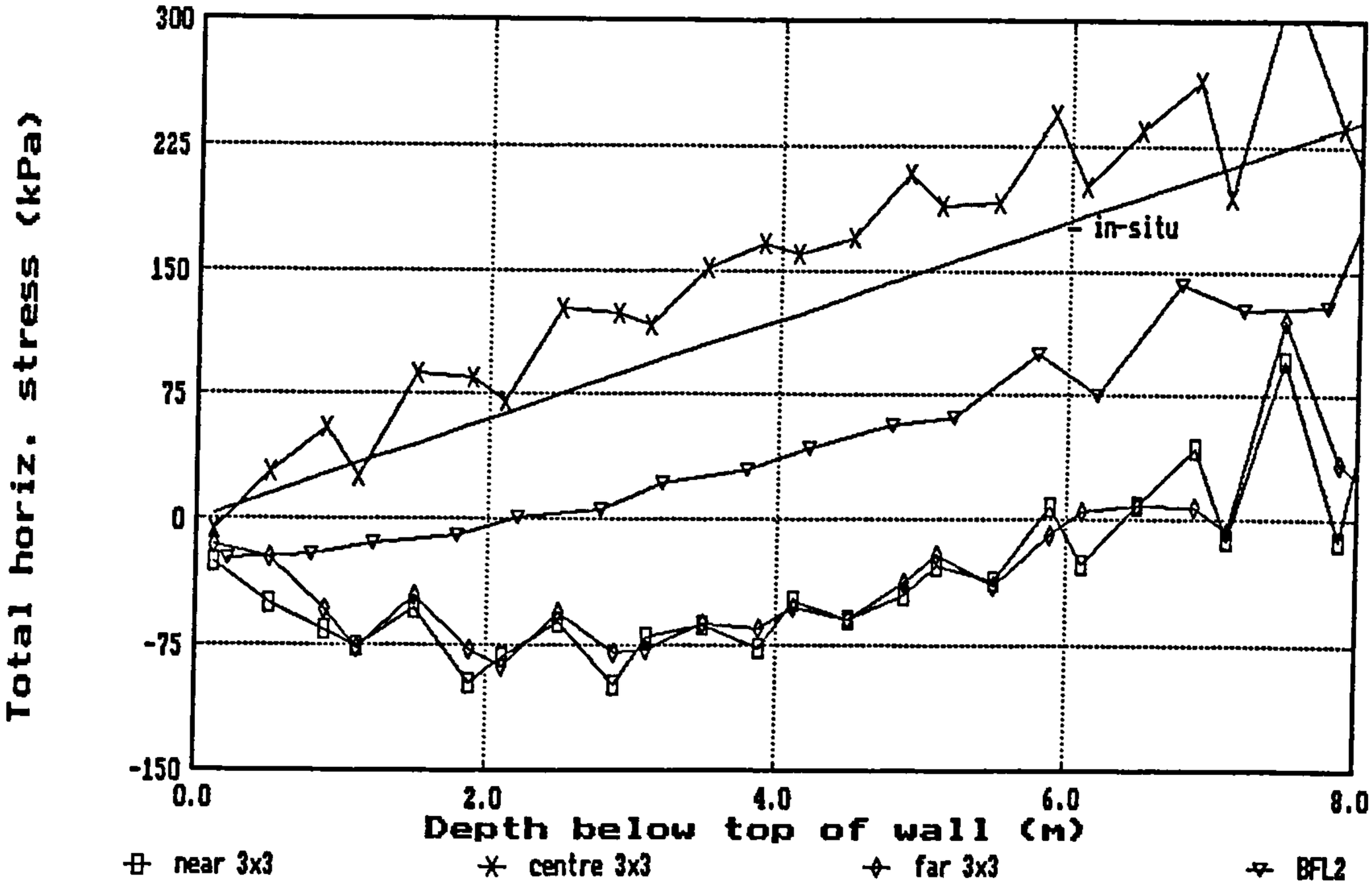

(c) Case RW3* - raw 3×3 stresses on near, centre and far sections compared with smoothed (BFL2) distribution

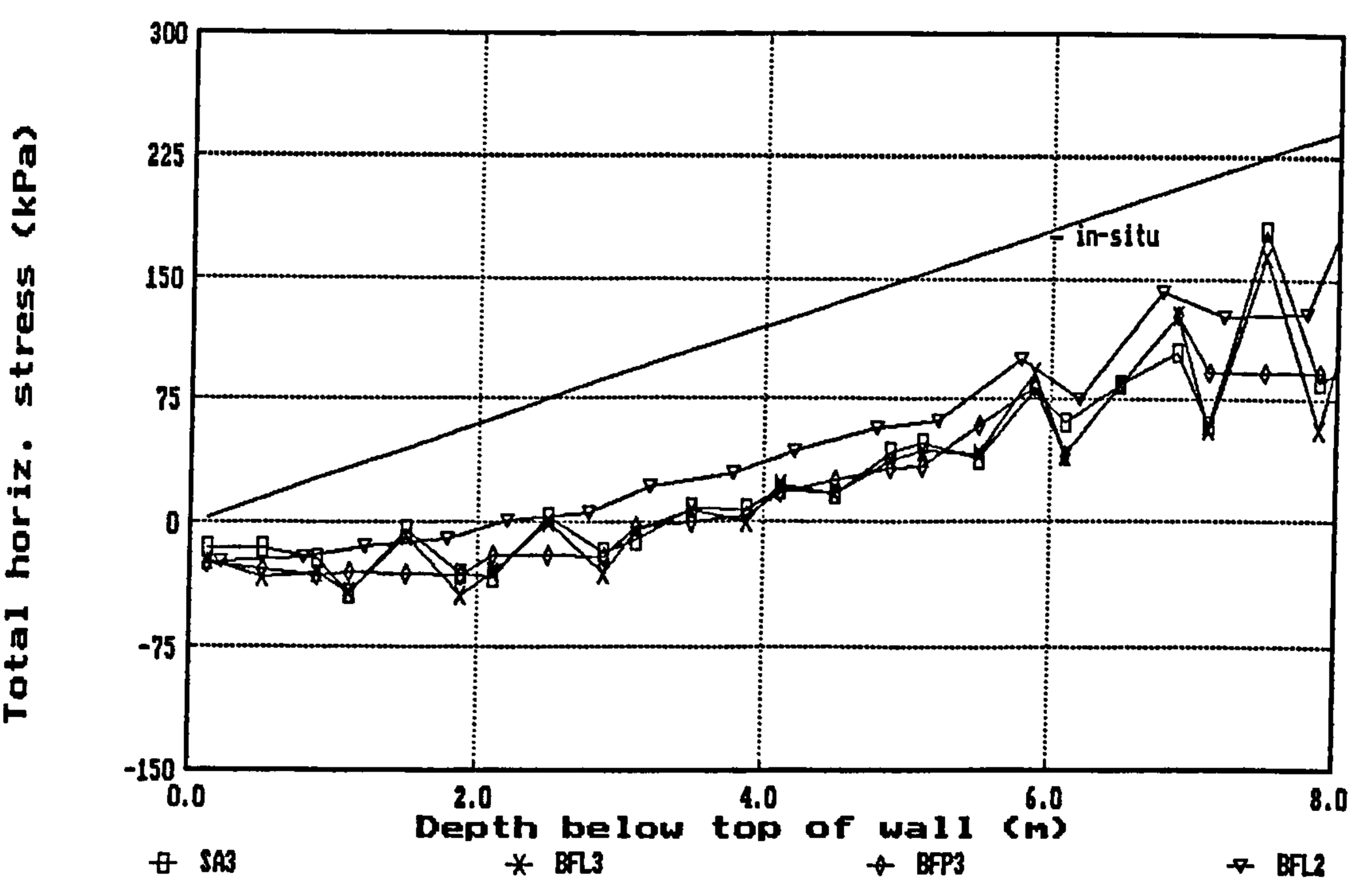

(d) Case RW3* - comparison of local smoothing methods

Fig 8.15 Total horizontal stress distributions on the retained side of an embedded wall - undrained elastic analysis (contd)

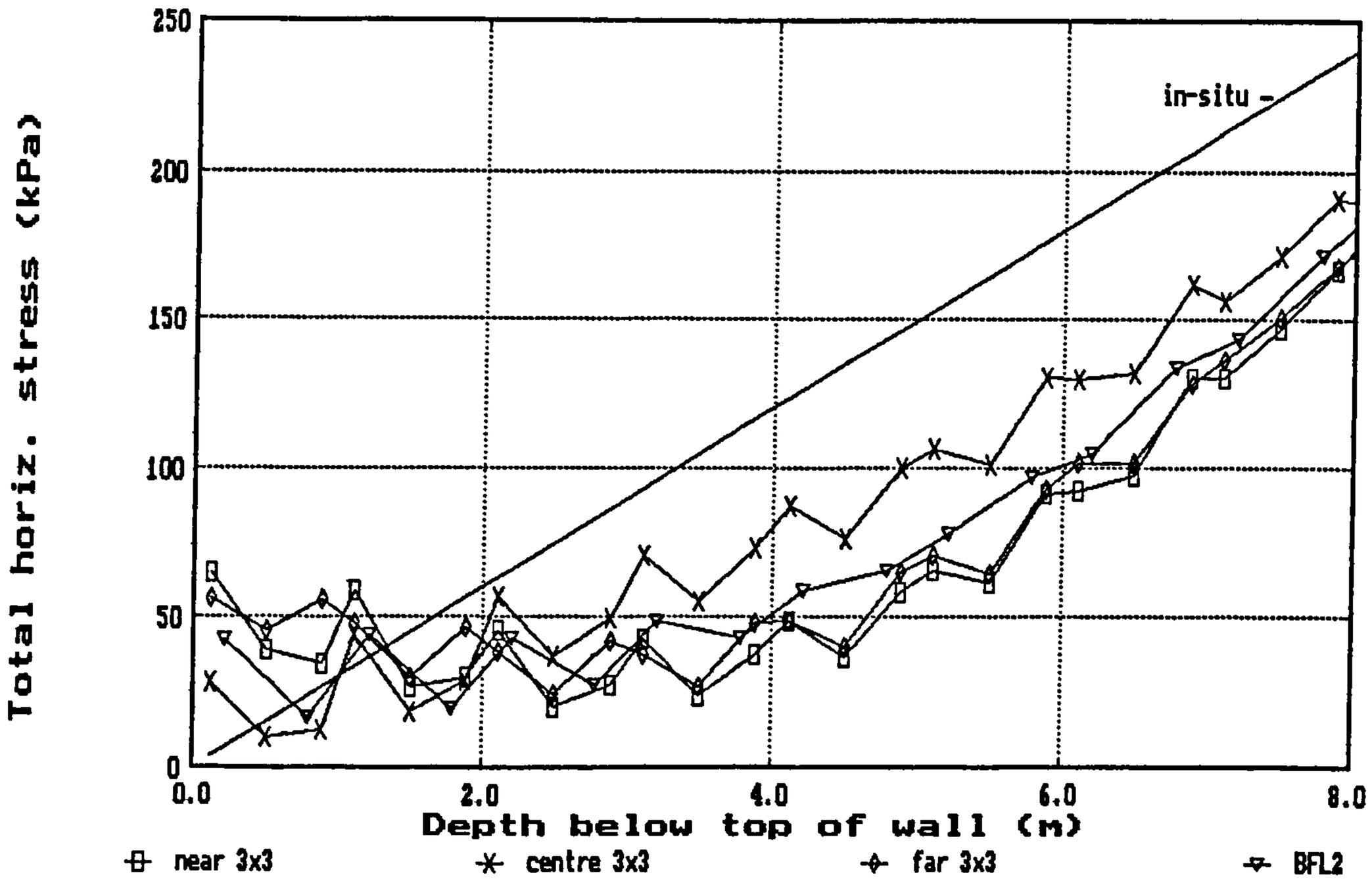

(e) Case RW11 - raw 3×3 stresses on near, centre and far sections, compared with smoothed (BFL2) distribution

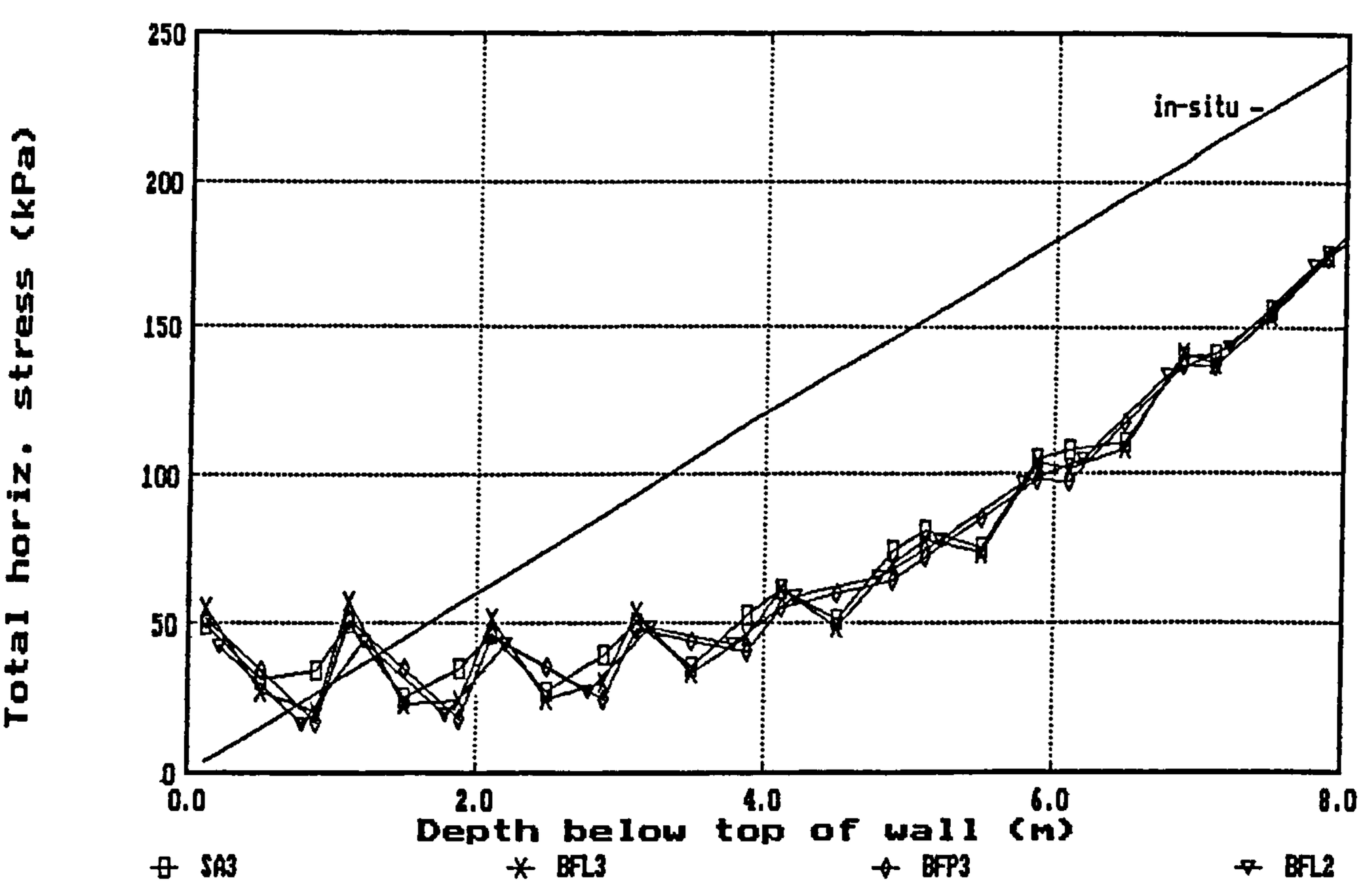

(f) Case RW11 - comparison of local smoothing methods

Fig 8.15 Total horizontal stress distributions on the retained side of an embedded wall - undrained elastic analysis (contd)

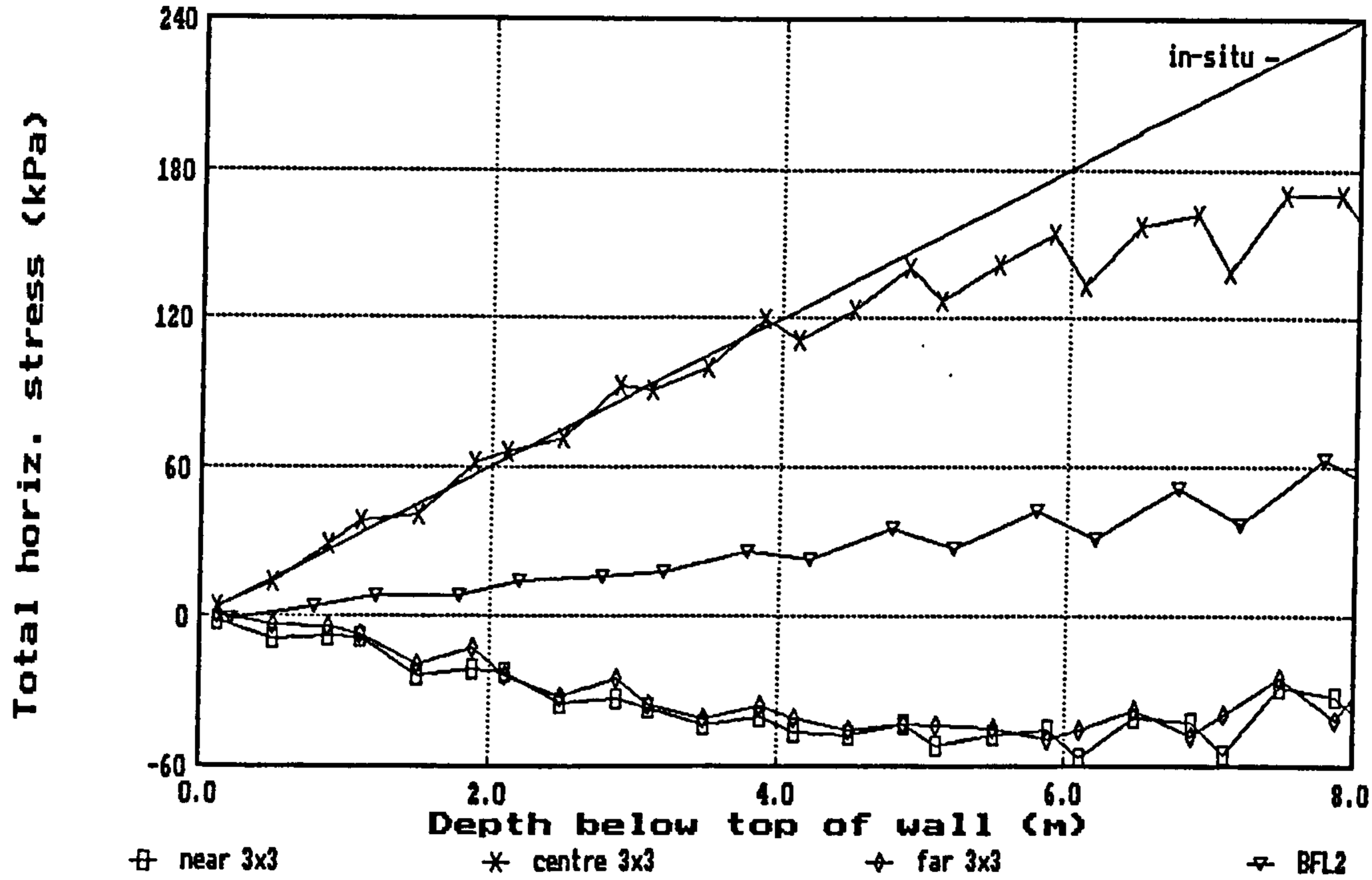

(a) Case RW103 - raw 3×3 stresses on near, centre and far sections raw 3×3 stresses compared with smoothed (BFL2) distribution

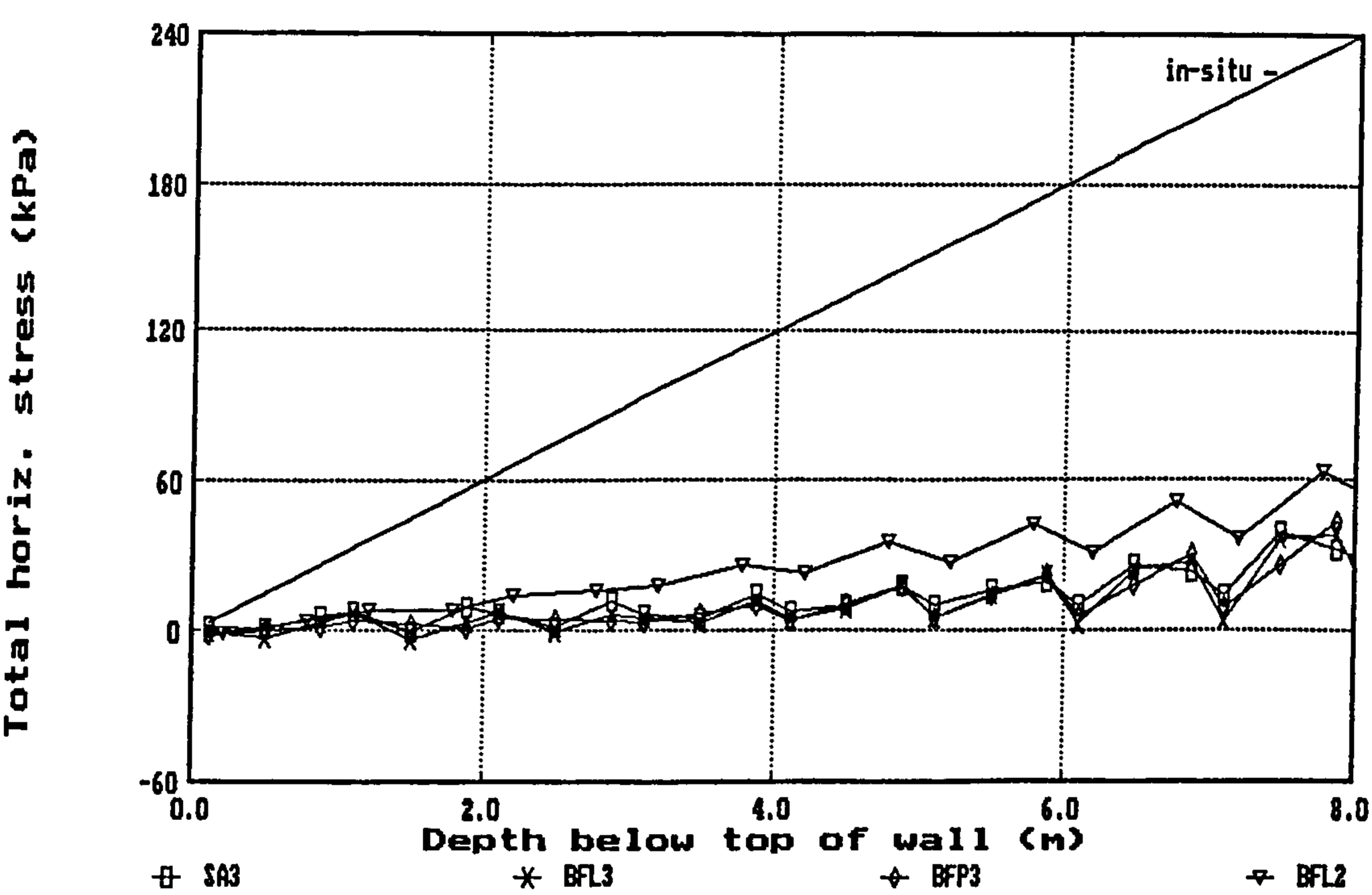

(b) Case RW103 - comparison of local smoothing methods

Fig 8.16 Total horizontal stress distributions on the retained side of an embedded wall - undrained elastic-perfectly plastic (Tresca) analysis

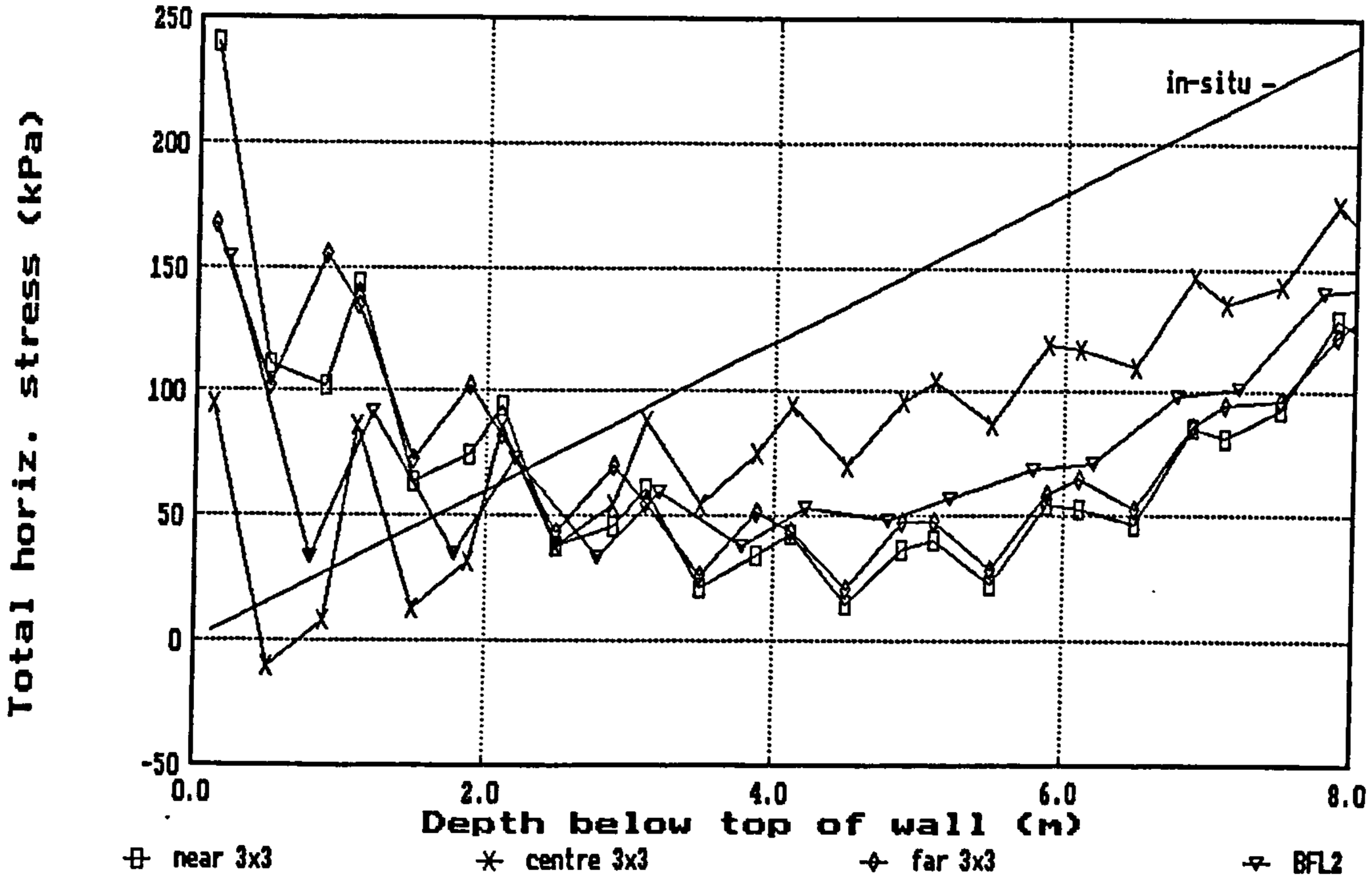

(c) Case RW112 - raw 3×3 stresses on near, centre and far sections compared with smoothed (BFL2) distribution

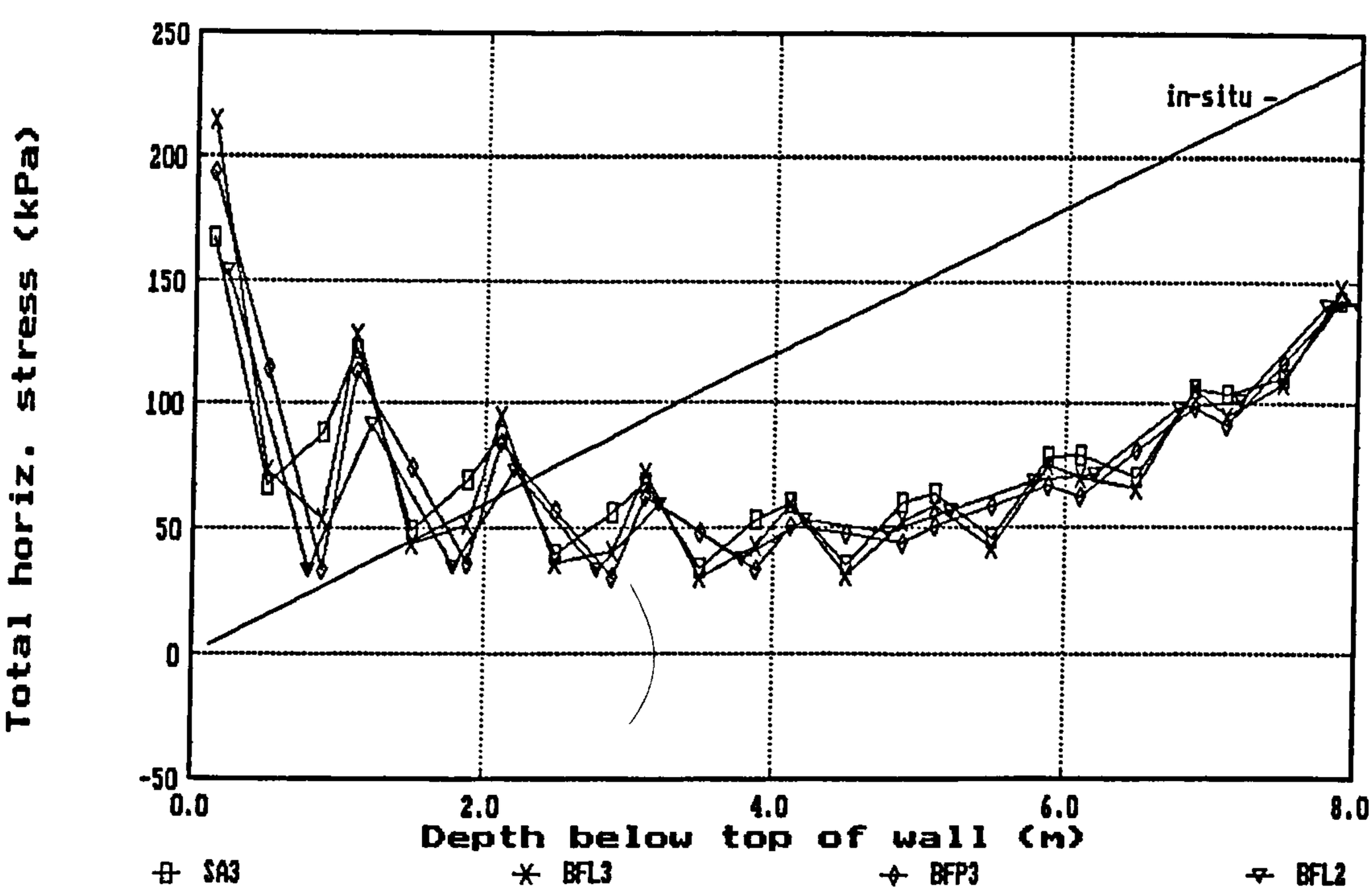

(d) Case RW112 - comparison of local smoothing methods

Fig 8.16 Total horizontal stress distributions on the retained side of an embedded wall - undrained elastic-perfectly plastic (Tresca) analysis (contd)

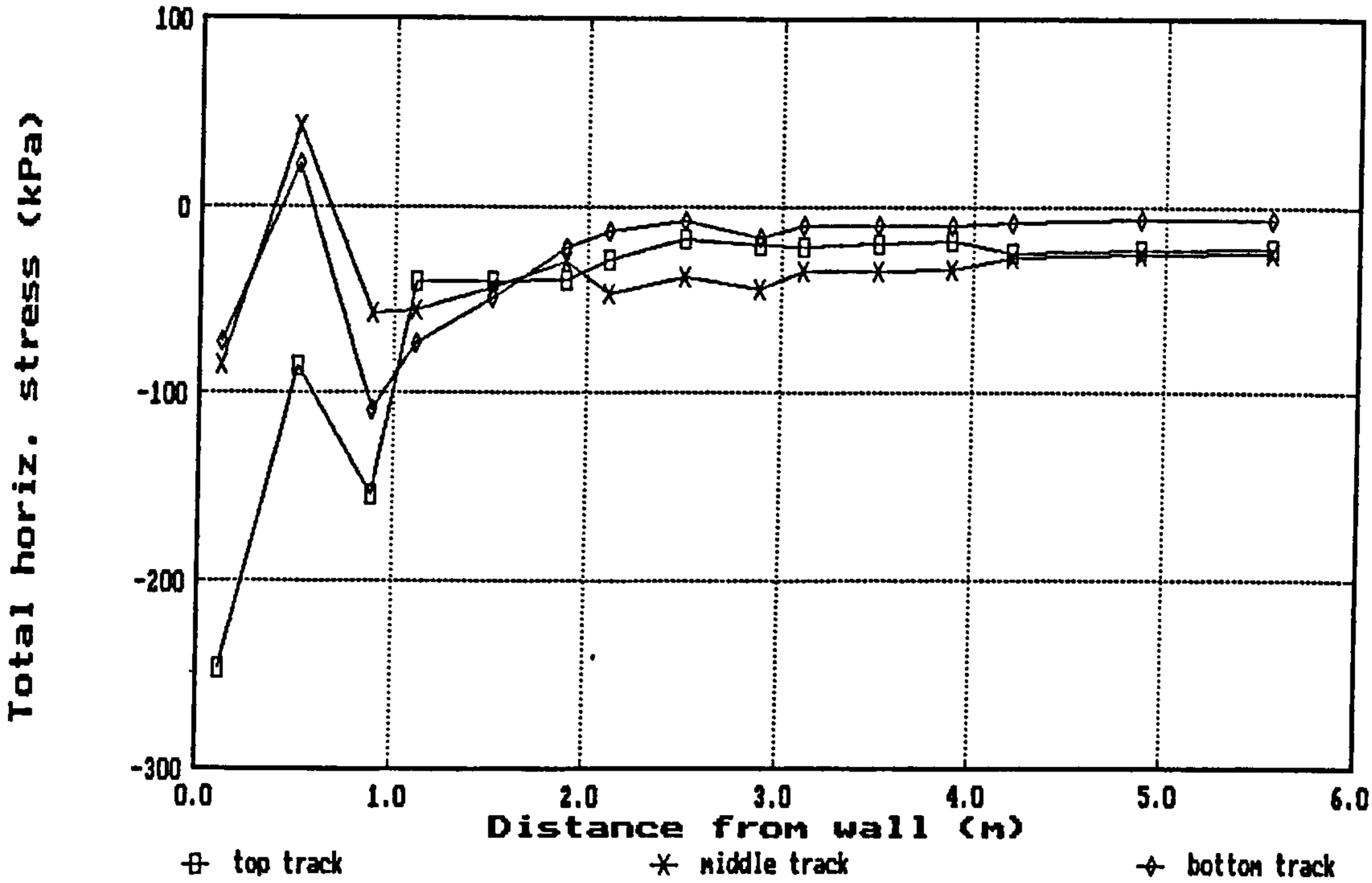

(a) Lateral variation of raw 3×3 stresses along horizontal "tracks" of Gauss points in row A (i.e. first row of elements below ground level)

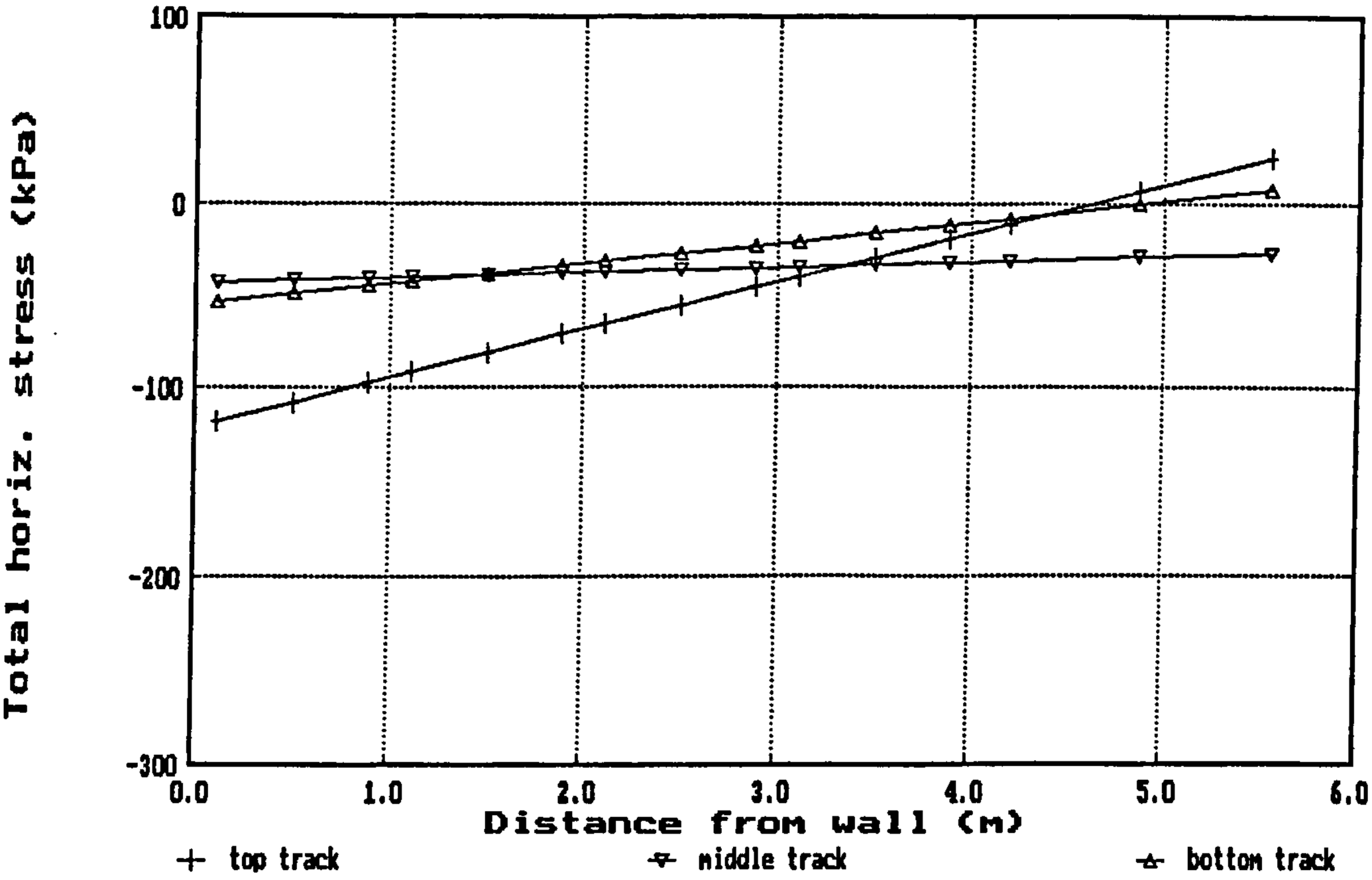

(b) best-fit lines to raw 3×3 stresses along horizontal "tracks" in row A

Fig 8.17 Total horizontal stresses on the retained side of an embedded wall - superlocal smoothing method -undrained elastic analysis - case RW1

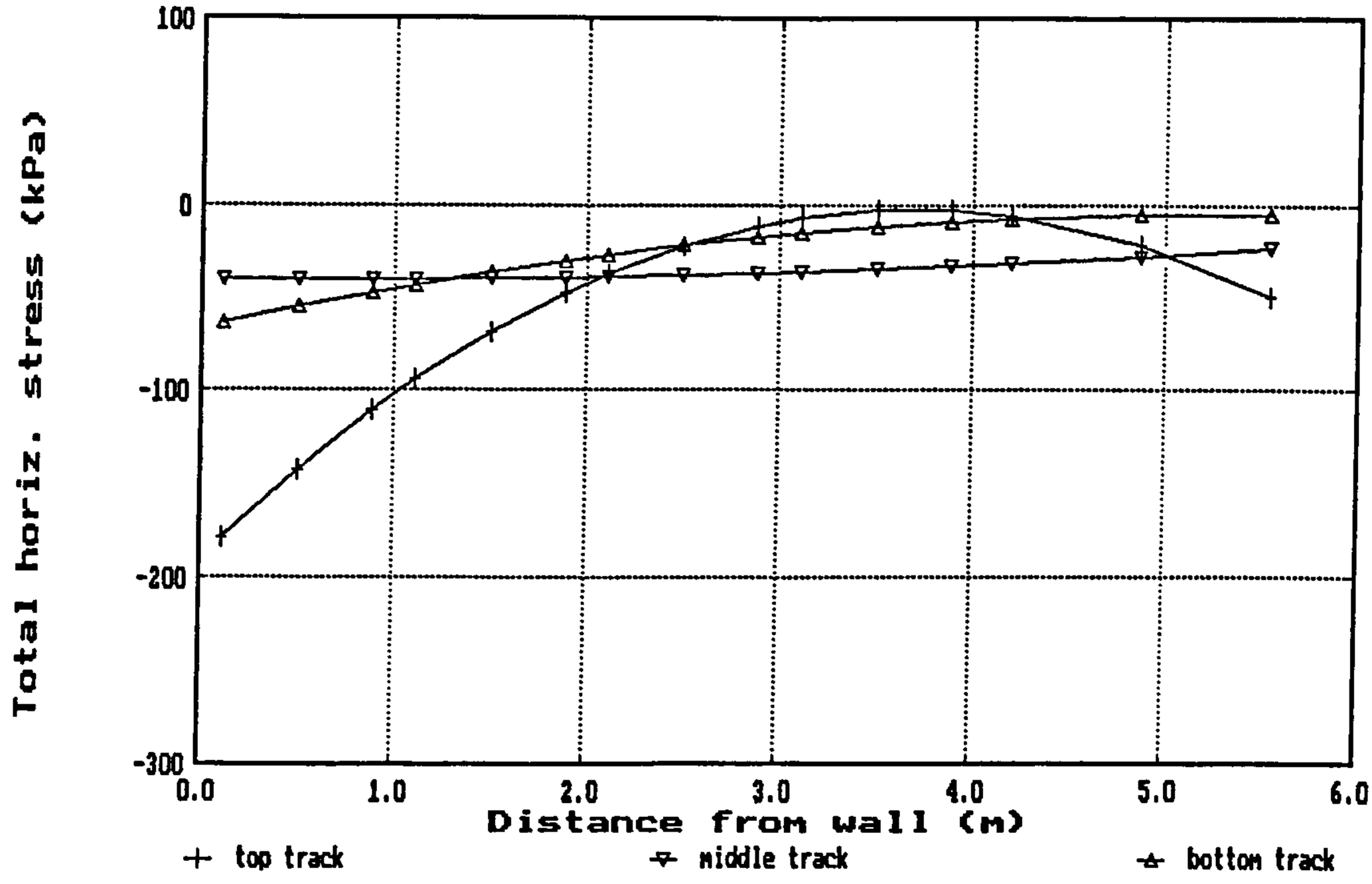

(c) best-fit curves to raw 3×3 stresses along horizontal "tracks" in row A

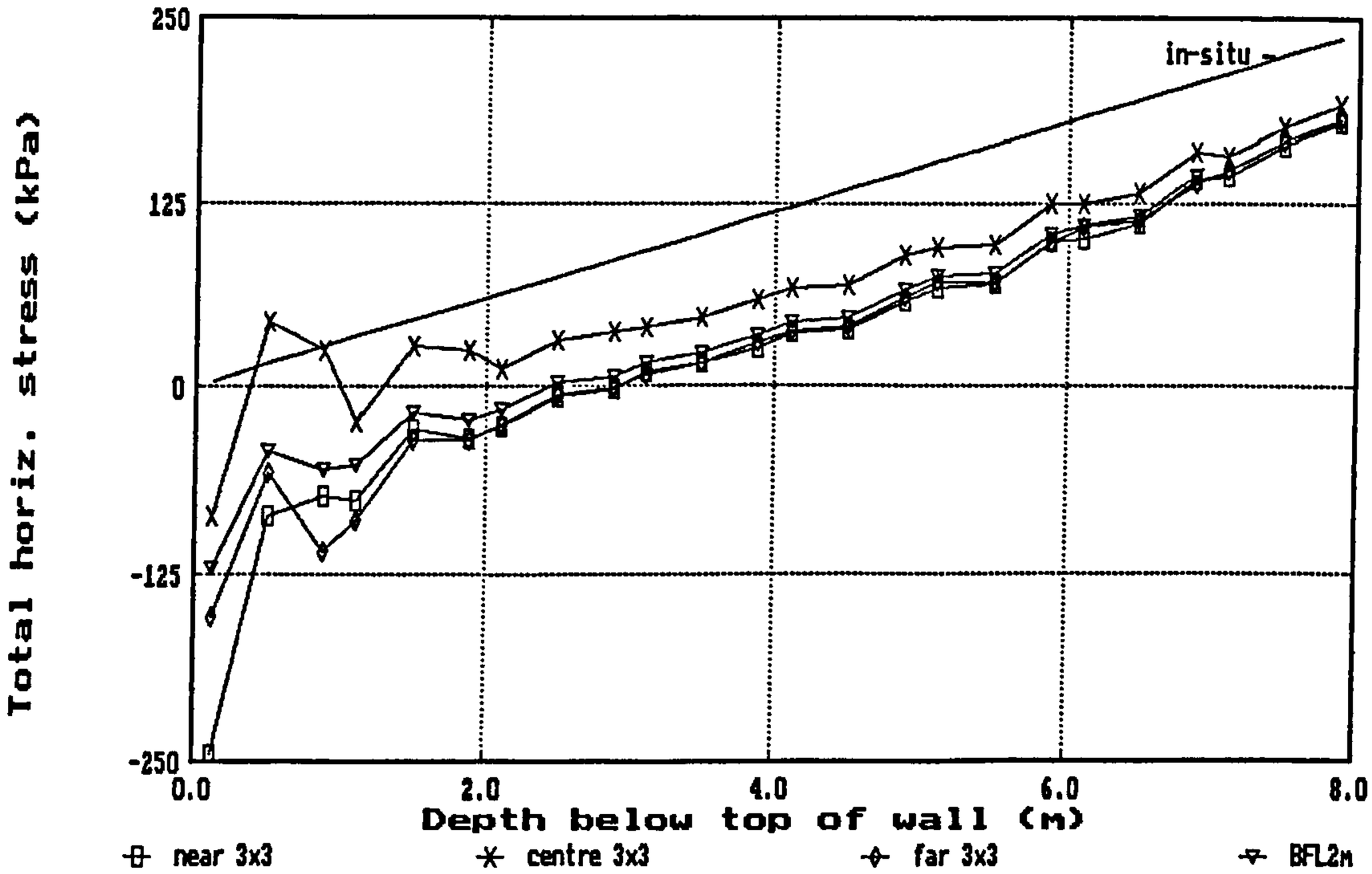

(d) Comparison of horizontal stress profiles - raw 3×3 stresses and BFL2m

Fig 8.17 Total horizontal stresses on retained side of an embedded wall - superlocal smoothing method - undrained elastic analysis - case RW1 (contd)

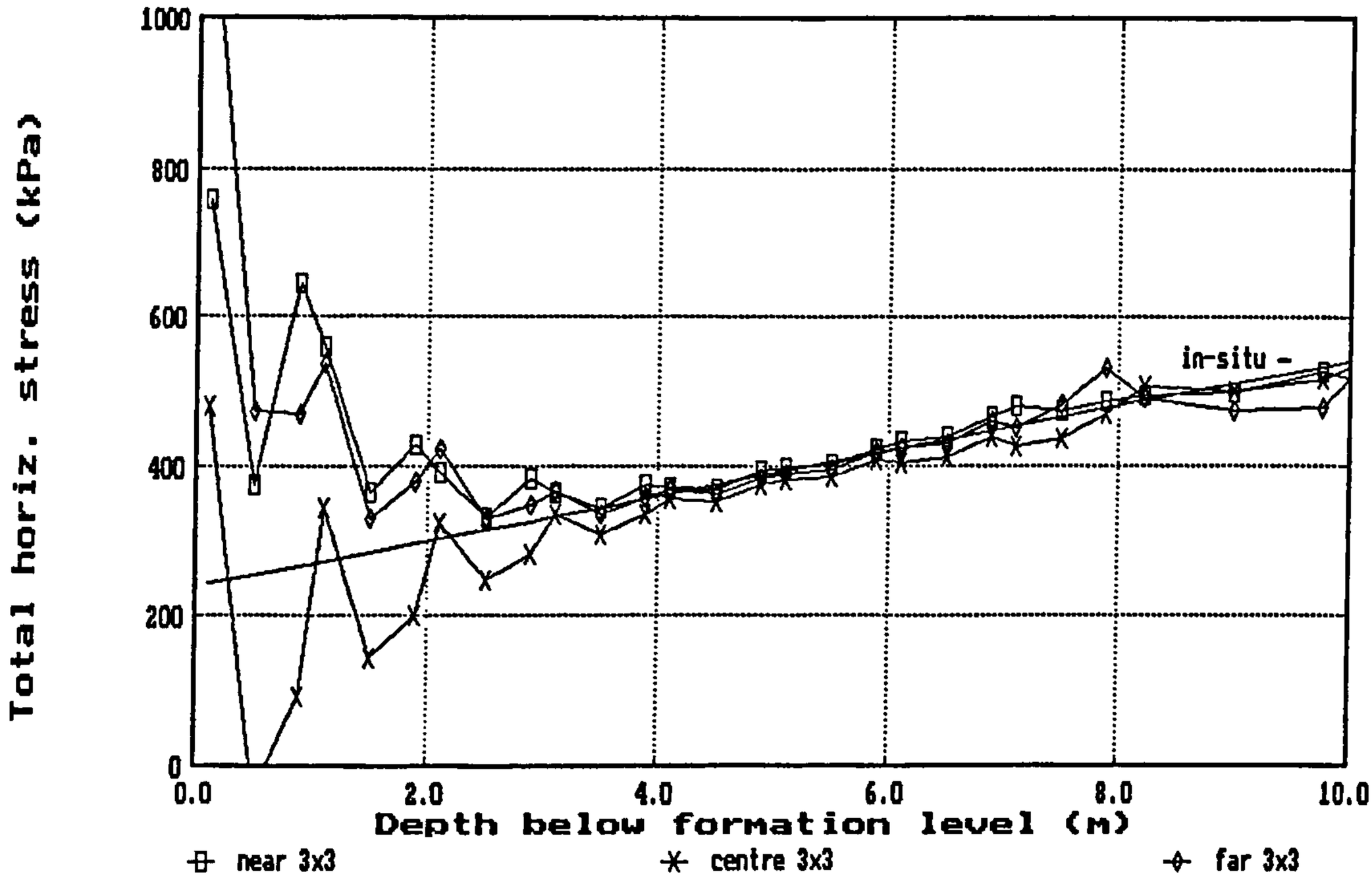

(a) raw 3×3 stresses on near, centre and far Gauss point sections

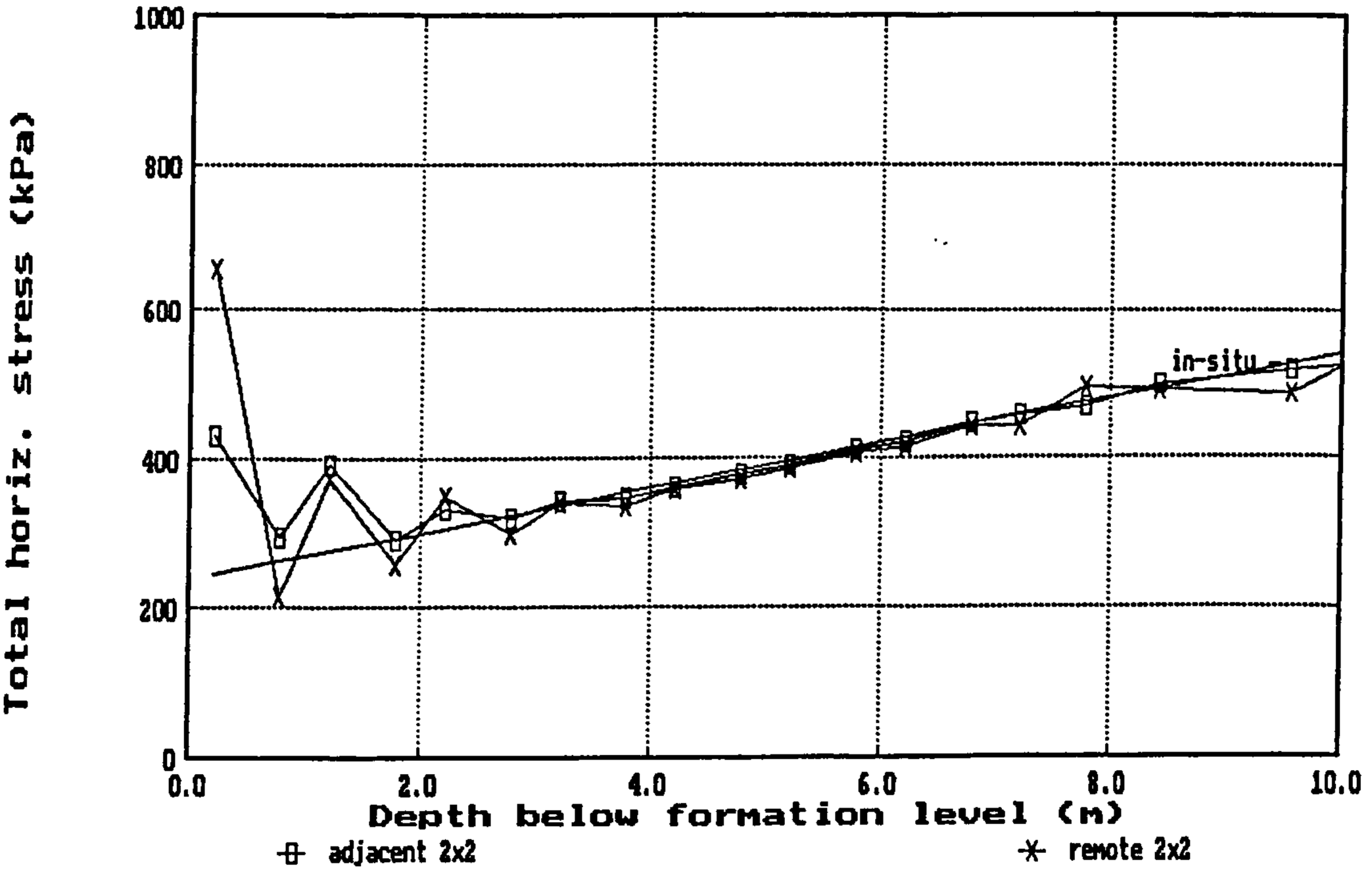

(b) interpolated 2×2 stresses on adjacent and remote sections

Fig 8.18 Total horizontal stress distributions on the excavated side of an embedded wall - undrained elastic analysis - case RW1

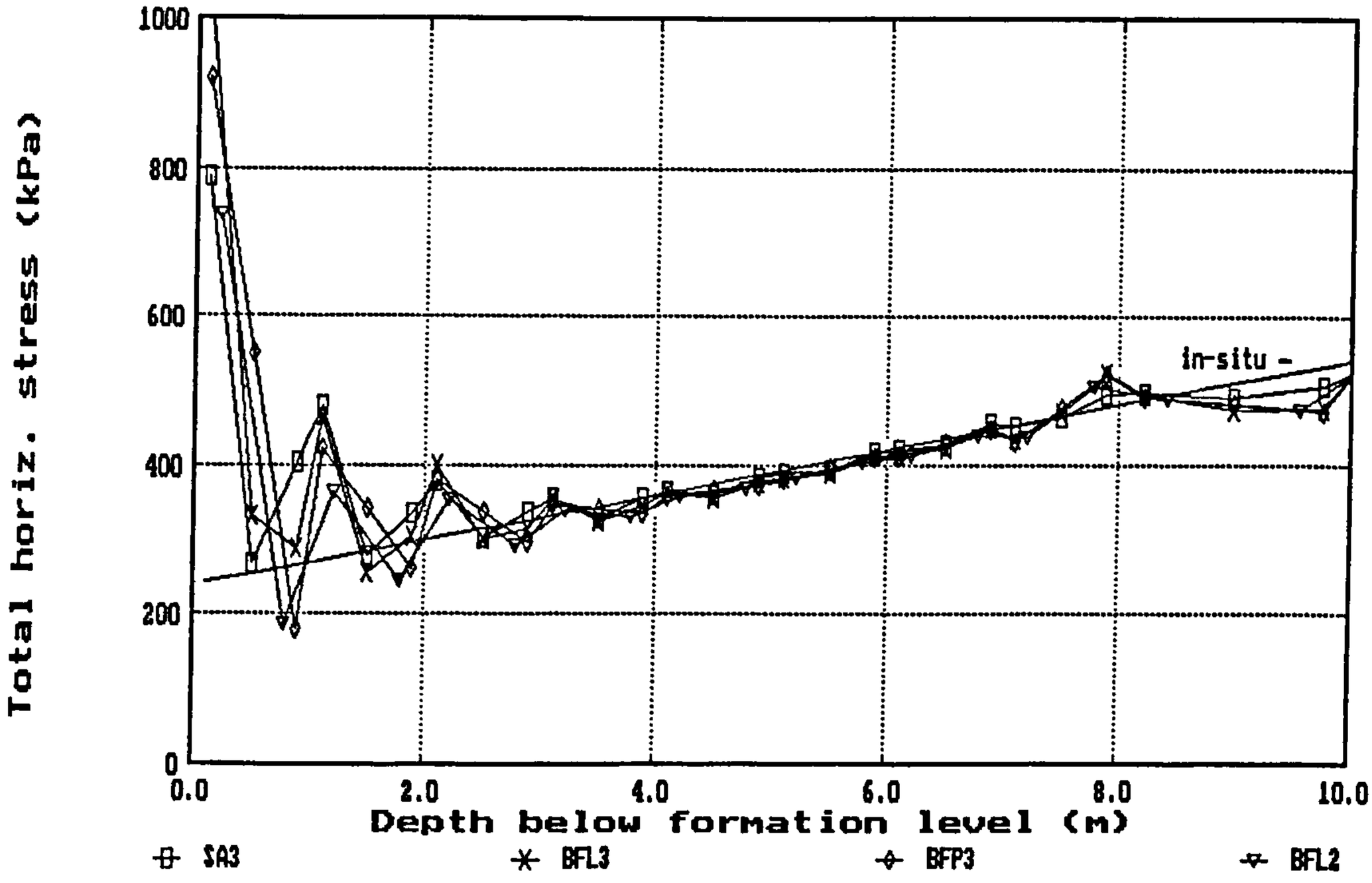

(c) comparison of local smoothing methods

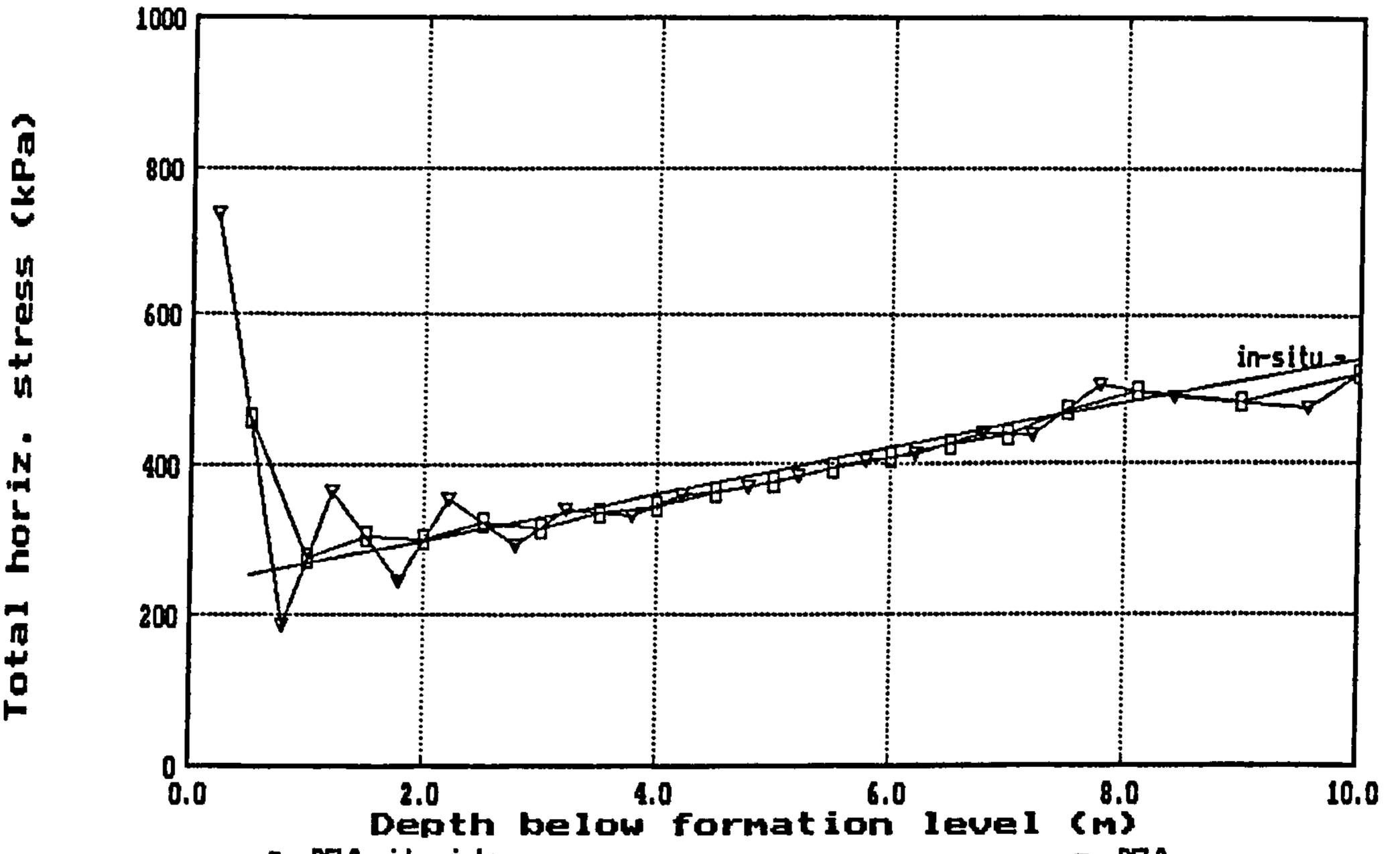

(d) interpolated 2×2 - best-fit line and simple joining up of mid-points

Fig 8.18 Total horizontal stress distributions on the excavated side of an embedded wall - undrained elastic analysis - case RW1 (contd)

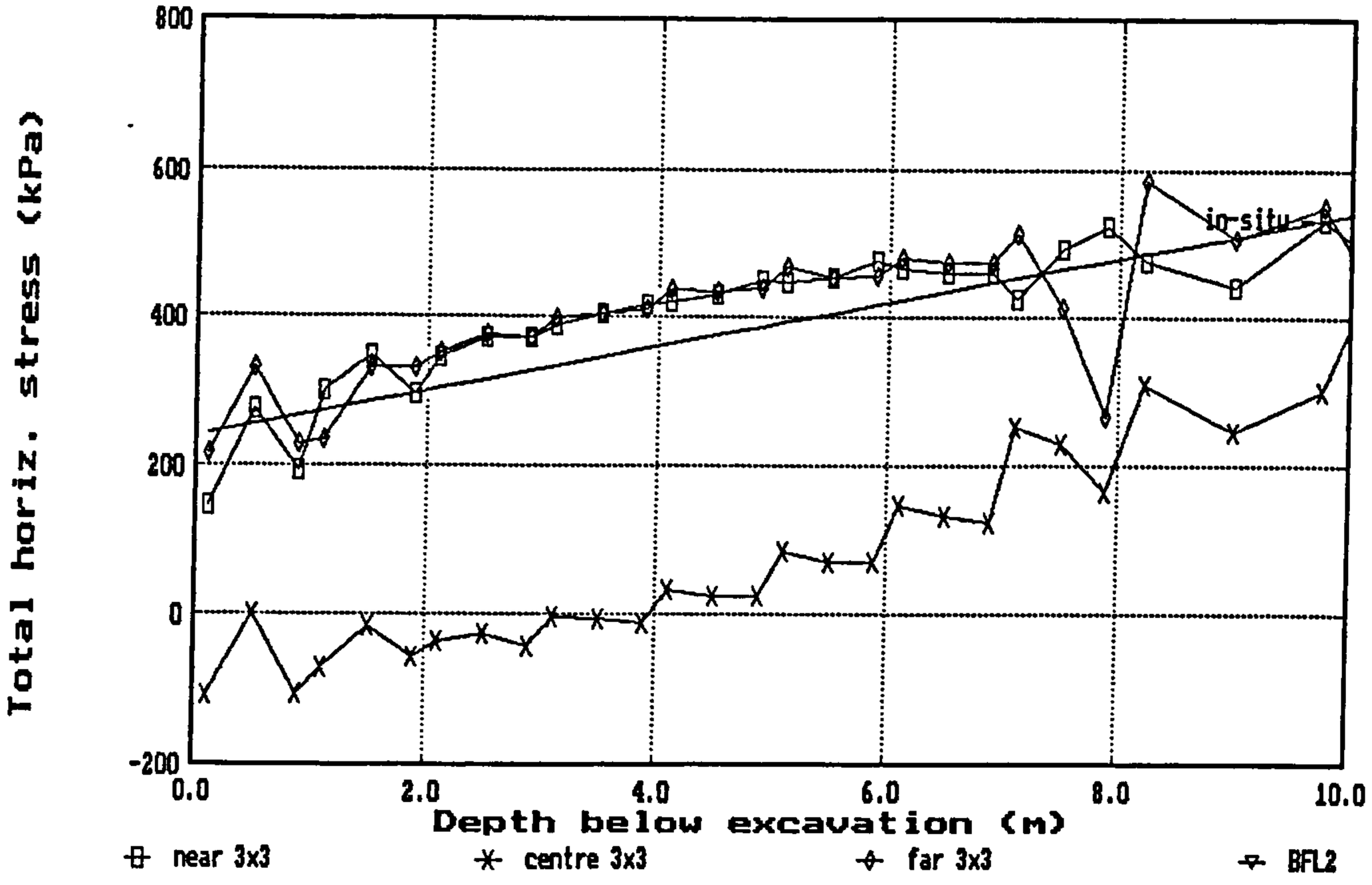

(a) raw 3×3 stresses on near, centre and far Gauss point sections

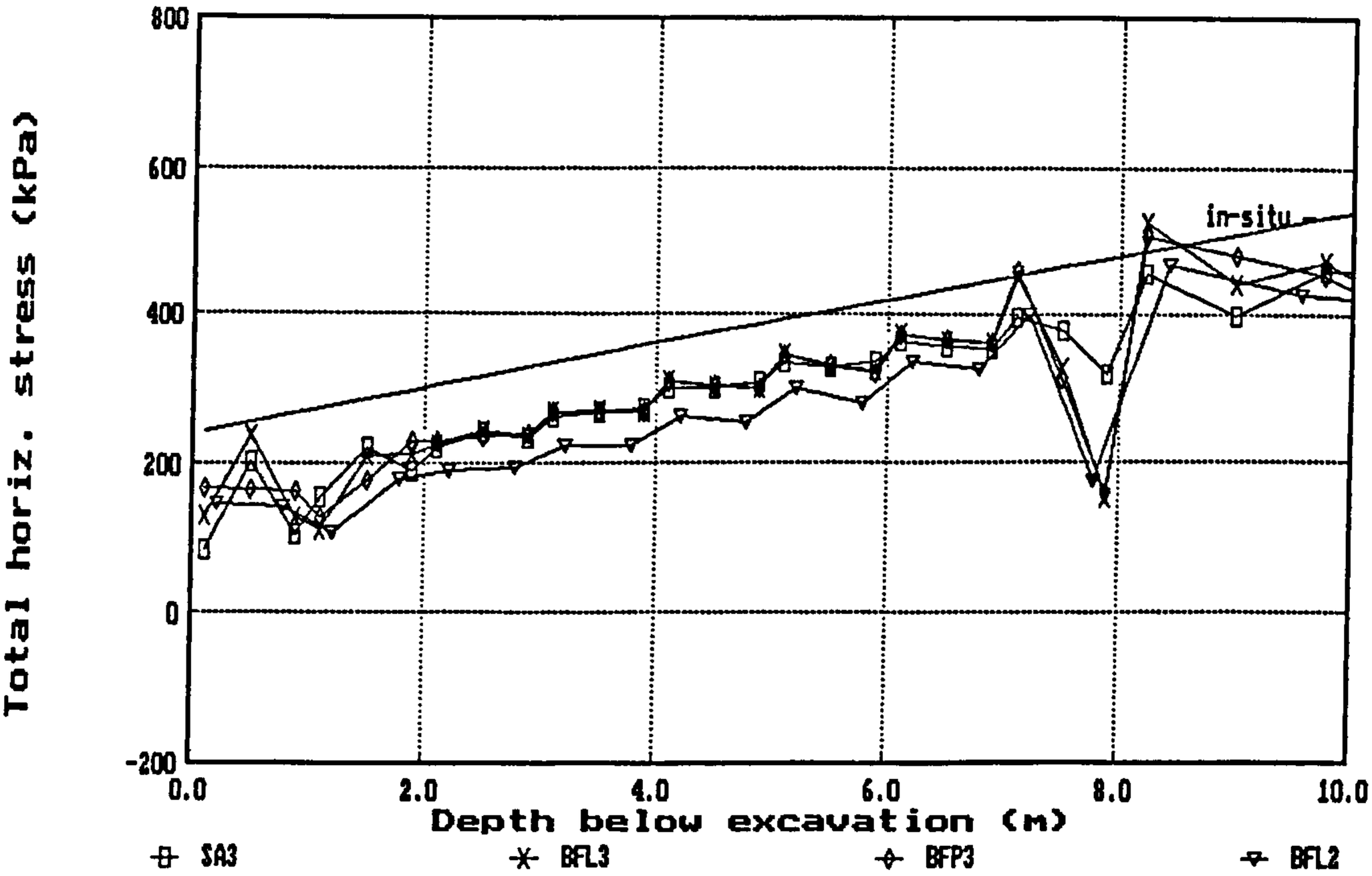

(b) comparison of local smoothing methods

Fig 8.19 Total horizontal stress distributions on the excavated side of an embedded wall - elasto-plastic analysis - case RW113

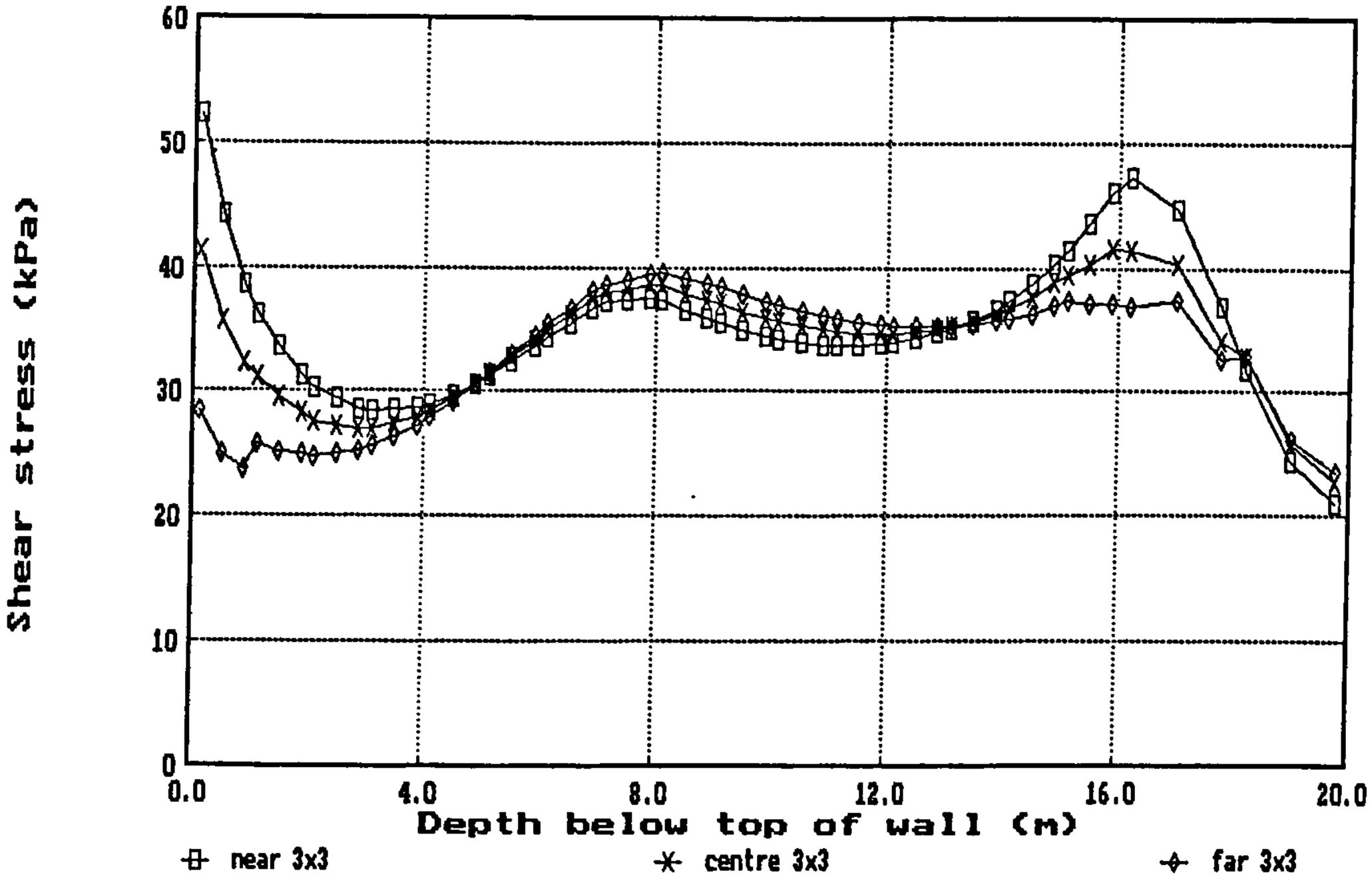

(a) raw 3×3 stresses on near, centre and far Gauss point sections

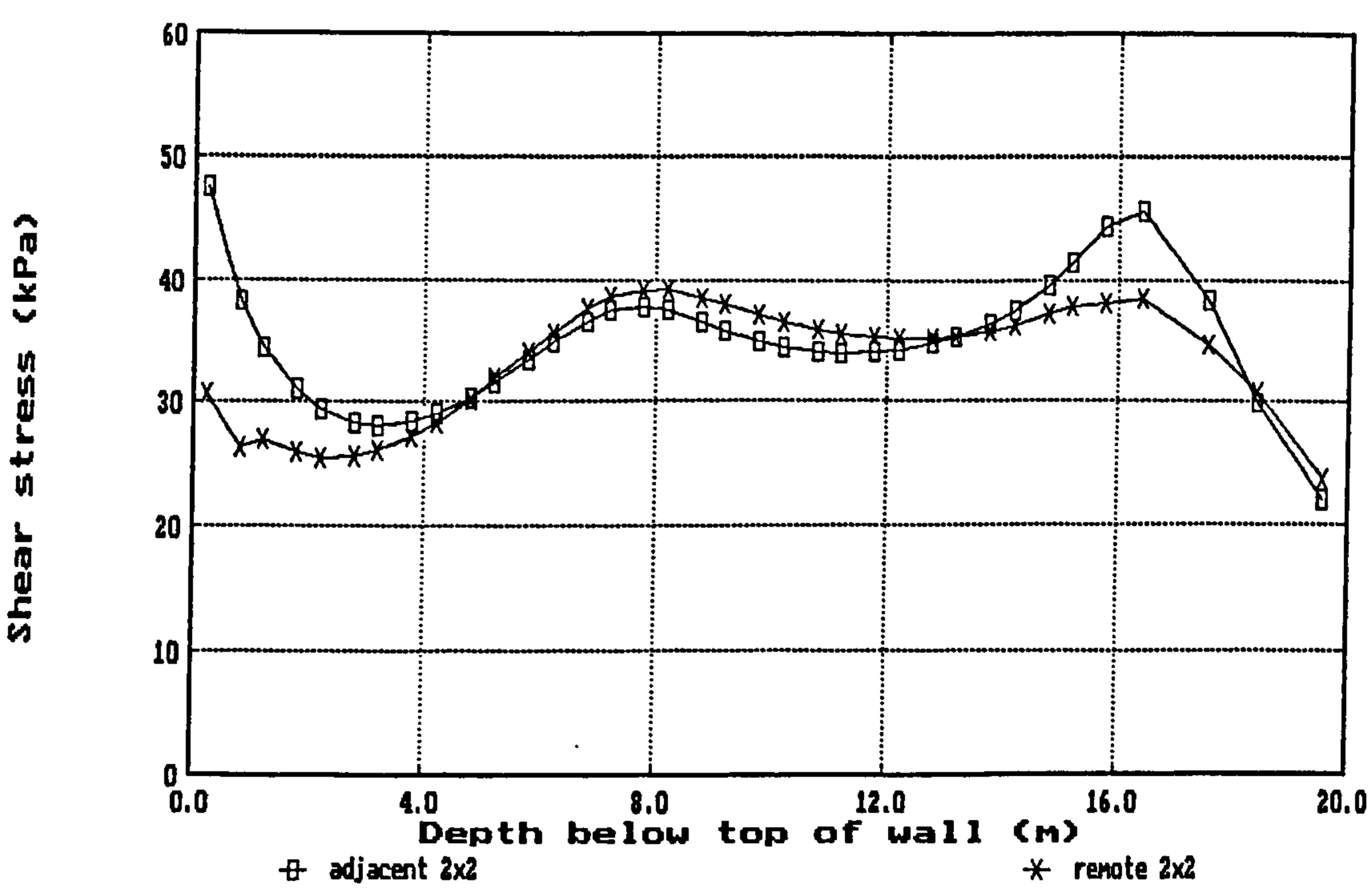

(b) interpolated 2×2 stresses on adjacent and remote sections

Fig 8.20 Soil-wall shear stress distributions on the retained side of an embedded wall - undrained elastic analysis - case RW1

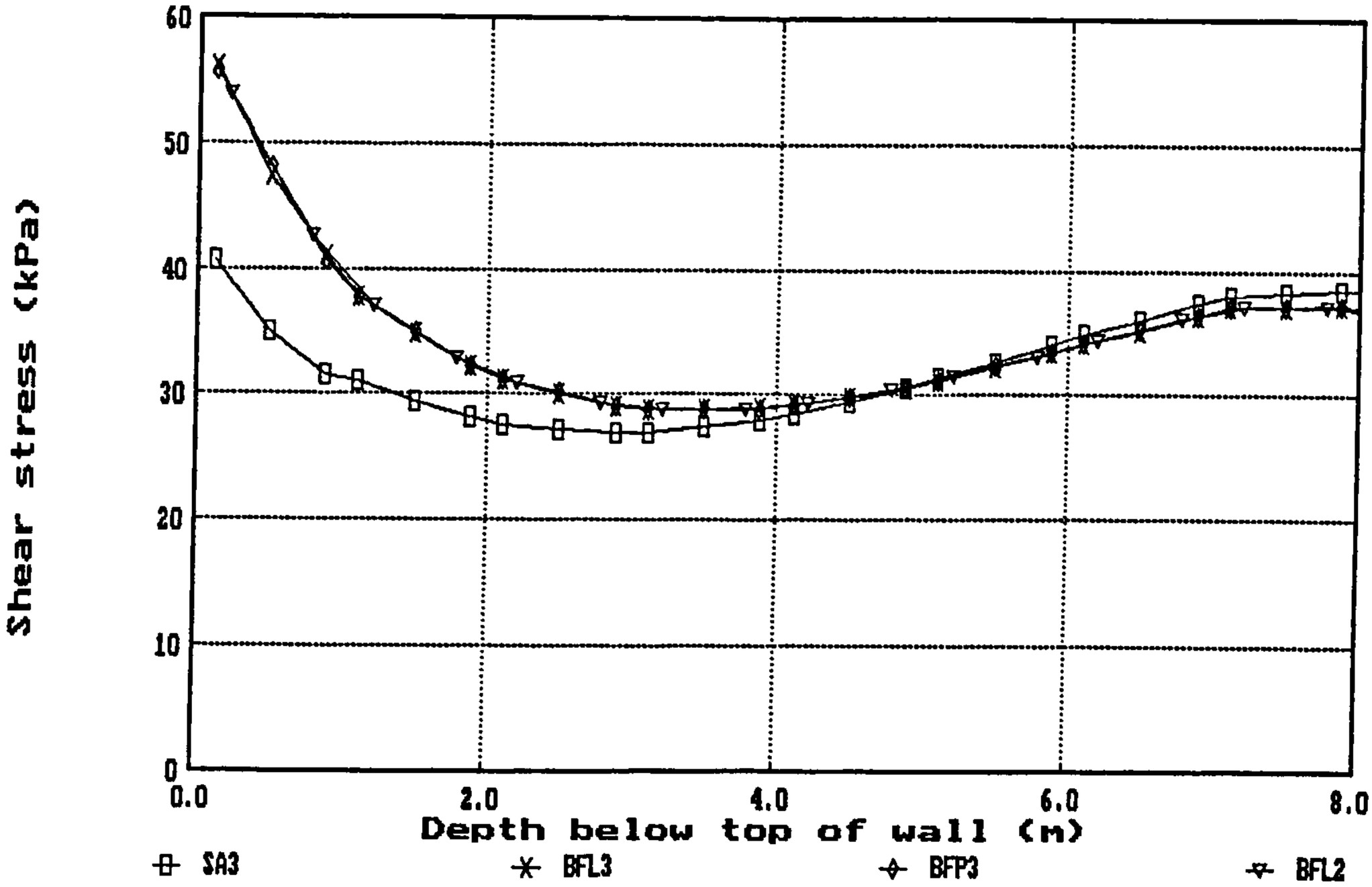

(c) comparison of local smoothing methods

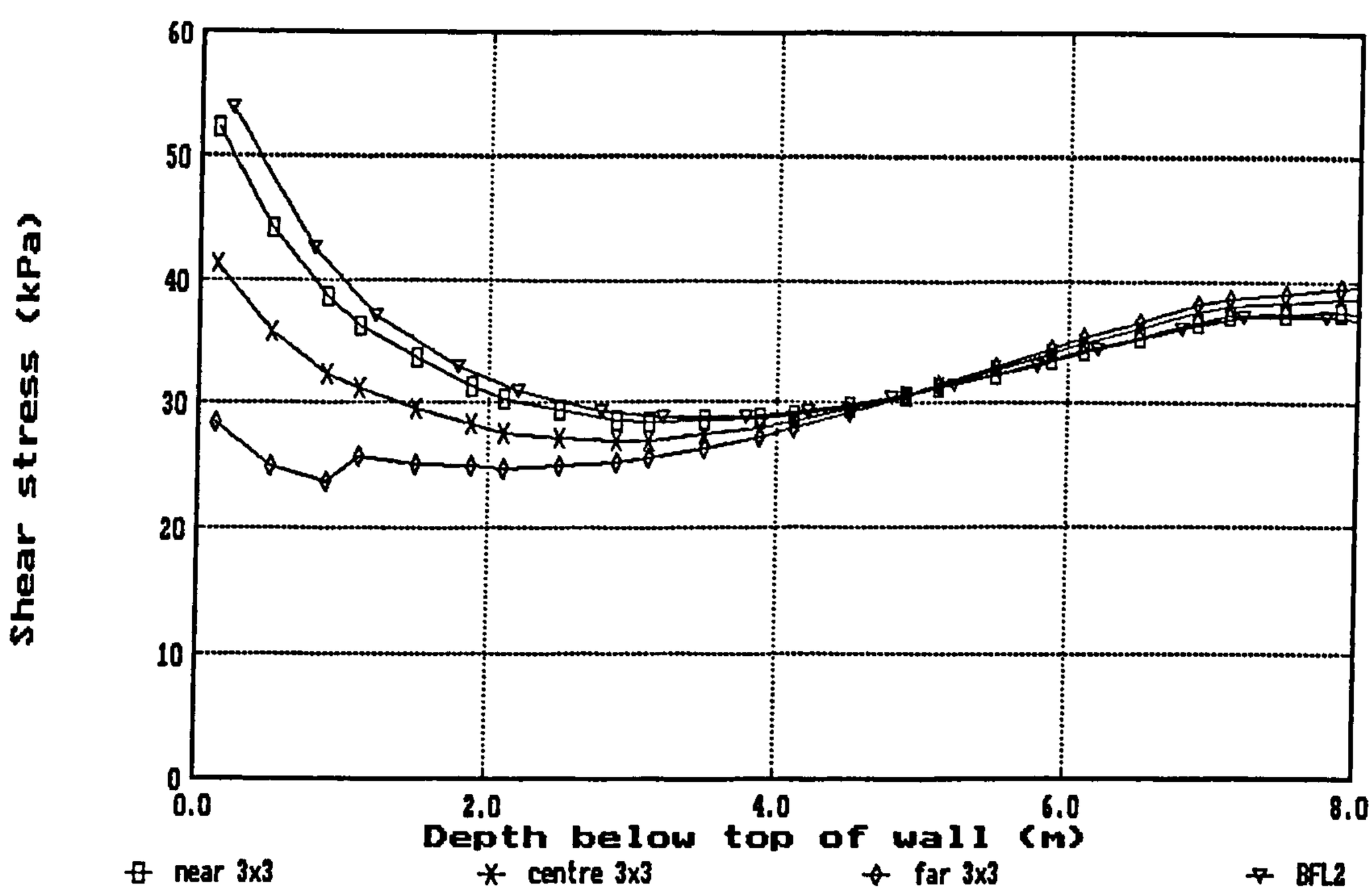

(d) raw 3×3 stresses compared with smoothed (BFL2) distribution

Fig 8.20 Soil-wall shear stress distributions on the retained side of an embedded wall - undrained elastic analysis - case RW1 (contd)

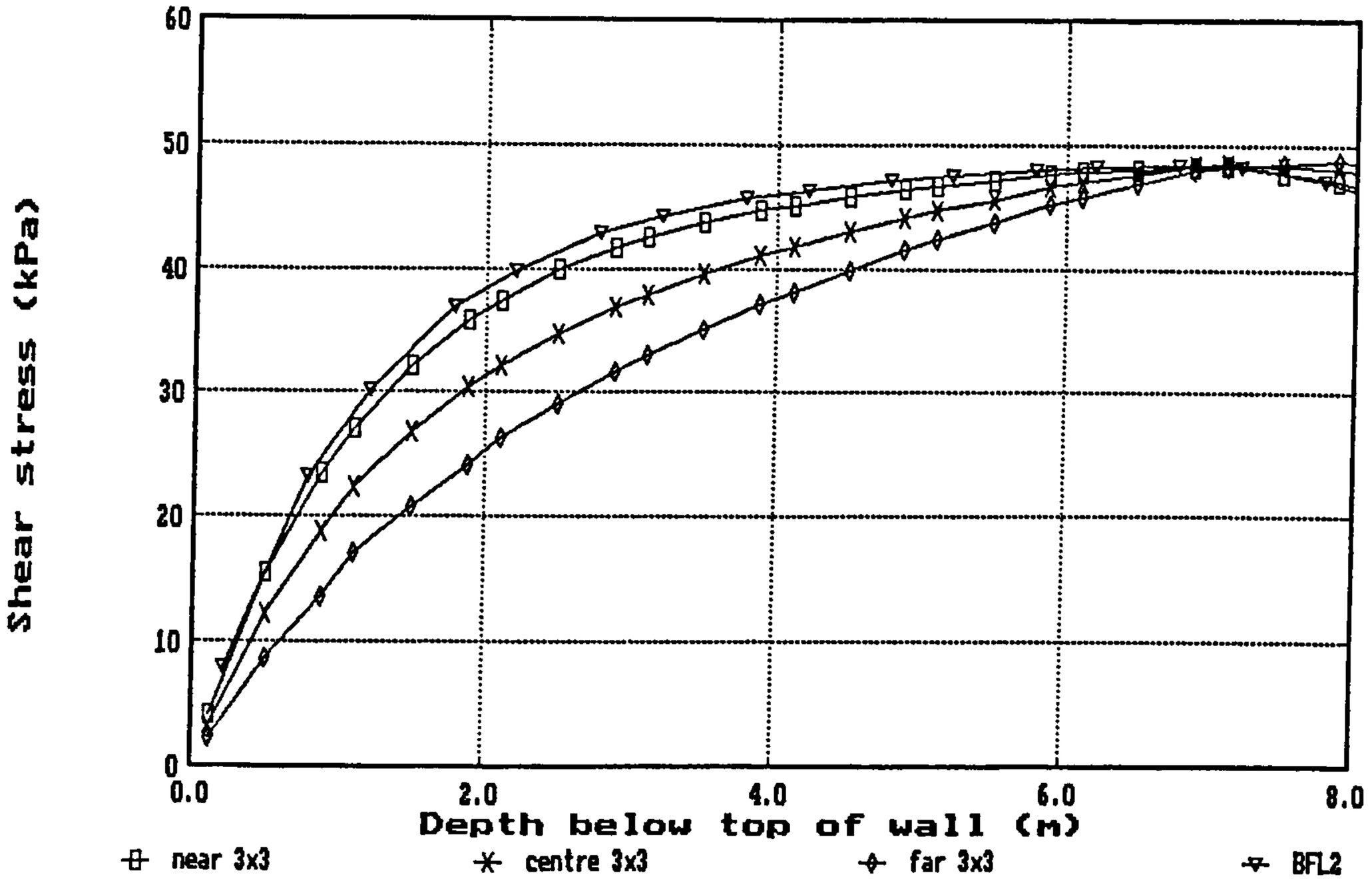

(a) Case RW3 - raw 3×3 stresses compared with smoothed (BFL2) distribution

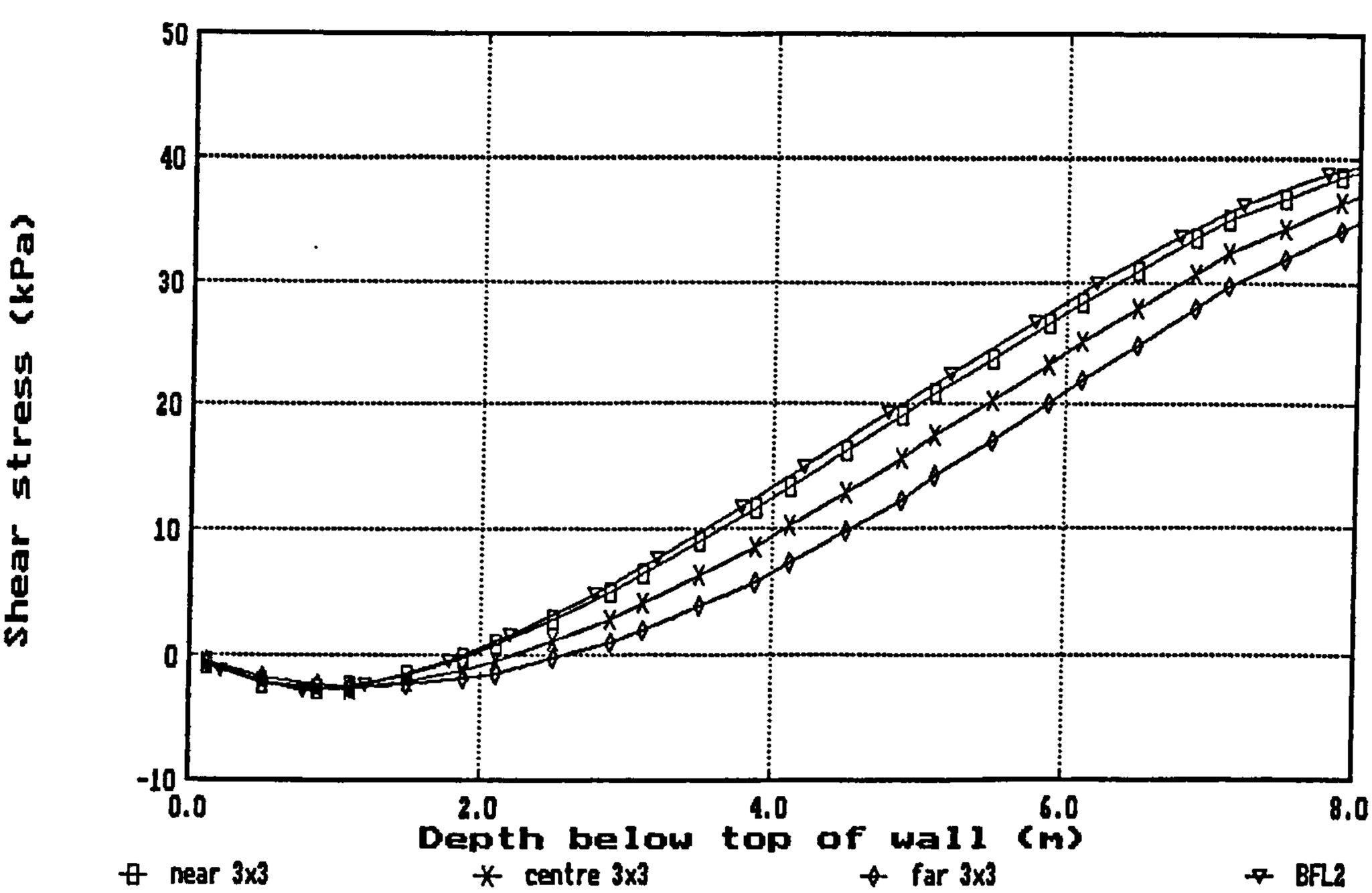

(b) Case RW13 - raw 3×3 stresses compared with smoothed (BFL2) distribution

Fig 8.21 Soil-wall shear stress distributions on the retained side of an embedded wall - undrained elastic analysis

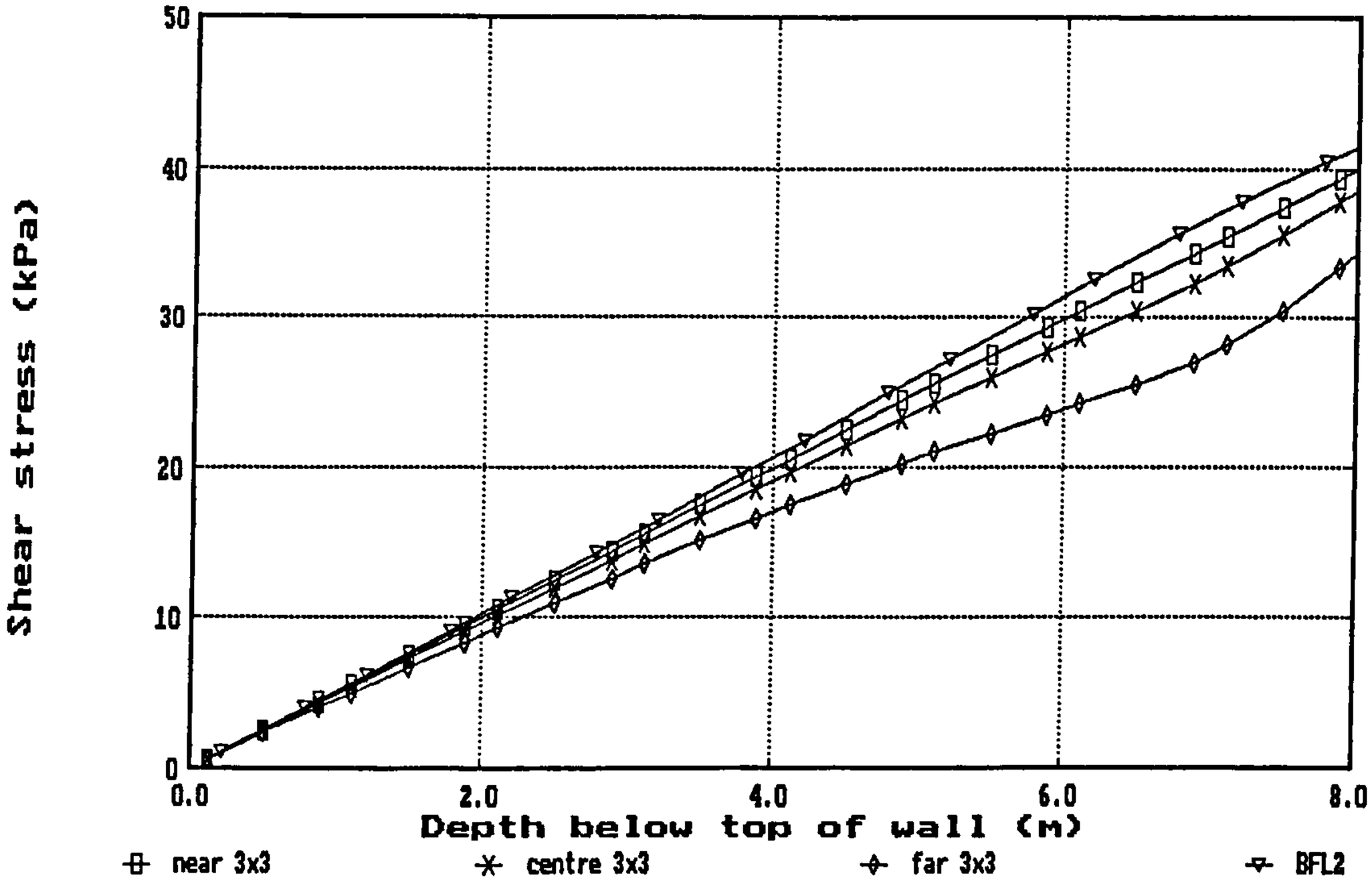

(c) Case RW103 - raw 3×3 stresses compared with smoothed (BFL2) distribution

Fig 8.21 Soil-wall shear stress distributions on the retained side of an embedded wall - undrained elastic analysis (contd)

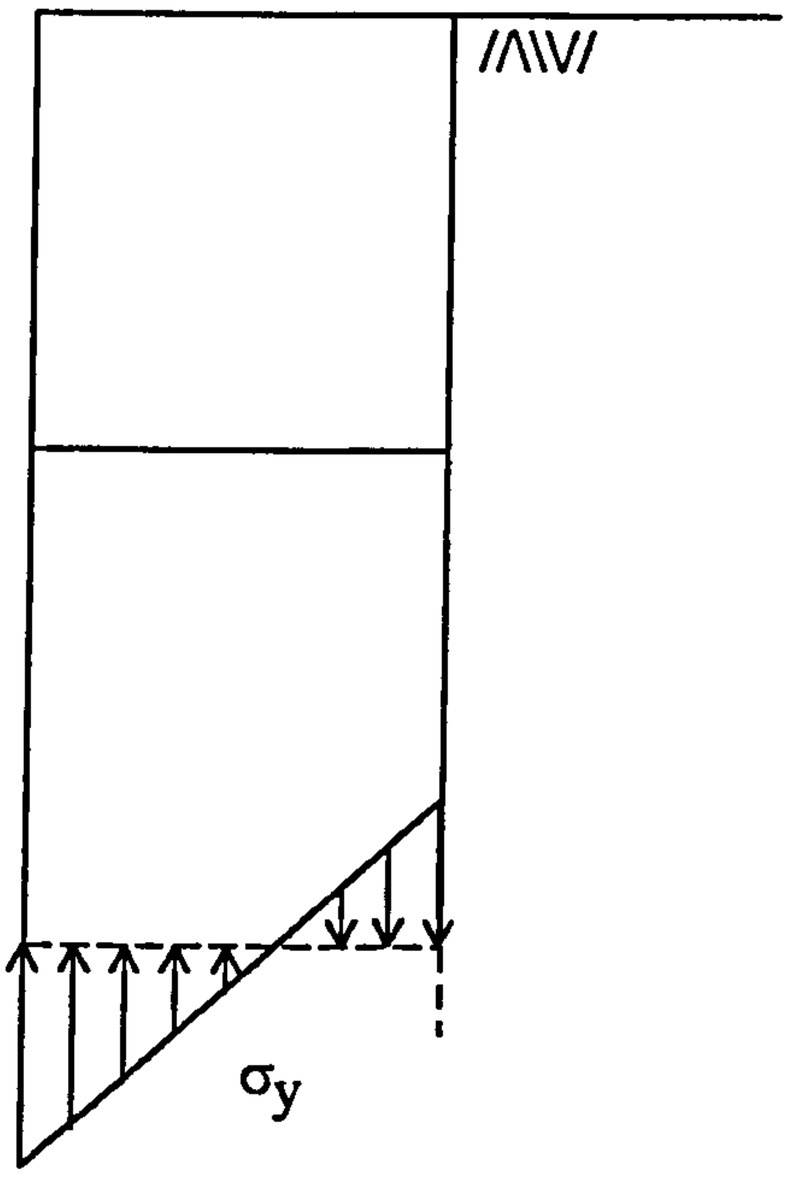

(a) using transverse stresses in wall (WSBM)

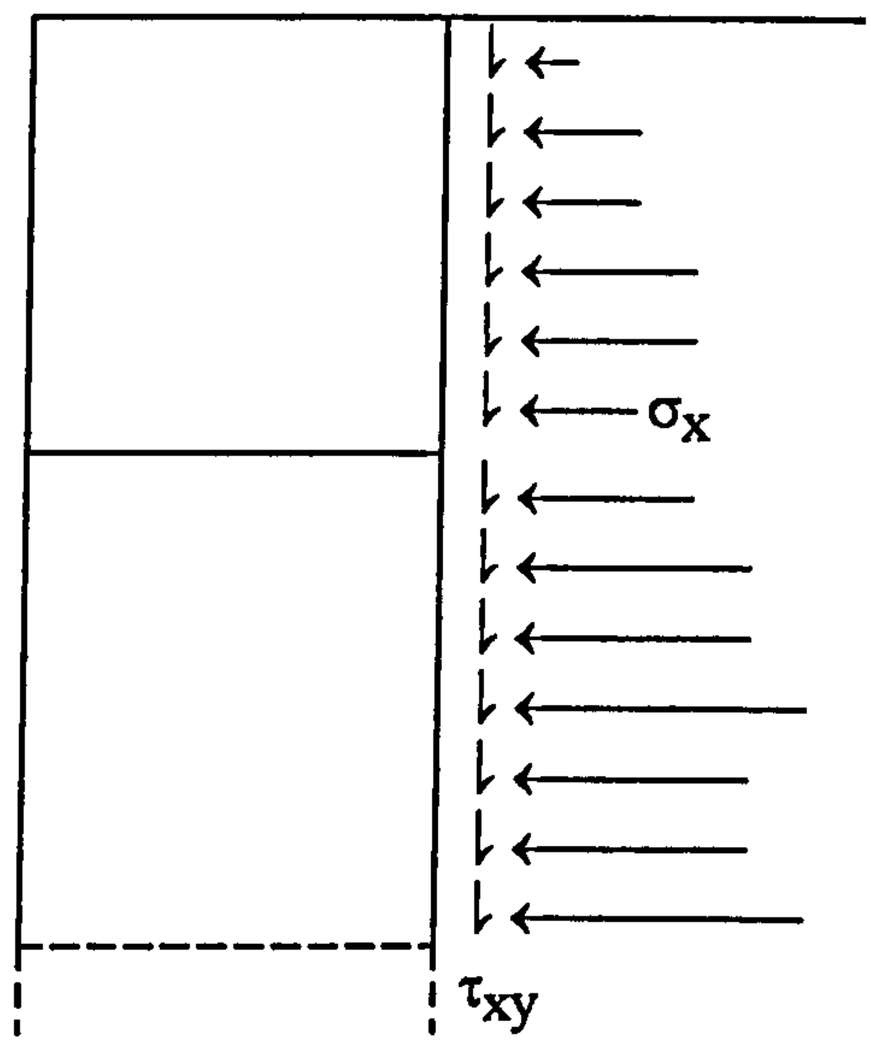

(b) using external earth pressures acting on wall (EPBM)

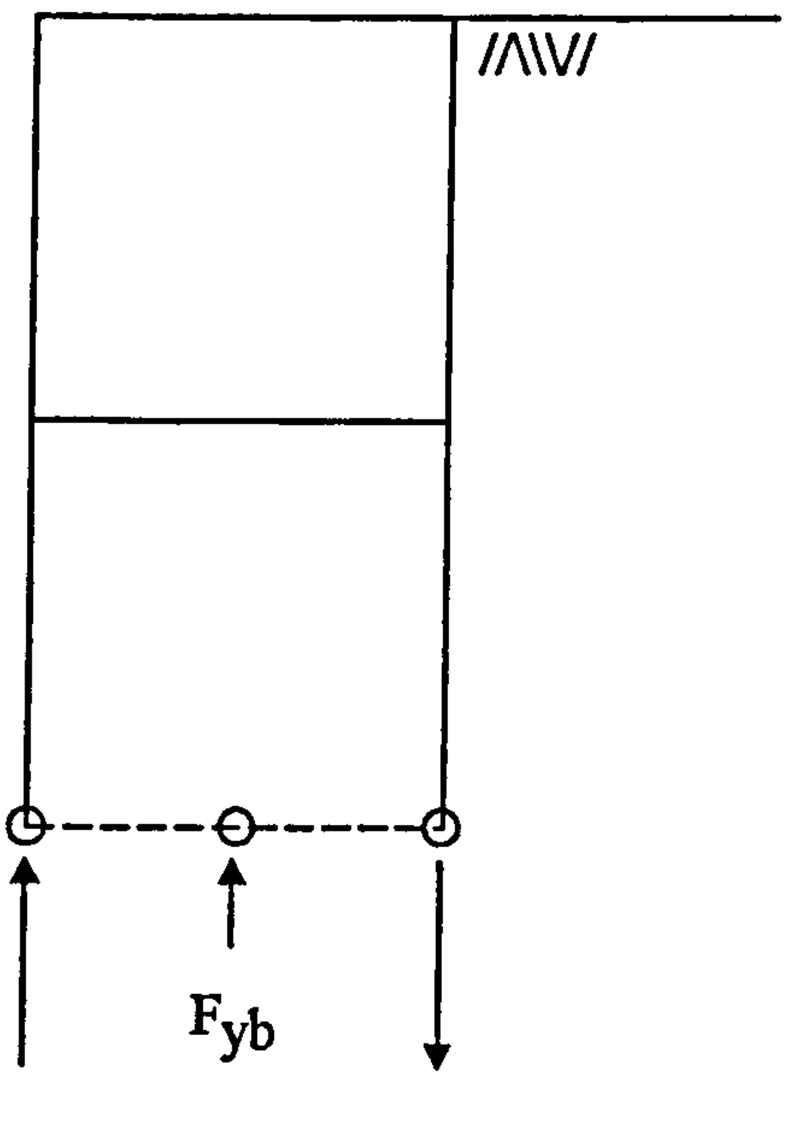

(c) using nodal forces between wall elements

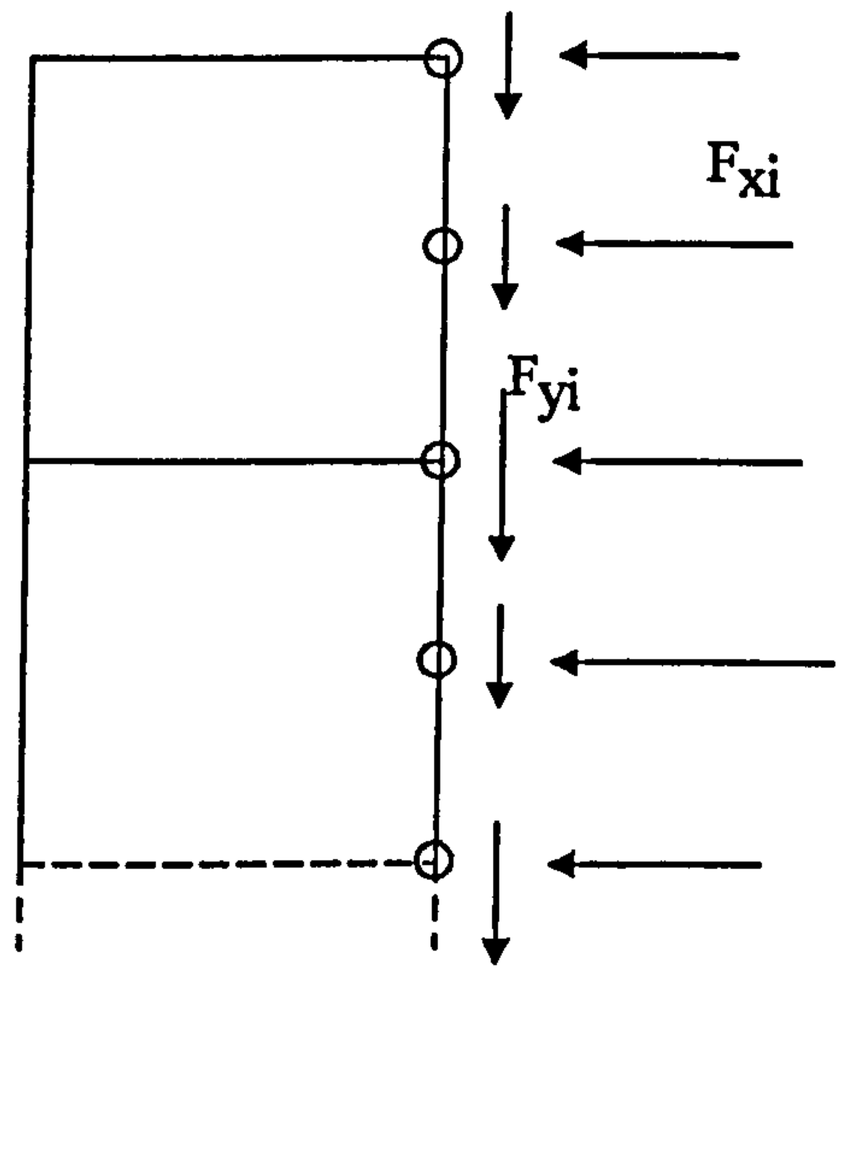

(d) using nodal forces equivalent to external earth pressures

Fig 8.22 Methods of calculating wall bending moments in 2D continuum elements

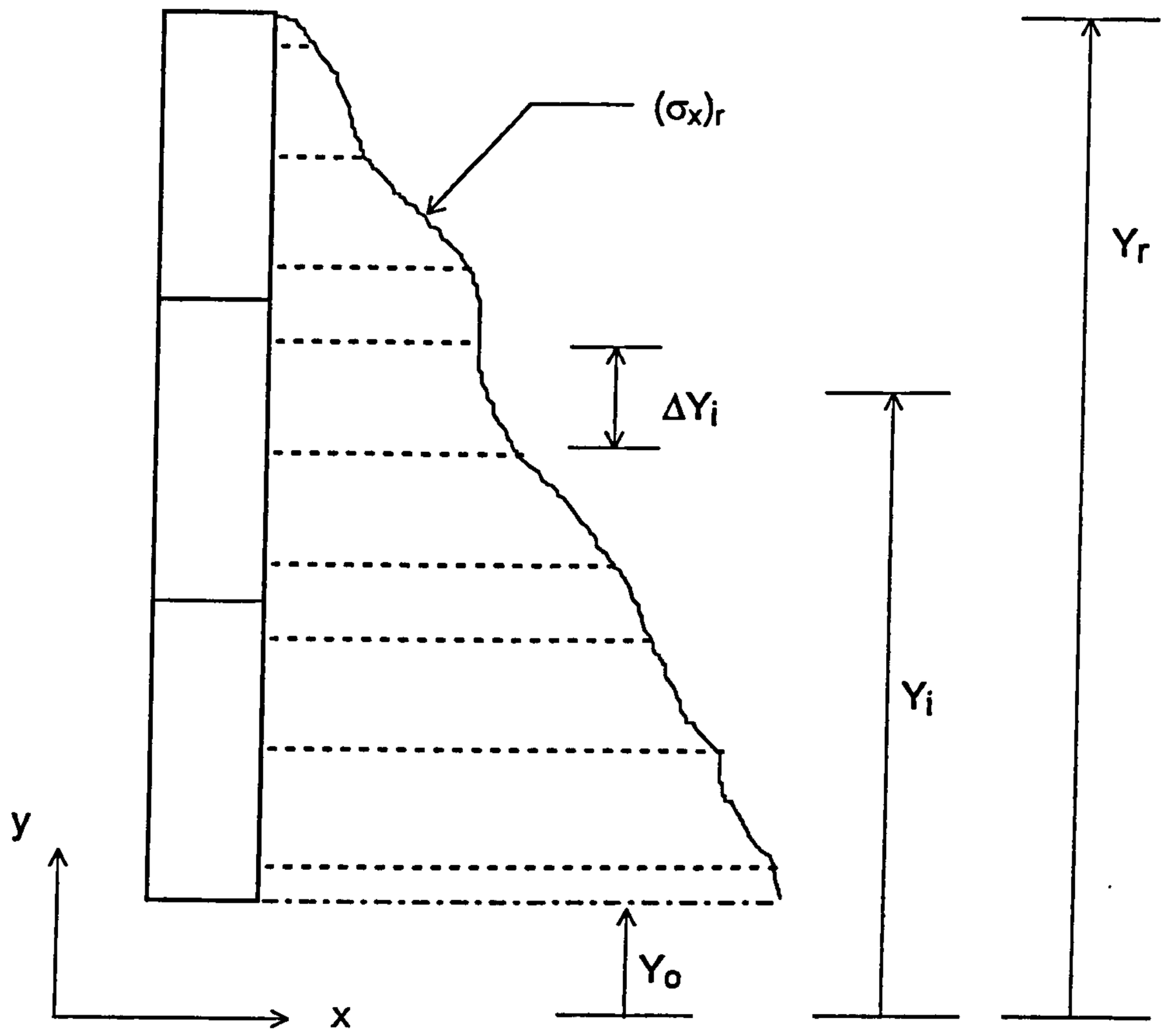

(a) using trapezoidal rule

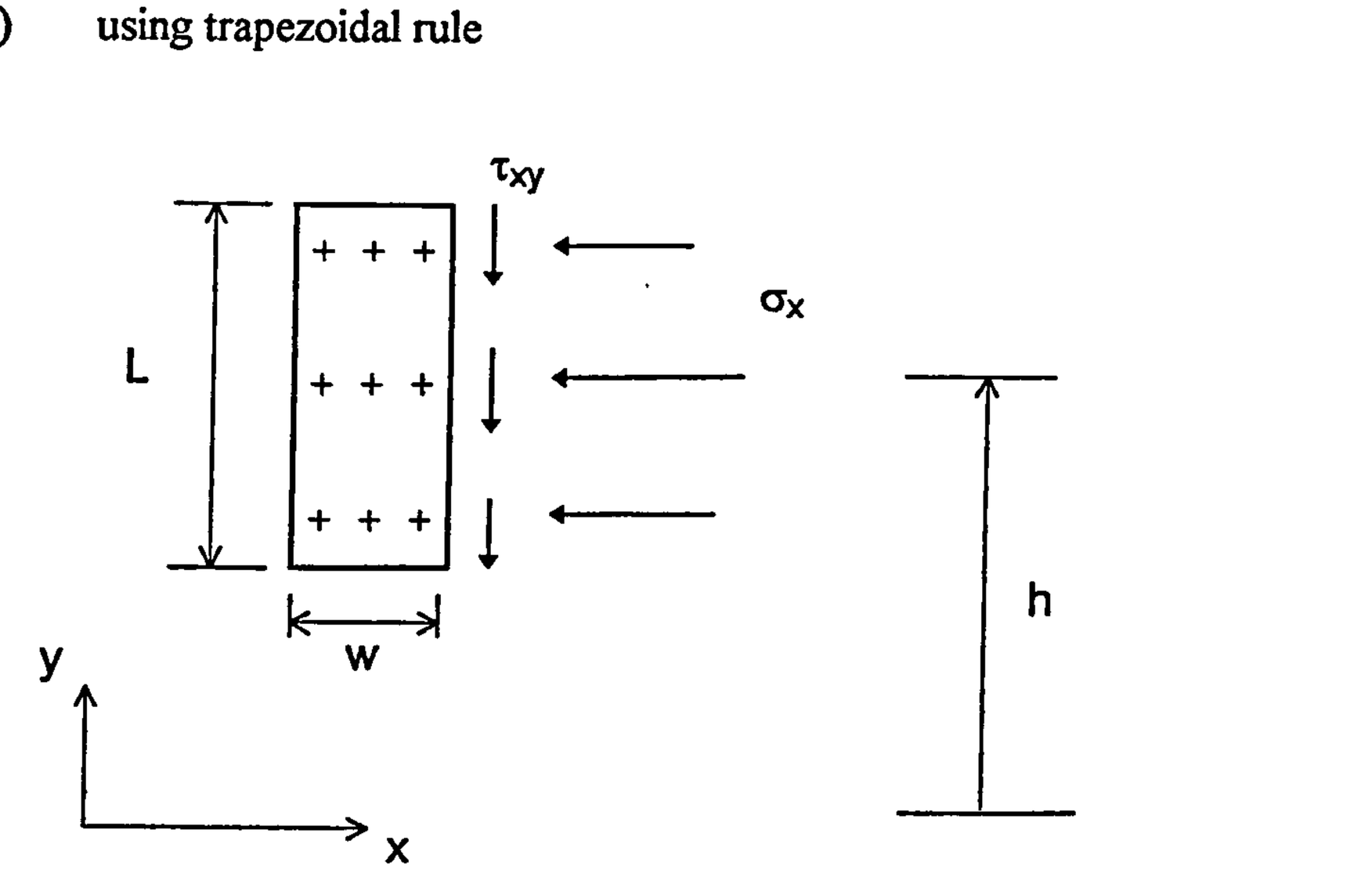

(b) using Gauss integration rules (+ = Gauss point)

Fig 8.23 Calculating wall bending moments from external earth pressures

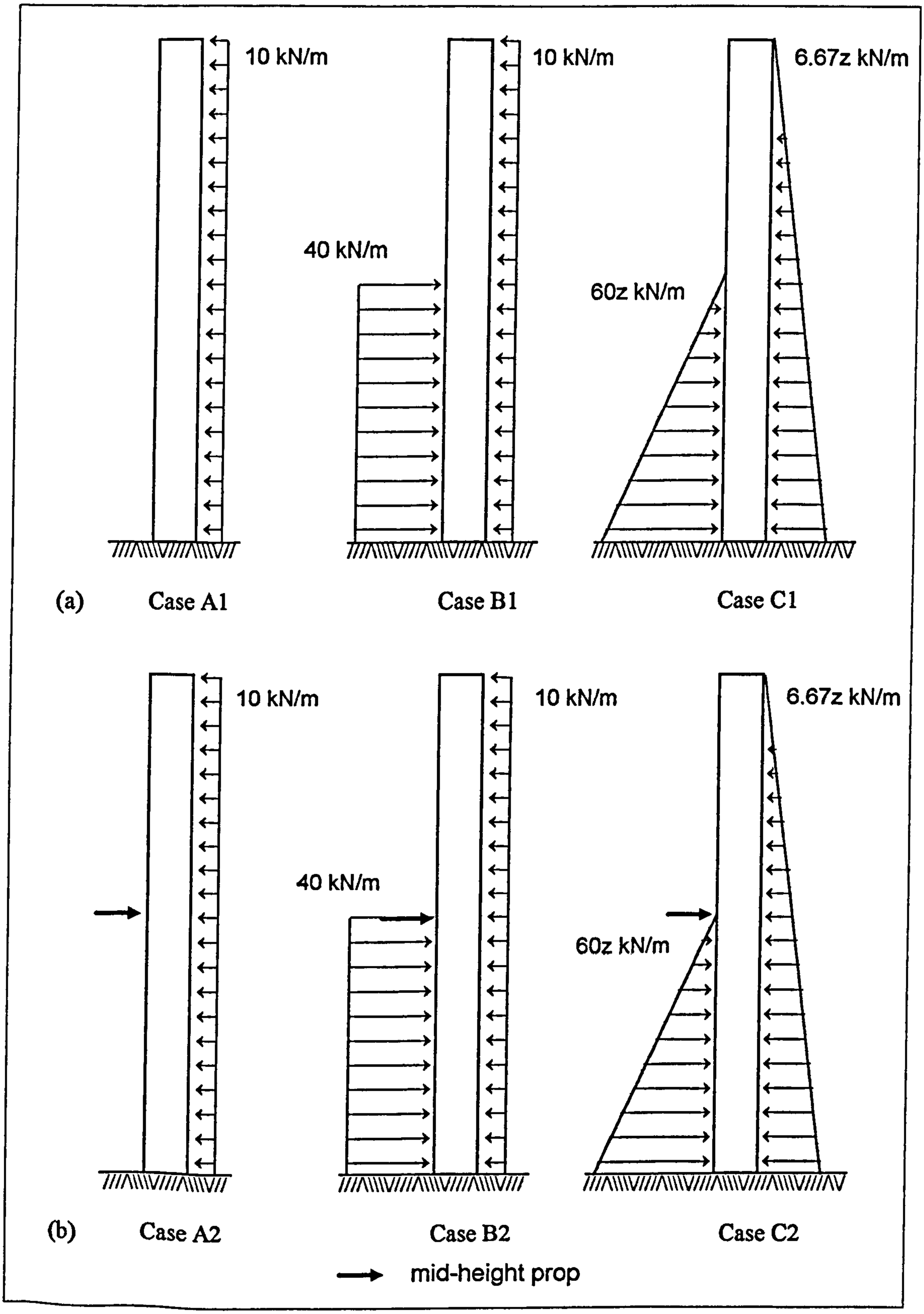

Fig 8.24 Load cases for benchmarking wall stress bending moments - single column of 16 LSQ elements fully-fixed at base, with optional mid-height prop

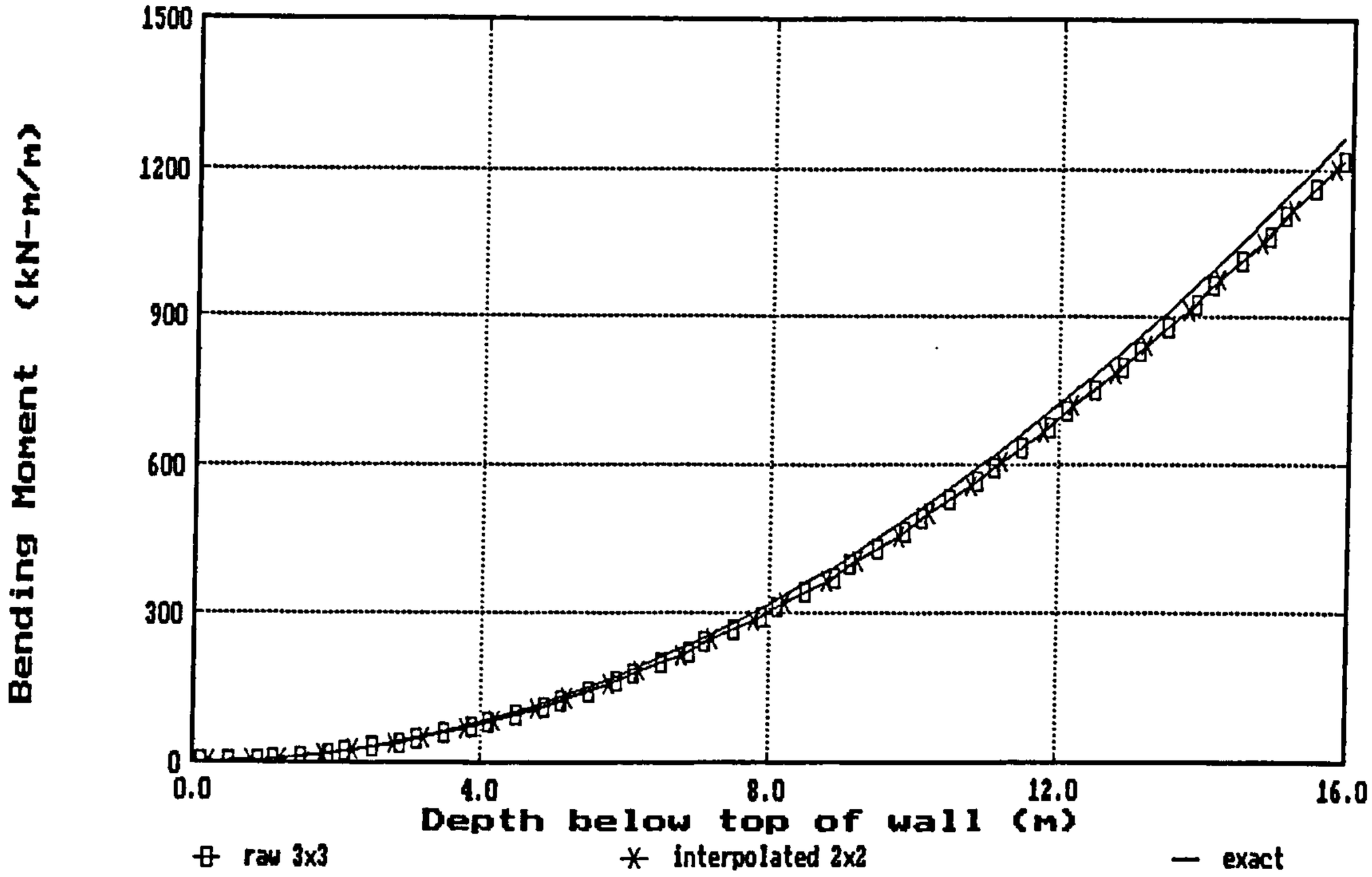

(a) Case A1 (cantilever with single UDL)

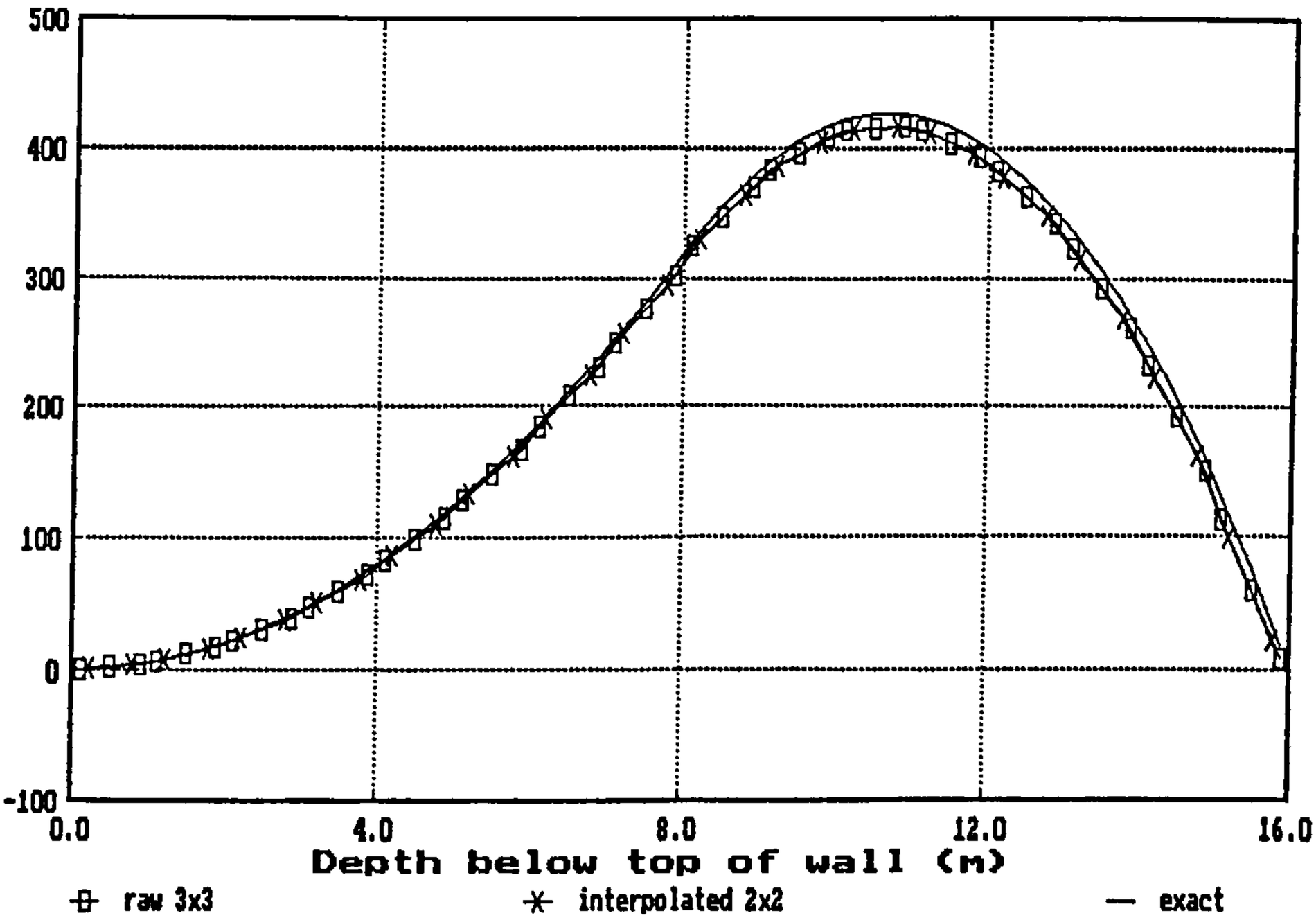

(b) Case B1 (cantilever with twin UDLs)

Fig 8.25 Wall stress bending moments for benchmark cases : calculations using 3×3 and 2×2 transverse stresses compared with exact solution

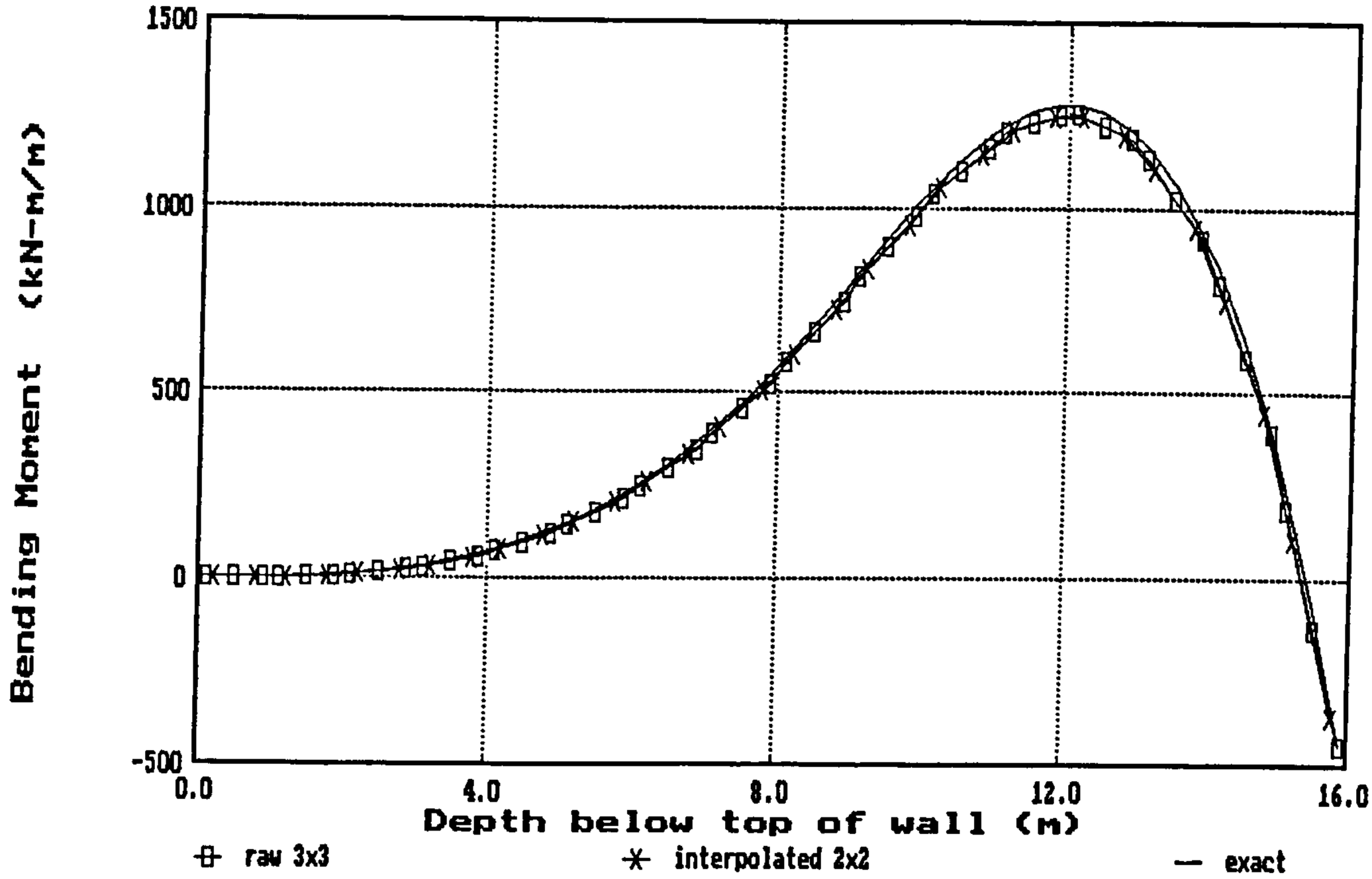

(c) Case C1 (cantilever with twin linearly varying loads)

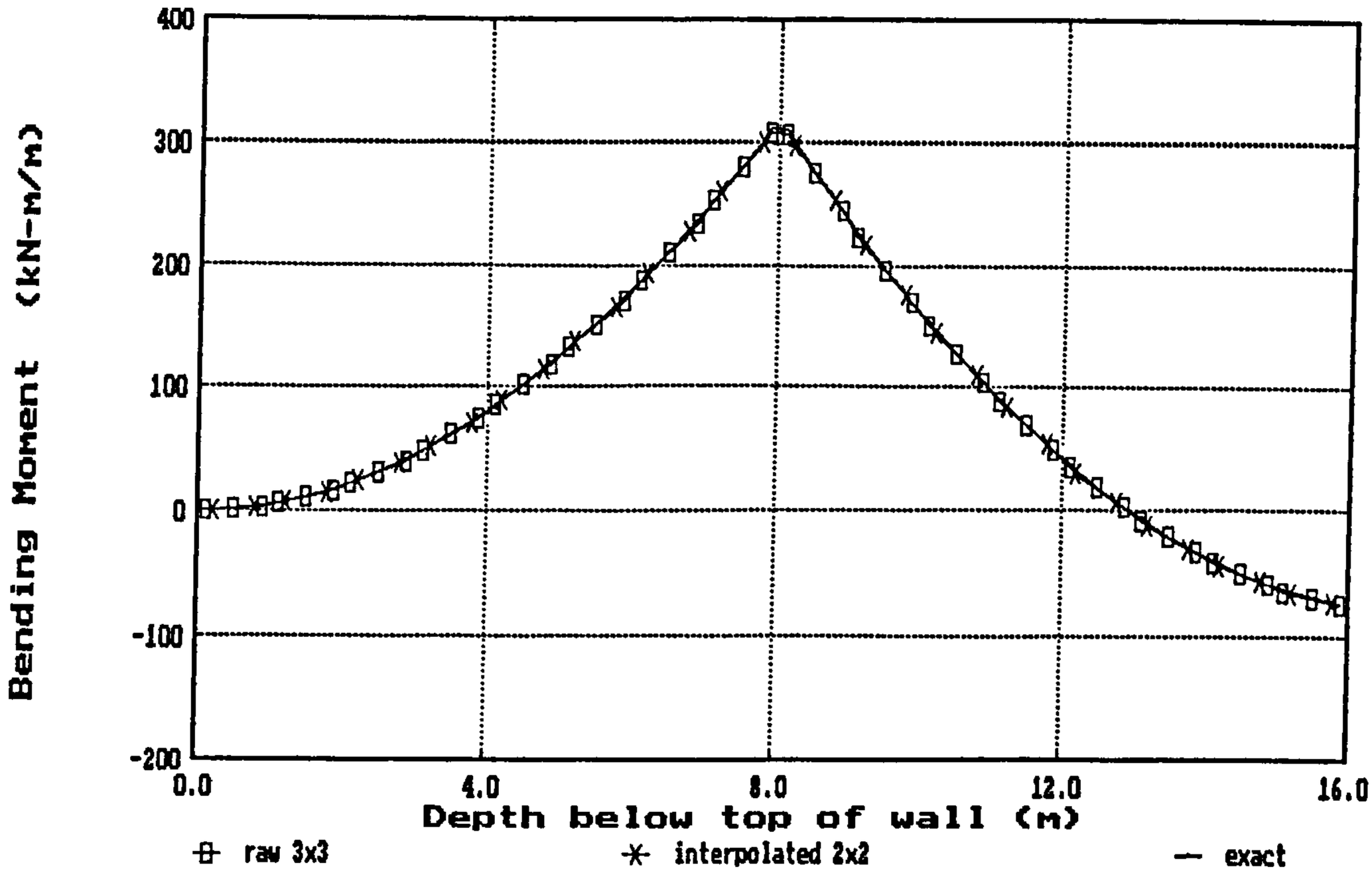

(d) Case A2 (mid-height propped cantilever with single UDL)

Fig 8.25 Wall stress bending moments for benchmark cases : calculations using 3×3 and 2×2 transverse stresses compared with exact solution (contd)

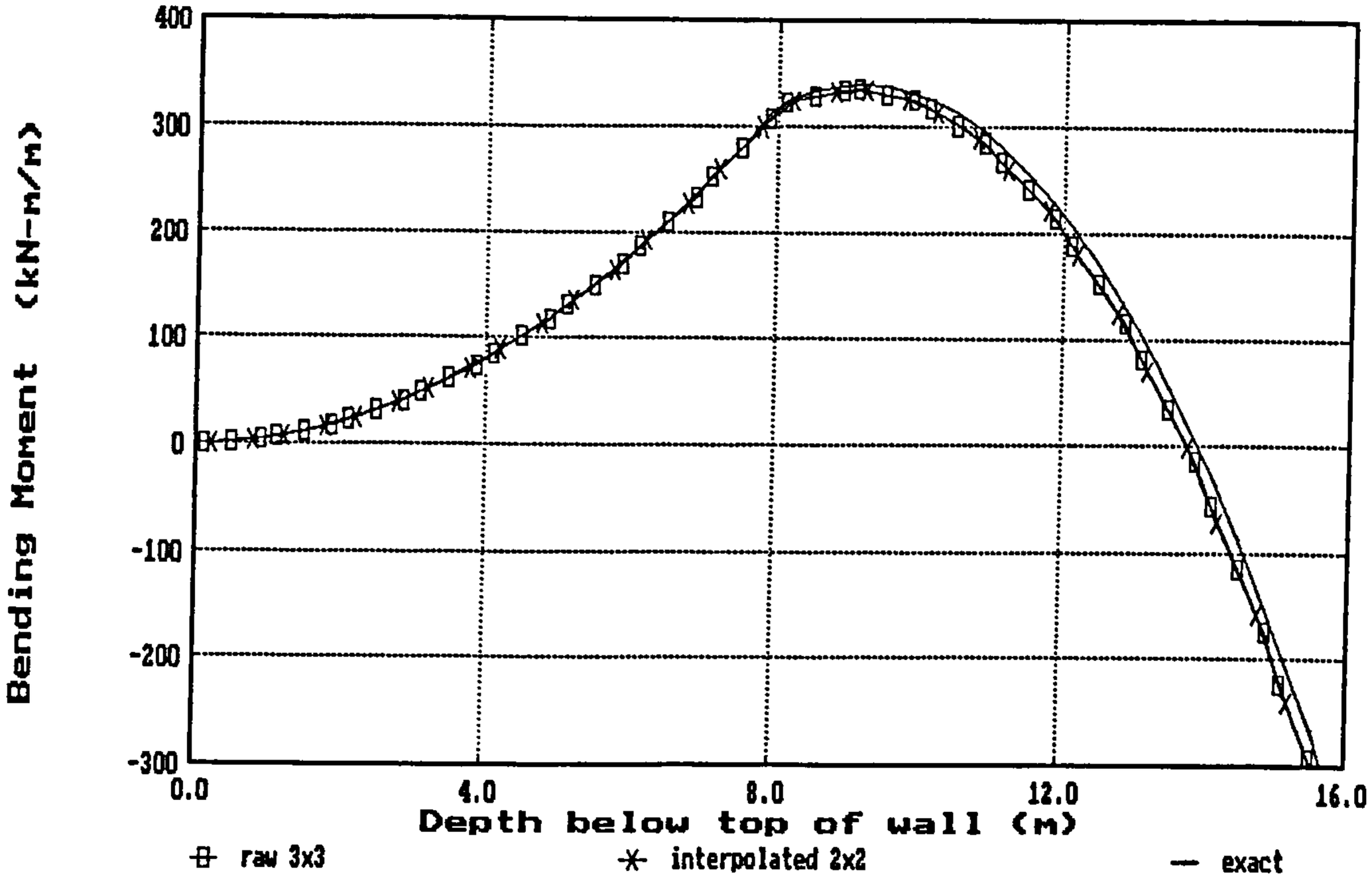

(e) Case B2 (mid-height propped cantilever with twin UDLs)

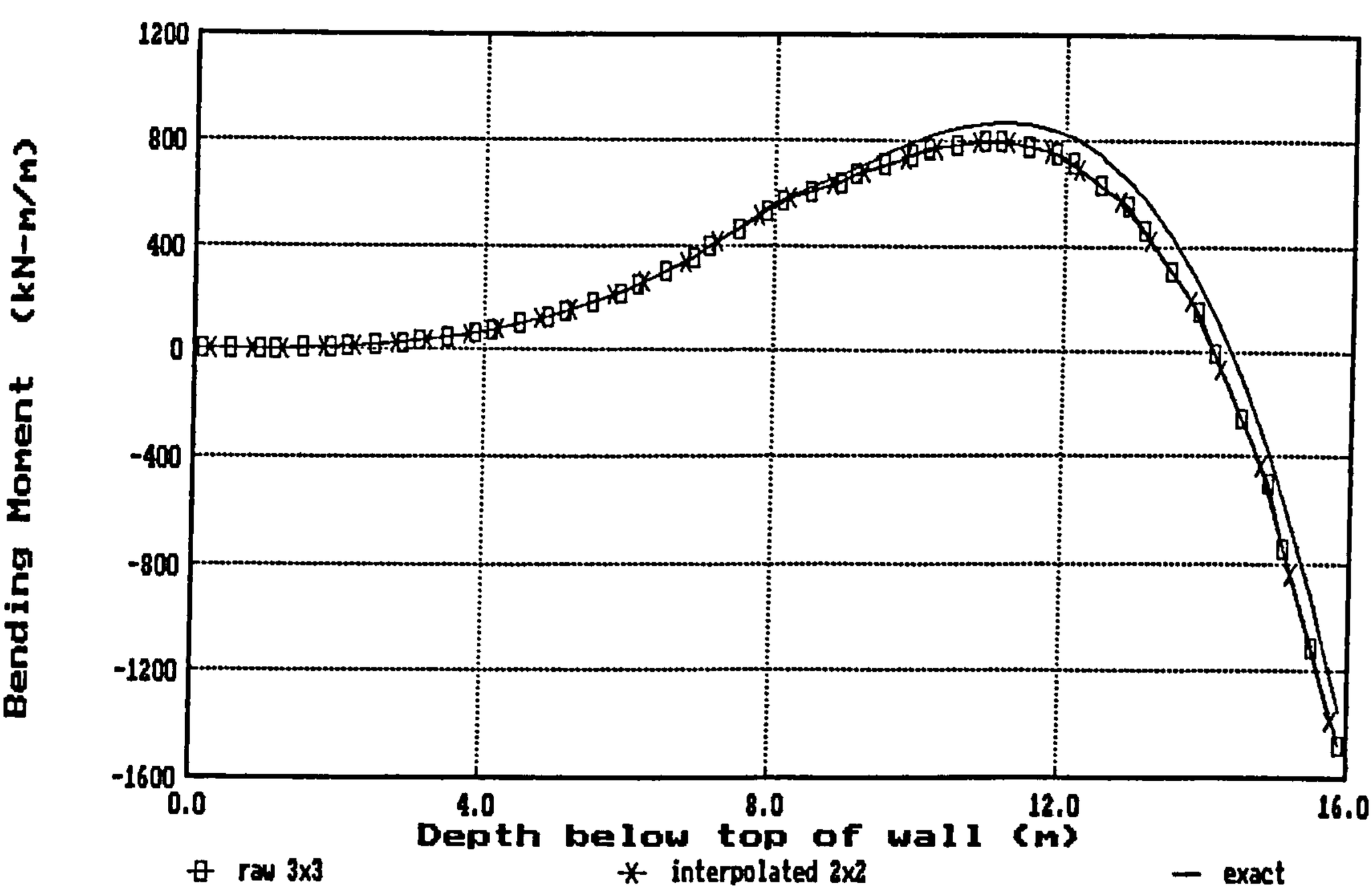

(f) Case C2 (mid-height propped cantilever with twin linearly varying loads)

Fig 8.25 Wall stress bending moments for benchmark cases : calculations using 3×3 and 2×2 transverse stresses compared with exact solution (contd)

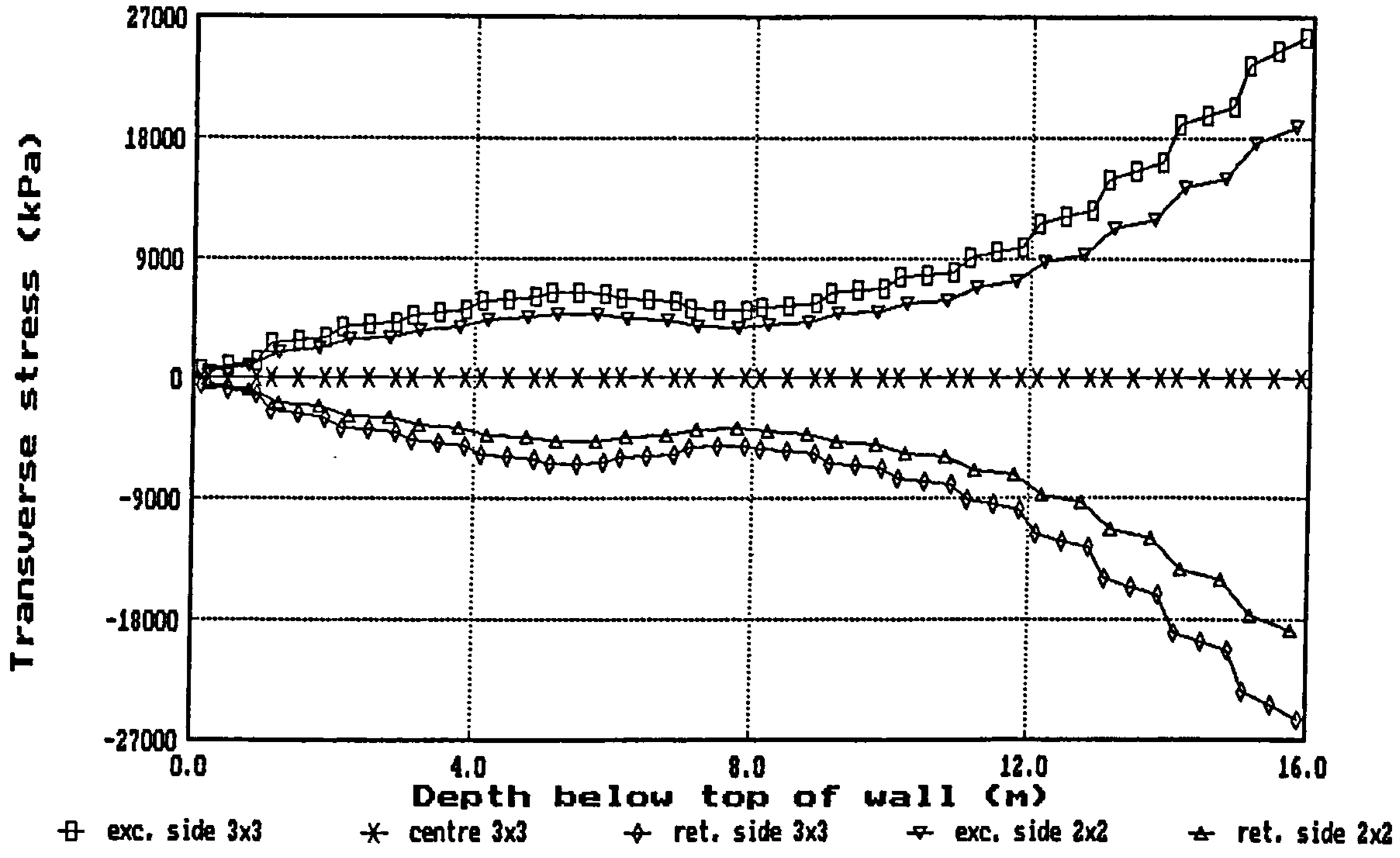

(a) Profiles of transverse stress : raw 3×3 and interpolated 2×2 Gauss points

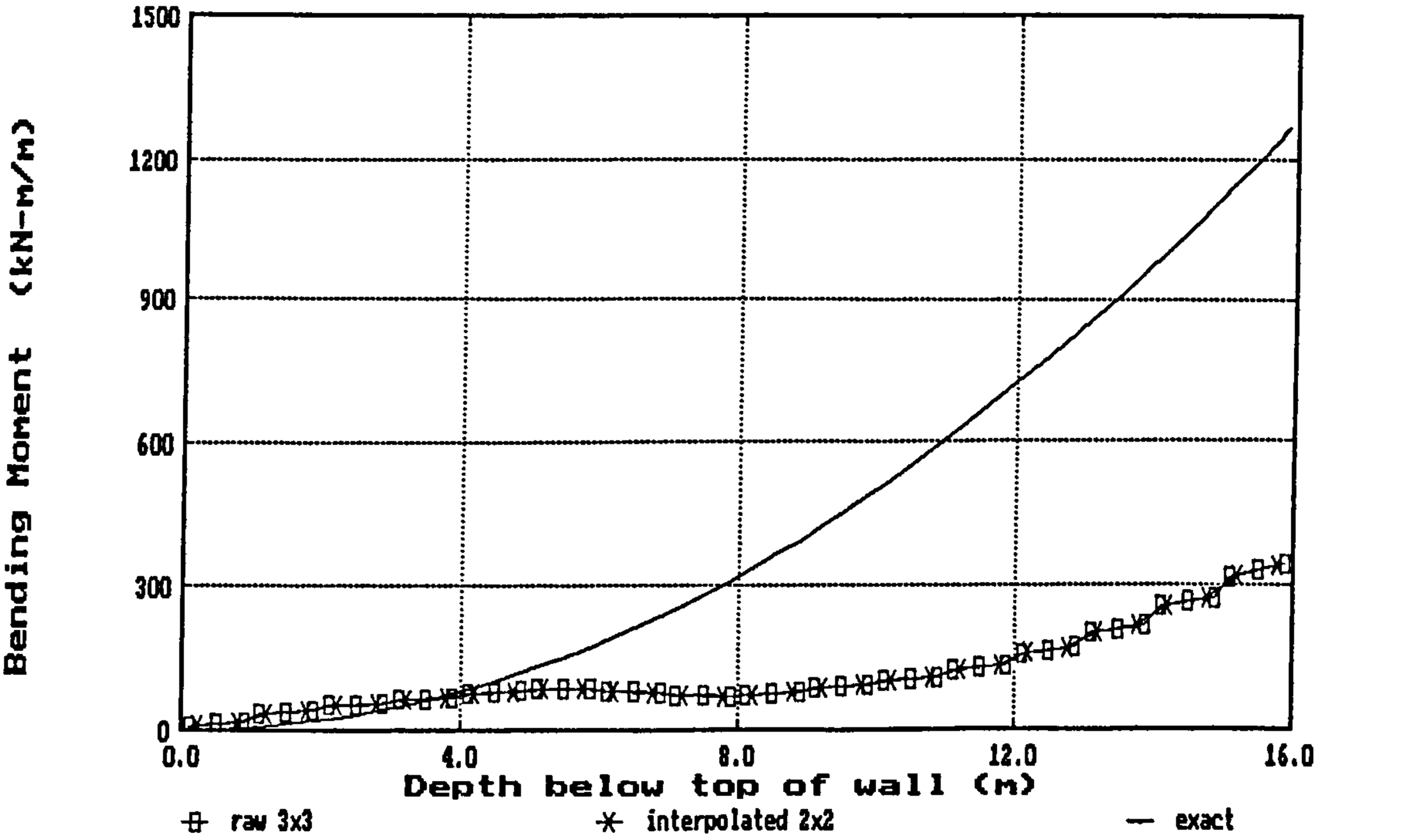

(b) Bending moment distribution - computed v analytical

Fig 8.26 Numerical problems with wall stress bending moments (Case A1 with element width reduced to give aspect ratio w/h = 1/4)

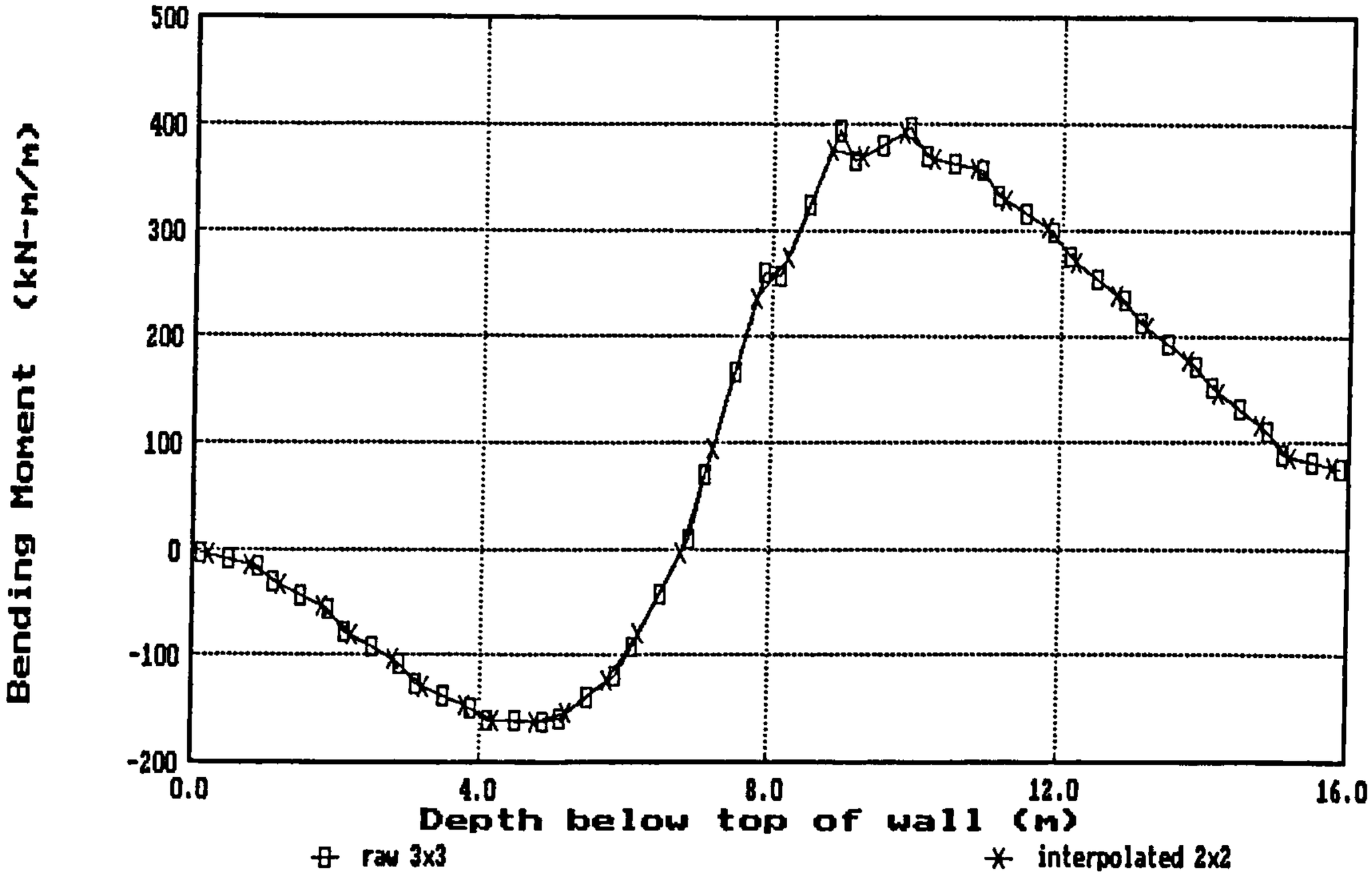

(a) Case RW3 : cantilever wall / undrained / elastic soil

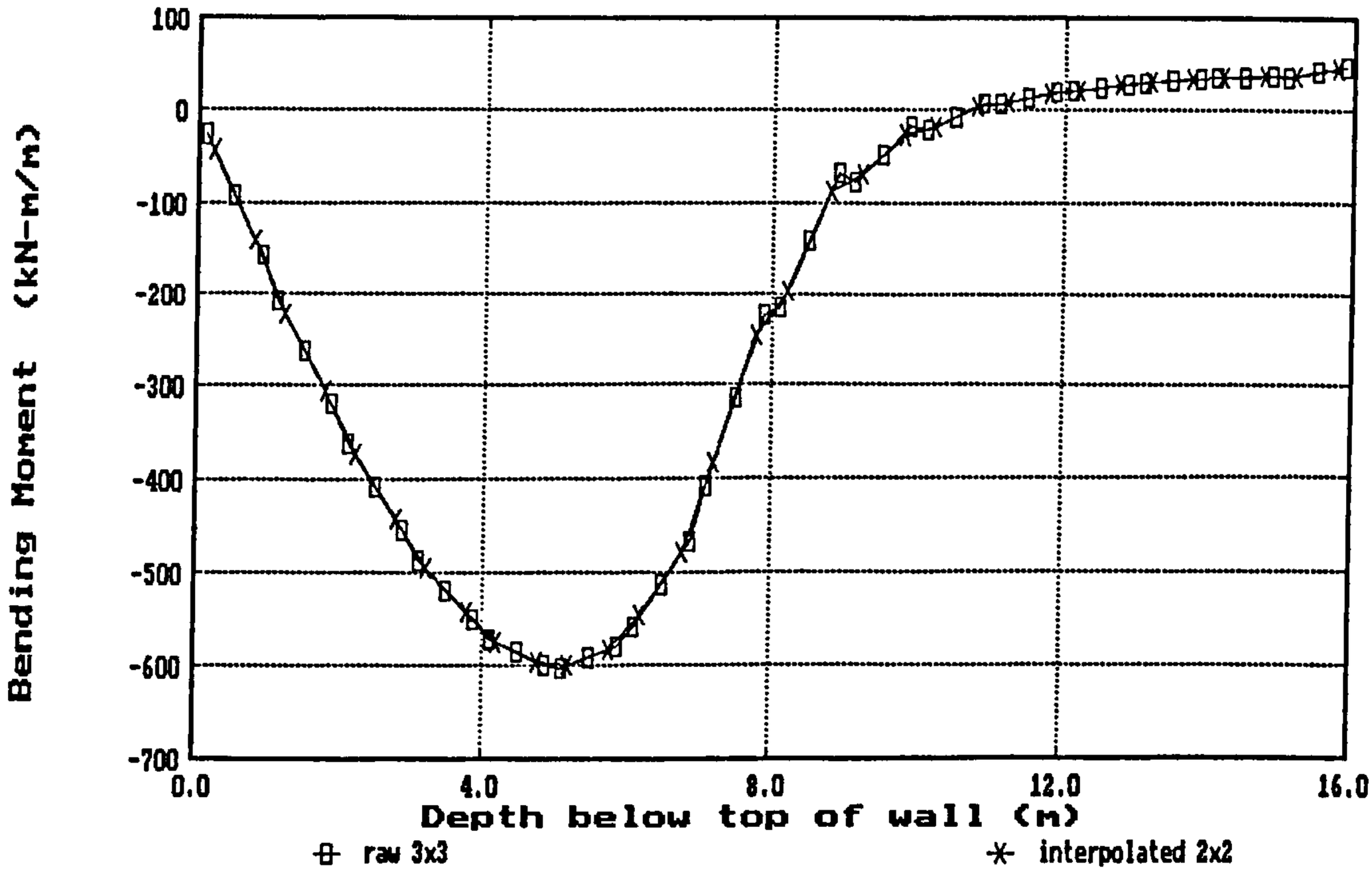

(b) Case RW11 : top-propped wall / undrained / elastic soil

Fig 8.27 Wall bending moments - comparison of wall stress methods using raw 3×3 and interpolated 2×2 Gauss point stresses

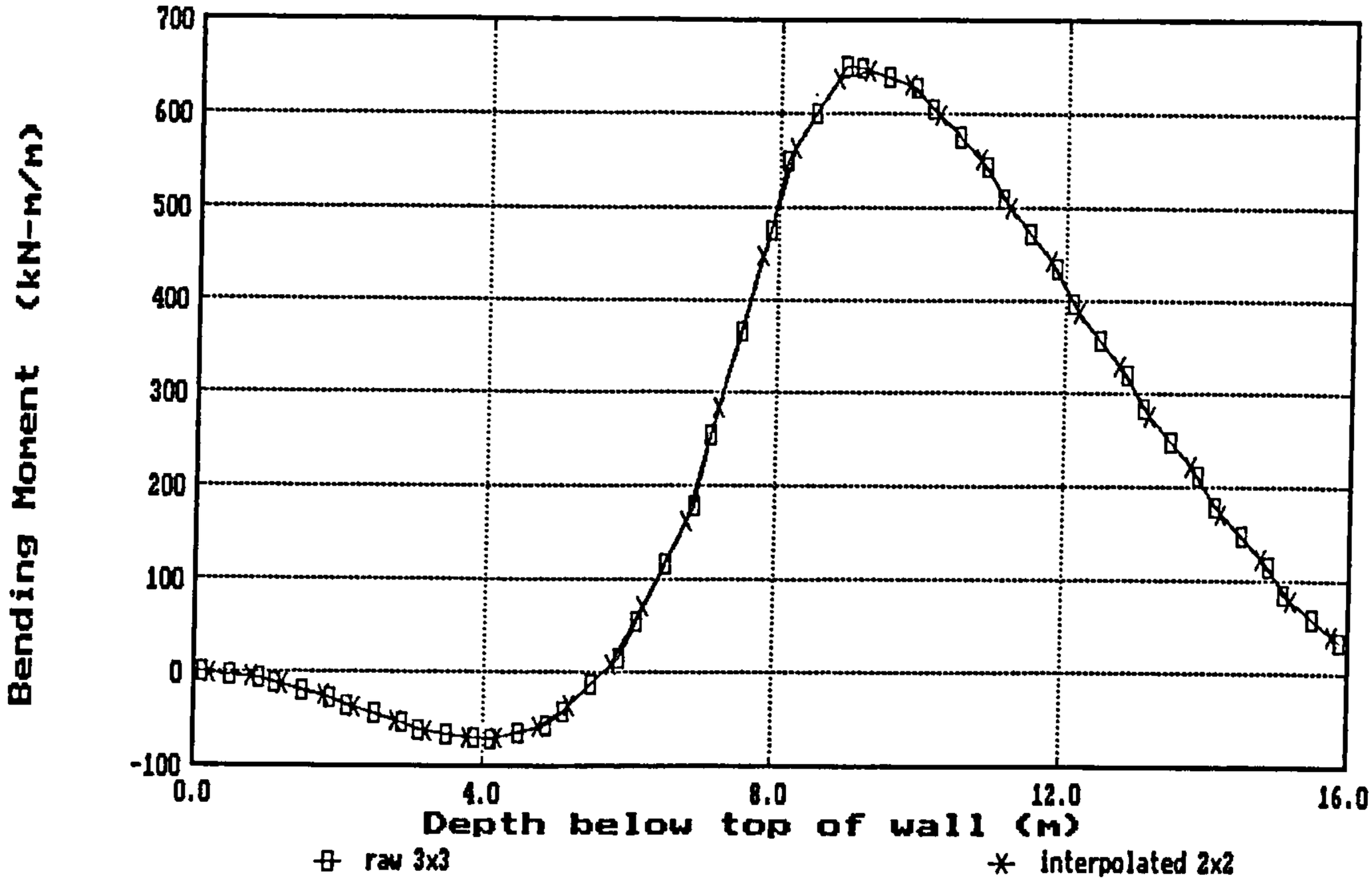

(c) Case RW53 : cantilever wall / drained / elastic soil

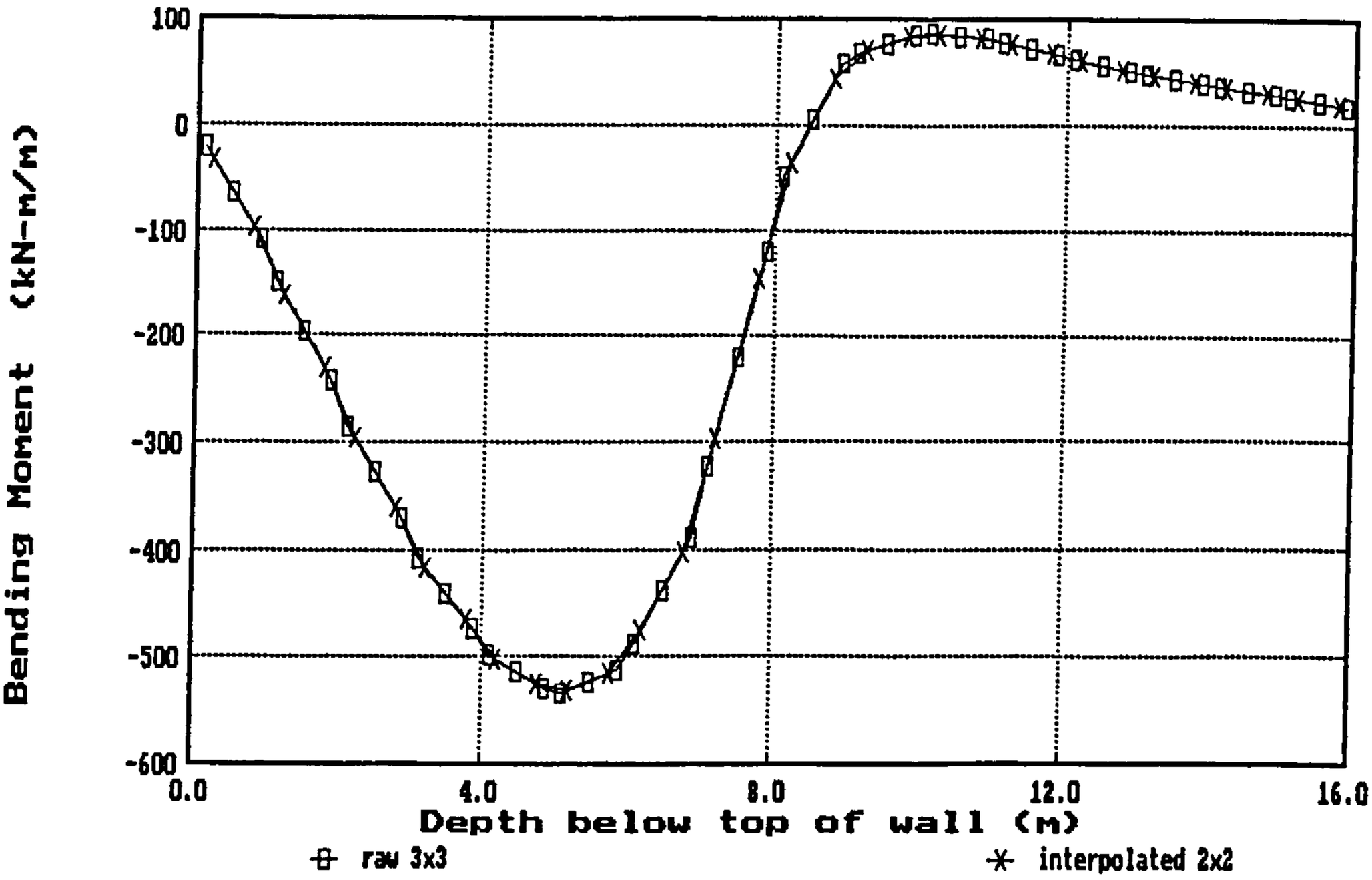

(d) Case RW61 : top-propped wall / undrained / elastic soil

Fig 8.27 Wall bending moments - comparison of wall stress methods using raw 3×3 and interpolated 2×2 Gauss point stresses (contd)

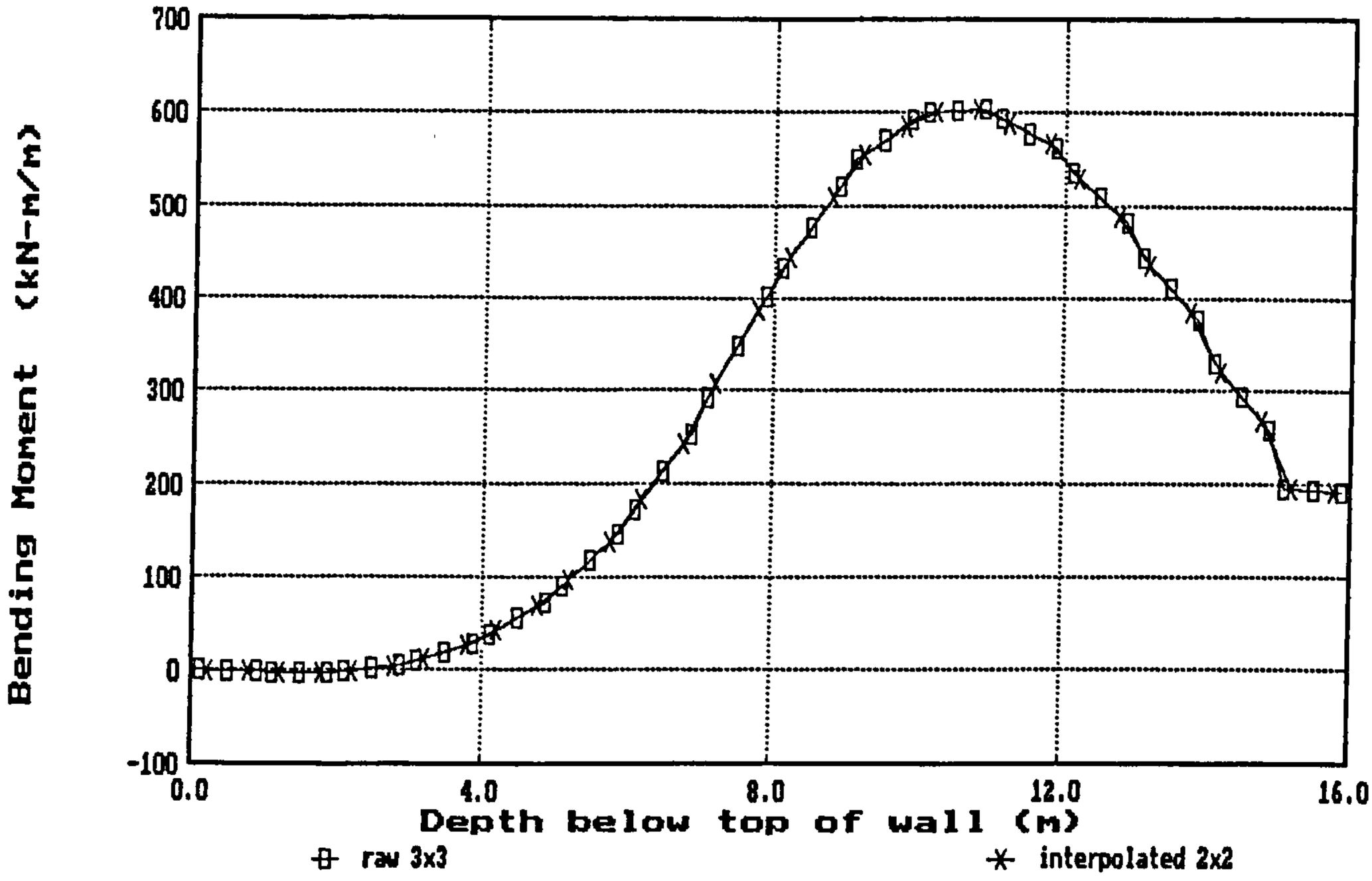

(e) Case RW103 : cantilever wall / undrained / elastic-perfectly plastic (Tresca)

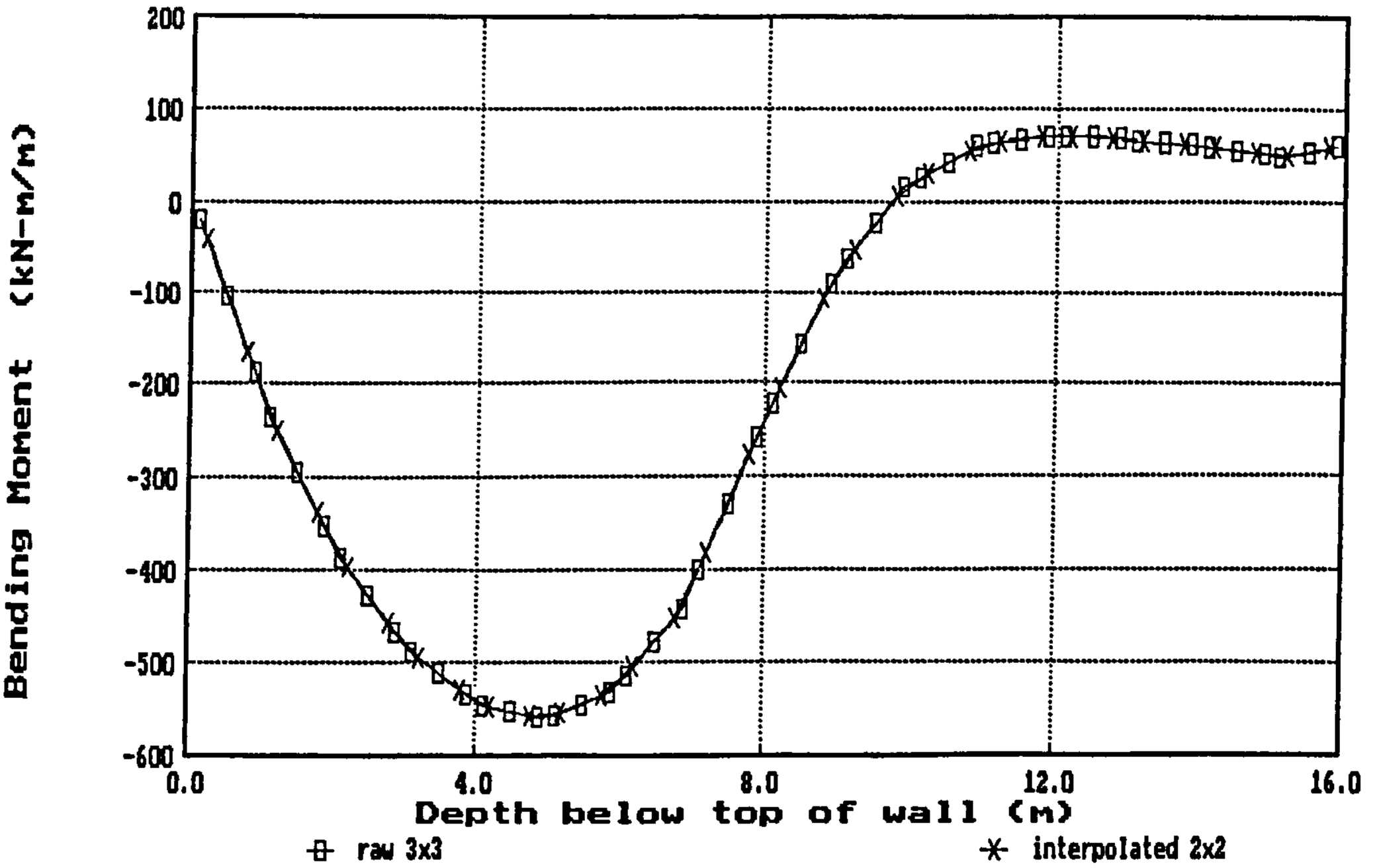

(f) Case RW112 : top-propped wall / undrained / elastic-perfectly plastic (Tresca)

Fig 8.27 Wall bending moments - comparison of wall stress methods using raw 3×3 and interpolated 2×2 Gauss point stresses (contd)

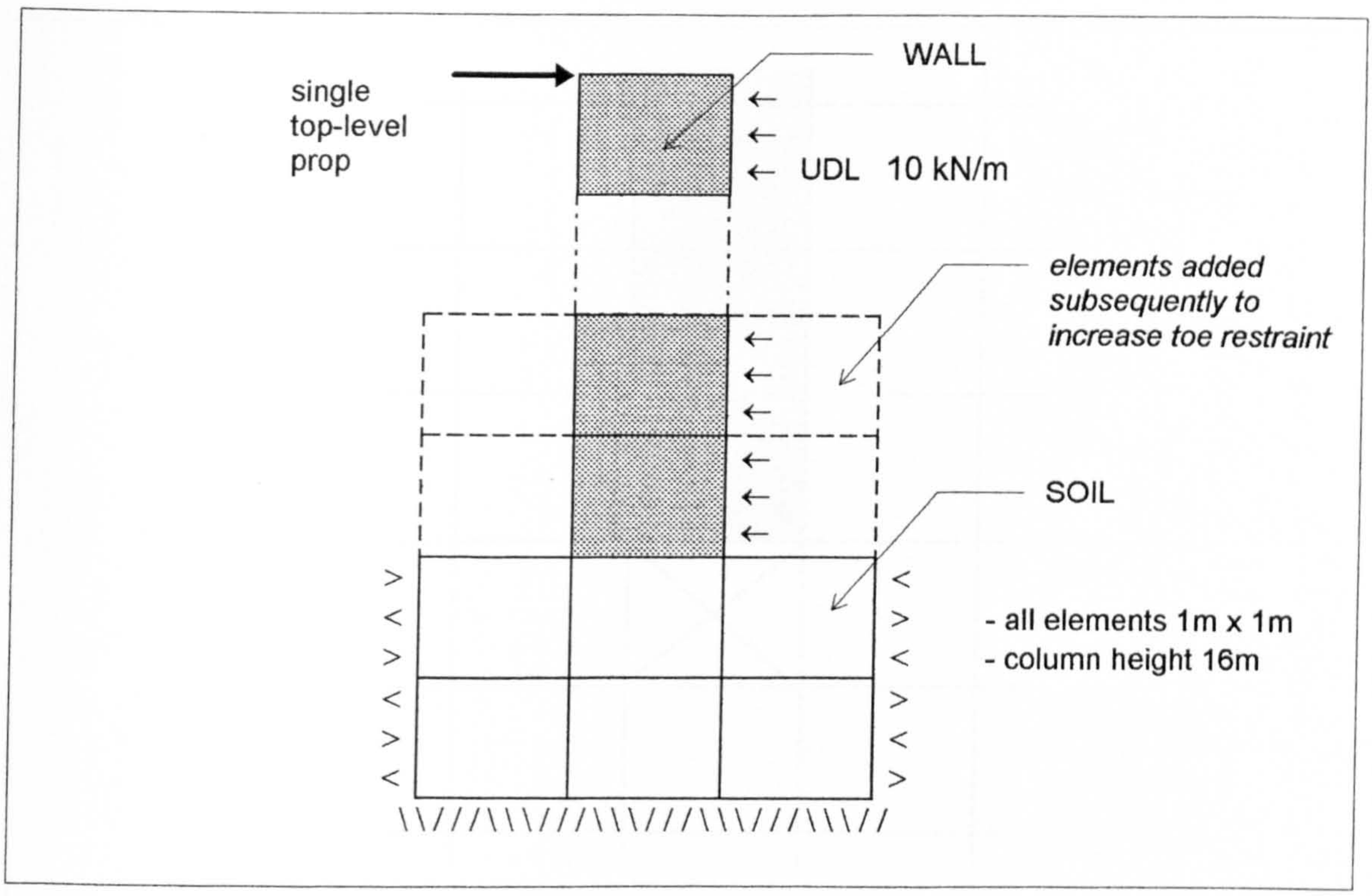

Fig 8.28 Single column of 16 LSQ elements with modifications at base (case A3)

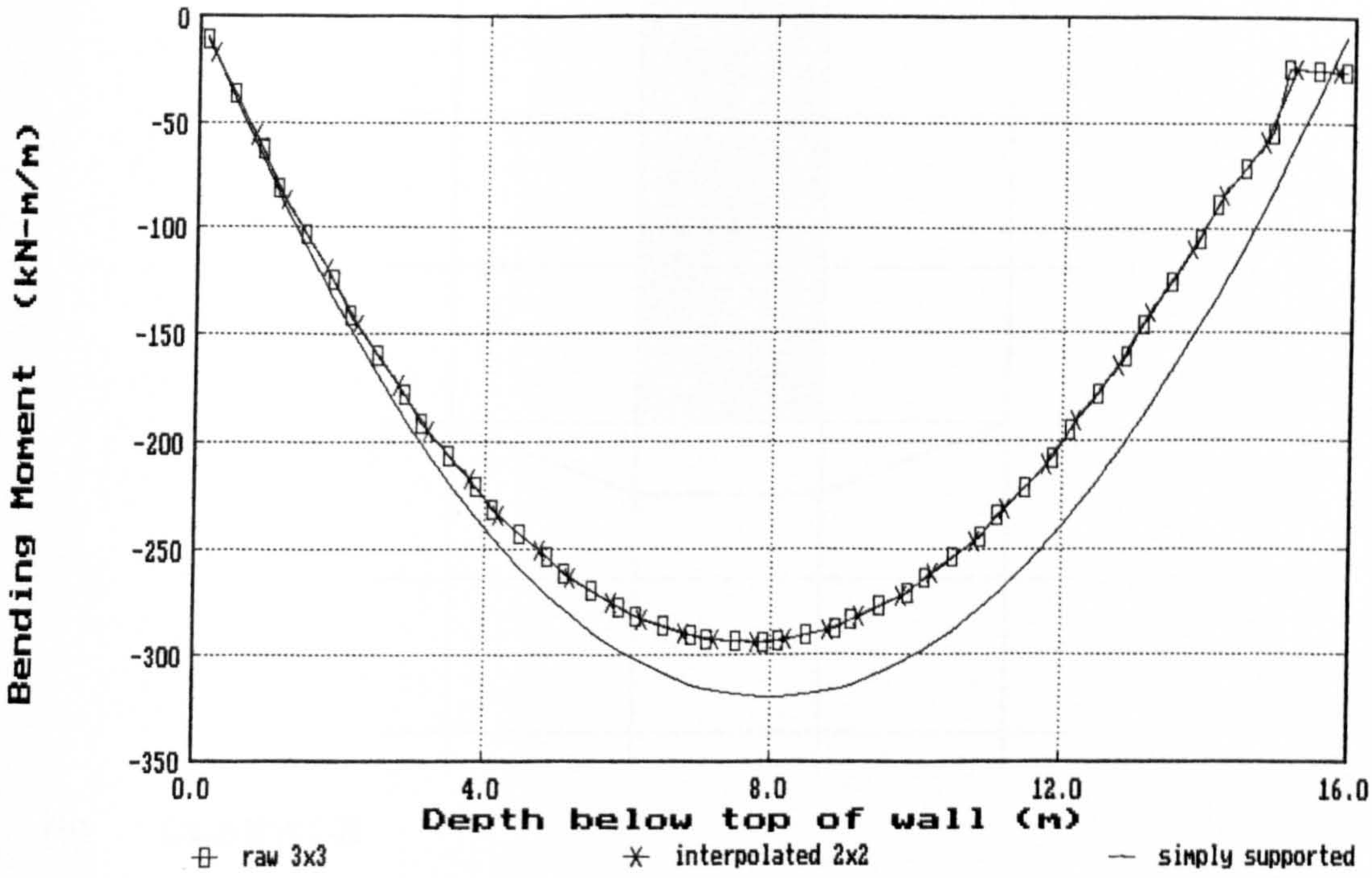

Fig 8.29 Wall stress bending moments for case A3, compared with exact solution for simply supported beam carrying a UDL.

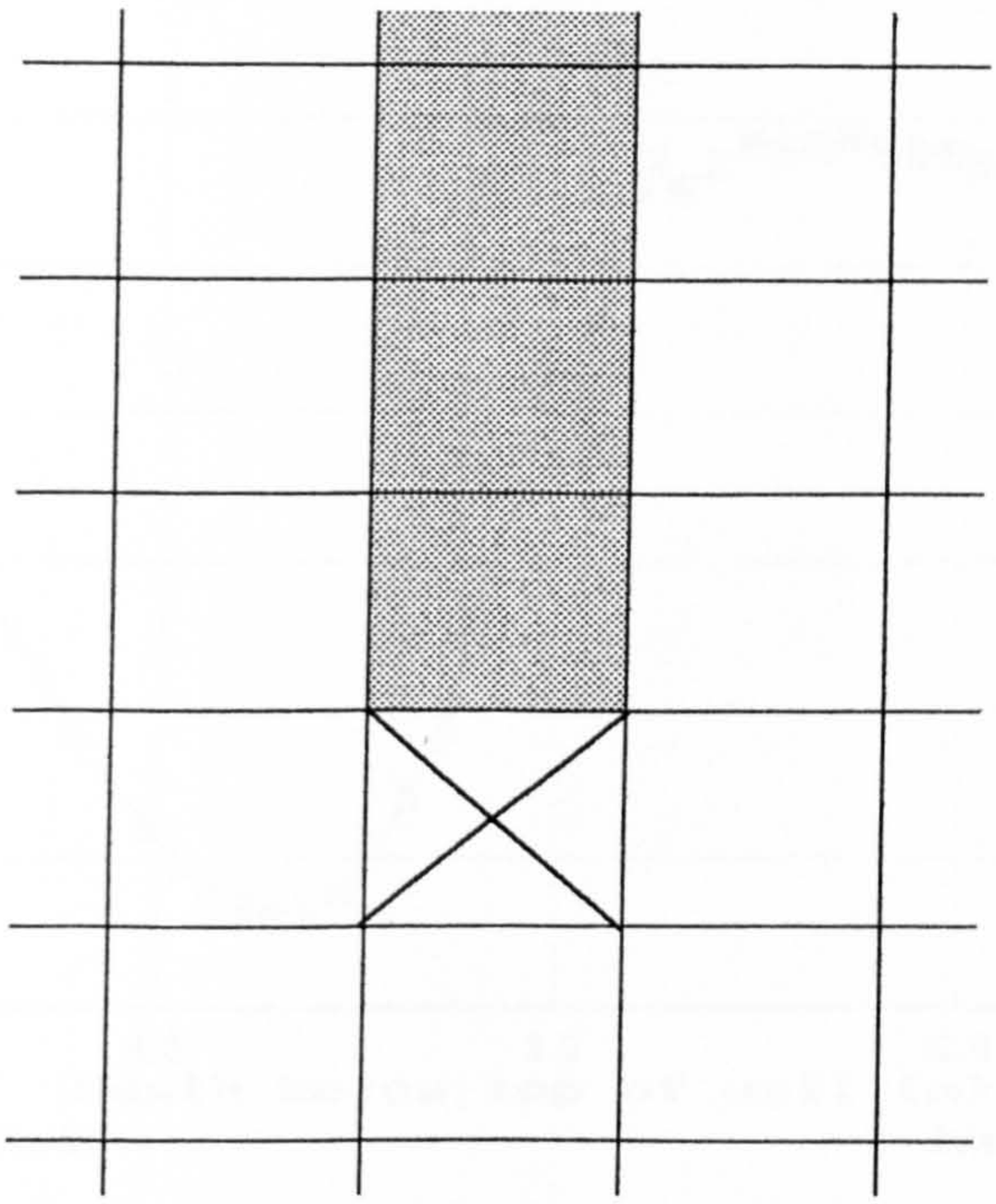

(a) Case RW1-A

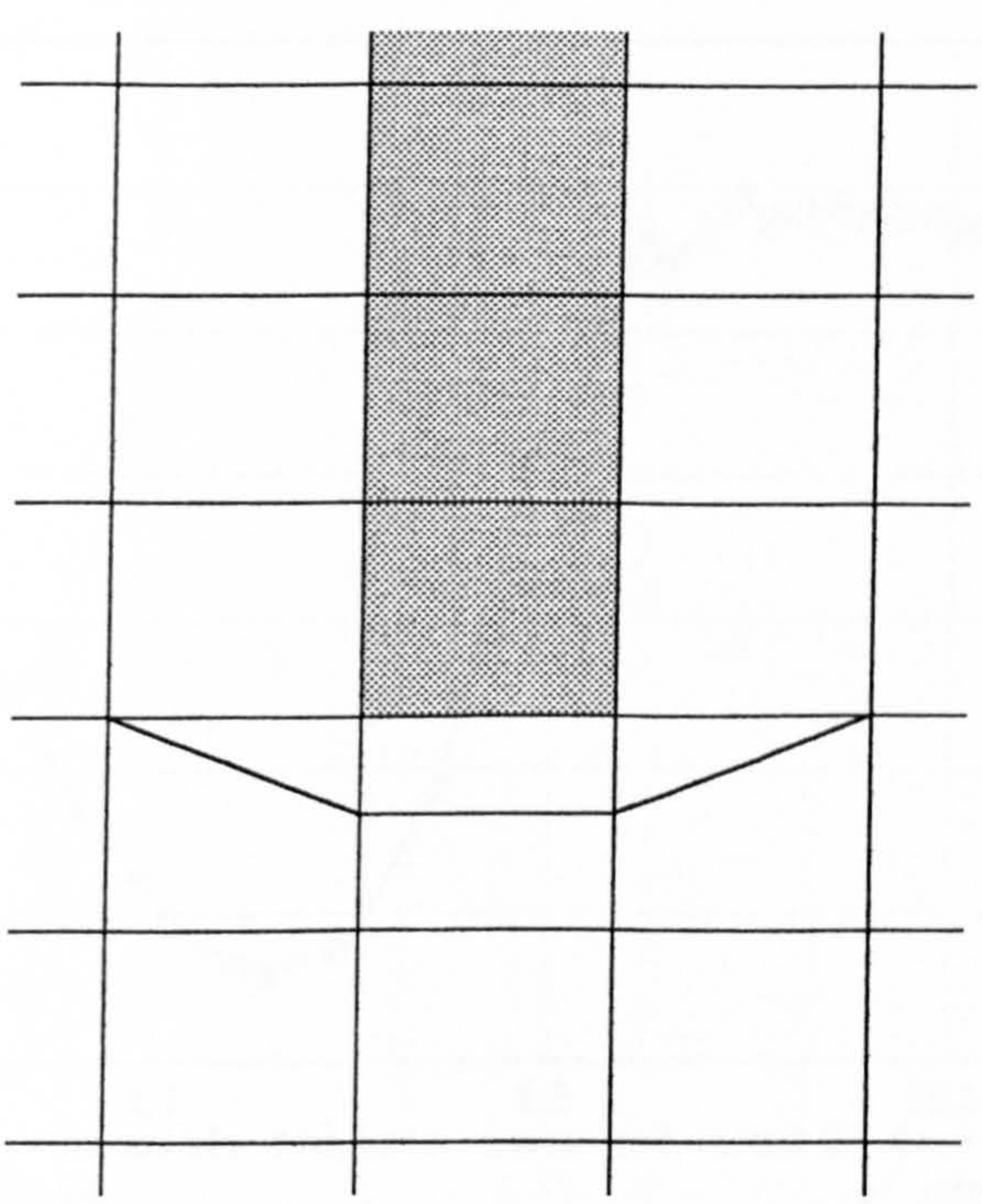

(b) Case RW1-B

Fig 8.30 Local mesh refinement schemes near the toe of an embedded wall

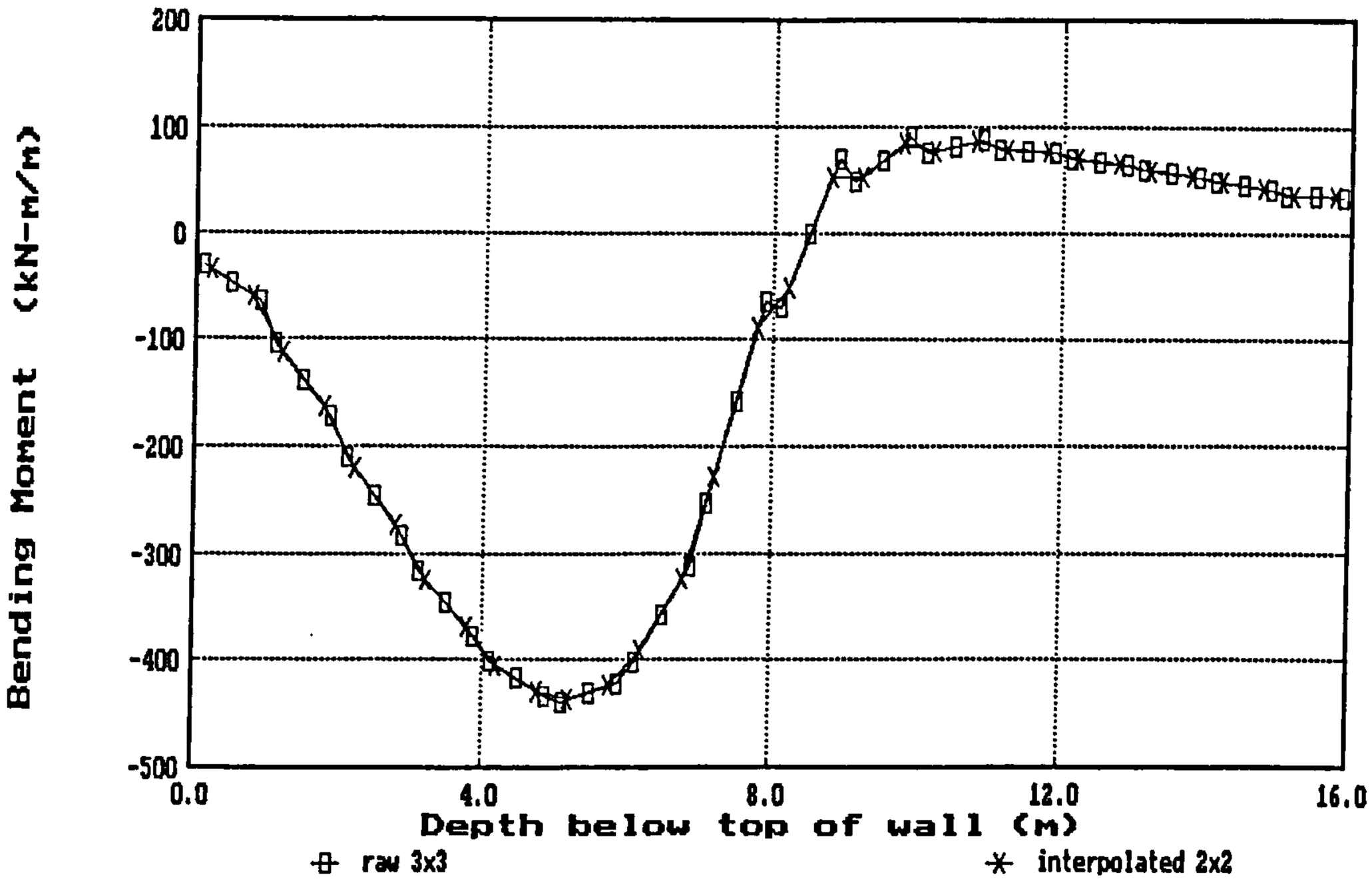

(a) Case RW1-A (one element below toe of wall wall subdivided)

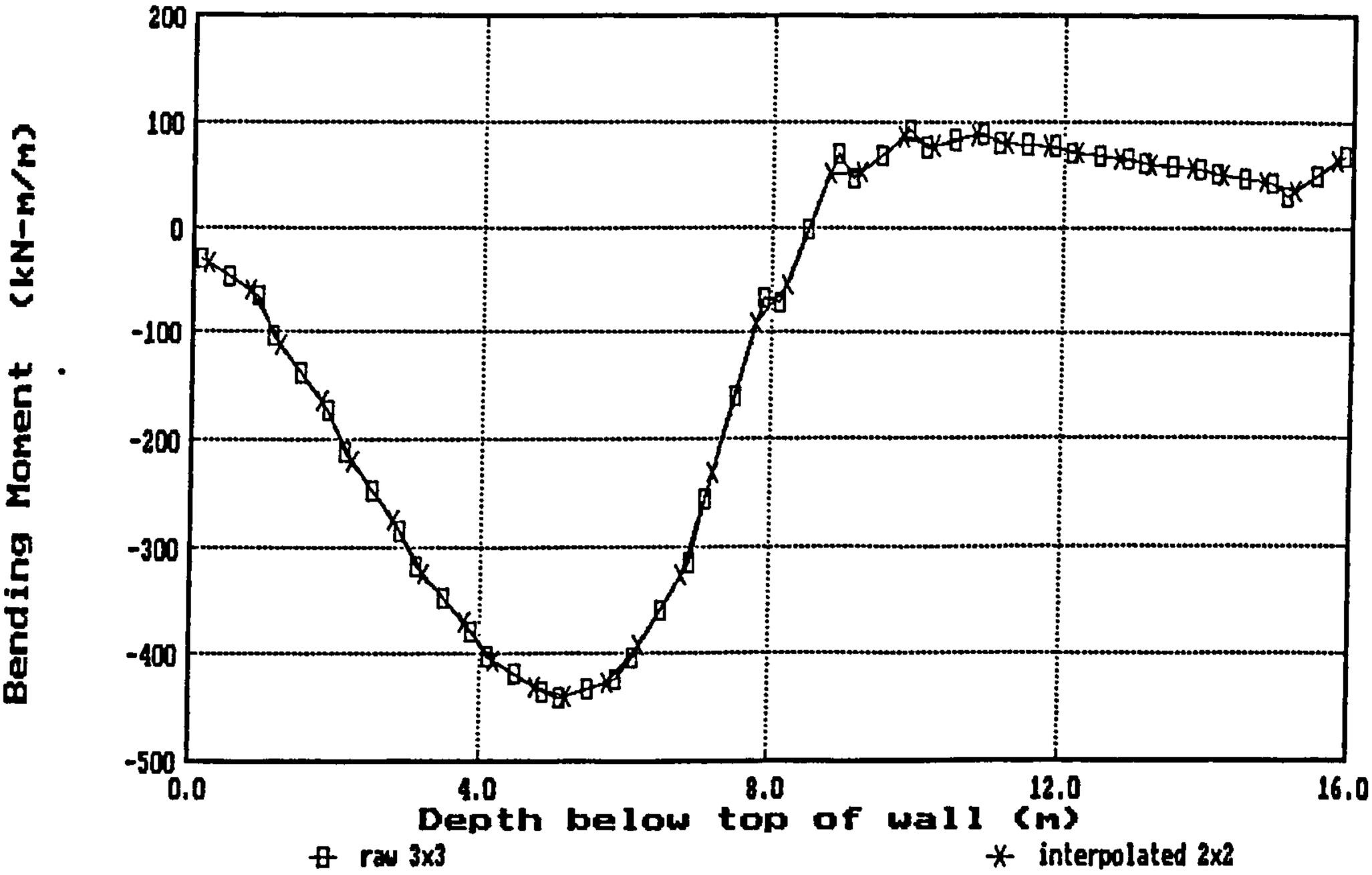

(b) Case RW1-B (three elements below toe of wall subdivided)

Fig 8.31 Wall stress bending moments following local mesh refinement near toe

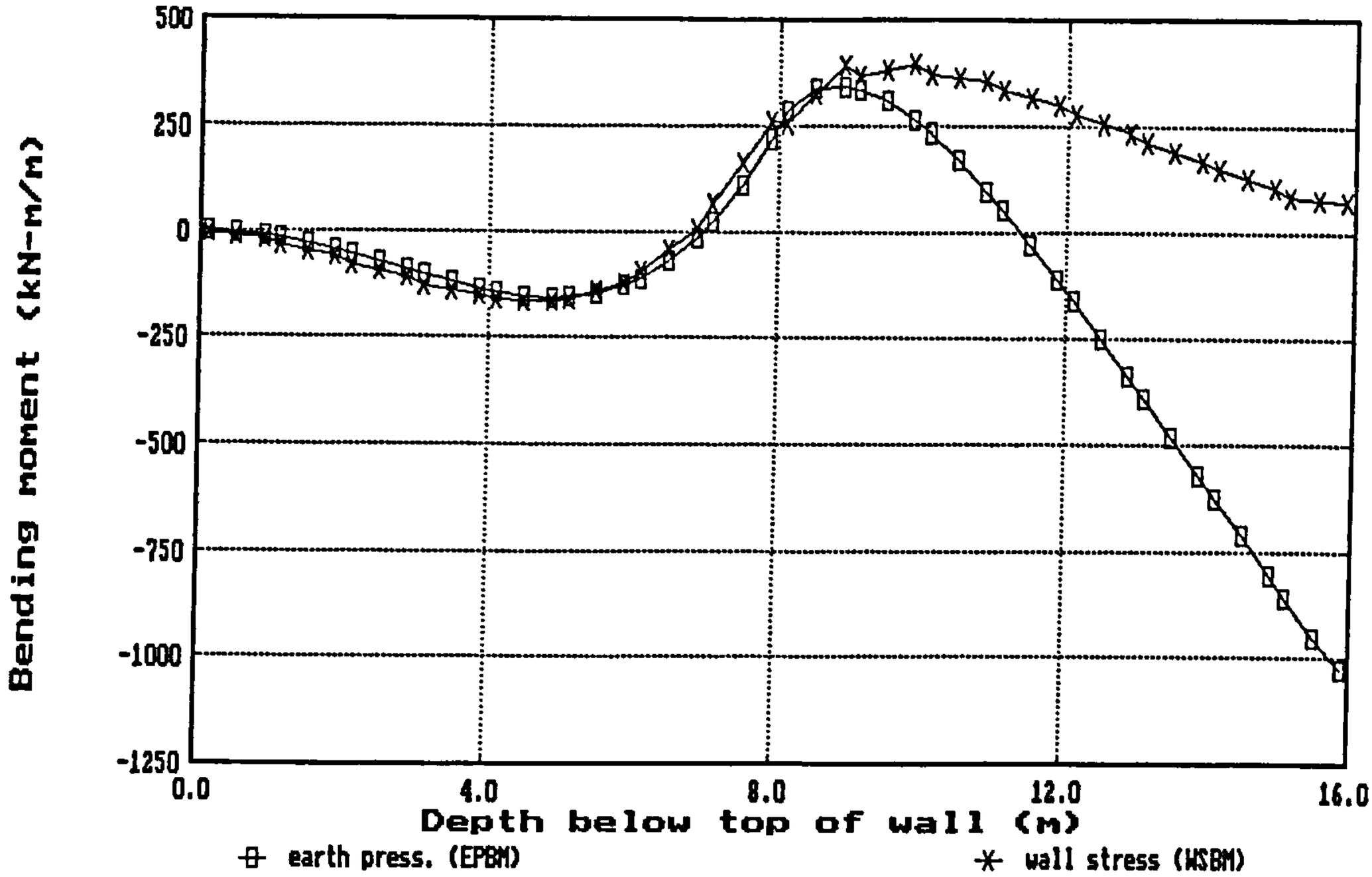

(a) Case RW3 : cantilever wall / undrained / elastic soil

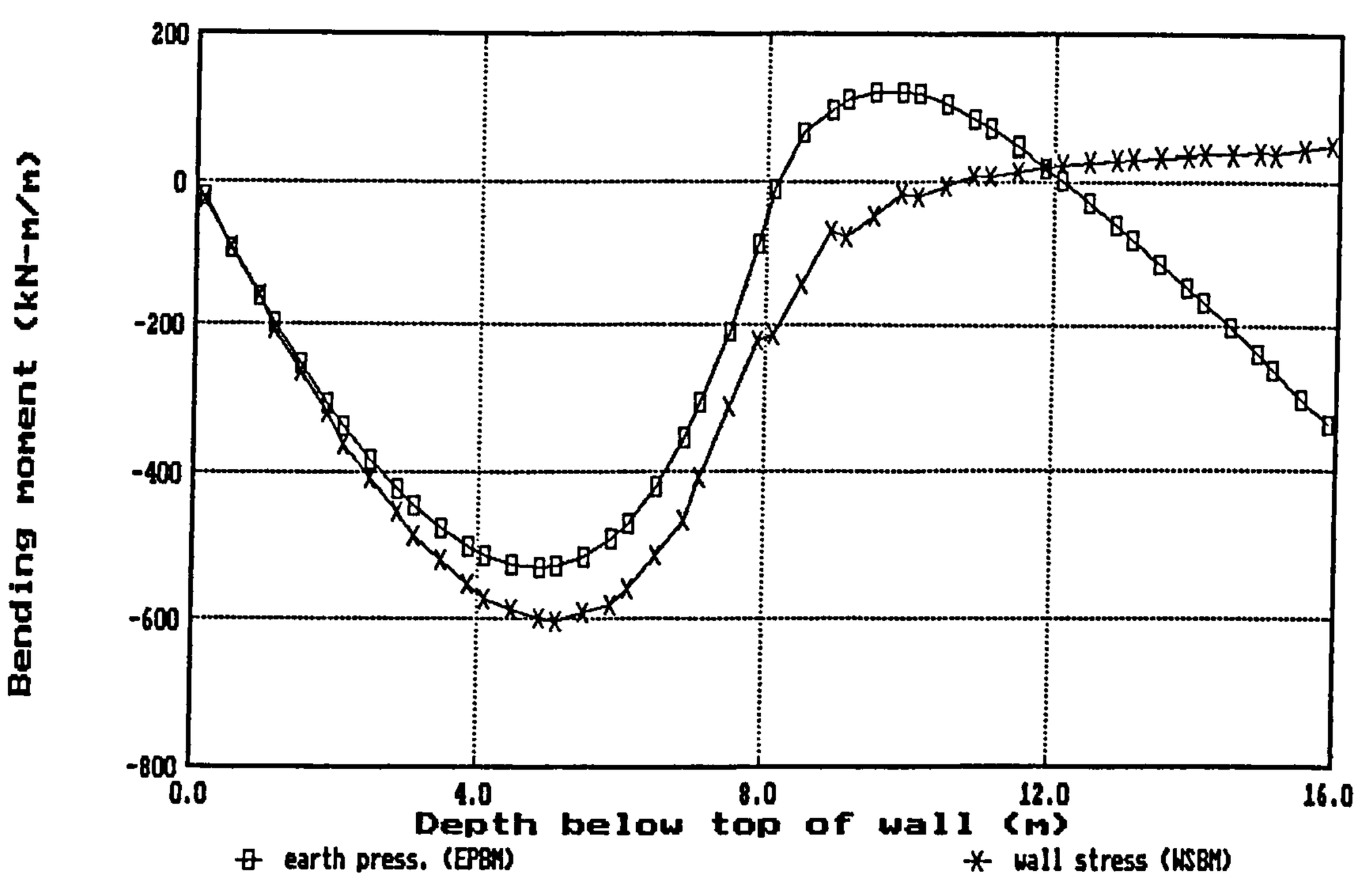

(b) Case RW11 : top-propped wall / undrained / elastic soil

Fig 8.32 Wall bending moments - comparison of wall stress and earth pressure methods

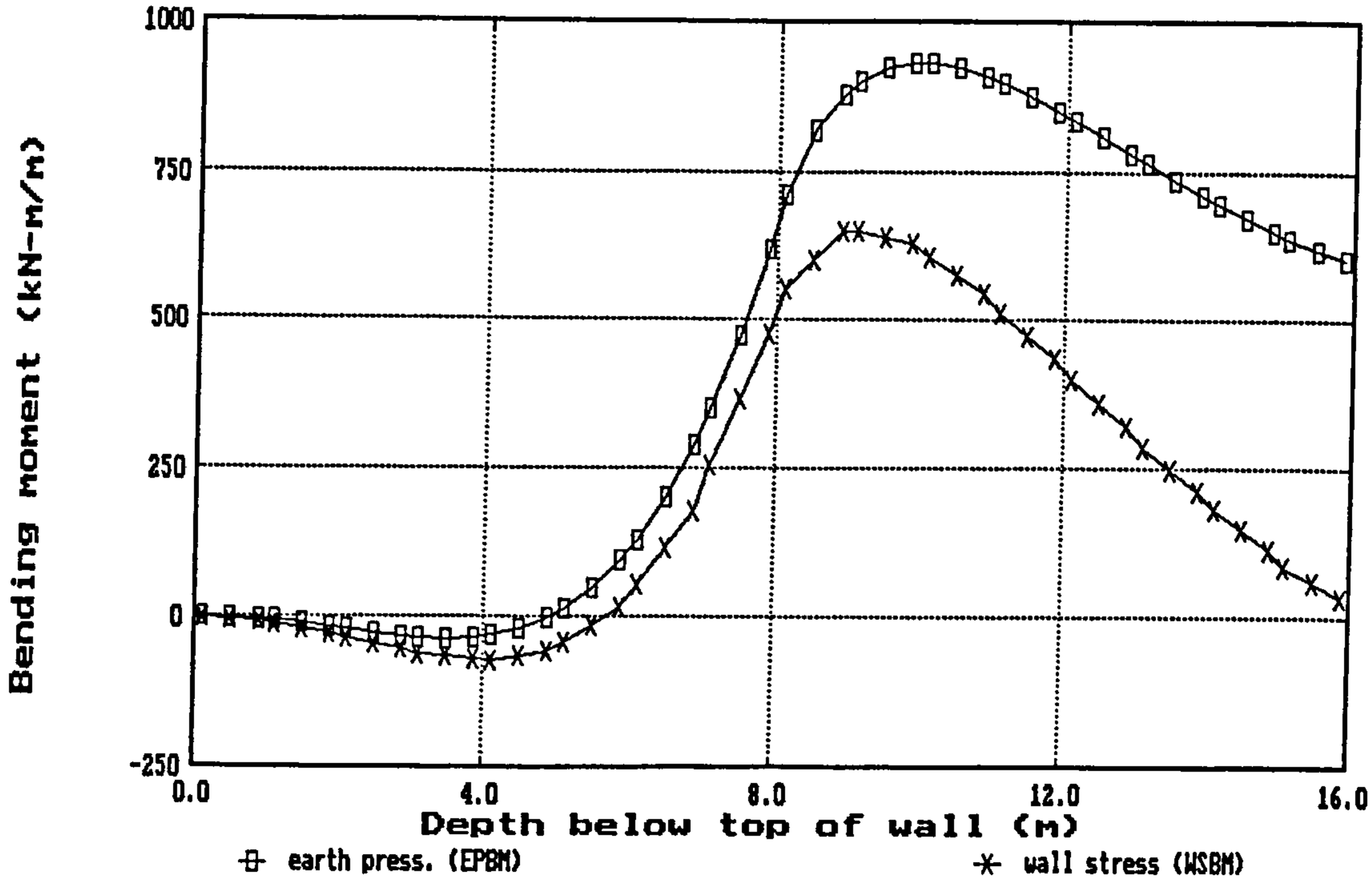

(c) Case RW53 : cantilever wall / drained / elastic soil

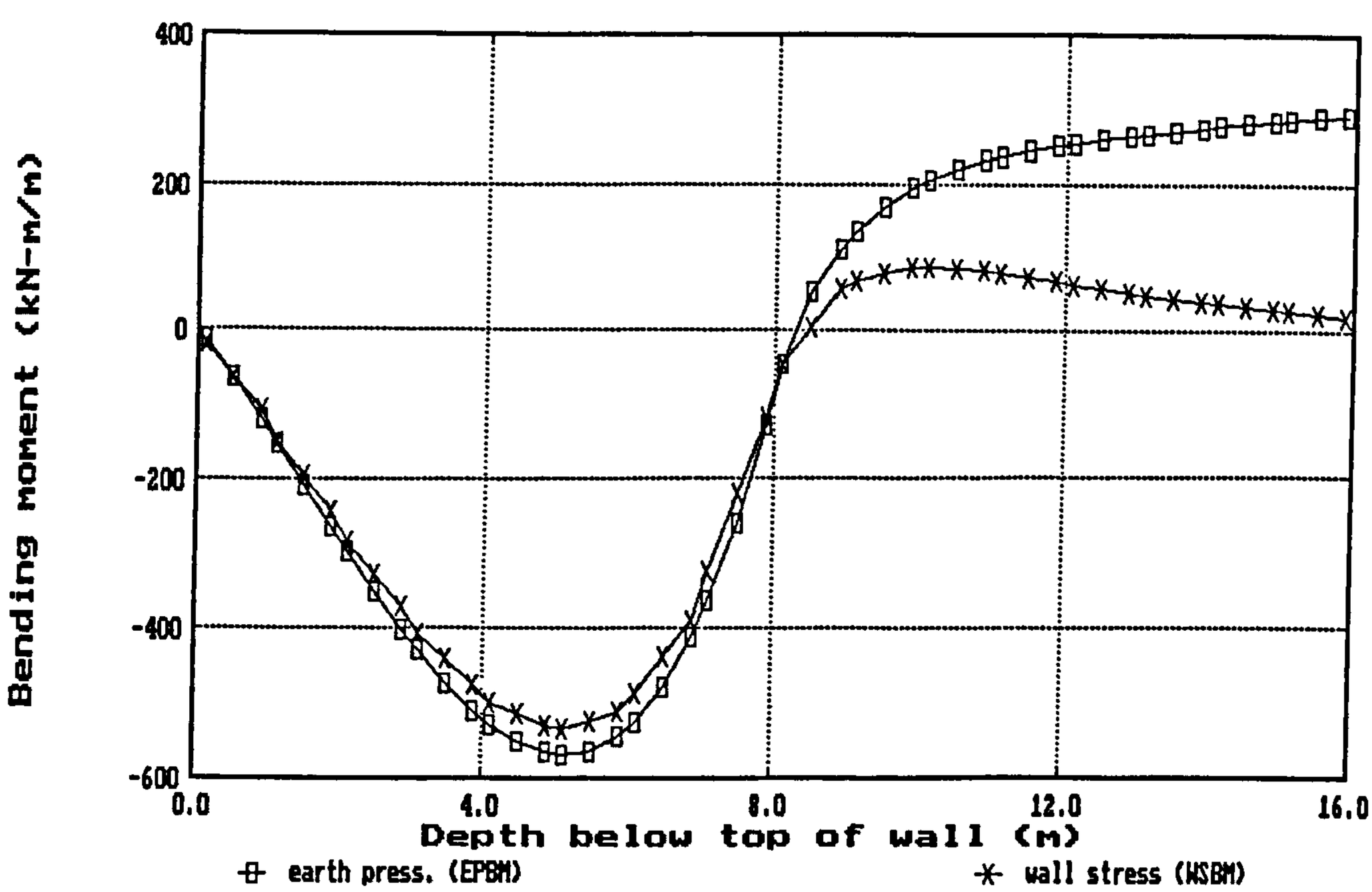

(d) Case RW61 : top-propped wall / drained / elastic soil

Fig 8.32 Wall bending moments - comparison of wall stress and earth pressure methods (contd)

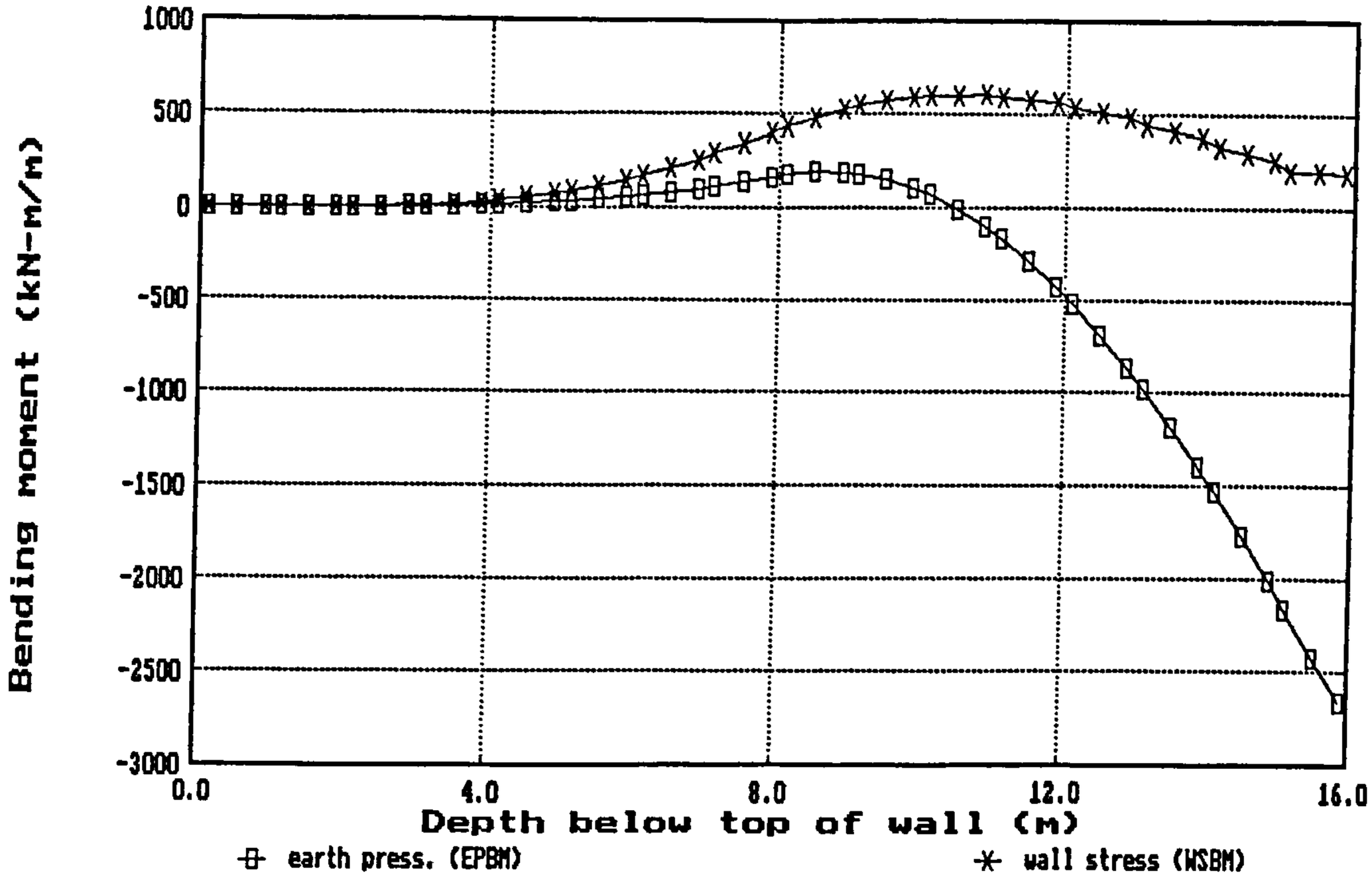

(e) Case RW103 : cantilever wall / undrained / elastic-perfectly plastic (Tresca)

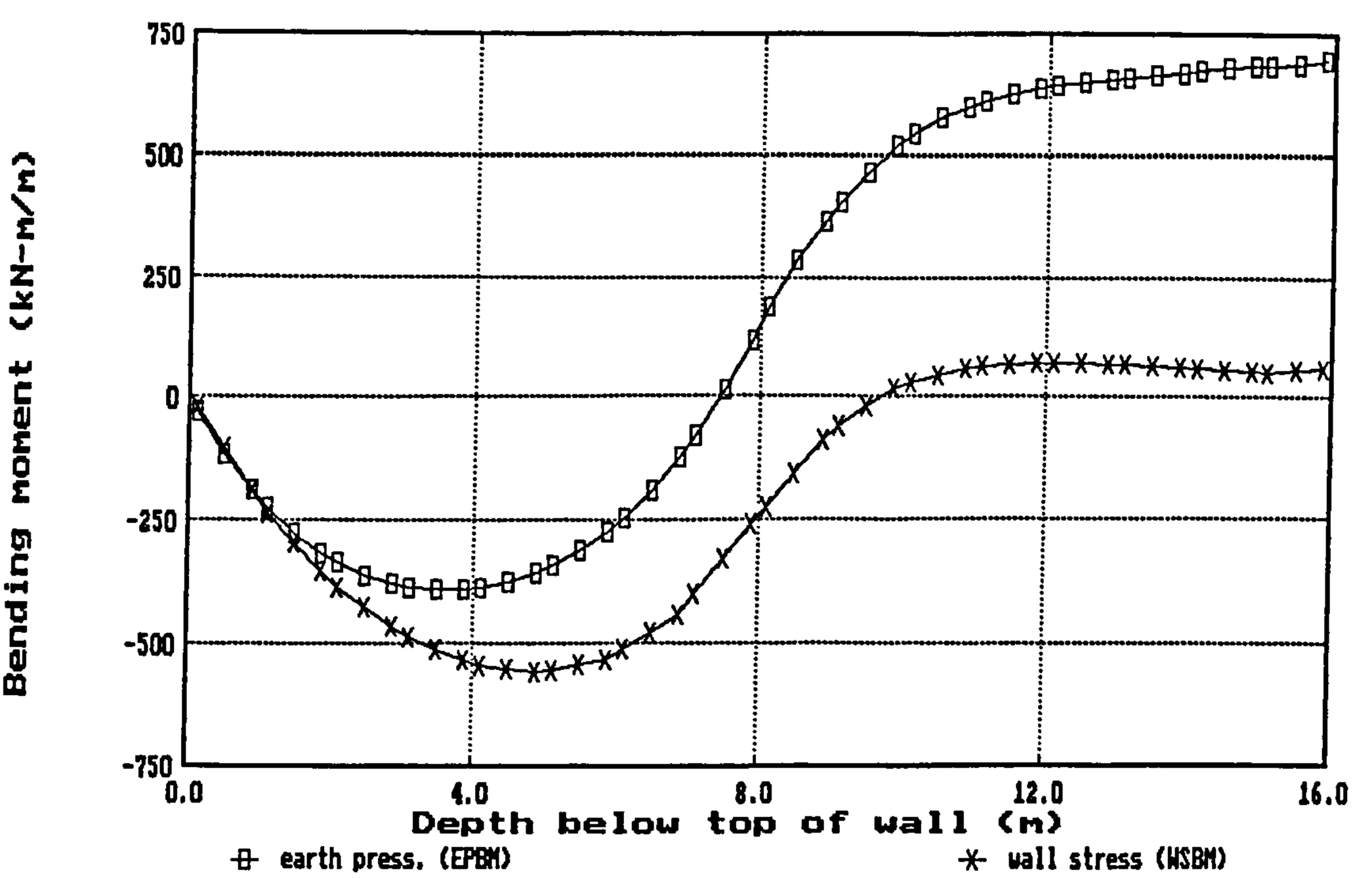

(f) Case RW112 : top-propped wall / undrained / elastic-perfectly plastic (Tresca)

Fig 8.32 Wall bending moments - comparison of wall stress and earth pressure methods (contd)

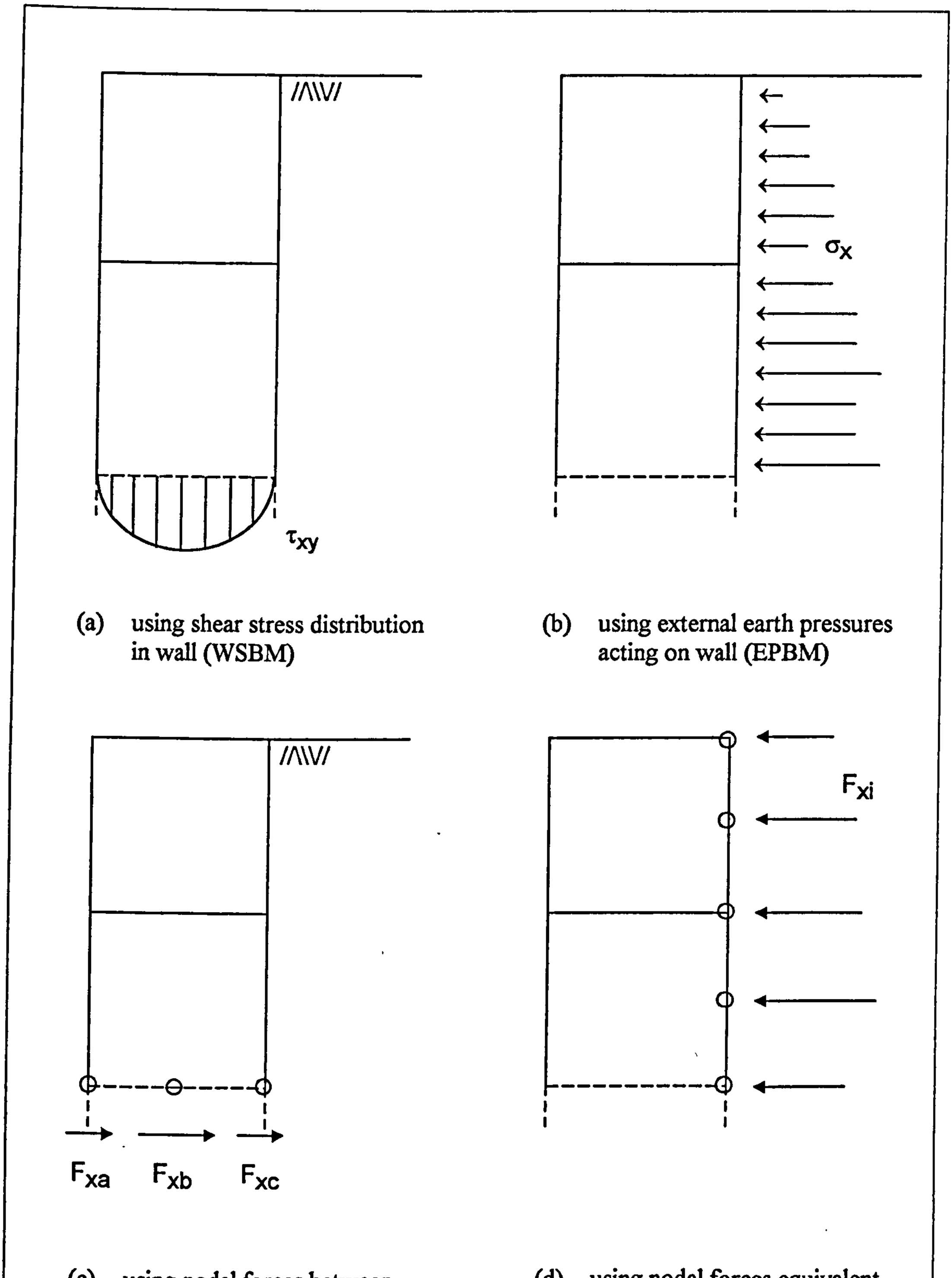

(a) using shear stress distribution in wall (WSBM)

(b) using external earth pressures acting on wall (EPBM)

(c) using nodal forces between wall elements

(d) using nodal forces equivalent to external earth pressures

Fig 8.33 Methods of calculating wall shear forces in 2D continuum elements

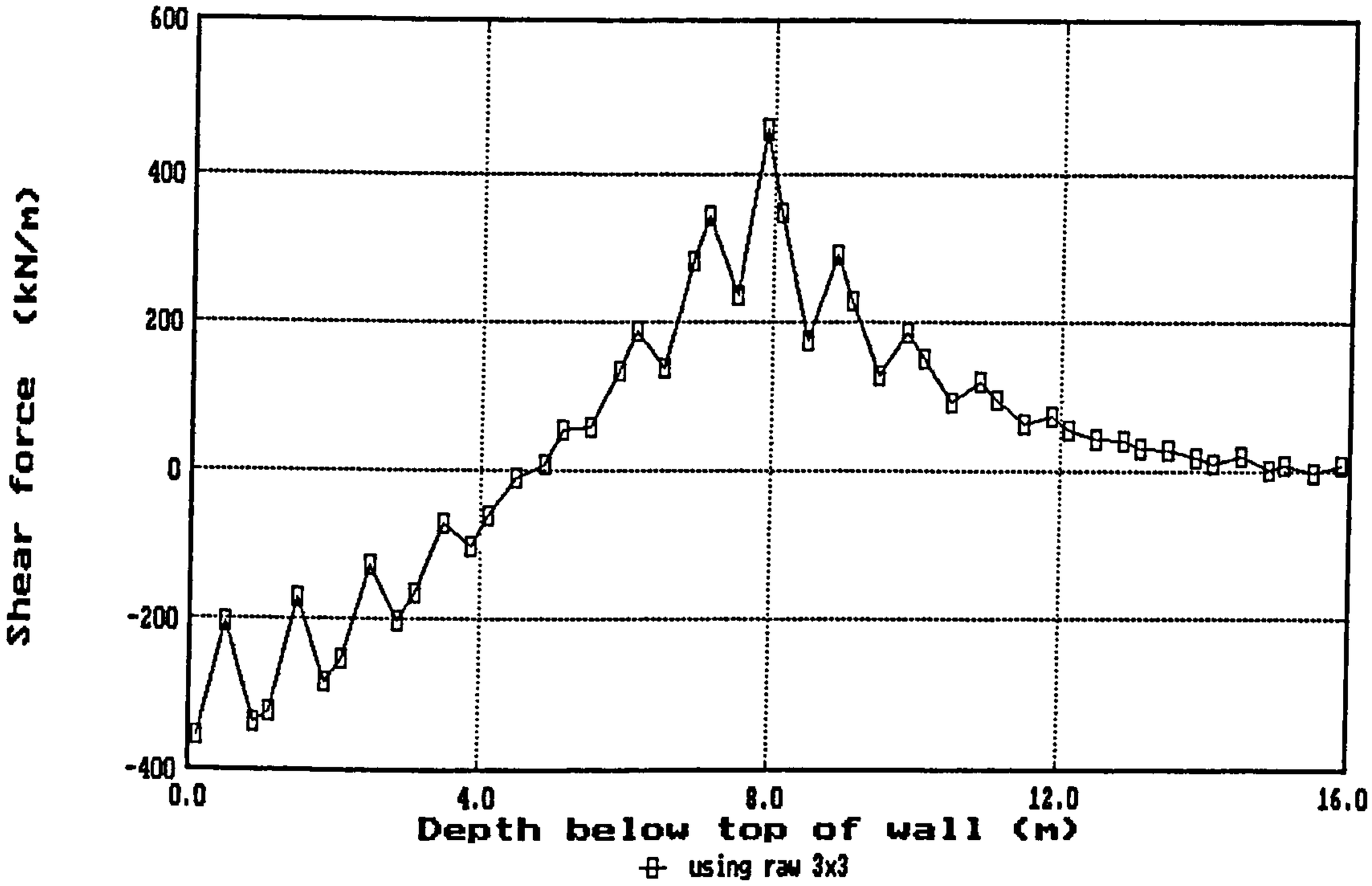

Fig 8.34 Typical wall shear force diagram based on raw Gauss point stresses

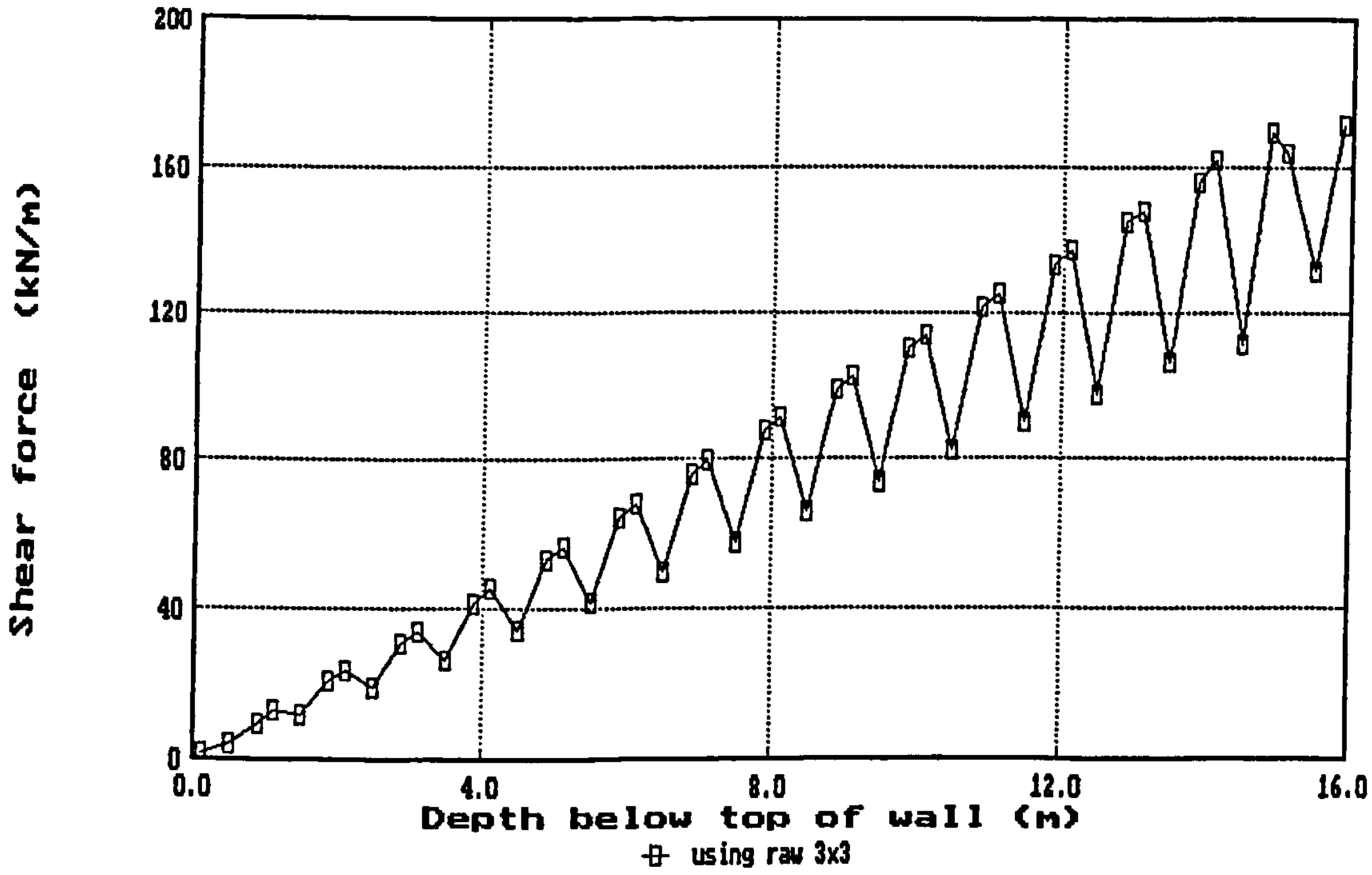

Fig 8.35 Wall stress shear force diagram for case A1 (unsmoothed τ_{xy})

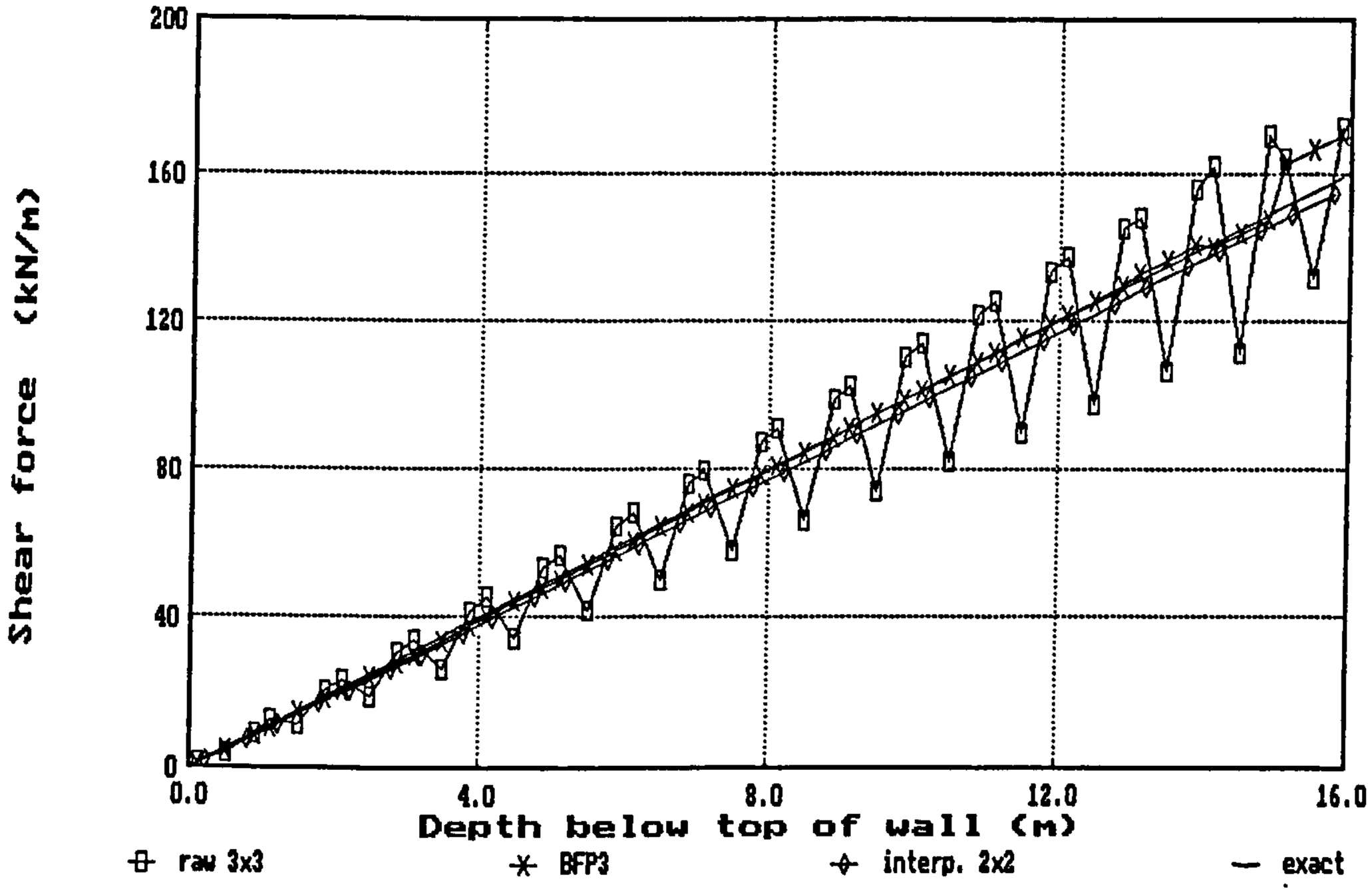

(a) Case A1 (cantilever with single UDL)

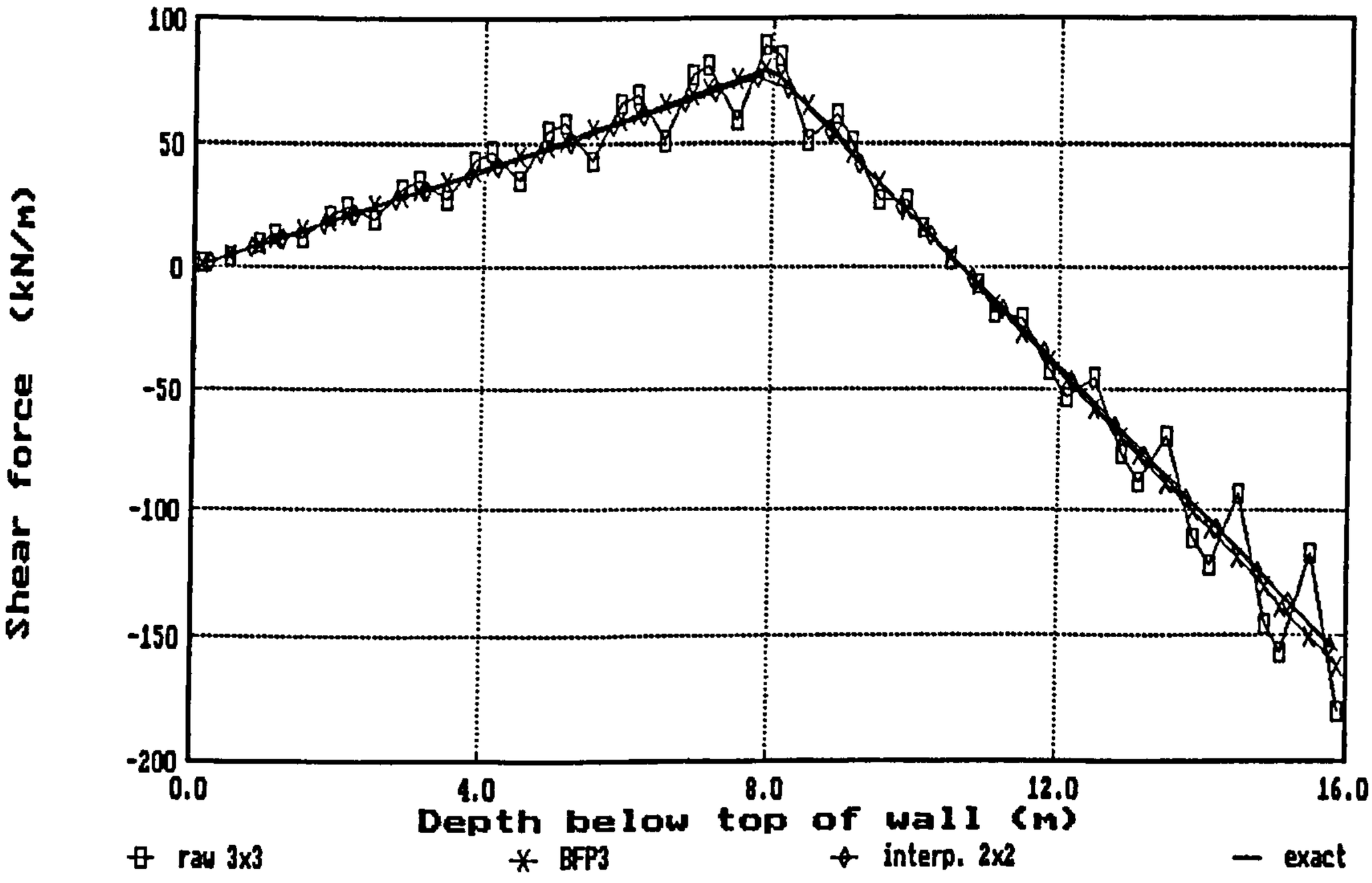

(b) Case B1 (cantilever with twin UDLs)

Fig 8.36 Wall stress shear forces for benchmark cases - best-fit plane (3×3) and interpolated (2×2) smoothing of τ_{xy}

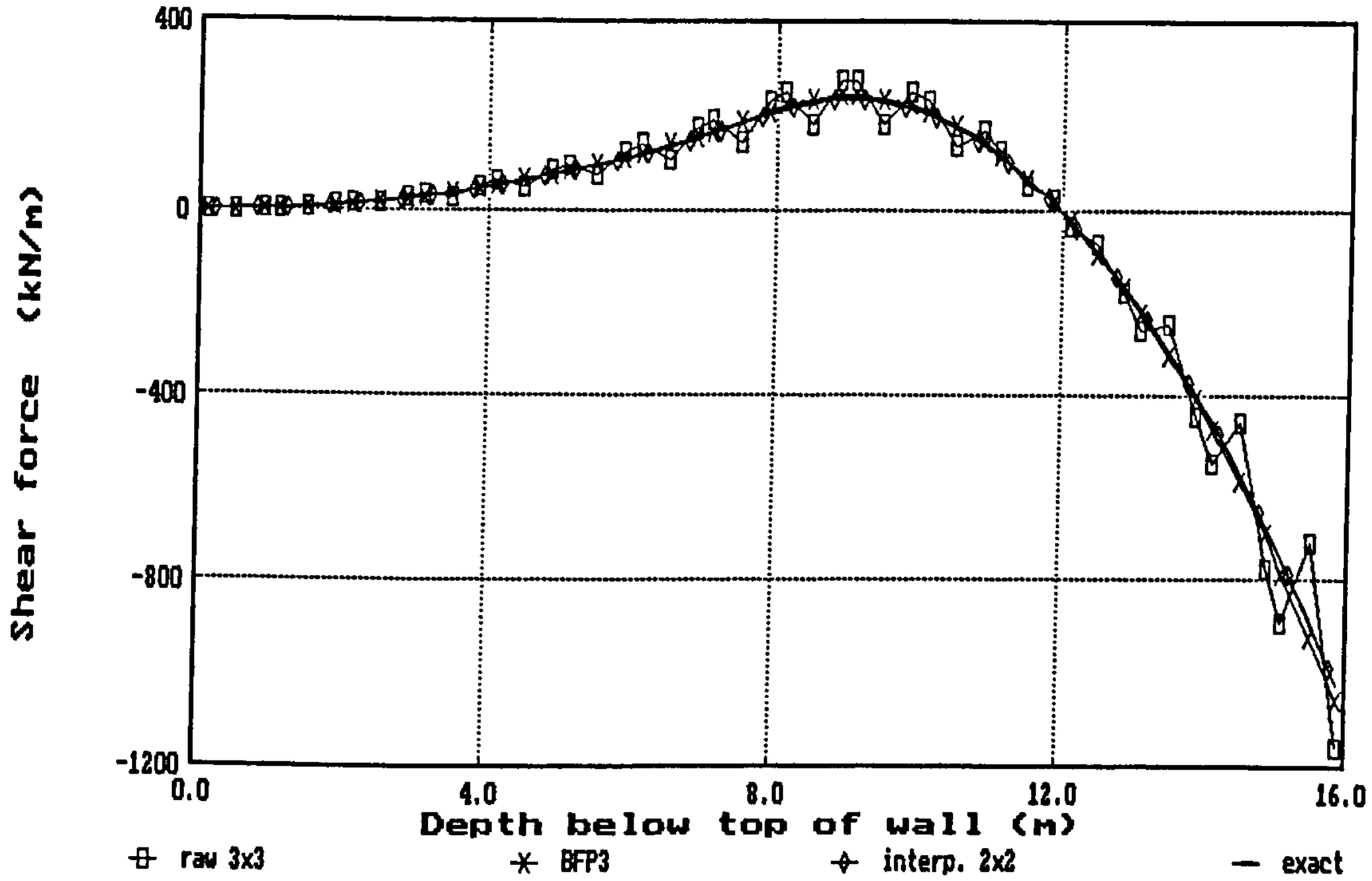

(c) Case C1 (cantilever with twin linearly varying loads)

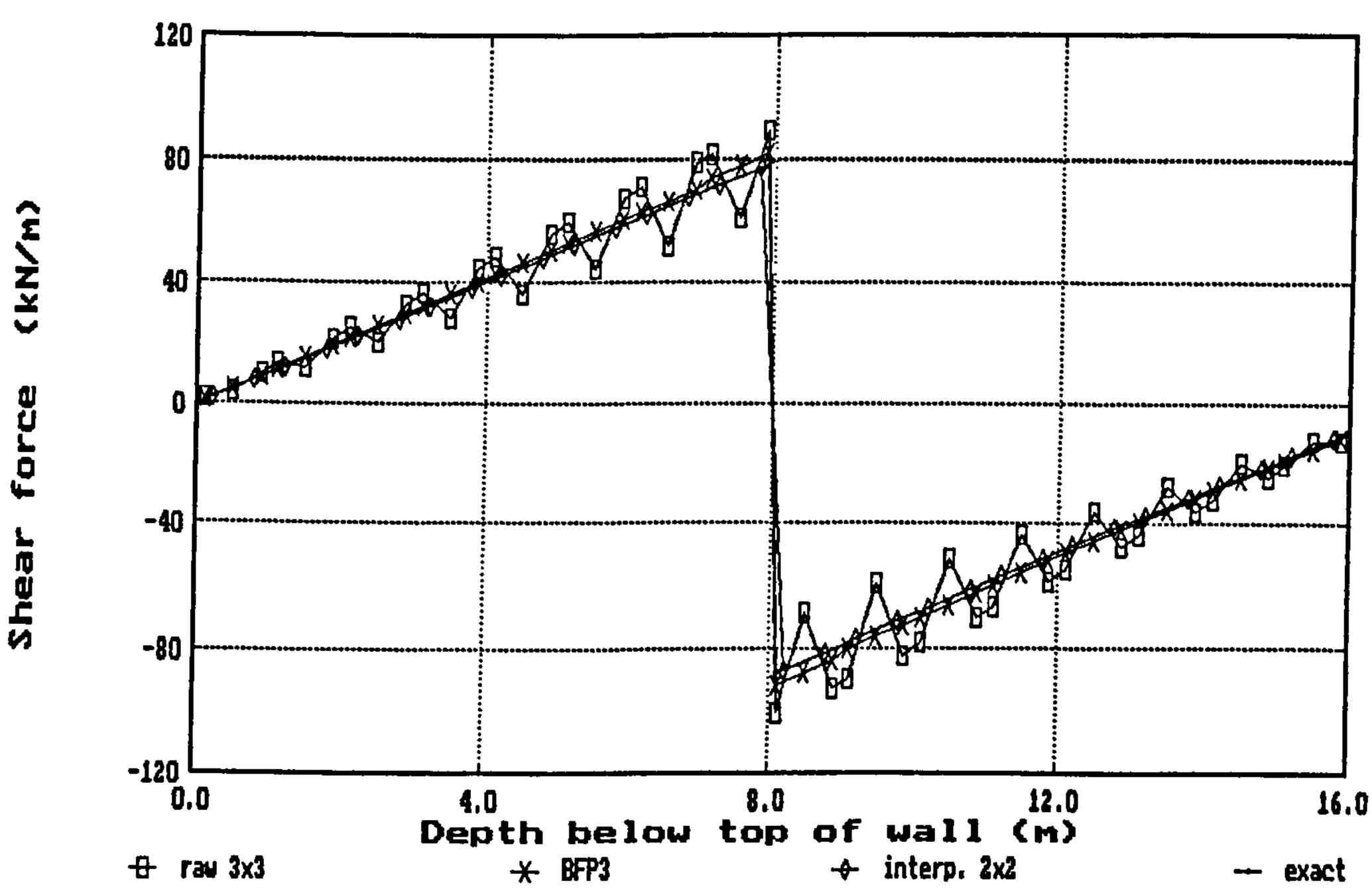

(d) Case A2 (mid-height propped cantilever with single UDL)

Fig 8.36 Wall stress shear forces for benchmark cases - best-fit plane (3×3) and interpolated (2×2) smoothing of τ_{xy}

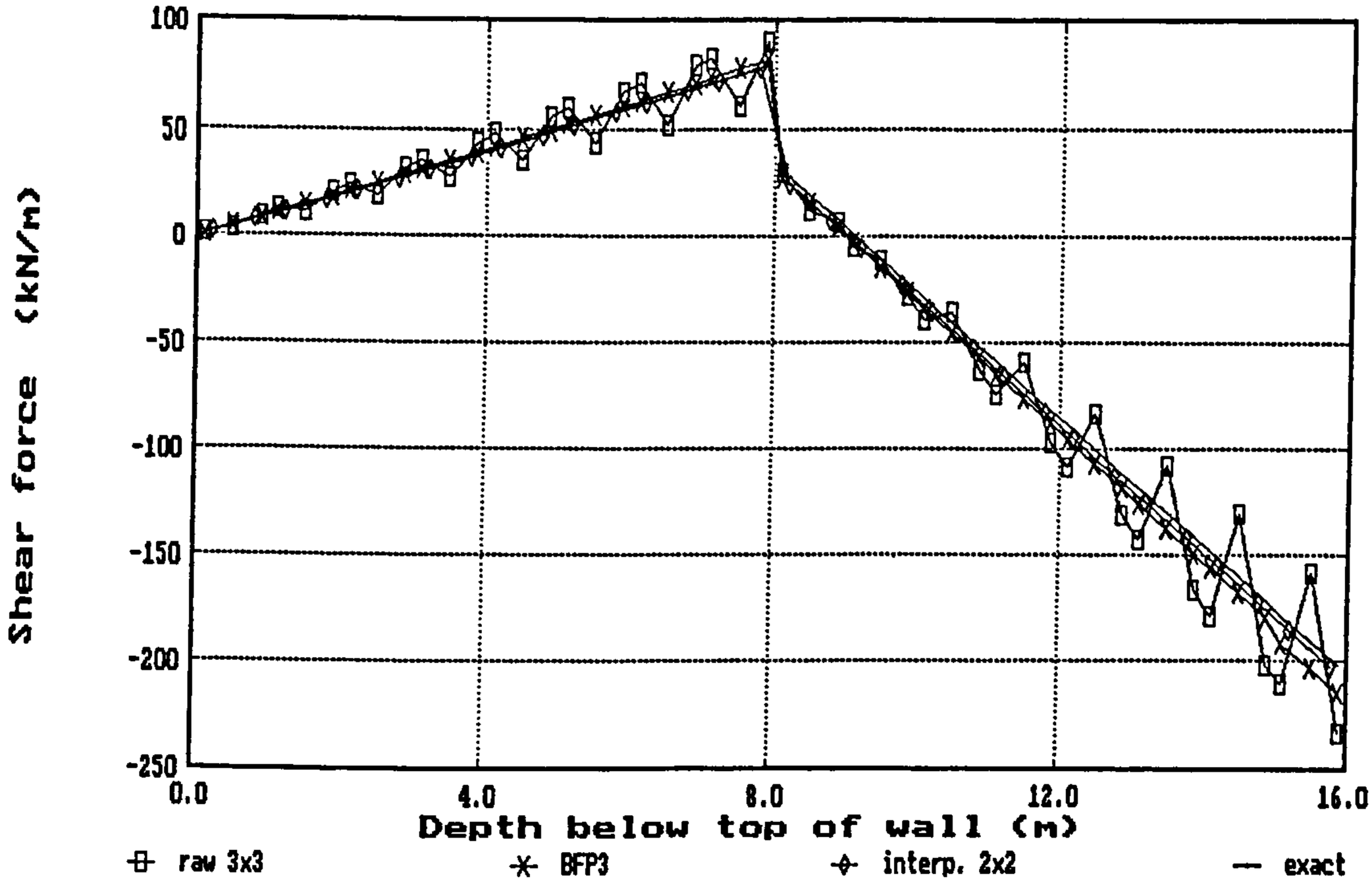

(e) Case B2 (mid-height propped cantilever with twin UDLs)

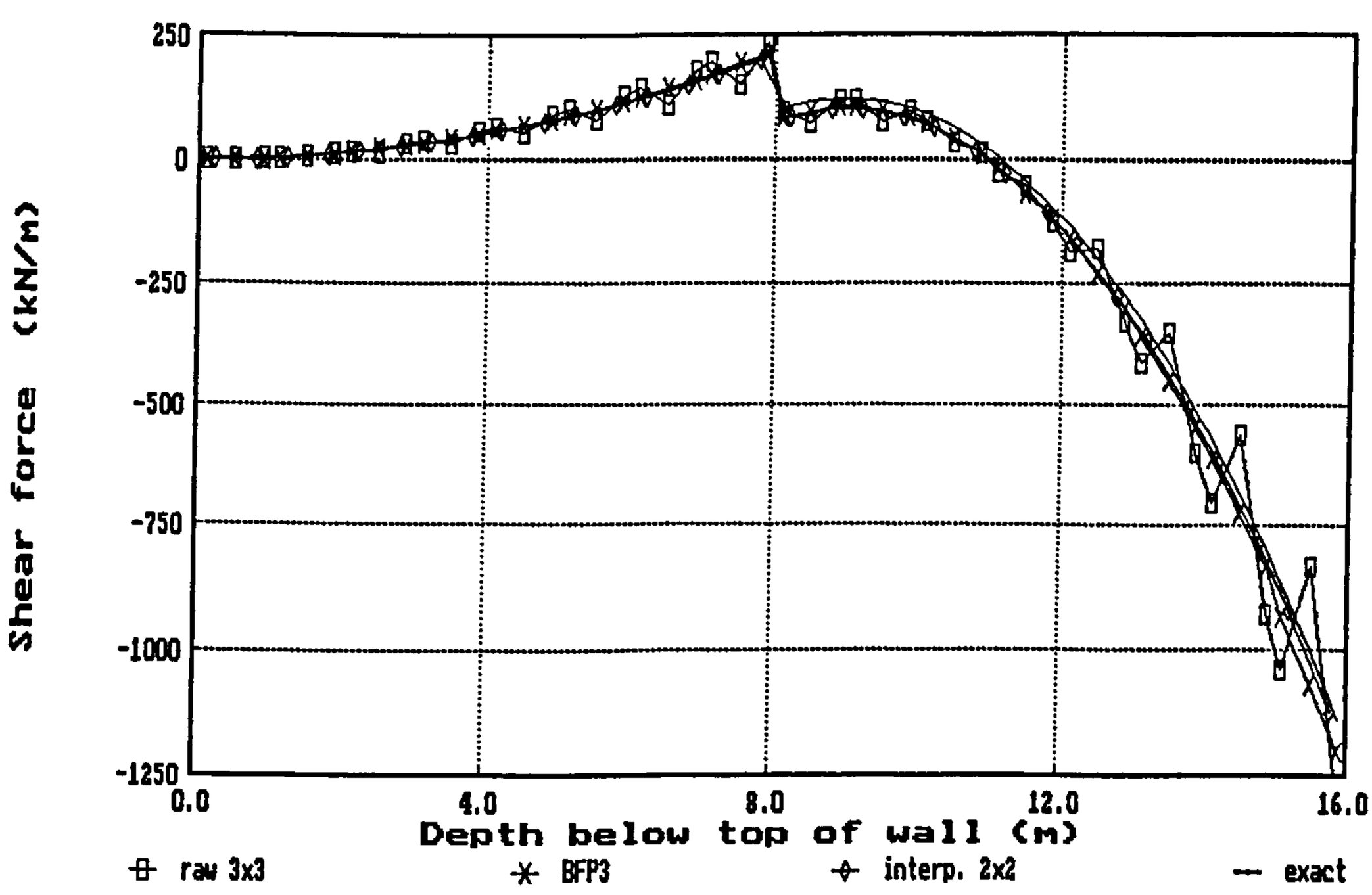

(f) Case C2 (mid-height propped cantilever with twin linearly varying loads)

Fig 8.36 Wall stress shear forces for benchmark cases - best-fit plane (3×3) and interpolated (2×2) smoothing of τ_{xy}

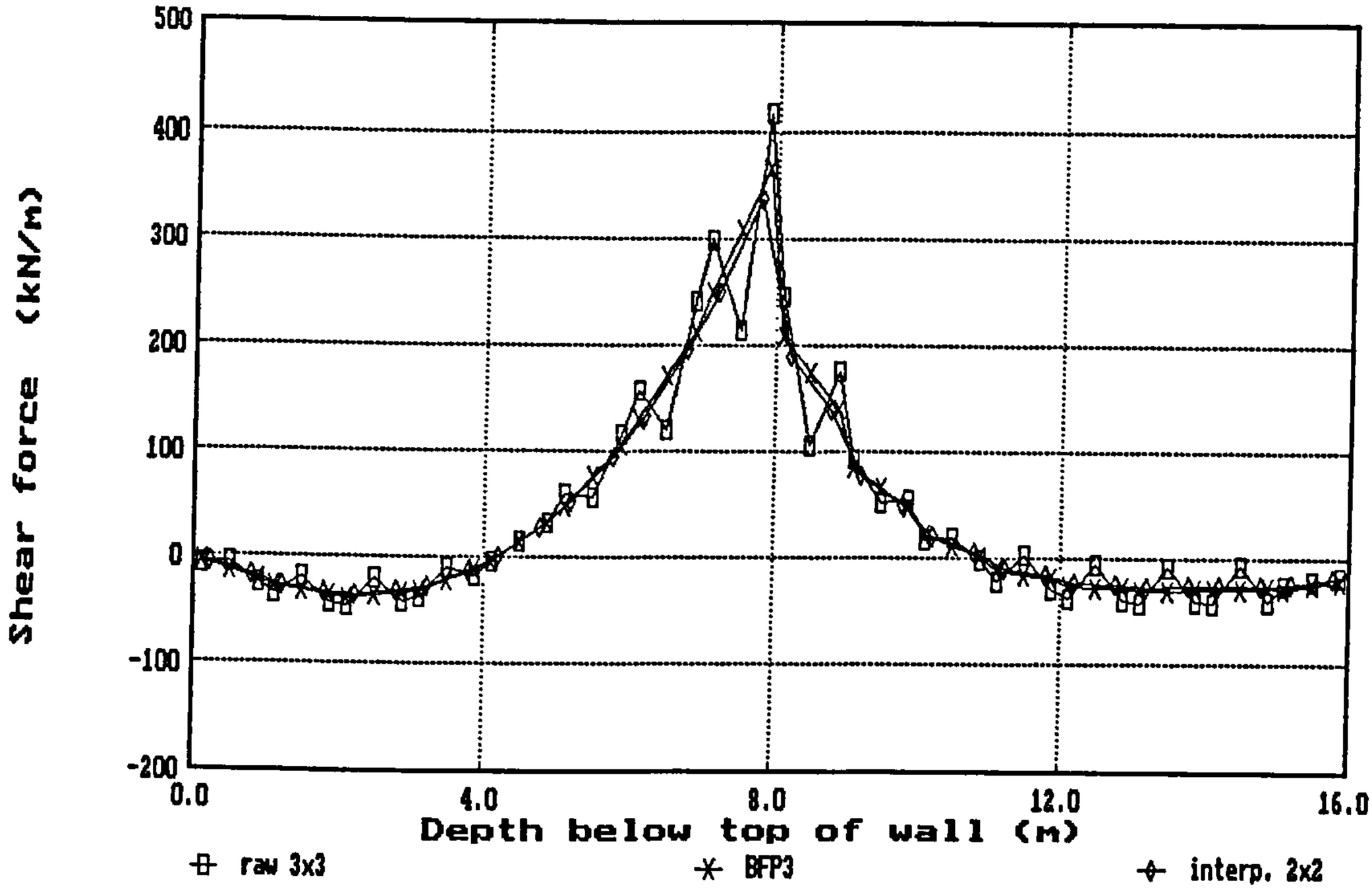

(a) Case RW3 : cantilever wall / undrained / elastic soil

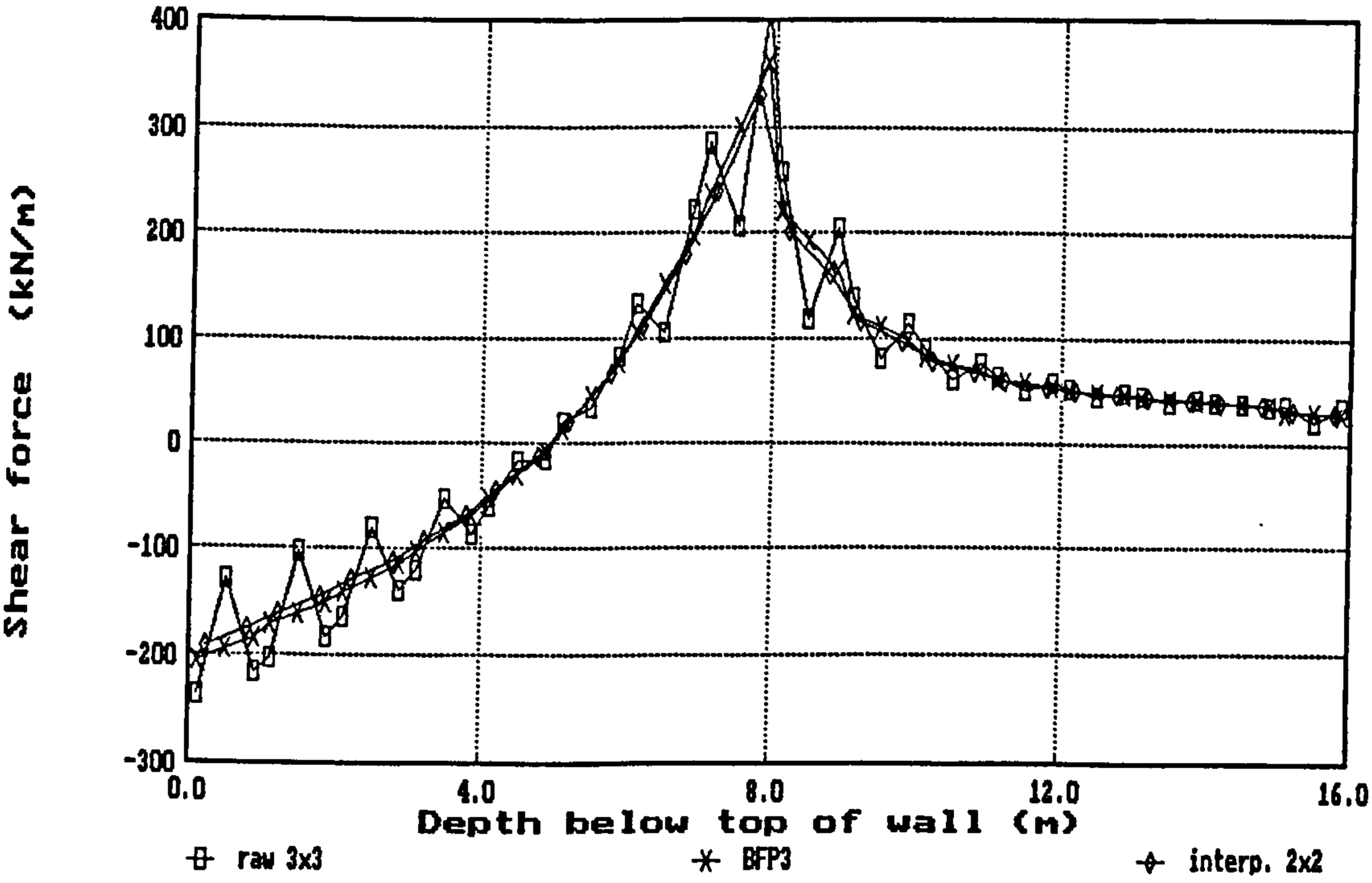

(b) Case RW11 : top-propped wall / undrained / elastic soil

Fig 8.37 Wall shear forces - comparison of wall stress methods using raw 3×3 and interpolated 2×2 Gauss point stresses

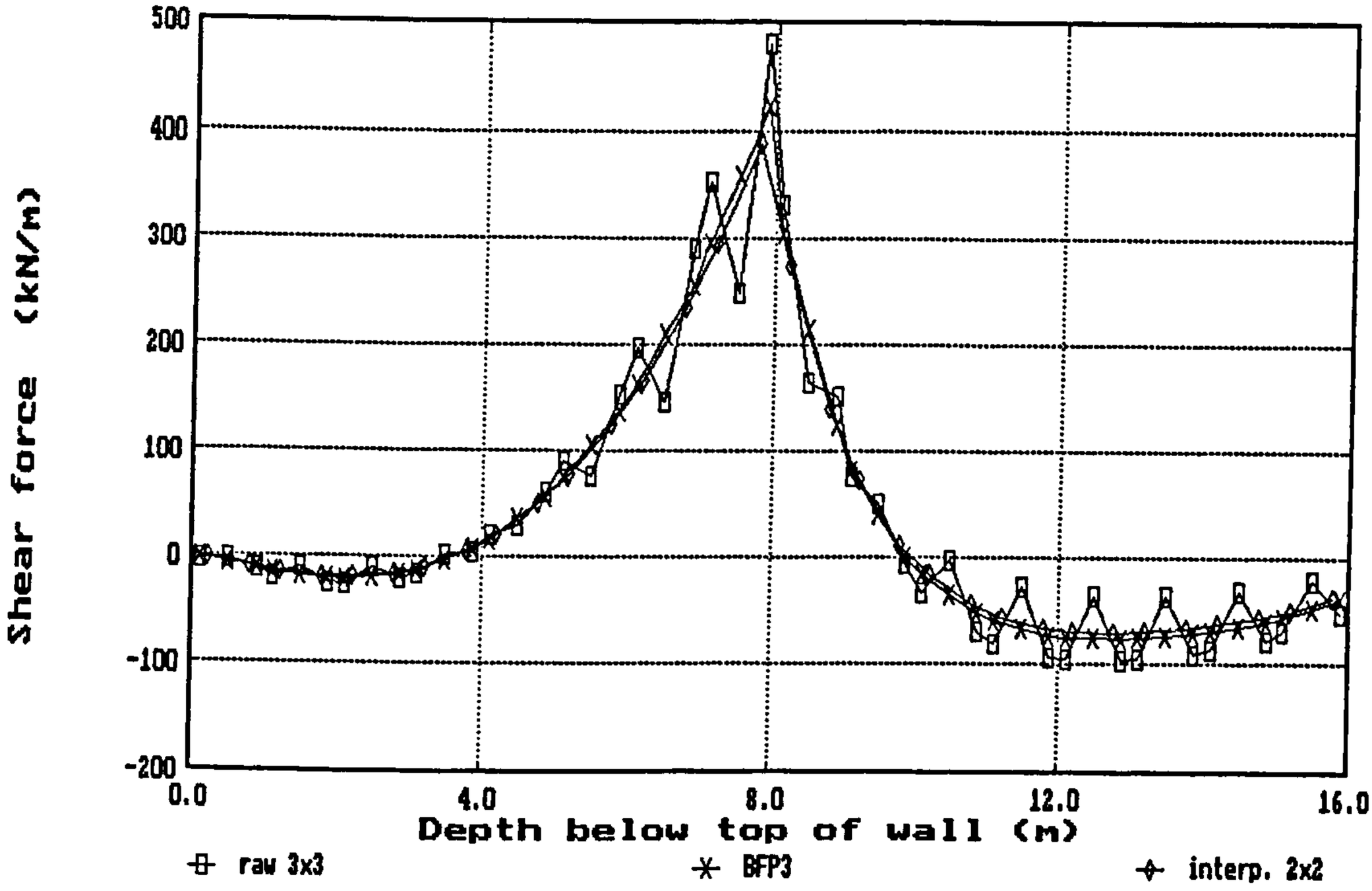

(c) Case RW53 : cantilever wall / drained / elastic soil

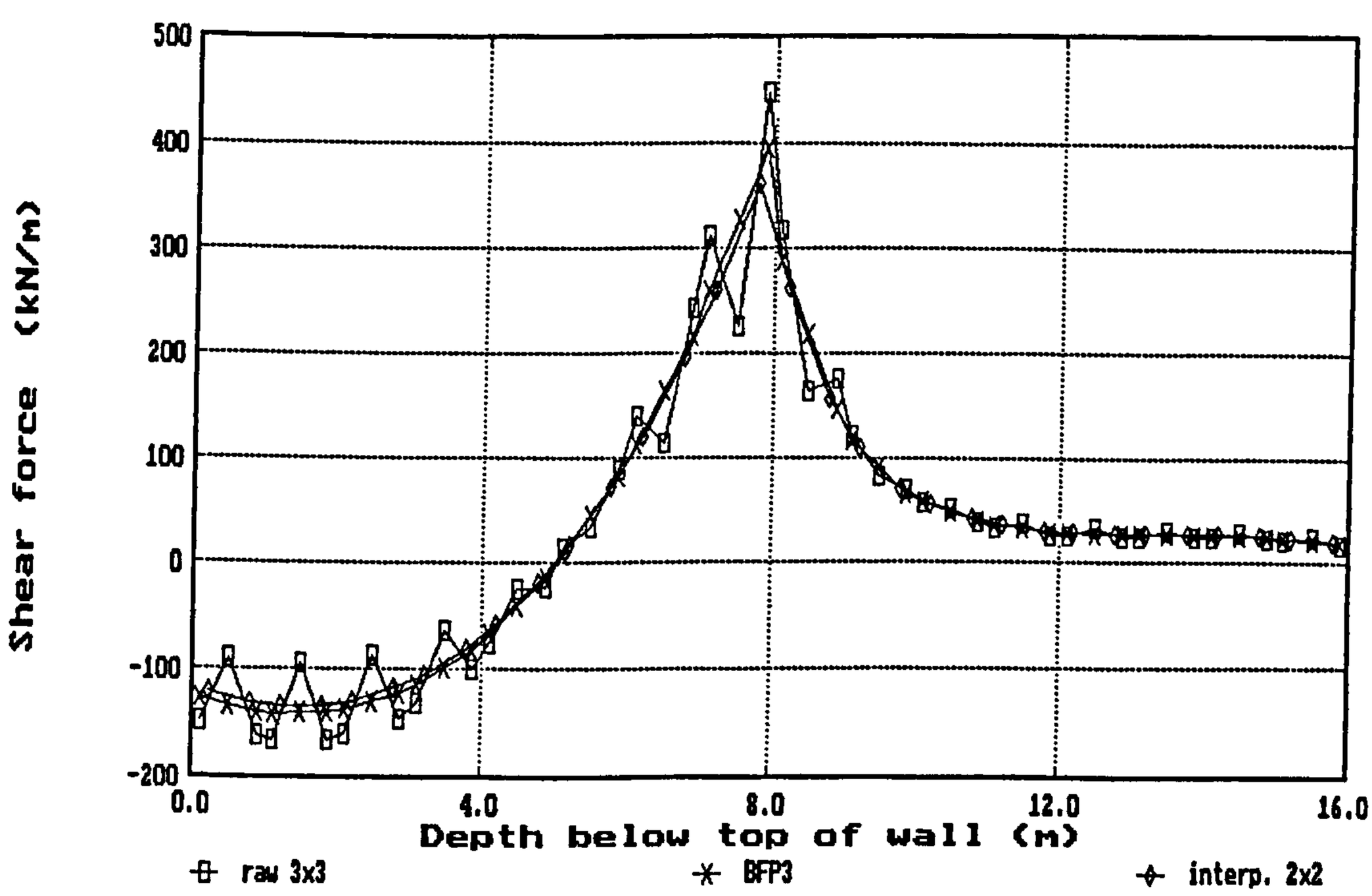

(d) Case RW61 : top-propped wall / drained / elastic soil

Fig 8.37 Wall shear forces - comparison of wall stress methods using raw 3×3 and interpolated 2×2 Gauss point stresses (contd)

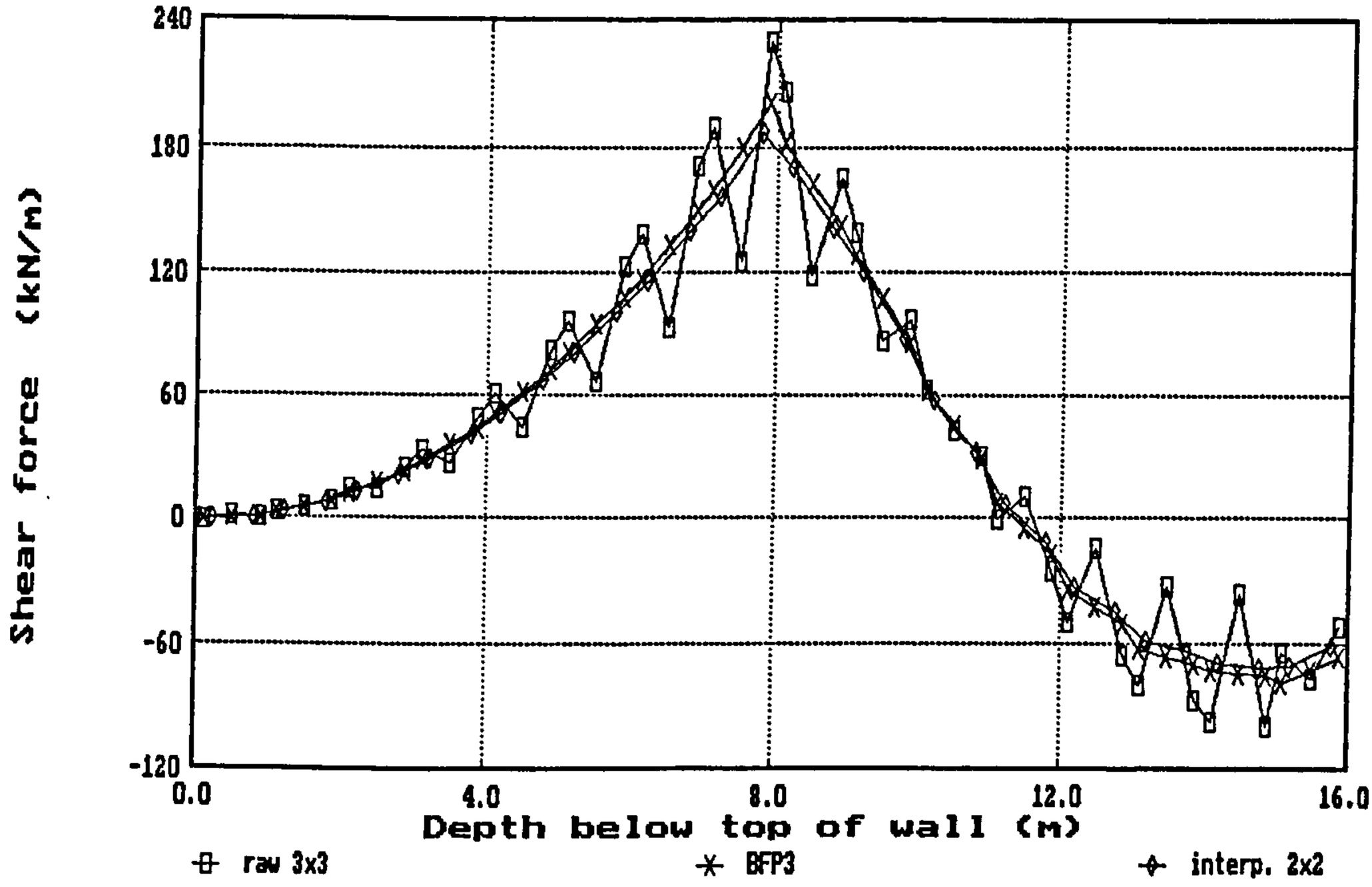

(e) Case RW103 : cantilever wall / undrained / elastic-perfectly plastic (Tresca)

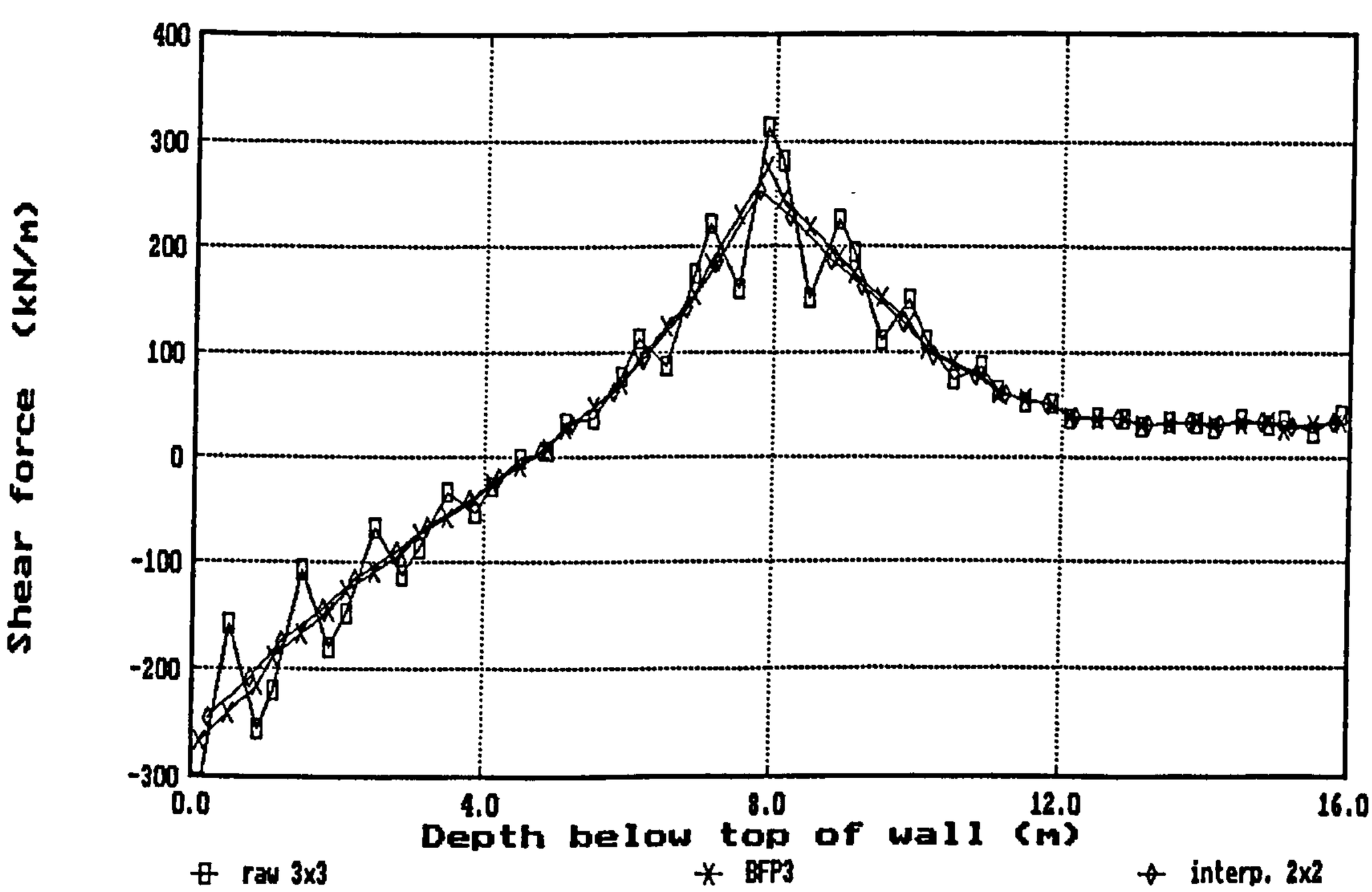

(f) Case RW112 : cantilever wall / undrained / elastic-perfectly plastic (Tresca)

Fig 8.37 Wall shear forces - comparison of wall stress methods using raw 3×3 and interpolated 2×2 Gauss point stresses (contd)

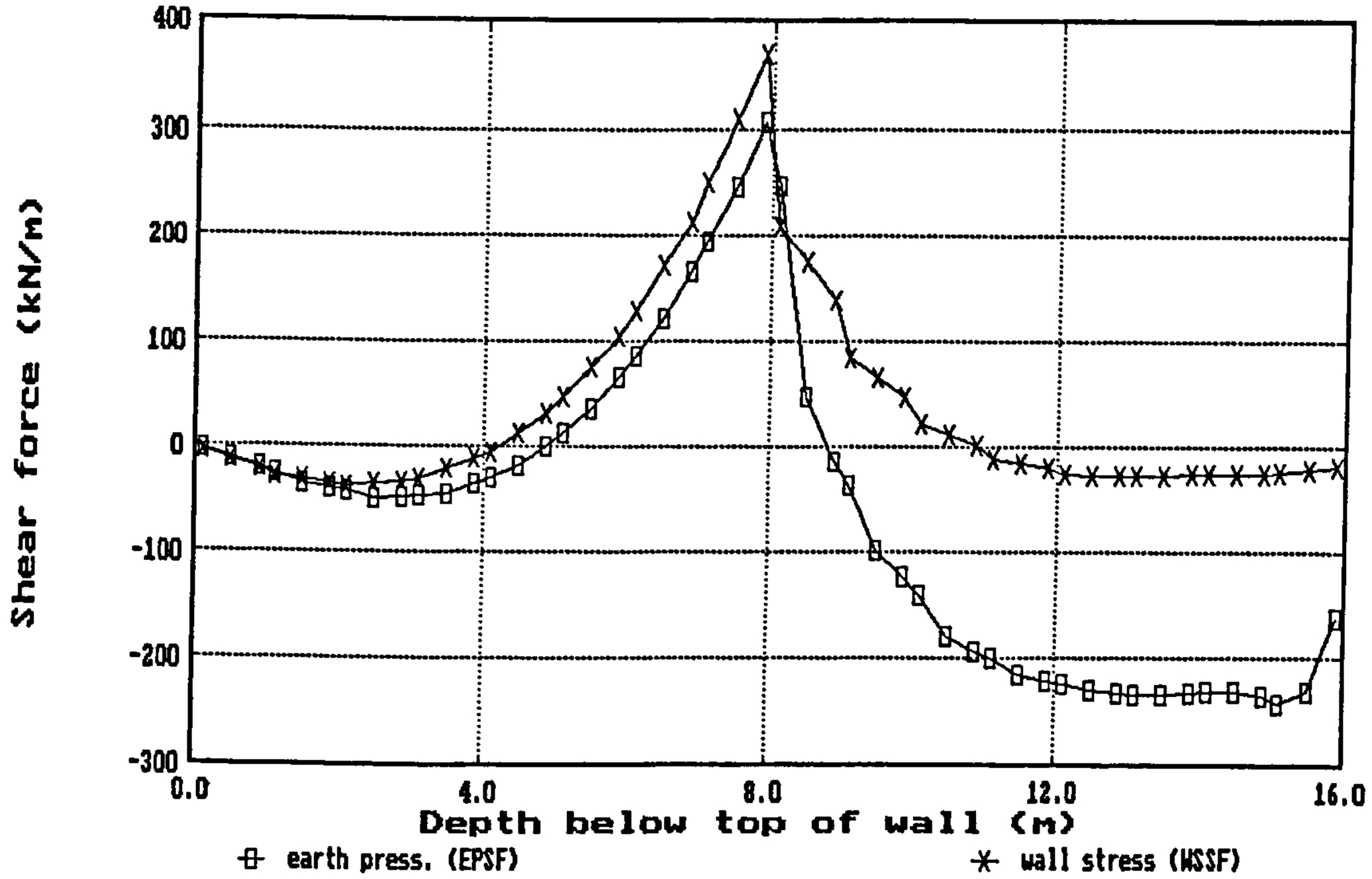

(a) Case RW3 : cantilever wall / undrained / elastic soil

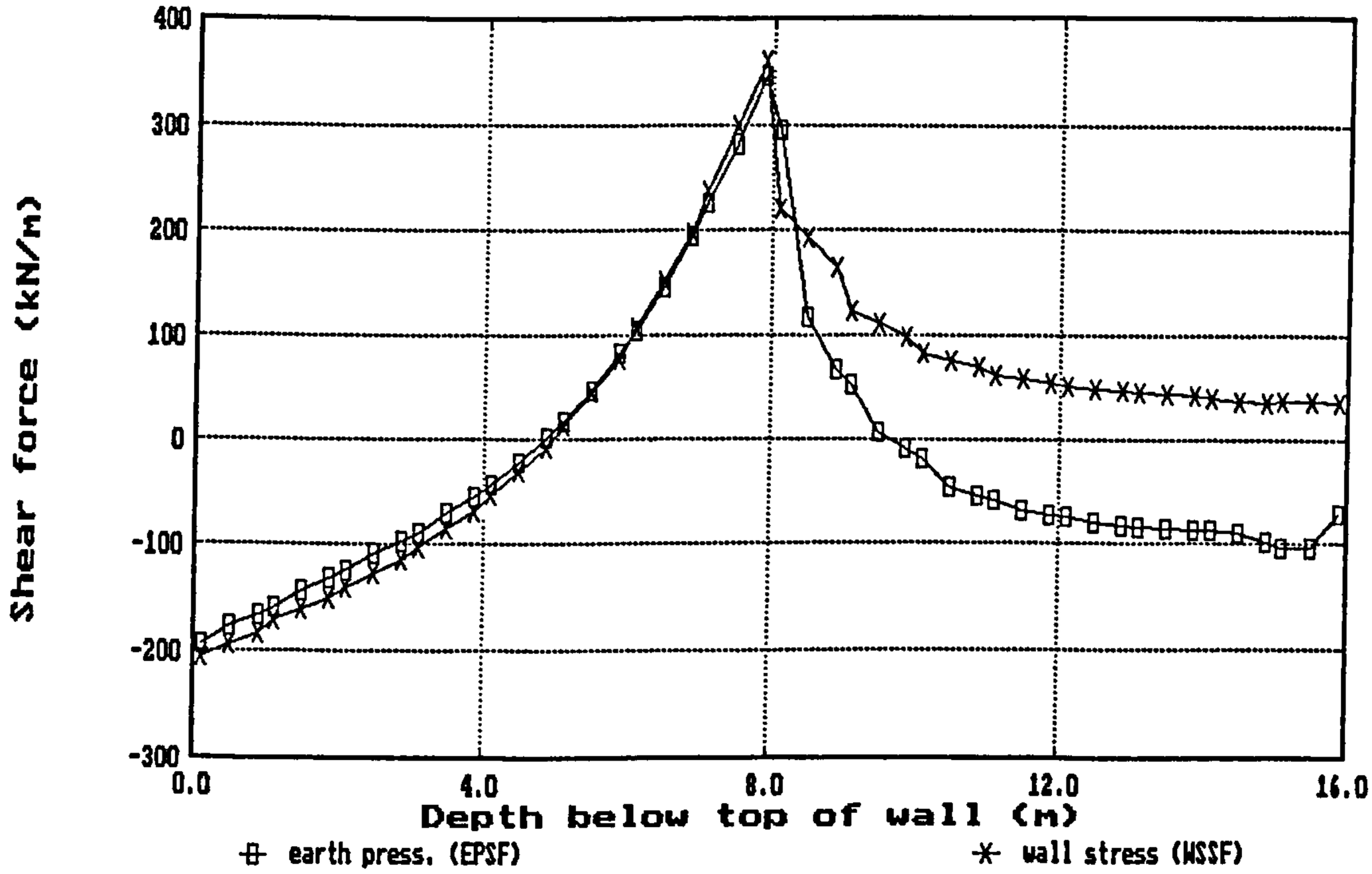

(b) Case RW11 : top-propped wall / undrained / elastic soil

Fig 8.38 Wall shear forces - comparison of wall stress and earth pressure methods

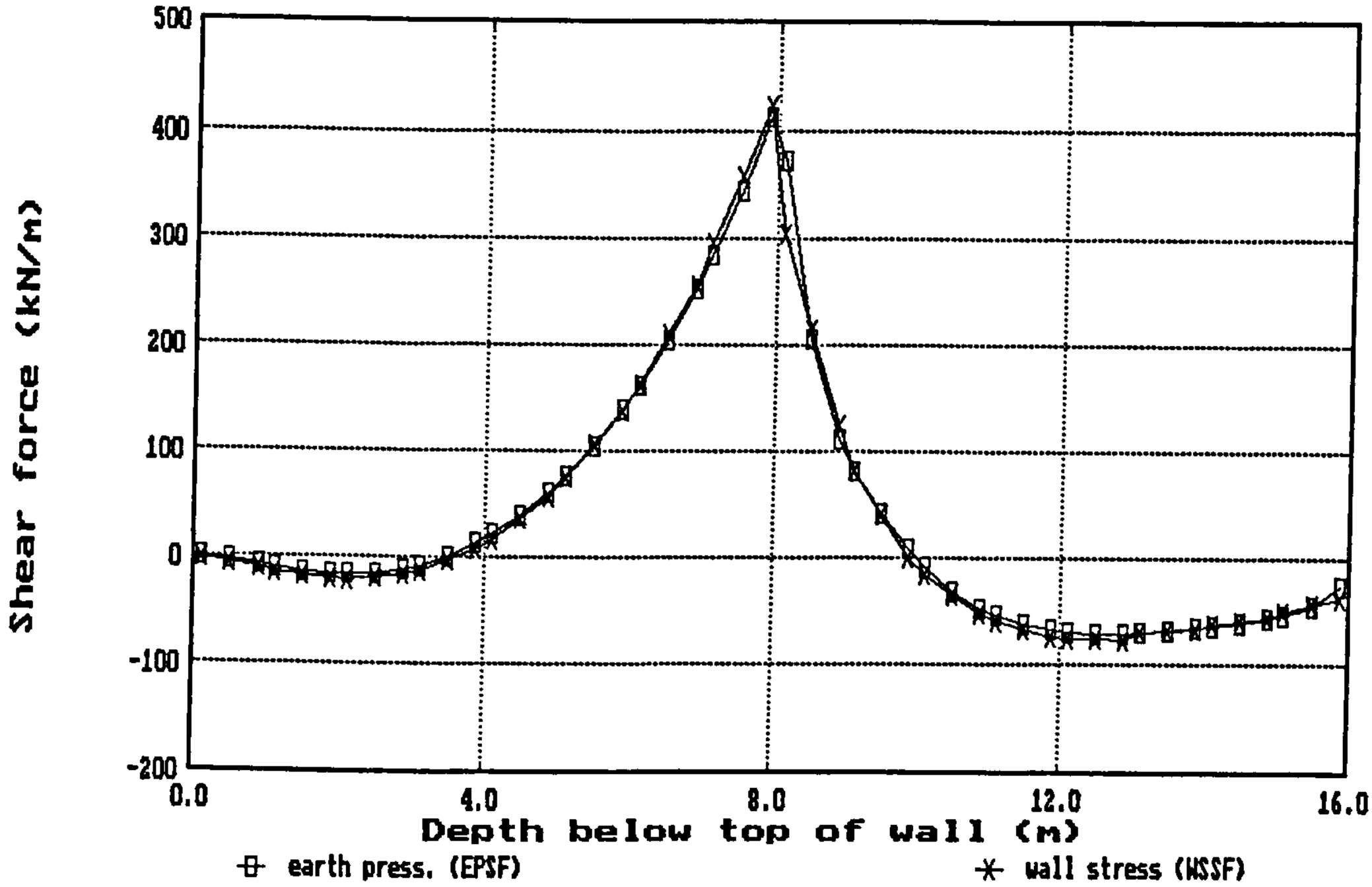

(c) Case RW53 : cantilever wall / drained / elastic soil

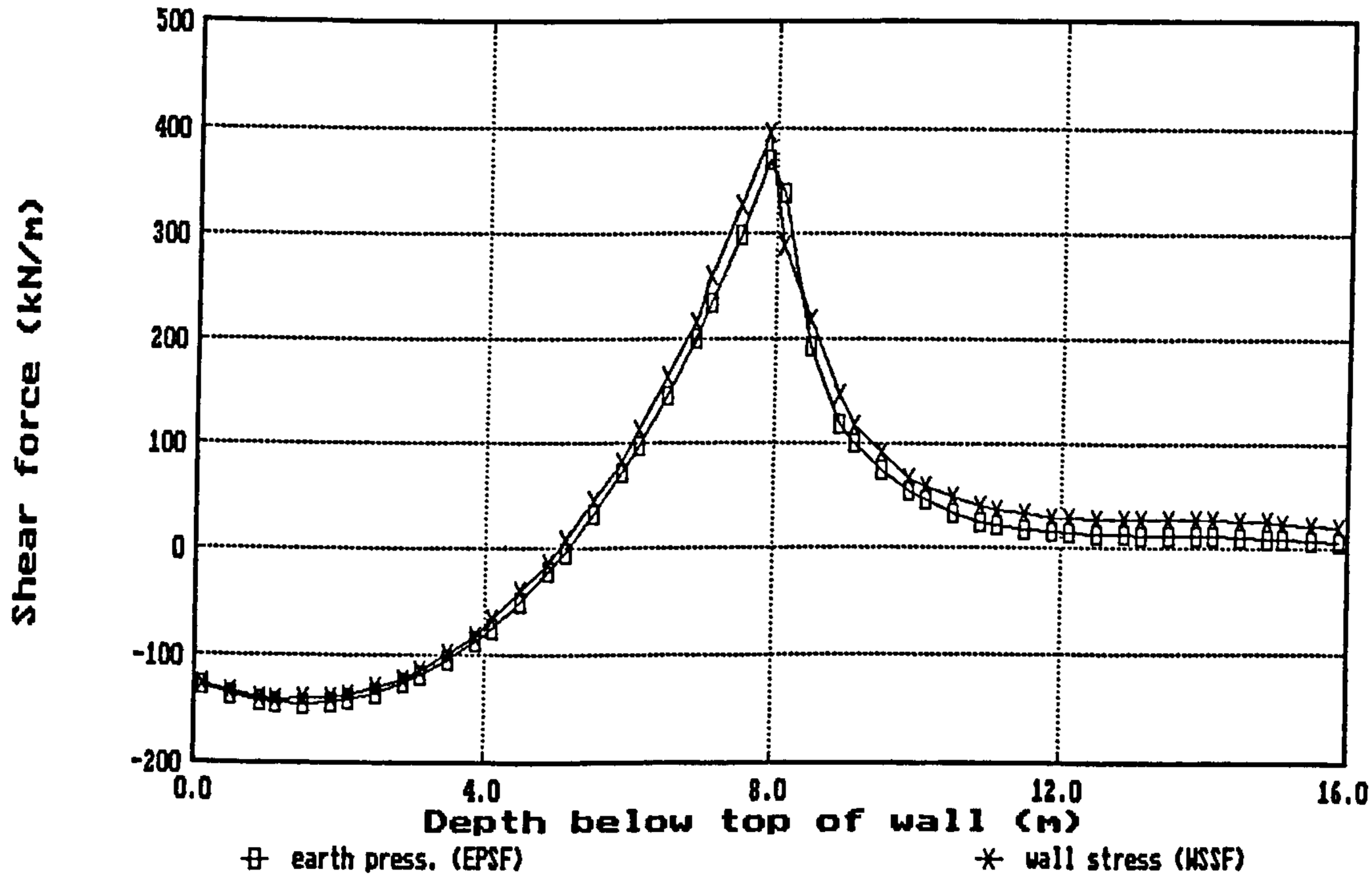

(d) Case RW61 : top-propped wall / drained / elastic soil

Fig 8.38 Wall shear forces - comparison of wall stress and earth pressure methods (contd)

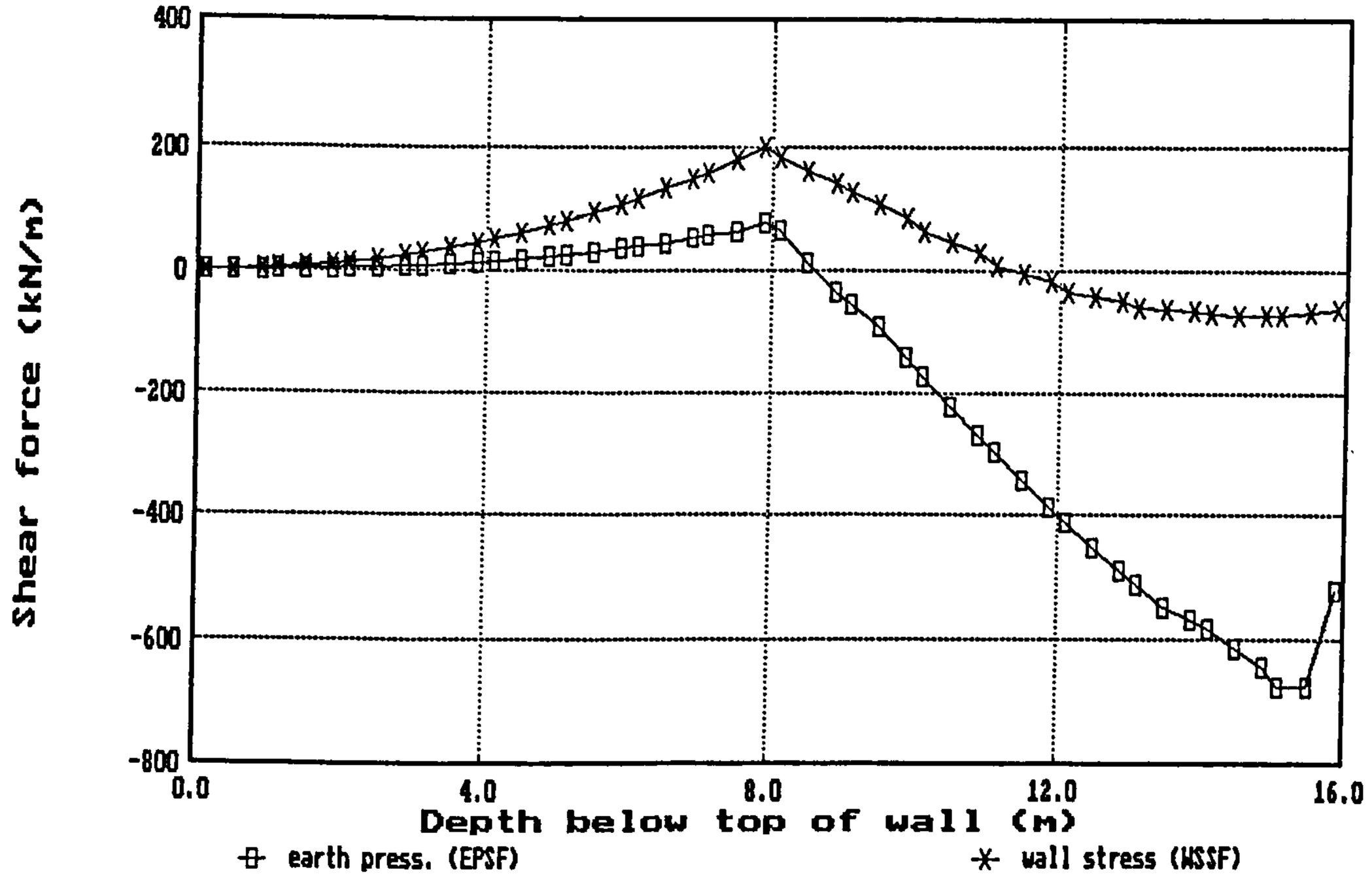

(e) Case RW103 : cantilever wall / undrained / elastic-perfectly plastic (Tresca)

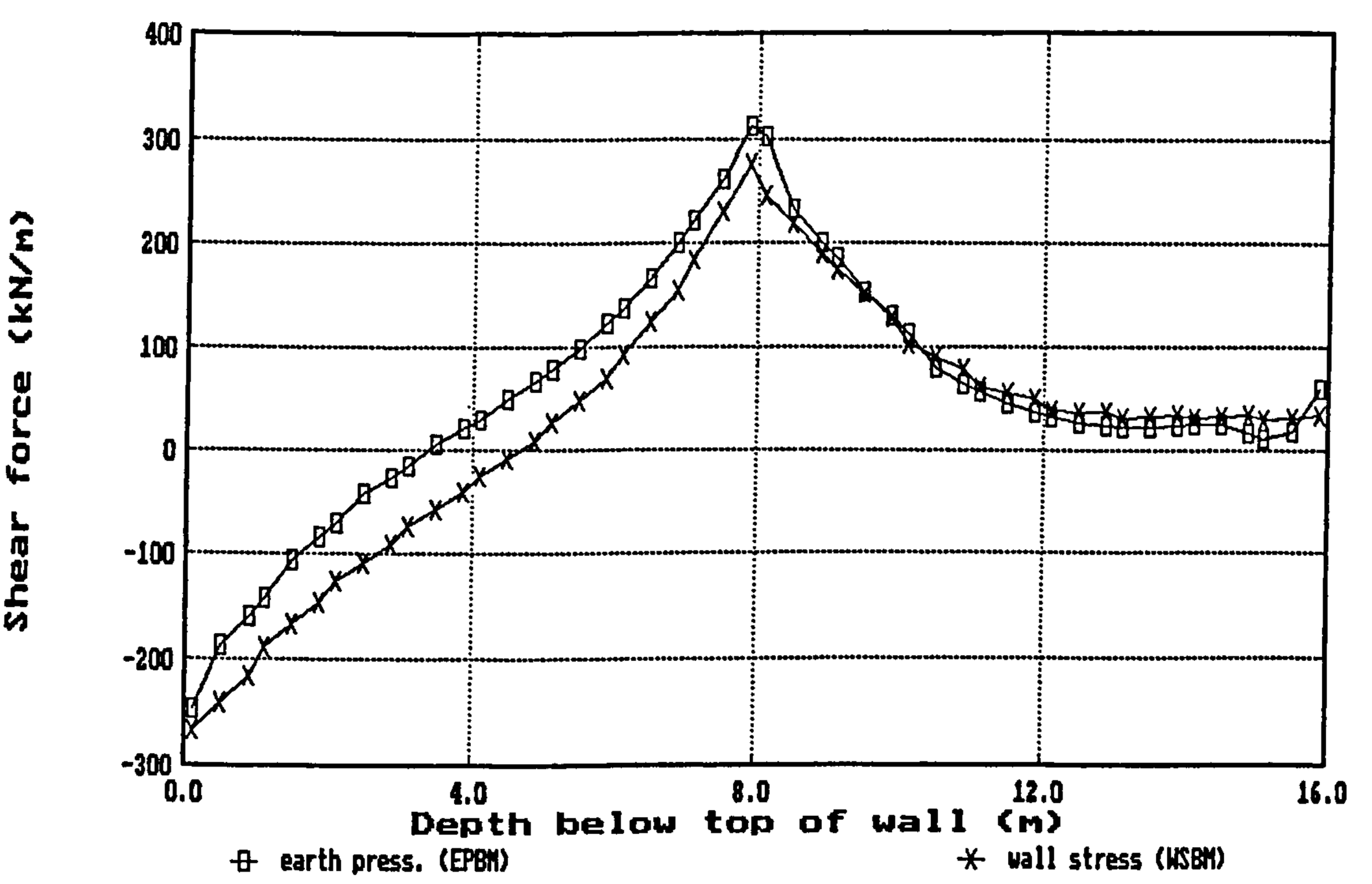

(f) Case RW112 : cantilever wall / undrained / elastic-perfectly plastic (Tresca)

Fig 8.38 Wall shear forces - comparison of wall stress and earth pressure methods (contd)

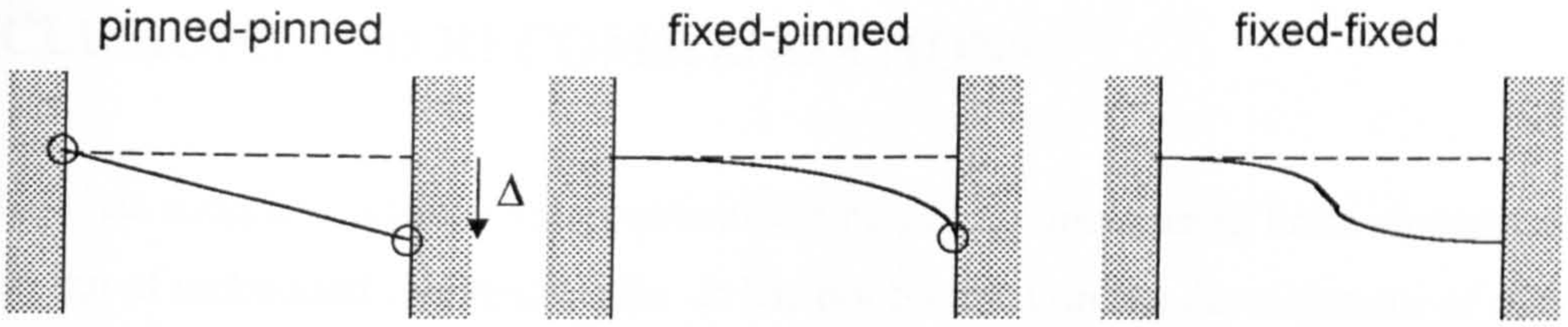

Transferable actions

P	✓	✓	✓	✓	✓	✓
S	#	#	✓	✓	✓	✓
M	×	×	✓	×	✓	✓

 # connection can take shear, but fixity needed at other end

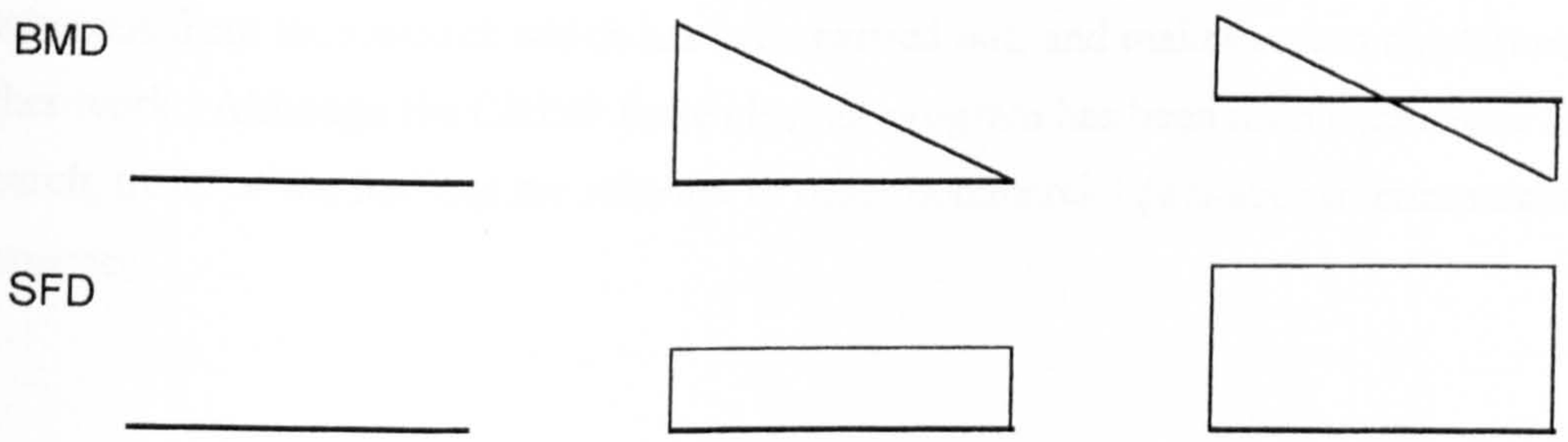

1-D 2-node bar not possible 2-node beam

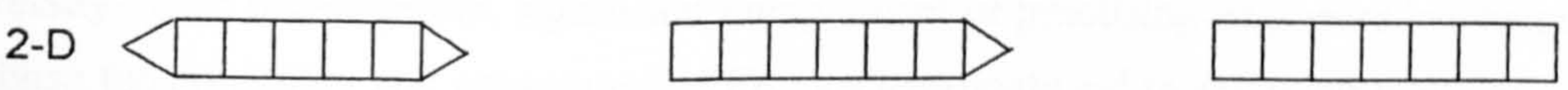

(concentric load) (concentric load)

(a) (b) (c)

Fig 8.39 Possible transferable actions in 1D and 2D elements used as retaining wall props : axial force (P), shear (S) and moment (M)

CHAPTER 9
CONCLUSIONS AND RECOMMENDATIONS

This thesis has sought to address the problems facing practitioners using finite element analysis in the design of embedded retaining walls. It has not focused on the development of new tools or techniques, but rather on the better (and/or more informed) application of those already in existence. Other investigators have put considerable effort into such topics as adaptive meshing, advanced constitutive modelling, 3D wall installation effects, and new non-linear solution methods. The writer's perception at the outset of the research was that there was considerable scope for investigating and clarifying a large number of basic modelling issues that could have a very significant effect on computed results.

Summary discussions have been presented at the end of all preceding chapters, highlighting the chief findings of each area of investigation in turn. This chapter draws together the main conclusions from the research which has been carried out, and makes recommendations for further work. Although the CRISP finite element program has been used exclusively for this research, many of the findings are relevant to other commercial packages of comparable complexity.

9.1 Previous Work and Established Practice

The major contributors and the different areas of progress in the application of finite elements to earth-retaining structures have been identified. Whilst most contribution has come from university-based investigators, significant involvement of practising engineers has helped to establish the credibility and acceptance of FE as a legitimate aid to retaining wall design. Data from centrifuge models and full-scale structures have led to an improved understanding of many aspects of embedded retaining wall behaviour, and have provided vital benchmarking for numerical models.

The first contribution made by this thesis is an analysis of the significant literature dealing with FE analysis of retaining walls. Key items from each published reference (wall type, support system, ground conditions, modelling assumptions, etc.) are summarized in tabular form, along with a "rating" of how useful and relevant the reference would be to a practising engineer (see

Table 2.3). About 40% of the tabulated references are considered very or highly relevant to practitioners, whereas some 30% are of limited usefulness (owing, for example, to insufficient detail of the modelling). Whilst somewhat subjective, this form of "filtering" and guidance on publications is invaluable for the novice analyst, but appears not to have been done previously.

Five areas of uncertainty in the use of finite elements in embedded retaining wall design have been identified as follows (Section 1.4):

a) geometric modelling and discretization
b) constitutive modelling and parameter selection
c) modelling of construction and long term effects
d) computational difficulties
e) obtaining design output

These are not mutually exclusive; for example, poor choices of mesh geometry can lead to numerical ill-conditioning and not just an inaccurate solution. However, the distinctions are considered helpful, and the sequence (a)-(e) corresponds to the order in which they are encountered in setting up, running, and interpreting an FE analysis. Numerical experiments conducted by the writer have provided insight into these issues and have helped to establish guidelines and rules that can be followed by practising engineers. Consequences of modelling decisions have been illustrated through their effect on output quantities generally sought by the designer, including wall displacement and bending moment, excavation heave, ground surface movement, horizontal soil stresses, and pore water pressures. Conclusions from these numerical experiments will now be summarized.

9.2 Geometric Modelling and Discretization

The element provision in CRISP is considered adequate for most embedded retaining wall problems, perhaps with the exception of a robust interface element and the option to employ reduced integration. Ultimately it is the actual mesh design (element grading, boundary location, etc.) which still causes the practitioner most difficulty - and this has received little attention in the literature. Consequently, investigations have been conducted into boundary location, mesh aspect ratio, boundary condition, and overall number and grading of elements.

Mesh boundary location must be selected with care, particularly if the profile of ground surface movement behind the wall is of primary concern (Section 4.2). If only wall displacements and bending moments are required, boundary location is less important. For the geometries considered in this work, reasonable accuracy was achieved with the remote vertical boundary at a distance of at least 8H from the back of the wall, and the bottom boundary a minimum of 8W from formation level (where H is the retained height of the excavation and W its half-width). Boundary location is particularly important for undrained conditions and/or where plastic yield occurs during the analysis. An increasing degree of elastic nonhomogeneity generally makes the results less sensitive to boundary location, whereas an increase in elastic anisotropy has the opposite effect. A mesh with boundaries that are shown to be sufficiently remote for an undrained elasto-plastic analysis should, in most cases, be more than adequate for other types of analysis. The corollary is that general purpose mesh adequacy cannot be established through drained analysis.

Closely linked with boundary location is the overall aspect ratio of the mesh (Section 4.3). If only one remote boundary is moved away from the retained excavation whilst the other is fixed, the mesh aspect ratio will change. Computed results will converge to different values than if both boundaries had been moved so as to preserve the original aspect ratio. If the unmoving boundary is too close to the excavation, convergence to a false maximum/ minimum value can occur. For example, if the bottom boundary is too close, the remote vertical boundary does not need to be moved very far before results reach steady values - but these will not be the same as those obtained when both remote boundaries were moved out together.

Boundary conditions are not normally specified at the meshing stage, but rather as part of the in-situ conditions (and perhaps also in later increments if element changes occur). However, there is clearly an interaction with boundary location; if boundaries are sufficiently remote, their roughness should not matter (Section 4.4). Therefore, switching boundary conditions from rough to smooth (and *vice versa*) can be used as a simple test of whether or not the far boundaries are sufficiently remote.

As regards the overall number of elements, a relatively modest sized mesh ($\approx$ 700 nodes) can produce results for an embedded retaining wall of reasonably simple geometry to within $\pm$5% of their expected value (Section 4.5). If this is to be reduced to within $\pm$1%, the number of

nodes must at least be doubled using some form of h-refinement (in which elements are subdivided). However, unless this is conducted in an orderly and consistent manner, the analysis may converge on an incorrect result. The location of the nodes within the mesh is also important and, for a given number of degrees of freedom (d.o.f.), there will be an optimum mesh grading which is situation dependent. A balance must be struck between the need to have a high density of nodes where stress gradients are high, whilst maintaining a reasonable transition to larger element sizes towards the remote boundaries (avoiding abrupt changes in size). Grading alteration through r-refinement (in which nodal positions are adjusted) provides another way of examining the adequacy of a mesh. If too few nodes are used, the analysis is particularly sensitive to their location; if the total number of d.o.f. is adequate, far less sensitivity to location is evident.

9.3 Constitutive Modelling and Parameter Selection

There is an abundance of constitutive models in CRISP, with more than adequate choice for the retaining wall analyst (Section 3.6). It is the understanding of how and when to use these different models, and how to select parameters for them, which is often lacking. The practitioner needs to know how much complexity is required to ensure a realistic result. More fundamentally, the practitioner needs to understand how different facets of constitutive behaviour (anisotropy, non-linearity, etc.) affect the outcomes of a retaining wall analysis. It is this need which the present work has addressed.

Modeling the nonhomogeneity of elastic stiffness with depth is very important - especially over the full depth of the wall itself (Section 5.2). Computed wall displacements and wall bending moments (distribution and/or magnitude) are particularly sensitive to nonhomogeneity under certain propping configurations. Predicted profiles of excavation heave and ground surface movement also depend very much on the degree of nonhomogeneity, which has implications for the assessment of damage to adjacent structures.

Anisotropy of elastic stiffness is not particularly important for embedded retaining wall analysis unless it is of a high degree (typically, $E_h/E_v > 2$). The form of anisotropy considered here is transverse anisotropy with a vertical plane of symmetry, requiring only five independent parameters (Section 5.3). Increasing the degree of anisotropy generally scales down the wall displacement profile (preserving its shape) and causes reductions in bending moment in some

propping cases. Excavation heave is largely unaffected by anisotropy, and significant reductions in ground surface movement occur only at high ratios of E_h/E_v under undrained conditions. Although not investigated in this thesis, anisotropy of permeability is probably more important owing to its effect on drainage rates during and after construction. Anisotropy of strength may be important if yielding is significant (e.g. in soft clays).

All output quantities of interest to the designer are affected by non-linearity of the elastic response - sometimes very dramatically (Section 5.4). However, the specific definition of non-linearity adopted is important; the use of a "reference strain" where all stiffness:strain curves pass through a common point is recommended. The impact of non-linearity depends not only on the absolute reduction in elastic stiffness with strain, but also the gradient with which this reduction takes place. The changes in computed wall displacement, bending moment and ground movement all depend on the rate of decay of stiffness with strain. Previous investigators have emphasized only the effect of non-linearity on the shape of the surface settlement trough. This thesis has shown that other quantities of interest to the designer are also influenced, such as wall displacement and bending moment, and that the nature of the influence is more subtle than is generally realized.

The introduction of plastic yielding leads to much larger wall displacements if the propping arrangement allows the development of zones of plastic yield (Section 5.5). Yielding allows stress redistribution to take place, which leads to a reduction in wall curvature and thus smoother bending moment profiles relative to the fully elastic case. Excavation heave profiles become more uniform across the excavation, as greater distortion of the soil takes place immediately in front of the wall. Settlement behind the wall is accentuated by yielding when the elastic nonhomogeneity is high, and the degree of propping becomes especially important. All of these effects are amplified by switching from undrained to drained conditions.

The incorporation of non-associated flow can, in extreme cases, double the predicted wall displacements and bending moments and cause large increases in predicted ground movements either side of the wall (Section 5.6). This is based on a comparison of analyses where dilation was totally suppressed ($\psi=0$) with those where full dilation was permitted ($\psi=\phi'$). However, it is unlikely that the potential for this much yield to occur during bulk excavation would be present in most real cases, so the implications for practical analyses may not be as dramatic. The ability to compare total (Tresca) and effective stress (Mohr-Coulomb) approaches to

undrained analysis depends on the differences introduced by the flow rules and the implied plastic volumetric strains.

Closely linked with constitutive model are drainage conditions and in-situ stresses. The facility in CRISP for drained, undrained and coupled-consolidation analyses covers every eventuality for saturated soils. The real uncertainty surrounds the choice of bulk modulus of water in an undrained analysis, and of time step in a coupled analysis; this is addressed later in Sections 9.4 and 9.5. Similarly, the way in which in-situ stresses can be defined is flexible enough for most practical cases, except in the presence of a sloping ground surface, which must be created at an early stage in the analysis.

The usefulness of complex models to the designer is questionable. An important part of the design process is being able to develop a "feel" for the relative importance of the different parameters. For example, most engineers have some understanding of undrained strength as it can be related to clay consistency and liquid limit, and the use of a single strength value in a yield criterion (e.g. Tresca) is very attractive. Those models which need only a few parameters with recognizable physical significance have a clear advantage over those which require specialized tests and/or curve fitting procedures. Advanced models, in the hands of their inventors, have been used to obtain good agreement between prediction and observations. Research and development of this nature should take place to improve our predictive capability, but the needs of practising geotechnical engineers must not be ignored. The work presented in this thesis should assist the retaining wall designer in deciding which aspects of soil behaviour may be important in the prediction of a particular quantity.

9.4 Modelling of Construction and Long Term Effects

Diaphragm wall installation can be modelled faithfully with fully-coupled three-dimensional analysis, but this complexity is not warranted in routine design. Alternative methods of varying rigour may be used, involving applied pressure distributions and multiple overlay element swapping - mostly plane strain in two-dimensions, but plane stress can also provide helpful insight (Section 6.2). The wished-in-place (WIP) method does not permit any relaxation of horizontal soil stresses prior to bulk excavation, leading to an upper bound on predicted wall displacements and bending moments. Conversely, the applied pressure method (plane strain) allows too much ground relaxation and provides a lower bound. The designer

may find it helpful to carry out both types of analysis to gain an appreciation of the significance of wall installation effects. Occasionally, coupled 3D analysis will be justified, if only to calibrate simpler methods such as the reduction of K_o to a post-installation value (K_i), or the prescription of a horizontal displacement at the soil-wall interface to mimic ground relaxation into the slurry trench.

Bulk excavation for embedded retaining walls should be carried out in layers whose thickness ΔH is no greater than one fifth (preferably one tenth) of the final retained height H, with each layer removed over at least 10-15 increments (Section 6.3). Layer thickness will, in many cases, be constrained by prop spacing; if the analysis is investigating the consequences of increasing this spacing, it is important that ΔH does not become too large. The independence of the final result on the number of increments used for excavation (Ishihara, 1970) only applies when the soil-structure response is elastic, and there are no changes to system stiffness (arising through, say, the introduction of props or anchors).

Virtually any kind of propping action and load transfer can be represented with 1D or 2D elements and appropriate connection details. The removal of a temporary prop or anchor causes a large horizontal total stress release on the earth-retaining structure, and the number of increments over which this happens must be selected with the same consideration as bulk excavation (Section 6.4). In overconsolidated clays, stress paths on the retained side will initially traverse the elastic region during wall installation and bulk excavation, moving towards (and possibly reaching) yield during prop removal.

To replicate undrained excavation in a coupled analysis, the time steps Δt need be no smaller than of the order of 0.1 days (2.5 hrs) per 1m layer of excavation in overconsolidated clay with a typical coefficient of permeability $k \approx 10^{-9}$ m/s (Section 6.5). Numerical instability (evidenced by equilibrium errors) will not occur unless time steps are reduced to 0.001 day (1.5 min) per 1m layer of excavation in the same clay, although pore water pressure profiles become erratic for $\Delta t < 0.1$ days. Partial drainage will begin to occur for $\Delta t \geq 1$ day per layer with this value of permeability, implying significant changes in effective stress. If this is the case, and the constitutive model permits a non-linear response, sufficient increments must be employed to ensure accurate representation.

The time required to reach long-term equilibration following construction (i.e. the time to equalization of pore water pressures t_e) will not be known *a priori* (Section 6.6). If insufficient time is allowed for equalization to occur, it would be possible to believe (incorrectly) that a small number of increments gave adequate accuracy. However, this insufficiency will be revealed through an insensitivity to the weightings of the time step, thus providing the basis for a simple test. If an insufficient number of increments is allowed for equalization, and only the wall displacement profiles are examined, then too short an equalization time will appear to have been adequate. Overlaying curves of maximum wall displacement against elapsed time will reveal the insufficiency of increments, which could serve as an alternative form of test.

If rising groundwater levels are a consideration, they should be included in the analysis as their effects on wall behaviour can be highly significant (Section 6.7). For embedded walls in clay, fluctuation of water levels might arise from the recharge of an underlying aquifer. The fully coupled saturated flow formulation is adequate in this situation, obviating the need for a nonsaturated approach. (It should be noted that rising groundwater is a different issue to that of the establishment of long-term steady seepage around a retaining wall or the investigation of different drainage schemes; etc.)

9.5 Computational Difficulties

A number of modelling difficulties arise because analysts do not always appreciate the limitations of the software and/or hardware used (Section 7.1). Some of these difficulties are obvious (e.g. high equilibrium errors) whereas others may remain hidden because their effects are only present in calculated quantities which the user has elected not to output.

Large stiffness contrasts between adjacent elements, possibly combined with high element aspect ratios, are a well-known source of numerical ill-conditioning. Embedded retaining walls present exactly this sort of problem, and ill-conditioning can affect results dramatically (Section 7.2). In practice, only slender walls constructed from steel (i.e. sheet pile) are likely to be at serious risk. If the analysis calls for slender members in regions of high stiffness contrast and stress gradients, element aspect ratios must not be allowed to exceed 1:4.

Effective stress analysis of undrained conditions by the technique of setting a high value for the bulk modulus of water, K_w, is very convenient (Section 7.3). There is an optimum value of K_w which avoids both partial saturation (K_w too low) and numerical instability (K_w too high). This optimum is approximately 100K′, where K′ is the effective stress bulk modulus of the soil. However, as the drained elastic stiffness often varies within a stratum, it is difficult to maintain the optimum ratio everywhere in the mesh with a single value of K′. Also, analysts may decide not to calculate K′ explicitly but rather opt for selecting an arbitrarily high value for K_w. The ability to specify K_w/K′ rather than K′ would help alleviate this difficulty.

Equivalence of coupled and uncoupled analyses at the undrained and drained limits can only be obtained in the elastic case (Section 7.4). In the presence of soil yielding, the coupled analysis permits patterns of volume change in the mesh which lead to results which cannot be matched by the uncoupled analysis. It would, therefore, be misleading to use an uncoupled analysis to benchmark a coupled analysis in the presence of plastic behaviour.

The development of tensile total stresses behind the wall arises from the combined response of the effective stresses and pore water pressures (Section 7.5.2). The constitutive law is not violated, as the stress state is well within the yield surface (when one is present). The effect is more pronounced with higher values of drained Young's modulus at the ground surface (E'_o) and when there is an elastic region of significant size. Forward wall displacement and bending moments are reduced; the latter very significantly around formation level.

Horizontal total stress anomalies can develop just below formation level, adjacent to the wall, in both fully elastic and elasto-plastic cases (especially the former, Section 7.5.3). The pore water pressure response in this area depends heavily on how much yielding occurs - but this is also true of the horizontal effective stress, and so the long term horizontal total stress is the same for both. Overconsolidation mechanisms are partly responsible, aided by the high vertical effective stresses in this region that can develop during equalization. Significant rotation of principal stresses also occurs just below formation level and this is a contributory factor.

Until very recently, only two options existed within CRISP for the solution scheme adopted in an elastic-perfectly plastic analysis (Section 7.6). Specifically, uniform load ratios (ULR - where 1/N of the load change occurs in each of N increments) or non-uniform load ratios

(NLR - where individual weightings are in the range 0-1 but must all sum to 1). In the context of bulk excavation in front of a retaining wall, the most effective form of NLR is where all the load is applied in the first increment of the block and the remaining increments are used for load iteration. This leads to better (faster) convergence of the analyses when increasing the number of increments used in a block. In addition, NLR produces more accurate results than ULR for a given number of increments - indeed NLR can produce better results for substantially fewer increments. A test for sufficiency of number of increment blocks would be to vary the load ratios adopted - if there are sufficient, the analysis will not be sensitive to the load ratio. (Users of Version 4 or later of SAGE CRISP have access to Newton-Raphson iteration, obviating the need for load ratio manipulation.)

9.6 Obtaining Design Output

Although displacement is the primary output of the finite element (displacement) method, the way in which it is viewed can be as important as the accuracy of its calculation (Section 8.2). Neither manipulation nor smoothing is necessary, but there are various ways in which displacement results can be presented graphically. Each of these can contribute to understanding the overall behaviour of the earth-retaining structure system and surrounding soil, and should be used. By isolating presumed features of interest too quickly, important points can be missed. Comparing profiles of horizontal and vertical movement with minima/maxima based on case studies is helpful in identifying anomalous behaviour. An inadmissible analysis can be approved unwittingly if all displacement information (deformed mesh, vectors, contours) is not scrutinized appropriately and thoroughly. There is a temptation to extract the wall deflection, ground surface settlement profile, etc as soon as the analysis is complete, but this is not responsible practice.

Engineers expect to be able to extract profiles of earth and water pressure acting on the wall, to compare with simplified design assumptions. However, the stress distributions output directly from CRISP (the "raw" Gauss point stresses) are not particularly useful in a design context (Section 8.3). Some form of smoothing is necessary. Methods which use a least-squares best-fit plane through the raw 3×3 Gauss point stresses, or which interpolate the 2×2 (reduced integration) point stresses from the 3×3, give a satisfactory degree of smoothing. Such local element-by-element methods are not ideal, as they still leave some degree of "raggedness" in the profiles of horizontal total stress or soil-wall shear stress. Approaches

using data outside of the immediate area would seem attractive, but the limited results presented in this thesis are not convincing. It would be useful to explore this more thoroughly in future research.

Wall bending moments calculated from external earth pressures are of limited reliability (Section 8.4). Toward the wall toe, (possible) errors in stress are being amplified by an increasing lever arm, thus compounding the error in bending moment. Calculating bending moments in this way is obvious and intuitive, but fails (at least in part) because of certain aspects of the finite element method. Instead, bending moments should be calculated from transverse stress distributions in the wall elements. The use of raw 3×3 or interpolated 2×2 stresses gives the same result, so the extra effort involved in interpolation is not warranted. This thesis has not considered wall bending moment computation when the wall is modelled with two or more columns of continuum elements. 8-noded quadrilaterals in a single column appear adequate, but if more than one column were used, a method based on transverse stress distributions would seem sensible.

The reliability of wall shear forces calculated from earth pressures is also limited, although the discrepancies are not quite as large as with bending moments (Section 8.5). As with bending moments, shear forces should be calculated from shear stress distributions in the wall elements themselves, but only after these stresses have gone through a preliminary stage of least-squares smoothing. Discontinuities in the shear force diagram should occur at (and only at) the location of props - the magnitude of the discontinuity providing a useful cross-check on calculated axial forces in those props. Zero shear force and maximum bending moment should, of course, be coincident in the wall (or any structural member) providing another cross-check on calculations.

The methods of obtaining the axial forces in props and anchors are straightforward (Section 8.6). The only factors to take into account when checking output veracity are whether or not shear stress transfer can occur (e.g. prop slab in contact with ground), and if any prestressing has been performed. To calculate bending moments and shear forces in 2-D elements, methods based on internal (transverse) stresses are preferred, as with the structural wall.

9.7 Recommendations for Further Work

Geometric modelling and discretization

Although reasonably comprehensive, the mesh boundary location studies presented in Chapter 4 should be extended to include the new generation of constitutive models which have been implemented recently in CRISP. The existing analyses could also be repeated for coupled analyses, as it is uncertain if this formulation is more or less demanding in terms of displacement boundary location. Furthermore, all meshes in Chapter 4 had level ground surfaces and horizontal bases; however, wall construction on sloping ground and or in strata with inclined bedrock is not uncommon, so the work on boundary locations could be usefully extended to these conditions. For the studies already completed herein, as well as for those additionally recommended, the key output values should be extended to include horizontal ground movement and possibly wall shear force. The former is particularly useful in assessing excavation-induced damage to structures.

Three-dimensional analysis is unlikely to feature in commercial embedded wall design for a number of years, and only then for prestigious projects where the additional time and cost can be justified. However, on the assumption that it will become cheaper and more convenient over the next decade to perform 3D analysis, now is the time to establish guidelines for mesh design (boundary location and condition, refinement and grading). Recently published meshes for 3D work seem rather coarse and of inadequate extent, and it would be unfortunate if this was adversely affecting the quality of the results and the conclusions based upon them.

The use of infinite elements could alleviate much of the uncertainty over boundary location, and it is recommended that a suitable form of infinite element is implemented in CRISP for numerical trials. There ought to be several satisfactory elements in existence for non-coupled work, although it may be necessary to create a special infinite element which can be used in a coupled analysis. Some embedded retaining wall cases will be more concerned with the interactions with other adjacent structures (e.g. tunnels or foundations) in which case boundary location will not be as important as the discretization between these structures.

A final recommendation under this heading is to investigate the potential benefits of adaptive meshing for embedded retaining wall analysis. There has been some work in this area for geomechanics applications, including the early work of Simpson specifically for retaining walls (Section 2.1.2). Adjacent buried structures might present a particular challenge to an adaptive

meshing algorithm, and there is always the danger that the FE code might become more like a "black box" to the user if the mesh is automatically refined. However, it is potentially a very useful tool and so it would be timely to revisit this topic.

Constitutive modelling and parameter selection

The studies reported in Chapter 5 for the basic constitutive models in CRISP should be augmented to "fill in" some of the gaps. For example, only three degrees of nonhomogeneity and of anisotropy were used, and whilst these covered the likely range that would be encountered in practice, the use of further intermediate values is recommended. Similar comments apply to the degrees of non-linear elasticity investigated with the Jardine model, with which there is considerable scope for further parametric study.

The studies of plastic yielding in the present work were quite limited, in so far as just two different yield criteria were used, together with a small number of shear strength parameters. Notwithstanding the fact that plastic yielding should not be a major issue for embedded walls in stiff overconsolidated clay, it is recommended that more comprehensive numerical studies are conducted. As well as different shear strength envelopes, it will be important to consider a greater range of in-situ stress conditions as this has a major influence on how soon yielding might occur in the wall construction process.

The effects of non-associated flow suggested by the results in Chapter 5 are significant and should be verified (or otherwise). It is recommended that the investigations of non-associated flow are repeated with the non-associated Mohr-Coulomb model now available in SAGE CRISP, taking advantage of the facility to specify angles of dilation ψ' between 0 and ϕ'.

New constitutive models have been incorporated in CRISP since this research work commenced, and others are certain to be implemented in future. Those considered applicable to embedded retaining wall design should be subject to the same sort of studies as described in Chapter 5, in order to guide practitioners on parameter selection. Ideally, designers would carry out these parametric studies themselves to develop a better understanding, but commercial time pressure will probably preclude it.

Modelling of construction and long term effects

3D wall installation is an obvious area for further research, extending the preliminary studies of Powrie and co-workers. As many design analyses will be 2D, the emphasis also needs to be on how 3D effects can be introduced into simpler 2D models. One example of this is in providing suitable values for K_i, the post-installation coefficient of earth pressure

Temporary berms have not been considered at all in this thesis, but the effect of their removal is not dissimilar to that of removing a temporary prop, and it is recommended that the type of studies conducted herein are repeated. Similar recommendations apply to a possible study of the effects of de-stressing temporary ground anchorages on embedded walls, as this has also been ignored in the present study.

The coupled analyses of bulk excavation in the present work should be repeated with drainage boundaries that evolve with excavation. This could provide useful insight into wall behaviour during construction delays. The analyses of partial drainage and long-term equalization used only limited constitutive behaviour, and there is considerable scope for extending these studies to include non-linear elasticity, etc. Finally, rising groundwater levels need to be investigated in a more generic way, as the results in Chapter 6 were from a specific commercial job and an idealised basement wall.

Computational difficulties

The ill-conditioning studies should be extended to full embedded retaining wall configurations to examine if the restrictions on modular and aspect ratio suggested in Chapter 7 can be relaxed. The implementation of K_w/K' as an input parameter to CRISP would simplify greatly the selection of a suitable pore fluid compressibility to ensure undrained behaviour, and would help avoid numerical problems with computed pore water pressures. The comparisons of coupled and uncoupled approaches could be taken much further; for example, the constitutive models used herein were rather limited and many other parameters in the problem were determined in an arbitrary way.

Tensile stresses (and excessive shear resistance) on the back of a retaining wall could be avoided with a suitably robust interface element; the Goodman-type element currently available in CRISP has not proven itself reliable in practical applications. Anomalies in horizontal stress will probably always be present and the only recommendation as such is for

users to be better educated in order to understand the origin of such features in an FE analysis, and their possible effect on the results as a whole. The recent implementation of Newton-Raphson iteration in (SAGE) CRISP creates the need for further parametric studies and benchmarking of the solution scheme.

Obtaining design output

The methods used for stress smoothing with CRISP output in Chapter 8, though seemingly effective, were fairly crude. There would be scope for re-examining this area of design output in the light of more recent developments in finite element analysis. The computation of bending moments and shear forces from nodal forces in the wall elements should be considered, although some modification of the program will be called for, and it is not apparent that methods using transverse stress distributions can be greatly improved on.

The creation of a purpose-built post-processor for retaining wall problems would be a very significant step forward for designers. In this respect, recent plans announced by the CRISP Consortium to produce what it terms "mesh setup wizards" are a welcome development. Although aimed more at the pre-processor end, setup wizards are a logical first-step in the provision of a package that practising engineers should find particularly helpful as they apply finite element analysis to the design of embedded retaining walls.

REFERENCES

Abedi, H., Porter, T.G., Lien, B.H. and Ramos, J.A. (1993)
Performance of a flexible earth retaining structure in soft clays - comparisons between finite element method and field measurements. in *Retaining Structures* (ed. Clayton), pp281-290. London: Thomas Telford.

Adenbrooke, T.I., Potts, D.M. and Puzrin, A.M. (1997)
The influence of pre-failure soil stiffness on numerical analysis of tunnel construction. *Géotechnique*, Vol 47, No 3, pp693-712.

AGS (1994)
Validation and Use of Geotechnical Software. London: Association of Geotechnical Specialists.

Al-Shlash, K.T. (1979)
Applications of the finite element method in assessing the behaviour of tied-back walls. PhD thesis, University of Sheffield.

Al-Tabbaa, A. (1987)
Permeability and stress-strain response of Speswhite kaolin. PhD thesis, Cambridge University.

Ali, S.R. (1993)
Numerical modelling of unsaturated soils at low stress levels. PhD thesis, University of Sheffield.

Almeida, M.S.S. (1984)
Stage constructed embankments on soft clays. PhD thesis, Cambridge University.

Arai, K. (1993)
Active earth pressure founded on displacement method. *Soils and Foundations*, Vol 33, No 3, pp54-67.

Arslan, U., Breth, H. and Wanninger, R. (1981)
An elasto-plastic analysis of anchored walls. *Proc. 10th ICSMFE*, Stockholm, Vol 2, pp21-28.

Athanasiu, C., Simonsen, A.S. and Ronning, S. (1991)
Back-calculation of case records to calibrate soil-structure interaction analysis by finite element method of deep excavations in soft clay. *Proc. 10th ECSMFE*, Florence, Vol 1, pp297-300.

Atkinson, J.H. (1973)
The deformation of undisturbed London Clay. PhD thesis, University of London.

Atkinson, J.H., Evans, J.S. and Ho, E.W.L. (1985)
Non-uniformity of triaxial samples due to consolidation with radial drainage. *Géotechnique*, Vol 35, No 3, pp353-356.

Azevedo, R. and Ko, H.Y. (1986)
Comparisons between centrifugal and numerical modelling of unsupported excavations in sand. *Proc. 2nd Int. Symp. Num. Models in Geomechanics* (eds Pande & Van Impe), Ghent, pp293-299. Redruth: M Jackson.

Babuska, I., Zienkiewicz, O.C., Gago, J. and Oliveira, E.R. De A. (1986)
Accuracy Estimates and Adaptive Refinements in Finite Element Computations. Chichester: J Wiley.

Bakeer, R.M. and Bhatia, S.K. (1989)
Earth pressure behind a gravity retaining wall. *Int. J. Num. Anal. Meth. Geomech.*, Vol 13, pp665-673.

Bakker, K.J. and Beem, R.C.A. (1994)
Modelling of the sheet pile wall test in Karlsruhe 1993. *Num. Meth. in Geot. Engg* (ed Smith), pp319-324. Rotterdam: Balkema.

Bakker, K.J. and Brinkgreve, R.B.J. (1991)
Deformation analysis of a sheetpile wall using a two dimensional model. *Proc. 10th ECSMFE*, Florence, Vol 2, pp655-658.

Bakker, K.J. and Vermeer, P. (1986)
Finite element analyses of sheetpile walls. *Proc. 2nd Int. Symp. Num. Models in Geomechanics* (eds Pande & Van Impe), Ghent, pp409-416. Redruth: M Jackson.

Barkhordari, K. (1998)
The influence of load transfer mechanisms on ground anchor design. PhD thesis, University of Surrey.

Barlow, J. (1976)
optimal stress locations in finite element models. *Int. J. Num. Meth. Engg.*, Vol 10, pp243-251.

Batten, M. and Powrie, W. (2000)
Measurement and analysis of temporary prop loads at Canary Wharf underground station, east London. *Proc. Instn Civ. Engrs, Geot. Engg,* Vol 143, No 3, pp151-164.

Berger, D.J. and Tryon, S.O. (1999)
Approach to designing structural slurry walls. *J. Geot. Geoenv. Engg Divn ASCE,* Vol 125, No GT11, pp1011-1022. [plus discussion by Haghayeghi and Alostaz, Vol 126, No GT2, p194.]

Bhatia, S.K. and Bakeer, R.M. (1989)
Use of the finite element method in modelling a static earth pressure problem. *Int. J. Num. Anal. Meth. Geomech.*, Vol 13, pp207-213.

Biot. M.A. (1941)
General theory of three-dimensional consolidation. *J. Applied Physics,* Vol 12, pp155-164.

Bishop, A.W. and Hight, D.W. (1977)
The value of Poisson's ratio in saturated soils and rocks stresses under undrained conditions. *Géotechnique*, Vol 27, No 3, pp369-384.

Bishop, A.W. and Wesley, L.D. (1975)
A hydraulic triaxial apparatus for controlled stress path testing. *Géotechnique*, Vol 25, No 4, pp657-670.

Bjerrum, L., Friman-Clausen, C.J. and Duncan, J.M. (1972)
Earth pressures on flexible structures, a state-of-the-art report. *Proc. 5th ECSMFE*, Madrid, Vol 2, pp169-196.

Bolton, M.D. and Powrie, W. (1987)
The collapse of diaphragm walls retaining clay. *Géotechnique*, Vol 37, No 3, pp335-353.

Bolton, M.D. and Powrie, W. (1988)
Behaviour of diaphragm walls in clay prior to collapse. *Géotechnique*, Vol 38, No 2, pp167-189.

Bolton, M.D., Britto, A.M., Powrie, W. and White, T.P. (1989)
Finite element analysis of a centrifuge model of a retaining wall embedded in a heavily over consolidated clay. *Computers and Geotechnics*, Vol 7, No 4, pp289-318.

Bolton, M.D., Powrie, W. and Symons, I.F. (1990)
The design of in-situ walls retaining overconsolidated clay: Parts I and II. *Ground Engineering*, Vol 22, pp34-40 & Vol 23, pp22-28.

Bond, A. (1996)
Private communication.

Booker, J.R. and Small, J.C. (1975)
An investigation of the stability of numerical solution of Biot's equations of consolidation. *Int. J. Solids & Structures*, Vol 11, pp907-911.

Borin, D.L. (1988)
WALLAP: Anchored and cantilevered retaining wall analysis program: User's Manual (Version 3). London: Geosolve.

Borja, R.I. (1990a)
Analysis of incremental excavation based on critical state theory. *J. Geot. Engg Divn ASCE*, Vol 116, No GT6, pp964-985.

Borja, R.I. (1990b)
Composite Newton-PCG and quasi-Newton iterations for non-linear consolidation. *Comp. Meth. Appl. Mech. Engg*, Vol 78.

Borja, R.I. and Kavazanjian, E. (1985)
A constitutive model for the stress-strain-time behaviour of 'wet' clays. *Géotechnique*, Vol 35, No 3, pp283-298.

Borja, R.I., Lee, S.R. and Seed, R.B. (1989a)
Excavation in cohesive soils: modelling the effects of creep on long-term performance. *Proc. 3rd Int. Symp. Num. Models in Geomechanics* (eds Pande & Pietruszczak), Niagara Falls, pp585-592.

Borja, R.I., Lee, S.R. and Seed, R.B. (1989b)
Numerical simulations of excavation in elastoplastic soils. *Int. J. Num. Anal. Meth. Geomech.*, Vol 13, pp231-249.

Boscardin, M.D. and Cording, E.J. (1989)
Building response to excavation-induced settlement. *J. Geot. Engg Divn ASCE*, Vol 155, GT1, pp1-21.

Bose, S.K. and Som, N.N. (1998)
Parametric study of a braced cut by finite element method. *Computers and Geotechnics*, Vol 22, No 2, pp91-107.

Brassinga, H.E. and Van Tol, A.F. (1991)
Deformation of a high-rise building adjacent to a strutted diaphragm wall. *Proc. 10th ECSMFE*, Florence, Vol 2, pp787-790.

Briaud, J.L. and Kim, N.K. (1998)
Beam-column method for tieback walls. *J. Geot. Geoenv. Engg Divn ASCE*, Vol 124, No GT1, pp67-79.

Briaud, J.L. and Lim, Y. (1999)
Tieback walls in sand: numerical simulation and design implications. *J. Geot. Geoenv. Engg Divn ASCE*, Vol 125, No GT2, pp101-110.

Britto, A.M. and Gunn. M.J. (1987)
Critical State Soil Mechanics via Finite Elements. Chichester: Ellis Horwood.

Britto, A.M. and Gunn. M.J. (1990)
CRISP Users and Programmers Guide. Internal report, Cambridge University Engineering Department.

Britto, A.M. and Kusakabe, O. (1984)
On the stability of supported excavations. *Can. Geot. J.*, Vol 21, No 2, pp338-348.

Broms, B.B., Wong, I.H. and Wong, K.S. (1986)
Experience with finite element analysis of braced excavations in Singapore. *Proc. 2nd Int. Symp. Num. Models in Geomechanics* (eds Pande & Van Impe), Ghent, pp309-324. Redruth: M Jackson.

Brooks, N.J. and Spence, J.F. (1993)
Design and recorded performance of a secant retaining wall in Croydon. in *Retaining Structures* (ed. Clayton), pp205-215. London: Thomas Telford.

Brown, P.T. (1969)
Numerical analysis of uniformly loaded circular rafts on deep elastic foundations. *Géotechnique*, Vol 19, No 3, pp399-404.

Brown, P.T. and Booker, J.R. (1985)
Finite element analysis of excavations. *Computers and Geotechnics*, Vol 1, No 3, pp207-220.

BSC (1992)
User manual for ReWaRD : Advanced retaining wall design and analysis.
Scunthorpe : British Steel Corporation.

Burland, J.B. (1975)
Session 1: Ground movement. *Proc. Symp. Design and Construction of Deep Basements* (ed Hancock), pp10-16. London: Instn Struct. Engrs.

Burland, J.B. (1978)
Application of the finite element method to prediction of ground movements. In *Developments in Soil Mechanics* (ed. C.R. Scott), pp69-101. London: Applied Science Publishers.

Burland, J.B. and Hancock, R.J.R. (1977)
Underground car park at the House of Commons, London: geotechnical aspects. *The Structural Engineer*, Vol 55, No 2, pp87-100.

Burland, J.B. and Wroth, C.P. (1975)
Settlement of buildings and associated damage. *Proc. BGS Conf. on Settlement of Structures, Cambridge*, pp611-654. Pentech Press, London.

Burland, J.B., Simpson, B. and St.John, H.D. (1979)
Movements around excavations in London Clay. *Proc. 7th ECSMFE*, Brighton, Vol 1, pp13-29.

Butler, F.G. (1975)
General Report and State of the Art Review, Session 3: 'Heavily over-consolidated clays'. *Proc Conf. Settlement of Structures, Cambridge*. London: Pentech Press.

Cai, F, Ugai, K. and Hagiwara, T. (2002)
Base stability of circular excavations in soft clay. *J. Geot. Geoenv. Engg Divn ASCE*, Vol 128, No 8, pp702-706.

Caliendo, J.A., Anderson, L.R. and Gordon, W.J. (1990)
A field study of a tieback excavation with a finite element analysis. *Design and Performance of Earth Retaining Structures* (eds Lambe & Hansen), Geot. Spec. Pub. 25, pp747-763. New York: ASCE.

Cantin, G., Loubignac, G. and Touzot, G. (1978)An iterative algorithm to build continuous stress and displacement solutions. *Int. J. Num. Meth. Engg.*, Vol 12, pp1493-1506.

Cappellari, G. and Ottaviani, M. (1981)
Finite element analysis of horizontal loading tests on a precast concrete diaphragm wall. *Implementation of Computer Procedures and Stress-Strain Laws in Geotechnical Engineering* (eds Desai and Saxena), Proc. Symp., Chicago, Vol 1, pp185-196. Durham: Acorn Press.

Carder, D. (1995)
Ground movements caused by different embedded retaining wall construction techniques. TRL Report 172. Crowthorne: Transport Research Laboratory.

Carder, D.R. and Symons, I.F. (1989)
Long term performance of an embedded cantilever retaining wall in stiff clay. *Géotechnique*, Vol 39, No 1, pp55-75.

Carder, D.R., Press, D.J., Morley, C.H., and Alderman, G.H. (1997)
Behaviour during construction of a propped diaphragm wall founded in London Clay at Aldershot Road underpass. TRL Report 239. Crowthorne: Transport Research Laboratory.

Carrier, W.D. and Christian, J.T. (1973)
Rigid circular plate resting on a non-homogeneous elastic half-space. *Géotechnique*, Vol 23, No 1, pp67-84.

Carrubba, P. and Colonna, P. (2000)
A comparison of numerical methods for multi-tied walls. *Computers and Geotechnics*, Vol 27, No 2, pp117-140.

Carswell, I.G., Carder, D.R. and Symons, I.F. (1991)
Long term performance of an anchored diaphragm wall embedded in stiff clay. TRRL Research Report 313. Crowthorne: Transport and Road Research Laboratory.

Chandler, R.J. (1995)
Field studies, analysis and numerical modelling of retaining walls propped at formation level. PhD thesis, University of London.

Chandrasekaran, V.S. and King, G:J.W. (1974)
Simulation of excavation using finite elements. *J. Geot. Engg Divn ASCE*, Vol 100, GT9, pp1086-1089.

Chang, C.S. and Abas, M.H.B. (1980)
Deformation analysis for braced excavation in clay. *Application of Plasticity and Generalized Stress-Strain in Geotechnical Engineering* (eds Yong & Selig), pp205-225. New York: ASCE.

Chang, C.Y. (1969)
Finite element analysis of soil movements caused by deep excavation and dewatering. PhD thesis, University of California, Berkeley, USA.

Chew, S.H., Yong, K.Y. and Lim, A.Y.K. (1996)
Three-dimensional FE analysis of a strutted excavation underlain by a deep deposit of soft clay. *Proc. 6th NTU-KU-KAIST Tri-lateral Seminar/Workshop on Civil Engineering*, Taejon, Korea, pp207-214.

Chow, Y.K. (1985)
Discussion on Desai and Sargand (Hybrid FE procedure for soil-structure interaction). *J. Geot. Engg Divn ASCE*, Vol 111, GT8, pp1057-1060.

Christian, J.T. and Wong, I.H. (1973)
Errors in simulating excavation in elastic media by finite elements. *Soils and Foundations*, Vol 13, No 1, pp1-10.

Christian, J.T., Hagmann, A.J. and Marr, W.A. (1977)
Incremental plasticity analysis of frictional soils. *Int. J. Num. Anal. Meth. Geomech.*, Vol 1, No 4, pp343-376.

CIRIA (2002)
Funder's Report CP96. London: CIRIA *(restricted circulation).*

Clarke, B.G. and Wroth, C.P. (1984)
Analysis of the Dunton Green retaining wall based on results of pressuremeter tests. *Géotechnique*, Vol 34, No 4, pp549-561.

Clarke, C. (1994)
Under Stress. *CADCAM.* Vol 13, No 11, pp45-46.

Clayton, C.R.I., and Heymann, G, (2001)
Stiffness of geomaterials at very small strains. *Géotechnique*, Vol 51, No 3, pp245-255.

Clough, G.W. (1969)
Finite element analysis of soil-structure interactions in U-frame locks. PhD thesis, University of California, Berkeley.

Clough, G.W. (1972a)
Application of finite element method to earth-structure interaction: State of the Art. *Proc. Symp. Applications of the Finite Element in Geotechnical Engineering*, Vicksburg, pp1057-1116.

Clough, G.W. and Denby, G.M. (1977)
Stabilizing berm design for temporary walls in clay. *J. Geot. Engg Divn ASCE*, Vol 103, GT2, pp75-90.

Clough, G.W. and Duncan, J.M. (1971)
Finite element analysis of retaining wall behaviour. *J. Soil Mech. Fndn Engg Divn ASCE*, Vol 97, SM12, pp1657-1673.

Clough, G.W. and Duncan, J.M. (1972)
Temperature effects on behaviour of Port Allen Lock. *Proc. Spec. Conf. on Performance of Earth and Earth-Supported Structures*, Purdue University, Vol 1, Pt 2, pp1467-1479. New York: ASCE.

Clough, G.W. and Hansen, L.A. (1981)
Clay anisotropy and braced wall behaviour. *J. Geot. Engg Divn ASCE*, Vol 107, GT7, pp893-913.

Clough, G.W. and Kuppusamy, T. (1985)
Finite element analysis of Lock and Dam 26 Cofferdam. *J. Geot. Engg Divn ASCE*, Vol 111, GT4, pp521-541.

Clough, G.W. and Mana, A.I. (1976)
Lessons learned in finite element analysis of temporary excavations in soft clay. *2nd Int. Conf. Num. Meth. in Geomechanics*, Blacksburg, Vol 1, pp496-510.

Clough, G.W. and Schmidt, B. (1981)
Design and performance of excavations and tunnels in soft clay. *Soft Clay Engineering* (eds Brand & Brenner), Chap. 8, pp569-602. Amsterdam: Elsevier.

Clough, G.W. and Tsui, Y. (1974)
Performance of tied-back walls in clay. *J. Geot. Engg Divn ASCE*, Vol 100, GT12, pp1259-1273.

Clough, G.W. and Tsui, Y. (1977)
Static analysis of earth retaining structures. *Numerical Methods in Geotechnical Engineering* (eds Desai & Christian), Chap. 15, pp506-527. New York: McGraw-Hill.

Clough, G.W., Hansen, L.A. and Mana, A.I. (1979)
Prediction of supported excavation movements under marginal stability conditions in clay. *Proc. 3rd Int. Conf. Num. Meth. in Geomechanics*, Aachen, Vol 4, pp1485-1502.

Clough, G.W., Webber, P.R. and Lamont, J. (1972)
Design and observation of a tied-back wall. *Proc. Spec. Conf. on Performance of Earth and Earth-Supported Structures*, Purdue University, Vol 1, Pt 2, pp1367-1389. New York: ASCE.

Clough, R.W. (1960)
The finite element method in plane stress analysis. *Proc. 2nd ASCE Conf. Electronic Computation*, Pittsburgh, pp345-378

Clough, G.W. and O'Rourke, T.D. (1990)
Construction induced movements of in-situ walls. *Proc. Spec. Conf. on Design and Performance of Earth-Retaining Structures*, Cornell, ASCE, Geotechnical Special Publication 25, Lambe PC and Hansen LA (eds), pp439-470.

Cole, K.W. and Burland, J.B. (1972)
Observation of retaining wall movements associated with a large excavation. *Proc. 5th ECSMFE*, Madrid, Vol 1, pp445-453.

Cook, R.D., Malkus, D.S. and Plesha, M.E. (1989)
Concepts and Applications of Finite Element Analysis (3rd ed). New York: J Wiley.

Creed, M.J. (1979)
Analysis of the deformations associated with anchored diaphragm walls. PhD thesis, University of Surrey.

Creed, M.J. and O'Brien, J. (1991)
Simplified finite element analysis of an embedded retaining wall. *Proc. 10th ECSMFE*, Florence, Vol 2, pp687-690.

Creed, M.J., Simons, N.E. and Sills, G.C. (1980)
Back analysis of the behaviour of a diaphragm wall supported excavation in the London Clay. *Proc. 2nd Int. Conf. Ground Movements and Structures*, Cardiff.

Cryer, C.W. (1963)
A comparison of the three-dimensional theories of Biot and Terzaghi. *Quart. J. Mech. Appl. Math.*, Vol 16, pp401-412.

Day, R.A. (1999)
Net pressure analysis of cantilever sheet-pile walls. *Géotechnique*, Vol 49, No 2, pp231-246. [plus discussion by Li, Vol 51, No 2, pp185-187.]

Day, R.A. (2001)
Earth pressure on cantilever walls at design retained heights. *Proc. Instn Civ. Engrs, Geot. Engg*, Vol 149, No 3, pp167-176.

Day, R.A. and Potts, D.M. (1989)
A Comparison of Design Methods for Propped Sheet Pile Walls. SCI Publication 077. Ascot: Steel Construction Institute.

Day, R.A. and Potts, D.M. (1991)
Finite element analysis of the Hatfield Wall. *Computer Methods and Advances in Geomechanics* (eds Beer et al), Vol 2, pp973-978. Rotterdam: Balkema.

Day, R.A. and Potts, D.M. (1993)
Modelling sheet pile retaining walls. *Computers and Geotechnics*, Vol 15, No 2, pp125-143.

De-Moor, E.K. (1994)
An analysis of bored pile/diaphragm wall installation effects. *Géotechnique*, Vol 44, No 2, pp341-348. [plus discussion in Vol 45, No 4, pp753-755.]

Dembicki, E. and Niemunis, A. (1991)
Deformation of cantilever retaining wall in preconsolidated anisotropic clay. *Proc. 10th ECSMFE*, Florence, Vol 2, pp691-694.

Desai, C.S. (1971)
Nonlinear analysis using spline functions. *J. Soil Mech. Fndn Engg Divn ASCE*, Vol 97, SM10, pp1461-1480.

Desai, C.S. and Sargand, S. (1984)
Hybrid FE procedure for soil-structure interaction. *J. Geot. Engg Divn ASCE*, Vol 110, GT4, pp473-486.

Desai, C.S., Zaman, M.M., Lightner, J.G. and Siriwadne, H.J. (1984)
Thin-layer element for interfaces and joints. *Int. J. Num. Anal. Meth. Geomech.*, Vol 8, No 1, pp19-43.

Dluzewski, J.M. (1991)
Soil-structure interaction in consolidation problems. *Computer Methods and Advances in Geomechanics* (eds Beer et al), Vol 2, pp1141-1146. Rotterdam: Balkema.

Dorn, W.S. and McCracken, D.D. (1972)
Numerical Methods with FORTRAN IV Case Studies. New York: John Wiley.

Duncan, J.M. and Chang, C.Y. (1970)
Nonlinear analysis of stress and strain in soils. *J. Soil Mech. Fndn Engg Divn ASCE*, Vol 96, SM5, pp1629-1653.

Duncan, J.M. and Clough, G.W. (1971)
Finite element analysis of Port-Allen lock. *J. Soil Mech. Fndn Engg Divn ASCE*, Vol 97, SM8, pp1053-1068.

Duncan, J.M., Clough, G.W. and Ebeling, R. (1990)
Behaviour and design of gravity earth retaining structures. *Design and Performance of Earth Retaining Structures* (eds Lambe & Hansen), Geot. Spec. Pub. 25, pp251-277. New York: ASCE.

Dysli, M. and Fontana, A. (1982)
Deformations around the excavations in clayey soil. *Proc. Int. Symp. Num. Models in Geomechanics (eds Pande et al)*, Zurich, pp634-642.

Egger, P. (1972)
Influence of wall stiffness and anchor prestressing on earth pressure distribution. *Proc. 5th ECSMFE*, Madrid, Vol 1, pp259-264.

Eisenstein, Z. and Medeiros, L.V. (1983)
A deep retaining structure in till and sand. Part II: performance and analysis. *Can. Geot. J.*, Vol 20, No 1, pp131-140.

Evgin, E. and Eisenstein, Z. (1985)
Performance of an elastoplastic model. *Can. Geot. J.*, Vol 22, No 2, pp177-185.

Fagan, M.J. (1992)
Finite Element Analysis. Harlow: Longman.

Faheem, H., Cai, F, Ugai, K. and Hagiwara, T. (2003)
Two-dimensional base stability of excavations in soft soils using FEM. *Computers and Geotechnics*, Vol 30, No 2, pp141-163.

FEA. (1998)
USAS System Version 14. Kingston on Thames: FEA Ltd.

Felix, B., Frank, R. and Kutniak, M. (1982)
F.E.M. calculations of a diaphragm wall, influence of the initial pressures and of the contact laws. *Int. Symp. Num. Models in Geomechanics* (eds Pande et al), Zurich. pp643-652.

Fernie, R., St.John, H.D. and Potts, D.M. (1991)
Design and construction of a 24m deep basement in London Clay to resist the effects of long term rise in ground water. *Proc. 10th ECSMFE*, Florence, Vol 2, pp699-702.

Finno, R.J. (1992)
Deep cuts and ground movements in Chicago Clay. *Excavation and Support for the Urban Infrastructure* (eds O'Rourke and Hobelman), pp119-143. Geotechnical Special Publication 33. New York, ASCE

Finno, R.J. and Harahap, I.S. (1991)
Finite element analysis of HDR-4 excavation. *J. Geot. Engg Divn ASCE*, Vol 117, No GT10, pp1590-1609.

Finno, R.J., Harahap, I.S. and Sabatini, P.J. (1991)
Analysis of braced excavations with coupled finite element formulations. *Computers and Geotechnics*, Vol 12, No 2, pp91-94.

Folic, R. and Pavlovic, P. (1986)
Numerical analysis of anchored reinforced concrete diaphragm walls. *Proc. 2nd Int. Symp. Num. Models in Geomechanics* (eds Pande & Van Impe), Ghent, pp423-431. Redruth: M Jackson.

Fourie, A.B. (1984)
The behaviour of retaining walls in stiff clay. PhD thesis, University of London.

Fourie, A.B. and Potts, D.M. (1988)
The estimation of design bending moments for retaining walls using finite elements. *Num. Meth. in Geomechanics* (ed Swoboda), pp1101-1107. Rotterdam: Balkema.

Fourie, A.B. and Potts, D.M. (1989)
Comparison of finite element and limiting equilibrium analyses for an embedded cantilever retaining wall. *Géotechnique*, Vol 39, No 2, pp175-188.

Fraser, R.A. (1992)
Mobilisation of stresses in deep excavations: the use of earth pressure cells at Sheung Wan crossover. *Predictive Soil Mechanics* (Proc. Wroth Memorial Symposium, Oxford) pp181-192. London: Thomas Telford.

Fried, I. (1971)
Discretization and computational errors in high-order finite elements. *J. AIAA*, Vol 9, No 10, pp2071-2073.

Fried, I. (1972)
Condition of finite element matrices generated from non-uniform meshes. *J. AIAA*, Vol 10, No 2, pp219-221.

Fried, I. (1973)
Influence of Poisson's ratio on the condition of the finite element stiffness matrix. *Int. J. Solids Structures*, Vol 9, No 3, pp323-329.

Gaba, A.R., Simpson, B., Beadman, D.R., and Powrie, W. (2003)
Embedded retaining walls: guidance for economic design. *Proc. Instn Civ. Engrs, Geot. Engg*, Vol 156, No 1, pp13-15.

Gallagher, R.H. (1977)
Accuracy in data input and in stress calculations. in *Finite Elements in Geomechanics* (ed Gudehus), Chapter 15. New York: Wiley.

Garrett, C. and Barnes, S.J. (1984)
The design and performance of the Dunton Green retaining wall. *Géotechnique*, Vol 34, No 4, pp533-548.

Georgiadis, M. and Anagnostopoulos, C. (1998)
Effect of berms on sheet-pile wall behaviour. *Géotechnique*, Vol 48, No 4, pp569-574.

Georgiadis, M. and Anagnostopoulos, C. (1999)
Displacement of structures adjacent to cantilever sheet pile walls. *Soils and Foundations*, Vol 39, No 2, pp99-104.

Ghaboussi, J. and Pecknold, D.A. (1984)
Incremental finite element analysis of geometrically altered structures. *Int. J. Num. Meth. Engg*, Vol 20, No 11, pp2061-2064.

Ghaboussi, J., Wilson, E.L. and Isenberg, J. (1973)
Finite element for rock joints and interfaces. *J. Soil Mech. Found. Engg Divn ASCE*, Vol 99, No SM10, pp1039-1054.

Gibson, R.E. (1974)
14th Rankine Lecture: The analytical method in soil mechanics. *Géotechnique*, Vol 24, No 2, pp115-140.

Gibson, R.E., Schiffman R.L. and Whitman R.V. (1989)
On two definitions of excess pore pressure. *Géotechnique*, Vol 39, No 1, pp169-171.

Girijavallabham, C.V. and Reese, L.C. (1968)
Finite element method for problems in soil mechanics. *J. Soil Mech. Fndn Engg Divn ASCE, Vol 94*, SM2, pp473-496.

Goh, A.T.C. (1990)
Assessment of basal stability for braced excavation systems using the finite element method. *Computers and Geotechnics*, Vol 10, pp325-338.

Goh, A.T.C. (1993)
Behaviour of cantilever retaining walls. *J. Geot. Engg Divn ASCE*, Vol 119, No GT11, pp1751-1770.

Goh, A.T.C. (1994)
Estimating basal-heave stability for braced excavations in soft clay. *J. Geot. Engg Divn ASCE*, Vol 120, No GT8, pp1430-1436.

Goh, A.T.C., Wong, K.S. and Broms, B.B. (1995)
Estimation of lateral wall movements in braced excavations using neural networks. *Can. Geot. J.*, Vol 32, No 6, pp1059-1064.

Goodman, R.E., Taylor, R.L. and Brekke, T.L. (1968)
A model for the mechanics of jointed rock. *J. Soil Mech. Fndn Engg Divn ASCE*, Vol 94, SM3, pp637-659.

Gourvenec, S.M. (1998)
Three dimensional effects of diaphragm wall installation and staged construction sequences. PhD thesis, University of Southampton.

Gourvenec, S.M. and Powrie, W. (1999)
Three-dimensional finite element analysis of diaphragm wall installation. *Géotechnique*, Vol 49, No 6, pp801-824.

Gourvenec, S.M. and Powrie, W. (2000)
Three-dimensional finite element analysis of embedded retaining walls supported by discontinuous earth berms. *Can. Geot. J.*, Vol 37, No 5, pp1062-1077.

Gourvenec, S.M., Powrie, W. and De-Moor, E.K. (2002)
Three-dimensional effects in the construction of a long retaining wall. *Proc. Instn Civ. Engrs Geot. Eng.*, Vol 155, No 3, pp163-174.

Griffiths, D.V. (1980a)
Finite element analyses of walls, footings and slopes. PhD thesis, University of Manchester.

Griffiths, D.V. (1980b)
Finite element analyses of walls, footings and slopes. *Proc. Conf. Computer Applications to Geotechnical Problems in Highway Engineering*, Cambridge, pp122-146.

Griffiths, D.V. and Koutsabeloulis, N.C. (1985)
Finite element analyses of excavations. *Computers and Geotechnics*, Vol 1, No 3, pp221-234.

Grose, W.J. and Toone, B.H. (1993)
The selection, design and performance of a multi-propped contiguous pile wall in Norwich. in *Retaining Structures* (ed. Clayton), pp24-36. London: Thomas Telford.

Gunn, M.J. (1982)
How not to analyse excavations. *Workshop on Critical State Soil Mechanics in Finite Elements*, Cambridge University.

Gunn, M.J. (1993)
The prediction of surface settlement profiles due to tunnelling. in *Predictive Soil Mechanics, Proc. Wroth Memorial Symposium, Oxford,* (eds. Houlsby and Schofield), pp 304-316. London: Thomas Telford.

Gunn, M.J. (1995)
Private Communication.

Gunn, M.J. and Britto, A.M. (1982), (1984) & (1990)
CRISP Users and Programmers Guide, Volumes 1 & 2. Cambridge: University Engineering Department.

Gunn, M.J. and Clayton, C.R.I. (1992)
Installation effects and their importance in the design of earth-retaining structures. *Géotechnique*, Vol 42, No 1, pp137-141.

Gunn, M.J. and Ponnampalam, A. (1990)
Calculation of bending moments from CRISP output in soil-structure interaction problems. *Proc 4th CRISP Users Workshop*, University of Surrey.

Gunn, M.J. and Rahim, A. (2003)
Private Communication (at 16th CRISP Users Workshop, South Bank University).

Gunn, M.J. and Woods, R.I. (1993)
The education of geotechnical finite element users. *Proc NAFEMS Seminar on Applications of Finite Elements in Geotechnical Engineering, London* (ed Peshkam), pp56-58.

Gunn, M.J., Satkunananthan, A. and Clayton, C.R.I. (1993)
Finite element modelling of installation effects. in *Retaining Structures* (ed. Clayton), pp46-55. London : Thomas Telford.

Gussmann, P. and Weber, K. (1994)
Limit state calculation of an anchored retaining wall. *Num. Meth. in Geot. Engg* (ed Smith), pp341-343. Rotterdam: Balkema.

Haliburton, T.A. (1968)
Numerical analysis of flexible retaining structures. *J. Soil Mech. Fndn Engg Divn ASCE*, Vol 94, SM6, pp1233-1251.

Hansen, L.A. and Clough, G.W. (1980)
Characterization of the undrained anisotropy of clays. *Application of Plasticity and Generalized Stress-Strain in Geotechnical Engineering* (eds Yong & Selig), pp253-276. New York: ASCE.

Hansen, L.A. and Clough, G.W. (1981)
The significance of clay anisotropy in finite element analyses of unsupported excavations. *Implementation of Computer Procedures and Stress-Strain Laws in Geotechnical Engineering* (eds Desai and Saxena), Proc. Symp., Chicago, Vol 1, pp73-92. Durham: Acorn Press.

Hansen, L.A. and Clough, G.W. (1982)
Finite element analysis of cofferdam behaviour. *Proc. 4th Int. Conf. Num. Meth. in Geomechanics*, Edmonton (ed Eisenstein), Vol 2, pp899-906. Rotterdam: Balkema.

Harris, D.I., Hight, D.W., Higgins, K.G., Potts, D.M. and Brady, K.C. (1993)
Finite element analysis of anchored earth retaining walls. in *Retaining Structures* (ed. Clayton), pp599-608. London: Thomas Telford.

Hashash, Y.M.A. and Whittle, A.J. (1996)
Ground movement prediction for deep excavations in soft clay. *J. Geot. Engg Divn ASCE*, Vol 122, No GT6, pp474-486.

Hashash, Y.M.A. and Whittle, A.J. (2002)
Mechanisms of load transfer and arching for braced excavations in clay. *J. Geot. Geoenv. Engg Divn ASCE*, Vol 128, No 3, pp187-197.

Hashash, Y.M.A., Marulanda, C, Ghaboussi, J. and Jung, S. (2003)
Systematic update of a deep excavation model using field performance data. *Computers and Geotechnics*, Vol 30, No 6, pp477-488.

Higgins, K.G, Potts, D.M. and Symons, I.F. (1989)
Comparison of predicted and measured performance of the retaining walls of the Bell Common tunnel. Report CR 124. Crowthorne: Transport and Road Research Laboratory.

Higgins, K.G., Potts, D.M. and Symons, I.F. (1993)
The use of laboratory derived soil parameters for prediction of retaining wall behaviour. in *Retaining Structures* (ed. Clayton), pp92-101. London: Thomas Telford.

Hillier, R.P. (1992)
The plate test on clay - a finite element study. PhD thesis, University of Surrey.

Hinton, E. and Campbell, J.S. (1974)
Local and global smoothing of discontinuous finite element functions using a least squares method. *Int. J. Num. Meth. Engg.*, Vol 8, pp461-480.

Hinton, E., Scott, F.C. and Ricketts, R.E. (1975)
Local least squares stress smoothing for parabolic isoparametric elements. *Int. J. Num. Meth. Engg.*, Vol 9, pp235-256.

Ho, D.K.H. and Smith, I.M. (1991)
Analysis of construction processes in braced excavations. *Proc. 10th ECSMFE*, Florence, Vol 1, pp213-218.

Holt, D.A. and Griffiths, D.V. (1992)
Transient analysis of excavations in soil. *Computers and Geotechnics*, Vol 13, No 3, pp159-174.

Hong, S.H., Lee, F.H. and Yong, K.Y. (2003)
Three-dimensional pile-soil interactions in soldier-piled excavations. *Computers and Geotechnics*, Vol 30, No 1, pp81-107.

Hsi, J.P. and Small, J.C. (1993)
Application of a fully coupled method to the analysis of an excavation. *Soils and Foundations*, Vol 33, No 4, pp36-48.

Hsieh, P.G. and Ou, C.Y. (1998)
Shape of ground surface settlement profiles caused by excavation. *Can. Geot. J.*, Vol 35, No 6, pp1004-1017.

Hubbard, H.W., Potts, D.M., Miller, D. and Burland, J.B. (1984)
Design of the retaining walls for the M25 cut and cover tunnel at Bell Common. *Géotechnique*, Vol 34, No 4, pp495-512.

Irons, B.M. (1970)
A frontal solution program for finite element analysis. *Int. J. Num. Meth. Engg.*, Vol 2, No 1, pp5-32.

Irons, B.M. and Ahmad, S. (1980)
Techniques of Finite Elements. Chichester: Ellis Horwood.

Ishihara, K. (1970)
Relations between process of cutting and uniqueness of solutions. *Soils and Foundations*, Vol 10, No 3, pp50-65.

ITASCA. (1991)
FLAC : Fast Lagrangian Analysis of Continua : User's Manual (Version 3). Minneapolis: ITASCA.

Itzumi, H., Kamemura, K. and Sato, S. (1976)
Finite element analysis of stresses and movements in excavations. *Proc. 2nd Int. Conf. Num. Meth. in Geomechanics*, Blacksburg, Vol 2, pp701-712.

Jardine, R., Potts, D.M., Fourie, A.B. and Burland, J.B. (1986)
Studies of the influence of non-linear stress-strain characteristics in soil-structure interaction. *Géotechnique*, Vol 36, No 3, pp377-396.

Jardine, R., Potts, D.M., St.John, H.D. and Hight, D.W. (1991)
Some practical applications of a non-linear ground model. *Proc. 10th ECSMFE*, Florence, Vol 1, pp223-228.

Jardine, R., Symes, M.J. and Burland, J.B. (1984)
The measurement of soil stiffness in the triaxial apparatus. *Géotechnique*, Vol 34, No 3, pp323-340.

Kerr, W.C. and Tamaro, G.J. (1990)
Diaphragm walls - update on design and performance. *Design and Performance of Earth Retaining Structures* (eds Lambe & Hansen), Geot. Spec. Pub. 25, pp576-594. New York: ASCE.

Kikuchi, N. (1985)
Finite Element Methods in Mechanics. Cambridge: University Press.

Krajewski, W., Edelmann, L. and Plamitzer, R. (2001)
Ability and limits of numerical methods for the design of deep construction pits. *Computers and Geotechnics*, Vol 28, Nos 6-7, pp425-444.

Kreyszig, E. (1999)
Advanced Engineering Mathematics, 8th Edition. Chichester: Wiley.

Kulathilaka, S.A.S. (1991)
Finite element analysis of earth retaining structures. PhD thesis, Monash University.

Kulathilaka, S.A.S. and Donald, I.B. (1991)
Finite element analysis of embedded walls. *Computer Methods and Advances in Geomechanics* (eds Beer et al), Vol 1, pp151-156. Rotterdam: Balkema.

Kulhawy, F.H. (1974)
Analysis of a high gravity retaining wall. *Proc. Speciality Conf. on Analysis and Design in Geot. Engg*, University of Texas, Austin, Vol 1, pp159-172. New York: ASCE.

Kutmen, G. (1986)
The influence of the construction process on bored piles and diaphragm walls : a numerical study. MPhil thesis, University of Surrey.

Lambe, T.W. (1972)
Predicting performance of braced excavations. *Proc. Speciality Conf. on Performance of Earth and Earth-Supported Structures*, Purdue University, Vol 3, pp255-256.

Lambe, T.W. (1973)
13th Rankine Lecture : Predictions in soil engineering. *Géotechnique*, Vol 23, No 2, pp149-202.

Lee, F H, Liu, K.X. and Yong, K.Y. (1997)
Prediction of ground movement around deep excavation. *Proc. 4th Regional Conference in Geot. Engg*, Johor Bahru, Malaysia, pp3-12

Lee, F.H., Yong, K.Y. and Liu, K.X. (1995)
Three-dimensional analyses of excavation in soft clay. *Proc.11th African Regional Conf. - Cairo '95*, Egyptian Geotech. Soc. Cairo, Egypt, pp167-180.

Lee, F.H., Yong, K.Y., Lee, S.L. and Toh, C.T. (1989)
Finite element modelling of a strutted excavation. *Proc. 3rd Int. Symp. Num. Models in Geomechanics* (eds Pande & Pietruszczak), Niagara Falls, pp577-584.

Lee, F.H., Yong, K.Y., Quan, K.C.N. and Chee, K.T. (1998)
Effect of corners in strutted excavations: field monitoring and case histories. *J. Geot. Geoenv. Engg Divn ASCE*, Vol 124, No GT4, pp339-349.

Lee, K.M., and Rowe, R.K. (1989)
Deformations caused by surface loading and tunnelling: the role of elastic anisotropy. *Géotechnique*, Vol 39, No 1, pp125-140.

Lee, T.C.K. (1990)
Finite element modelling of deep excavation in London Clay. PhD thesis, University of London.

Lee, T.C.K. and Butler, F.G. (1993)
Estimation of earth pressures in the design of a deepened quay wall formed of an existing relieving platform. in *Retaining Structures* (ed. Clayton), pp702-710. London: Thomas Telford.

Li, E.S.F. (1990)
On the analysis of singly-propped diaphragm walls. PhD thesis, University of London.

Li, E.S.F., Nyirenda, Z.M. and Pickles, A.R. (1993)
Design and measured performance of diaphragm walls at Waterloo International Terminal. in *Retaining Structures* (ed. Clayton), pp237-247. London: Thomas Telford.

Lightner, J.G. (1981)
A mixed finite element procedure for soil-structure interaction including construction sequences. PhD thesis, Virginia Polytechnic Institute, Blacksburg, VA.

Likar, J. and Vukadin, V. (2003)
Time-dependent back analysis of a multi-anchored pile retaining wall. *J. Geot. Geoenv. Engg Divn ASCE*, Vol 129, No 1, pp91-95.

Lings, M.L., Ng, C.W.W. and Nash, D.F.T. (1994)
The lateral pressure of wet concrete in diaphragm wall panels cast under bentonite. *Proc. Instn Civ. Engrs, Geot. Engg*, Vol 107, No 3, pp163-172.

Livesely, R.K. (1983)
Finite Elements: an Introduction for Engineers. Cambridge: University Press

Long, M. (2001)
A case history of a deep basement in London Clay. *Computers and Geotechnics*, Vol 28, Nos 6-7, pp397-444.

Lorig, L.J. (1991)
Analysis of novel retaining structures using explicit finite difference codes. *Computer Methods and Advances in Geomechanics* (eds Beer et al), Vol 1, pp157-164. Rotterdam: Balkema.

Mana, A.I. and Clough, G.W. (1981)
Prediction of movements for braced cuts in clay. *J. Geot. Engg Divn ASCE*, Vol 107, GT6, pp759-777.

Mandel, J. (1957)
Consolidation des sols (etude mathematique), *Géotechnique*, Vol 3, No 3, pp287-299.

Mar, A. (1993)
Adaptive mesh refinement for nonlinear problems in geomechanics. PhD thesis, University of Manchester.

Matos-Fernandes, M. (1985)
Performance and analysis of a deep excavation in Lisbon. *Proc. 11th ICSMFE*, San Francisco, Vol 4, pp2073-2078.

Matos-Fernandes, M. (1986)
Three dimensional analysis of flexible earth-retaining structures. *Proc. 2nd Int. Symp. Num. Models in Geomechanics* (eds Pande & Van Impe), Ghent, pp433-438. Redruth: M Jackson.

Matos-Fernandes, M., Cardoso, A.J.S., Trigo, J.F.C. and Marques, J.M.M.C. (1993)
Bearing capacity failure of tied-back walls - a complex case of soil-structure interaction. *Computers and Geotechnics*, Vol 15, No 2, pp87-103.

Matsuo, M., Kamei, T. and Ohta, H. (1982)
Deformation of an underground cellular structure and foundation. *Proc. 4th Int. Conf. Num. Meth. in Geomechanics*, Edmonton (ed Eisenstein), Vol 2, pp921-927. Rotterdam: Balkema.

Matsuo, M., Kenmochi, S. and Yagi, H. (1978)
Experimental study on earth pressure of retaining wall by field tests. *Soils and Foundations*, Vol 18, No 3, pp27-41.

Matsuzawa, H. and Hazarika, H. (1996)
Analyses of active earth pressure against rigid retaining wall subjected to different modes of movement. *Soils and Foundations*, Vol 36, No 3, pp51-65.

Mavroulidou, M. (1999)
Numerical modelling of seepage in the presence of phreatic surfaces. PhD thesis, University of Surrey.

Medeiros, L.V., El-Nahhas, F., Smith, L.B. and Eisenstein, Z. (1982)
Modelling of construction of an underground station. *Proc. 4th Int. Conf. Num. Meth. in Geomechanics*, Edmonton (ed Eisenstein), Vol 2, pp929-934. Rotterdam: Balkema.

Melosh, R.J. (1963)
Basis of derivation of matrices for the direct stiffness method. *AIAA J*, Vol 1, pp1631-1637.

Meyer, C.J. (1975)
Special problems related to linear equation solvers. *Proc. ASCE J. Struct. Div.*, No ST6, pp869-890.

Morgenstern, N.R. and Eisenstein, Z. (1970)
Methods of estimating lateral loads and deformations. *Speciality Conf. on Lateral Stresses in the Ground and Design of Earth-Retaining Structures*, Cornell University, pp51-102. New York: ASCE.

Morgenstern, N.R. and Price, V.E. (1965)
The analysis of the stability of general slip surfaces. *Géotechnique*, Vol 15, No 2, pp79-93.

Morris, D.V. and Crockford, W.W. (1990)
Cement stabilized soil retaining walls. *Design and Performance of Earth Retaining Structures* (eds Lambe & Hansen), Geot. Spec. Pub. 25, pp307-321. New York: ASCE.

Moulds, R.I. (1998)
Analysis of double-wall cofferdams. MSc dissertation, University of Surrey.

Mroz, Z., Norris, V.A., and Zienkiewicz, O.C. (1979)
Application of an anisotropic hardening model in the analysis of elasto-plastic deformation of soils. *Géotechnique*, Vol 29, No 1, pp1-34.

Murphy, D.J., Clough, G.W. and Woolworth, R.S. (1975)
Temporary excavations in varved clay. *J. Geot. Engg Divn ASCE*, Vol 101, GT3, pp279-295.

NAFEMS (1984)
Guidelines to Finite Element Practice. East Kilbride: National Engineering Laboratory/ Dept of Trade and Industry.

NAFEMS (2001)
Guidelines for Geotechnical Finite Element Practice (Draft for Consultation). London: National Agency for Finite Element Methods and Standards.

Nakai, T. (1981)
Analyses of soil-footing and soil-wall interaction. *Proc. 10th ICSMFE*, Stockholm, Vol 2, pp205-208.

Nakai, T. (1985)
Finite element computations for active and passive earth pressure problems of retaining walls. *Soils and Foundations*, Vol 25, No 3, pp98-112.

Nakai, T., Kawano, H., Murata, K., Banno, M. and Hashimoto, T. (1999)
Model tests and numerical simulation of braced excavation in sandy ground: influences of construction history, wall friction, wall stiffness, strut position and strut stiffness. *Soils and Foundations*, Vol 39, No 3, pp1-12.

Naylor, D.J. (1974)
Stresses in nearly incompressible materials by finite elements with application to the calculation of excess pore pressures. *Int. J. Num. Meth. Engg*, Vol 8, pp443-460.

Naylor, D.J. (1975)
Non-linear finite element models for soil. PhD thesis, University of Wales, College of Swansea.

Naylor, D.J. (1985)
A continuous plasticity version of the critical state model. *Int. J. Num. Meth. Engg*, Vol 21, pp1187-1204.

Naylor, D.J., Pande, G.N., Simpson, B. and Tabb, R. (1984)
Finite Elements in Geotechnical Engineering. Swansea: Pineridge Press.

Newman, R.L and Cǫvil, C.S. (1993)
A temporary secant mini-pile wall propped by a deep jet grout raft. in *Retaining Structures* (ed. Clayton), pp478-487. London: Thomas Telford.

Newson, T.A. (1992)
Constitutive modelling of anisotropically consolidated clay. PhD thesis, University of Wales, College of Cardiff.

Ng, C.W.W. (1992)
An evaluation of soil-structure interaction associated with a multi-propped excavation in stiff clay. PhD thesis, University of Bristol.

Ng, C.W.W. and Lings, M.L. (1995)
Effects of modelling soil nonlinearity and wall installation on back-analysis of deep excavations in stiff clay. *J. Geot. Engg Divn ASCE*, Vol 121, No GT10, pp687-695.

Ng, C.W.W. and Yan, R.W.M. (1998)
Stress transfer and deformation mechanisms around a diaphragm wall panel. *J. Geot. Geoenv. Engg Divn ASCE*, Vol 124, No GT7, pp638-648.

Ng, C.W.W. and Yan, R.W.M. (1999)
Three-dimensional modelling of a diaphragm wall installation sequence. *Géotechnique*, Vol 49, No 6, pp825-834.

Ng, C.W.W., Lings, M.L., Simpson, B. and Nash, D.F.T. (1995)
An approximate analysis of three-dimensional effects of diaphragm wall installation. *Géotechnique*, Vol 45, No 3, pp497-507. [plus discussion in Vol 46, No 4, pp775-777]

Ng, C.W.W., Simpson, B., Lings, M.L. and Nash, D.F.T. (1998)
Numerical analysis of a multi-propped excavation in stiff clay. *Can. Geot. J.*, Vol 35, No 1, pp115-130.

Ng, P.C.F., Pyrah, I.C. and Anderson, W.F. (1997)
Assessment of three interface elements and modification of the interface element in CRISP 90. *Computers and Geotechnics*, Vol 21, No 4, pp315-339.

O'Rourke, T.D. and O'Donnell, C.J. (1997)
Deep rotational stability of a tiedback excavation in clay. *J. Geot. Geoenv. Engg Divn ASCE*, Vol 123, No GT6, pp506-515. [plus discussion in Vol 123, No GT6, pp1221-1228.]

Oblozinsky, P., Ugai, K., Katagiri, M., Saitoh, K., Ishii, T., Masuda, T. and Kuwabara, K. (2001)
A design method for slurry trench wall stability in sandy ground based on the elasto-plastic FEM. *Computers and Geotechnics*, Vol 28, No 2, pp145-159.

Oden, J.T. and Brauchli, H.J. (1971)
On the calculation of consistent *stress distributions in finite element approximations. Int. J. Num. Meth. Engg.*, Vol 3, pp317-325.

Oden, J.T. and Reddy, J.N. (1973)
Note on an approximation method for computing consistent conjugate stresses in elastic finite elements. *Int. J. Num. Meth. Engg.*, Vol 6, pp55-61.

Onishi, K. and Sugawara, T. (1999)
Behaviour of an earth retaining wall during deep excavation in Shanghai soft ground. *Soils and Foundations*, Vol 39, No 3, pp89-97.

Ooi, P.S.K., Walker, M.P. and Smith, J.D. (2002)
Performance of a single-propped wall during excavation and during freezing of the retained soil. *Computers and Geotechnics*, Vol 29, No 5, pp387-409.

Osaimi, A.E. and Clough, G.W. (1979)
Pore pressure dissipation during excavation. *J. Geot. Engg Divn ASCE*, Vol 105, GT4, pp481-498.

Ou, C.Y. and Lai, C.H. (1994)
Finite element analysis of deep excavation in layered sandy and clayey soil deposits. *Can. Geot. J.*, Vol 31, No 2, pp204-214.

Ou, C.Y. and Shiau, B.Y. (1998)
Analysis of the corner effects on excavation behaviour. *Can. Geot. J.*, Vol 35, No 3, pp532-540.

Ou, C.Y., Chiou, D.C. and Wu, T.S. (1996a)
Three-dimensional finite element analysis of deep excavations. *J. Geot. Engg Divn ASCE*, Vol 122, No GT5, pp337-345. [plus discussion in Vol 122, No GT5, pp458-460.]

Ou, C.Y., Hsieh, P.G. and Chiou, D.C. (1993)
Characteristics of ground surface settlement during excavation. *Can. Geot. J.*, Vol 30, No 5 Oct, pp758-767.

Ou, C.Y., Shiau, B.Y. and Wang, I.W. (2002)
Three-dimensional deformation behaviour of the Taipei National Enterprise Center (TNEC) excavation case history. *Can. Geot. J.*, Vol 37, No 2, pp438-448.

Ou, C.Y., Wu, T.S. and Hsieh, H.S. (1996b)
Analysis of deep excavation with column type of ground improvement in soft clay. *J. Geot. Engg Divn ASCE*, Vol 122, No GT9, pp709-716.

Owen, D.R.J. (1991)
An academic view of FE education as preparation for future practice. *Proc. Ist Int. Conf. Education and Training in Finite Element Analysis*, Glasgow, pp1-13.

Owen, D.R.J. and Hinton, E. (1980)
Finite Elements in Plasticity : Theory and Practice. Swansea: Pineridge Press.

Ozawa, Y. and Duncan, J.M. (1976)
Elasto-plastic finite element analyses of sand deformation. *2nd Int. Conf. Num. Meth. in Geomechanics*, Blacksburg, Vol 1, pp243-263.

Padfield, C.J. and Mair, R.J. (1984)
Design of retaining walls embedded in stiff clay. CIRIA Report 104. London: Construction Industry Research and Information Association.

Palmer, J.H.L. and Kenney, T.C. (1972)
Analytical study of a braced excavation in weak clay. *Can. Geot. J.*, Vol 9, No 2, pp145-164.

Pande, G.N., Beer, G. and Williams, J.R. (1990)
Numerical Methods in Rock Mechanics. Chichester: J Wiley.

Pappin, J.W., Simpson, B., Felton, P.J. and Raison, C. (1986)
Numerical analysis of flexible retaining walls. *Proc. Conf. Num. Meth. in Engg Theory and Application (NUMETA)*, Swansea, pp789-802.

Parry, R.G. (1982)
Private Communication, cited by Britto and Gunn (1987) in *Critical State Soil Mechanics via Finite Elements.*

Peck, R.B. (1969)
Advantages and limitations of the observational method in applied soil mechanics. *Géotechnique*, Vol 19, No 2, pp171-187.

Peck, R.B. (1985)
The last sixty years. Special Lecture, *Proc. 11th ICSMFE, San Francisco*. Golden Jubilee Volume, pp123-133. Rotterdam: Balkema

Peshkam, V. (1993)
Proc NAFEMS Seminar on Applications of Finite Elements in Geotechnical Engineering, Someplace. London: National Agency for Finite Element Methods and Standards.

Phillips, A., Ho, K.K.S. and Pappin, J.W. (1993)
Long-term toe stability of multi-propped basement walls in stiff clays. in *Retaining Structures* (ed. Clayton), pp333-342. London: Thomas Telford.

Pian, T.H.H. (1973)
Hybrid models. in *Numerical and Computational Methods in Structural Engineering*, (eds Fenves *et al.*). New York: Academic Press.

Pickles, A.R. and Woods, R.I. (1989)
Finite element studies of an embankment on soft ground. *Proc Third Int. Symp. Numerical Models in Geomechanics*, Niagara Falls, (eds. Pande & Pietruszack), pp628-635. London: Elsevier Science Publishers.

Pierpoint, N.D. (1996)
The prediction and back-analysis of excavation behaviour in Oxford Clay. PhD thesis, University of Sheffield.

Pinelo, A. and Matos-Fernandes, M. (1981)
Anchors behaviour and tied back wall analysis. *Proc. 10th ICSMFE*, Stockholm, Vol 2, pp219-225.

Ponnampalam, A. (1990)
MPhil/PhD Transfer Report, University of Surrey.

Potts, D.M. (1991)
Finite element simulation of embedded retaining walls. *Advanced Geotechnical Analysis, Developments in Soil Mechanics and Foundation Engineering - 4* (eds. Banerjee and Butterfield), Chap. 4. London: Elsevier.

Potts, D.M. (1993)
The analysis of earth-retaining structures. in *Retaining Structures* (ed. Clayton), pp167-186. London: Thomas Telford.

Potts, D.M. (2003)
42nd Rankine Lecture: Numerical analysis: a virtual dream or a practical reality?. *Géotechnique*, Vol 53, No 6, pp533-573.

Potts, D.M. and Burland, J.B. (1983)
A numerical investigation of the retaining walls of the Bell Common Tunnel. TRRL Supplementary Report 783. Crowthorne: Transport and Road Research Laboratory.

Potts, D.M. and Day, R.A. (1990)
The use of sheet pile retaining walls for deep excavations in stiff clay. *Proc. Instn Civ. Engrs*, Part 1, Vol 88, pp899-927.

Potts, D.M. and Fourie, A.B. (1984)
The behaviour of a propped retaining wall: results of a numerical experiment. *Géotechnique*, Vol 34, No 3, pp383-404.

Potts, D.M. and Fourie, A.B. (1985)
The effect of wall stiffness on the behaviour of a propped retaining wall. *Géotechnique*, Vol 35, No 3, pp347-352.

Potts, D.M. and Fourie, A.B. (1986)
A numerical study of the effects of wall deformation on earth pressure. *Int. J. Num. Anal. Meth. Geomech.*, Vol 10, pp383-405.

Potts, D.M. and Gens, A. (1985)
A critical assessment of methods of correcting for drift from the yield surface in elastoplastic finite element analysis. *Int. J. Num. Anal. Meth. Geomech.*, Vol 9, pp 149-159.

Potts, D.M. and Knights, M.C. (1985)
Finite element techniques for preliminary assessment of a cut and cover tunnel. *Tunnelling '85*, Fourth Int. Symp., Brighton, pp83-92.

Potts, D.M., Addenbrooke, T.I. and Day, R.A. (1993)
The use of soil berms for temporary support of retaining walls. in *Retaining Structures* (ed. Clayton), pp440-447. London: Thomas Telford.

Potts, D.M., Adenbrooke, T. and Day, R. (1990)
Convergence criteria for Cam-clay constitutive models. *Proc 4th CRISP Users Workshop*, University of Surrey.

Potts, D.M., Axelsson, K., Grande, L., Schweiger, H., and Long, M. (2002)
Guidelines for the use of Advanced Numerical Analysis. London: Thomas Telford.

Potts, D.M., Fourie, A.B. and Burland, J.B. (1984)
The influence of in-situ soil stresses on the behaviour of propped retaining walls. *Soil-Structure Interaction*, pp43-46. London: Instn Struct. Engrs.

Powrie, W. and Batten, M. (2000)
Comparison of measured and calculated temporary-prop loads at Canada Water Station. *Géotechnique*, Vol 50, No 2, pp127-140.

Powrie, W. and Chandler, R.J. (1998)
The influence of a stabilizing platform on the performance of an embedded retaining wall: a finite element study. *Géotechnique*, Vol 48, No 3, pp403-410.

Powrie, W. and Daly, M.P. (2002)
Centrifuge model tests on embedded retaining walls supported by earth berms. *Géotechnique*, Vol 52, No 2, pp89-106.

Powrie, W. and Kantartzi, C. (1996)
Ground response during diaphragm wall installation in clay: centrifuge model tests. *Géotechnique*, Vol 46, No 4, pp725-739.

Powrie, W. and Li, E.S.F. (1990a)
Design study of an in situ wall propped at formation level. *Workshop on Advanced Geotechnical Analysis*, Cambridge University.

Powrie, W. and Li, E.S.F. (1990b)
Private communication.

Powrie, W. and Li, E.S.F. (1991a)
Finite element analysis of an in situ wall propped at formation level. *Géotechnique*, Vol 41, No 4, pp499-514.

Powrie, W. and Li, E.S.F. (1991b)
Analysis of in-situ retaining walls propped at formation level. *Proc. Inst. Civ. Engrs*, Part 2, Vol 91, Dec, pp853-873.

Powrie, W., Chandler, R.J., Carder, D.R. and Watson, G.V.R. (1999)
Back-analysis of an embedded retaining wall with a stabilizing base slab. *Proc. Instn Civ. Engrs, Geot. Engg*, Vol 137, No 2, pp75-86.

Powrie, W., Davies, J.N. and Britto, A.M. (1993)
A cantilever retaining wall supported by a berm during temporary works activities. in *Retaining Structures* (ed. Clayton), pp418-428. London: Thomas Telford.

Rampello, S., Tamagnini, C. and Calabresi, G. (1992)
Observed and predicted response of a braced excavation in soft to medium clay. in Predictive Soil Mechanics, *Proc. Wroth Memorial Symposium*, Oxford, pp420-433.

Reissner, E. (1950)
On a variational theorem of elasticity. *J. Math. Phys.* Vol 29, pp90-98.

Richards, D.J. (1995)
Centrifuge and numerical modelling of twin- propped retaining walls. PhD thesis, University of London.

Richards, D.J. and Powrie, W. (1994)
Finite element analysis of construction sequences for propped retaining walls. *Proc. Instn Civ. Engrs, Geot. Engg*, Vol 107, No 4, pp207-216.

Richards, D.J., Holmes, G. and Beadman, D.R. (1999)
Measurement of temporary prop loads at Mayfair car park. *Proc. Instn Civ. Engrs, Geot. Engg*, Vol 137, No 3, pp165-174.

Robinson, J. (1976)
A single element test. *Comp. Meth. Appl. Mech. Engg.*, Vol 7, No 2, pp191-200.

Rodrigues, J.S.N. (1975)
The development and application of a finite element program for the solution of geotechnical problems. PhD thesis, University of Surrey

Rosanoff, R.A., Gloudemann, J.F., and Levy, S. (1968)
Numerical conditioning of stiffness matrix formulations for frame structures. *Proc. 2nd Air Force Conf. on Matrix Methods in Struct. Mech.*, AFFDL-TR-68-150, pp1020-1060.

Roscoe, K.H. and Burland, J.B. (1968)
On the generalised strain-strain behaviour of 'wet' clay. in *Engineering Plasticity* (eds Heyman & Leckie), pp535-609. Cambridge University Press.

Roscoe, K.H. and Schofield, A.N. (1963)
Mechanical behaviour of an idealised 'wet' clay. *Proc 2nd ECSMFE, Wiesbaden*, pp47-54.

Roth, W.H. and Crandall, L. (1981)
Non linear elastic finite element analysis of lateral pressure against a basement wall. *Int. J. Num. Anal. Meth. Geomech.*, Vol 5, pp327-344.

Roth, W.H., Lee, K.L. and Crandall, L. (1979)
Calculated and measured earth pressures on a deep basement wall. *Proc. 3rd Int. Conf. Num. Meth. in Geomechanics*, Aachen, Vol 4, pp1179-1191.

Rudykh, D.L. (1981)
Use of the finite element method for determining fill earth pressure on retaining walls. *Osnovaniya, Fundamenty i Mekhanika Gruntov*, Vol 2, March, pp20-22.

SAGE. (1996)
SAGE CRISP - Volume 1 - Users Guide. SAGE Engineering Ltd, Bath.

Sargand, S.M. (1981)
A hybrid finite element procedure for soil-structure interaction including construction sequences. PhD thesis, Virginia Polytechnic Institute, Blacksburg, VA.

Schad, H. (1985)
Computing costs for FEM analysis of foundation engineering problems and possible ways of increasing efficiency. *Int. J. Num. Anal. Meth. Geomech.*, Vol 9, pp261-275.

Schoenwolf, D.A., Whitman, R.V., Abbott, E.L. and Becker, J.M. (1992)
Post Office Square garage project - a case history of instrumented slurry wall performance. *Slurry Walls : Design, Construction and Quality Control* (eds Paul, Davidson and Cavalli), pp361-376. Philadelphia: ASTM Special Tech. Publ. 1129.

Schofield, A.N. (1980)
Cambridge geotechnical centrifuge operations. *Géotechnique*, Vol 30, No 3, pp227-268.

Schofield, A.N. and Wroth, C.P. (1968)
Critical State Soil Mechanics. Maidenhead: McGraw-Hill.

Schweiger, H.F. (1994)
Deep excavations in soft soil - finite element analysis and in-situ measurements. *Num. Meth. in Geot. Engg* (ed Smith), pp369-376. Rotterdam: Balkema.

Seed, R.B. and Duncan, J.M. (1986)
FE Analyses: compaction-induced stresses and deformations. *J. Geot. Engg Divn ASCE*, Vol 112, No GT1, pp22-43.

Sills, G.C., Burland, J.B. and Czechowski, M.K. (1977)
Behaviour of anchored diaphragm wall in stiff clay. *Proc. 9th ICSMFE*, Tokyo, Vol 2, pp147-154.

Simpson B., Blower T., Craig, R.N., and Wilkinson, W.B. (1989)
The engineering implications of rising groundwater levels in the deep aquifer beneath London. CIRIA Special Publications, London

Simpson, B. (1973)
Finite elements applied to problems of plane strain deformation in soils. PhD thesis, Cambridge University.

Simpson, B. (1980)
Use of finite element method for analysis of ground movements. *Proc. Conf. Computer Applications to Geotechnical Problems in Highway Engineering*, Cambridge, pp101-121.

Simpson, B. (1981)
Finite element design with particular reference to deep basements in London Clay. Chapter 12 of *Finite Elements in Geotechnical Engineering* (Naylor *et al*). Swansea: Pineridge Press.

Simpson, B. (1992)
32nd Rankine Lecture. Retaining structures - displacement and design. *Géotechnique*, Vol 42, No 4, pp539-576.

Simpson, B. and Ng, C.W.W. (1995)
Discussion on 'An analysis of bored pile/diaphragm wall installation effects'. *Géotechnique*, Vol 45, No 4, p753.

Simpson, B. and Wroth, C.P. (1972)
Finite element computations for a model retaining wall in sand. *Proc. 5th ECSMFE*, Vol 1, pp85-93.

Simpson, B., O'Riordan, N.J. and Croft, D.D. (1979)
A computer model for the analysis of ground movements in London Clay. *Géotechnique*, Vol 29, No 2, pp149-175.

Skempton, A.W. (1954)
The pore pressure coefficients A and B. *Géotechnique*, Vol 4, No 4, pp143-147.

Sloan, S.W. and Randolph, M.F. (1982)
Numerical prediction of collapse loads using finite element methods. *Int. J. Num. and Anal. Meth. in Geomechanics*, Vol 6, pp47-76.

Sloan, S.W. and Randolph, M.F. (1983)
Automatic element reordering for finite element analysis with frontal solution schemes. *Int. J. Num. Meth. Engg.*, Vol 19, pp1153-1181

Smith, I.M. (1970)
A finite element approach to elastic soil-structure interaction. *Can. Geot. J.*, Vol 7, No 2, pp95-105.

Smith, I.M. (1973)
Numerical analysis of plasticity in soils. *Proc. Symp. Plasticity and Soil Mechanics*, Cambridge, pp279-289. [plus oral discussion, pp290-296.]

Smith, I.M. and Boorman, R. (1974)
The analysis of flexible bulkheads in sands. *Proc. Instn Civ. Engrs*, Part 2, Vol 57, pp413-436.

Smith, P.R., Jardine, R., and Hight, D.W. (1992)
The yielding of Bothkennar clay. *Géotechnique*, Vol 42, No 2, pp257-274.

St John, H.D., Higgins, K.G., and Potts, D.M. (1995)
Discussion on 'An analysis of bored pile/diaphragm wall installation effects'. *Géotechnique*, Vol 45, No 4, pp753-755.

St.John, H.D. (1975)
Field and theoretical studies of the behaviour of ground around deep excavations in London Clay. PhD thesis, Cambridge University.

St.John, H.D., Harris, D.I., Potts, D.M. and Fernie, R. (1993)
Design study for a cantilever bored pile retaining wall with relieving slabs. in *Retaining Structures* (ed. Clayton), pp363-372. London: Thomas Telford.

St.John, H.D., Potts, D.M., Jardine, R.J. and Higgins, K.G. (1992)
Prediction and performance of ground response due to construction of a deep basement at 60 Victoria Street. in Predictive Soil Mechanics, *Proc. Wroth Memorial Symposium*, Oxford, pp449-465.

Stallebrass, S.E. (1990)
The effect of recent stress history on the deformation of over-consolidated soils. PhD thesis, City University.

Stallebrass, S.E. and Taylor, R.N. (1997)
The development and evaluation of a constitutive model for the prediction of ground movements in overconsolidated clay. *Géotechnique*, Vol 47, No 2, pp235-254.

Stevens, A., Corbett, B.O. and Steele, A.J. (1977)
Barbican Arts Centre: the design and construction of the substructure. *The Structural Engineer*, Vol 55, No 11, pp473-485.

St.John, H.D., Harris, D.I., Potts, D.M. and Fernie, R. (1993)
Design study for a cantilever bored pile retaining wall with relieving slabs. in *Retaining Structures* (ed. Clayton), pp363-372. London: Thomas Telford.

Stroh, D. (1974)
Finite element analysis of tied-back walls (in German). DSc thesis, Technische Hochscule Darmstadt.

Stroh, D. (1975)
Discussion - Performance of tied-back walls in clay (Clough & Tsui). *J. Geot. Engg Divn ASCE*, Vol 101, No GT8, pp833-836.

Stroh, D. and Breth, H. (1976)
Deformation of deep excavations. *Proc. 2nd Int. Conf. Num. Meth. in Geomechanics*, Blacksburg, Vol 2, pp686-700.

Swain, A. (1989)
Private communication.

Symons, I.F. (1990)
The behaviour of embedded retaining walls. *Design and Performance of Earth Retaining Structures* (eds Lambe & Hansen), Geot. Spec. Pub. 25, pp562-575. New York: ASCE.

Symons, I.F. and Carder, D.R. (1991)
The behaviour in service of a propped retaining wall embedded in soft clay. *Proc. 10th ECSMFE*, Florence, Vol 2, pp761-766.

Symons, I.F. and Carder, D.R. (1993)
Stress changes in stiff clay caused by the installation of embedded walls. in *Retaining Structures*, (ed C.R.I. Clayton), pp227-236. London: Thomas Telford

Symons, I.F., Little, J.A., McNulty, T.A., Carder, D.R. and Williams, S.G.O. (1987)
Behaviour of a temporary anchored sheet pile wall on A1(M) at Hatfield. TRRL Research Report 99. Crowthorne: Transport and Road Research Laboratory.

Symons, I.F., Potts, D.M. and Charles, J.A. (1985)
Predicted and measured behaviour of a proposed embedded retaining wall in stiff clay. *Proc. 11th ICSMFE*, San Francisco, Vol 4, pp2265-2268.

Tamano, T., Fukui, S., Kadota, S. and Ueshita, K. (1991)
Mechanical behaviour of bottom ground heave due to excavation. *Computer Methods and Advances in Geomechanics* (eds Beer et al), Vol 1, pp199-204. Rotterdam: Balkema.

Tan, S.B., Tan, S.L. and Chin, Y.K. (1985)
A braced sheetpile excavation in soft Singapore marine clay. *Proc. 11th ICSMFE*, San Francisco, Vol 3, pp1671-1674.

Tan, T.S., Leong, P.H., Yong, K.Y., Kamata, R., Wei, J. Chua, K.C. and Loh, Y.H. (2001)
A case study of the behaviour of a vertical sea wall. *Soils and Foundations*, Vol 41, No 5, pp103-115.

Taylor, R.E. and Meadows, D.F. (1990)
Cellular sheetpile floodwall in cohesive material at Williamson, West Virginia. *Design and Performance of Earth Retaining Structures* (eds Lambe & Hansen), Geot. Spec. Pub. 25, pp217-231. New York: ASCE.

Tedd, P., Chard, B.M., Charles, J.A. and Symons, I.F. (1984)
Behaviour of a propped embedded retaining wall in stiff clay at Bell Common Tunnel. *Géotechnique*, Vol 34, No 4, pp513-532.

Templeton, J.S. (2002)
The role of finite elements in suction foundation design analysis. *Proc Offshore Technology Conference*, Houston, Paper OTC 14235.

Terzaghi, K. (1943)
Theoretical Soil Mechanics. John Wiley & Sons, New York.

Thompson, S.A. (1976)
Finite elements in soils. PhD thesis, Cambridge University.

Tong, P. (1971)
On the numerical problems of finite elements. in *Computer Aided Engineering* (ed. G.L. Gladwell), pp539-558. University of Waterloo Press.

Tsui, Y. and Cheng, Y.M. (1989)
A fundamental study of braced excavation construction. *Computers and Geotechnics*, Vol 8, No 1, pp39-64.

Tsui, Y. and Clough, G.W. (1974)
Plane strain approximations in finite element analysis of temporary walls. *Proc. Conf. on Analysis and Design in Geot. Engg*, University of Texas, Austin, Vol 1, pp173-197. New York: ASCE.

Turner, M.J., Clough, R.W., Martin, H.C. and Topp, L.J. (1956)
Stiffness and deflection analyses of complex structures. *J. Aeronautical Sciences*, Vol 23, No 9, p805-823.

Ugai, K. (1991)
Analyses of active earth pressure problems base on simple constitutive equations for granular materials. *Computer Methods and Advances in Geomechanics* (eds Beer et al), Vol 1, pp527-532. Rotterdam: Balkema.

Van Den Berg, P. (1991)
Effects of surface loading on earth retaining walls. *Proc. 10th ECSMFE*, Florence, Vol 2, pp767-770.

Van Weele, A.F. (1989)
Prediction versus performance. *Proc. 12th ICSMFE*, Rio de Janeiro, Supplementary Volume, pp1-15.

Vaziri, H.H. (1996)
Numerical study of parameters influencing the response of flexible retaining walls. *Can. Geot. J.*, Vol 33, No 2, pp290-308.

Vaziri, M. (1988)
An Experimental and Theoretical Investigation of Screw Plate Testing. PhD thesis, University of Surrey.

Vermeer, P.A., Punlor, A. and Ruse, N. (2001)
Arching effects behind a soldier pile wall. *Computers and Geotechnics*, Vol 28, Nos 6-7, pp379-396.

Wallace, J.C., Ho, C.E. and Long, M.M. (1993)
Retaining wall behaviour for a deep basement in Singapore marine clay. in *Retaining Structures* (ed. Clayton), pp195-204. London: Thomas Telford.

Ward, W.H. and Burland, J.B. (1973)
The use of ground strain measurements in civil engineering. *Phil. Trans. R. Soc. London*, A274, pp421-428.

Watson, G.V.R. and Carder, D.R. (1994)
Comparison of the measured and computed performance of a propped bored pile wall at Walthamstow. *Proc. Instn Civ. Engrs, Geot. Engg*, Vol 107, No 2, pp127-133. [plus discussion Vol 113, No 1, pp58-59]

Wheeler, P. (1998)
Value of geotechnics in construction : meeting client needs. *Ground Engineering*, supplement, November, pp6-7.

Wheeler, S.J., Näätänen, A. and Karstunen, M. (2003)
An anisotropic elasto-plastic model for natural soft clay. *Can. Geot. J.*, Vol 40, No 3, pp403-418.

Whittle, A.J. (1993)
Evaluation of a constitutive model for overconsolidated clays. *Géotechnique*, Vol 43, No 2, pp289-314.

Whittle, A.J. and Hashash, Y.M.A. (1993)
Analysis of the behaviour of propped diaphragm walls in a deep clay deposit. in *Retaining Structures* (ed. Clayton), pp131-139. London: Thomas Telford.

Whittle, A.J. and Kavvadas, M.J. (1994)
Formulation of the MIT-E3 constitutive model for overconsolidated clays. *J. Geot. Engg Divn ASCE*, Vol 120, No GT1, pp173-198.

Whittle, A.J. and Ladd, C.C. (1998)
discussion on Deep rotational stability of a tiedback excavation in clay (O'Rourke and O'Donnell). *J. Geot. Engg Divn ASCE*, Vol 123, No GT6, pp1222-1227.

Whittle, A.J., Hashash, Y.M.A. and Whitman, R.V. (1993)
Analysis of deep excavation in Boston. *J. Geot. Engg Divn ASCE*, Vol 119, No GT1, pp69-90. [plus discussion by Koutsoftas in Vol 120, No GT10, pp1909-1912.]

Winkler, E. (1867)
Die Lehre von der Elastizitat und Festigkeit. Prague: Dominicus.

Wong, K.S. and Broms, B.B. (1989)
Lateral wall deflections of braced excavations in clay. *J. Geot. Engg Divn ASCE*, Vol 115, No GT6, pp853-870.

Wood, L.A. and Forbes-King, C.J. (1989)
Behaviour of flexible earth retaining walls at full-scale. *Computer and Physical Modelling in Geot. Engg* (eds Balasubramaniam et al), pp535-544. Rotterdam: Balkema.

Woods, R.I. (1986)
Finite element analysis of coupled consolidation. *Proc. 2nd Int. Symp. Numerical Models in Geomechanics*, (eds. Pande and Van Impe), pp709-717. Redruth: Jackson & Son.

Woods, R.I. (1990)
A Users Guide to the CRISP Suite at University of Surrey. Internal Report, Department of Civil Engineering, University of Surrey.

Woods, R.I. (1993)
Finite element analysis of Jamaica Flour Mills. Report to Engineering Geology Ltd, Godalming (in confidence).

Woods, R.I. (1995)
Finite element analysis of Queensberry House. Report to Laing Technology Group Ltd, Mill Hill (in confidence).

Woods, R.I. and Clayton, C.R.I. (1993)
Application of the CRISP finite element program to practical retaining wall design. in *Retaining Structures* (ed. Clayton), pp102-111. London: Thomas Telford.

Woods, R.I. and Contreras, L.F. (1988)
Numerical modelling of plate loading tests - Part II. *Research Report GE/88/8*, City University, London.

Woods, R.I. and Miller, K.S. (1997)
Finite element analysis of the demolition and reconstruction of Queensberry House. *Proc 10th CRISP Users Workshop*, City University.

Woods, R.I., Gunn, M.J. and Hillier, R.P. (1992)
The influence of nonlinearity on the interpretation of stiffness parameters from field plate load tests. *Proc Fourth Int. Symp. On Numerical Models In Geomechanics*, Swansea (Eds. G.N. Pande and S. Pietruszack). Rotterdam; Balkema, Vol 2, pp999-1011.

Wroth, C.P. (1972)
General theories of earth pressure and deformation. General Report, *Proc. 5th ECSMFE*, Madrid, Vol 1, pp33-52.

Yong, K.Y., Lee, F.H., Parnploy, U. and Lee, S.L. (1989)
Elasto-plastic consolidation analysis for strutted excavation in clay. *Computers and Geotechnics*, Vol 8, No 4, pp311-328.

Yoo, C.S. (2001)
Behaviour of braced and anchored walls in soils overlying rock. *J. Geot. Geoenv. Engg Divn ASCE*, Vol 127, No 3, pp225-233.

Young, D.K. and Ho, E.W.L. (1994)
The observational approach to design of a sheet-pile retaining wall. *Géotechnique*, Vol 44, No 4, pp637-654.

Zienkiewicz, O.C. (1971)
The Finite Element Method (2nd Ed). Chichester: J Wiley.

Zienkiewicz, O.C. (1977)
The Finite Element Method (3rd Ed). Chichester: J Wiley.

Zienkiewicz, O.C. (1987)
Computer prediction in engineering. *University of Wales Science and Technical Review*, Vol 2, Autumn, pp5-19.

Zienkiewicz, O.C. and Taylor, R.L. (1989)
The Finite Element Method (4th Ed), Volume I. Maidenhead: McGraw-Hill.

Zienkiewicz, O.C., Emson, C. and Bettess, P. (1983)
A Novel Boundary Infinite Element. *Int. J. Num. Meth. Engg.*, Vol 19, pp393-404.

Zytynski, M. (1976)
First Year Research Report, Cambridge University, Engineering Department.

APPENDIX A

Details of Case Histories

(Commercial retaining wall analyses conducted by the writer)

APPENDIX A
DETAILS OF CASE HISTORIES

Throughout this thesis, reference has been made to specific retaining wall analyses when discussing particular modelling issues. This Appendix gives full details of these analyses - all of which were performed by the writer for a variety of clients[1] (contractors, consultants, local authorities, research organizations) between 1989-1996. With one exception, the analyses have one important feature in common; namely, that they were performed as part of the design process for a real retaining structure - with the associated time/cost constraints. There was no time for the continuous refinement of modelling details which is possible in the research environment - each analysis had to be more or less "right first time". A rapid turn-around was required, with results being faxed to the client concerned as soon as they were available. Thus the writer is well-placed to understand the pressures and difficulties experienced in a commercial design context. Prior to the first case in 1989, the writer had not carried out a full retaining wall analysis, although had had 5 years experience with CRISP in the analysis of other geotechnical problems.

In all cases, the client was responsible for specifying overall geometry, material parameters, and desired output. The writer was responsible for discretization, selection of constitutive model, construction modelling, identifying (and fixing) numerical problems, and post-processing. On occasion, the writer had the opportunity to indicate what in-situ and laboratory tests should be carried out to obtain parameters for the finite element analysis - but this was the exception rather than the rule.

Sensitivity studies were often carried out - sometimes to explore variations in soil parameters (in which there may have been little confidence), or perhaps to study alterations to the excavation/propping sequence. A number of these sensitivity studies were part of the analysis specification initially given to the writer - in other instances, they arose from considering the results of a preliminary analysis, and evolved in a more open-ended manner.

Most of the time, the writer acted essentially as a form of FE subcontractor with clearly defined tasks, deadlines and liabilities. Ultimately the client was responsible for deciding how

---

[1] "client" in this context is the party which commissioned the analyses - not the client for the overall engineering project.

to act upon the results, although was always able to seek clarification from the writer. In one or two instances, a staff member of the client worked alongside the writer in order to be trained and educated in the finite element analysis process - with the intention of doing subsequent analyses him/herself.

Details of each case have been given in a standard format:

a) project summary
b) analysis overview
c) analysis details
d) specific comments
e) finite element mesh

In several cases, one or more significantly different cross-sections were analysed, and as these were beyond mere sensitivity studies, they have been noted separately within each case.

The cases are reported in chronological order, and all except the last were completed before the bulk of numerical investigations detailed in this thesis were finished. Consequently, none of the recommendations which have emerged from the investigations herein were available when these commercial analyses were conducted. Indeed, the absence of such guidelines was a contributory factor to this research work being conducted in the first place.

Case	Title
1	A406 Walthamstow
2	Neasden Lane Underpass
3	A6(M) Stockport
4A	Southwark Station Ticket Hall
4B	Southwark Station Concourse
5	Greenside Place
6A	RPR (Regents Park Road) Junction Tunnels
6B	RPR Junction Approaches
6C	RPR Junction Slip Road 3
6D	RPR Junction Slip Road 5
7	A322 Aldershot Road Underpass
8A	Queensberry House : Transverse
8B	Queensberry House : Longitudinal

CASE 1 - A406 Walthamstow

Project Details / Analysis Overview						
Full title	A406 Chingford Rd to Hale End Rd					
Location	Walthamstow, NE London					
Client	Bullen & Partners, Croydon					
Description	depressed elevation road corridor, 2.8 km long, 28.8m wide					
Wall type	contiguous bored piles (1800 dia. @ 2000 c/c)					
Wall dimensions (m)	retained height	11.0	overall length	22.0	width/diam.	1.8
Support (temporary)	single high-level row of tubular steel props					
Support (permanent)	single articulated concrete slab at formation level					
Ground conditions	made ground and drift deposits overlying London clay to depth					
Pore pressures	hydrostatic to 10m depth; underdrained below 10m					
Unusual aspects	hinged prop slab / long term recharge of pore pressures expected					
Design variations	possibility of narrower road corridor (21.4m wide)					
Other comments	construction completed in 1991					
Publications/articles	"Cut and dried", *New Civil Engineer*, 29 Sep 1991, pp22-23					
Type of analysis	coupled consolidation (construction + long term + recharged p.w.p.)					
Purpose of analysis	to check contractors alternative design					
Soil model	non-homogeneous isotropic linear elastic-perfectly plastic					
Structural materials	linear elastic (concrete walls/slabs and steel tubular props)					
Recent history	no previous construction/excavation to model					
Wall installation	element swopping					
Excavation sequence	sequential with installation/removal of propping					
Long term behaviour	equilibration to present p.w.p. profile with foundation level drainage, followed by equilibration to future (recharged) distribution					
Output required	wall deflections, wall bending moments, lateral earth pressures, permanent prop slab axial loads and bending moments, swelling pressures on underside of slab, shear stresses on back of wall					
Field measurements	none taken or made available					

CASE 1 - A406 Walthamstow (contd)

CRISP Analysis details

Mesh details	**NN**	193	**NEL**	189	**X/H**	5.24	**Y/W**	2.72

Element types	**soil**	LSQ/u	**wall**	LSQ	**supports**	LSQ

Soil parameters (London clay)	E_o	50	MPa	m_E	5	MPa/m	y_o	50	m
	ν	0.200		c_o	8	kPa	m_C	0	kPa/m
	ϕ	23	°	γ	20	kN/m^3			
	γ_w	10	kN/m^3	k_X	.015	m/yr	k_Y	.003	m/yr
Concrete parameters	E	28	GPa	ν	0.150		γ	24	kN/m^3
Prop parameters	E	210	GPa	A	.01047	m^2/m			

In-situ stresses (kPa)	pt	y (m)	σ'_X	σ'_Y	σ'_Z	K_O	u	p'_C
	1	50.	0.	0.	0.	3.5	0.	-
	2	47.	140.	40.	140.	3.5	20.	-
	3	45.	174.	60.	174.	2.9	40.	-
	4	40.	209.	110.	209.	1.9	90.	-
	5	35.	304.	190.	304.	1.6	110.	-
	6	0.	1200.	750.	1200.	1.6	250.	-

Boundary fixities	**cent.line**	smooth	**base**	smooth	**remote**	smooth

Block	**Incs**	**Time (yrs)**	**Activity**
1	1	0.	set up initial p.w.p. boundary conditions
2	5	.25	install wall (swop elements)
3	4	.2	excavate to +48m and install temporary props
4	4	.2	excavate to +44.4m
5	6	.3	excavate to +39.4m
6	2	.1	excavate to +39m (FL) and install permanent prop slab
7	5	.25	remove temporary props
8	2	.1	apply 25 kPa surcharge on prop slab (≡ carriageway load)
9	7	120.	fix under-slab drain and allow equilibration to present p.w.p. profile
10	7	120.	allow equilibration to recharged (hydrostatic) p.w.p. profile

CASE 1 - A406 Walthamstow (contd)

Comments

- Contractor (Cementation) used ICFEP (via GCG) in their design work - Category III checking was performed by Maunsell & Partners, who also used CRISP

- The FE mesh used by the writer was based on that used by GCG, although the writer had no access to the ICFEP predictions

- The hinge detail was varied in thickness to study the effects of moment transfer at the connection - a "bow tie" arrangement worked well in eliminating moment transfer:

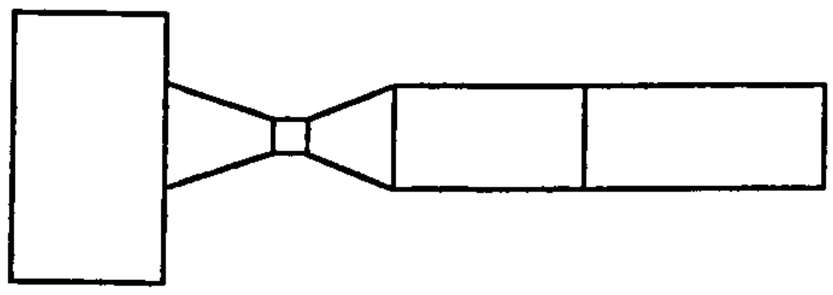

- The writer's analyses showed that the wall crest movements were greater if equilibration was allowed to the existing p.w.p. profile **first**; i.e. before recharging groundwater levels. The contractor had not shown this intermediate stage. Recharging ground water actually pushed the wall crest back towards the retained soil (the resultant line of thrust of the extra water pressure acted below the permanent formation level prop)

- Stress path tests had been carried out on London clay samples to obtain appropriate stiffness parameters for the soil around the retaining wall

- Self-boring pressuremeter data had been used to infer the profile of Ko with depth

CASE 2 - Neasden Lane Underpass

Project Details / Analysis Overview						
Full title	Neasden Lane Underpass					
Location	Neasden, NW London					
Client	Transport & Road Research Laboratory, Crowthorne					
Description	underpass beneath A406 North Circular Road, 29.65m wide					
Wall type	diaphragm panels					
Wall dimensions (m)	retained height	8.6	overall length	13.0	width/diam.	0.6
Support (temporary)	four levels of prestressed ground anchorages at 20° to horizontal					
Support (permanent)	same as temporary					
Ground conditions	London clay overlying Woolwich and Reading Beds at depth					
Pore pressures	hydrostatic; GWL 1m below ground surface					
Unusual aspects	one of the earliest anchored diaphragm walls to be built					
Instrumentation	inclinometers, piezometers, spade cells, and load cells (in wall)					
Other comments	construction completed in 1972; TRL instrumentation installed 1988					
Publications/articles	Sills *et al.* (1977), Carswell *et al.* (1991)					
Type of analysis	coupled consolidation (construction + long term up to 15 years)					
Purpose of analysis	to compare predicted and observed performance					
Soil model	non-homogeneous isotropic linear elastic-perfectly plastic					
Structural materials	linear elastic (concrete wall and steel anchor tendons)					
Recent history	no previous construction to model					
Wall installation	element swopping					
Excavation sequence	sequential with installation/stressing of anchors					
Long term behaviour	equilibration to present p.w.p. profile with formation level drainage					
Output required	wall deflections, wall bending moments, lateral earth pressures, pore water pressure profiles, anchor tendon loads, horizontal ground movements					
Field measurements	wall and ground movements, pore water pressures, anchor loads					

CASE 2 - Neasden Lane Underpass (contd)

CRISP Analysis details

Mesh details	**NN**	169	**NEL**	154	**X/H**	5.24	**Y/W**	2.72

Element types	**soil**	LSQ/u	**wall**	LSQ	**supports**	CSB

Soil parameters (London clay)	E_o	32	MPa	m_E	8.4	MPa/m	y_o	40.2	m
	ν	0.200		c_o	10	kPa	m_c	0	kPa/m
	ϕ	24	°	γ	19.4	kN/m^3			
	γ_w	9.81	kN/m^3	k_X	.015	m/yr	k_Y	.003	m/yr
Concrete parameters	E	30	GPa	ν	0.150		γ	22.6	kN/m^3
Tendon parameters	E	200	GPa	A	243e-6	m^2/m	θ	20	°

In-situ stresses (kPa)	**pt**	**y (m)**	**σ'x**	**σ'y**	**σ'z**	**Ko**	**u**	**p'c**
	1	42.65	0.	0.	0.	2.0	0.	-
	2	8.0	644.6	322.3	644.6	2.0	346.5	-

Boundary fixities	**cent.line**	smooth	**base**	smooth	**remote**	smooth

Block	**Incs**	**Time (yrs)**	**Activity**
1	1	0.	set up initial p.w.p. boundary conditions
2	5	.2	install wall (swop-in elements)
3	4	.1	excavate to +40.2m
4	4	.08	apply tensioning force for 1st level of anchors
5	1	.02	install 1st level of anchors
6	4	.1	excavate to +38.2m
7	4	.08	apply tensioning force for 2nd level of anchors
8	1	.02	install 2nd level of anchors
9	4	.1	excavate to +36.2m
10	4	.08	apply tensioning force for 3rd level of anchors
11	1	.02	install 3rd level of anchors
12	4	.1	excavate to +34.2m
13	4	.08	apply tensioning force for 4th level of anchors
14	1	.02	install 4th level of anchors
15	7	15.	set FL drainage and allow equilibration to original p.w.p. profile

CASE 2 - Neasden Lane Underpass (contd)

Comments

- The Neasden Lane Underpass is a well-known case, reported by Sills *et al.* in the 9th ICSMFE (Tokyo, 1977) and by Burland *et al.* the 9th ECSMFE (Brighton, 1979)

- The underpass was also featured in Creed's 1980 PhD thesis on the numerical modelling of diaphragm walls, in which he developed his own FE code - however as his analyses were uncoupled (undrained) and assumed anisotropic linear behaviour for the soil, limited comparison with the writer's results was possible

- The TRL instrumentation was not installed at the time of construction, but some 16 years after the wall was completed - so no data exists on ground, wall or anchor behaviour during or immediately after construction

- The TRL requested sensitivity studies on E' and Ko in order to see which would give the best match between some aspects of the measured behaviour could be matched by parametric variation, but not all at the same time - so it was not possible to establish an unambiguous set of parameters

- Mid-way through the analyses it was discovered that there was a bug in the Mohr-Coulomb model, which effectively suppressed dilation at yield - this was corrected and made a noticeable difference to those analyses where significant yielding took place (i.e. those with high Ko values)

- A complete set of field data is given by Carswell *et al.* (1991) in TRRL Research Report 313

CASE 3 - A6(M) Stockport

Project Details / Analysis Overview						
Full title	A6(M) Stockport N/S Bypass - Bredbury Walls					
Location	Stockport, Manchester					
Client	L G Mouchel & Partners, Manchester					
Description	depressed elevation road corridor, 40m wide					
Wall type	diaphragm panels					
Wall dimensions (m)	retained height	11.2	overall length	16.9	width/diam.	0.9
Support (temporary)	three levels of prestressed ground anchors at 30° to horizontal					
Support (permanent)	as per temporary					
Ground conditions	stiff clay overlying medium dense to dense sand					
Pore pressures	hydrostatic; GWL at 9.5m below original ground level					
Unusual aspects	carriageway line on sidelong ground at 1:12 slope					
Design variations	original wall sections at Kingsway - cantilever T-section diaphragms used at Forty Acre Drive (7m ret. ht), Osborne Street (8m ret. ht), and Red Hill Drive (6m ret. ht)					
Other comments	construction completed in 199?					
Publications/articles	none known					
Type of analysis	coupled consolidation (construction + long term)					
Purpose of analysis	to calibrate simpler wall design software (WALLAP) and provide estimates of ground movement behind the wall					
Soil model	homogeneous isotropic linear elastic-perfectly plastic					
Structural materials	linear elastic (concrete walls/slabs and steel anchor tendons)					
Recent history	no previous construction/excavation to model					
Wall installation	element swopping					
Excavation sequence	sequential with installation/stressing of anchors					
Long term behaviour	equilibration to present p.w.p. profile, with FL drainage					
Output required	wall deflections, wall bending moments, anchor tendon loads, and ground movements behind wall					
Field measurements	none taken or made available					

CASE 3 - A6(M) Stockport (contd)

CRISP Analysis details

Mesh details	**NN**	307	**NEL**	283	**X/H**	7.19	**Y/W**	3.05

Element types	**soil**	LSQ/u	**wall**	LSQ	**supports**	CSB

Soil parameters (stiff clay)	E_o	30	MPa	m_E	0	MPa/m	y_o	84.0	m
	ν	0.200		c_o	0	kPa	m_C	0	kPa/m
	ϕ	24.5	°	γ	21	kN/m^3			
	γ_w	9.81	kN/m^3	k_X	.019	m/yr	k_Y	.019	m/yr
(dense sand)	E_o	50	MPa	m_E	0	MPa/m	y_o	78.5	m
	ν	0.250		c_o	0	kPa	m_C	0	kPa/m
	ϕ	32	°	γ	21	kN/m^3			
	γ_w	9.81	kN/m^3	k_X	315	m/yr	k_Y	315	m/yr
Concrete parameters	E	30	GPa	ν	0.150		γ	22.6	kN/m^3
Tendon parameters	E	200	GPa	A	140e-6	m^2	θ	30	°

In-situ stresses (kPa)

pt	y (m)	σ'_X	σ'_Y	σ'_Z	K_O	u	p'_C
1	94.	0.	0.	0.	0.7	0.	-
2	82.	29.4	42.0	29.4	0.7	0.	-
3	81.	44.1	63.0	44.1	0.7	0.	-
4	80.	84.0	84.0	84.0	1.0	0.	-
5	79.	87.2	105.	87.2	0.83	0.	-
6	78.	75.6	126.0	75.6	0.6	0.	-
7	77.	73.5	147.0	73.5	0.5	0.	-
8	74.	90.8	190.0	90.8	0.478	10.	-
9	70.	104.8	234.0	104.8	0.448	50.	-
10	66.	116.2	278.0	116.2	0.418	90.	-
11	60.	172.0	344.0	172.0	0.5	150.	-
12	10.	447.0	894.0	447.0	0.5	650.	-

Boundary fixities	**cent.line**	smooth	**base**	smooth	**remote**	smooth

CASE 3 - A6(M) Stockport (contd)

Block	Incs	Time (yrs)	Activity
1	1	.003	set up initial p.w.p. boundary conditions
2	5	.02	excavate to top of wall (+82.0m)
3	10	.115	install wall (swop elements)
4	10	.01	excavate to +81.0m
5	20	.015	apply tensioning force for 1st level of anchors
6	1	.005	install 1st level of anchors
7	20	.02	excavate to +78.5m
8	20	.015	apply tensioning force for 2nd level of anchors
9	1	.005	install 2nd level of anchors
10	20	.02	excavate to +76.0m
11	20	.015	apply tensioning force for 3rd level of anchors
12	1	.005	install 3rd level of anchors
13	20	.03	excavate to +73.5m
14	20	.03	excavate to +71.0m
15	19	50	allow equilibration to original p.w.p. profile

Comments

- The soil parameters were rather vague (triaxial data were unreliable; one borehole log with SPT 'N' values was made available), but it was still possible to do a meaningful analysis - appropriate "limits of range" values were used, inferred from subgrade modulus values adopted by Mouchel in the WALLAP analyses

- The presence of side-long ground was ignored in the analyses - to have incorporated it would have necessitated starting with a level surface (where in-situ stress could be conveniently defined), and then excavating to the required profile

- Wall movements were generally 50% of those predicted by WALLAP, and were thought to be more realistic

- The high EI of the T-section diaphragms used on some sections gave an equivalent plane strain thickness of ≈ 2m - T-sections are highly three-dimensional and an equivalent plane strain thickness would only be appropriate on a long stretch of wall

CASE 4A - Southwark Station Ticket Hall

Project Details / Analysis Overview						
Full title	Jubilee Line Extn Contract 104 - Southwark Station Ticket Hall					
Location	Southwark, SE London					
Client	L G Mouchel & Partners, West Byfleet					
Description	underground station ticket hall, built within a secant pile "box"					
Wall type	secant bored piles (male piles 750 dia. @ 900 c/c)					
Wall dimensions (m)	retained height	5.0	overall length	14.0	width/diam.	0.75
Support (temporary)	single row of props 1m below crest					
Support (permanent)	2 levels of slabs: roof and formation level					
Ground conditions	made ground, alluvium and gravel overlying London clay					
Pore pressures	hydrostatic; GWL 4m b.g.l.					
Unusual aspects	female secant piles ignored in calculating wall EI					
Design variations	4m and 6m retained heights					
Other comments	construction completed in 1998					
Publications/articles	"Jubillee Jackpot", *New Civil Engineer*, 8 Oct 1992, pp22-23					
Type of analysis	coupled consolidation (construction + long term)					
Purpose of analysis	to check contractors alternative design					
Soil model	non-homogeneous isotropic linear elastic-perfectly plastic					
Structural materials	linear elastic (concrete walls and slabs; steel props)					
Recent history	no previous construction/excavation to model					
Wall installation	element swopping					
Excavation sequence	sequential with installation/removal of propping					
Long term behaviour	equilibration to present p.w.p. profile, assuming under-slab drainage					
Output required	wall deflections, wall bending moments, settlements outside site					
Field measurements	none taken or made available					

CASE 4A - Southwark Station Ticket Hall (contd)

CRISP Analysis details

Mesh details	**NN**	323	**NEL**	307	**X/H**	9.48	**Y/W**	3.50

Element types	**soil**	LSQ/u	**wall**	LSQ	**supports**	LSQ / T

Soil parameters (Alluvium/peat)	E_o	5	MPa	m_E	0	MPa/m	y_o	101	m
	ν	0.25		c_o	0	kPa	m_C	0	kPa/m
	ϕ	25	°	γ	16	kN/m^3			
	γ_w	9.81	MPa	k_X	3.0	m/yr	k_Y	3.0	m/yr
(London clay)	E_o	40	MPa	m_E	8	MPa/m	y_o	95	m
	ν	0.20		c_o	1.5	kPa	m_C	0	kPa/m
	ϕ	22	°	γ	20	kN/m^3			
	γ_w	9.81	MPa	k_X	.019	m/yr	k_Y	.019	m/yr
Concrete parameters	E	30	GPa	ν	0.15		γ	22.6	kN/m^3
Prop parameters	E	200	GPa	A	.0054	m^2/m			

In-situ stresses (kPa)	pt	y (m)	σ'_X	σ'_Y	σ'_Z	K_O	u	p'_C
	1	104	0.	0.	0.	0.5	0.	-
	2	101	28.5	57.0	28.5	0.5	0.	-
	3	100	36.5	73.0	36.5	0.5	0.	-
	4	97	45.5	91.0	45.5	0.5	30.0	-
	5	95	54.5	109.0	54.5	0.5	50.0	-
	6	94.9	165.0	110.0	165.0	1.5	51.0	
	7	64.0	628.5	419.0	628.5	1.5	360.0	-

Boundary fixities	**cent.line**	smooth	**base**	smooth	**remote**	smooth

Block	**Incs**	**Time (yrs)**	**Activity**
1	1	.003	set up initial p.w.p. boundary conditions
2	10	.115	install wall - swop elements
3	10	.02	apply 10 kPa surcharge and excavate to +103.0m
4	10	.02	install temp prop and excavate to +102.0m
5	10	.02	excavate to +101.0m

CASE 4A - Southwark Station Ticket Hall (contd)

Block	Incs	Time (yrs)	Activity
6	10	.02	excavate to +100.0m
7	10	.02	excavate to +99.0m
8	10	.02	excavate to +97.8m
9	1	.02	remove prop / install base and roof slabs
10	10	.02	apply 50 kPa surcharge on crest
11	5	.05	set drainage boundary on underside of base slab
12	14	50	march forward in time for 50 years

Comments

- Initial analyses were conducted in Autumn 1991, with additional work requested in Spring 1992 - variations in design necessitated further analyses in Spring 1994.

- The writer was also involved in checking the design of a large piled raft foundation at Southwark Station, though with a semi-analytical elastic method rather than finite element analysis.

- A second section was analysed on the station concourse, linking the ticket hall with the escalators and platforms.

CASE 4B - Southwark Station Concourse

Project Details / Analysis Overview	*(only where different to case 4A)*					
Full title	Jubilee Line Extn 104 - Southwark Station Upper East Concourse					
Description	underground station passenger concourse					
Wall type	diaphragm panels					
Wall dimensions (m)	retained height	11.0	overall length	24.0	width/diam.	1.2
Support (temporary)	two levels of props 1m and 6m below crest					
Support (permanent)	three levels of slab; roof, intermediate and formation level					
Unusual aspects	none					
Design variations	none					
Long term behaviour	equilibration to present p.w.p. profile, assuming under-slab drainage					
Output required	wall deflections, wall bending moments, settlements outside site					

CRISP Analysis details	*(only where different to case 4A)*							
Mesh details	**NN**	340	**NEL**	339	**X/H**	4.25	**Y/W**	4.52

Block	**Incs**	**Time (yrs)**	**Activity**
1	1	.003	set up initial p.w.p. boundary conditions
2	10	.115	install wall - swop elements
3	10	.02	apply 10 kPa surcharge, excavate to +102.2m, install top-level prop
4	10	.02	excavate to +99.7m
5	10	.02	excavate to +97.2m, and install low-level prop
6	10	.02	excavate to +95.2m
7	10	.02	excavate to +94.0m
8	10	.02	excavate to +92.7m
9	1	.02	excavate to +92.2, remove temp props, install permanent slabs
10	10	.02	apply 50 kPa surcharge
11	5	.05	apply drainage condition to base of slab
12	14	50	march forward in time to t=50 years

CASE 5 - Greenside Place

Project Details / Analysis Overview						
Full title	Greenside Place basement walls					
Location	Greenside Place, Edinburgh					
Client	Tarmac Construction Engineering Services, Wolverhampton					
Description	multi-level basement for proposed office/shopping development					
Wall type	contiguous bored piles (1200 dia. @ 1350 c/c)					
Wall dimensions (m)	retained height	15.6	overall length	21.5	width/diam.	1.2
Support (temporary)	five levels of prestressed ground anchors at 15° to horizontal					
Support (permanent)	from basement floors (built bottom-up), though most anchors left in					
Ground conditions	made ground over clayey sand and sandy clay, overlying bedrock					
Pore pressures	hydrostatic; GWL at ground surface					
Unusual aspects	truly 3-dimensional in plan / side-long ground / shallow rock head at variable depth across site / some anchors removable					
Design variations	anchor inclination increased / anchor length increased / bored piles extended to bedrock / assumed Ko varied					
Other comments	construction completed in 199? / Keller SBMA anchors used					
Publications/articles	none known					
Type of analysis	undrained, total stress - construction (temporary works stage) only					
Purpose of analysis	to prove adequacy of temporary works design					
Soil model	non-homogeneous isotropic linear elastic-perfectly plastic					
Structural materials	linear elastic (concrete walls/slabs and steel anchor tendons)					
Recent history	no previous construction/excavation to model					
Wall installation	element swopping					
Excavation sequence	sequential with installation/stressing of anchors					
Long term behaviour	not examined					
Output required	wall deflections, wall bending moments, anchor tendon loads					
Field measurements	none taken or made available					

CASE 5 - Greenside Place (contd)

CRISP Analysis details

Mesh details	**NN**	378	**NEL**	358	**X/H**	3.65	**Y/W**	1.00

Element types	**soil**	LSQ	**wall**	LSQ	**supports**	CSB

Soil parameters (Made ground)	E_o	40	MPa	m_E	0	MPa/m	y_o	54.5	m
	ν'	0.497		c_o	80	kPa	m_c	0	kPa/m
	ϕ	0	°	γ	18	kN/m^3			
	K_w	-	MPa	k_X	-	m/yr	k_Y	-	m/yr
(Clayey sand)	E_o	70	MPa	m_E	0	MPa/m	y_o	38.8	m
	ν	0.497		c_o	140	kPa	m_c	0	kPa/m
	ϕ	0	°	γ	18	kN/m^3			
	K_w	-	MPa	k_X	-	m/yr	k_Y	-	m/yr
Concrete parameters	E	28.8	GPa	ν	0.150		γ	24	kN/m^3
Tendon parameters	E	200	GPa	A	381e-6	m^2/m	θ	15	°

In-situ stresses (kPa)	**pt**	**y (m)**	**σ'_X**	**σ'_Y**	**σ'_Z**	**K_o**	**u**	**p'_c**
	1	54.5	0.	0.	0.	-	0.	-
	2	24.0	244.0	244.0	244.0	1.0	305.0	-

Boundary fixities	**cent.line**	smooth	**base**	rough	**remote**	smooth

Block	**Incs**	**Time (yrs)**	**Activity**
1	10	-	install bored-pile wall (swop elements)
2	10	-	excavate to +53.5m
3	8	-	apply tensioning force for 1st level of anchors
4	1	-	install 1st level of anchors
5	10	-	excavate to +50.5m
6	8	-	apply tensioning force for 2nd level of anchors
7	1	-	install 2nd level of anchors
8	10	-	excavate to +47.0m
9	8	-	apply tensioning force for 3rd level of anchors
10	1	-	install 3rd level of anchors

CASE 5 - Greenside Place (contd)

Block	Incs	Time (yrs)	Activity
11	10	-	excavate to +43.5m
12	8	-	apply tensioning force for 4th level of anchors
13	1	-	install 4th level of anchors
14	10	-	excavate to +40.5m
15	8	-	apply tensioning force for 5th level of anchors
16	1	-	install 5th level of anchors
17	10	-	excavate to +43.5m (final dig level)

Comments

- Initial analyses conducted in Spring 1993, with additional work requested in Autumn 1994 when the Consultant requested ground anchors to be inclined more steeply (25° instead of 15°)

- The results of the analyses were used in an interactive refinement of the temporary works design

- Two other sections through the bored-pile "box" were examined, largely because the depth to rock varied enormously across the site - on Section HH, for example, the excavated height was 13.2m but the bored piles were only required to be 9m long (with 3 levels of anchors) as the lower 5m of the excavation was in rock

- The rather low Y/W ratio for the mesh tabulated above is due to the relatively shallow depth of the rock head - a deeper mesh was simply not required

- This is one case where there was an opportunity to specify further laboratory tests for analysis parameters

CASE 6A - RPR Junction Tunnels

Project Details / Analysis Overview						
Full title	A1/A406/A598 Regents Park Rd Jct. Improvements - Tunnel Walls					
Location	Regents Park, NW London					
Client	Kennedy & Donkin Transportation, Godalming					
Description	cut and cover tunnels for complex road junction scheme					
Wall type	contiguous bored piles (900 dia. @ 900 c/c)					
Wall dimensions (m)	retained height	8.5	overall length	11.5	width/diam.	0.90
Support (temporary)	roof prop slab (concrete)					
Support (permanent)	roof and formation level (road) prop slabs					
Ground conditions	made ground overlying weathered and unweathered London clay					
Pore pressures	hydrostatic; GWL at ground surface					
Unusual aspects	none in particular					
Design variations	depth of clay softening post-excavation / degree of moment transfer between wall and slabs / drawdown of GWL behind walls					
Other comments	design never built - project shelved by DTp					
Publications/articles	none known					
Type of analysis	(a) uncoupled undrained (constr.) and drained (long term) analyses, and (b) coupled consolidation (construction + long term)					
Purpose of analysis	to calibrate routine wall design software (FREW), and to predict movements of the adjacent ground					
Soil model	non-homogeneous isotropic linear elastic-perfectly plastic					
Structural materials	linear elastic (concrete walls/slabs)					
Recent history	no previous construction/excavation to model					
Wall installation	element swopping					
Excavation sequence	sequential with installation/removal of props					
Long term behaviour	softening of clay beneath excavation (using stop-restart), then equilibration to present p.w.p. profile, assuming under-slab drainage					
Output required	wall deflections, wall bending moments, excavation heave, vertical swelling pressures on road slab, settlement profile behind wall					
Field measurements	none taken - project never built					

CASE 6A - RPR Junction Tunnels (contd)

CRISP Analysis details

Mesh details	**NN**	420	**NEL**	407	**X/H**	8.12	**Y/W**	4.15

Element types	**soil**	LSQ/u	**wall**	LSQ	**supports**	LSQ	

Soil parameters (London clay - weathered)	E_o	28	MPa	m_E	6.3	MPa/m	y_o	19.0	m
	ν	0.20		c_o	0	kPa	m_C	0	kPa/m
	ϕ	22	°	γ	20	kN/m^3			
	γ_w	9.81	MPa	k_X	1e-3	m/yr	k_Y	.25e-3	m/yr
(London clay - unweathered)	E_o	91	MPa	m_E	1.75	MPa/m	y_o	9.0	m
	ν	0.20		c_o	0	kPa	m_C	0	kPa/m
	ϕ	22	°	γ	20	kN/m^3			
	γ_w	9.81	MPa	k_X	1e-3	m/yr	k_Y	.25e-3	m/yr
Concrete parameters	E	15.5	GPa	ν	0.150		γ	24	kN/m^3

In-situ stresses (kPa)	**pt**	**y (m)**	**σ'_X**	**σ'_Y**	**σ'_Z**	**K_o**	**u**	**p'c**
	1	20	30	30	30	1	0.	-
	2	19	50	50	50	1	10	-
	3	18.99	75	50	75	1.5	10	-
	4	-15	570	380	570	1.5	350	-

Boundary fixities	**cent.line**	smooth	**base**	smooth	**remote**	smooth

Block	**Incs**	**Time (yrs)**	**Activity**
1	1	.01	set up initial p.w.p. boundary conditions
2	9	.1	install wall (swop elements)
3	10	.02	excavate to +17.5m AOD
4	10	.04	install roof slab
5	10	.01	excavate to +16.0m AOD
6	10	.01	excavate to +14.0m AOD
7	10	.01	excavate to +11.5m AOD
8	10	.1	install formation level (road) slab
9	15	120	set up under-road drainage, and step forward 120 years

CASE 6B - RPR Junction Approaches

Project Details / Analysis Overview	*(only where different to case 6A)*					
Full title	A1/A406/A598 Regents Pk Rd Jct. Improvements - Approach Walls					
Description	approach walls for complex road junction scheme					
Wall type	contiguous bored piles (1500mm dia. @ 1500mm c/c)					
Wall dimensions (m)	retained height	8.5	overall length	15.0	width/diam.	1.5
Support (temporary)	single row of high level props					
Support (permanent)	formation level (road) prop slab					
Unusual aspects	none in particular					
Design variations	clay softening post-excavation / drawdown of GWL behind walls					
Type of analysis	(a) uncoupled undrained (constr.) and drained (long term) analyses, and (b) coupled consolidation (construction + long term)					

CRISP Analysis details								
Mesh details	**NN**	423	**NEL**	405	**X/H**	7.71	**Y/W**	2.02
Element types	**soil**	LSQ/u	**wall**	LSQ	**supports**	LSB		
Prop parameters	E	15.5	GPa	A	.026	m^2/m		

Block	Incs	Time (yrs)	Activity
1	1	.01	set up initial p.w.p. boundary conditions
2	9	.1	install wall (swop elements)
3	10	.02	excavate to +17.5m AOD
4	5	.04	install temporary prop
5	10	.01	excavate to +16.0m AOD
6	10	.01	excavate to +14.0m AOD
7	10	.01	excavate to +11.5m AOD
8	5	.07	install permanent formation level (road) slab
9	10	.01	remove temporary prop
10	15	120	set under-road drainage, and step forward 120 years

CASE 6C - RPR Junction Slip Road 3

Project Details / Analysis Overview	*(only where different to case 6A)*
Full title	A1/A406/A598 Regents Pk Rd Jct. Improvements - Slip Road 3
Description	retaining walls for split-level slip road, in a complex road junction
Wall type - North	contiguous bored piles (1350 dia. @ 1200 c/c)
- South	contiguous bored piles (900 dia. @ 1050 c/c)

Wall dimensions (m)	**N**	retained height	8.5	overall length	13.6	width/diam.	1.35
	S		7.1		10.5		0.90

Support (temporary)	single high-level prop from North wall to South wall
Support (permanent)	formation level (road) prop slab
Unusual aspects	asymmetric in cross section, requiring both North and South walls to be modelled / "cranked" permanent prop slab
Design variations	degree of moment transfer between walls and slab / drawdown of GWL behind walls
Type of analysis	coupled consolidation (construction + long term) <u>only</u>
Recent history	need to create existing raised ground level on north side
Excavation sequence	sequential with installation/removal of props
Long term behaviour	equilibration to present p.w.p. profile, assuming under-slab drainage and drawdown behind walls (due to seepage between piles)

CRISP Analysis details

Mesh details	**NN**	846	**NEL**	804	**X/H**	4.59	**Y/W**	8.75

Element types	**soil**	LSQT/u	**wall**	LSQ	**supports**	LSB

Soil parameters	all as before except:	m_E	3.15	MPa/m	ϕ	20	°

Prop parameters	E	210	GPa	A	.216e-4	m^2/m			

CASE 6C - RPR Junction Slip Road 3 (contd)

Block	Incs	Time (yrs)	Activity
1	1	.001	set up initial p.w.p. boundary conditions
2	9	20	build up raised ground surface & apply surcharges (N & S sides)
3	10	.02	excavate to -1.0m
4	10	.02	excavate to -2.0m
5	1	.04	install top level prop
6	9	.025	excavate to -3.4m
7	10	.025	excavate to -4.7m
8	10	.025	excavate to -5.8m
9	10	.025	excavate to -6.8m
10	10	.025	excavate to -7.8m
11	10	.15	excavate to -8.5m and install road slab
12	10	.02	remove temporary prop
13	5	2	set under-road and behind-wall drainage and step forward 2 yrs
14	5	.02	apply equivalent surcharge for new housing development
15	10	118	step forward in time to 120 years

Comments

- The asymmetry of the walls, prop slab and ground profile (about the carriageway centreline) necessitated the modelling of a full section and hence rather more elements/ nodes than usual

- The results of the analyses produced some unexpected trends in terms of the relative movements of the North and South walls - retrospective attempts to explain the mechanisms involved were not wholly satisfactory

- In-situ geophysical testing to determine G_{max} was carried out by the University of Surrey (under a separate contract) for comparison with laboratory stiffnesses *(this comment applies to cases 6A-6D)*

CASE 6D - RPR Junction Slip Road 5

Project Details / Analysis Overview							*(only where different to case 6C)*
Full title	A1/A406/A598 Regents Pk Rd Jct. Improvements - Slip Road 5						
Description	retaining walls for a slip road, in a complex road junction						
Wall type - **North** - **South**	contiguous bored piles (1800 dia. @ 1500 c/c) contiguous bored piles (750 dia. @ 800 c/c)						
Wall dimensions (m) N S	retained height	8.5 0.0	overall length	15.0 10.0	width/diam.	1.8 0.75	
Support (temporary)	raking prop from wall crest to row of lateral piles						
Support (permanent)	formation level (road) slab, propped against lateral piles						
Unusual aspects	asymmetric in cross section with wall (north) and lateral piles (south) / side-long ground / temporary berms used during construction						
Design variations	depth of clay softening post-excavation / degree of moment transfer between wall and slabs / possible drainage between piles						
Type of analysis	coupled consolidation (pre-history, construction + long term)						
Recent history	creation of existing side-long ground surface profile						
Excavation sequence	complex - berms formed to accommodate raking props, then removed to allow installation of road slab						
Long term behaviour	equilibration to present p.w.p. profile, assuming under-slab drainage and drawdown behind walls (due to seepage between piles)						

CRISP Analysis details									
Mesh details	**NN**	545	**NEL**	540	**X/H**	4.76	**Y/W**	4.18	
Element types	**soil**	LSQT/u	**wall**	LSQ	**supports**	CSB			
Prop parameters	E	210	GPa	A	.885e-4	m^2/m			

CASE 6D - RPR Junction Slip Road 5 (contd)

Block	Incs	Time (yrs)	Activity
1	1	.01	set up initial p.w.p. boundary conditions
2	4	.01	create present day (sloping) ground surface
3	10	120	step forward 120 years
4	5	.1	install north wall (swop elements)
5	5	.1	install south wall (swop elements)
6	5	.1	excavate berm (I)
7	10	.1	excavate berm (II)
8	8	.1	excavate berm (III)
9	5	.2	excavate berm (IV)
10	1	.04	install temporary prop
11	4	.1	remove LHS berm (I)
12	10	.1	remove LHS berm (II)
13	1	.15	install formation level (road) slab
14	14	.02	remove temporary prop
15	10	.1	remove RHS berm
16	15	120	set under-road drainage, and step forward 120 years

Comments

- As with Slip Road 3, the asymmetry of the walls and ground profile necessitated the modelling of a full section

- The row of piles forming the South "wall" were not acting as a wall at this stage of the analysis/design but rather as lateral reaction piles for both the temporary and permanent props - later on, it was intended that excavation would take place to the south of the South "wall" two form a separate (lower) level of carriageway

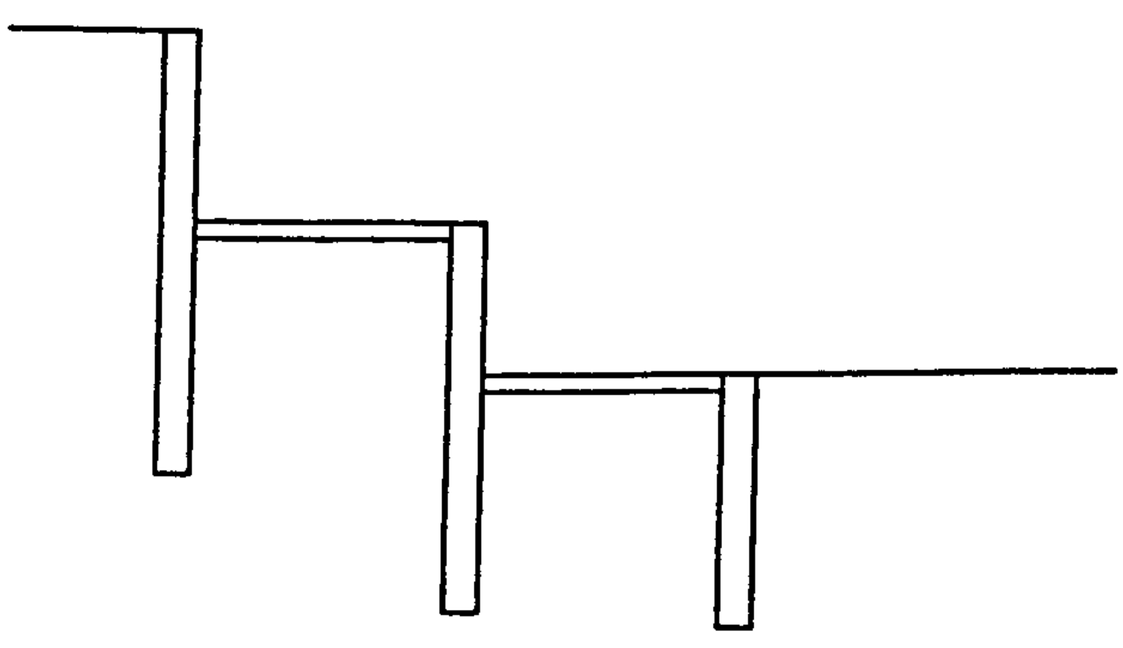

CASE 7 - A331 Aldershot Rd Underpass

Project Details / Analysis Overview						
Full title	A331 Black Water Valley Route - Aldershot Road Underpass					
Location	Junction with A323, Aldershot, Surrey					
Client	Surrey County Council, Ewell					
Description	trunk road underpass at grade-separated interchange, 28.4m wide					
Wall type	T-section diaphragm walls					
Wall dimensions (m)	retained height	10.0	overall length	19.0	width/diam.	1.2*
Support (temporary)	double row of tubular steel props					
Support (permanent)	single articulated concrete slab at formation level					
Ground conditions	made ground, alluvium and gravels overlying London clay to depth					
Pore pressures	hydrostatic; high local water table; suspected artesian conditions					
Unusual aspects	hinged prop slab					
Design variations	anchors for temporary support / wall and ground stiffness / Ko in London clay / rigidity of carriageway slab					
Other comments	completed and open to traffic in Sept 1996					
Publications/articles	"Holding water", *NCE Roads Supplement* June 1995, pp25-28. Carder *et al.* (1997), TRL Report 239					
Type of analysis	coupled consolidation (construction + long term)					
Purpose of analysis	to calibrate routine wall design software (FREW and WALLAP), and investigate long-term soil-wall-slab interaction					
Soil model	non-homogeneous isotropic linear elastic-perfectly plastic					
Structural materials	linear elastic (concrete walls/slabs and steel tubular props)					
Recent history	no previous construction/excavation to model					
Wall installation	element swopping					
Excavation sequence	sequential with installation of props					
Long term behaviour	equilibration to existing p.w.p. profile, with under-road drainage					
Output required	wall deflections, wall bending moments, prop loads, slab axial thrusts and bending moments, swelling pressures on slab, settlements and horizontal ground movements behind wall, p.w.p. profiles					
Field measurements	extensive - both during and after construction					

CASE 7 - A331 Aldershot Rd Underpass (contd)

CRISP Analysis details

Mesh details	**NN**	480	**NEL**	456	**X/H**	6.02	**Y/W**	2.42

Element types	**soil**	LSQT/u	**wall**	LSQ	**supports**	CSB

Soil parameters (alluvium)	E_o	12.5	MPa	m_E	0	MPa/m	y_o	70.5	m
	ν	0.20		c_o	0	kPa	m_c	0	kPa/m
	ϕ	28	°	γ	18	kN/m^3			
	γ_w	9.81	MPa	k_X	31.5	m/yr	k_Y	31.5	m/yr
(London clay)	E_o	30	MPa	m_E	6	MPa/m	y_o	67.0	m
	ν	0.15		c_o	5	kPa	m_c	0	kPa/m
	ϕ	22	°	γ	21	kN/m^3			
	γ_w	9.81	MPa	k_X	.0315	m/yr	k_Y	.0032	m/yr
Concrete parameters	E	27	GPa	ν	0.15		γ	23	kN/m^3
Prop parameters	E	210	GPa	A		m^2/m			

In-situ stresses (kPa)	**pt**	**y (m)**	**σ'_X**	**σ'_Y**	**σ'_Z**	**K_o**	**u**	**p'_c**
	1	72.6	0.	0.	0.	0.6	0.	-
	2	67.1	26.4	44.0	26.4	0.6	55	-
	3	67.0	67.2	44.8	67.2	0.4	56	-
	4	24.0	583.2	388.8	583.2	1.5	486	-

Boundary fixities	**cent.line**	smooth	**base**	smooth	**remote**	smooth

Block	**Incs**	**Time (yrs)**	**Activity**
1	*1*	-	set up initial p.w.p. boundary conditions
2	*5*	-	apply HA surcharge at existing ground level
3	*1*	-	install wall (swop elements)
4	*5*	-	excavate to +68.6m
5	*1*	-	install temporary high level prop
6	*25*	-	excavate to +60.8m (formation level)
7	*5*	-	backfill behind capping beam to +72.6m
8	*5*	-	change surcharge from HA to HB

CASE 7 - A331 Aldershot Rd Underpass (contd)

Block	Incs	Time (yrs)	Activity
9	*2*	-	install under-carriageway drainage blanket
10	*5*	-	install permanent carriageway prop slab
11	*15*	-	remove temporary props
12	*20*	-	allow equilibration to present p.w.p. profile, with under-slab drain

Comments

- Involvement was from an early stage, as the client appointed the University of Surrey to be the Technical Approval consultant for the Approval in Principal (AIP) document for the ARU in December 1991

- Following adoption of the final AIP, advice was given on FE analyses used in the design process, and the data given above for this case is based on these analyses

- Much more detailed and refined analyses were carried out during and subsequent to construction by University of Surrey, in which the full wall installation process was modelled and Simpson's "brick" model was used for the London clay - however, such retrospective refinement is always possible in a research contract, and this is rather different to the design environment which this thesis is focusing on.

- As with the A6(M) Stockport Bypass, 2D idealisation of a T-section diaphragm wall produced a high equivalent plane-strain wall thickness because of the high EI

- Soil parameters for the finite element analysis at the design stage were reasonably comprehensive and were obtained by Surrey CC Materials Laboratory - subsequently, the University of Surrey obtained block samples for stress path testing as part of the research contract

- Full details of wall performance up to 1996 can be found in Carder *et al.* (1997).

CASE 8A - Queensberry House Transverse

Project Details / Analysis Overview						
Full title	Queensberry House : transverse section					
Location	Saville Row, London W1					
Client	Laing Technology Group, Mill Hill					
Description	multi-level deep basement demolition and deepening/widening					
Wall type	contiguous bored piles (750 dia. @ 900 c/c)					
Wall dimensions (m)	retained height	19.5	overall length	25.8	width/diam.	0.75
Support (temporary)	six levels of tubular steel props					
Support (permanent)	eight levels of concrete floor slabs/ramps (underground car park)					
Ground conditions	made ground and gravel, overlying London clay to depth					
Pore pressures	hydrostatic from 6m to 19m b.g.l.; underdrained beneath this					
Unusual aspects	truly 3-dimensional in plan / extremely complex construction sequence / need to model construction of original building					
Design variations	temporary propping arrangements and unsupported heights / nonlinearity of soil stiffness parameters					
Other comments	construction completed in 1998					
Publications/articles	Woods and Miller (1997)					
Type of analysis	fully coupled (original construction, 30-year equilibration, sequential demolition and construction + long term)					
Purpose of analysis	to predict movements of (and hence damage to) adjacent structures					
Soil model	non-homogeneous isotropic nonlinear elastic-perfectly plastic					
Structural materials	linear elastic (concrete walls/slabs, steel columns & tubular props)					
Recent history	construction of previous Queensberry house in 1966					
Wall installation	element swopping					
Excavation sequence	extremely complex; sequential with demolition and the installation of temporary props and permanent floor slabs					
Long term behaviour	equilibration to existing p.w.p. profile, with under-slab drainage					
Output required	wall deflections, bending moments and shear forces; horizontal and vertical ground movements; slab axial thrusts					
Field measurements	horizontal and vertical movements in and around site					

CASE 8A - Queensberry House Transverse (contd)

CRISP Analysis details

Mesh details	**NN**	983	**NEL**	1242	**X/H**	3.69	**Y/W**	1.65

Element types	**soil**	LSQ/T/u	**wall**	LSQ	**supports**	CSB/LSQ

Soil parameters (London clay)	E_O	74.5	MPa	m_E	2	MPa/m	y_O	16.14	m
	ν	0.20		c_O	5	kPa	m_C	0	kPa/m
	ϕ	20	°	γ	20	kN/m^3			
	γ_W	9.81	MPa	k_X	6e-4	m/wk	k_Y	6e-4	m/wk
Concrete parameters	E	20	GPa	ν	0.15		γ	24	kN/m^3
Prop parameters	E	207	GPa	A	593e-5	m^2/m			

In-situ stresses (kPa)	pt	y (m)	σ'_X	σ'_Y	σ'_Z	K_O	u	p'_C
	1	23.6	0.	0.	0.		0.	-
	2	17.5	61.0	122.0	61.0	0.5	0.	-
	3	16.15	67.8	135.5	67.8	0.5	13.5	-
	4	16.14	271.2	135.6	271.2	2	13.6	-
	5	11.15	371.0	185.5	371.0	2	63.5	-
	6	11.14	278.4	185.6	278.4	1.5	63.6	
	7	-15	468.0	312.0	468.0	1.5	190.0	
	8	-17.5	1233.0	822.0	1233.0	1.5	0.	
	9	-30.0	1608.0	1072.0	1608.0	1.5	0.	-

Boundary fixities	**cent.line**	smooth	**base**	rough	**remote**	rough

Block	**Incs**	**Time (wks)**	**Activity** (week nos)
1	1	.005	set up initial p.w.p. boundary conditions
2	9	26.	install existing basement
3	9	20.	apply loads from existing superstructure
4	11	1560.	allow 30 years post construction equilibrium
5	10	21.	cancel existing superstructure loads (1-21)
6	1	3.	install prop A (+ support) (22-24)
7	5	1.	breakout for sheet piles (25)
8	1	3.	install sheet piles and contiguous piles (26-28)

CASE 8A - Queensberry House Transverse (contd)

Block	Incs	Time (wks)	Activity	(week nos)
9	5	1.	excavate central well to +8.34 : remove prop A / install B	(29)
10	5	1.	excavate central well to +5.64 : install prop C	(30)
11	5	1.	excavate central well to +1.74 : install prop D and base slab	(31)
12	1	2.	install plunge columns/piles and cast base (level 13) slab	(32-33)
13	2	5.	construction elsewhere	(34-38)
14	4	2.	build up internal shear walls to +17.5	(39-40)
15	3	4.	internal shear walls up to +23.1 : break out upper foundation	(41-44)
16	3	3.	floor slabs cast within shear walls : props E,F,G replace B,C,D	(45-47)
17	3	4.	construction elsewhere	(48-51)
18	1	1.	prop H installed	(52)
19	4	16.	apply new superstructure loads	(53-68)
20	1	1.	prop K installed / upper wall broken out	(69)
21	1	2.	construction elsewhere	(70-71)
22	1	3.	level 1 slab installed	(72-74)
23	3	3.	excavate outer section to +14.24 : remove prop K / install L	(75-77)
24	2	4.	construction elsewhere	(78-81)
25	1	2.	level 3 slab installed	(82-83)
26	3	2.	exc. outer section to +11.54 / remove props H & L / install M	(84-85)
27	2	2.	construction elsewhere	(86-87)
28	1	2.	level 5 slab installed	(88-89)
29	3	4.	exc. outer section to +8.84 / remove props E & M / install N	(90-93)
30	2	2.	construction elsewhere	(94-95)
31	1	2.	level 7 slab installed	(96-97)
32	3	2.	exc. outer section to +6.14 / remove props F & N / install O	(98-99)
33	1	1.	construction elsewhere	(100)
34	1	1.	level 9 slab installed	(101-102)
35	3	2.	exc. outer section to +2.94 / remove props G & O / install P	(103-104)
36	3	2.	excavate outer section to +1.74	(105-106)
37	1	1.	place no fines concrete	(107)
38	1	2.	base (level 13) slab installed	(108-109)
39	1	1.	construction elsewhere	(110)
40	1	2.	level 11 slab installed / remove prop P	(111-112)
41	11	1560.	allow for a further 30 years after construction	

CASE 8B - Queensberry House Longitudinal

Project Details / Analysis Overview	*(only where different to case 8A)*
Full title	Queensberry House : longitudinal section
Design variations	fixity between existing basement and party wall

CRISP Analysis details *(only where different to case 8A)*

Mesh details	**NN**	1150	**NEL**	1434	**X/H**	3.39	**Y/W**	1.21

Block	**Incs**	**Time (wks)**	**Activity** (week nos)
1-5	40	1627	*as per case 8A*
6	1	1.	install prop 1 (22)
7	1	1.	demolish upper ramp / install prop 2 (23)
8	3	2.	cut slot for contig. piles / install props 3 & 4 / remove prop 1 (24-25)
9	2	3.	cut slot for sheet piles (26-28)
10	2	.5	install sheet piles and contiguous piles (29a)
11	1	.5	replace props 3 & 4 with 5 & 6 / install prop 7 (29b)
12	1	1.	excavate central well to +7.00 / install prop 8 (30)
13	4	1.	excavate central well to +4.30 / install prop 9 (31)
14	3	2.	excavate central well to +2.49 / place blinding slab (13L) (32-33)
15	1	5.	construction elsewhere (34-38)
16	1	1.	cast base (level 13) slab / install prop 10 (39)
17	2	3.	erect shear walls (cl),(24)(29) to +17.5 (40-42)
18	2	1.	demolish upper shelf (43)
19	2	4.	internal shear walls up to +23.1 (41-44)
20	3	.5	excavate outer section to +12.8 / remove prop 2 (45a)
21	1	.5	install prop 11 / construct internal floor levels 11 & 9 (45b)
22	3	.5	exc. outer section to +9.8 / remove prop 7 & top of sheet pile (46a)
23	1	.5	install prop 12 / construct internal floor levels 7 & 5 (46b)
24	3	.5	excavate outer section to +7.0 (47a)
25	1	.5	install prop 13 / construct internal floor levels 3 & 1 (47b)
26	3	.5	excavate outer section to +4.4 (48a)
27	1	.5	install prop 14 / construct internal roof (level 0) (48b)
28	3	1.	exc. outer section to +2.49 (FL) / place blinding (49)
29	1	1.	cast remaining base (level 13) slab (50)

CASE 8B - Queensberry House Longitudinal (contd)

Block	Incs	Time (yrs)	Activity	(week nos)
30	1	2.	erect shear wall (33) to +17.5	(51-52)
31	1	1.5	install level 11 slab	(53-54a)
32	1	.5	install level 9 slab / shear wall (33) to +23.1	(54b)
33	1	1.	install level 7 slab	(55)
34	1	1.	install level 5 slab	(56)
35	3	1.5	remove prop 10 & support	(57-58a)
36	1	.5	install level 3 slab	(58b)
37	2	1.	install level 1 slab / commence superstructure loading	(59)
38	3	2.	further superstructure loads	(60-61)
39	4	3.	install roof slab / further loads / remove props 5 & 6	(62-64)
40	4	25.	further superstructure loads	(65-89)
41	2	1.	remove prop 11 & support	(90)
42	1	7.	construction elsewhere	(91-97)
43	2	1.	remove prop 12 & support	(98)
44	1	4.	construction elsewhere	(99-102)
45	2	1.	remove prop 13 & support	(103)
46	1	4.	construction elsewhere	(104-107)
47	2	1.	remove prop 14 & support	(108)
48	11	1560.	allow for a further 30 years after construction	

Comments

- Probably the most complex basement analysis ever undertaken with CRISP (based on discussions with the authors and other users of CRISP)

- Many different zones of concrete (contiguous piles, internal shear walls, plunge piles, floor slabs, etc.) and steel (sheet piles, tubular props, plunge columns, etc.) were required - the values quoted in the table above are only representative, as different values had to be used to take account of spacings in the third dimension, etc.

- The non-linear elastic stiffness model used was based on the Jardine *et al.* Imperial College logarithmic-periodic function - implemented in CRISP by the writer for this job

- Comparative analyses were conducted with PLAXIS by the consultant (Buro Happold) in order to check LTG's work, although these analyses were not as sophisticated

- Stiffness v strain data were obtained from both laboratory triaxial tests and also in-situ pressuremeter tests, with the latter giving a much more consistent pattern

- This is the only commercial analysis with which the writer was involved where horizontal ground movements towards the wall were required (as part of the damage prediction exercise)

- Computed wall movements were used to set trigger levels as part of the Observational Method adopted for the construction

- Comparisons of computed and observed wall movements were very favourable, with computed always a little greater than observed

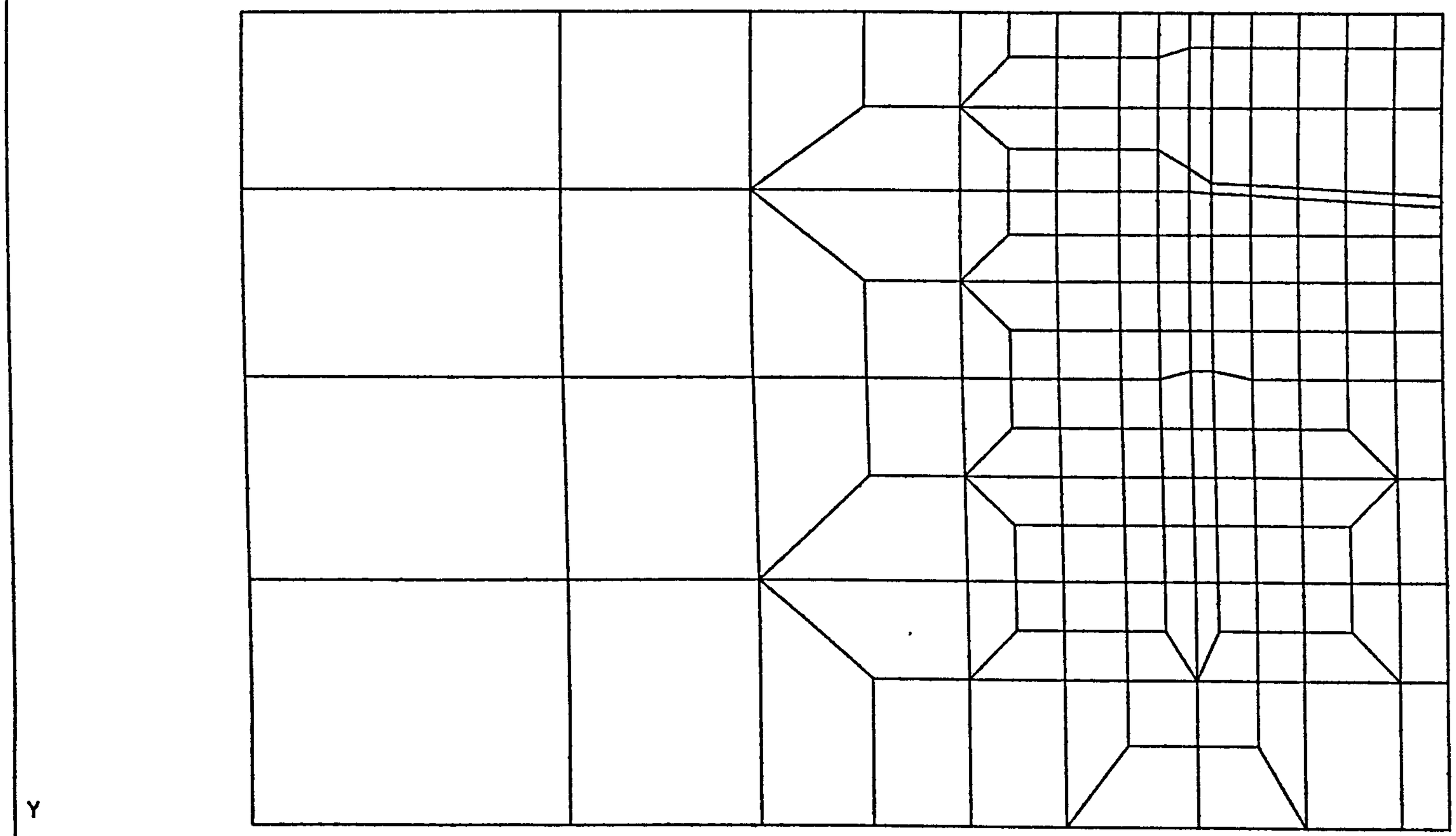

CASE 1 - A406 WALTHAMSTOW - IN-SITU STAGE

FINITE ELEMENT MESH

GEOM SCALE 0 20.00 metre

XMIN : -13.232 XMAX : 88.232 YMIN :-0.121E-05 YMAX : 50.000

CRISP-94	CUED TRL	18/12/98 02:20	UNIVERSITY OF SURREY	FIG. 1

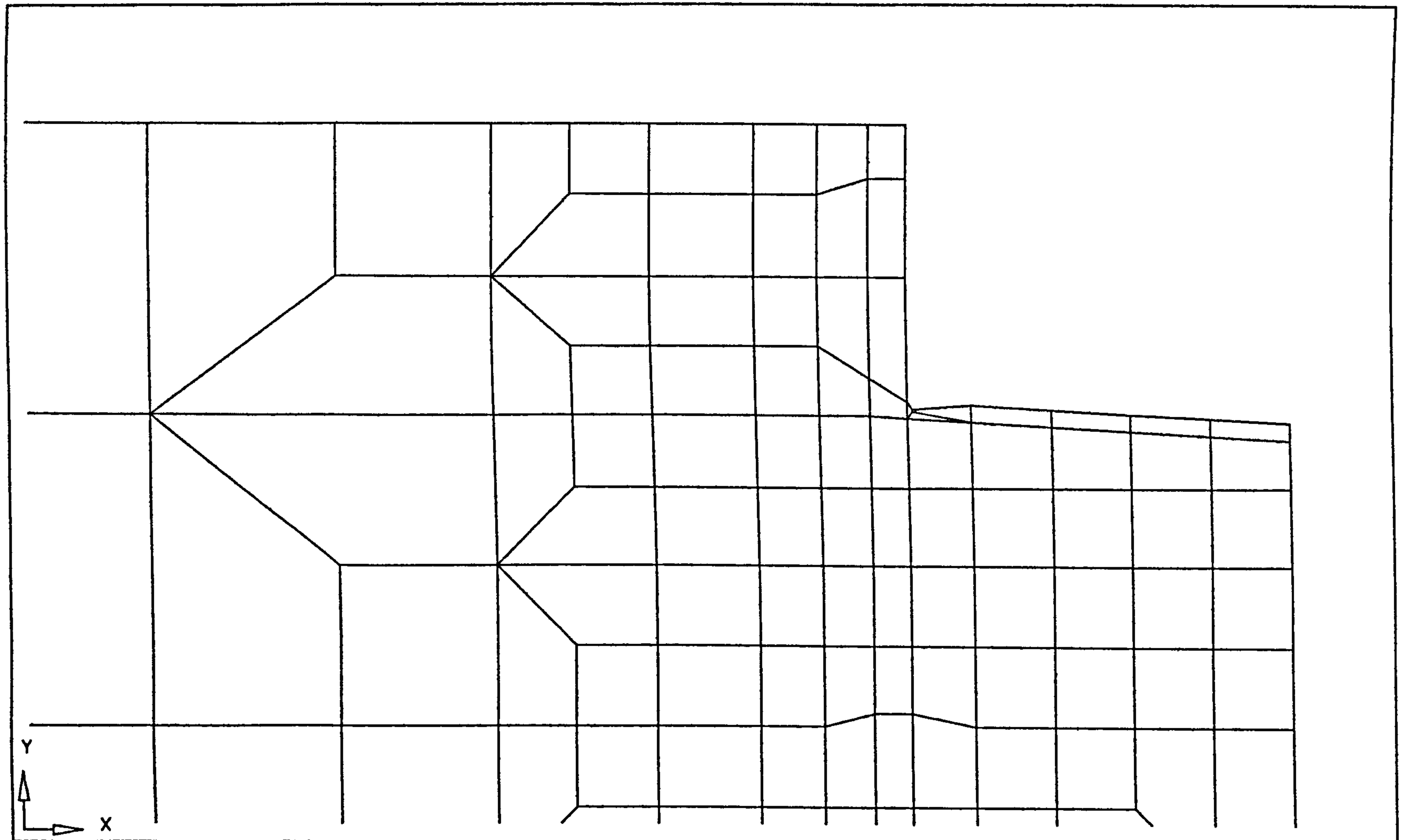

CASE 1 - A406 WALTHAMSTOW - FINAL GEOMETRY

FINITE ELEMENT MESH

GEOM SCALE 0 8.00 metre

XMIN : 27.354 XMAX : 78.085 YMIN : 26.250 YMAX : 51.250

CRISP-94	CUED TRL	18/12/98 02:25	UNIVERSITY OF SURREY	FIG. 1

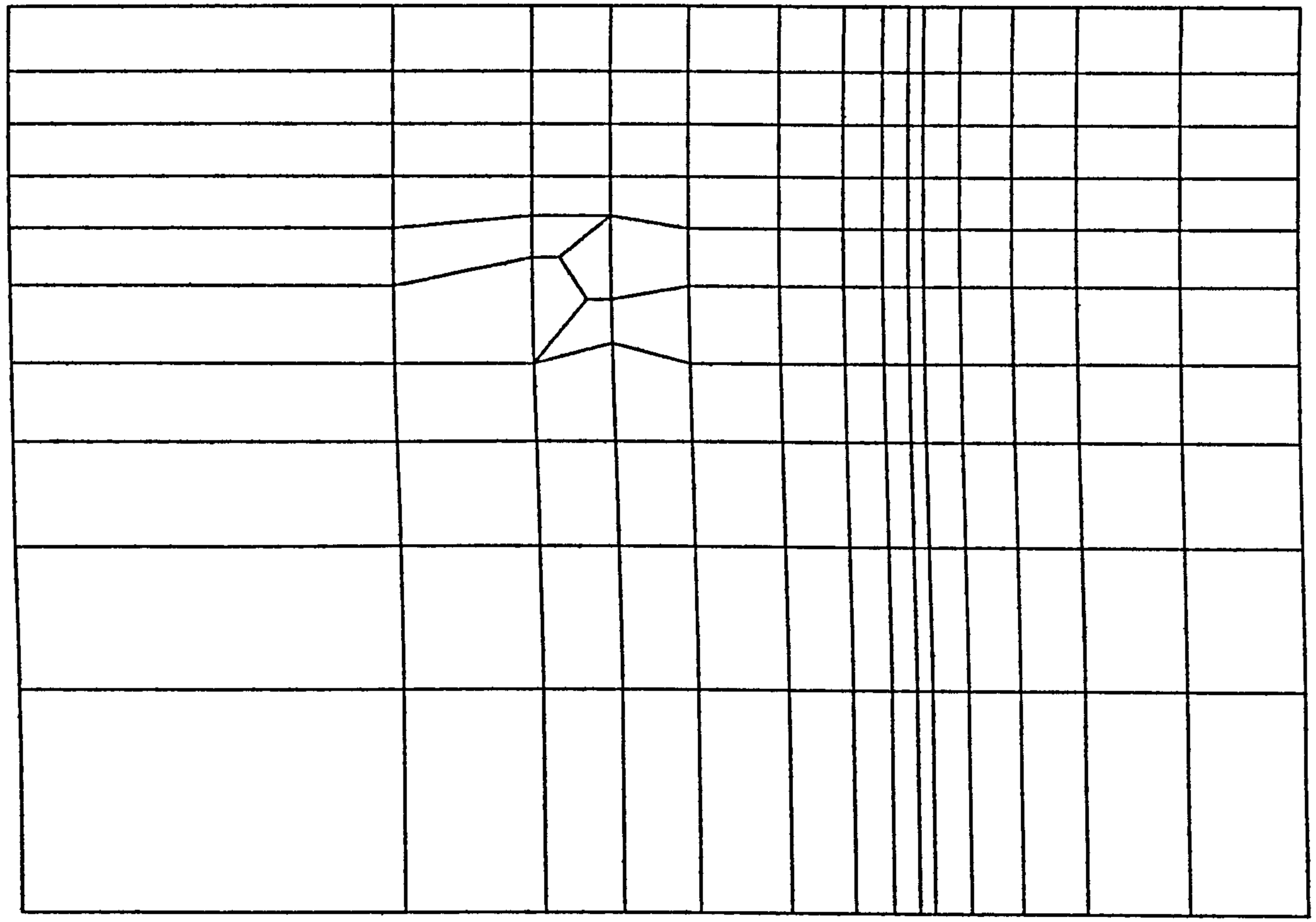

CASE 2 - NEASDEN LANE UNDERPASS - IN-SITU STAGE

FINITE ELEMENT MESH

GEOM SCALE 0 16.00 metre

XMIN : -10.097 XMAX : 60.217 YMIN : 8.000 YMAX : 42.650

CRISP-94	CUED TRL	18/12/98 02:32	UNIVERSITY OF SURREY

FIG. 1

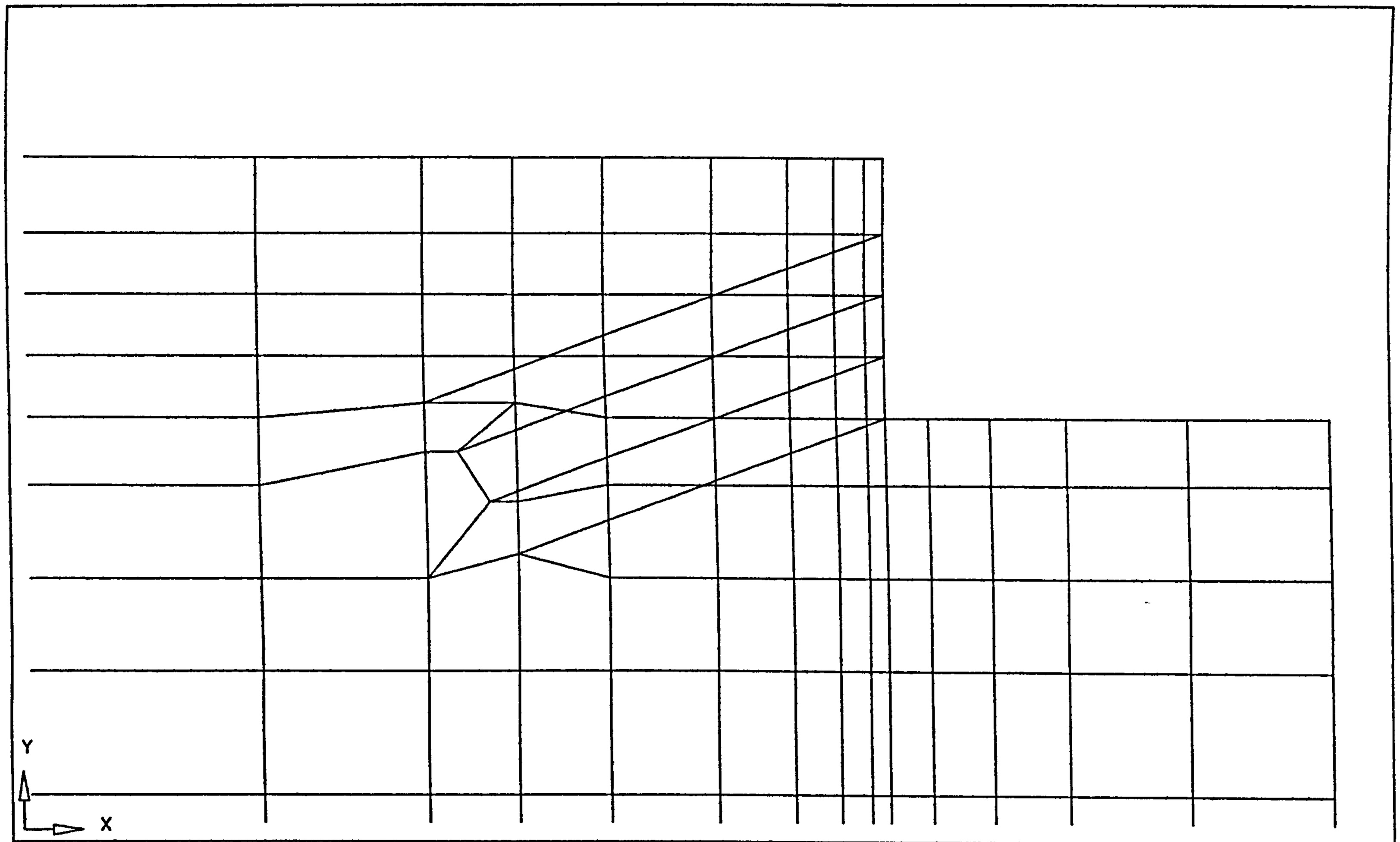

CASE 2 - NEASDEN LANE UNDERPASS - FINAL GEOMETRY

FINITE ELEMENT MESH

GEOM SCALE 0 8.00 metre

XMIN : 7.481 XMAX : 51.428 YMIN : 23.159 YMAX : 44.816

CRISP-94	CUED TRL	18/12/98 02:37	UNIVERSITY OF SURREY	FIG. 1

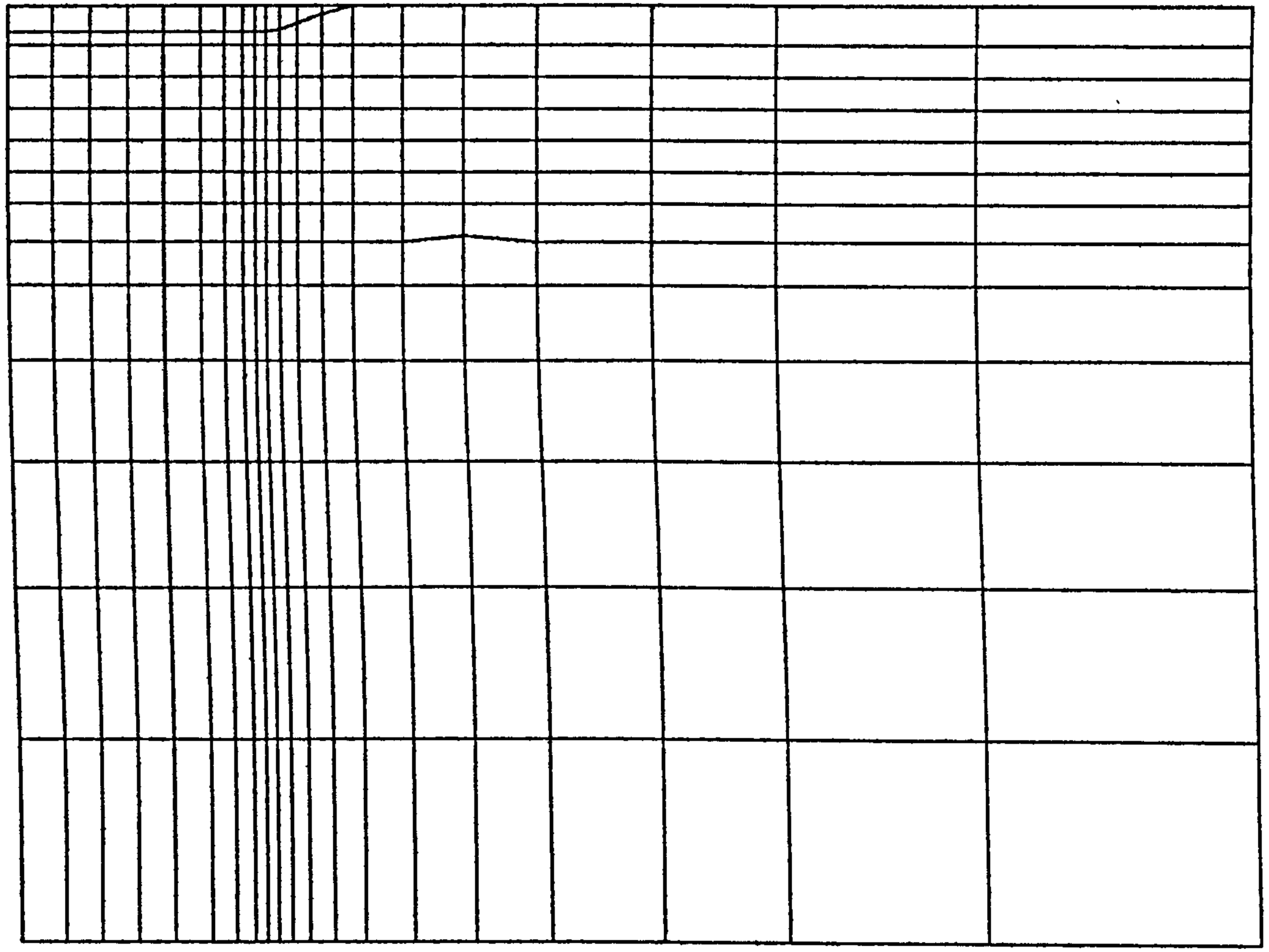

CASE 3 - A6(M) STOCKPORT BYPASS - IN-SITU STAGE

FINITE ELEMENT MESH

GEOM SCALE 0 32.00 metre

XMIN : -25.083 XMAX : 125.083 YMIN : 10.000 YMAX : 84.000

CRISP-94	CUED TRL	18/12/98 02:46	UNIVERSITY OF SURREY	FIG. 1

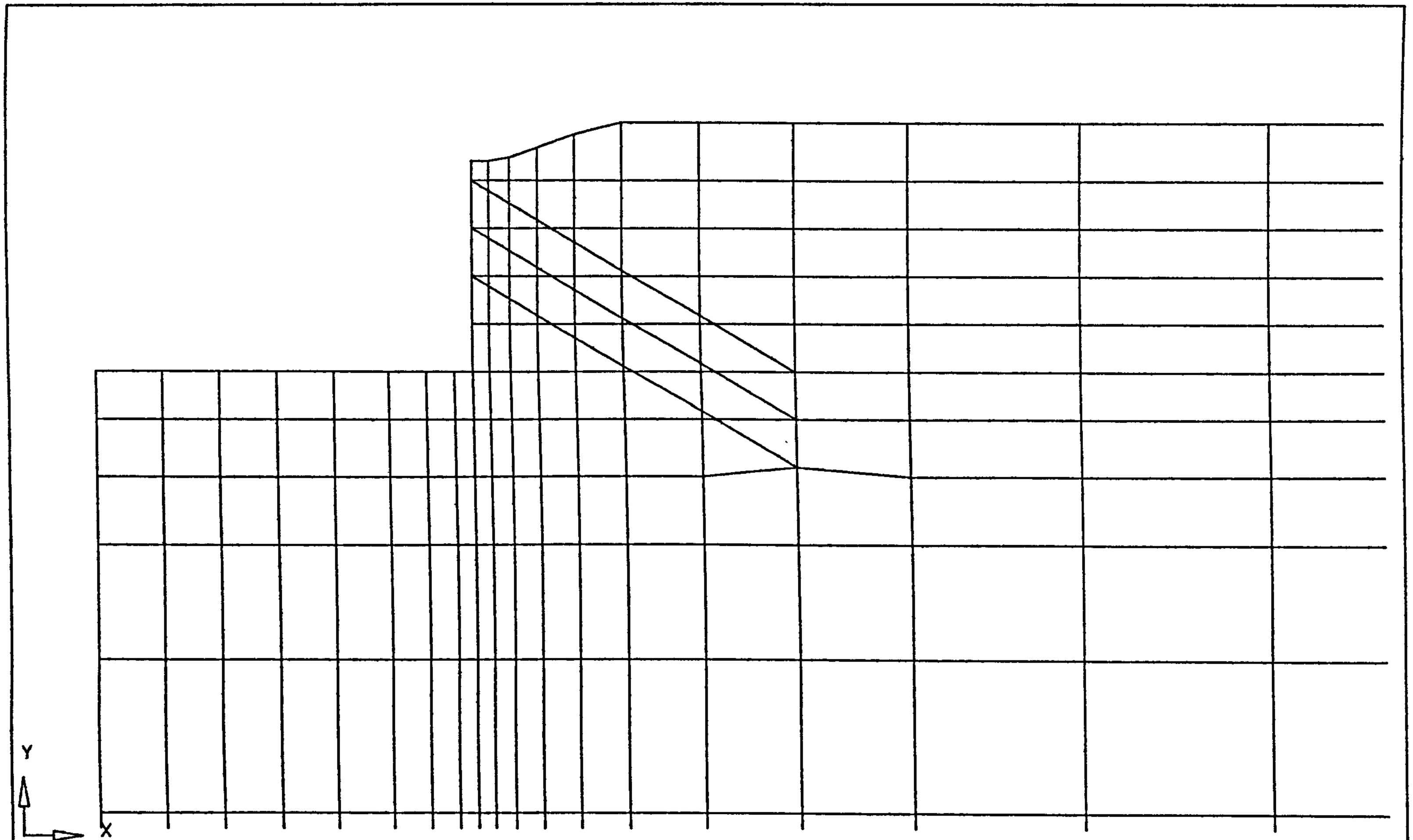

CASE 3 - A6(M) STOCKPORT BYPASS - FINAL GEOMETRY

FINITE ELEMENT MESH

GEOM SCALE 0 16.00 metre

XMIN : -3.631 XMAX : 67.877 YMIN : 50.524 YMAX : 85.762

CRISP-94	CUED TRL	18/12/98 02:44	UNIVERSITY OF SURREY	FIG. 1

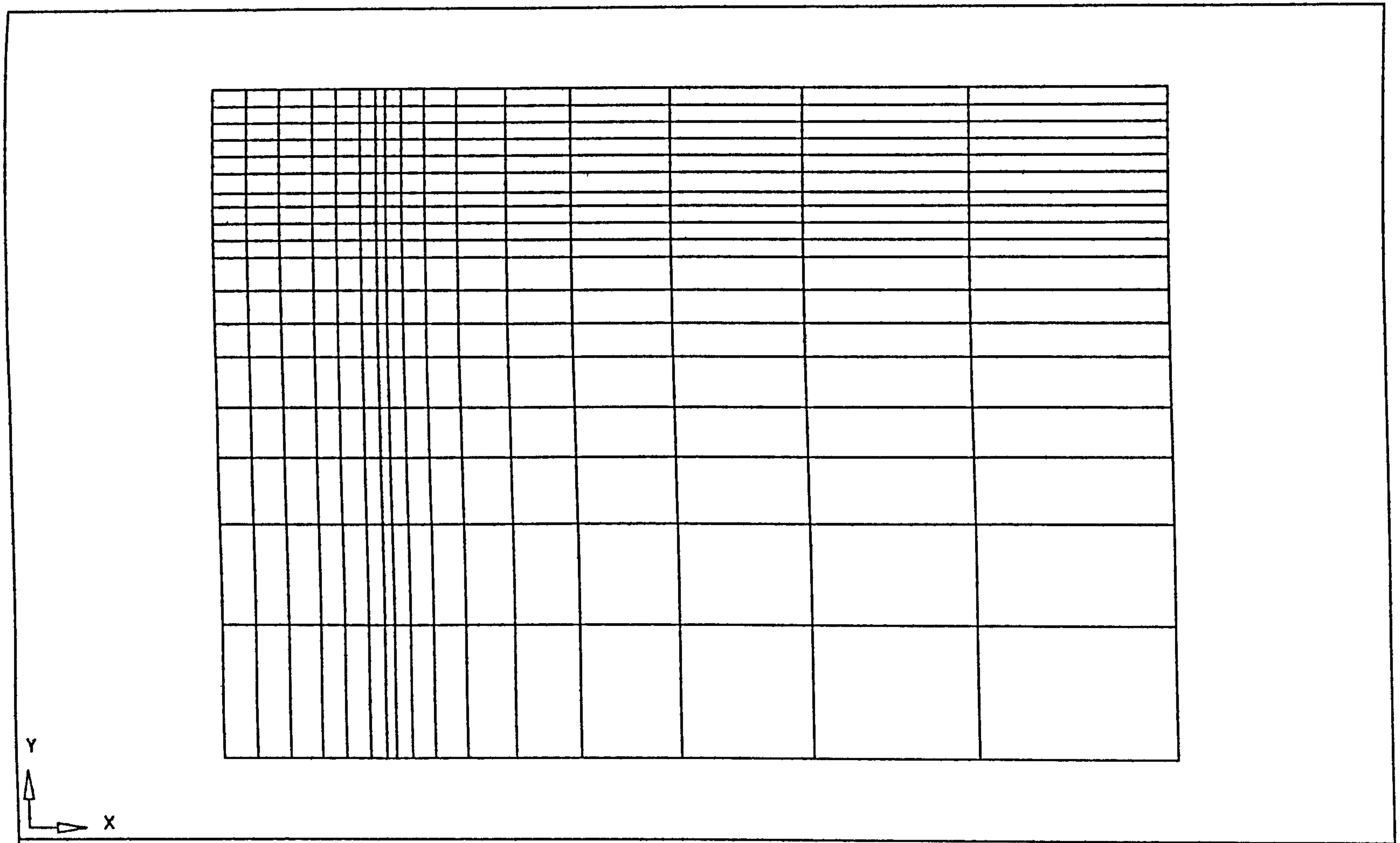

CASE 4A - JLE SOUTHWARK STATION TICKET HALL - IN-SITU STAGE

FINITE ELEMENT MESH

GEOM SCALE 0 16.00 metre

XMIN : -11.585 XMAX : 69.585 YMIN : 64.000 YMAX : 104.000

CRISP-94	CUED TRL	18/12/98 02:47	UNIVERSITY OF SURREY

FIG. 1

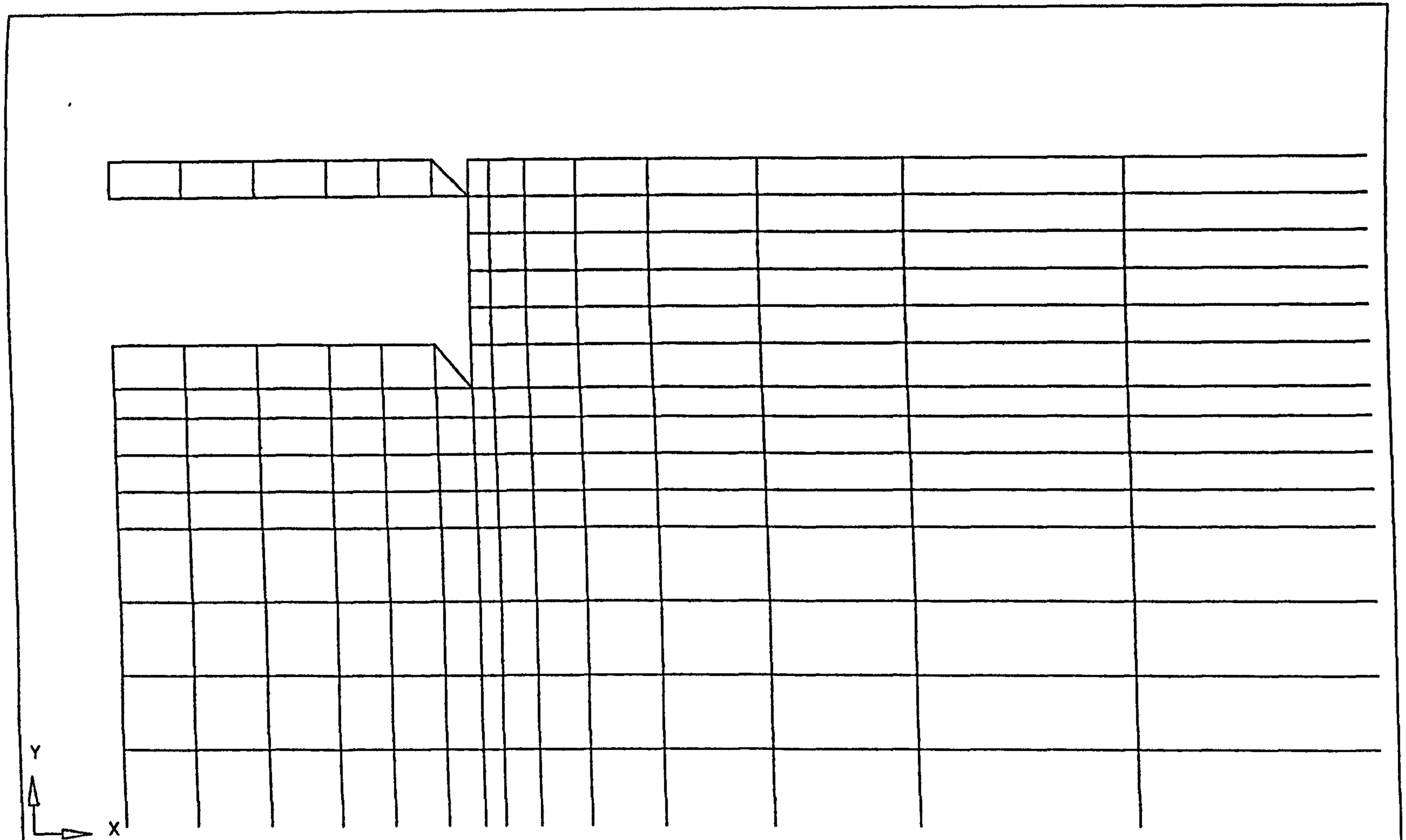

CASE 4A - JLE SOUTHWARK STATION TICKET HALL - FINAL GEOMETRY

FINITE ELEMENT MESH

GEOM SCALE 0 8.00 metre

XMIN : -2.361 XMAX : 34.534 YMIN : 87.636 YMAX : 105.818

CRISP-94	CUED TRL	18/12/98 02:54	UNIVERSITY OF SURREY	FIG. 1

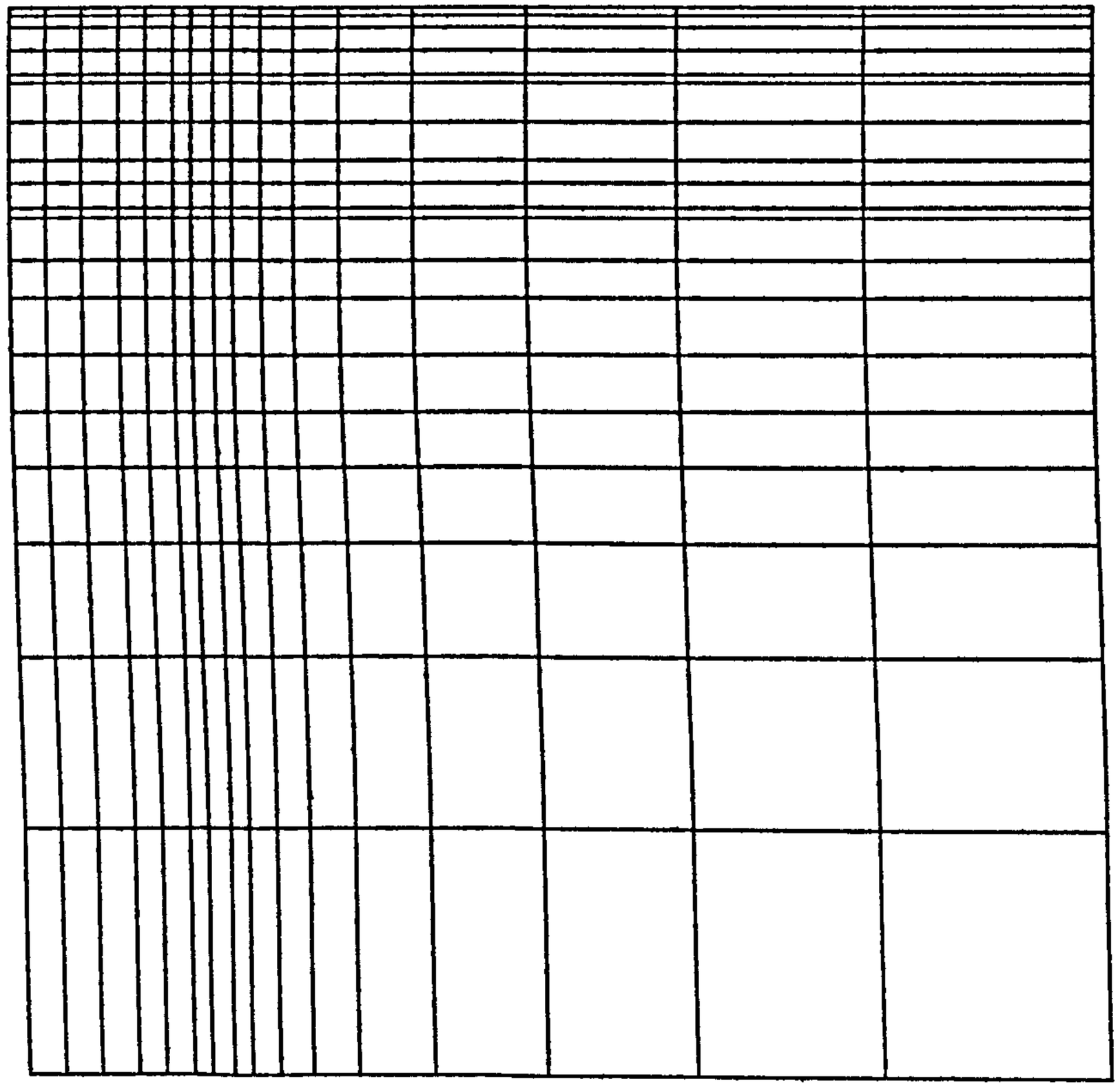

CASE 4B - JLE SOUTHWARK STATION UPPER CONCOURSE - IN-SITU STAGE

FINITE ELEMENT MESH

GEOM SCALE 0 24.00 metre

XMIN : -28.023 XMAX : 86.023 YMIN : 47.000 YMAX : 103.200

CRISP-94	CUED TRL	18/12/98 02:56	UNIVERSITY OF SURREY	FIG. 1

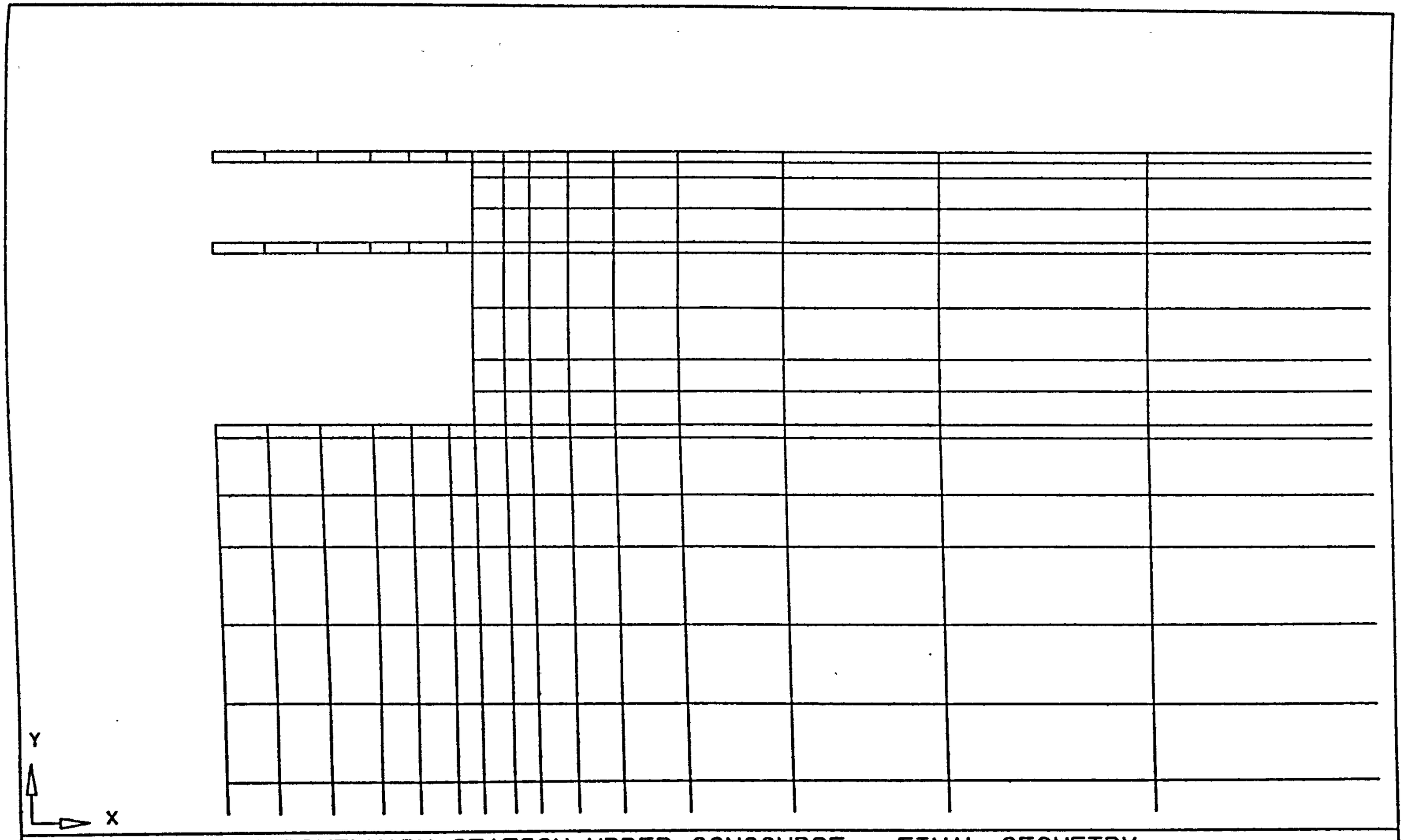

CASE 4B - JLE SOUTHWARK STATION UPPER CONCOURSE - FINAL GEOMETRY

FINITE ELEMENT MESH

GEOM SCALE 0 8.00 metre

XMIN : -7.287 XMAX : 44.552 YMIN : 80.209 YMAX : 105.755

CRISP-94	CUED TRL	18/12/98 02:59	UNIVERSITY OF SURREY

FIG. 1

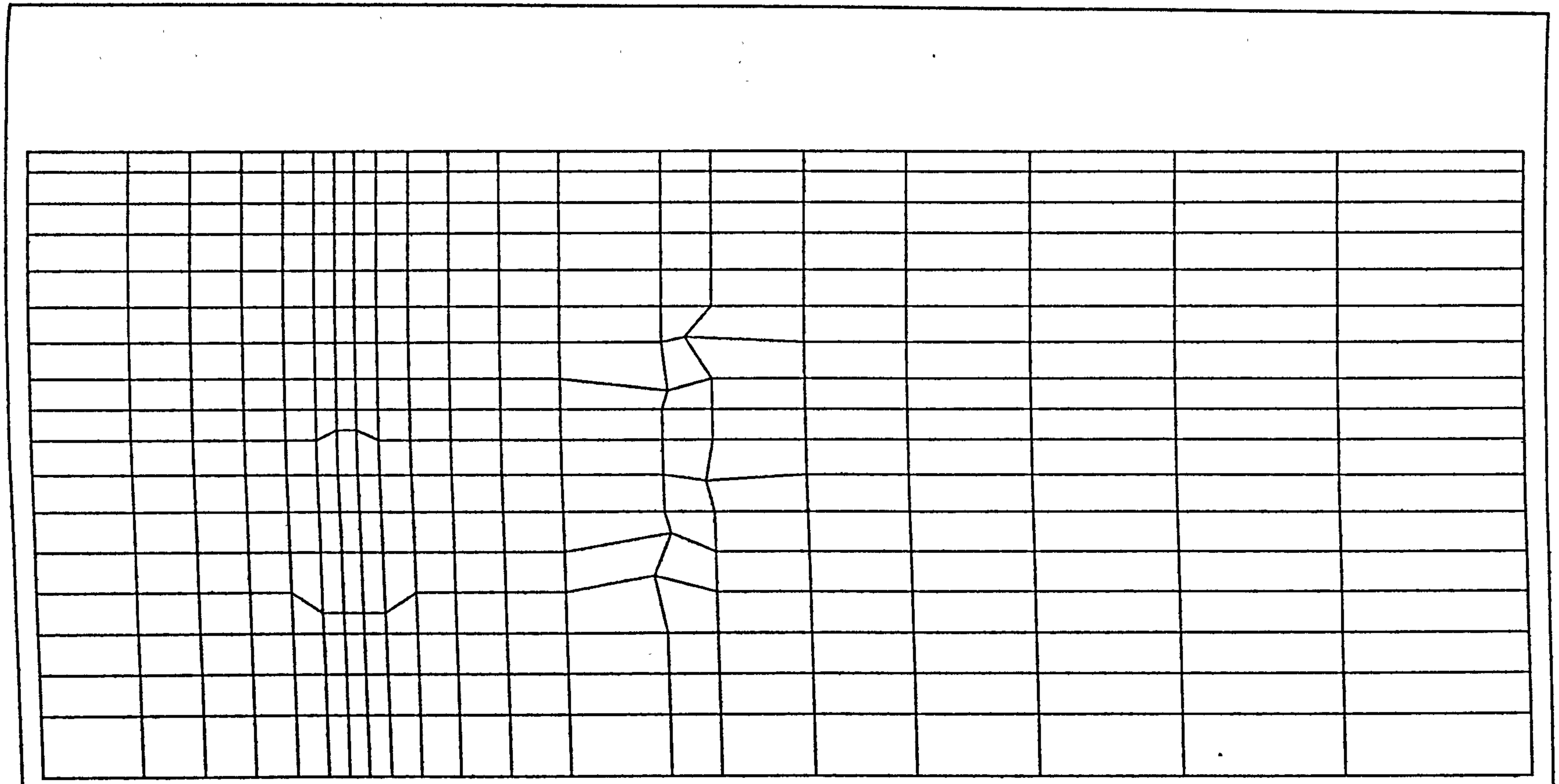

CASE 5 - GREENSIDE PLACE (SECTION AA) - IN-SITU STAGE

FINITE ELEMENT MESH

GEOM SCALE 0 16.00 metre

XMIN :-0.271E-06 XMAX : 73.000 YMIN : 21.263 YMAX : 57.237

CRISP-94	CUED TRL	18/12/98 03:03	UNIVERSITY OF SURREY

FIG. 1

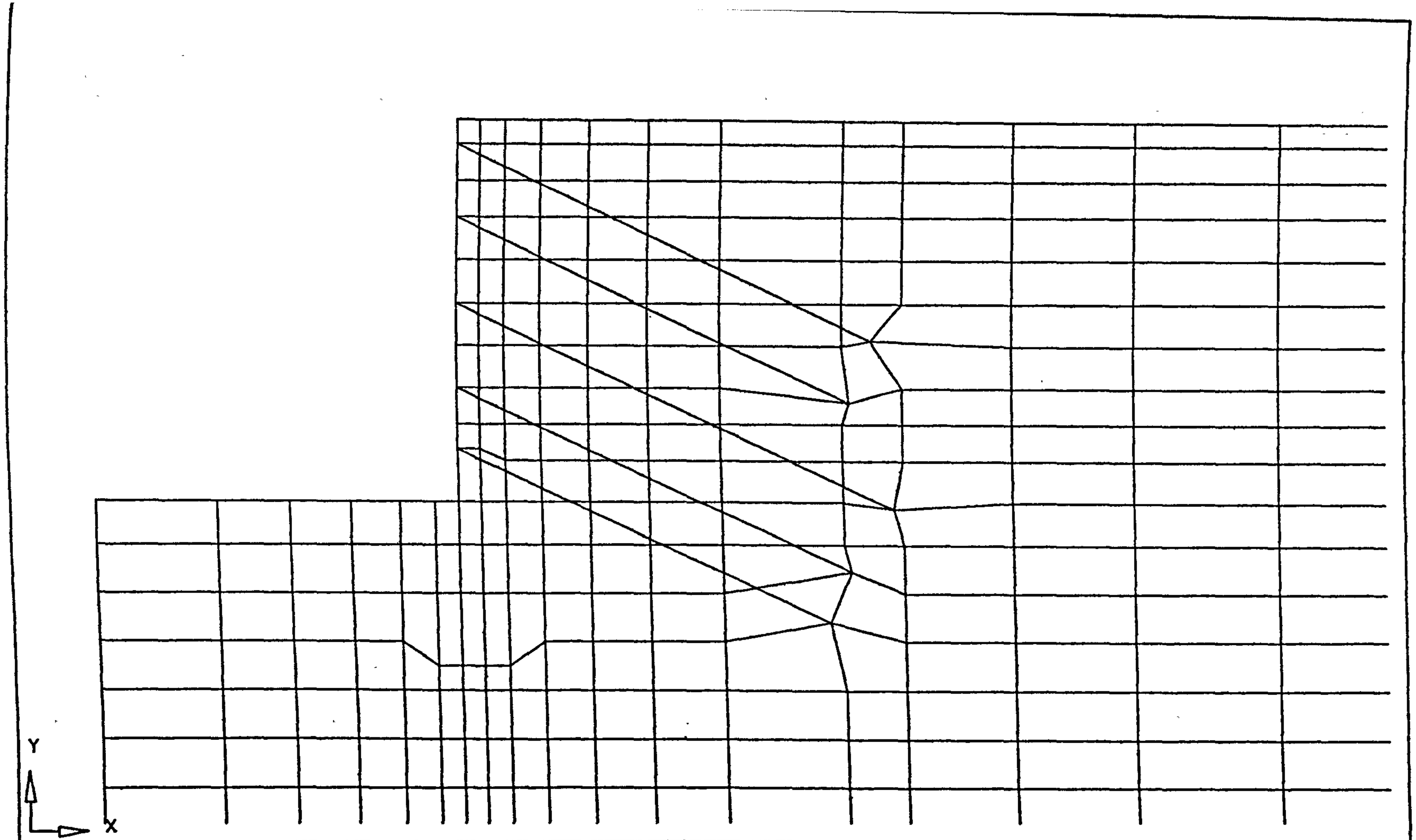

CASE 5 - GREENSIDE PLACE (SECTION AA) - FINAL GEOMETRY

FINITE ELEMENT MESH

GEOM SCALE 0 12.00 metre

XMIN : -2.808 XMAX : 53.346 YMIN : 28.181 YMAX : 55.853

CRISP-94	CUED TRL	18/12/98 03:08	UNIVERSITY OF SURREY	FIG. 1

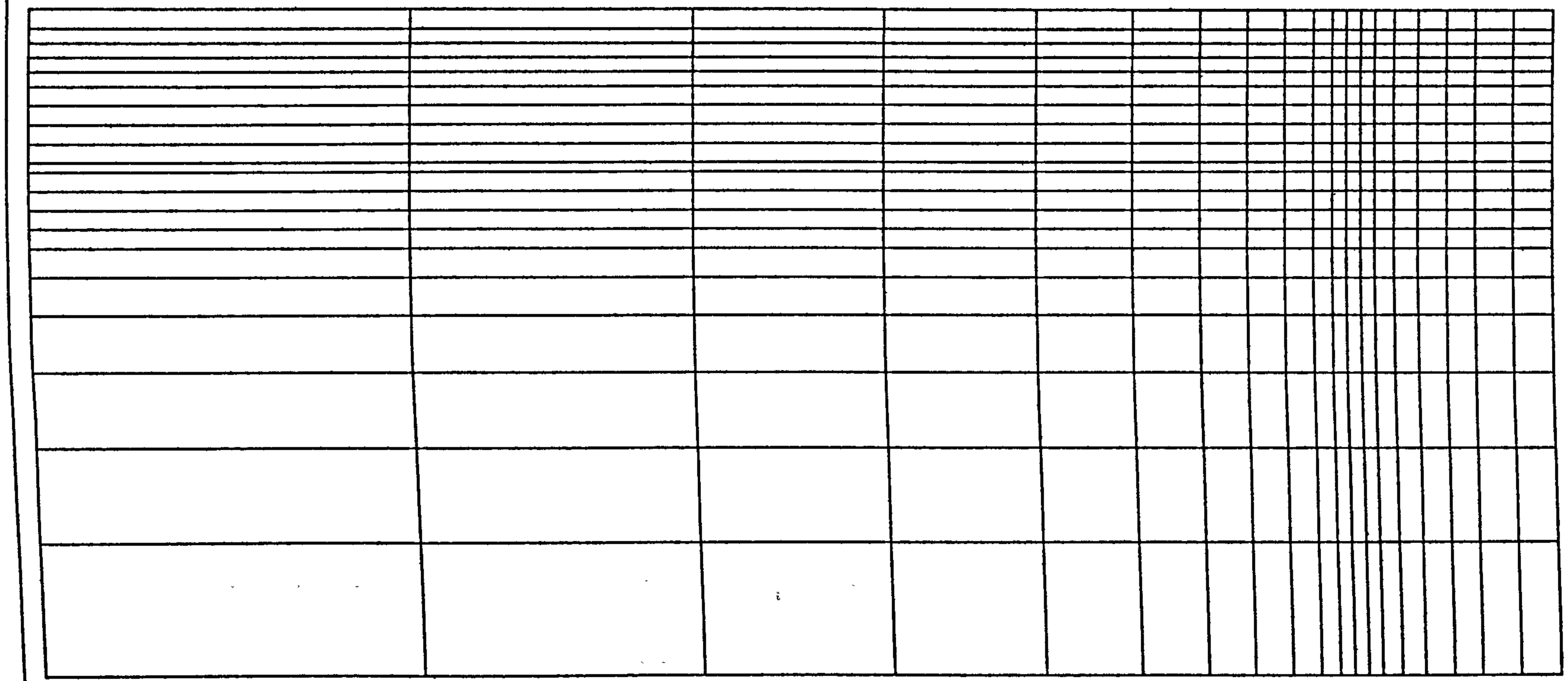

CASE 6A - RPR JUNCTION TUNNEL WALLS - IN-SITU STAGE

FINITE ELEMENT MESH

GEOM SCALE 0 16.00 metre

XMIN : -80.000 XMAX :-0.298E-06 YMIN : -17.212 YMAX : 22.212

CRISP-94	CUED TRL	18/12/98 01:18	UNIVERSITY OF SURREY	FIG. 1

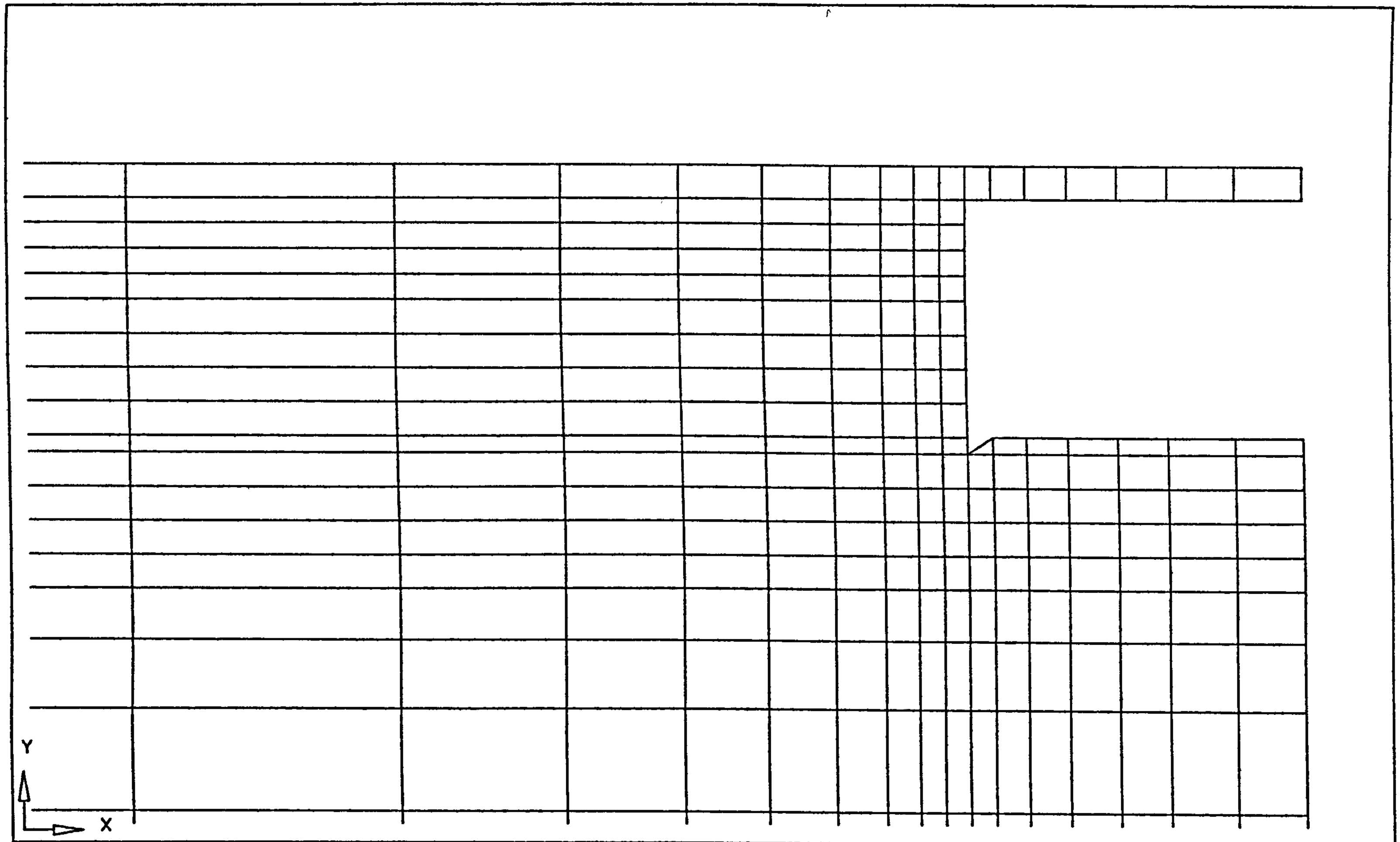

CASE 6A - RPR JUNCTION TUNNEL WALLS - FINAL GEOMETRY

FINITE ELEMENT MESH

GEOM SCALE 0 8.00 metre

XMIN : -38.000 XMAX : 2.000 YMIN : 2.500 YMAX : 22.212

CRISP-94	CUED TRL	18/12/98 01:21	UNIVERSITY OF SURREY

FIG. 1

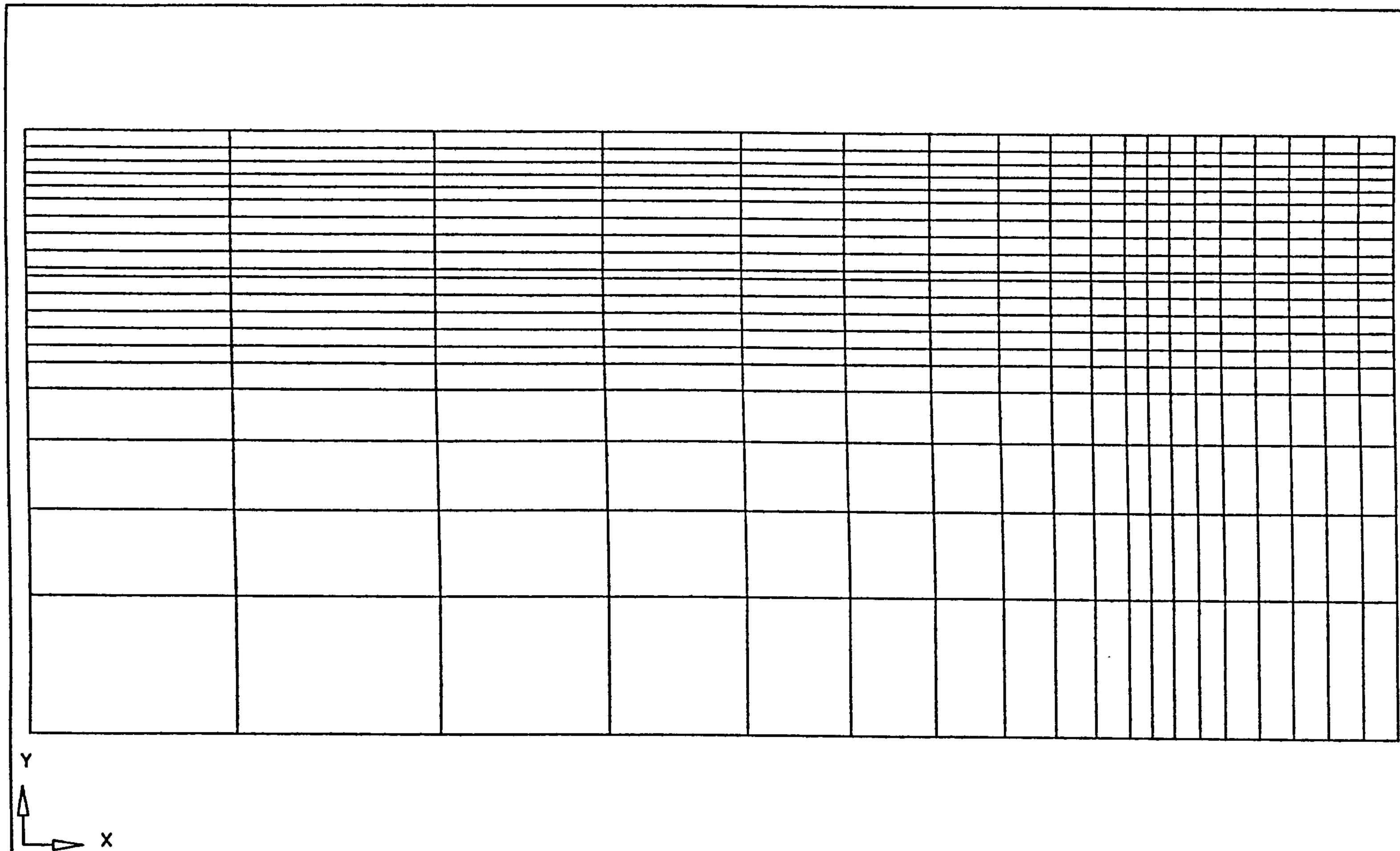

CASE 6B - RPR JUNCTION APPROACH WALLS - IN-SITU STAGE

FINITE ELEMENT MESH

GEOM SCALE 0 16.00 metre

XMIN : -80.000 XMAX : 0.250 YMIN : -17.273 YMAX : 22.273

CRISP-94	CUED TRL	18/12/98 01:15	UNIVERSITY OF SURREY

FIG. 1

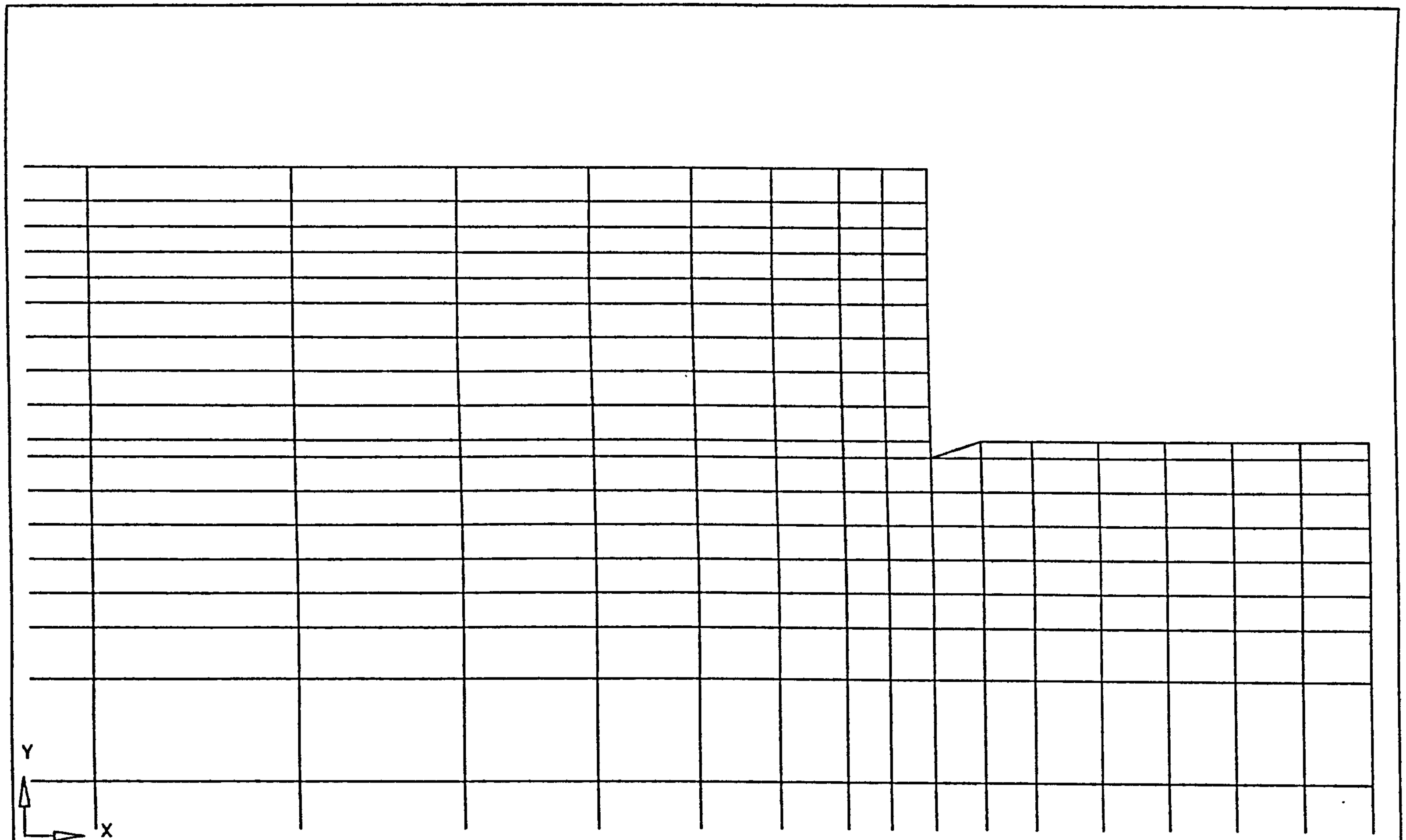

CASE 6B - RPR JUNCTION APPROACH WALLS - FINAL GEOMETRY

FINITE ELEMENT MESH

GEOM SCALE 0 8.00 metre

XMIN : -39.875 XMAX : 0.250 YMIN : 2.500 YMAX : 22.273

CRISP-94	CUED TRL	18/12/98 01:17	UNIVERSITY OF SURREY

FIG. 1

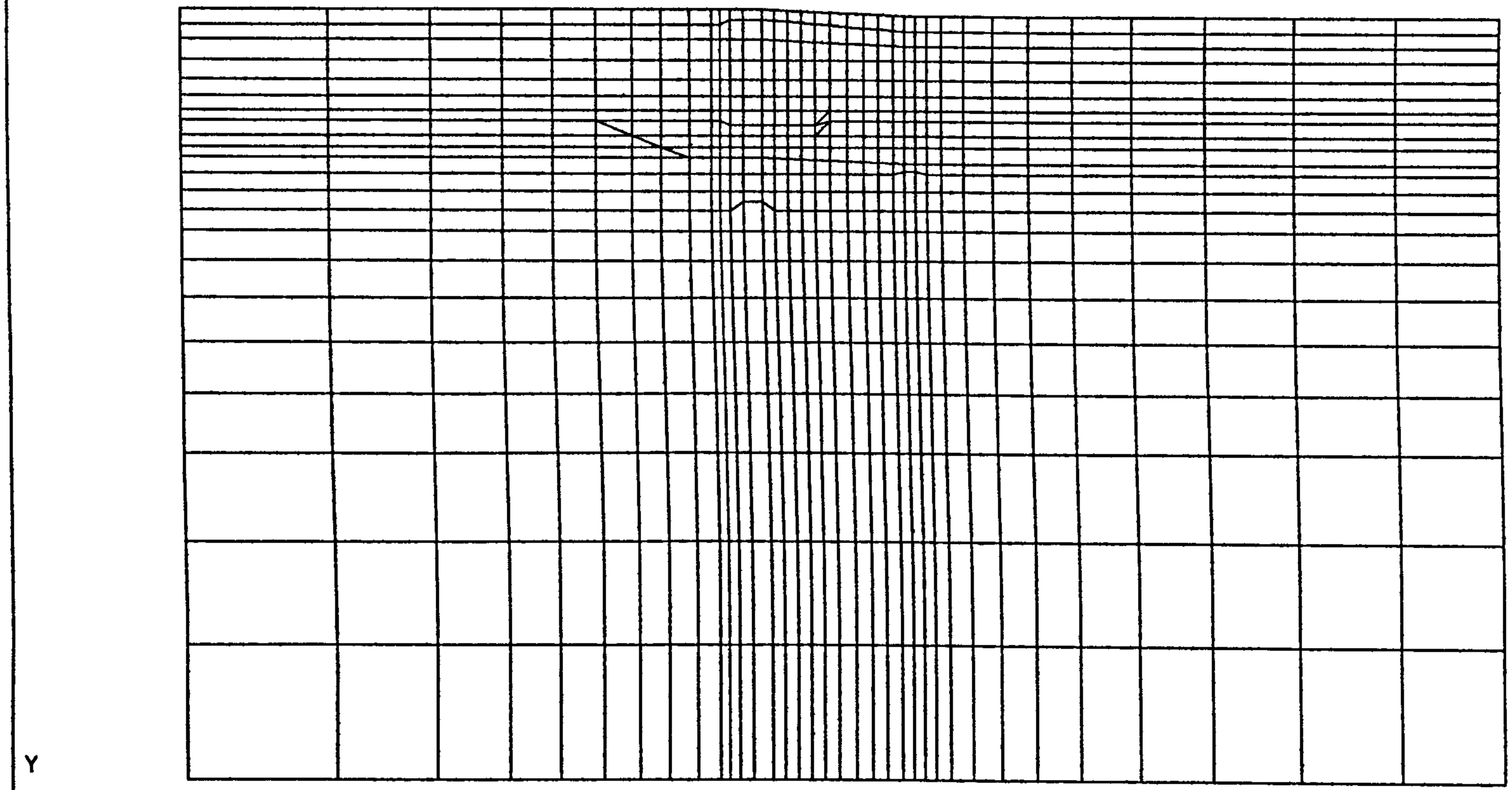

CASE 6C - RPR JUNCTION SLIP ROAD 3 (CH 805m) - IN-SITU STAGE

FINITE ELEMENT MESH

GEOM SCALE 0 24.00 metre

XMIN : -50.298 XMAX : 60.298 YMIN : -52.000 YMAX : 2.500

CRISP-94	CUED TRL	18/12/98 00:48	UNIVERSITY OF SURREY	FIG. 1

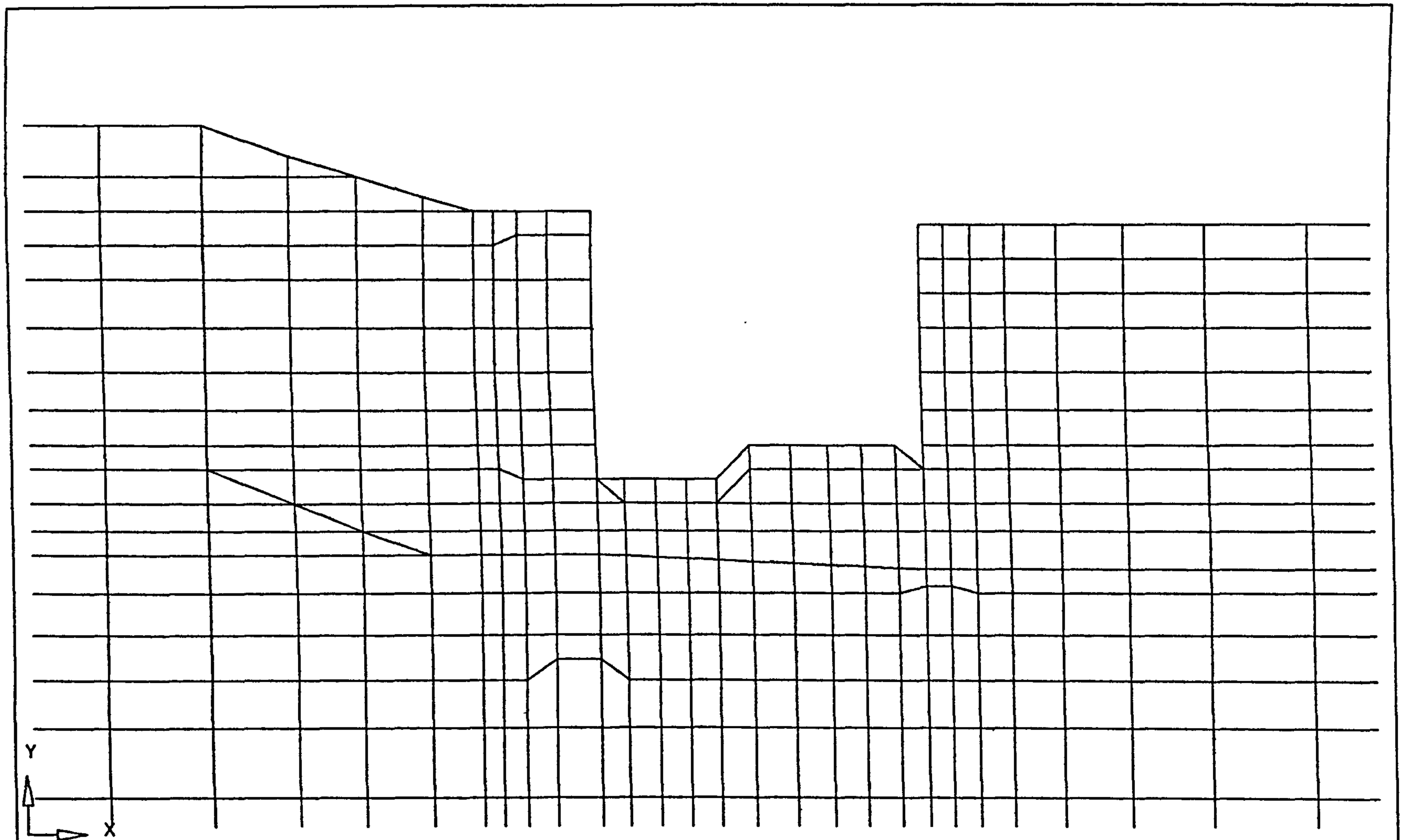

CASE 6C - RPR JUNCTION SLIP ROAD 3 (CH 805m) - FINAL GEOMETRY

FINITE ELEMENT MESH

GEOM SCALE 0 8.00 metre

XMIN : -16.724 XMAX : 22.774 YMIN : -15.991 YMAX : 3.473

CRISP-94	CUED TRL	18/12/98 00:56	UNIVERSITY OF SURREY	FIG. 1

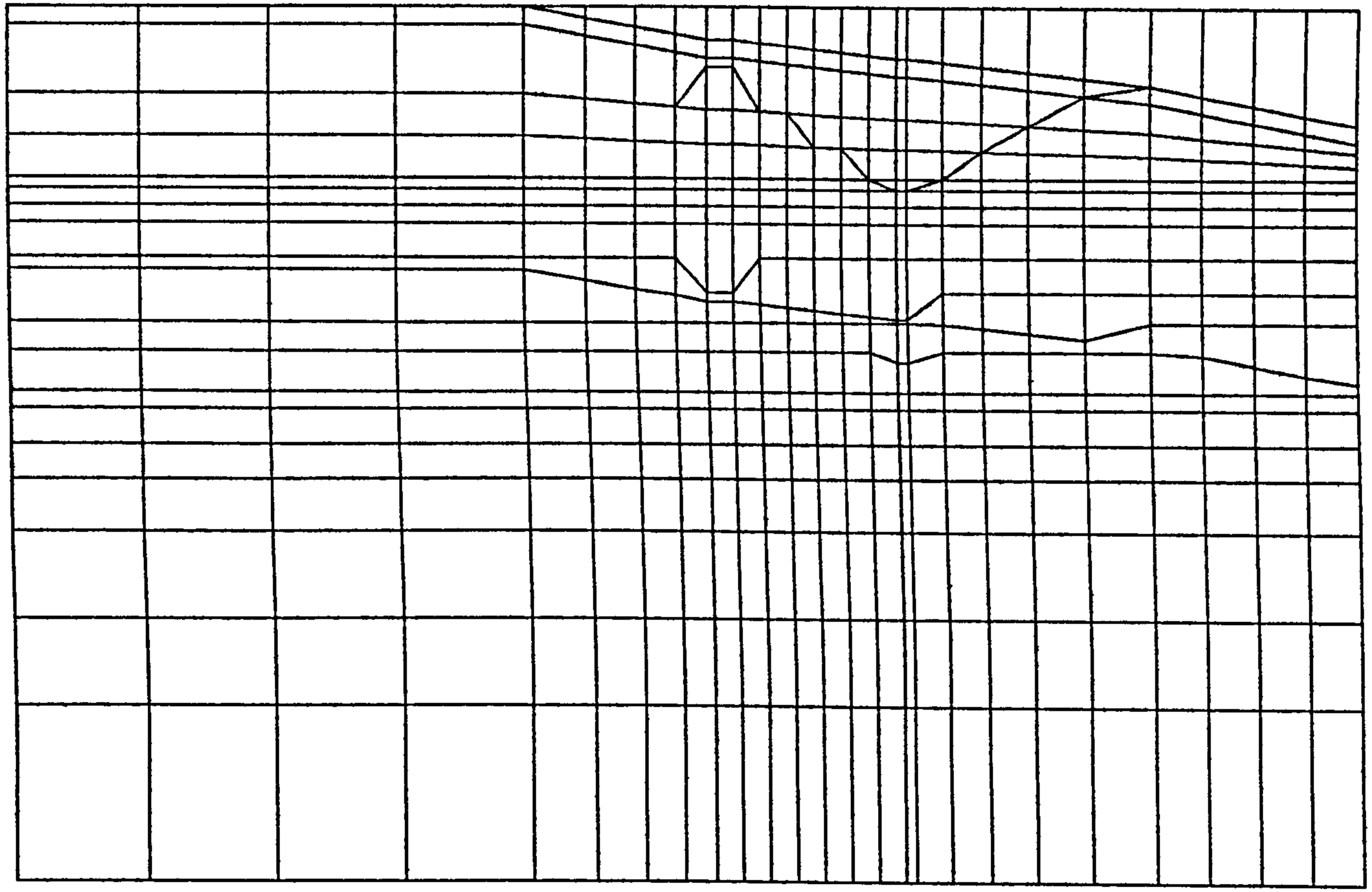

CASE 6D - RPR JUNCTION SLIP ROAD 5 (CH 1670m) - IN-SITU STAGE

FINITE ELEMENT MESH

GEOM SCALE 0 20.00 metre

XMIN : -53.732 XMAX : 47.732 YMIN : -50.000 YMAX : 0.121E-05

CRISP-94	CUED TRL	17/12/98 23:56	UNIVERSITY OF SURREY	FIG. 1

A-52

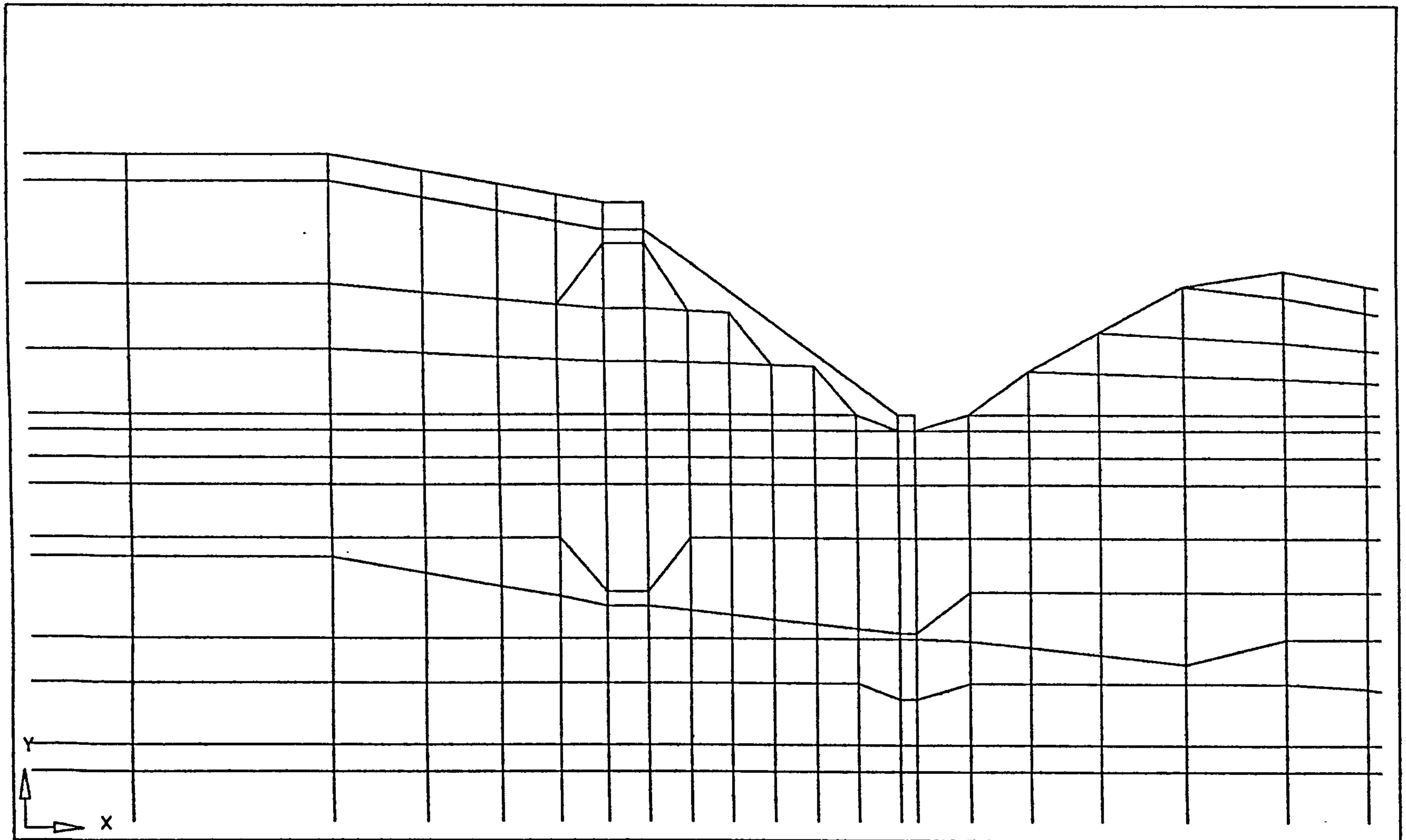

CASE 6D - RPR JUNCTION SLIP ROAD 5 (CH 1670m) - TEMPORARY STAGE

FINITE ELEMENT MESH

GEOM SCALE 0 8.00 metre

XMIN : -23.293 XMAX : 27.439 YMIN : -22.500 YMAX : 2.500

CRISP-94	CUED TRL	18/12/98 01:47	UNIVERSITY OF SURREY	FIG. 1

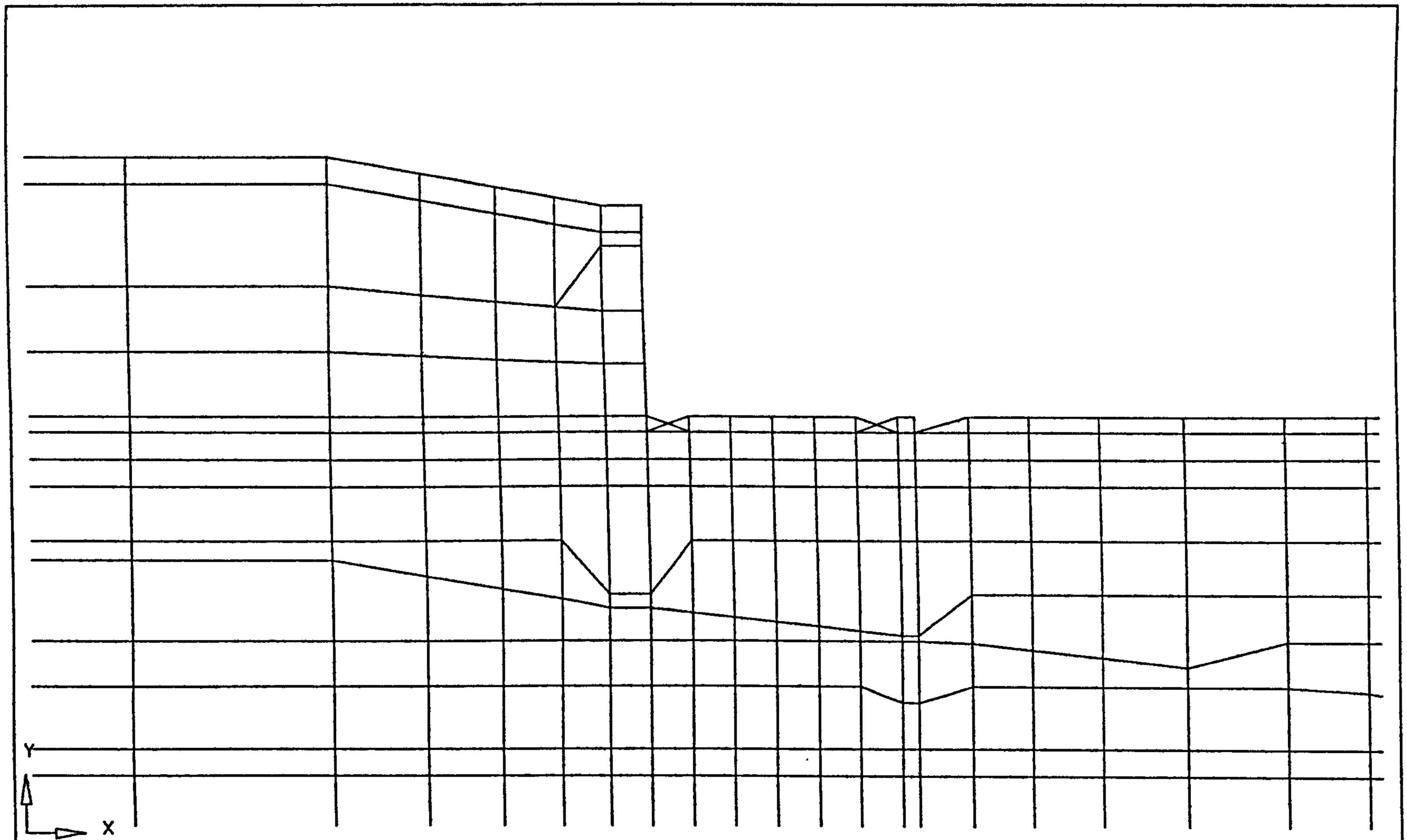

CASE 6D - RPR JUNCTION SLIP ROAD 5 (CH 1670m) - FINAL GEOMETRY

FINITE ELEMENT MESH

GEOM SCALE 0 8.00 metre

XMIN : -23.293 XMAX : 27.439 YMIN : -22.500 YMAX : 2.500

CRISP-94	CUED TRL	18/12/98 01:37	UNIVERSITY OF SURREY	FIG. 1

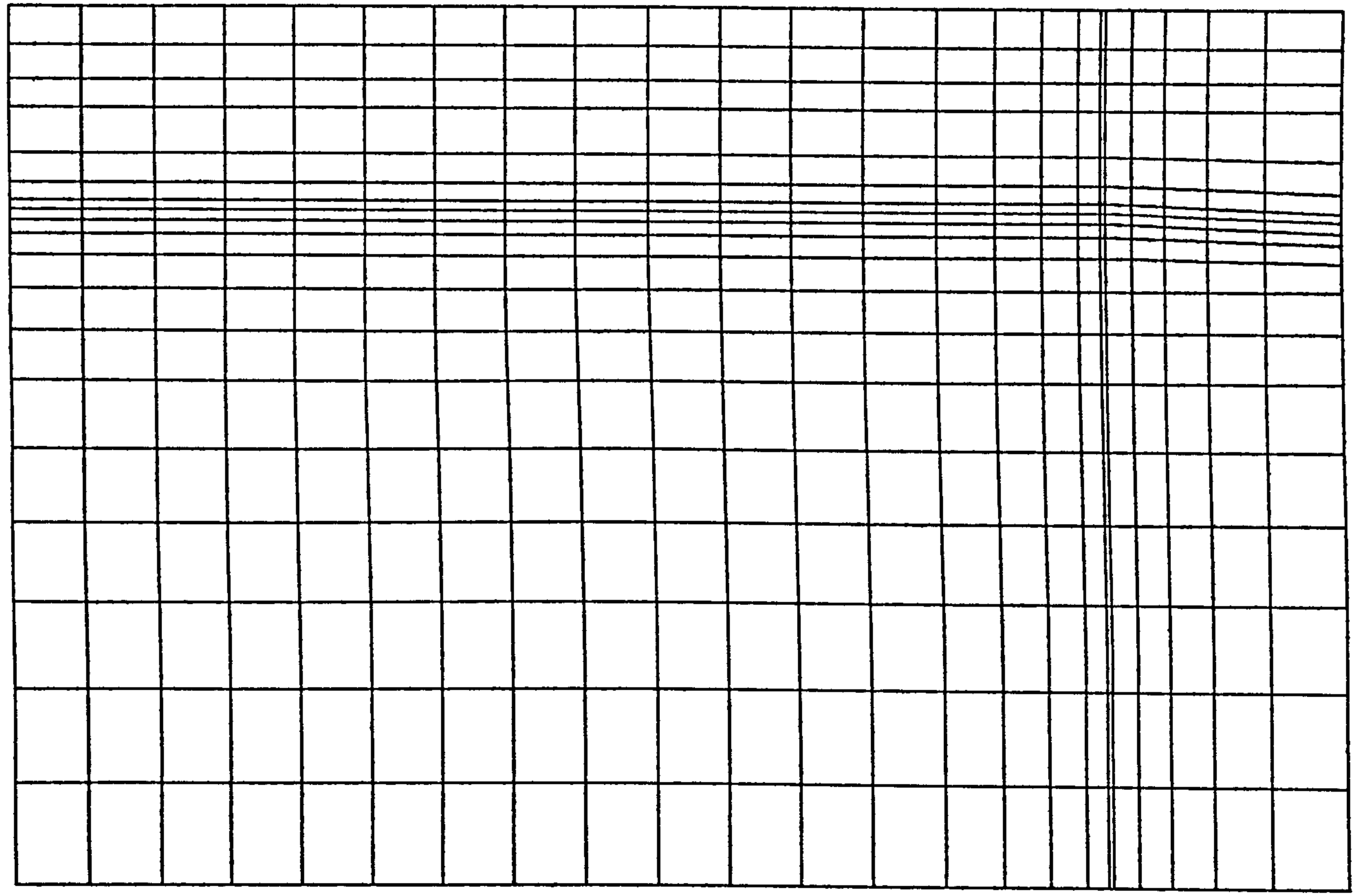

CASE 7 - BVR ALDERSHOT ROAD UNDERPASS - IN-SITU STAGE

FINITE ELEMENT MESH

GEOM SCALE 0 20.00 metre

XMIN : -86.811 XMAX : 11.811 YMIN : 24.000 YMAX : 72.600

CRISP-94	CUED TRL	27/12/98 02:45	UNIVERSITY OF SURREY	FIG. 1

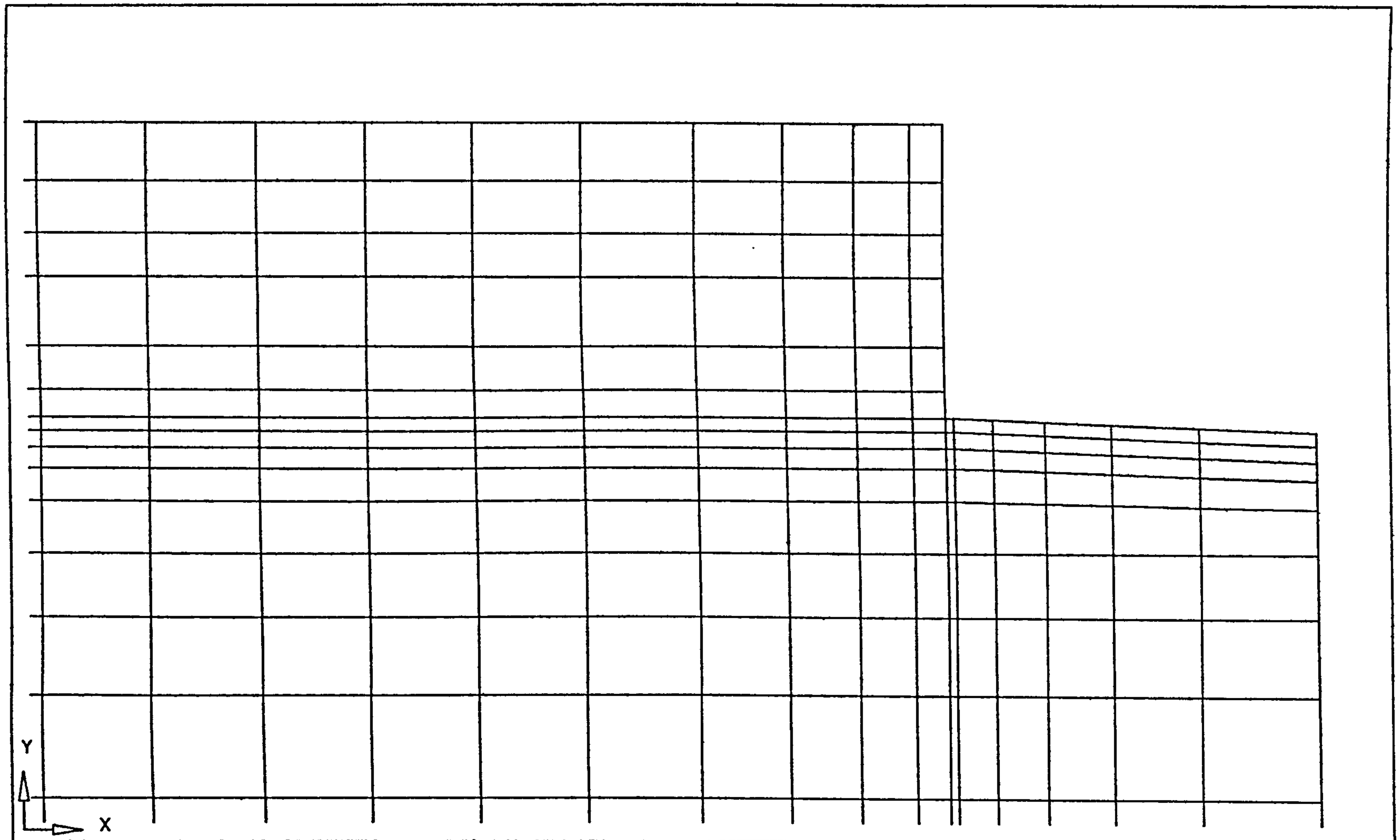

CASE 7 - BVR ALDERSHOT ROAD UNDERPASS - FINAL GEOMETRY

FINITE ELEMENT MESH

GEOM SCALE 0 8.00 metre

XMIN : -47.362 XMAX : 1.949 YMIN : 49.515 YMAX : 73.815

CRISP-94	CUED TRL	27/12/98 02:54	UNIVERSITY OF SURREY	FIG. 1

A-56

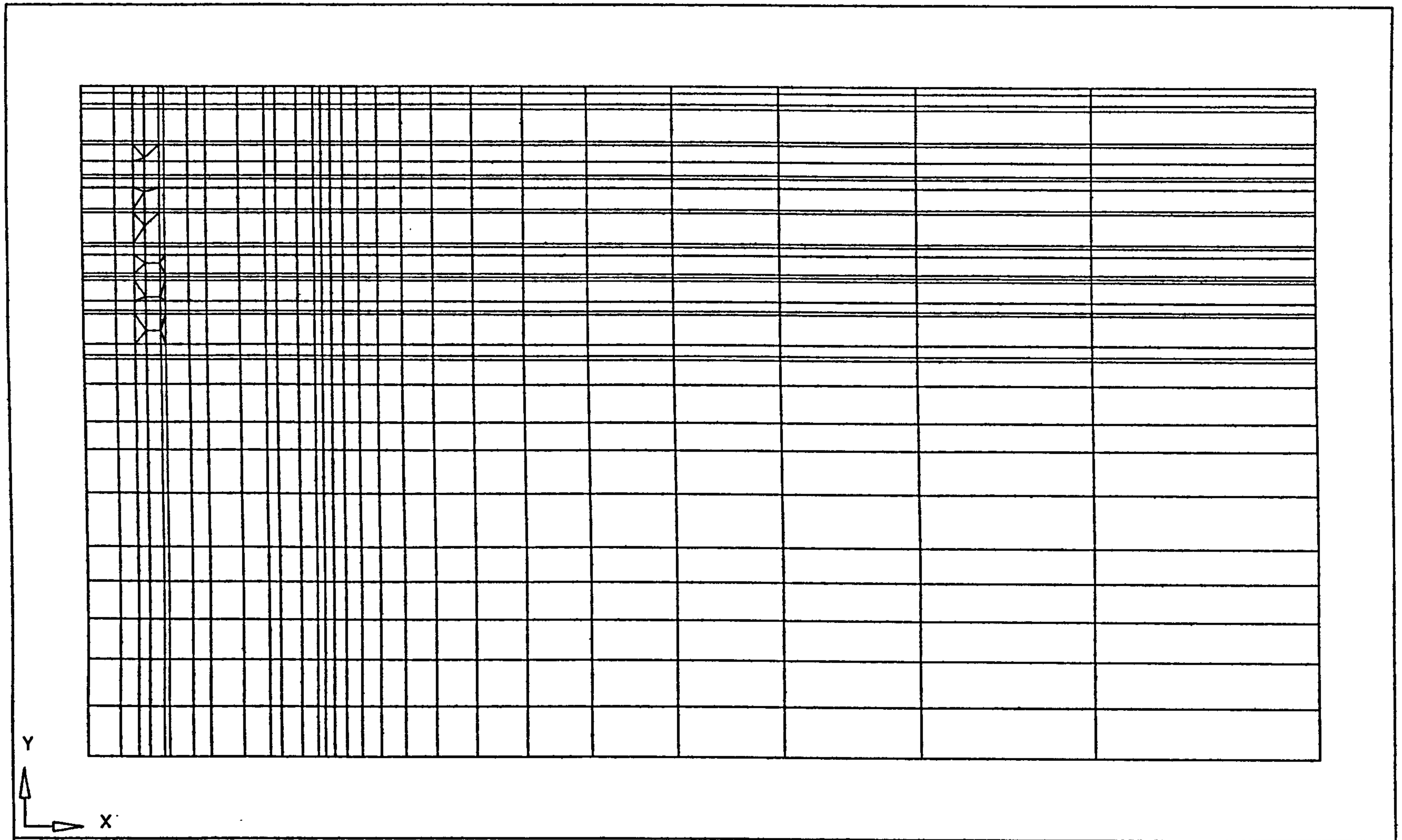

CASE 8A - QUEENSBERRY HOUSE TRANSVERSE SECTION - IN-SITU STAGE

FINITE ELEMENT MESH

GEOM SCALE 0 24.00 metre

XMIN : -4.628 XMAX : 103.938 YMIN : -30.000 YMAX : 23.500

CRISP-94	CUED TRL	23/12/98 18:49	UNIVERSITY OF SURREY	FIG. 1

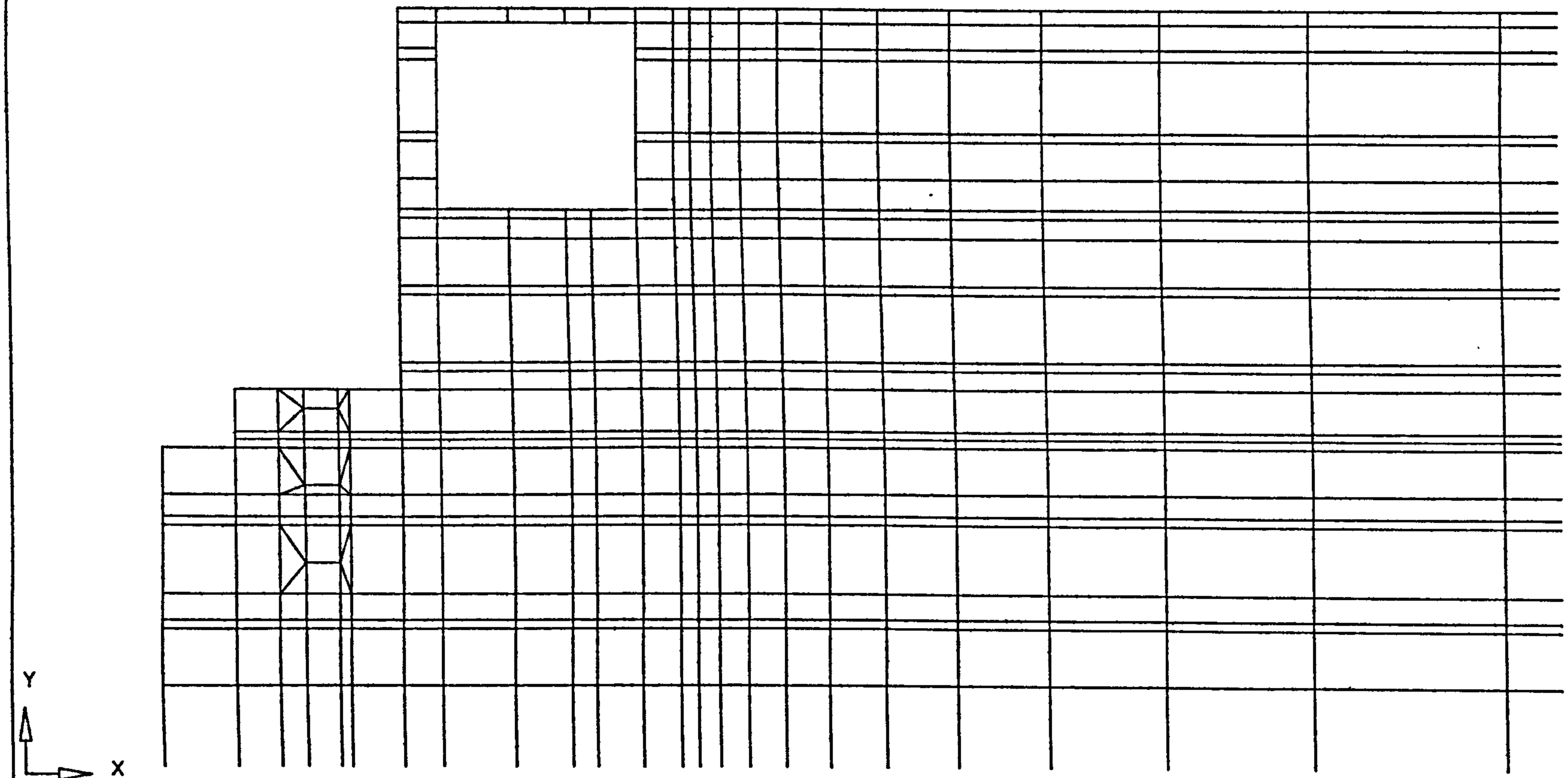

CASE 8A - QUEENSBERRY HOUSE TRANSVERSE SECTION - INC BLOCK

FINITE ELEMENT MESH

GEOM SCALE 0 12.00 metre

XMIN : -4.628 XMAX : 49.655 YMIN : -0.575 YMAX : 26.175

CRISP-94	CUED TRL	23/12/98 19:01	UNIVERSITY OF SURREY	FIG. 1

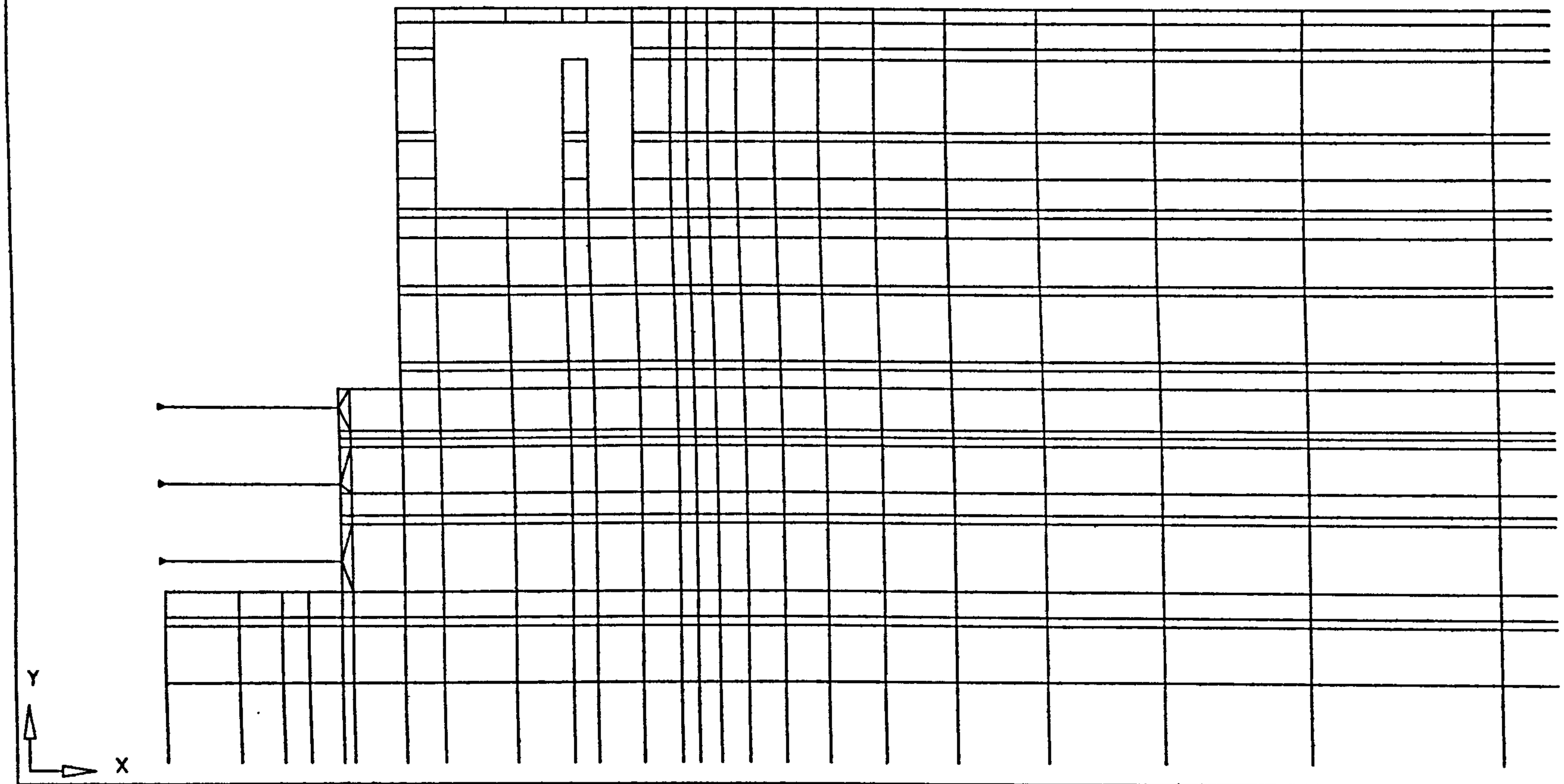

CASE 8A - QUEENSBERRY HOUSE TRANSVERSE SECTION - INC BLOCK

FINITE ELEMENT MESH

GEOM SCALE 0 12.00 metre

XMIN : -4.628 XMAX : 49.655 YMIN : -0.575 YMAX : 26.175

CRISP-94	CUED TRL	23/12/98 19:01	UNIVERSITY OF SURREY	FIG. 2

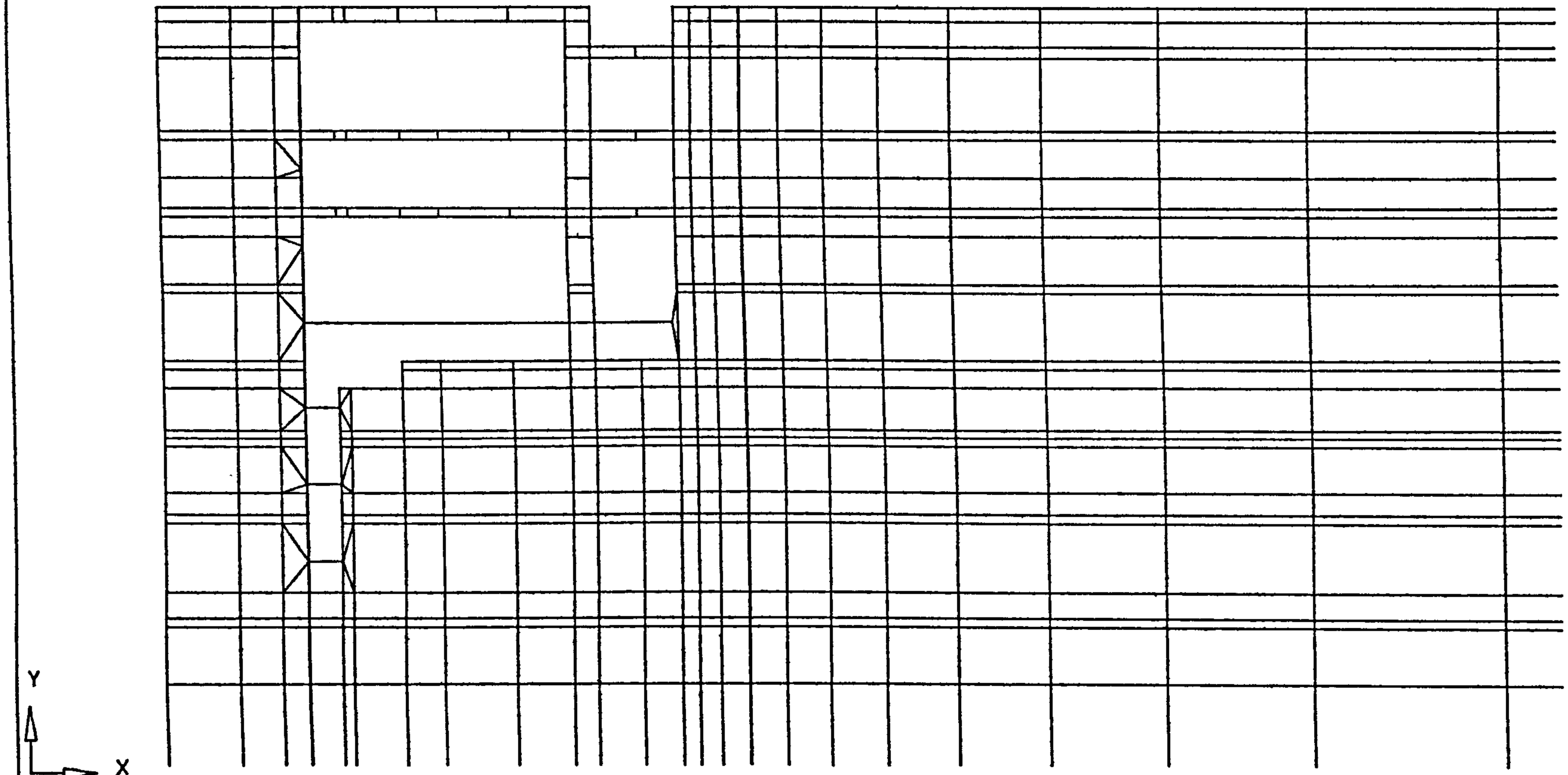

CASE 8A - QUEENSBERRY HOUSE TRANSVERSE SECTION - INC BLOCK

FINITE ELEMENT MESH

GEOM SCALE 0 12.00 metre

XMIN : -4.628 XMAX : 49.655 YMIN : -0.575 YMAX : 26.175

CRISP-94	CUED TRL	23/12/98 19:01	UNIVERSITY OF SURREY	FIG. 3

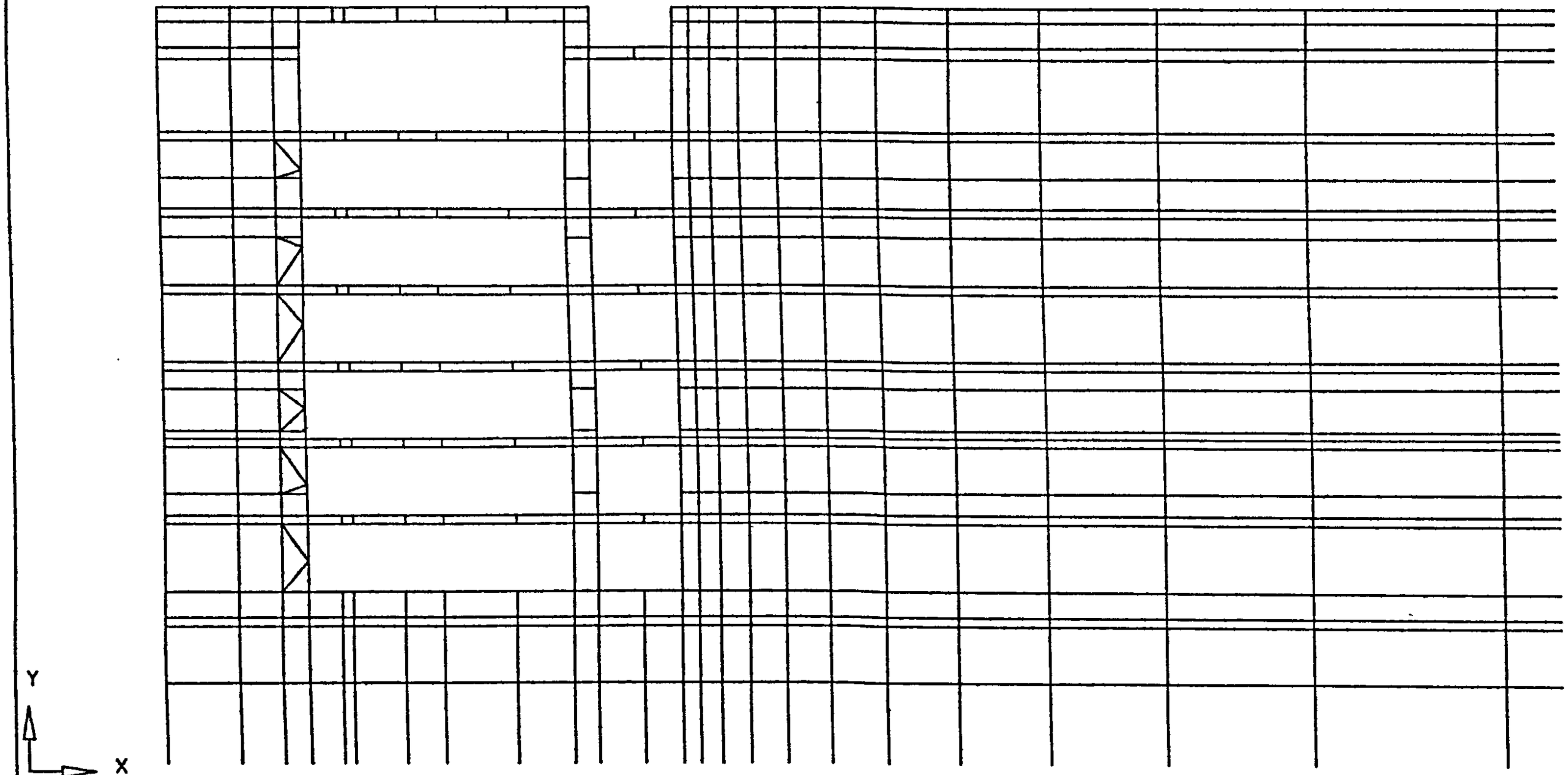

CASE 8A - QUEENSBERRY HOUSE TRANSVERSE SECTION - INC BLOCK

FINITE ELEMENT MESH

GEOM SCALE 0 12.00 metre

XMIN : -4.628 XMAX : 49.655 YMIN : -0.575 YMAX : 26.175

CRISP-94	CUED TRL	23/12/98 19:02	UNIVERSITY OF SURREY	FIG. 4

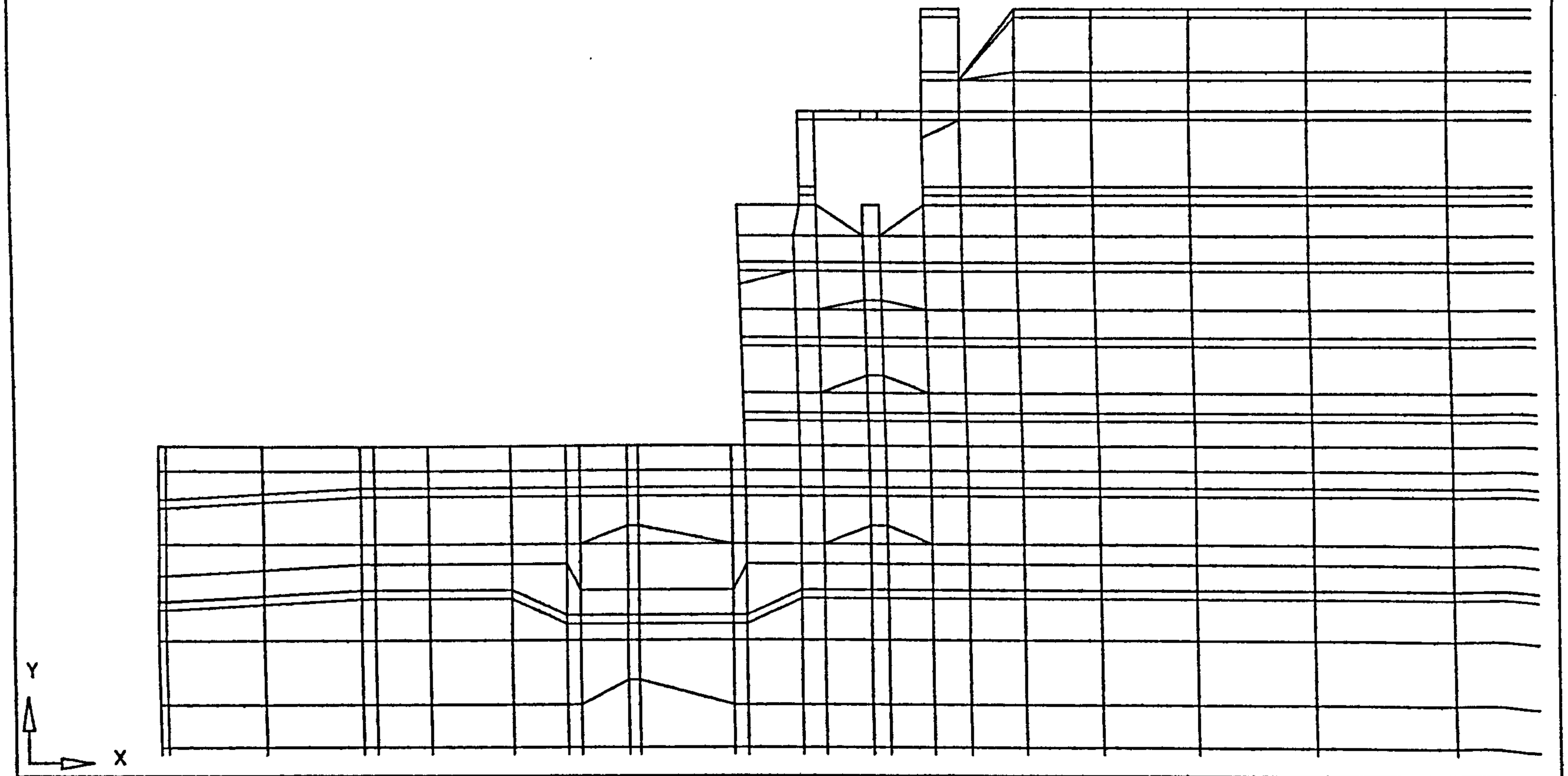

CASE 8B - QUEENSBERRY HOUSE LONGITUDINAL SECTION - INC BLOCK

FINITE ELEMENT MESH

GEOM SCALE 0 12.00 metre

XMIN : -4.484 XMAX : 49.900 YMIN : -0.520 YMAX : 26.280

CRISP-94	CUED TRL	23/12/98 20:32	UNIVERSITY OF SURREY	FIG. 1

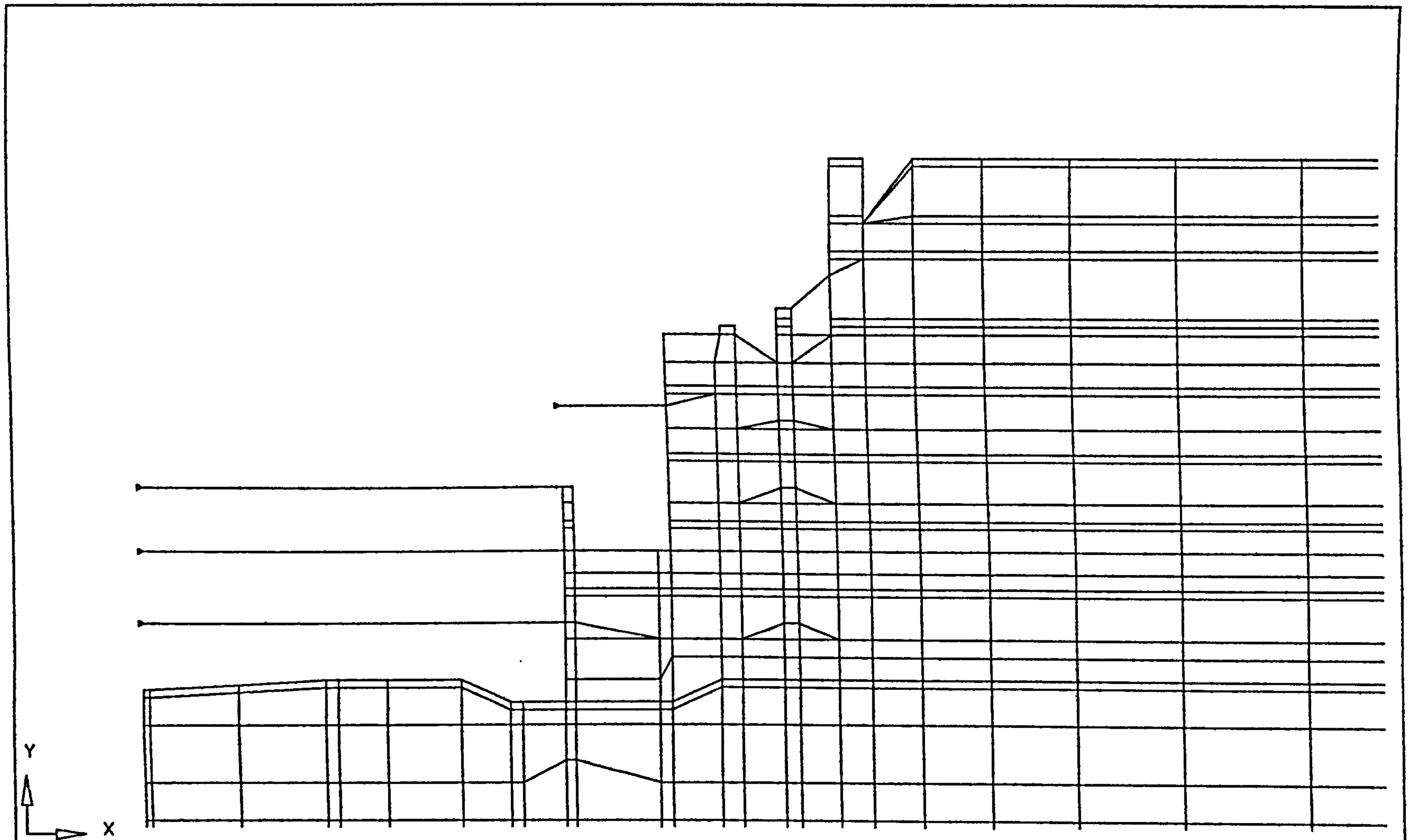

CASE 8B - QUEENSBERRY HOUSE LONGITUDINAL SECTION - INC BLOCK

FINITE ELEMENT MESH

GEOM SCALE 0 12.00 metre

XMIN : -4.484 XMAX : 49.900 YMIN : -0.520 YMAX : 26.280

CRISP-94	CUED TRL	23/12/98 20:33	UNIVERSITY OF SURREY	FIG. 2

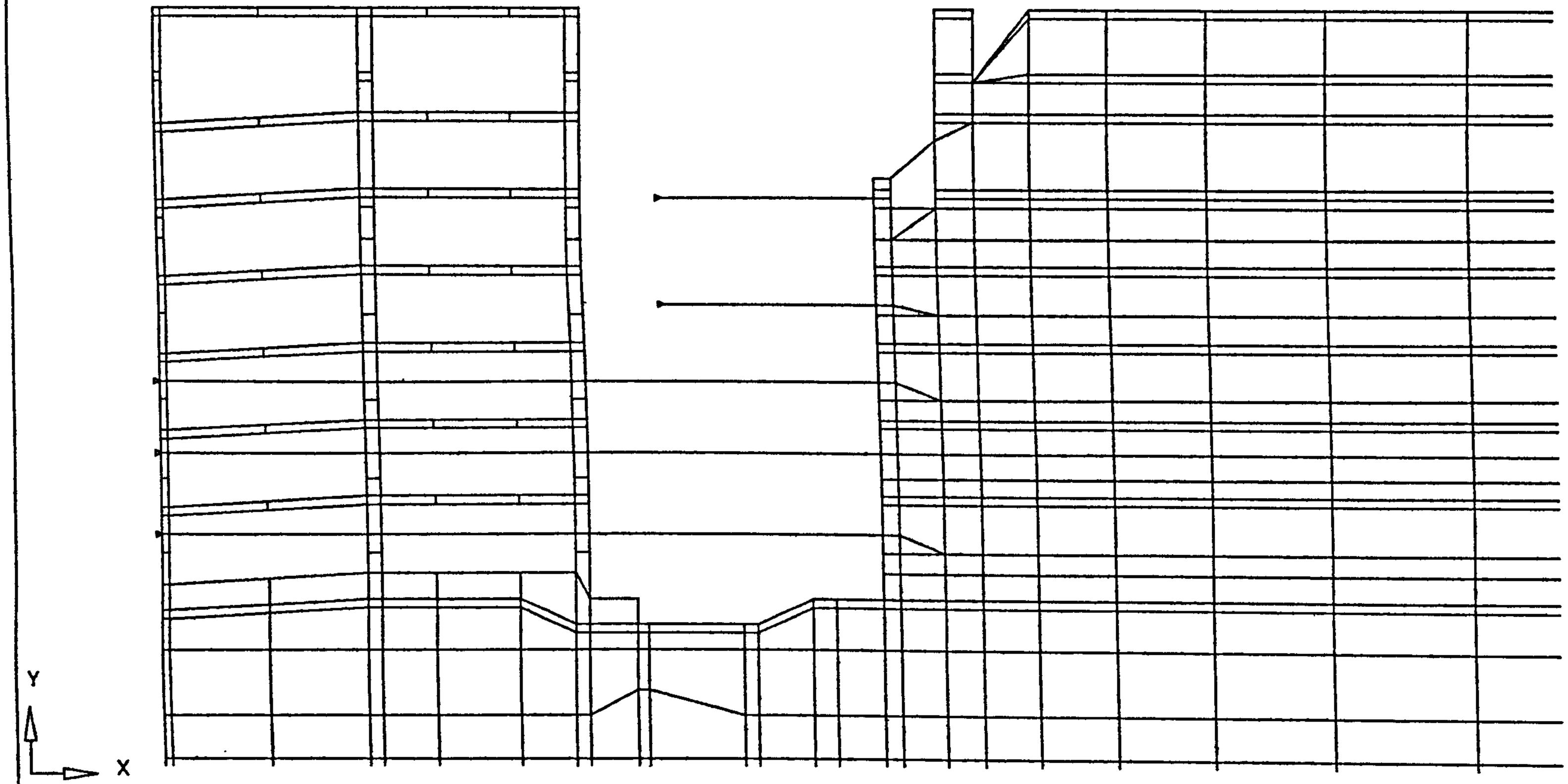

CASE 8B - QUEENSBERRY HOUSE LONGITUDINAL SECTION - INC BLOCK

FINITE ELEMENT MESH

GEOM SCALE 0 12.00 metre

XMIN : -4.484 XMAX : 49.900 YMIN : -0.520 YMAX : 26.280

CRISP-94	CUED TRL	23/12/98 20:33	UNIVERSITY OF SURREY	FIG. 3

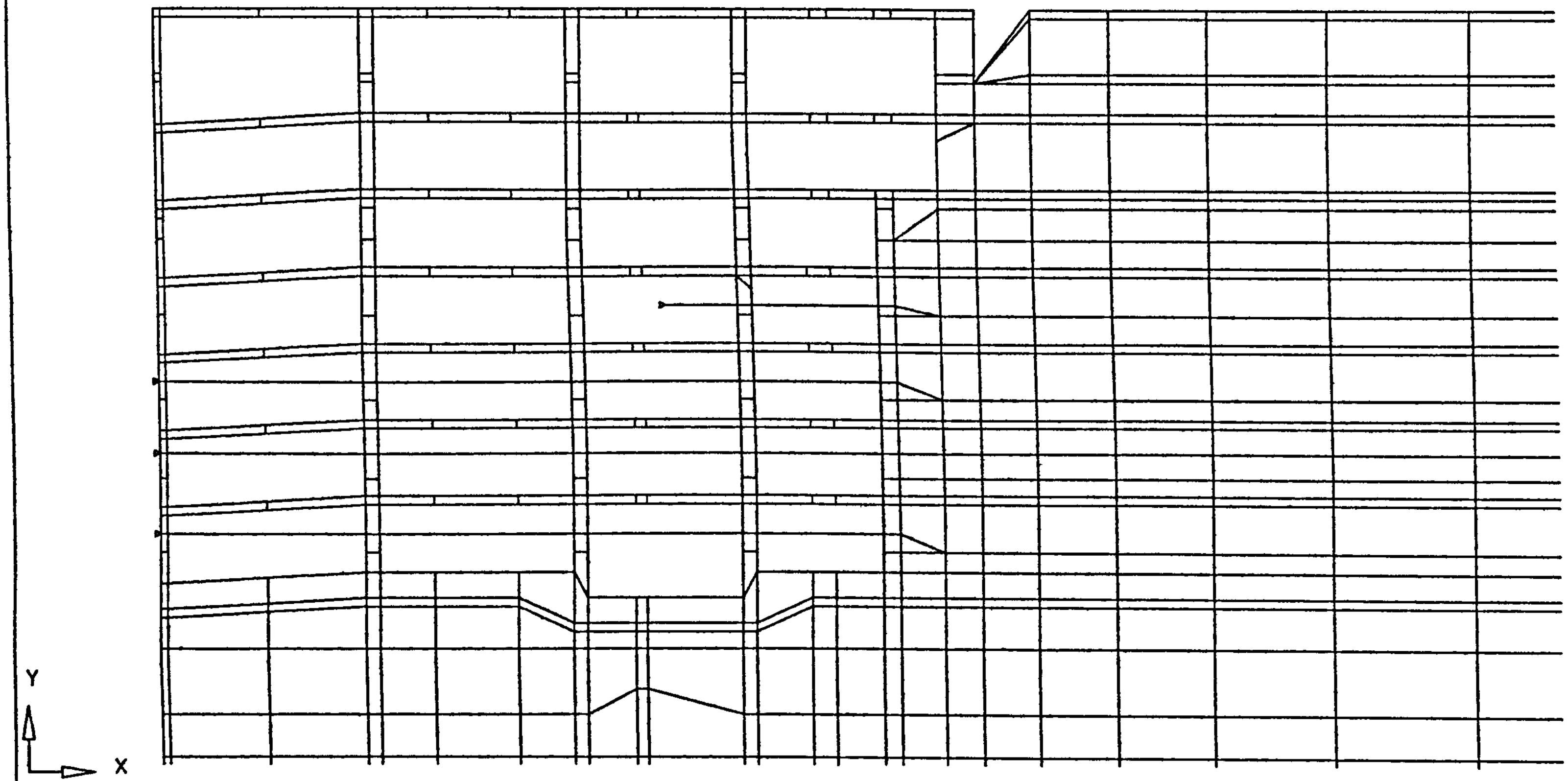

CASE 8B - QUEENSBERRY HOUSE LONGITUDINAL SECTION - INC BLOCK

FINITE ELEMENT MESH

GEOM SCALE 0 12.00 metre

XMIN : -4.484 XMAX : 49.900 YMIN : -0.520 YMAX : 26.280

CRISP-94	CUED TRL	23/12/98 20:33	UNIVERSITY OF SURREY	FIG. 4

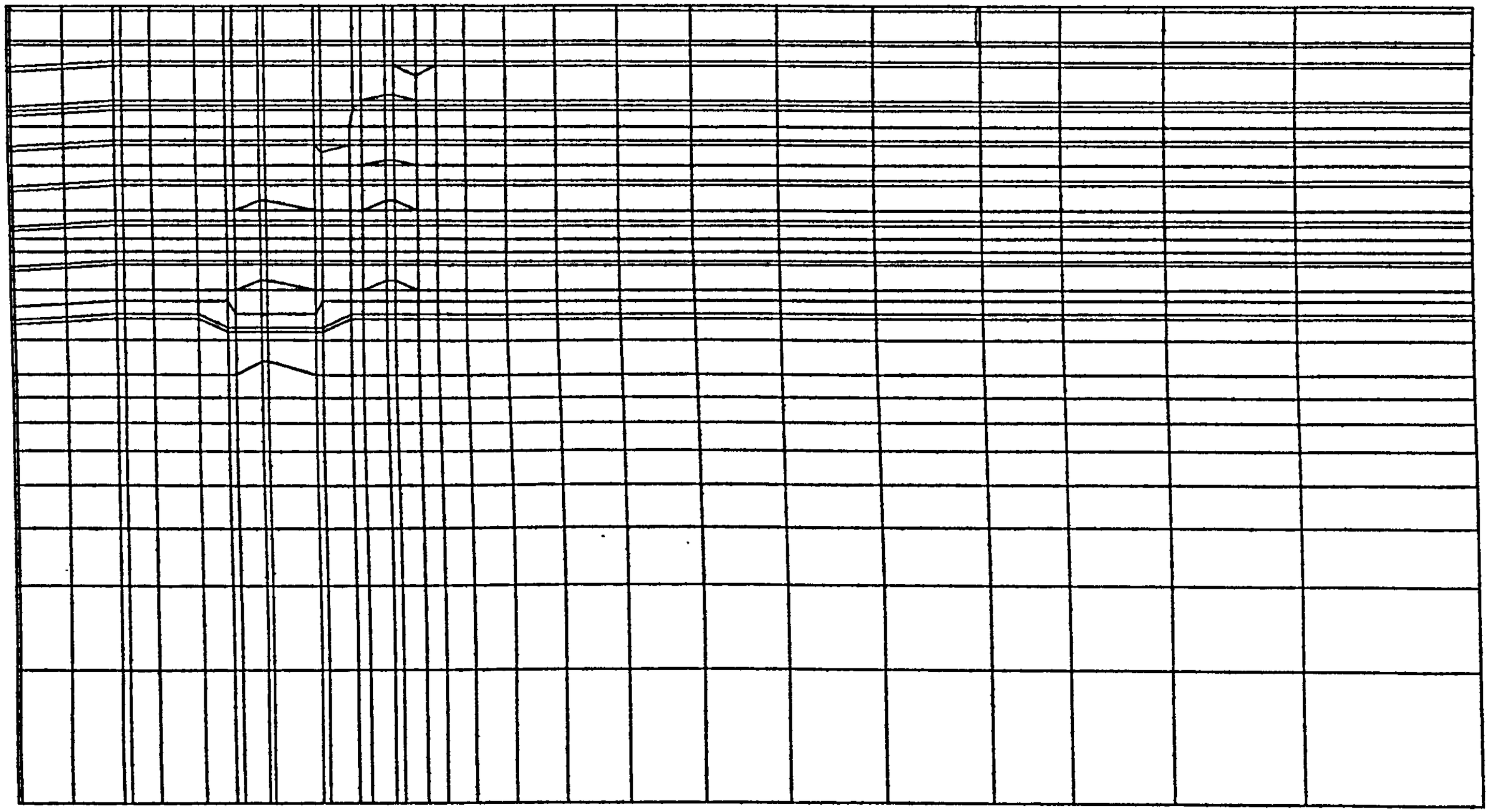

CASE 8B - QUEENSBERRY HOUSE LONGITUDINAL SECTION - IN-SITU STAGE

FINITE ELEMENT MESH

GEOM SCALE 0 24.00 metre

XMIN : -4.484 XMAX : 104.284 YMIN : -30.000 YMAX : 23.600

CRISP-94	CUED TRL	23/12/98 20:28	UNIVERSITY OF SURREY	FIG. 1

APPENDIX B

Supplementary Plots for Numerical Studies

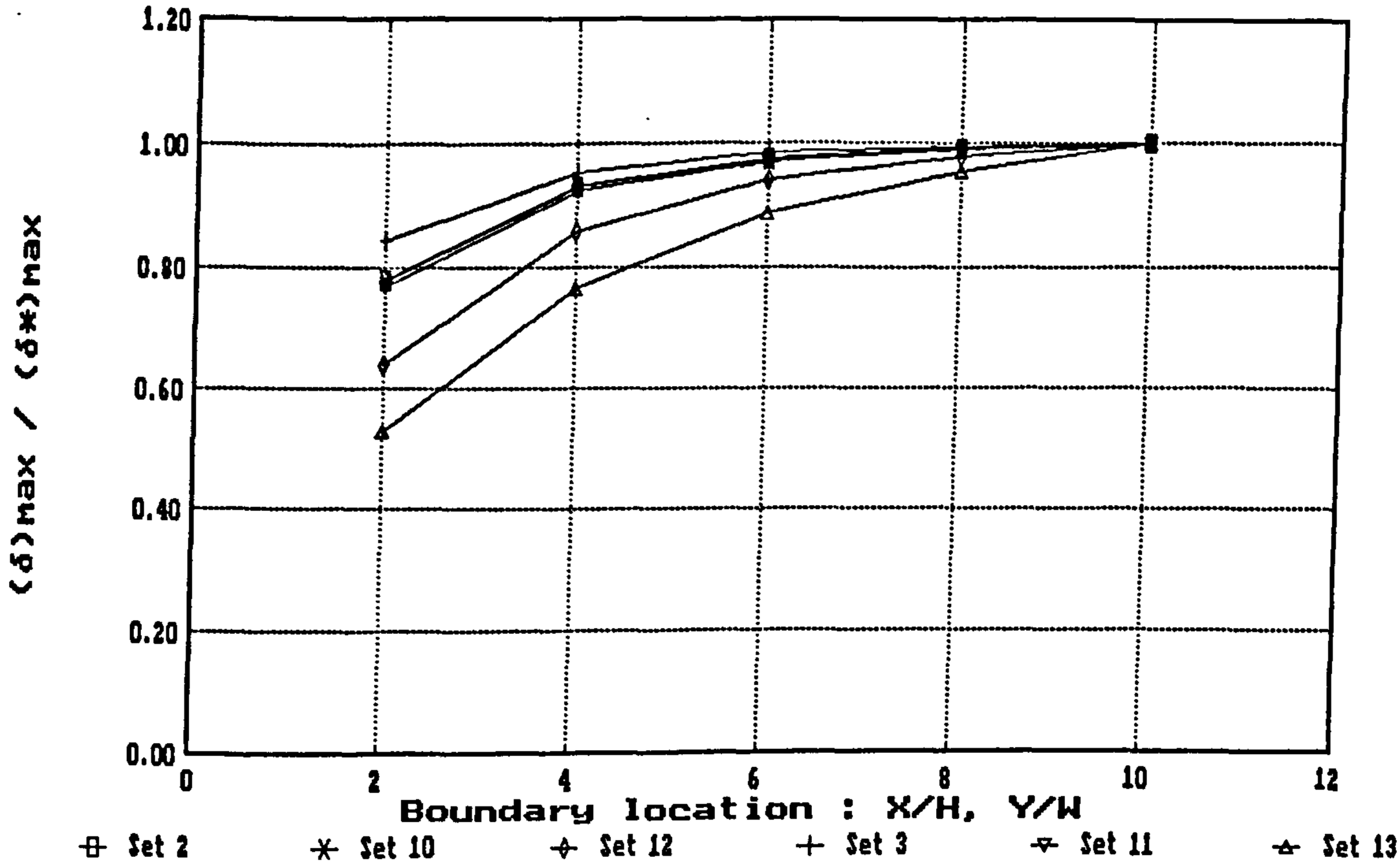

(a) top-propped wall / undrained / elastic and elastic-perfectly plastic analyses

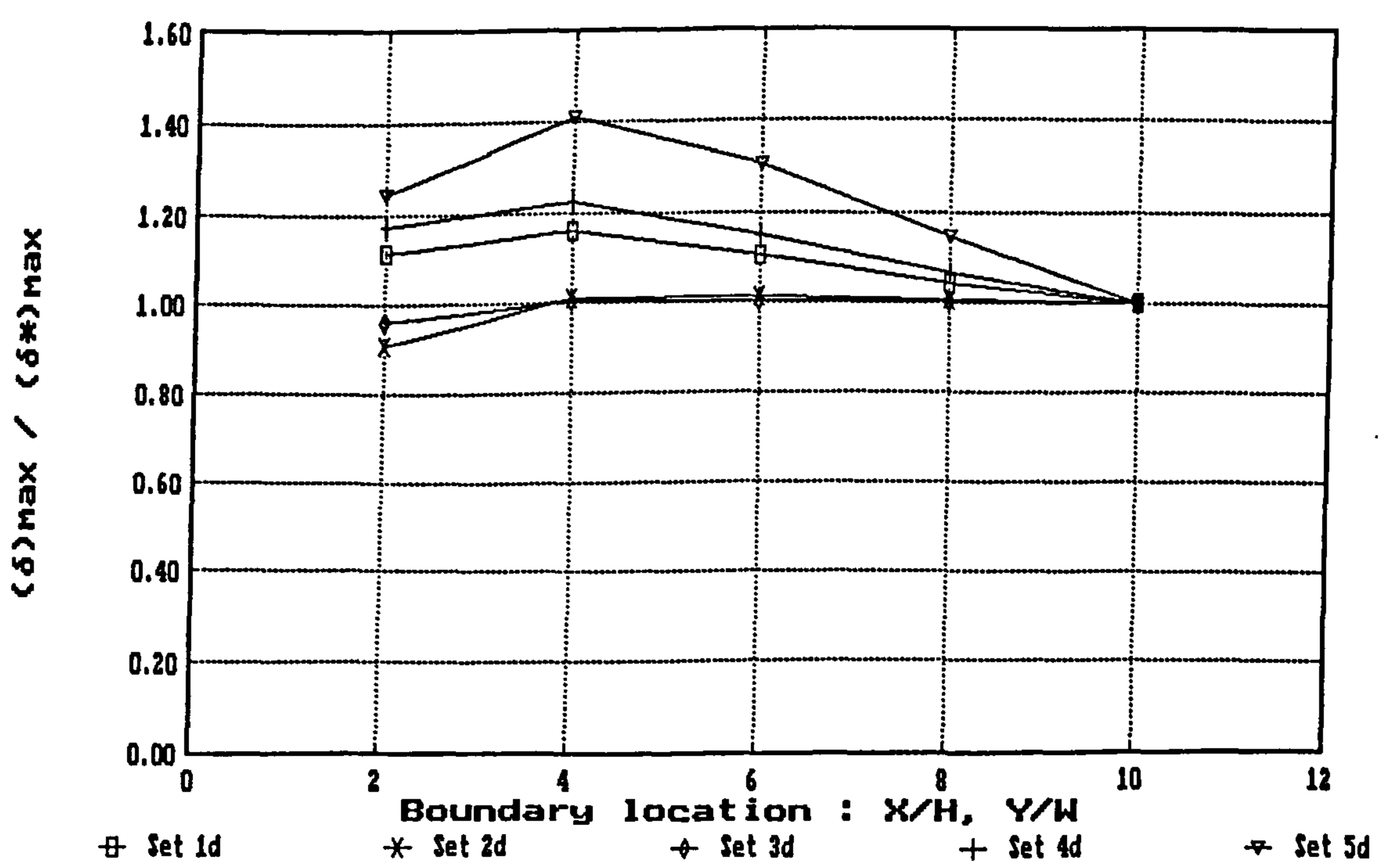

(b) cantilever wall / drained / elastic analysis

Fig. B1 Influence of remote boundary location on maximum wall displacement (Series A) : selected convergence plots

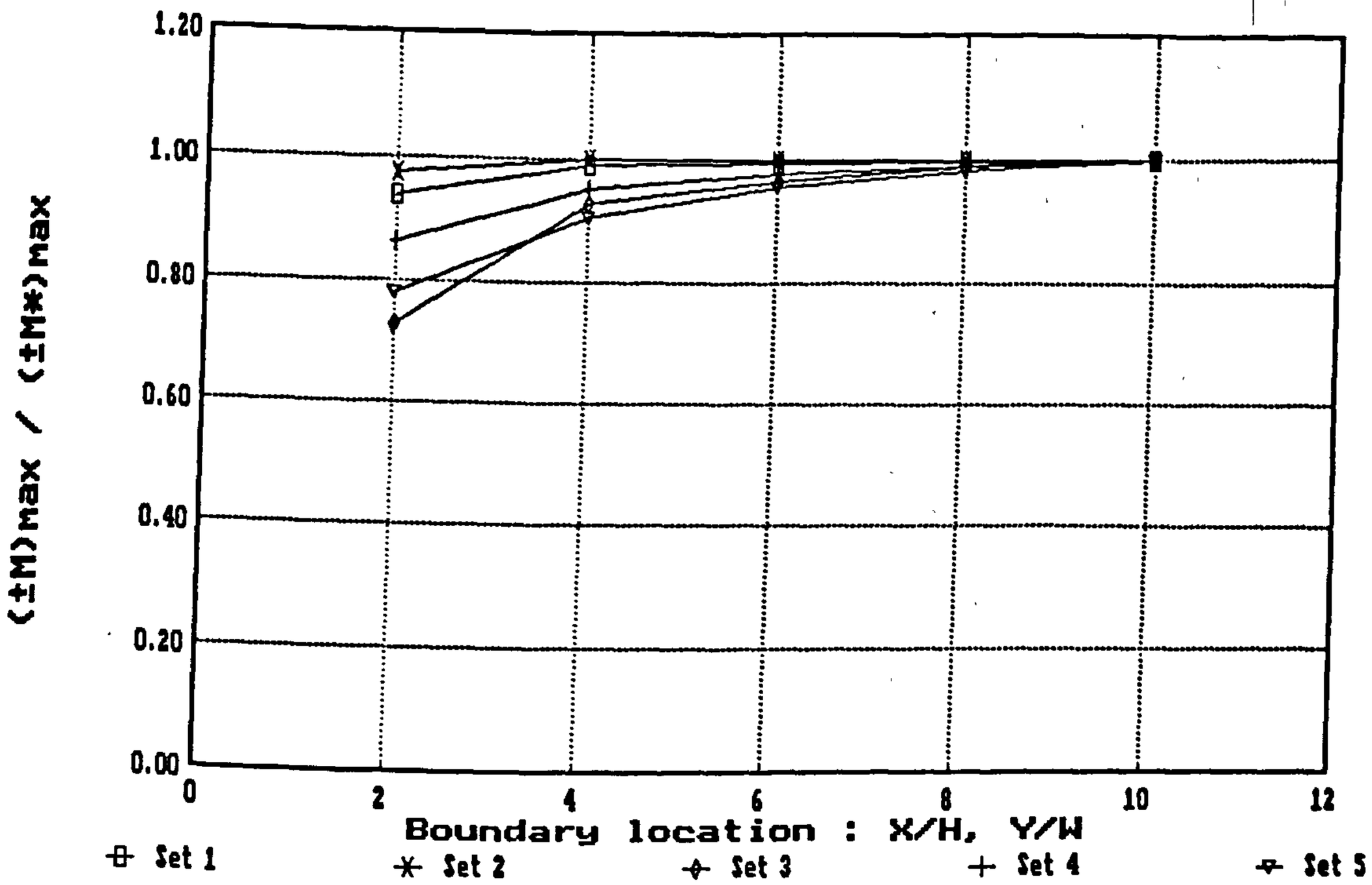

(a) alternately-propped wall / undrained / elastic analysis

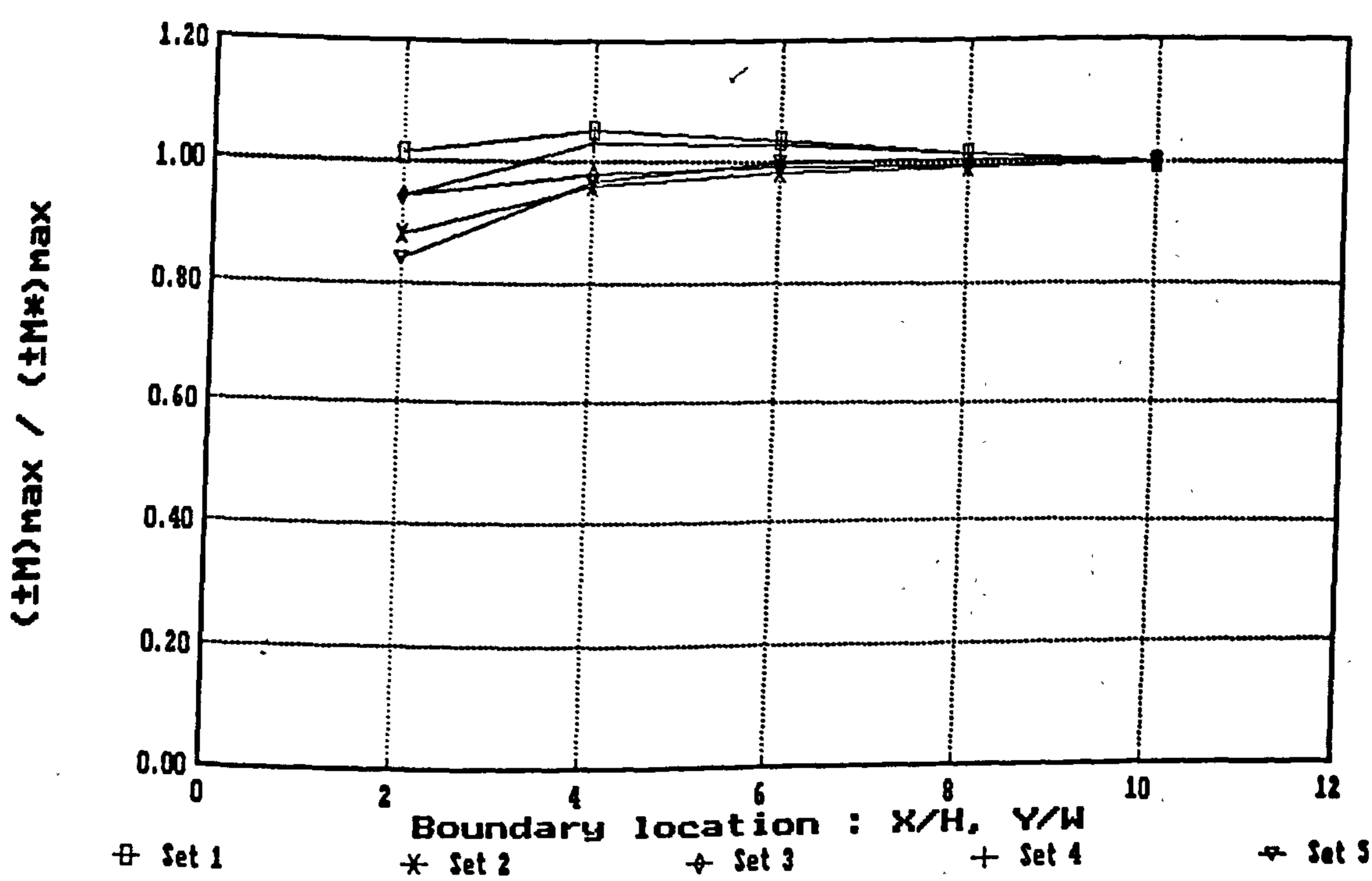

(b) bottom-propped wall / undrained / elastic analysis

Fig. B2 Influence of remote boundary location on maximum wall bending moment (Series A) : selected convergence plots

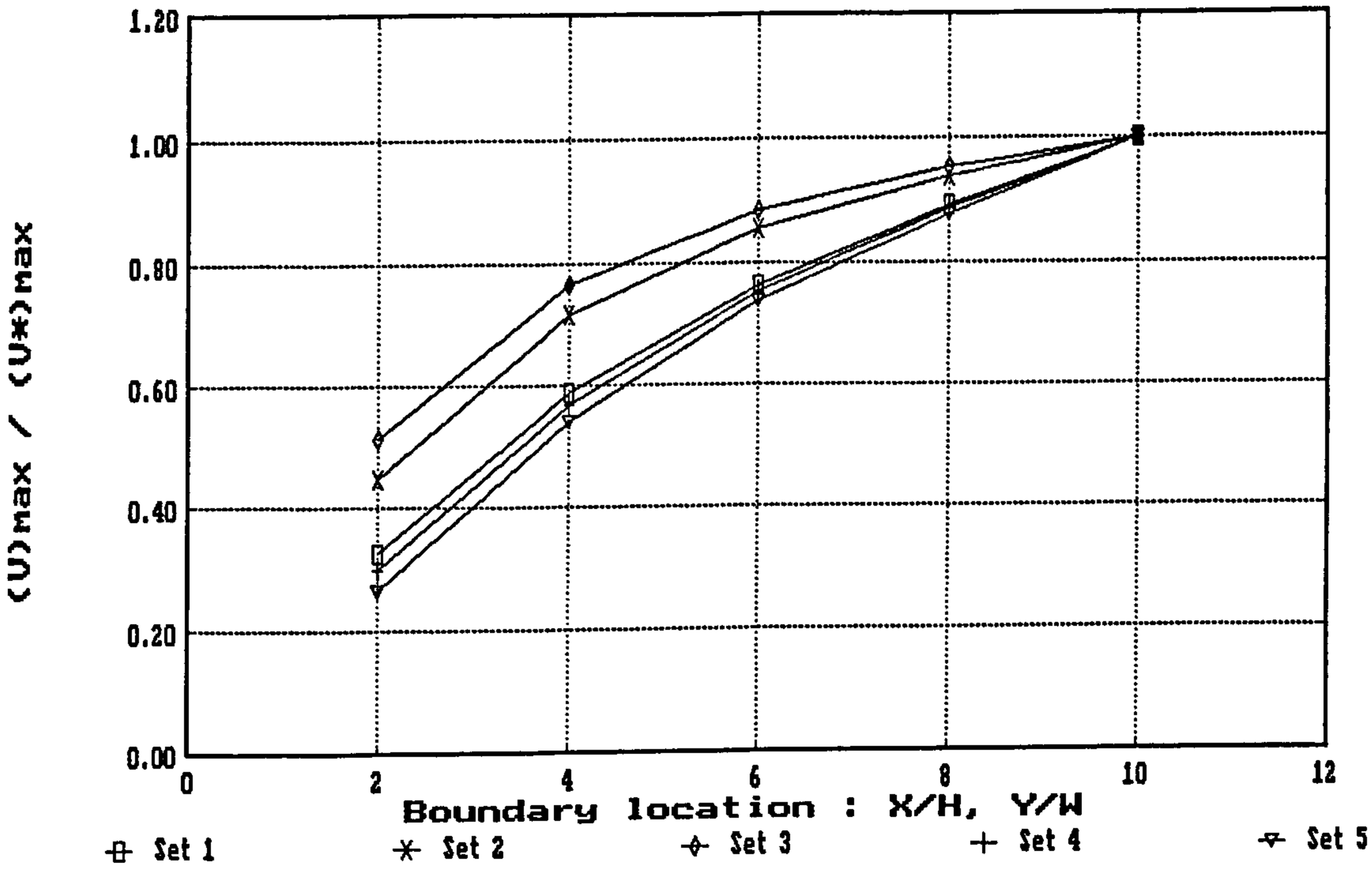

(a) alternately-propped wall / undrained / elastic analysis

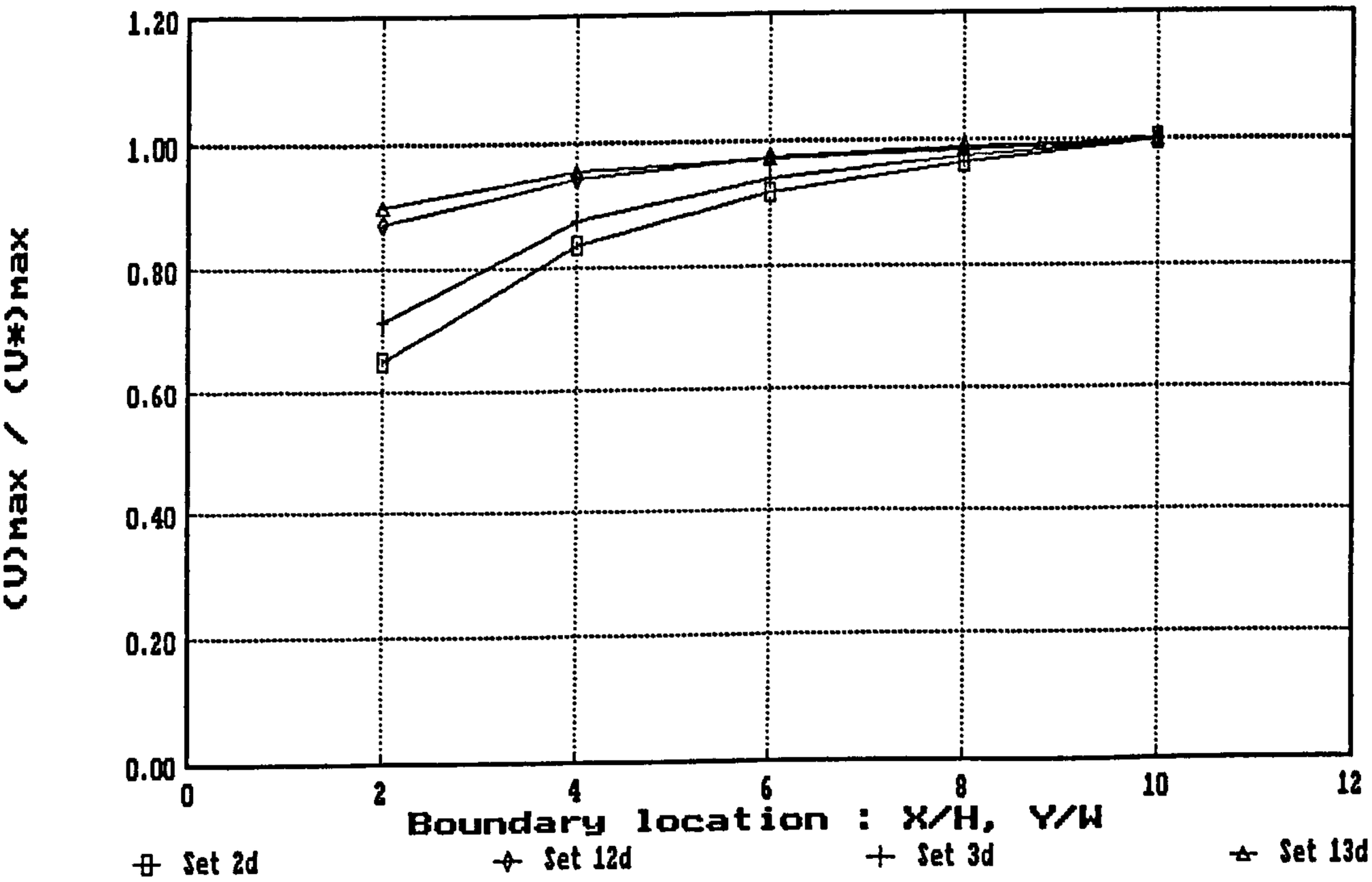

(b) doubly-propped wall / drained / elastic and elastic-perfectly plastic analyses

Fig. B3 Influence of remote boundary location on maximum excavation heave (Series A) : selected convergence plots

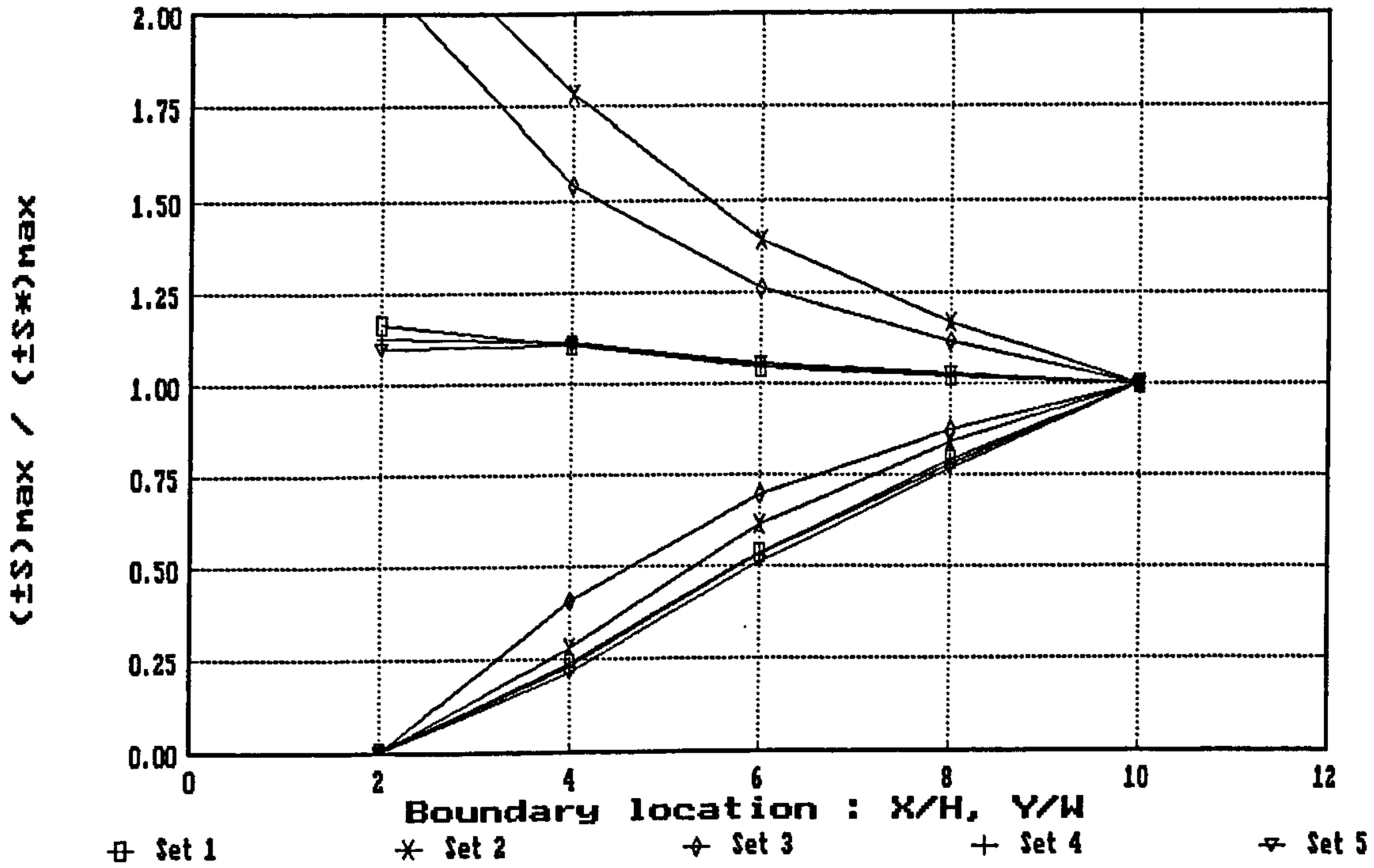

(a) cantilever wall / undrained / elastic analysis

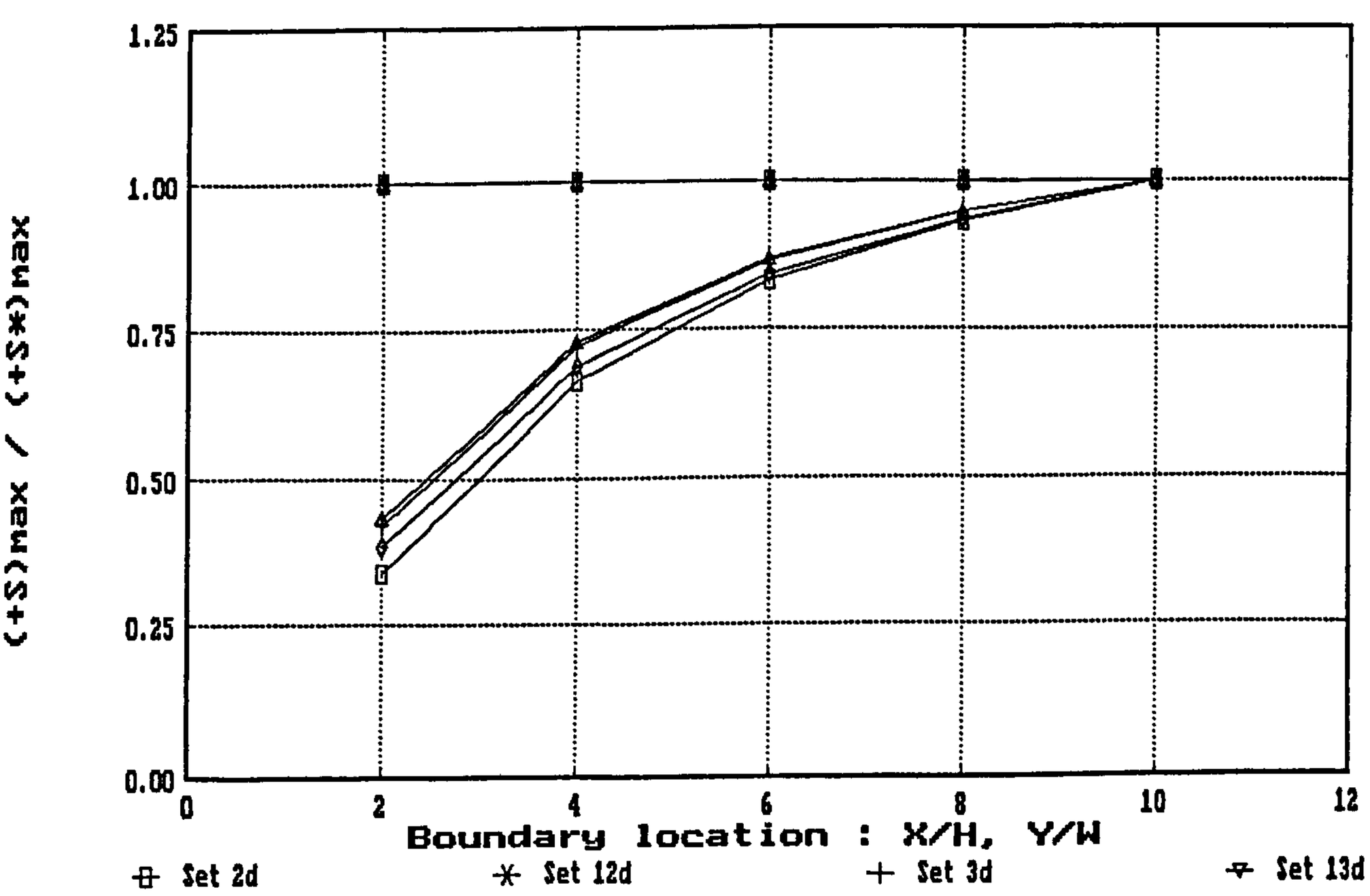

(b) bottom-propped wall / drained / elastic-perfectly plastic analysis

Fig. B4 Influence of remote boundary location on maximum ground surface movement (Series A) : selected convergence plots

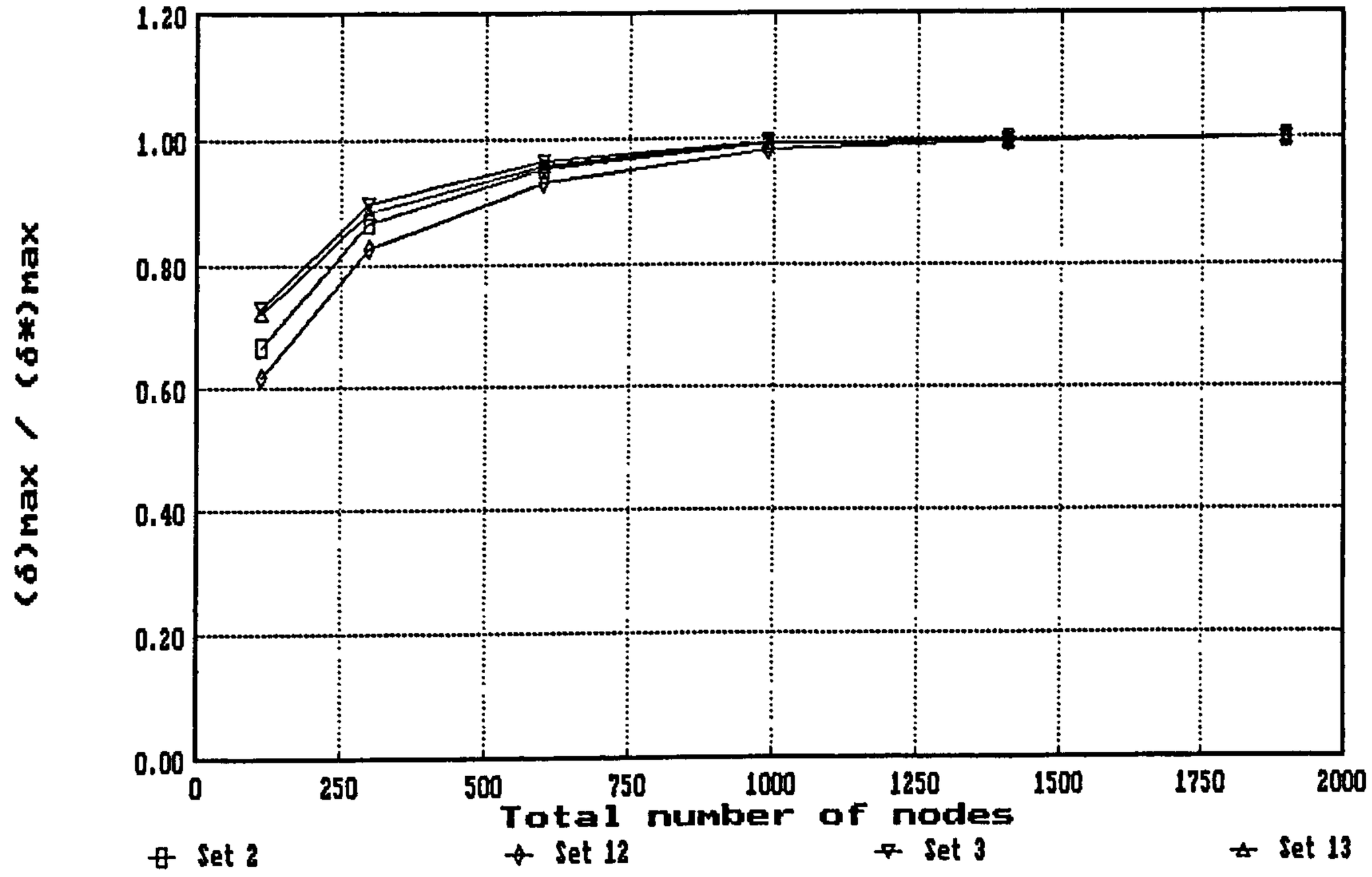

(a) wall displacement / top-propped wall / elastic-perfectly plastic analyses

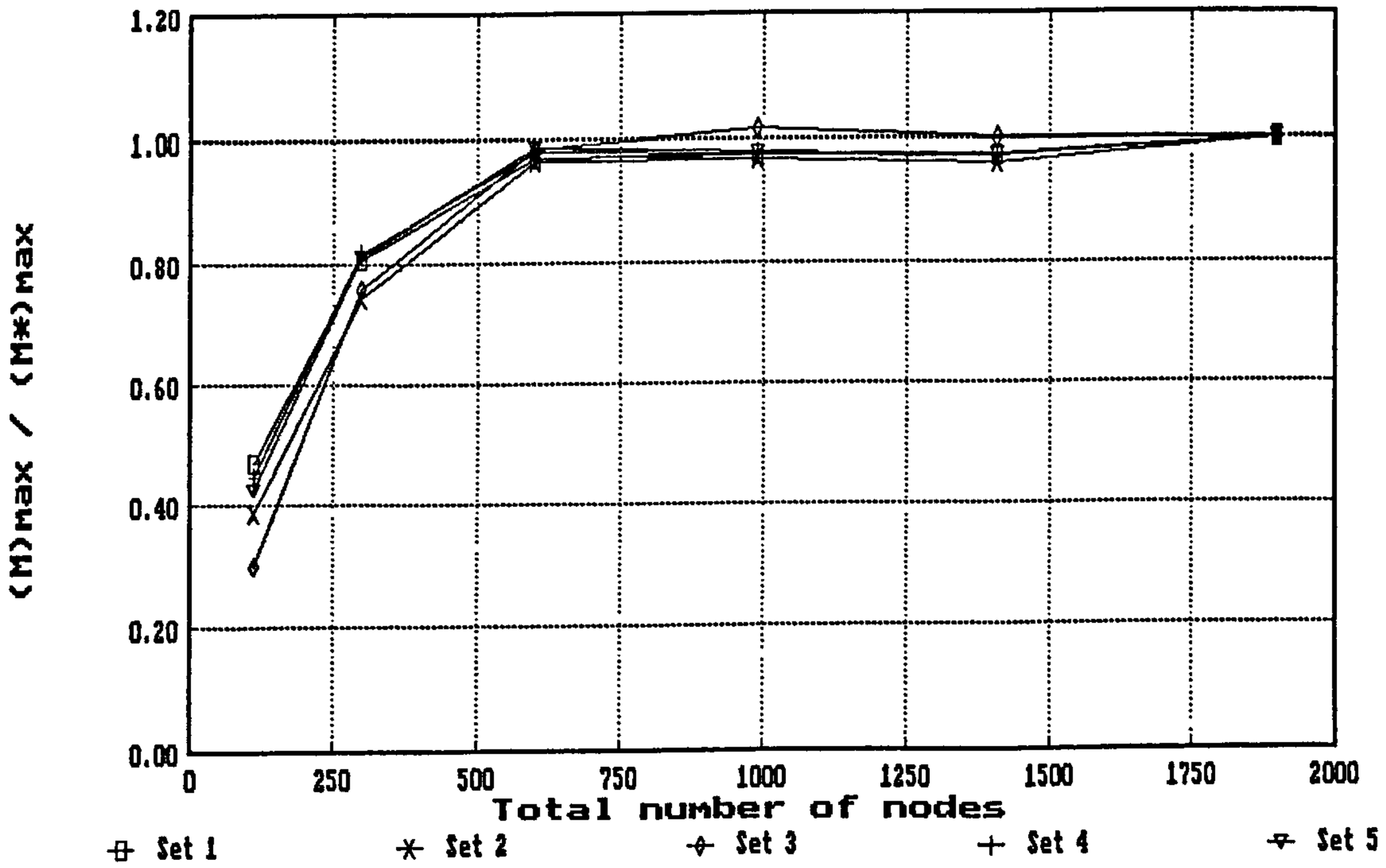

(b) wall bending moment / cantilever wall / elastic analysis

Fig. B5 Influence of mesh grading (Series III h-refinement) : selected convergence plots for undrained analyses

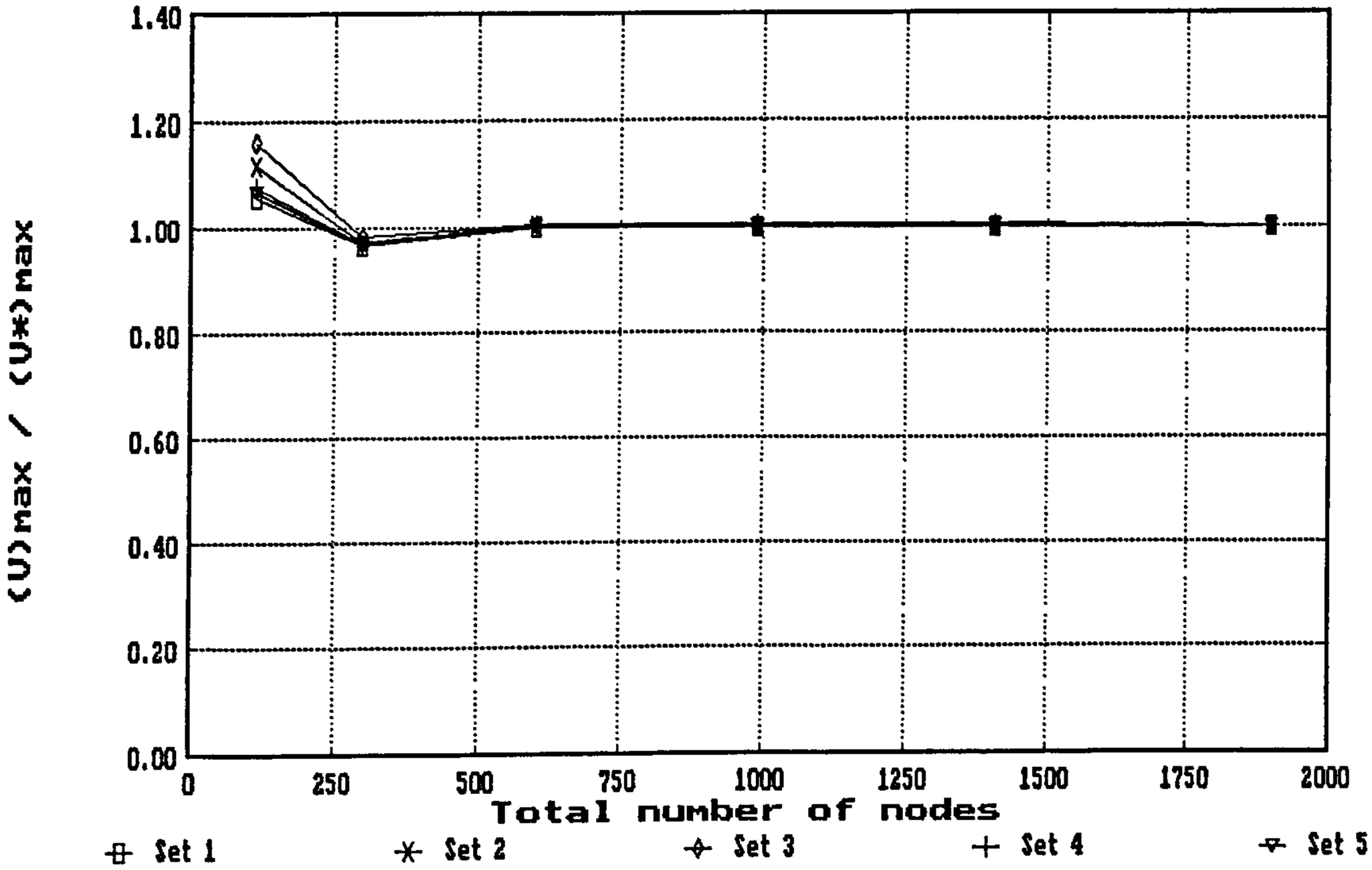

(c) excavation heave / top-propped wall / elastic analysis

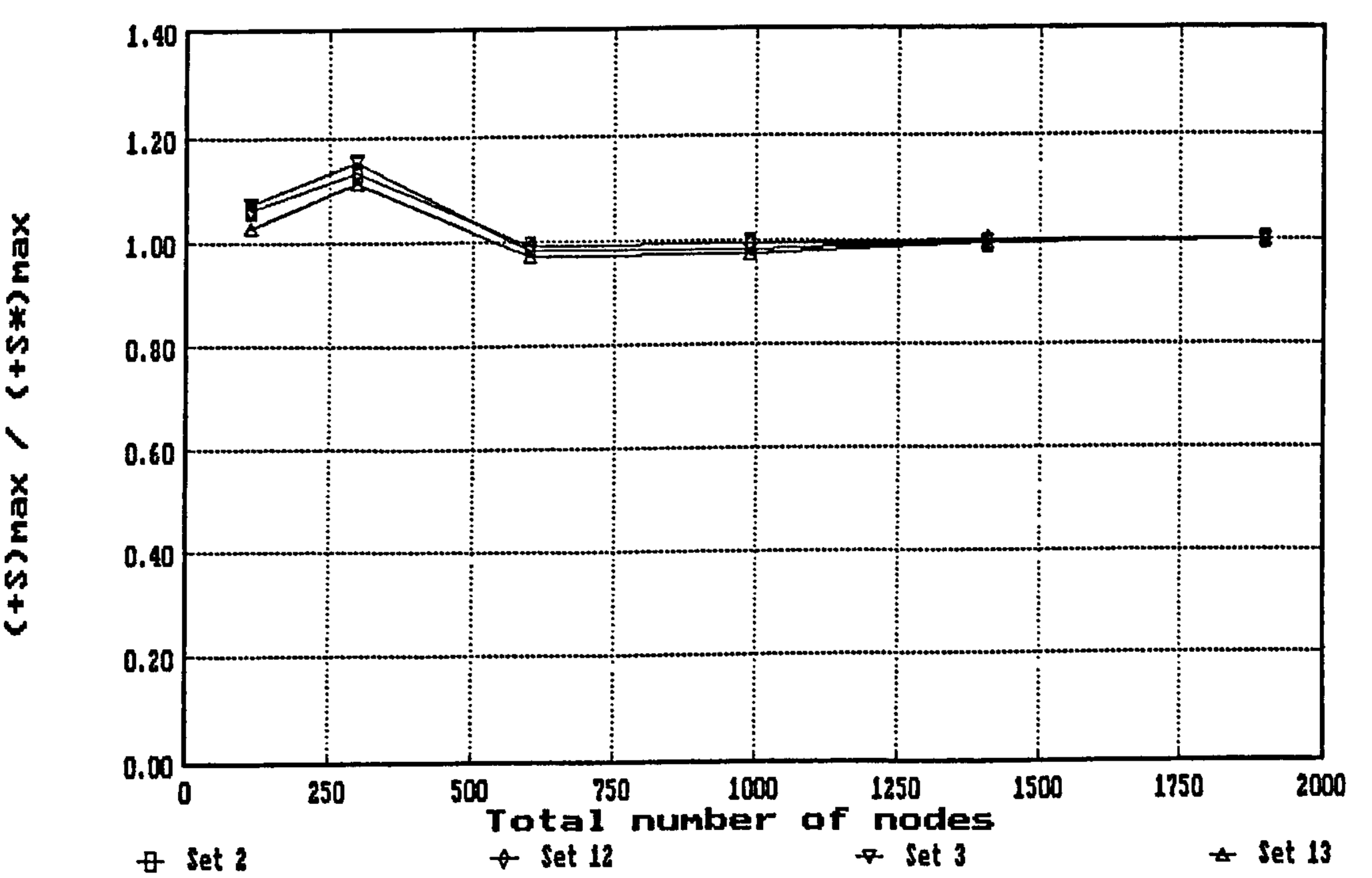

(d) ground surface movement / bottom-propped wall / elastic-perf. plastic analyses

Fig. B5 Influence of mesh grading (Series III h-refinement) : selected convergence plots for undrained analyses (contd)

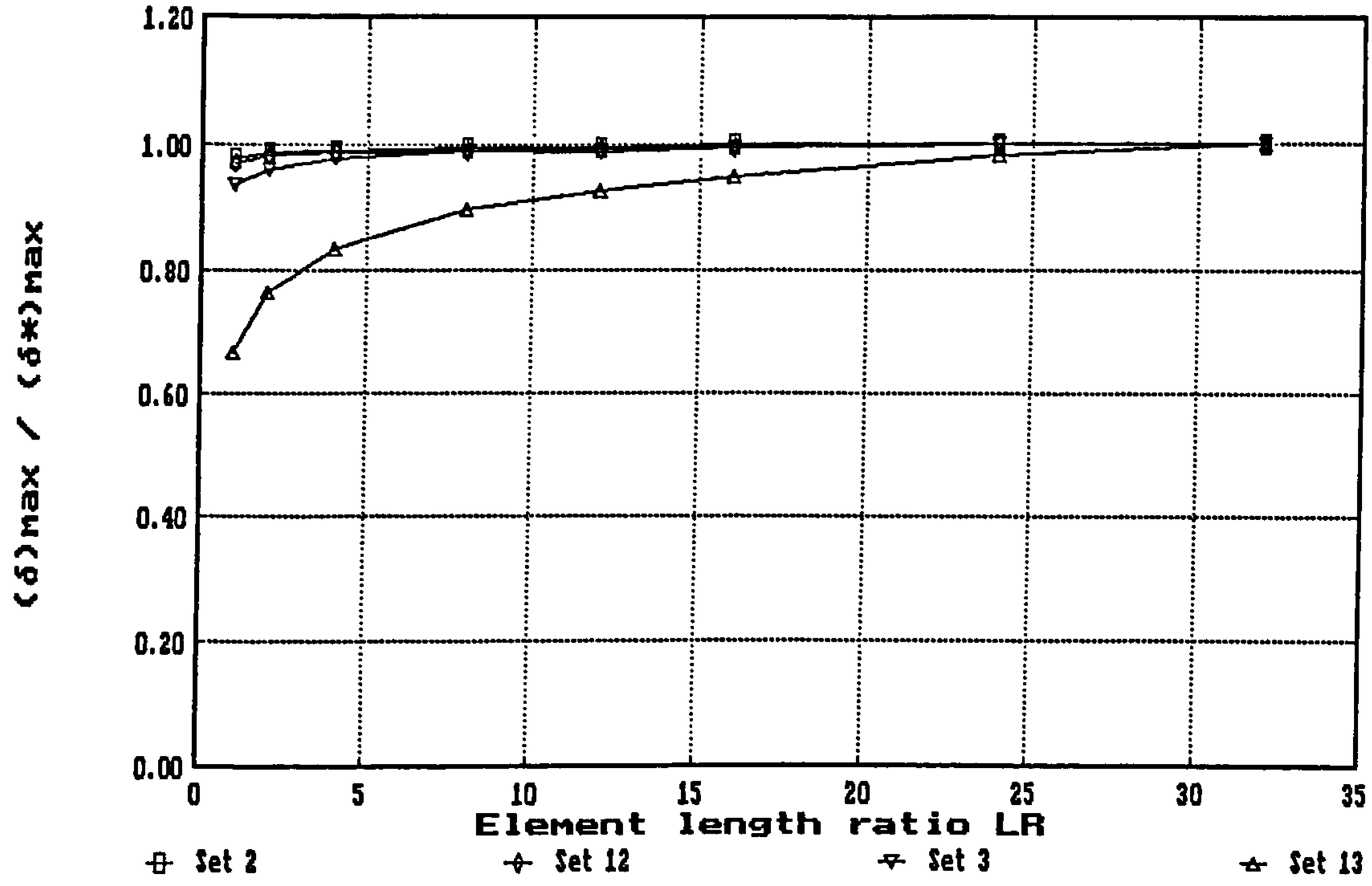

(a) wall displacement / cantilever wall / elastic-perfectly plastic analyses

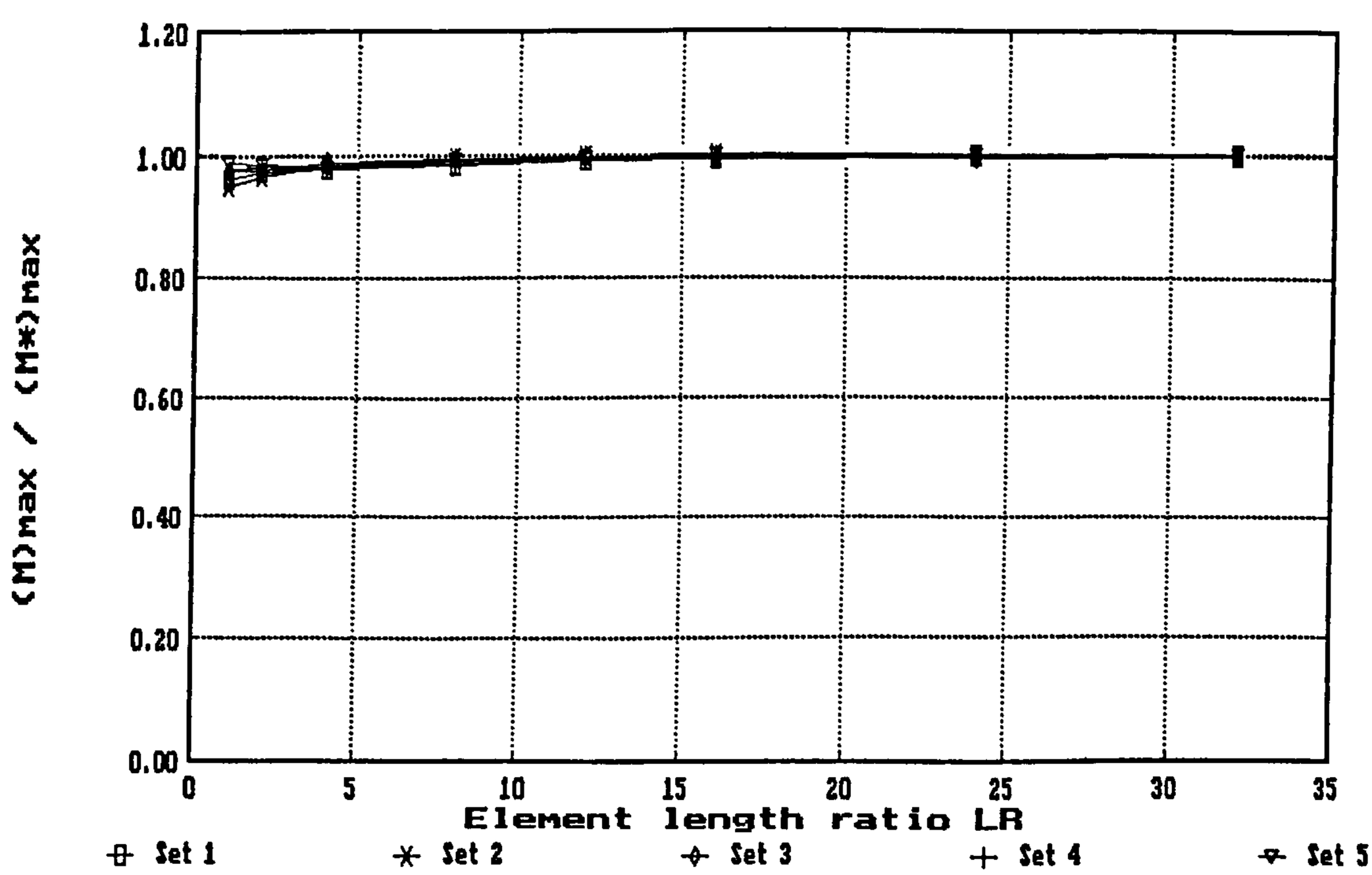

(b) wall bending moment / top-propped wall / elastic analysis

Fig. B6 Influence of mesh grading (Series I r-refinement) : selected convergence plots for undrained analyses

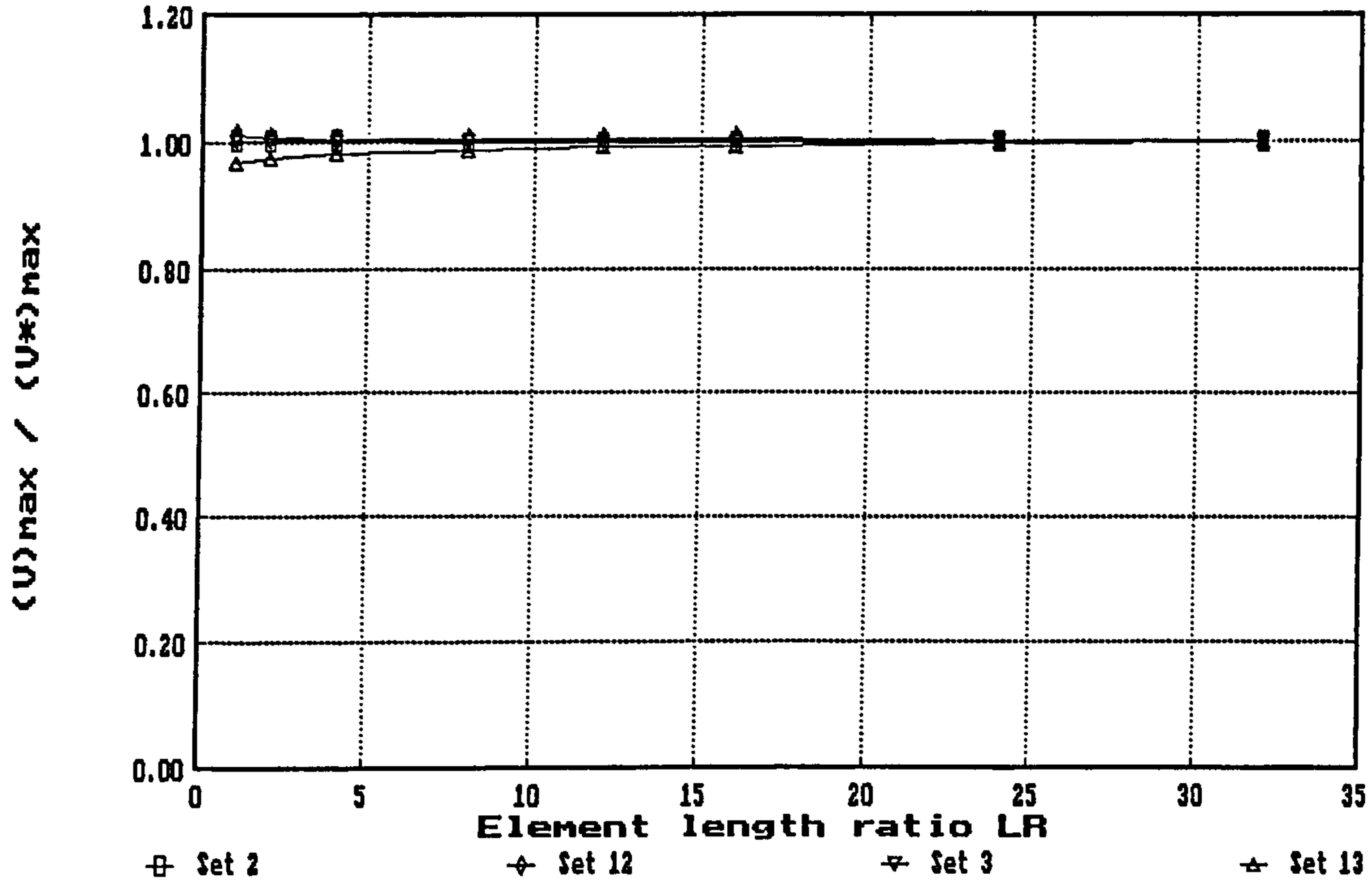

(c) excavation heave / cantilever wall / elastic-perfectly plastic analyses

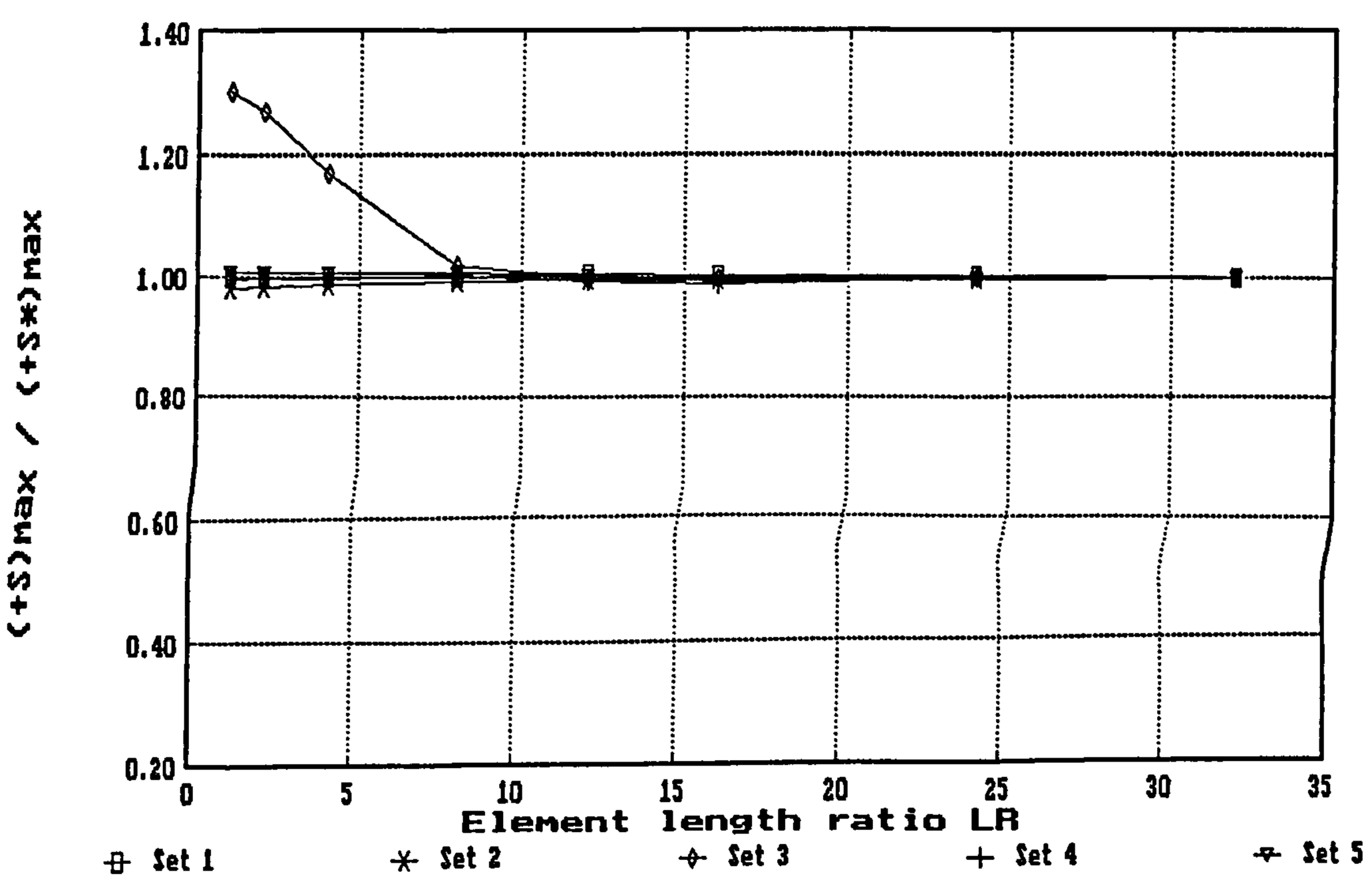

(d) ground surface movement / cantilever wall / elastic analysis

Fig. B6 Influence of mesh grading (Series I r-refinement) : selected convergence plots for undrained analyses (contd)

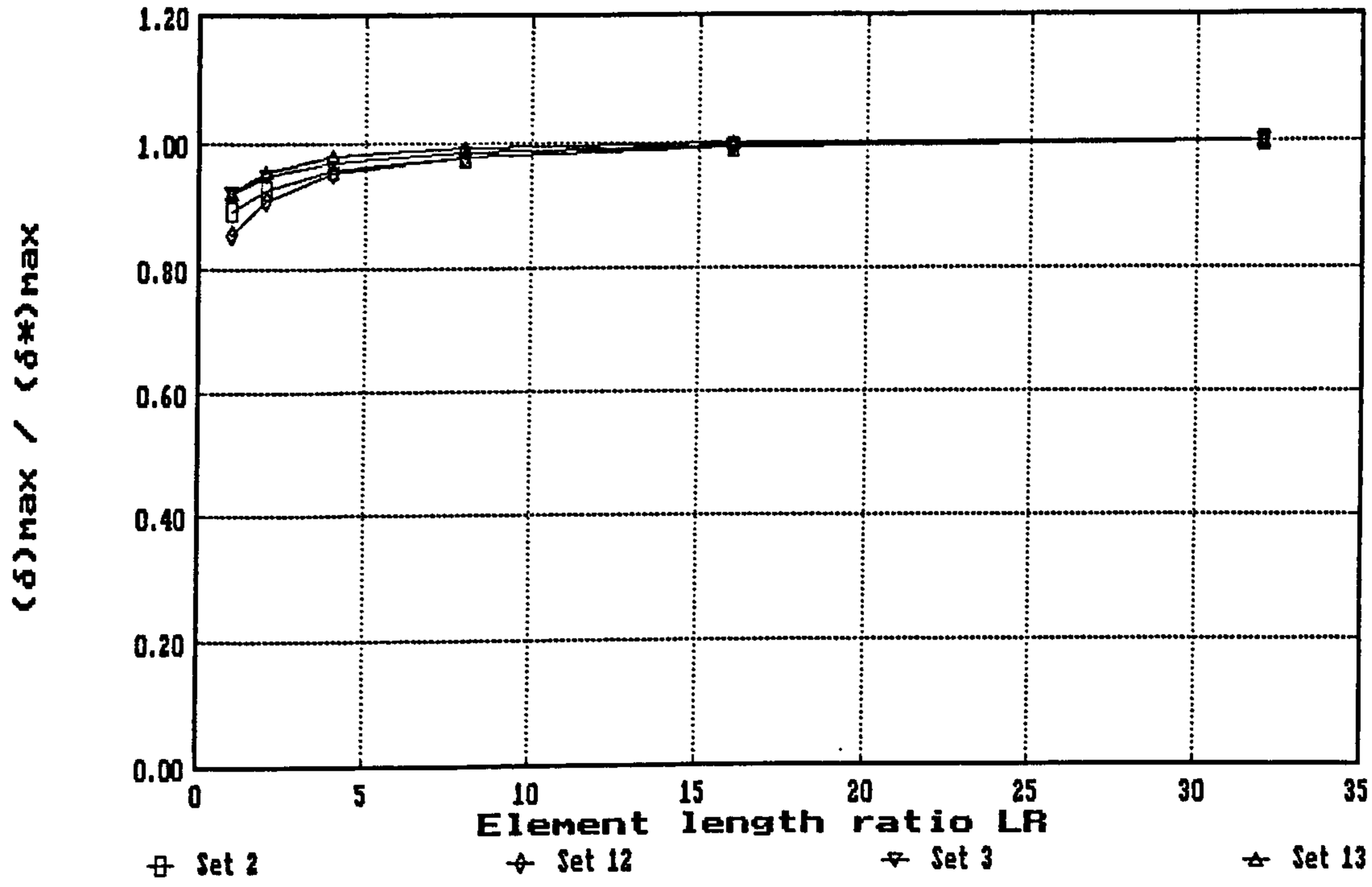

(a) wall displacement / top-propped wall / elastic-perfectly plastic analyses

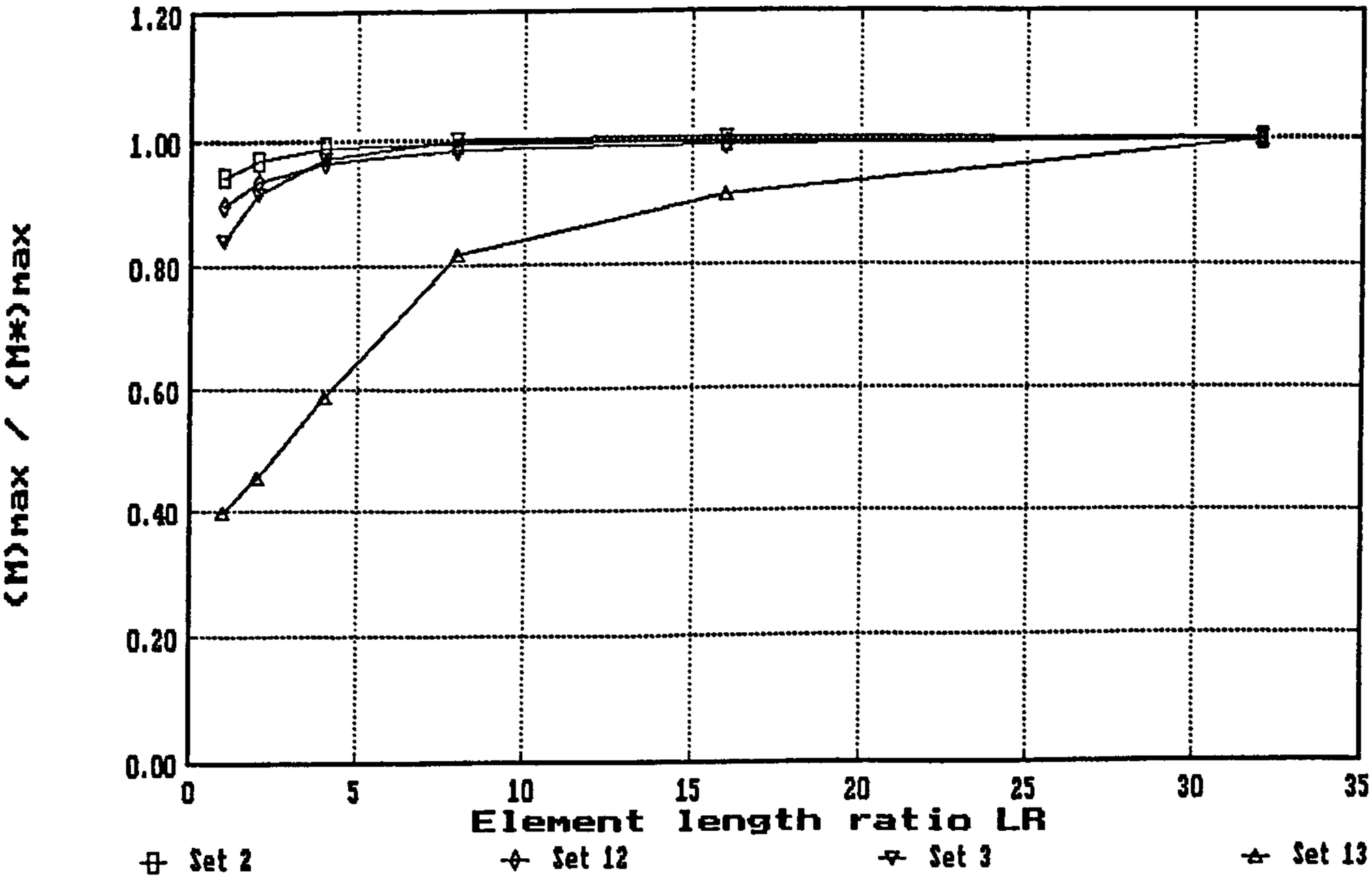

(b) wall bending moment / cantilever wall / elastic-perfectly plastic analyses

Fig. B7 Influence of mesh grading (Series II r-refinement) : selected convergence plots for undrained analyses

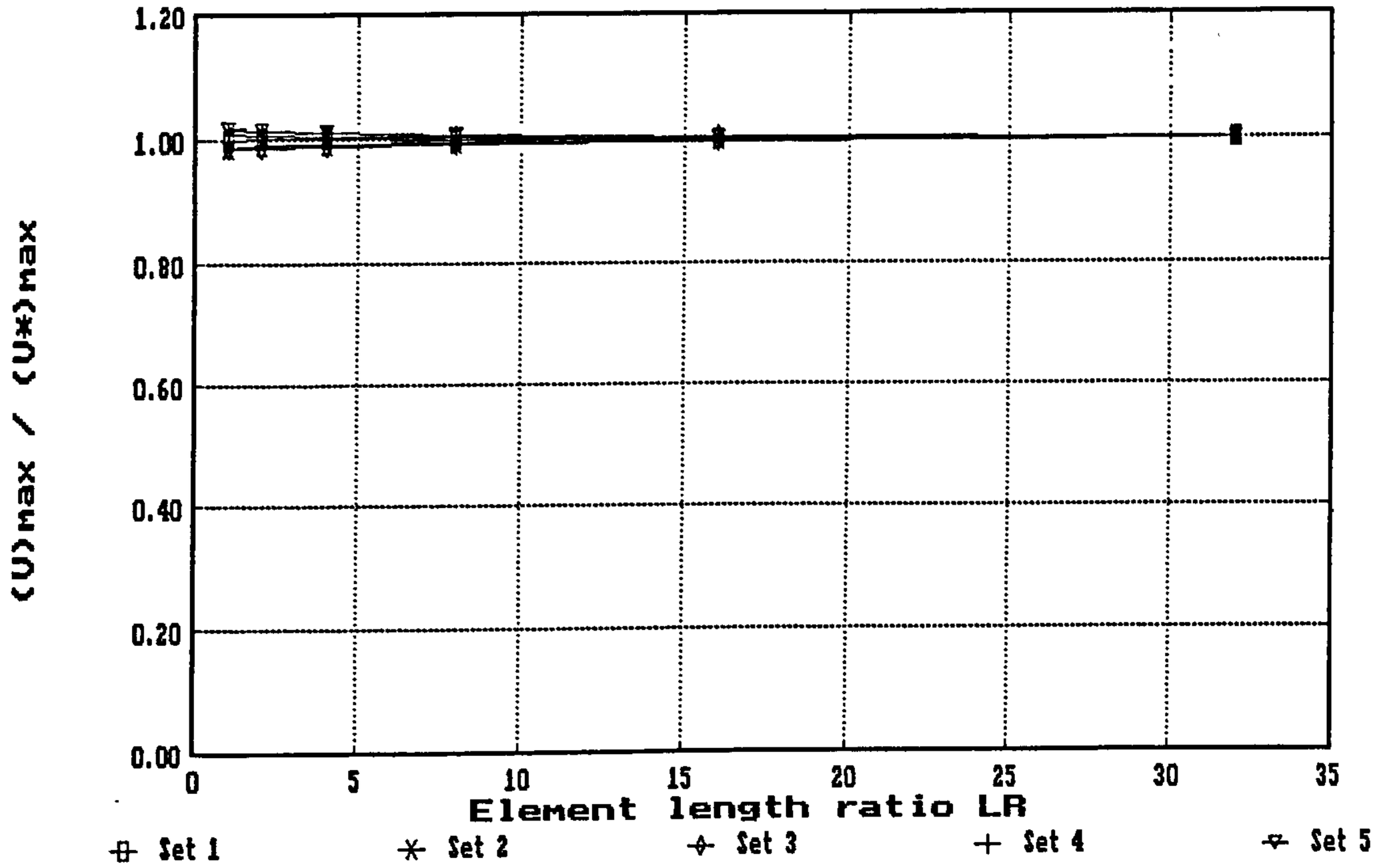

(c) excavation heave / top-propped wall / elastic analysis

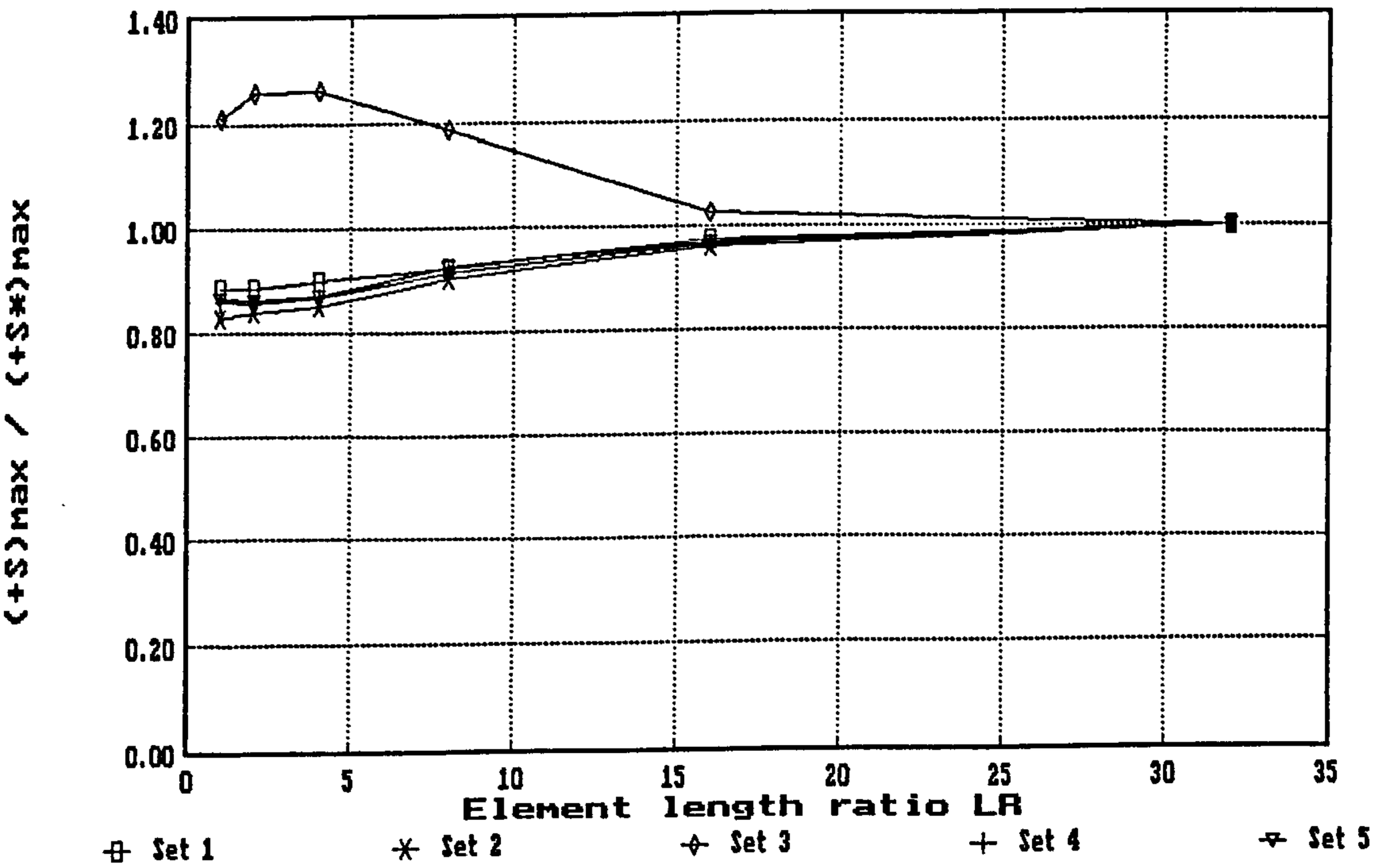

(d) ground surface movement / cantilever wall / elastic analysis

Fig. B7 Influence of mesh grading (Series II r-refinement) : selected convergence plots for undrained analyses (contd)

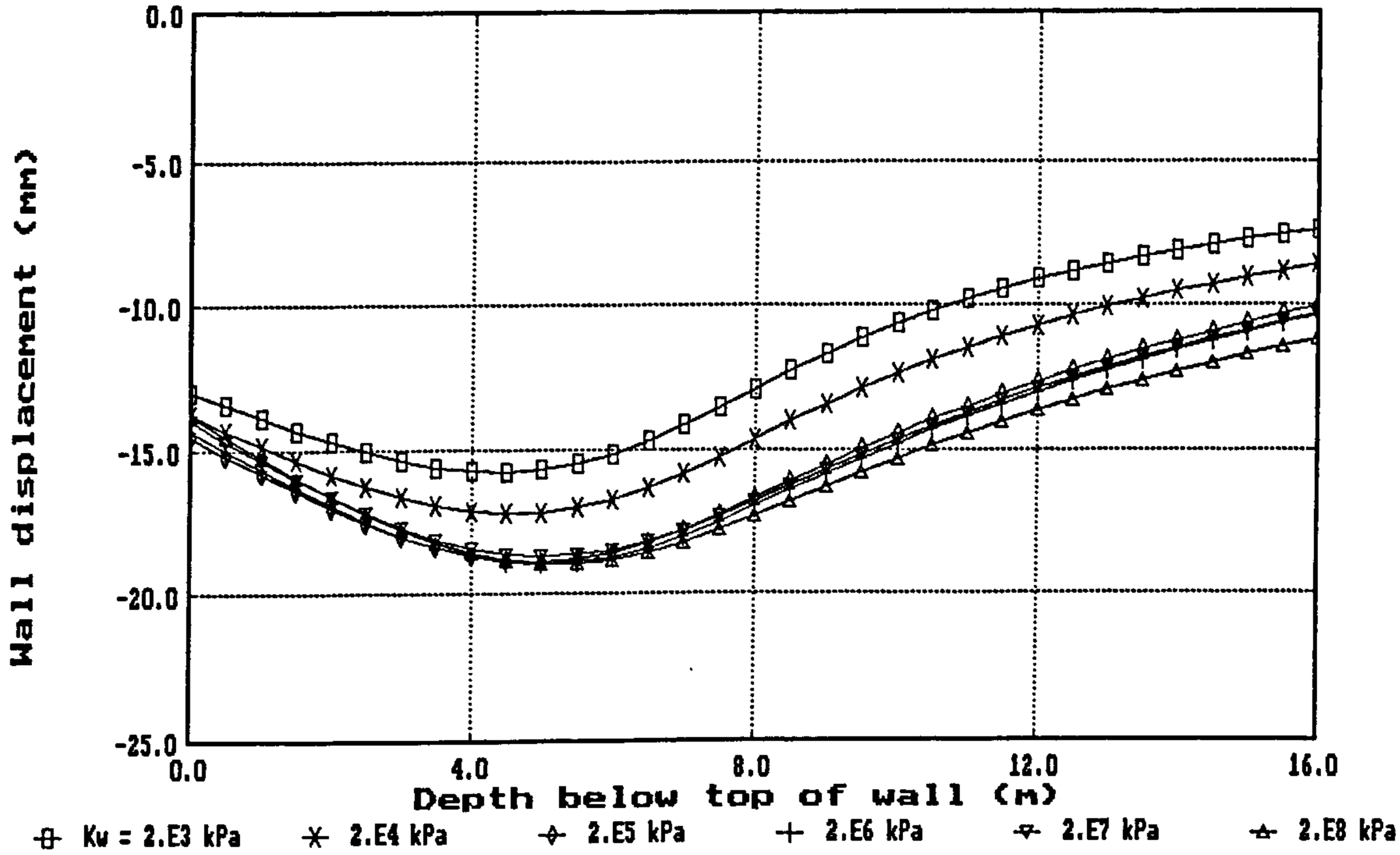

(a) elastic soil (set 1)

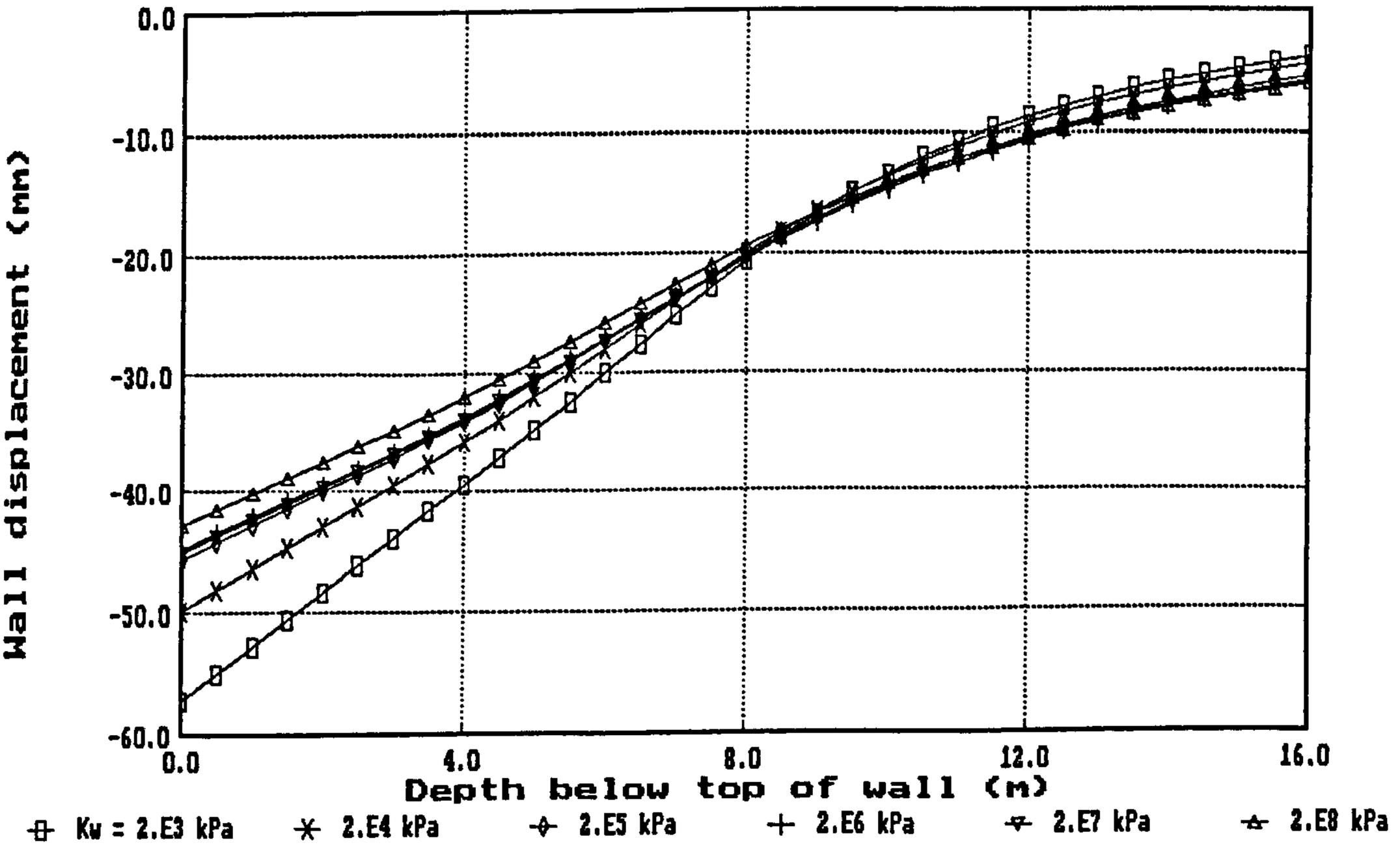

(b) elastic soil (set 3)

Fig. B8 Influence of pore fluid compressibility on an effective stress analysis of a cantilever wall : profiles of wall displacement

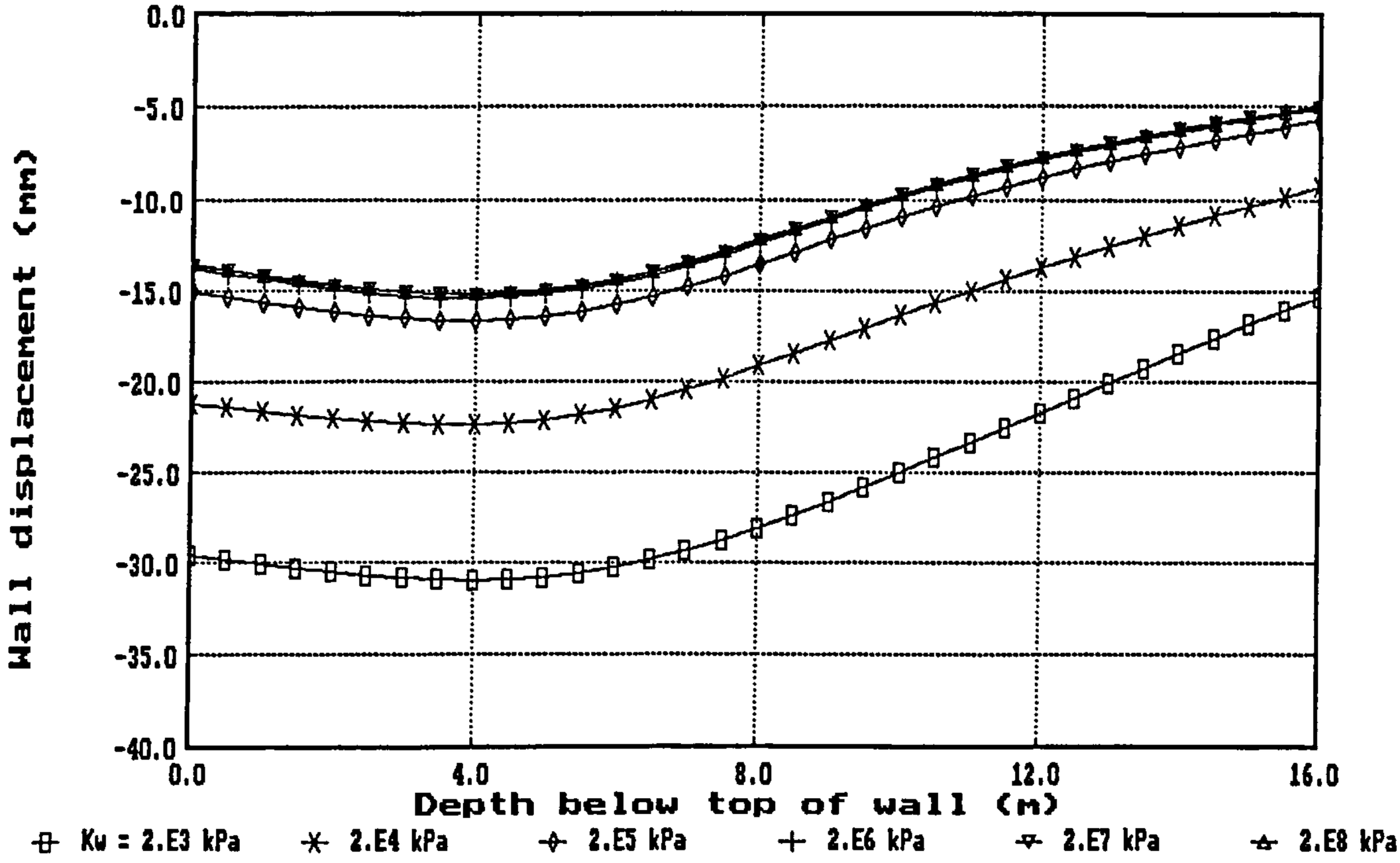

(c) *elastic-perfectly* plastic soil (set 12)

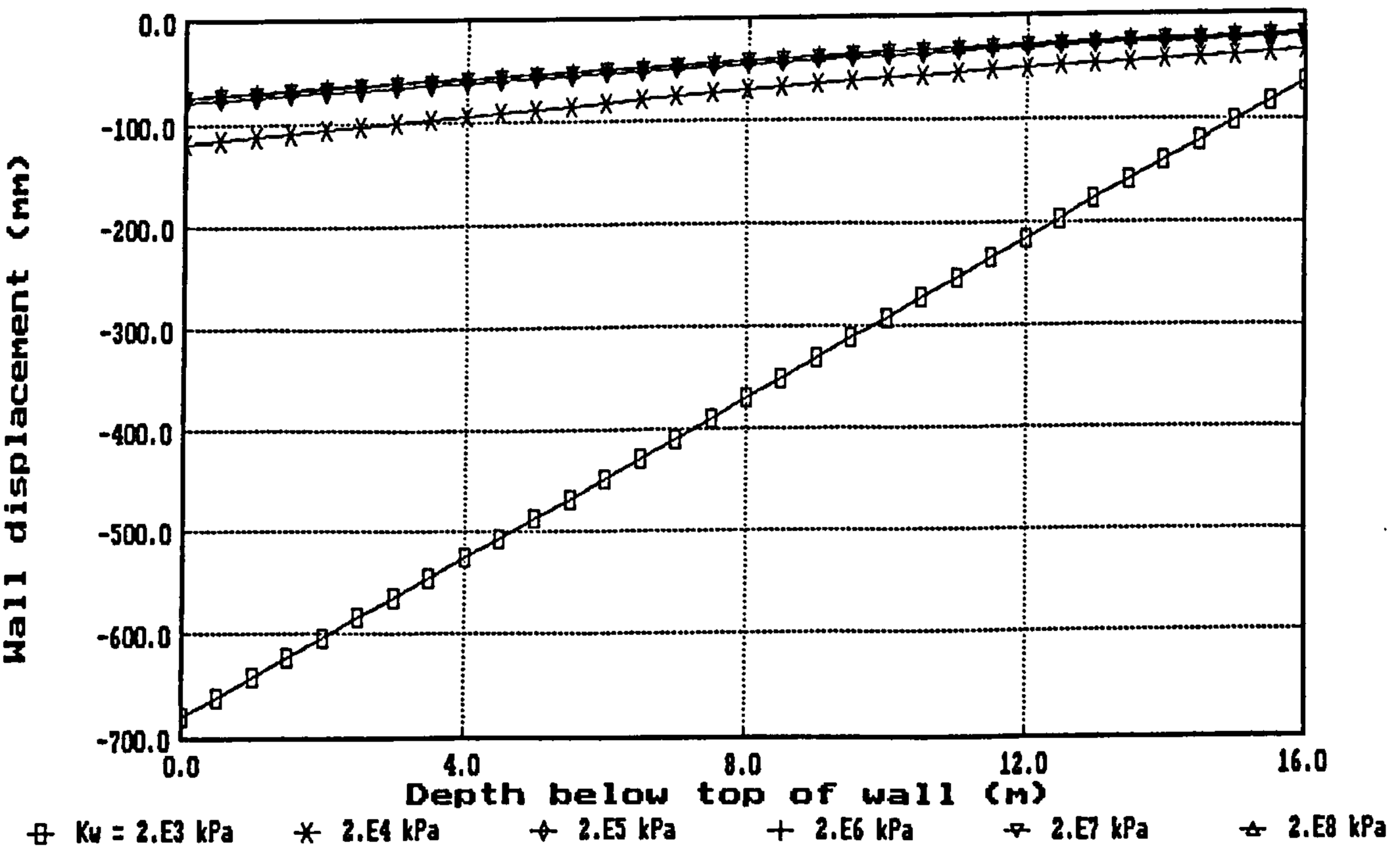

(d) elastic-perfectly plastic soil (set 13)

Fig. B8 Influence of pore fluid compressibility on an effective stress analysis of a cantilever wall : profiles of wall displacement (contd)

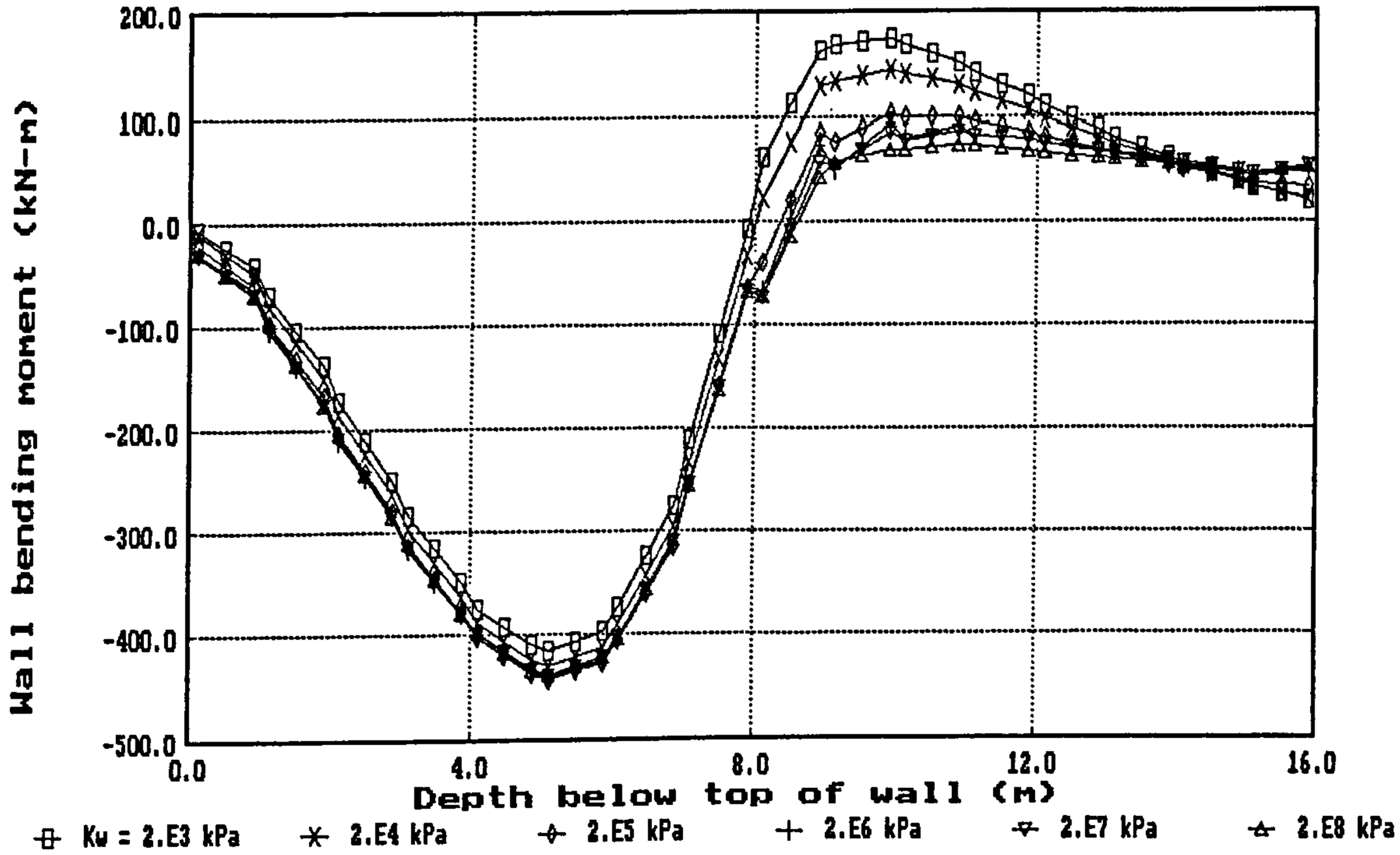

(a) elastic soil (set 1)

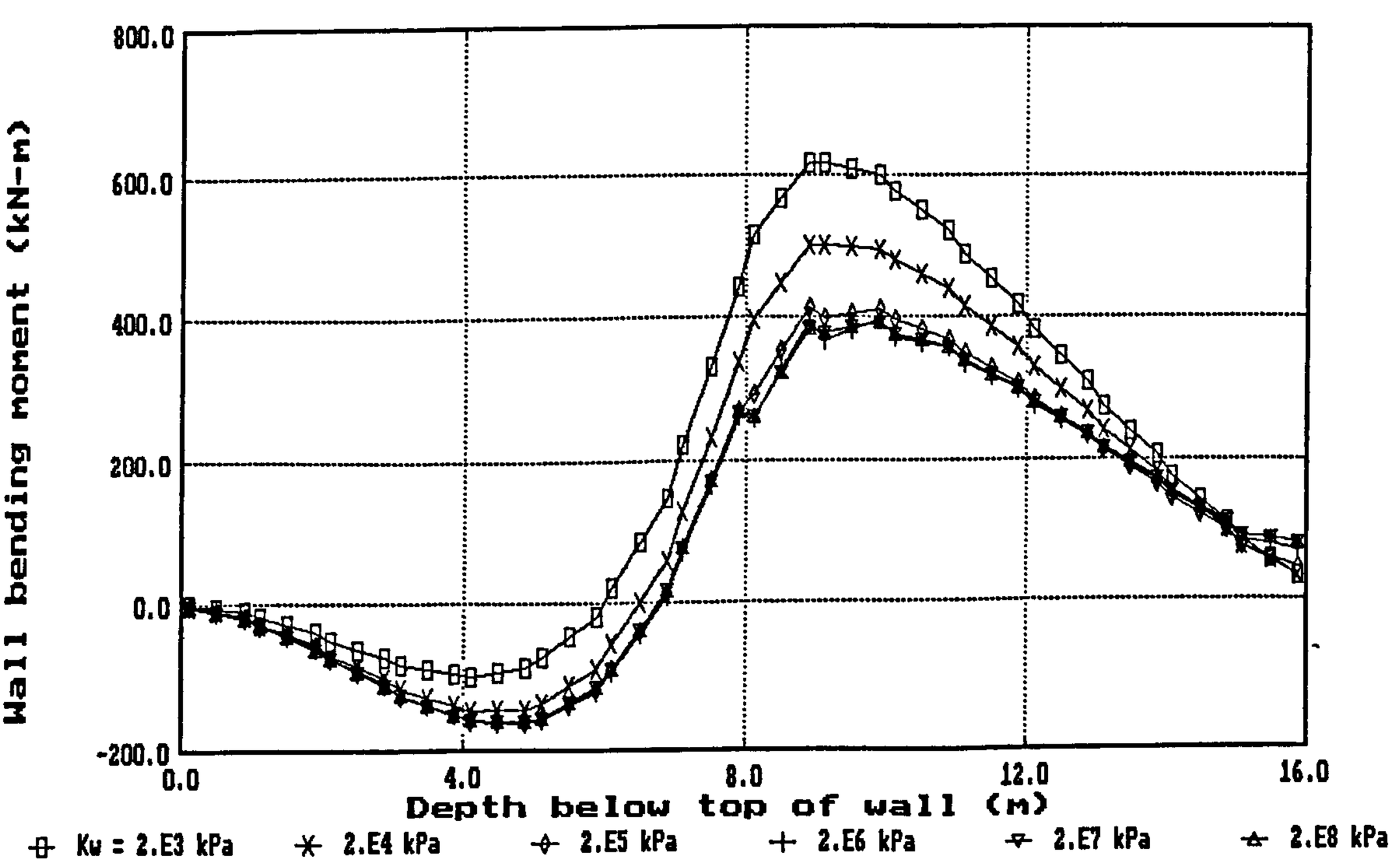

(b) elastic soil (set 3)

Fig. B9 Influence of pore fluid compressibility on an effective stress analysis of a cantilever wall : profiles of wall bending moment

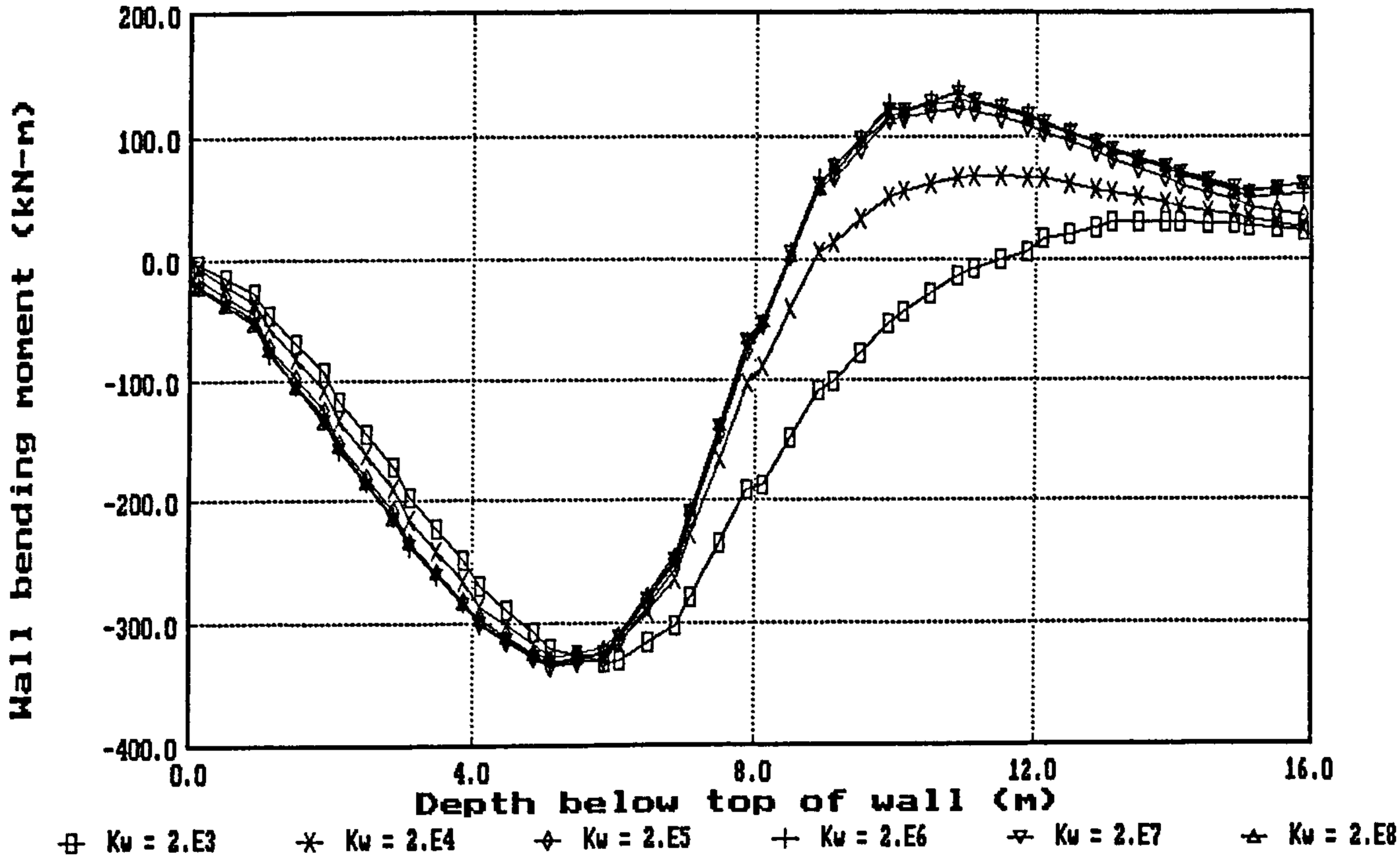

(c) elastic-perfectly plastic soil (set 12)

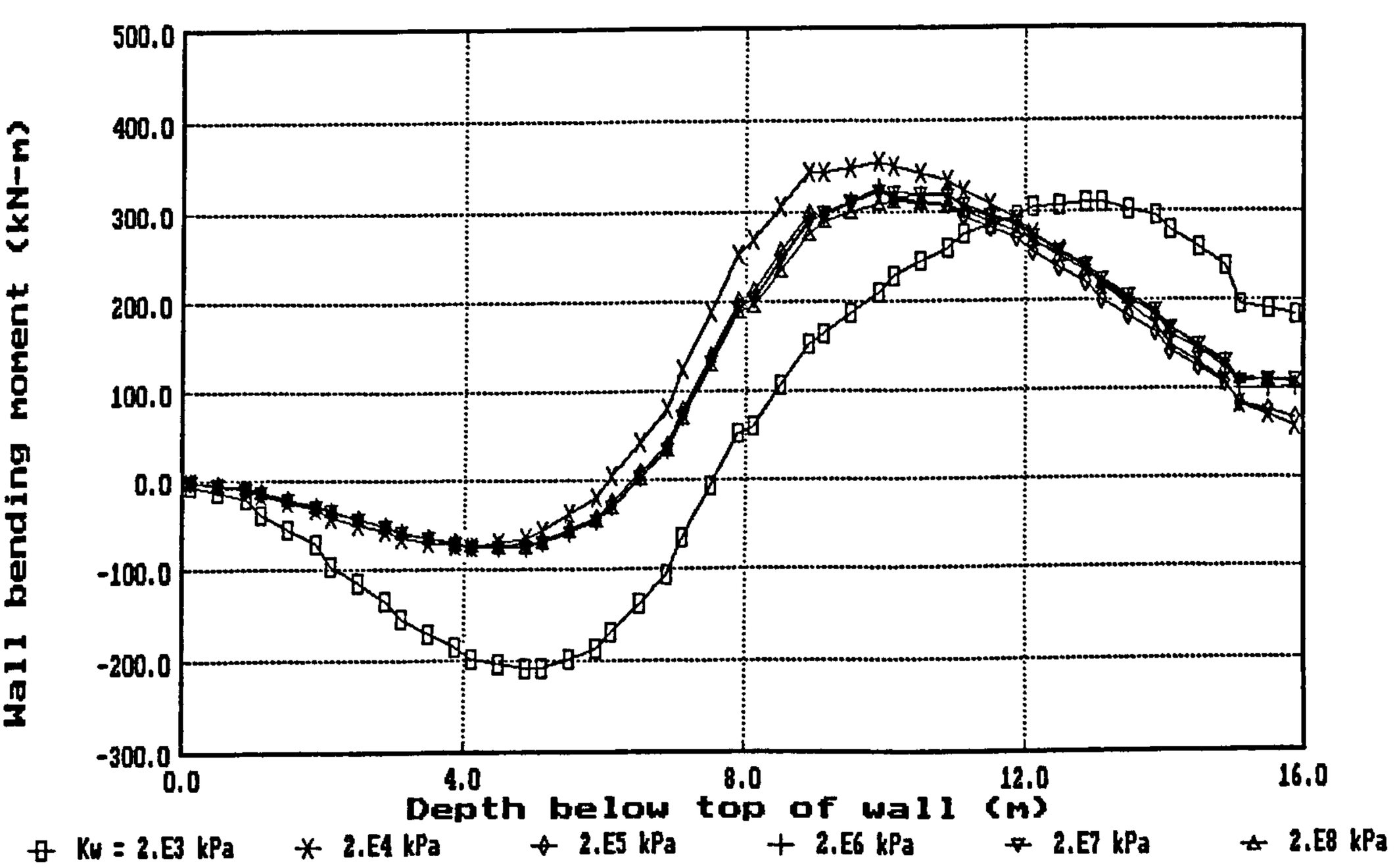

(d) elastic-perfectly plastic soil (set 13)

Fig. B9 Influence of pore fluid compressibility on an effective stress analysis of a cantilever wall : profiles of wall bending moment (contd)

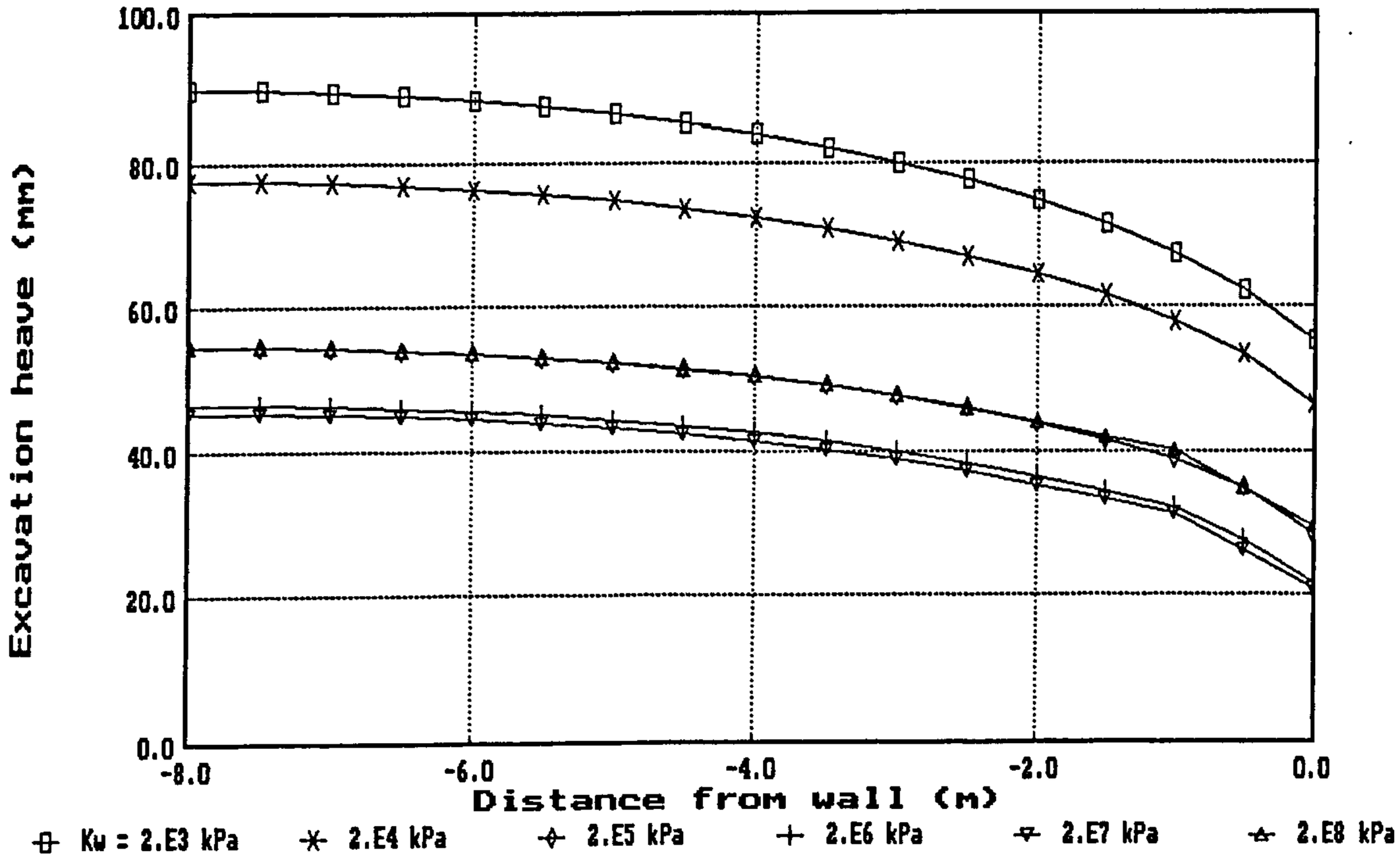

(a) elastic soil (set 1)

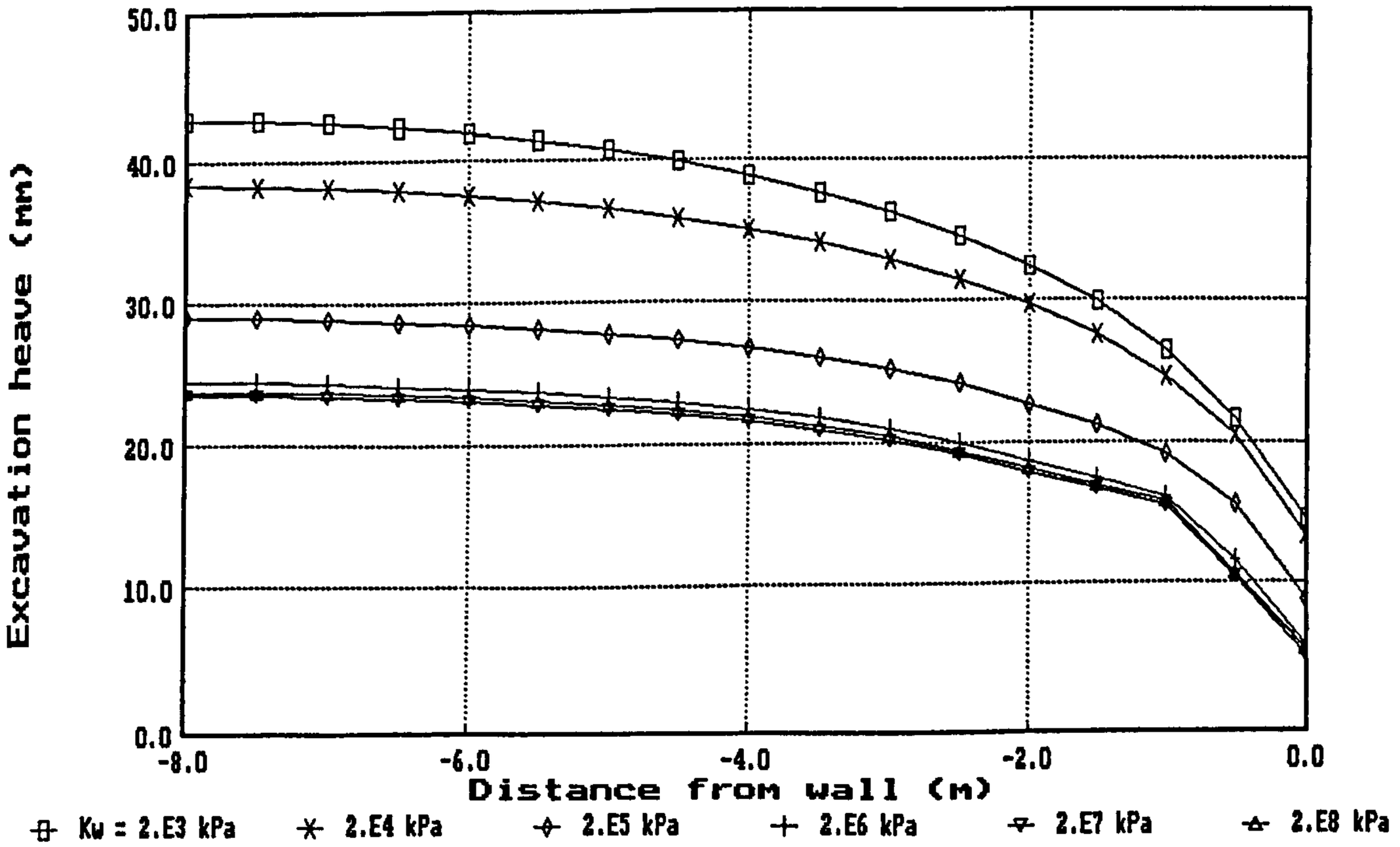

(b) elastic soil (set 3)

Fig. B10 Influence of pore fluid compressibility on an effective stress analysis of a cantilever wall : profiles of excavation heave

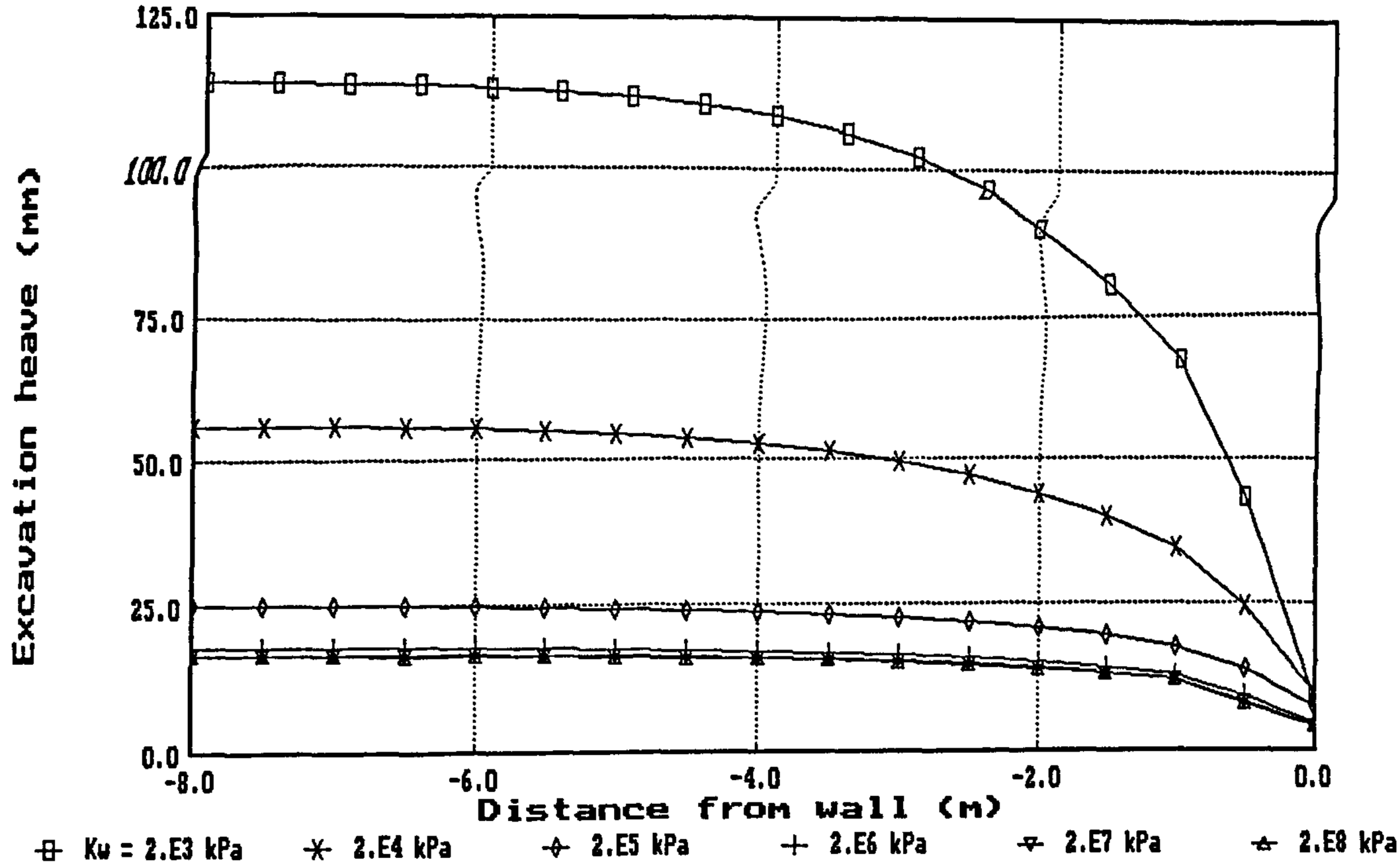

(c) elastic-perfectly plastic soil (set 12)

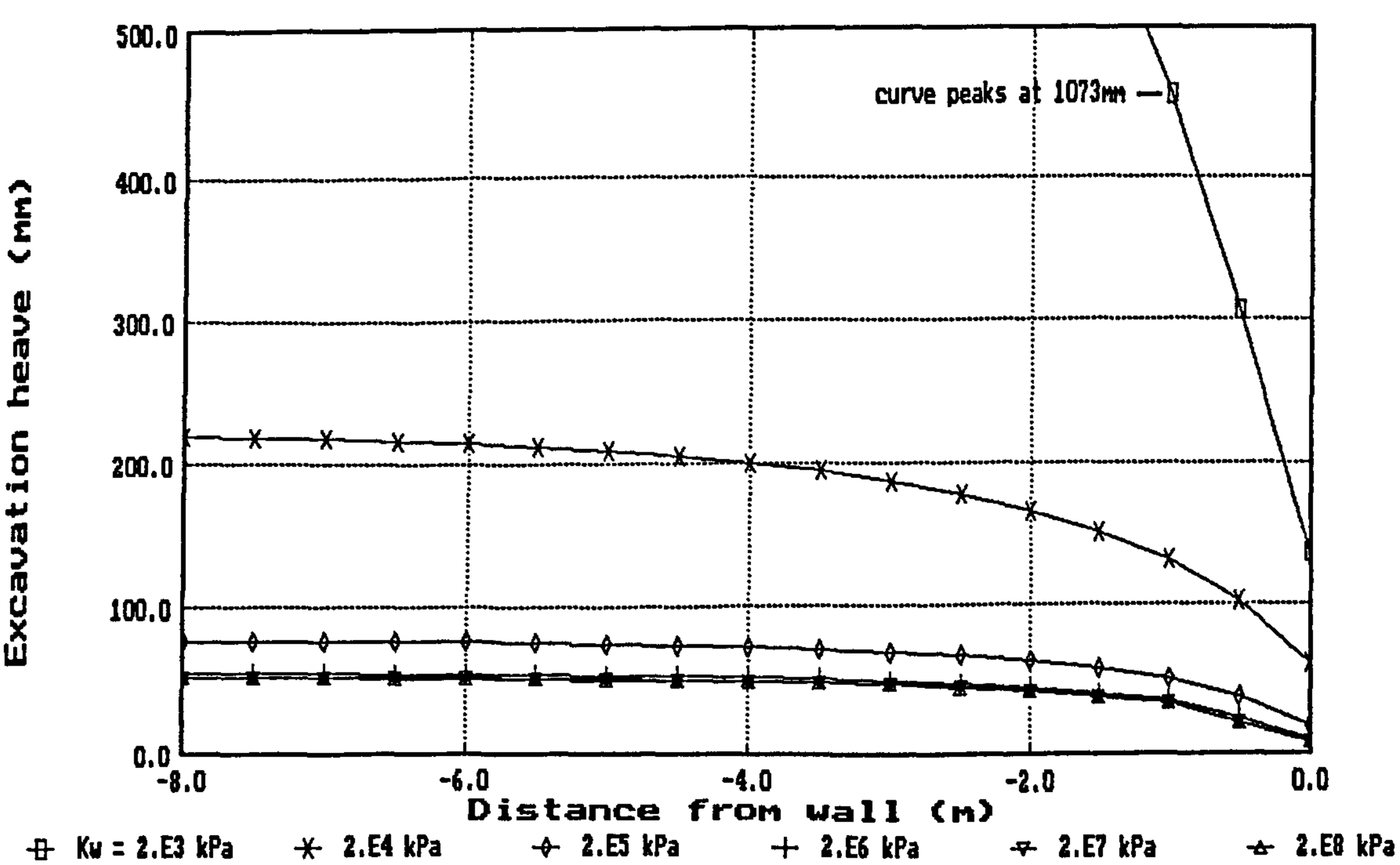

(d) elastic-perfectly plastic soil (set 13)

Fig. B10 Influence of pore fluid compressibility on an effective stress analysis of a cantilever wall : profiles of excavation heave (contd)

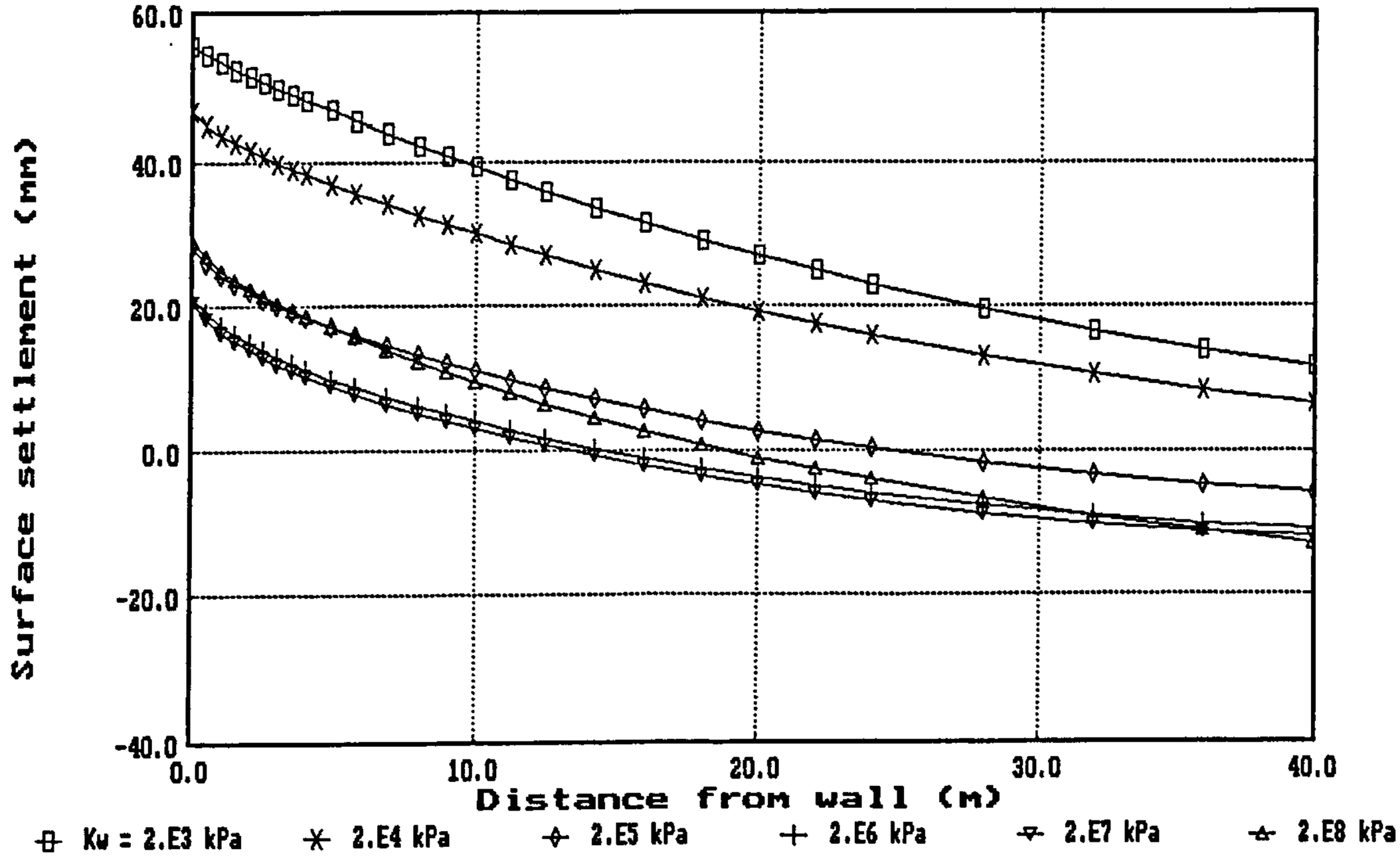

(a) elastic soil (set 1)

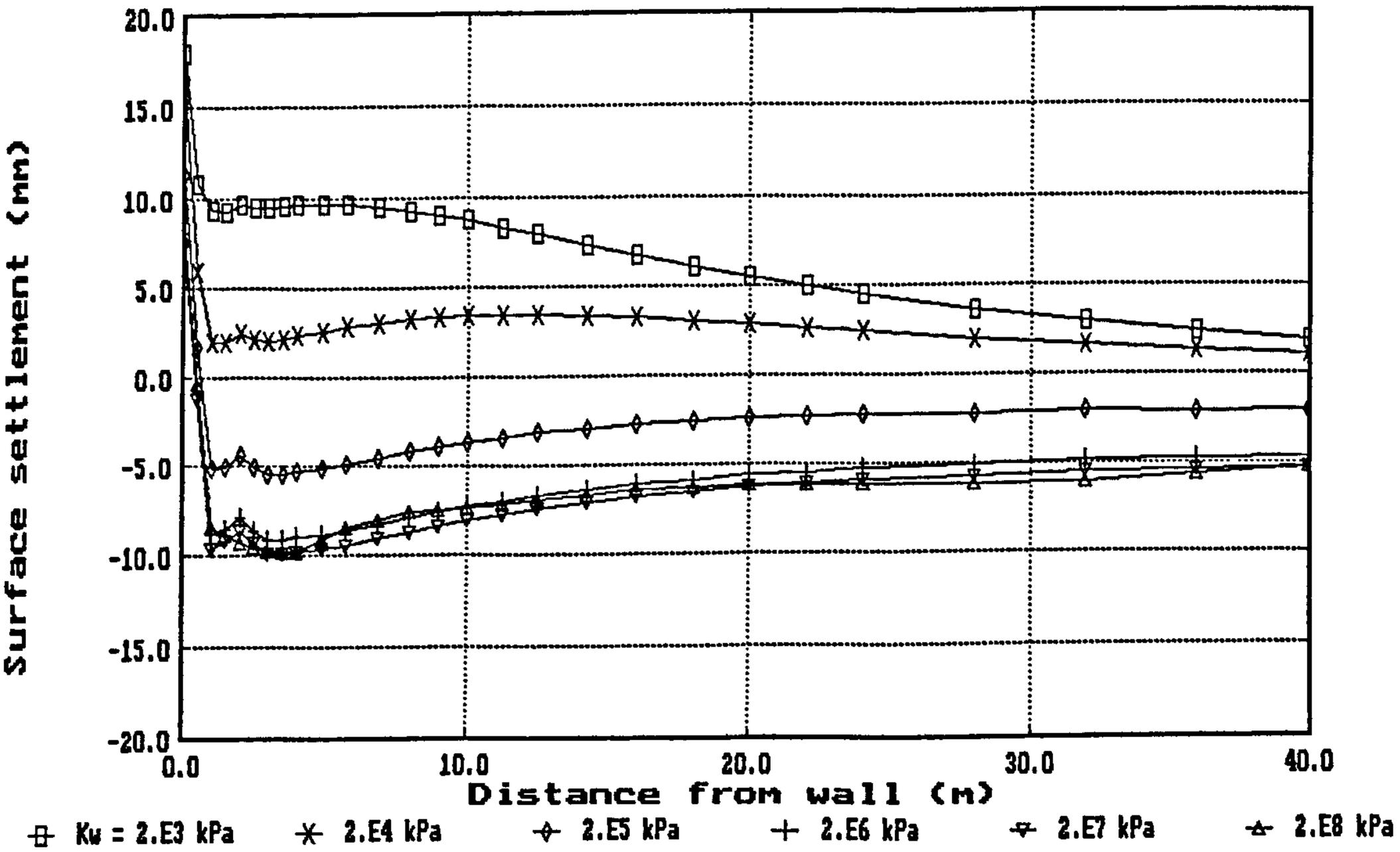

(b) elastic soil (set 3)

Fig. B11 Influence of pore fluid compressibility on an effective stress analysis of a cantilever wall : profiles of ground surface movement

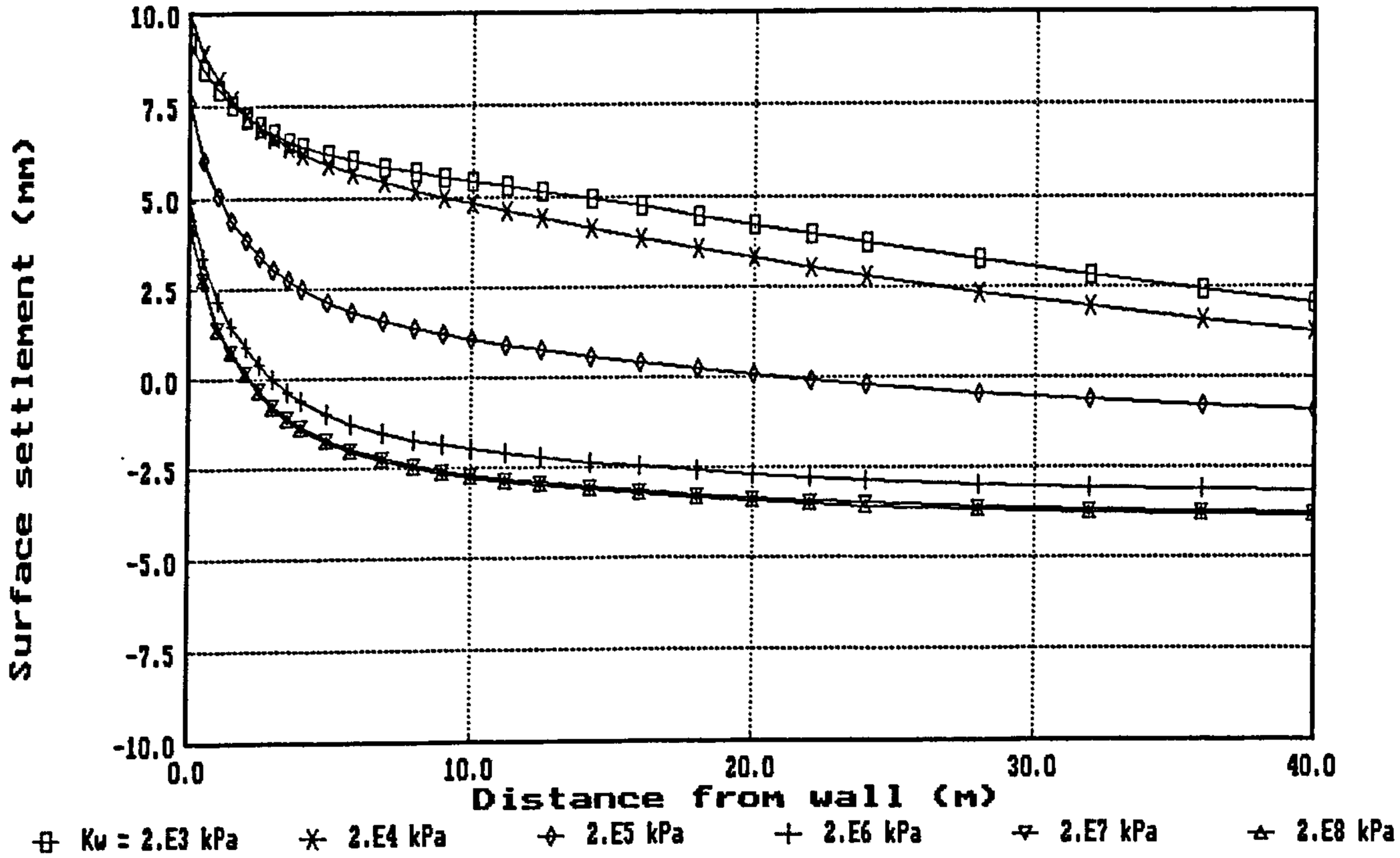

(c) elastic-perfectly plastic soil (set 12)

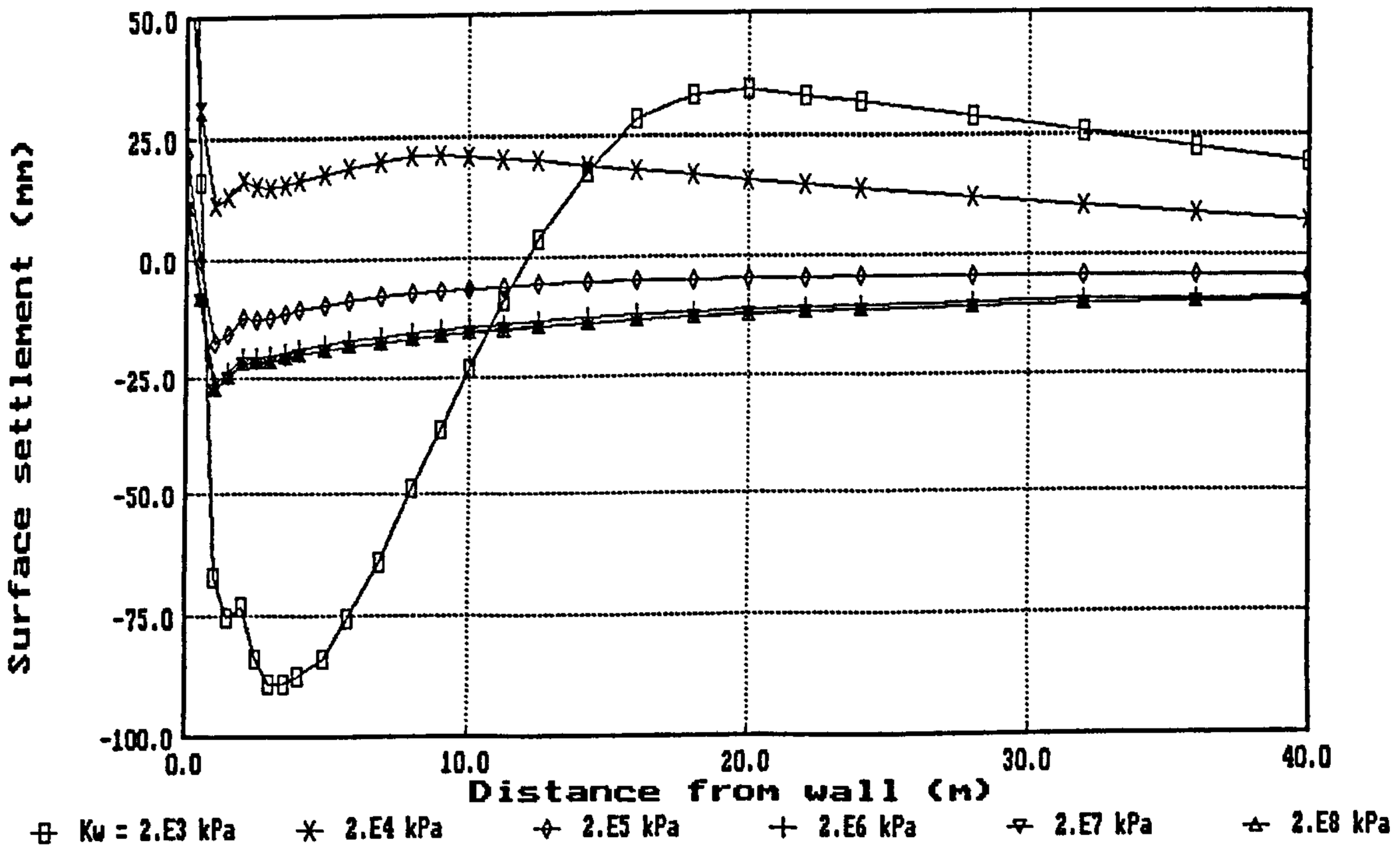

(d) elastic-perfectly plastic soil (set 13)

Fig. B11 Influence of pore fluid compressibility on an effective stress analysis of a cantilever wall : profiles of ground surface movement (contd)

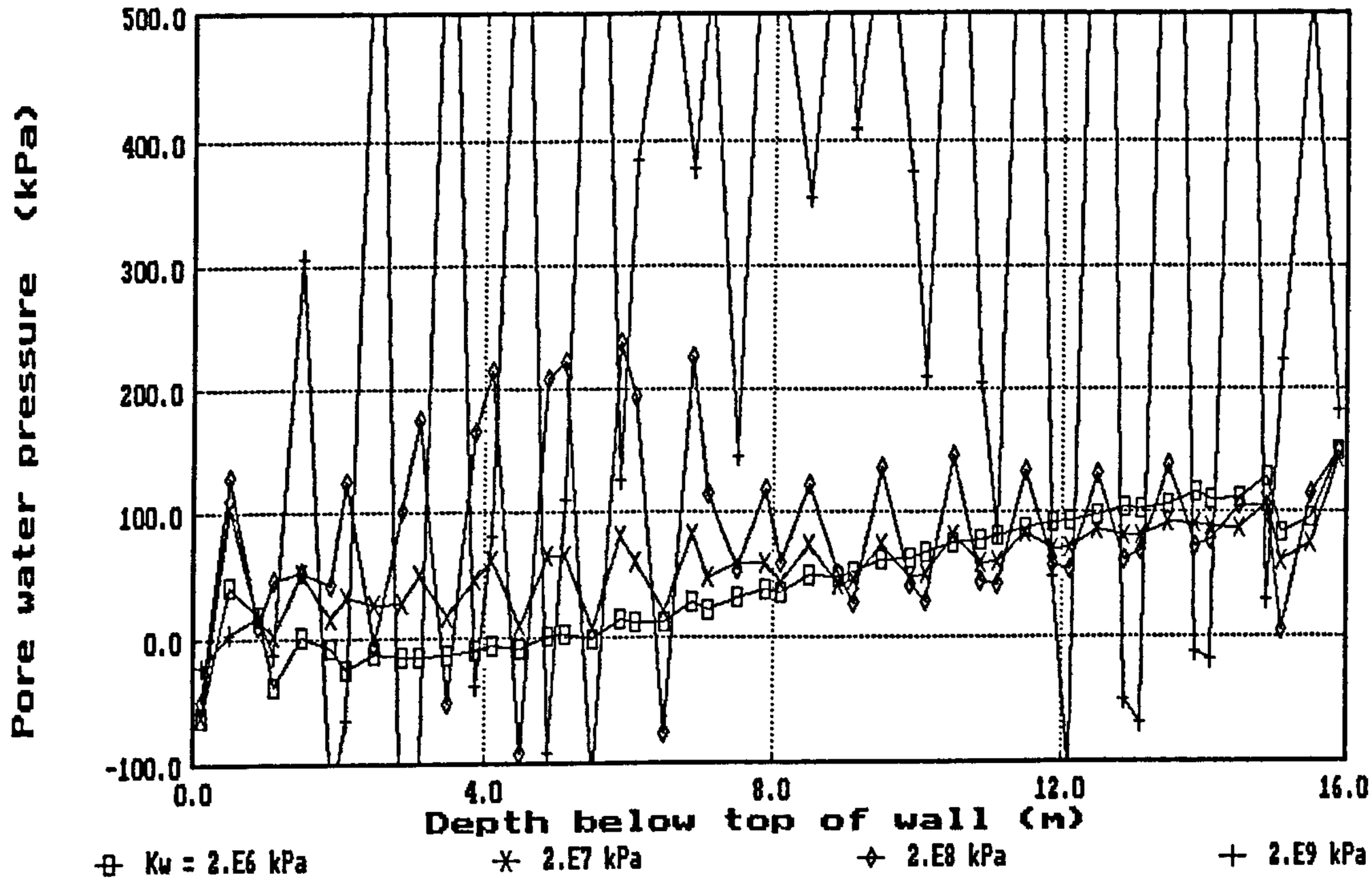

(a) elastic soil (set 1)

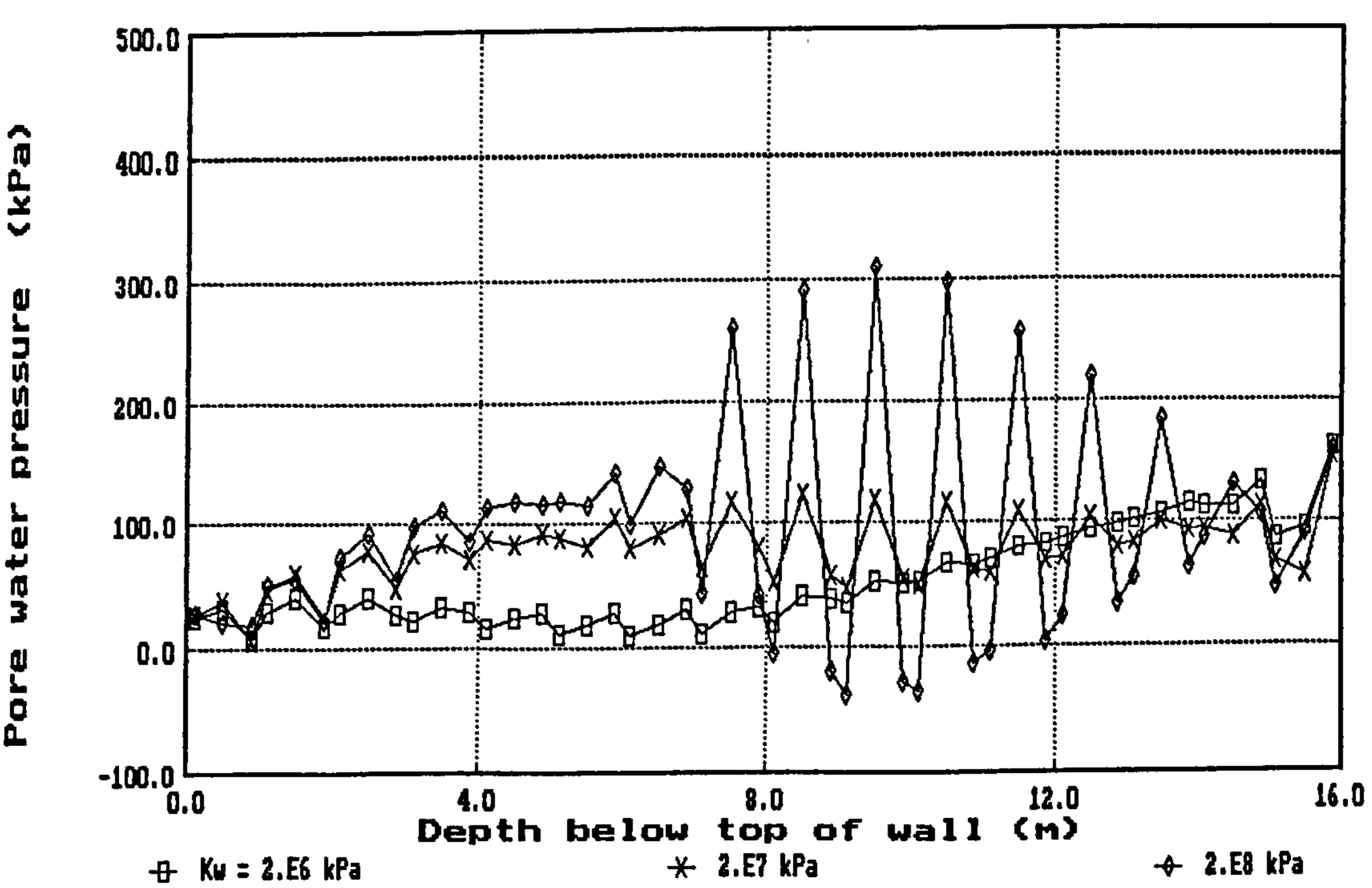

(b) elastic soil (set 3)

Fig. B12 Influence of pore fluid compressibility on an effective stress analysis of a cantilever wall : profiles of pore water pressure on retained side

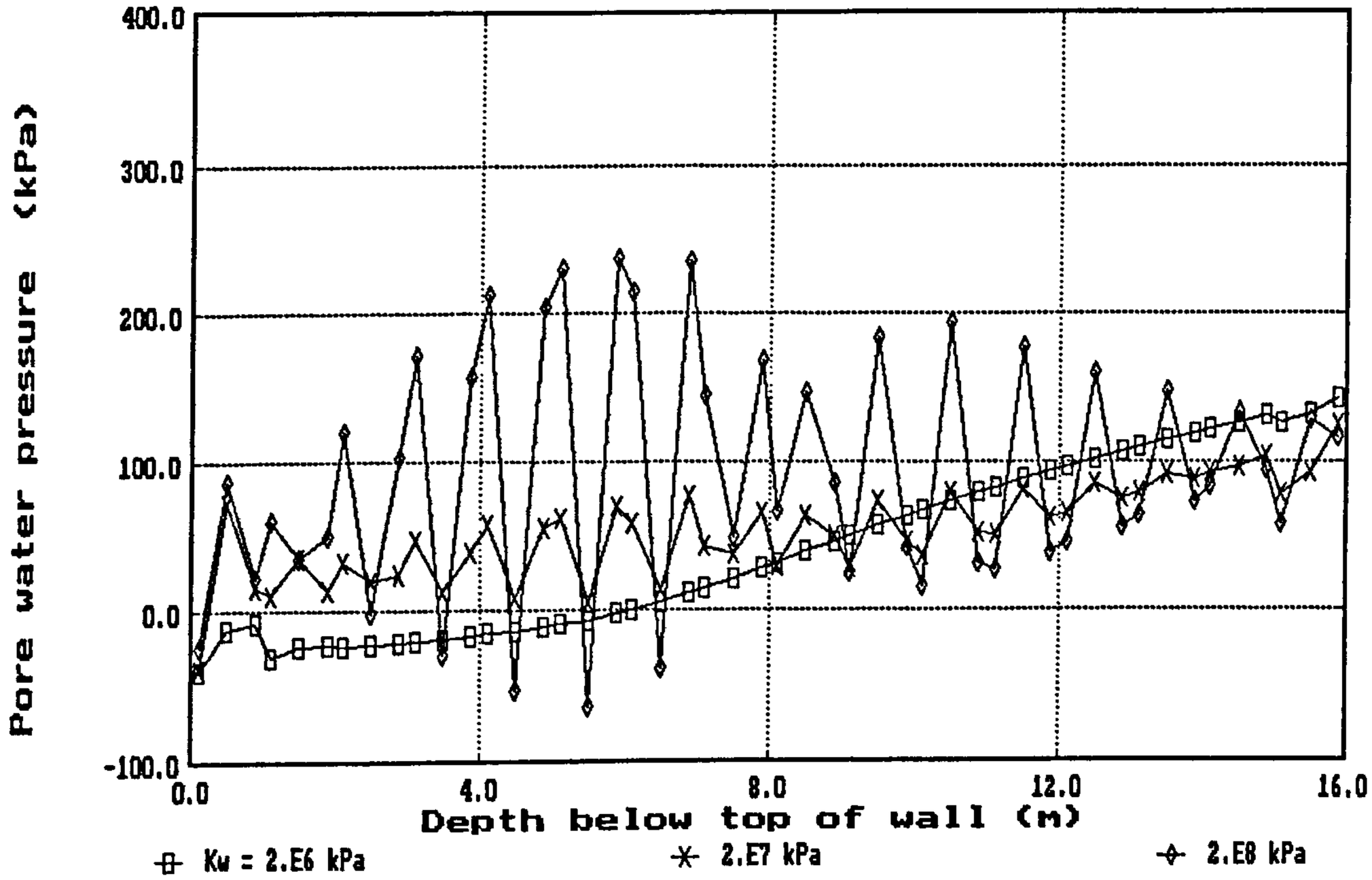

(c) elastic-perfectly plastic soil (set 12)

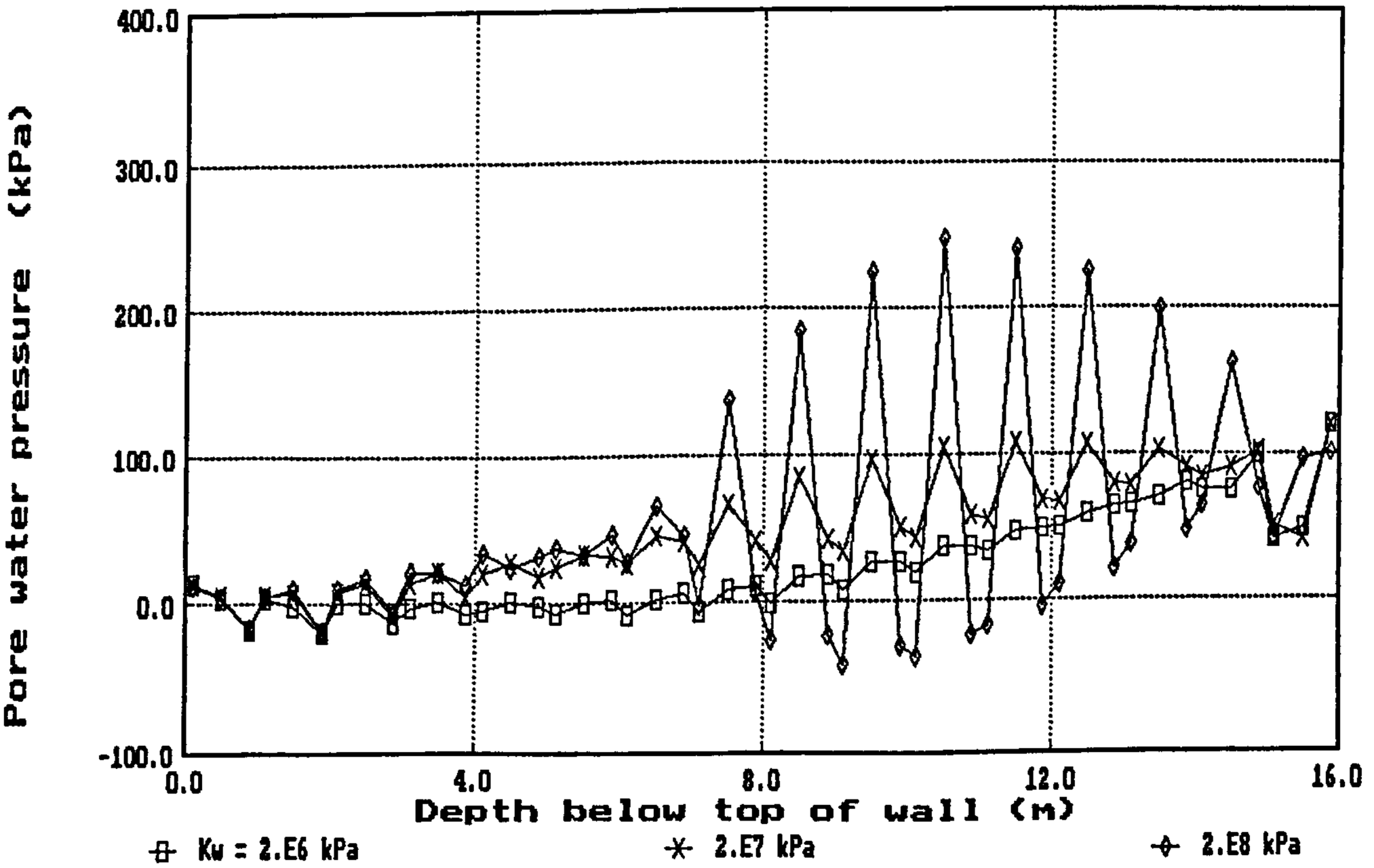

(d) elastic-perfectly plastic soil (set 13)

Fig. B12 Influence of pore fluid compressibility on an effective stress analysis of a cantilever wall : profiles of pore water pressure on retained side (contd)

APPENDIX C

Derivation of Equations for Stress Smoothing

APPENDIX C

Derivation of Equations for Stress Smoothing

C1 Best-fit plane $y = a+bx+cy+dxy$

Such a plane is required as an approximation to the stress values in an element integrated with a 3×3 Gauss point rule. Assume that the approximated stress σ^* is given by:

$$\sigma^* = a + bx + cy + dxy \qquad \text{(C1)}$$

Let the error between the true stress σ and σ^* equal e:

$$e = \sigma - \sigma^* = \sigma - a - bx - cy - dxy \qquad \text{(C2)}$$

Thus the sum of the errors squared (E) taken over all N data points (x_i, y_i) is:

$$E = \Sigma e^2 = \sum_{1}^{N} (\sigma - a - bx_i - cy_i - dx_i y_i)^2 \qquad \text{(C3)}$$

To determine the values of the coefficients a, b, c and d which will minimise E (the least-squares solution), partially differentiate Eqn (C3) w.r.t. to each coefficient, and equate to zero:

$$\begin{aligned} \partial E/\partial a &= 2\Sigma (\sigma - a - bx_i - cy_i - dx_i y_i) \,.\, -1 &&= 0 \\ \partial E/\partial b &= 2\Sigma (\sigma - a - bx_i - cy_i - dx_i y_i) \,.\, -x_i &&= 0 \\ \partial E/\partial c &= 2\Sigma (\sigma - a - bx_i - cy_i - dx_i y_i) \,.\, -y_i &&= 0 \\ \partial E/\partial d &= 2\Sigma (\sigma - a - bx_i - cy_i - dx_i y_i) \,.\, -x_i y_i &&= 0 \end{aligned} \qquad \text{(C4)}$$

Rearranging (C4) leads to:

$$\begin{aligned} \Sigma(a + bx_i + cy_i + dx_i y_i) &= \Sigma \sigma_i \\ \Sigma(ax_i + bx_i^2 + cx_i y_i + dx_i^2 y_i) &= \Sigma \sigma_i x_i \\ \Sigma(ay_i + bx_i y_i + cy_i^2 + dx_i y_i^2) &= \Sigma \sigma_i y_i \\ \Sigma(ax_i y_i + bx_i^2 y_i + cx_i y_i^2 + dx_i^2 y_i^2) &= \Sigma \sigma_i x_i \end{aligned}$$

In matrix form (dropping the subscripts 'i' for clarity):

$$\begin{bmatrix} N & \Sigma x & \Sigma y & \Sigma xy \\ \Sigma x & \Sigma x^2 & \Sigma xy & \Sigma x^2 y \\ \Sigma y & \Sigma xy & \Sigma y^2 & \Sigma xy^2 \\ \Sigma xy & \Sigma x^2 y & \Sigma xy^2 & \Sigma x^2 y^2 \end{bmatrix} \begin{bmatrix} a \\ b \\ c \\ d \end{bmatrix} = \begin{bmatrix} \Sigma\sigma \\ \Sigma\sigma.x \\ \Sigma\sigma.y \\ \Sigma\sigma.x.y \end{bmatrix} \qquad \text{(C5)}$$

where $N (= \Sigma 1) = 9$ for a 3×3 data set).

C2 Best-fit line $y = a+bx$

The derivation is exactly the same as for the best-fit plane, except that coefficients c and d are no longer required. By eliminating the 3rd and 4th row and column from Eqn (C5):

$$\begin{bmatrix} N & \Sigma x \\ \Sigma x & \Sigma x^2 \end{bmatrix} \begin{bmatrix} a \\ b \end{bmatrix} = \begin{bmatrix} \Sigma\sigma \\ \Sigma\sigma.x \end{bmatrix} \qquad \text{(C6)}$$

C3 Best-fit curve $y = a+bx+cx^2$

The error between σ and σ^* is now:

$$e = \sigma - \sigma^* = \sigma - a - bx - cx^2 \qquad \text{(C7)}$$

and the sum of the errors squared E:

$$E = \Sigma e^2 = \sum_{1}^{N} (\sigma - a - bx_i - cx_i^2)^2 \qquad \text{(C8)}$$

Differentiating w.r.t. to each coefficient:

$$\begin{aligned} \partial E/\partial a &= 2\Sigma (\sigma - a - bx_i - cx_i^2) \,.\, -1 = 0 \\ \partial E/\partial b &= 2\Sigma (\sigma - a - bx_i - cx_i^2) \,.\, -x = 0 \\ \partial E/\partial c &= 2\Sigma (\sigma - a - bx_i - cx_i^2) \,.\, -x^2 = 0 \end{aligned} \qquad \text{(C9)}$$

Rearranging (C9) leads to:

$$\begin{aligned} \Sigma(a + bx_i + cx_i^2) &= \Sigma\,\sigma_i \\ \Sigma(ax_i + bx_i^2 + cx_i^3) &= \Sigma\,\sigma_i x_i \\ \Sigma(ax_i^2 + bx_i^3 + cx_i^4) &= \Sigma\,\sigma_i x_i^2 \end{aligned}$$

In matrix form (dropping the subscripts 'i' for clarity):

$$\begin{bmatrix} N & \Sigma x & \Sigma x^2 \\ \Sigma x & \Sigma x^2 & \Sigma x^3 \\ \Sigma x^2 & \Sigma x^3 & \Sigma x^4 \end{bmatrix} \begin{bmatrix} a \\ b \\ c \end{bmatrix} = \begin{bmatrix} \Sigma\sigma \\ \Sigma\sigma.x \\ \Sigma\sigma.x^2 \end{bmatrix} \qquad \text{(C10)}$$